Design, synthesis, and biological evaluation of new RNA ligands : inhibition of miRNA-210 maturation

Marc-Antoine Panosetti

▶ **To cite this version:**

Marc-Antoine Panosetti. Design, synthesis, and biological evaluation of new RNA ligands : inhibition of miRNA-210 maturation. Organic chemistry. Université Côte d'Azur, 2023. English. NNT : 2023COAZ4128 . tel-04461299

HAL Id: tel-04461299

https://theses.hal.science/tel-04461299

Submitted on 16 Feb 2024

HAL is a multi-disciplinary open access archive for the deposit and dissemination of scientific research documents, whether they are published or not. The documents may come from teaching and research institutions in France or abroad, or from public or private research centers.

L'archive ouverte pluridisciplinaire **HAL**, est destinée au dépôt et à la diffusion de documents scientifiques de niveau recherche, publiés ou non, émanant des établissements d'enseignement et de recherche français ou étrangers, des laboratoires publics ou privés.

Conception, synthèse et évaluation biologique de nouveaux ligands d'ARN: inhibition de la maturation du miRNA-210

Marc-Antoine Panosetti

Institut de Chimie de Nice (ICN) et Istituto Italiano di Tecnologia (IIT)

Présentée en vue de l'obtention du grade de docteur en Chimie **d**'Université Côte d'Azur

Dirigée par:
Maria Duca et Benedetto Grimaldi

Co-encadrée par:
Audrey Di Giorgio

Soutenue le: 21 Décembre 2023

Devant le jury, composé de:

Ruth Brenk, Professeure,
University of Bergen
Stefano Moro, Professeur,
University of Padova
Alexandre David, Directeur de Recherche,
Institut de Génomique Fonctionnelle
Audrey Di Giorgio, Maître de Conférences,
Université Côte d'Azur
Benedetto Grimaldi, Senior Researcher,
Italian Institute of Technology
Maria Duca, Directrice de Recherche,
Université Côte d'Azur

DOCTOR COMUNITATIS EUROPEAE

ISTITUTO ITALIANO DI TECNOLOGIA

Design, Synthesis, and Biological Evaluation of new RNA ligands: inhibition of miRNA-210 maturation

PhD Thesis Defense Committee

Reviewers:

Ruth Brenk, Professor, University of Bergen, Norway

Stefano Moro, Professor, University of Padova, Italy

Examiner:

Alexandre David, Director of Research at CNRS, Institute of Functional Genomics, France

PhD Thesis Directors:

Maria Duca, Director of Research at CNRS, Institute of Chemistry of Nice, France

Benedetto Grimaldi, Senior Researcher, Italian Institute of Technology, Italy

PhD Thesis Co-Supervisor:

Audrey Di Giorgio, Associate Professor, Institute of Chemistry of Nice, France

Design, synthesis, and biological evaluation of new RNA ligands: inhibition of miRNA-210 maturation.

The increasing knowledge of functional non-coding RNAs (ncRNA) has outlined their significance in functional biology and their association with various diseases. This has stimulated the need to design and identify small molecules that can selectively interact with RNAs, serving as potential chemical probes and therapeutic agents. MicroRNAs are one of the most widely studied classes of ncRNAs. They play crucial roles in gene expression regulation, and their overexpression is related to several diseases, such as cancers. More specifically, miRNA-210 has been described to play a critical role in the adaptive response of cancer cells toward low oxygen conditions (hypoxia). Therefore, inhibiting its overexpression by using small molecules could lead to new and innovative anticancer agents.

This manuscript discusses the design and preparation of new series of heterocyclic compounds that possess affinity and selectivity toward unique RNA structures, as well as the optimization and biological evaluation of such molecules as RNA ligands *in vitro* and *in cellulo*.

An approach based on using the precursor forms of miRNA-210 as targets for small molecule interaction was developed, thus allowing for direct inhibition of miRNA-210 biogenesis, which impeded its gene regulation function. Through comprehensive structure-activity relationships studies, combined with biochemical measurement of the affinity and selectivity of the newly generated compound, we identified several compounds that proved to be efficient miRNA-210 inhibitors. Further cellular assessment of these compounds correlated their *in vitro* activity with *in cellulo* reversion of hypoxic adaptive response in cancer cells through miRNA inhibition. These small molecules provide suitable chemical scaffolds for developing innovative miR-210 inhibitors for treating hypoxia-related tumors.

Keywords: RNA-ligands; Anticancer agents; Drug Discovery

Conception, synthèse et évaluation biologique de nouveaux ligands d'ARN: inhibition de la maturation du miRNA-210.

L'accroissement des connaissances sur les ARN non codants fonctionnels (ARNnc) a mis en évidence leur importance en biologie fonctionnelle et leur association avec diverses maladies. Cela a stimulé le besoin de concevoir et d'identifier des petites molécules capables d'interagir sélectivement avec ces ARN, servant ainsi de sondes chimiques ou d'agents thérapeutiques potentiels. Les micro-ARN (miR) sont l'une des classes d'ARNnc les plus largement étudiées ; ils jouent un rôle crucial dans la régulation de l'expression des gènes, et leur surexpression est liée à plusieurs maladies telles que les cancers. Plus précisément, le miR-210 a été décrit comme jouant un rôle clé dans la réponse adaptative des cellules cancéreuses aux conditions de faible teneur en oxygène (hypoxie). Par conséquent, l'inhibition de sa surexpression à l'aide de petites molécules pourrait conduire à de nouveaux agents anticancéreux innovants.

Ce manuscrit décrit la conception et la préparation de nouvelles séries de composés hétérocycliques qui présentent une affinité et une sélectivité envers des structures d'ARN uniques, ainsi que de l'optimisation et de l'évaluation biologique de ces molécules en tant que ligands d'ARN *in vitro* et *in cellulo*.

Une approche basée sur l'utilisation des précurseurs du miR-210 en tant que cibles pour l'interaction avec de petites molécules a été développée, permettant ainsi d'inhiber directement la biogenèse du miR-210, ce qui empêcherait sa fonction de régulation génique. Grâce à des études approfondies de relations structure-activité, associées à l'évaluation biochimique de l'affinité et de la sélectivité des nouveaux composés générés, nous avons pu identifier plusieurs composés qui se sont révélés être des inhibiteurs efficaces du miR-210. Une évaluation cellulaire ultérieure de ces composés a permis de corréler leur activité *in vitro* avec la réversion *in cellulo* de la réponse adaptative à l'hypoxie de cellules cancéreuses grâce à l'inhibition du miR. Ces petites molécules représentent des nouveaux inhibiteurs innovants du miR-210 pour le traitement des tumeurs liées à l'hypoxie.

Mot clés : Ligands d'ARN ; Agents anticancéreux ; Drug Discovery

Acknowledgments

First, I would like to thank all the PhD Thesis Committee members for agreeing to spend precious time evaluating this manuscript. I want to begin by thanking Prof. Ruth Brenk and Prof. Stefano Moro for accepting to thoroughly review this manuscript, and I am deeply honored to have the opportunity to discuss my project with both of you. I am also sincerely grateful to Dr. Alexandre David for accepting to join the committee and examine my work.

I must thank the Italian Institute of Technology (IIT) for giving me the opportunity to spend two fruitful working periods abroad in their state-of-the-art laboratories in the beautiful city of Genova. IIT allowed me to spend half of my PhD abroad, which translated into greater independence, adaptability, and resilience. IIT's exciting and open-minded working environment allowed me to meet outstanding researchers and collaborate with amazing colleagues.

I want to express my sincere gratitude to all the people who supported me and played an invaluable role during these three years. To be more personal, I preferred to thank each of them in their respective languages in the following paragraphs.

Ce manuscrit, ce projet, cette collaboration avec l'IIT, ces 3 (voire 5) incroyables années n'auraient pas pu avoir lieu sans ma direction de thèse au sein de l'Institut de Chimie de Nice. Premièrement, Maria, je me dois de commencer ce paragraphe par un grand MERCI. Nous nous sommes connus il y a maintenant 5 ans, je n'étais alors qu'un étudiant de M1 qui probablement n'avait pas encore les idées claires sur son futur professionnel. Tu m'as alors accepté dans ton équipe pour effectuer mon stage de 2 mois, et là, tu as su tout de suite me convaincre d'y rester ! Tellement bien, que je décidai alors de retourner dans ton équipe pour mon stage de M2. Après 3 mois de stage, la pandémie de Covid a malheureusement fortement entravé la suite du projet que tu m'avais confié avec le premier confinement total… Malgré tout il nous a été possible de retourner au labo avant la fin du stage, me permettant de prendre mes derniers repères au labo et de me convaincre qu'une poursuite en thèse serait le bon choix pour moi ! Et voilà qu'il a fallu en chercher une de thèse, je ne vais pas te cacher que j'ai craint de ne pas pouvoir rester dans l'équipe, car à ce moment-là, tu n'avais pas de financement disponible… Quelques semaines plus tard me voilà presque parti pour Rouen, super projet mais quitter le soleil de Nice, mmhh… Et là, un mail de ta part, tu me proposes un projet de thèse en collaboration avec l'IIT à Genova ! Et 3 années plus tard voilà que celui-ci se termine déjà… Alors tout en terminant cette thèse, je te dis merci de m'avoir fait confiance, merci d'avoir cru en moi, merci de toujours avoir trouvé les bons mots dans les moments compliqués ou les moments de doutes. En effet, plus que jamais tu auras su me faire comprendre qu'une thèse n'est pas un sprint, mais plutôt une épreuve d'endurance, avec ses hauts… et ses bas ! Au cours de ces 3 ans, tu as, je crois, même eu peur que je perde ma motivation du début. Mais non, et ça, je le dois à

tes précieux conseils et tes idées arrivées à point nommé quand plus rien ne fonctionnait au labo… Je prends maintenant du recul, et me rends compte que ton exigence et ta rigueur ont fait de moi le jeune chercheur que je suis aujourd'hui. Tu as toujours essayé de répondre à tous nos besoins, que ce soit professionnel avec un labo qui n'a jamais manqué de rien et aussi d'un point de vue personnel, nous laissant la liberté de gérer nos journées de façon autonome. Grâce à toi j'ai découvert le domaine de la chimie médicinale et surtout de l'ARN, et en voici le résultat, qui, j'espère, te rend aussi fier que moi. Sur un plan plus personnel, merci d'avoir toujours tout fait pour faire régner la bonne ambiance dans l'équipe (avec de sacrés repas d'équipes aussi !) et j'espère y avoir contribué aussi, ces lignes ne suffiront pas à exprimer tout le respect et la considération que j'ai pour toi.

Audrey, tout d'abord un grand MERCI à toi aussi, qui vaut plus que tout. Comment ne pas oublier la première fois que je t'ai eu en TD, j'étais alors en L2, et je découvrais alors ta précision et ta rigueur avec toutes ces fiches et ces explications au cordeau. Cette précision et franchise font de toi une personne qui a toujours su nous tirer vers le haut, en nous poussant à nous remettre en question constamment. Sans toi, je n'aurai probablement pas intégré l'équipe en M1, et sans nos discussions tout au long de ces années, je ne serai probablement pas le jeune scientifique que je suis aujourd'hui. Merci pour avoir toujours été là, pour la chimie avec ta patience sans faille lorsque personne ne vient te dire que la manip a fonctionné, mais uniquement que le produit n'est pas pur, ou bien quand tu acceptais de passer des heures avec mes spectres RMN… Dans ces cas-là, tu as toujours eu le commentaire ou la blague qu'il faut, m'ayant permis d'affronter ces 3 années de la meilleure des manières. Sur un plan plus personnel, merci aussi d'avoir cru en moi pour réaliser ce projet que vous m'avez confié et merci pour ta bonne humeur imperturbable même dans les moments plus compliqués que d'autre. Comme pour Maria, je ne peux exprimer entièrement combien j'ai été honoré de travailler avec toi, mais je peux te garantir que tu m'as fait grandir sur le plan pro et perso et je tiens à t'exprimer ma profonde reconnaissance pour cela. Dernier mot, je te promets de te tenir au courant des choses qui fonctionneront pour moi par la suite !

Benedetto, prima di tutto un enorme GRAZIE. Mi ricorderò quando mi avete mandato la mail per il progetto in collaborazione con IIT. Ero incredibilmente felice e onorato, ma anche spaventato devo ammettere… 3 anni fa, non avrei mai pensato poter andare a lavorare in un laboratorio di biologia così, senza tanti problemi. Prima di tutto, grazie per aver sempre creduto nel chimico che ero allora, e grazie per avermi aiutato a diventare il biochimico che sono adesso. La tua grandissima esperienza e la tua capacità a risolvere un problema in un attimo rimarranno sempre un esempio per me, sin dall'inizio sei sempre stato disponibile per qualsiasi domanda o richiesta da parte mia. Non dimenticherò i meeting caffè/sigarette in giro per l'IIT, e devo dire che terrò presente questa cosa in quanto molto utile per cambiare delle solite riunioni in ufficio! I due periodi passati in IIT hanno rappresentato, e rappresentato tuttora, esperienze che hanno cambiato la mia

visione della ricerca e che hanno che hanno avuto un'influenza importante nella mia crescita personale e professionale. Pensare che 3 anni fa non avevo una minima idea di come crescono le cellule… e adesso non mi vedo continuare in progetti senza biologia. Poche righe non basteranno mai a esprimere tutta la mia gratitudine nei tuoi confronti e quanto questa esperienza in IIT mi abbia arricchito personalmente e professionalmente facendomi sentire sempre parte attiva di un grande progetto di collaborazione scientifica.

Nadia, comment te remercier pour tout ce que tu as fait en quelques lignes… Tu m'as connu en L1 et depuis, tu as toujours été incroyable, imprévisible, drôle, simple, sincère ! Tu les aimes tes étudiants et ça se ressent, sache qu'ils t'aiment aussi et ils te remercient pour ta joie de vivre infaillible. Je ne sais comment te remercier pour toujours avoir eu le mot juste, que ce soit pour la manip qui ne marche pas ou pour me remonter le moral pendant la rédaction ! Beaucoup de souvenirs me reviennent en écrivant ces mots, mais je crois que je n'oublierai jamais notre intervention au collège sur le SIDA… Que de situations mémorables, où tu me regardais pour voir comment j'allais m'en sortir avec les questions des 3èmes parfois un peu limite ! Bon vu que tu me l'as répété toujours les jours depuis que tu le sais, je me dois aussi de t'en vouloir pour avoir préféré escalader sur l'Himalaya plutôt que d'assister à ma soutenance, mais sache que ça ne me donne qu'une bonne raison de revenir te voir !!!

Stéphane, nous n'avons peut-être pas échangé très souvent sur le plan professionnel, mais tu as toujours été disponible pour tout ce qui est équipement et autre au labo. Merci, car tout cela a permis de mener à bien ce projet. Bon, je ne peux pas non plus oublier ton fameux gâteau au chocolat (meilleur que celui de Maria mais on ne va pas lui dire) et ton accueil lors des barbecues chez vous, qui ont toujours été un succès.

Christophe, merci pour ton aide tout au long de ces 3 ans. Mes comités de thèses ont toujours été très enrichissants avec tes conseils et tes idées pour faire avancer le projet. Merci, aussi pour nos discussions lors des barbecues chez Maria, ta bonne humeur a aussi participé à la réussite de cette thèse.

Vient maintenant le tour des membres non-permanents de l'équipe. D'abord merci aux « anciens », Benjamin, Sylvain, Mélanie, Alessandro, Lauriane, Mathieu, vous avez tous participé à la bonne ambiance collective qui a été essentielle pour ces 3 années. Chloé, tout d'abord un grand merci pour ton boulot sur les bis-thiazole qui a été source d'inspiration pour mes tris-thiazole et ce fût un honneur de prendre la suite, en quelque sorte, de la doctorante qui a été un exemple au début de ma thèse. Merci aussi pour l'excellente ambiance au labo avec Céline ! Céline, tu es probablement la raison pour laquelle j'ai décidé de poursuivre en thèse, tu as été une encadrante incroyable, parfois psychorigide, mais tu fais partie des personnes qui ont fait de moi le jeune chercheur que je suis maintenant. Sache que ton tiroir a toujours été parfaitement rangé et que tous tes conseils m'ont permis de mener à bien ce projet ! A vous deux, un grand merci et hâte de vous revoir.

Maurinne, Sandra, ou bien la cyclopropane team, merci pour votre bonne humeur et vos précieux conseils au quotidien. Ce fameux congrès à Rome restera dans mes souvenirs, comme les pavés du Vatican sous les roues de la trottinette. Maurinne, la voisine de paillasse parfaite, rien à dire, toujours le sourire et prête à aider l'autre. Ce fût un plaisir de partager avec toi ces 3 années, maintenant faut que je vienne aux USA… ! Sandra, grazie di cuore per la tua simpatia e la tua disponibilità. È stato un onore lavorare con te, e pubblicare con te! In bocca al lupo per la brillantissima carriera che ti aspetta.

Eleonora, Jihed, merci à tous les deux pour votre soutient au cours de ces 3 ans. Eleonora, grazie per la tua onestà e semplicità, è stato un piacere averti come collega. Jihed, merci pour toutes les fois où j'ai oublié de faire ci, de faire ça, et tu as toujours été là ! Ta joie de vivre et ta disponibilité m'ont beaucoup servi pour mener à bien ces 3 années. La thèse ce n'est pas simple c'est sûr, et avoir un collègue sur qui compter c'est si précieux. Nul doute que tu as une brillante carrière qui t'attends !

Marc-Alexandre, Enzo, sans ces deux ingénieurs cette thèse aurait été très différente… Sûrement plus tranquille, mais c'est synonyme d'ennui pour moi, alors merci d'avoir participé à la réussite de ces 3 années. Marc-A on a commencé ensemble, et depuis, tu es le collègue parfait au labo toujours dispo pour tout, réparer un truc ou aider quelqu'un ! Enzo, on n'était peut-être pas dans le même labo (tu as essayé…) mais que de fous rires (après 16h bien entendu). Merci pour ton aide et pour tes conseils. Merci aussi pour avoir été le DJ attitré du 6éme étage ! Trop de souvenirs avec vous, que dire de plus que merci pour ces moments passés ensemble, toujours plein de rebondissements comme à Dublin ou à Florence, pour ceux qui s'en souvienne. Vous êtes grands les mecs, hâte de recommencer !

Je me dois maintenant de remercier le sale stagiaire que j'ai eu à supporter, pardon, encadrer... ! Et dire que le sale stagiaire c'était moi il n'y a pas si longtemps. Merci pour ta précieuse aide, sans laquelle je n'aurai pas pu terminer ma dernière série de composés. Tu as été le plus procédurier des stagiaires mais aussi le plus curieux et rigoureux, ce qui, je le sais te sera très utile pour la suite de ta vie professionnelle.

Vient ensuite le tour des autres membres de l'ICN, il me faudrait 25 pages pour tous vous remercier alors je vais essayer d'être bref. Merci, aux « anciens », Guillaume, Laure, Aurélien, Lorenzo, Steve, Lou, Julien, Mathilde, votre bonne humeur et vos conseils ont été précieux pendant ces 3 années. Pour les plus récents, je dois d'abord exprimer ici mon immense considération pour les deux meilleurs, les deux sans qui je n'aurai pas tenu, sans qui je n'aurai pas su avec qui faire le con, sans qui les 8 ans d'études auraient été infiniment longues… Je pense qu'ils se sont reconnus, Kevin, Philippe, GRAZIE MA. Merci d'avoir toujours été là, à n'importe quel moment, dans n'importe quelle situation improbable. Nous sommes liés tant par nos accidents de voitures que par notre amitié sans faille. Les copains, vous êtes sans doute les deux personnes les plus incroyables que j'ai rencontrées en arrivant

à Nice, je sais qu'il va falloir que je parte bientôt et j'ai la gorge nouée rien que d'y penser, et là ce petit trio prendra encore plus son importance. Mon aventure à l'ICN n'aurait pas été aussi mémorable, voire éprouvante sans le reste de la bande Dia Duit. Rowan, merci pour m'avoir fait rire avec tes oublis ou tes siestes improbables. Julie, merci pour ton soutien quotidien, pour tes conseils (qui aurait été cherché HATU sinon…) et ta franchise. Ta bonne humeur a largement contribué au bon déroulement de cette thèse et tout ce qui va avec. Alexis, le voisin champenois, quelle rencontre ! Merci de m'avoir fait rire pendant ces années et merci pour tes délires avec Philippe qui ont probablement marqué à jamais ces 3 années. Emilie, merci d'abord pour le cadeau mémorable de l'année dernière… un grand merci à notre organisatrice préférée et merci pour tous les moments passés ensemble. Quentin, le calme de la bande, mais tu caches bien ton jeu pour t'avoir vu quelques fois t'ambiancer ! Merci aussi pour les quelques soirées passées chez toi ! Je vais rajouter ici un merci aux deux petites nouvelles de la bande, Emma et Eden, qui en 2 semaines parmi nous, ont prouvé que la relève était assurée de la meilleure des manières. Merci à vous tous, avec du recul, je me rends vraiment compte de la chance que j'ai de vous avoir connu, alors hâte d'être au prochain épisode.

Comment pourrais-je ne pas remercier le groupe historique, celui du master, celui avec qui les souvenirs sont interminables et pas forcément racontables ici. Chris, Julie, Tony, Dorian, Julie, un grand merci pour nos les nombreux moments ensembles qui ont permis de passer ces 3 années intenses de la meilleure des façons. Chris, merci pour ton accueil dans le canton, toujours mémorable. Julie, il en faudrait des lignes, mais en tout cas merci pour avoir toujours été là, depuis le début. N'importe quel moment je pouvais t'écrire, et je savais que tu allais me donner la plus honnête des réponses, parfois dure mais vraie. Avoir quelqu'un comme toi sur qui compter est inestimable. Dorian, mon corse préféré, que de bons souvenirs à refaire le monde autour d'un bon verre ! Julie, merci pour ta bonne humeur constante et pour nous avoir reçus à maintes reprises chez vous. Tony, merci d'avoir toujours été toi-même, merci pour tes blagues toujours les bienvenues. A vous tous, merci d'être là, et merci de faire partie de cette histoire.

Non posso non ringraziarvi, il gruppo IIT, per la vostra accoglienza e estrema simpatia ! Michela, Ale, Francesco, Michele, Vera, Marco, Luce, Andrea, Alessandra, Matteo, Cristiano, Raffaele, Alessio, Federico, Gabriele, Rachele, Francesca... Spero di non dimenticare nessuno, è stato un piacere conoscervi e lavorare con voi. Una menzione speciale per il gruppetto dei diversi viaggi, Roma, Grenoble... Quanti ricordi che hanno reso questi tre anni indimenticabili e mi hanno fatto sorridere; tutti insieme siamo un bel gruppo, mi avete subito messo a mio agio e fatto sentire parte di qualcosa di bello

Trois années de thèse, ce sont des hauts et des bas, et si j'ai pu garder le cap, c'est aussi grâce au soutien de ma famille. Je suis loin de vous géographiquement, mais je sais pouvoir compter sur vous à n'importe quel moment. Ce n'est pas sans être nostalgique que je vois la fin de cette thèse, mais aussi de ces 8 années d'études arriver. Rédiger une thèse,

devoir s'enfermer et rester devant un ordinateur pendant des heures, c'est une souffrance, c'est sûr… Mais finalement, en prenant du recul, je dois dire que je suis heureux, certes soulagé d'avoir terminé toutes ces pages, et surtout fier du manuscrit qui suit. Cher Parents, Maman, Papa, votre éducation, vos encouragements, votre soutien quotidien tout simplement, m'ont permis d'en arriver là. Cette thèse vous est entièrement dédiée, probablement sans vous, je ne me serai jamais lancé dans des études si longues, mais vous m'avez donné les clés pour y arriver en me montrant ce que travailler et gagner sa vie signifiait, dès le début. C'est cela qui m'a définitivement donné envie d'y aller, de me lancer dans une licence, un master, une thèse, et j'espère vous rendre fiers. Aucun mot n'exprimera toute la reconnaissance que je porte aux valeurs que vous m'avez transmise et à tout ce que vous m'avez permis de réaliser jusqu'à présent.

Table of Contents

Table of Figures

Table of Schemes

Table of Tables

List of Abbreviations

ACI	*Acute Cerebral Infarction*
ADME	*Absorption, Distribution, Metabolism, and Excretion*
AI	*Artificial Intelligence*
AIDS	*Acquired ImmunoDeficiency Syndrome*
ALDHSA1	*Aldehyde Dehydrogenase 1*
ASC	*Human Adipose Stromal Cells*
ASO	*Antisense Oligonucleotides*
ATP	*Adenosine Triphosphate*
BCL2	*B-cell Lymphoma 2*
BDNF	*Brain Derived Neurotrophic Factor*
BMAL1	*Basic helix-loop-helix ARNT like 1*
BNIP	*BCL2 Interacting Protein 3*
CA9	*Carbonic Anhydrase 9*
CASP8AP2	*Caspase-8-Associated Protein-2*
CCG	*Clock-Controlled Genes*
Chem-CLIP	*Chemical Cross-Linking and Isolation by Pull-Down*
CLOCK	*Circadian Locomotor Output Cycles Kaput*
CNE	*Cellosaurus cell line*
COVID-19	*Coronavirus Disease of 2019*
CRISPR	*Clustered Regularly Interspaced Short Palindromic Repeats*
CRY	*Cryptochromes*
Cryo-EM	*Cryogenic Electron Microscopy*
CSC	*Cancer Stem Cells*
DCM	*Dichloromethane*
2-DCS	*2-Dimensional Combinatorial Screening*
DDQ	*2,3-Dichloro-5,6-Dicyano-1,4-benzoQuinone*
DECP	*Diethyl Chlorophosphate*
DGCR8	*DiGeorge Syndrome Critical Region 8*
DMF	*Dimethylformamide*
DMSO	*Dimethyl sulfoxide*
DNA	*Deoxyribonucleic Acid*
DSB	*Double-Strand Break*
DSF	*Differential Scanning Fluorimetry*
EC_{50}	*Half maximal effective concentration*
EDC	*1-Ethyl-3-(3-dimethylaminopropyl) carbodiimide*
EDQ	*Eclipse Dark Quencher*
ELCCA	*Enzyme-Linked Click Chemistry Assay*
EMSA	*Electrophoretic Mobility Shift Assay*
ESCC	*Esophageal Squamous Cell Carcinoma*
FAM	*6-Carboxyfluorescein*
FBDD	*Fragment-Based Drug Discovery*

FDA	*Food and Drug Administration*
FGFRL1	*Fibroblast growth Factor Receptor-Like 1*
FOXP3	*Forkhead box P3*
FRET	*Förster Resonance Energy Transfer*
GD	*Grave's Disease*
GFP	*Green Fluorescent Protein*
GPD1L	*Glycerol-3-Phosphate Dehydrogenase 1 Like*
GSK	*GlaxoSmithKline*
HATU	*Hexafluorophosphate Azabenzotriazole Tetramethyl Uronium*
HCT-116	*Human Colorectal Carcinoma-116*
HER2	*Human Epidermal growth factor Receptor 2*
HIF	*Hypoxia-Inducible Factor*
HIV	*Human Immunodeficiency Virus*
HOAt	*1-Hydroxy-7-Azabenzotriazole*
HOSu	*N-Hydroxysuccinimide*
HOXA1	*Homeobox A1*
HPASMC	*Human Pulmonary Artery Smooth Muscle Cells*
HPLC	*High-Performance Liquid Chromatography*
HRM	*Hypoxia-regulated miRNAs*
HRMS	*High-Resolution Mass Spectrometry*
HRP	*Horseradish Peroxidase*
HTS	*High-Throughput Screening*
IC_{50}	*Half maximal Inhibitory Concentration*
IPF	*Idiopathic Pulmonary Fibrosis*
JUN	*Transcription Factor JUN*
K_D	*Dissociation Constant*
$KHSO_4$	*Potassium Bisulfate*
LATS2	*Large Tumor Suppressor Kinase 2*
LEF	*Local Environment of Fluorine*
LNA	*Locked Nucleic Acid*
LON	*Mitochondrial LON Protease*
LYN	*Tyrosine-Protein Kinase Lyn*
MAX	*MYC Associated Factor X*
MCF	*Michigan Cancer Foundation*
MEC	*Mammary Epithelial Cells*
miR	*MicroRNA*
miRNA	*MicroRNA*
MNT	*MAX Network Transcriptional Repressor*
NAFLD	*Non-Alcoholic Fatty Liver Disease*
NMR	*Nuclear Magnetic Resonance*
NOESY	*Nuclear Overhauser Effect Spectroscopy*
PCR	*Polymerase Chain Reaction*
PDCD4	*Programmed Cell Death Protein 4*
PER	*Period*
PHD	*Prolyl Hydroxylase Domain enzyme*

PIK1	*Phosphatidylinositol 4-Kinase*
PR	*Progesterone Receptor*
PTEN	*Phosphatase and Tensin Homolog*
PTPN2	*Protein Tyrosine Phosphatase Non-receptor type 2*
RAD52	*Radiation Sensitive 52*
RIBOTAC	*Ribonuclease Targeting Chimeras*
RISC	*RNA-induced Silencing Complex*
RNA	*Ribonucleic Acid*
ROS	*Reactive Oxygen Species*
RT-qPCR	*Reverse Transcription Quantitative Real-Time Polymerase Chain Reaction*
SAR	*Structure-Activity Relationship*
SFDA	*Chinese Food and Drug Administration*
SHAPE	*Selective 2′-hydroxyl Acylation analyzed by Prime Extension*
SMA	*Spinal Muscular Atrophy*
SMM	*Small Molecule Microarray*
STAT	*Signal Transducer and Activator of Transcription*
STD	*Saturation-Transfer Difference*
TAR	*HIV Trans-Activation Response RNA*
TGP	*TargapremiR*
THF	*Tetrahydrofuran*
Th17	*T helper 17 cells*
TLC	*Thin Layer Chromatography*
TNBC	*Triple-Negative Breast Cancer*
TRBP	*TAR RNA-binding Protein*
UTR	*Untranslated Region*
UV	*Ultraviolet*
VEGF	*Vascular Endothelial Growth Factor*
VHL	*Von Hippel-Lindau Protein*

Preface

From drug discovery to small molecules targeting RNA

Preface | From drug discovery to small molecules targeting RNA

The discovery and development of novel drugs is a critical aspect of modern healthcare, as it plays a vital role in preventing, treating, and curing various diseases. As our understanding of disease mechanisms grows, there is a pressing need for drugs that target such disorders more precisely and with fewer side effects. Given the limitations of current therapies and the emergence of drug-resistant pathogens, innovative therapeutic solutions are of the most significant importance. Despite challenges, ongoing novel drug research has the potential to transform the way we treat diseases and improve the health outcomes of patients. Over the years, technological advances, and new insights into the biological mechanisms of diseases have provided opportunities to discover novel drugs[1,2]. Today, drug discovery involves a multidisciplinary approach integrating diverse research fields, including chemistry, biology, pharmacology, and computational sciences.

The development of new therapeutics that target proteins has been a significant focus of the pharmaceutical industry for several decades, resulting in a vast array of successful drugs that target human and pathogenic proteins. Despite advances, the number of targetable macromolecules has remained limited, prompting a shift towards exploring non-protein drug targets[3,4]. One promising avenue of exploration is the use of new medicines to modulate RNA, which could significantly broaden the landscape of targetable macromolecules by more than an order of magnitude.

Once considered to be only a passive intermediary between DNA and proteins, RNA has become a key player in the fields of medicinal chemistry and chemical biology. Since the discovery of ribosomal and transfer RNA (rRNA and tRNA, respectively) in the 1950s[5], the concept of non-coding RNA (ncRNA) with precise biological functions has been studied. After sequencing the human genome, it became apparent that only a tiny percentage (1.5%) of transcribed DNA codes for proteins[6,7], (***Figure 1***) and an even lower part is the actual target of marketed drugs. This realization has sparked a growing interest in expanding the scope of drug targets beyond proteins. Indeed, this leaves a vast amount of non-coding RNA that could be explored as therapeutic targets, thus widening the landscape of current medicinal chemistry. Non-coding RNAs are now recognized to have various roles in cellular processes such as transcriptional and post-transcriptional gene expression regulation (riboswitches, siRNA, piRNA)[8], catalysis (ribozymes)[9], and splicing (lncRNA, snRNA)[10]. As more research has uncovered the critical roles RNAs play in various cellular processes, it has become increasingly evident that RNA is also a significant player in the development and progression of diseases. Several RNA-implicating disorders have been identified, including

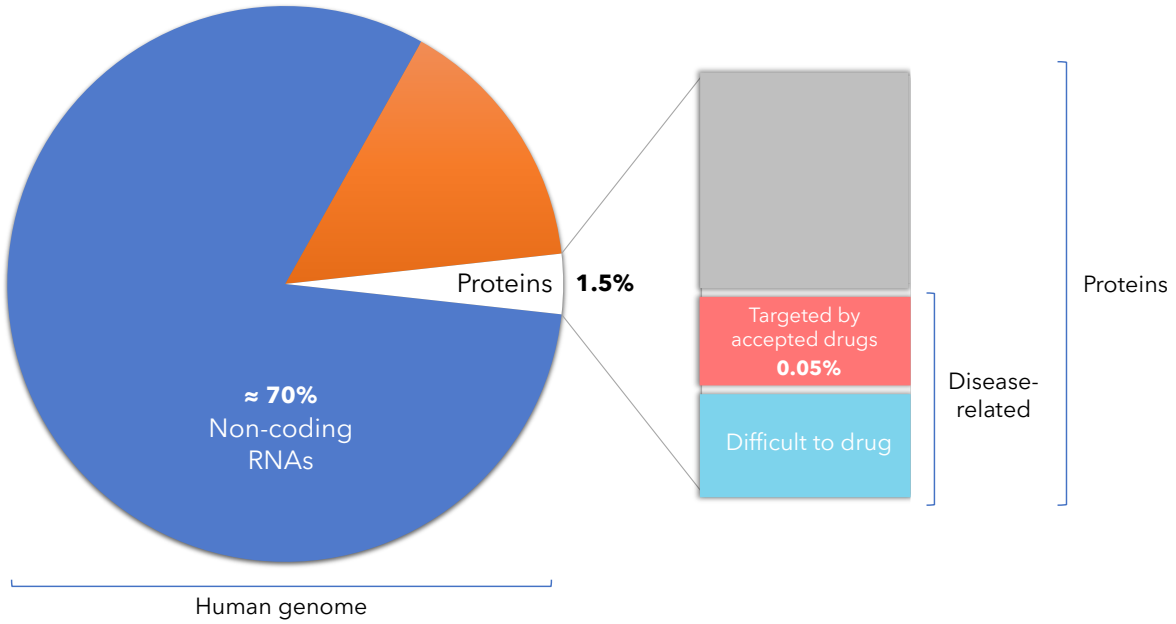

Figure 1 *- The druggable RNA world.*

cancer[11], genetic disorders[12], and viral infections[13]. The growing understanding of RNA's diverse and essential functions has led to a greater appreciation of its involvement in disease states, and ongoing research in this area is uncovering new insights into the mechanisms by which RNA contributes to pathophysiology.

Researchers are exploring new ways to target these biomolecules based on these observations. Among the approaches being investigated, antisense oligonucleotides (ASOs) have shown promising results in inhibiting the function of specific ncRNAs[14]. ASOs recognize RNAs by sequence complementarity thanks to the formation of Watson-Crick-Franklin hydrogen bonds with single-stranded RNAs. Oligonucleotides are essential tools for studying RNA functions and their potential therapeutic applications. However, their use remains limited due to bioavailability, delivery issues, and pharmacodynamic and pharmacokinetic drawbacks[15]. Furthermore, since biologically relevant ncRNAs are highly structured, oligonucleotides cannot access and interact efficiently with these structures. Nevertheless, some solutions have been found, leading to various ASOs being approved by regulatory agencies[16]. Yet, a complementary approach using small molecules has been developed and holds great promise for chemical intervention on RNA biological functions and treating various diseases[17].

While ASOs recognize a linear sequence of RNA, small molecules target specific sites in structured ncRNAs that fold into specific three-dimensional structures, facilitated by the association of single-stranded and double-stranded regions[18,19]. Binding typically occurs in the structural pockets or cavities formed within the ncRNA molecule;

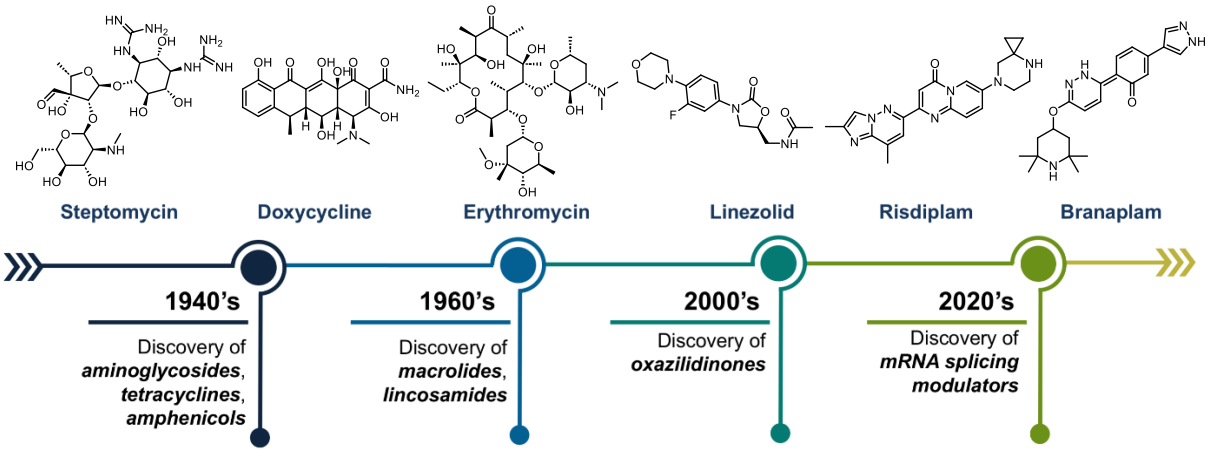

Figure 2 *- Timeline of RNA binders.*

these binding pockets are analogous to the binding sites found in proteins. By interacting with such structured ncRNAs, small molecules can affect their folding, stability, localization, and interactions with other molecules. This can lead to the modulation of ncRNA functions, such as regulating gene expression, RNA processing, and cellular signaling pathways. The development of small molecules is an active area of research, very well documented in the literature[18,20-23], as these molecules have the potential to be used as therapeutic agents for various diseases.

The beginning of RNA-targeting ligands can be traced back to the early 1940s (***Figure 2***) with the discovery of aminoglycoside natural compounds, whose streptomycin is the earliest example[24]. Aminoglycosides bind to prokaryotic ribosomal RNA and inhibit bacterial protein synthesis, which is the basis for their mechanism of action as antibiotics. Chemical compounds like streptomycin are composed of positively charged aminooligosaccharides that can interact with the negatively charged RNA backbone, this electrostatic interaction being essential for their excellent binding. In addition, the three-dimensional shape of aminoglycosides allows them to interact selectively with a specific pocket in the A-site region of prokaryotic ribosomal RNA[22,25]. The discovery of aminoglycosides and their interaction with RNA provided the first insights into the potential of RNA as a therapeutic target.

After discovering aminoglycosides as ribosome binders with antimicrobial activities, many other classes of natural and synthetic compounds were found to interact with RNA and inhibit protein synthesis. These compounds include tetracyclines (e.g., doxycycline, ***Figure 2***), macrolides (e.g., erythromycin, ***Figure 2***), and oxazolidinones (e.g., linezolid, ***Figure 2***), which have diverse chemical structures ranging from highly positively charged aminoglycosides to smaller heterocyclic and heteroaromatic compounds. In recent years, the RNA-targeting field has gained increased attention, and the FDA approval of risdiplam

as an RNA-splicing modulator for treating spinal muscular atrophy (SMA) highlighted the therapeutic potential of RNA-targeting drugs[26,27].

Overall, looking at the success of small molecules targeting RNA in both the private and academic sectors, small molecules targeting RNAs hold excellent potential for developing novel therapeutics for a wide range of diseases, including antiproliferative activity on different cancers. Therefore, our group, *Targeting Nucleic Acids* in the Institute of Chemistry of Nice (ICN), is working on the design, synthesis, and biological evaluation of small-molecule RNA binders for the targeting of non-coding RNAs toward anticancer and antimicrobial strategies. Accordingly, my PhD project is based on a collaboration with the *Molecular Medicine Research Line* of the Italian Institute of Technology (IIT). It aims to synthesize small molecules as inhibitors of the biogenesis of a specific miRNA to repress its oncogenic role. To that extent, my PhD thesis is organized in four different chapters.

Chapter I provides a literature review in the context of targeting RNA. The first sections detail how and why the historical therapeutic targets, proteins, are gradually being replaced by RNA. More specifically, non-coding microRNAs, their role in several diseases, and their potential as therapeutic targets will be extensively reviewed. A non-exhaustive presentation of their known ligands and their *in vitro*, *in cellulo*, or even *in vivo* evaluations highlight the challenges that medicinal chemists are still facing in this fast-evolving field of drug discovery and the tools developed to address them. The last section focuses on a specific miRNA referred to as miRNA-210. The whys and hows of this latter are presented, outlining its crucial role in the adaptation to low oxygen levels of cancer cells. Conclusive remarks show how miRNA-210 inhibition can be an innovative therapeutic approach in cancer chemotherapy.

Chapter II describes the optimization process of a previously identified miRNA-210 inhibitor. To improve this published compound's affinity and inhibition activity, 7 new analogs were prepared and evaluated *in vitro via* biochemical assays for their effective inhibition of miRNA-210. An *in cellulo* toxicity pattern of each of the newly generated analogs was obtained, highlighting strict links between chemical structure and biological activity.

Chapter III details the design, synthesis, and biological evaluation of new miRNA ligands possibly capable of reducing oncogenic miRNA-210 levels and impeding any resistance mechanisms in cancer cells. The synthesis of 31 innovative compounds and the rational design process that led to their preparation are described. The following sections present *in vitro* assessments of their affinity and inhibition activity toward the RNA target. The ability of the new compounds to inhibit miRNA-210 levels and its related downstream targets is described, correlating *in vitro* results with *in cellulo* response.

Chapter IV concludes the study by summarizing the key research findings related to the project aims and challenges and discussing the value and contribution to the field of RNA targeting. Limitations of this study are also presented, and outlooks for future research are proposed.

Chapter I

Literature Review

Chapter I | Literature review

The work presented in this manuscript focuses on developing small molecules to target oncogenic miRNAs. Harnessing the power of miRNAs as therapeutic targets has emerged as a promising strategy for developing innovative treatments. Targeting miRNAs offers a unique therapeutic approach due to their ability to modulate multiple genes and pathways simultaneously. By manipulating the levels of specific miRNAs, it becomes possible to modify their activity, leading to changes in the expression of target genes involved in disease pathways. However, developing effective miRNA-targeted therapies requires a thorough understanding of the biological mechanisms. Additionally, careful consideration of delivery methods to reduce potential off-target effects and a deep understanding of the structure of the miRNA target are essential. While miRNA-based treatments are in their early stages of development and face obstacles before widespread clinical development, the continuous progress in miRNA research provides valuable information into this exciting field[28,29]. It paves new ways for personalized medicine and the treatment of diverse diseases but also uses the developed chemical tools better to understand miRNAs' structure, roles, and functions. This sub-chapter aims to explore strategies employed in targeting miRNAs for therapeutic applications. It will encompass techniques for identifying disease-associated miRNAs, approaches to modulate miRNA expression and activity, and the challenges associated with miRNA-based therapies.

I.1 microRNAs: micromessengers of the genome

As mentioned earlier in this manuscript, ncRNAs play essential roles in various disease pathways. NcRNAs can be divided into long non-coding RNAs (lncRNAs) and small ncRNAs. Initially, "small RNA" was associated with any ncRNA from 50-250 nucleotides (nt). This term has been used to encompass every "very" small ncRNA, such as siRNA, piRNA, and microRNAs (miRNA or miR) (***Figure 3***), on which I will focus in this work[30].

I.1.1 A class of non-coding RNAs

MicroRNAs are single-stranded RNA molecules that typically range in length from 20 to 25 nucleotides. They regulate post-transcriptional gene silencing by interfering with the translation of mRNAs into proteins. The discovery of the first microRNA goes back to 1993

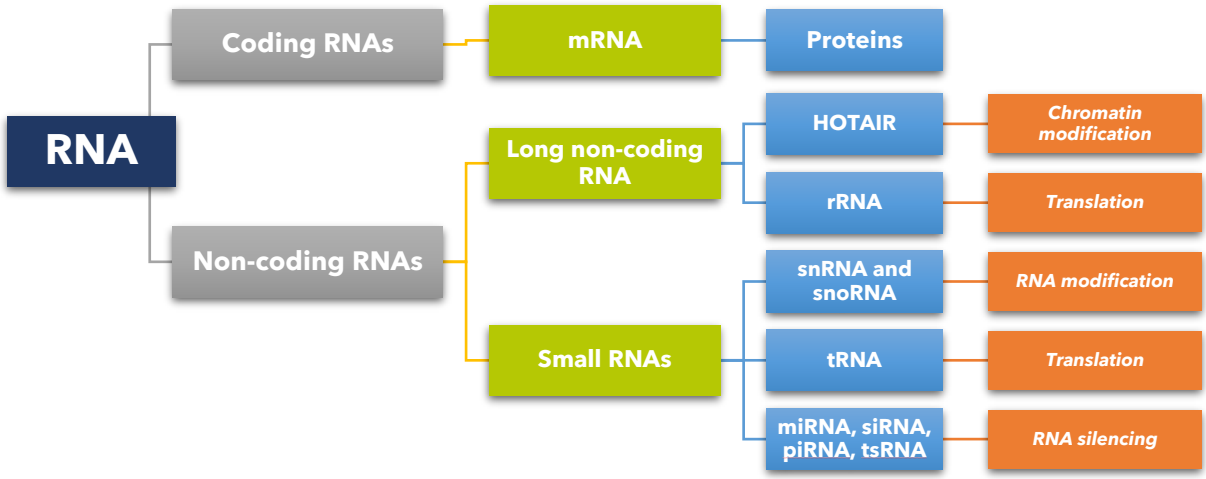

Figure 3 *- Eukaryotic RNA nomenclature and function.*

when Ambros and Ruvkun's research groups highlighted *lin-4* in *Caenorhabditis elegans*[31,32]. Firstly, they discovered that the *lin*-4 gene was coding for a pair of small RNAs, one longer than the other, and proposed that the longer one was a precursor of the shorter one. Then, they realized that both RNAs had antisense complementarity with regions of the 3'-untranslated region (UTR) of the *lin-14* gene. They went on to demonstrate that the shorter *lin-4* regulated *lin-14* by reducing *lin-14* protein levels but no significant decrease in the levels of the corresponding mRNA. *Lin-4* has since then been known to translationally repress the *lin-14* biological pathway, along with being the first member of the most widely studied class of ncRNAs.

Today, the microRNA databank called miRbase (www.mirbase.org) has the complete and confirmed sequences of 38 589 miRNAs in different species, 2 654 being mature human miRNAs that regulate approximately 60% of protein-coding genes[33]. When working with such a vast number of biomolecules, proper nomenclature is essential to distinguish each miRNA from the other. The nomenclature of microRNAs follows a standardized system that allows for their efficient identification and categorization. MiRNAs are named based on their species of origin, followed by a unique number assigned to each unique sequence. For instance, in humans, miRNAs are denoted as hsa-miR (*Homo sapiens*), followed by a three-digit number. This number is assigned chronologically, ensuring each identified miRNA has a distinct identifier[34,35]. MicroRNAs are synthesized (see section I.1.2) as a duplex, giving rise to miRNA-#-5p and miRNA-#-3p; the 5p strand arises from the 5' end of the precursor miRNA hairpin while the 3p strand originates from the 3' end. Hence, miRNAs can have

different isoforms (nearly identical sequences), denoted by a lowercase letter following the number. For example, miR-181a and miR-181b share the same sequence, except for three nucleotides (nt).

Their role in many processes has now been confirmed in many cellular pathways such as apoptosis, proliferation, hematopoiesis, differentiation, or embryonic development; some of them are known to regulate a few genes, but others, called *master regulators*, are key miRNAs playing a role in the regulation of hundreds of genes[36]. Complex networks of activation or repression exist since each miRNA acts on different mRNA targets; new techniques are now used to understand and assess miRNA expression levels, highlighting new biological and cellular pathways. Reverse Transcription Quantitative Polymerase Chain Reactions (RT-qPCR) or hybridization-based microarrays have revolutionized miRNA expression profiling to gain knowledge on disease progression. MiRNAs can be either underexpressed, leading to protein upregulation, or overexpressed, causing a repressive activity on protein levels. Given those profiling efforts, many miRNAs are now linked to being the cause, or significant contributors, of several diseases like arrhythmia, Alzheimer's, or deafness (***Table 1***).

Disease	Engaged miRNA	Reference
Alzheimer's disease	miR-107	Wang *et al.*[37]
Parkinson's disease	miR-184, let-7	Gehrke *et al.*[38]
Spinal motor neuron disease	miR-9	Haramati *et al.*[39]
Arrhythmia / Hypertension	miR-1	Yang *et al.*[40]
Deafness	miR-96	Lewis *et al.*[41]
Cardiac disorder	miR-21	Thum *et al.*[42]
Rett's syndrome	miR-382, miR-29, miR-146	Urdinguio *et al.*[43]

Table 1 *– List of miRNAs involved in non-cancer diseases.*

A subclass of miRNA recently roused researchers' interest after discovering that such miRNA expression is dysregulated in human cancer through various mechanisms. MicroRNAs can act either as tumor suppressors or oncogenes in cancer, depending on their specific targets and functions[44-46]. Tumor suppressor miRNAs inhibit the expression of oncogenic proteins, thereby acting as a defense mechanism against cancer. For example, let's consider miR-34a, a well-known tumor suppressor miRNA. It is frequently downregulated in various cancers and plays a critical role in inhibiting the expression of genes, like MYC or BCL2, involved in cell proliferation and survival[47,48]. MiR-21 can be cited as the most widely studied; it represses the expression of tumor-suppressing genes like PTEN and PDCD4[49,50]. Notably, it must be noted that the roles of miRNAs in cancer are often tissue and tumor-specific. For instance, in solid cancers originating from epithelial cells, as

well as in lymphomas and leukemia, miR-155 is frequently upregulated and acts as an oncogene, promoting tumor proliferation. However, miR-155 is often downregulated in endocrine tumors, suggesting a potential tumor-suppressive role in this context[51]. These tissue-specific variations in miRNA expression and function highlight the complex and diverse nature of miRNA involvement in cancer, where their effects can vary depending on the specific type of cancer and cellular context. Understanding these multiple roles of miRNAs can provide valuable insights into the tumorigenesis mechanisms and may lead to the development of targeted therapeutic approaches tailored to specific cancer types.

I.1.2 MicroRNA biogenesis

MicroRNAs (miRNAs) are formed through a complex biogenesis pathway (***Figure 4***). The process starts with the transcription of miRNA genes by RNA polymerase II or III, generating primary miRNA transcripts (pri-miRNAs)[52,53]. Pri-miRNAs are typically several hundred nucleotides long and contain specific structures that are recognized and cleaved by an enzyme complex made of an RNA binding protein, DiGeorge Syndrome Critical Region 8 (DGCR8), and a ribonuclease III (RNase III) enzyme, Drosha; they work cooperatively to produce a precursor miRNA (pre-miRNA), which is approximately 70-100 nucleotides long[54,55]. The pre-miRNA is then exported from the nucleus to the cytoplasm with the help of the exportin-5 protein. Another RNase III enzyme called Dicer recognizes

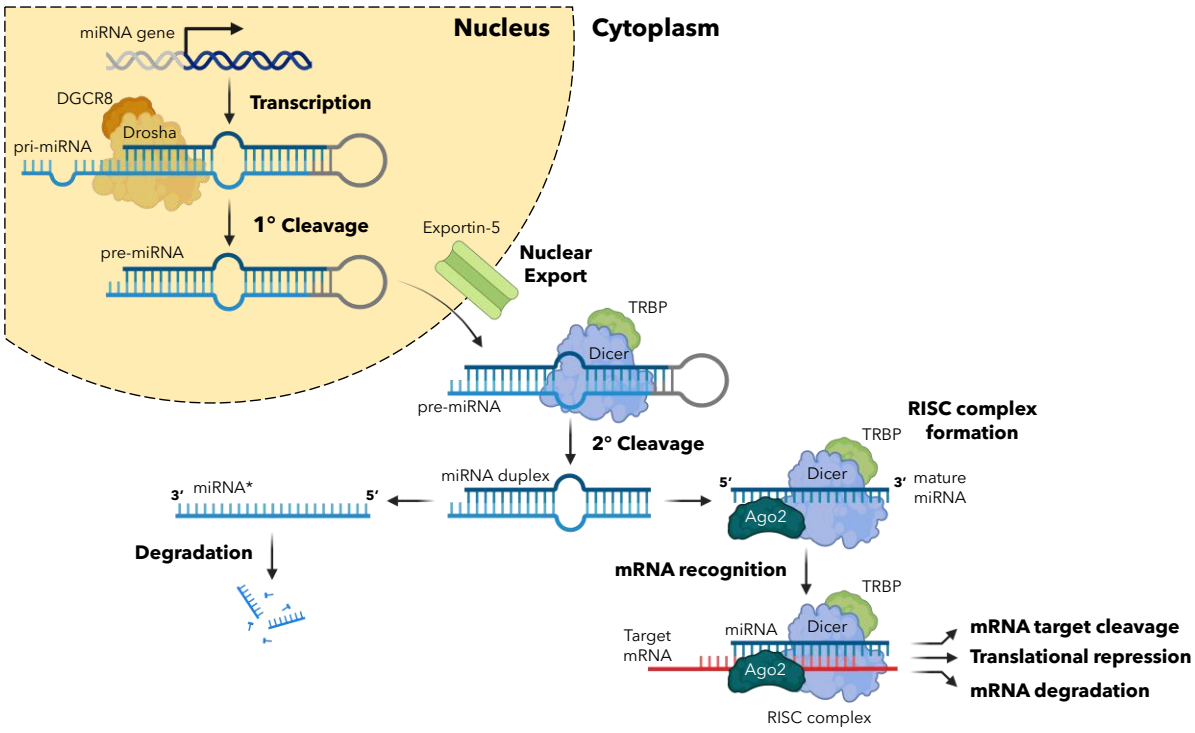

Figure 4 *– Canonical microRNA biogenesis and mechanism of action.*

and cleaves the pre-miRNA in the cytoplasm, forming a double-stranded RNA molecule[56]. Unlike Drosha, Dicer can act alone, but a protein partner, TRBP, has been identified to ensure the perfect processing of pre-miRNAs. The resulting double-stranded RNA is approximately 20-24 nucleotides in length and consists of a miRNA duplex.

Argonaute proteins, key RNA-induced silencing complex (RISC) components, bind to the miRNA duplex. The duplex is unwound, and one strand called mature miRNA, is selectively loaded into the Argonaute (Ago) protein. The other strand, the passenger strand (or miRNA*), is typically degraded. A mature miRNA sequence consists of a 5' and a 3' end; the 5' end of the miRNA contains a phosphate group protecting the biomolecule from degradation. Whereas the 3' end is less stable but is a recognition site for the loading into the RISC complex. The miRNA duplex's thermodynamic stability and structural features guide the selection process[57]. At this point, Dicer, TRBP, Ago, and the mature miRNA form the RNA-induced silencing complex (see RISC complex in *Figure 4*). The mature miRNA guides the RISC complex to target messenger RNAs (mRNAs) with complementary sequences[58].

The binding of the mature miRNA to the target mRNA at the 3'-UTR extremity can lead to translational repression or degradation of the mRNA, resulting in post-transcriptional gene silencing[59]. This regulation of gene expression by miRNAs is involved in numerous cellular processes, including development, differentiation, and response to various stimuli, as mentioned earlier in this manuscript.

It is worth noting that while this is a general overview of miRNA biogenesis, known as the canonical pathway, there can be some variations and additional regulatory steps depending on the specific miRNA and cell type[60]. To date, different non-canonical pathways have been highlighted, mainly reporting a different role or function of the proteins involved in the canonical pathway. Some documented processes are described as Dicer-independent or Drosha/DGCR8-independent[61,62].

I.1.3 From Structure to Therapeutic Targeting of miRNAs

While a single-stranded short stretch of oligonucleotides constitutes miRNAs, miRNA precursors adopt unique and complex 3D structures based on different levels of organization. They usually fold as a hairpin-like structure with a stem-loop configuration. The stem region of the miRNA is formed by Watson-Crick-Franklin base-pairing between complementary nucleobases (***Figure 5A***), thus creating a duplex; this stem region provides stability to the molecule. Unpaired nucleotides form what are known as loops. For example,

small internal loops can be found at the base of the stem. Loop regions are typically shorter in length than the stem and can adopt different structural patterns, such as bulges, internal loops, or hairpin loops (***Figure 5B***). Noteworthy, miRNA structure can vary; not all miRNAs possess the same features. The general structure outlined above represents the typical characteristics of the majority of miRNAs[63,64].

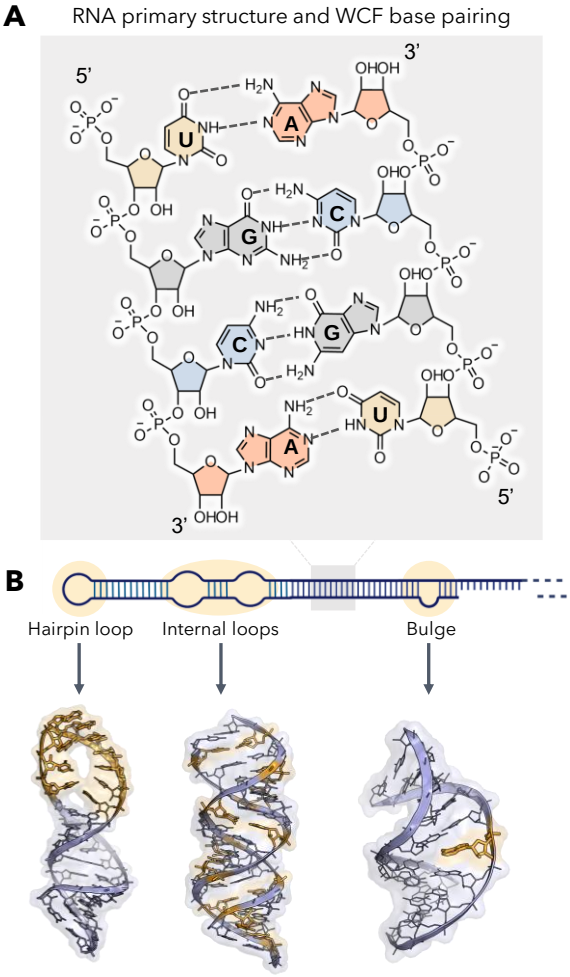

Figure 5 *- Overview of RNA primary and secondary structures. (A) Nucleotide building blocks of RNA primary structure. Each consists of a ribose sugar, containing a 2′ hydroxyl unique to RNA over DNA; phosphodiester groups, which connect the 5′ and 3 ′ hydroxyl groups of the ribose sugars; and adenine, guanine, uracil, and cytosine nucleobases, which define the sequence of an RNA molecule. Canonical Watson–Crick–Franklin hydrogen bonding patterns are shown in the middle. Dashed lines represent hydrogen bonds. (B) Example of canonical RNA secondary structures.*

Two strategies are employed to target miRNAs: antisense oligonucleotides (ASOs) and small molecules (***Figure 6***). The first is a straightforward way of targeting a disease-related, linear sequence of a mature miRNA with a complementary sequence of nucleotides. Still, as mentioned earlier in the manuscript, ASOs need better pharmacokinetic and pharmacodynamic properties. On the other hand, small molecule inhibitors are also being explored as another recent means of targeting highly structured miRNAs. In this approach,

as shown in ***Figure 6***, small molecules can target a precise RNA structure, hardly accessible by ASOs, of one of the precursors of miRNA biogenesis to prevent the maturation of overexpressed miRNAs.

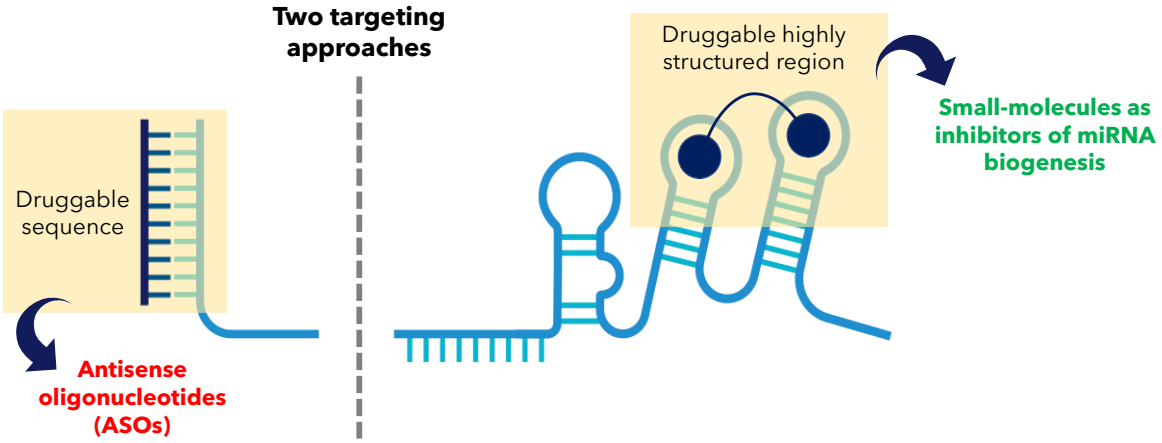

Figure 6 *- Two major ways to affect miRNA by lead medicines.*

Antisense Oligonucleotides (ASOs)

ASOs have already been extensively studied as gene-silencing agents and can be designed to have a sequence that is complementary to the specific mature miRNA target. They usually range from 15 to 22 nucleotides in length and can be employed to target disease-related miRNAs. They are generally referred to as antimiRs, and their function is based on complementary base pairing to sequester the mature miRNA[65]. Hence, antimiRs are in competition with the target mRNA, but when bound, they inhibit the miRNA and allow for the restoration of normal gene expression patterns [66].

The first appearance of antimiRs in the literature goes back to the mid-2000s, with unmodified sequences and thus low stability towards nucleases and poor cellular uptake[67,68]. In the following years, significant progress was made in antimiR chemistry, leading to various modifications. One promising idea was locked nucleic acids (LNAs), where the ribose sugar is conformationally blocked by a bridge between the 2′ oxygen and the 4′ carbon. Ribose, now blocked in *endo* conformation, provides increased cellular stability to the ASO. Other modifications came from the 2′ position on the sugar; methyl groups, fluorine, or methoxyethyl groups were inserted to improve stability and cellular uptake[68]. All these modifications (and others not reviewed here) led to clinical trials initiated to assess the safety and efficacy of ASOs targeting miRNAs in human patients. Ongoing

trials are exploring the use of antimiRs in cancer therapy, hepatitis C viral infection, and other diseases (***Table 2***). These trials aim to validate the therapeutic potential of ASOs for miRNA modulation and establish their safety profiles.

Disease	Name of antimiR	Engaged miRNA	Reference
Lymphoma	Cobomarsen	miR-155	Seto *et al.*[69]
Non-alcoholic fatty liver disease (NAFLD)	RG-125 (AZD4076)	miR-103, miR-107	Regulus Therapeutics and AstraZeneca[70]
Hepatitis C	Miravirsen	miR-122	Gebert *et al.*[71]
Fibrosis	MRG-229	miR-29	Chioccioli *et al.*[72]
Alport nephropathy	Lademirsen	miR-21	Gomez *et al.*[73]

Table 2 *– List of ASOs under clinical trials.*

The development and implementation of ASO therapies targeting miRNAs may pave the way for future clinical approval, but antimiRs still face several problems and challenges. The major one is off-target effects; antimirs may bind to an unrelated miRNA and lead to potential unintended consequences and interferences with normal cellular pathways. ASOs must overcome various physiological barriers, such as the blood-brain barrier, to reach their intended site of action. Then, delivery issues need to be cited; indeed, dispatching ASOs to the specific tissues or cells where the target miRNA is expressed can be challenging.

In conclusion, antimiRs show great potential for further research and clinical investigations. However, since the heterogeneity of diseases may not allow for a single "magic bullet" approach, small molecule targeting the biogenesis or miRNAs is another strategy that has attracted scientists in recent years.

Small molecules

The use of small molecules to target miRNAs involves several strategies. Given these premises and having precisely in mind miRNAs' structure, the design of selective binders as potential drugs or chemical probes can start. With their short length and absence of noticeable secondary structural features, mature miRNAs present a significant challenge for direct binding. Making it exceptionally difficult to target with high specificity other than direct complementary sequence binding. This led researchers to look upstream into miRNA biogenesis and design innovative bioactive molecules or probes.

One direct approach is identifying small molecules that can directly bind to specific precursors of miRNA structures instead of linear sequences, as ASOs do. These small

molecules can disrupt miRNA biogenesis, stability, or binding to target mRNAs, thereby modulating miRNA-mediated gene regulation. Another less specific approach involves targeting the proteins in miRNA processing and function. Several proteins, as described before, are critical for miRNA biogenesis (e.g., Dicer, Drosha, and Argonaute), and small molecules can be designed to specifically bind to these proteins, either inhibiting their function or promoting their activity, thus modulating miRNA expression and activity indirectly.

Accordingly, one promising strategy to reverse disease-related miRNA upregulation is to inhibit its maturation by developing binders of the corresponding pre-miRNA or pri-miRNA. While mature miRNA contains low structural elements, the longer pri-miRNA and pre-miRNA sequences adopt the aforementioned distinctive hairpin secondary structures with internal bulges and loops (***Figure 5B***). By targeting these particular structural features, especially those near the enzymatic processing sites, the biogenesis process of miRNA can be effectively impeded. While conventional ASO-based methods typically function to stoichiometrically restrict the activity of the mature miRNA species, targeting precursor forms offers the unique advantage of limiting the production of mature miRNA. With this perspective, targeting miRNA function with small molecules provides an alternate exploration strategy.

I.1.4 Targeting miRNAs biogenesis using synthetic small molecules

The field of targeting RNAs by small molecules is underexplored and yet very promising, as highlighted by recent reviews[18–20,23]. Many examples of RNA ligands and methodologies to target other biologically relevant RNAs exist, event binders of non-human RNAs. For example, ribosomal RNA was one of the first targets, but inhibition of the replication of viral RNAs also became an attractive approach for designing small molecules[74]. Several viruses, like hepatitis C or the human immunodeficiency virus (HIV), were studied. For HIV, Wang *et al.* started to work on the Tat/TAR model at the end of the 1990s, showing that a well-known aminoglycoside (neomycin) could inhibit the interaction between the two biomolecules[75]. Further studies led to the discovery of verapamil and different analogs as new inhibitors of Tat/TAR interaction[76].

However, in this section, we decided exclusively to focus on the most important examples of small-molecule RNA binders targeting the biogenesis of human miRNAs. Drug discovery approaches usually involve either a systematic screening of a chemical library or a rational drug design process. However, when it comes to miRNA, it is essential to note that the scarcity of structural data has often led to the use of screening methods, while the advent

of precise 3D modeling enabled the enrichment of these screening strategies. To make up for this knowledge gap, conventional techniques typically employed in the design of small molecules targeting proteins and macromolecules have yet to be noticed in the field of miRNA[77,78]. Bottom-up approaches that go from the identification of the molecular target to the discovery of inhibitors and finally to the detection of *in cellulo* activity benefited the successful strategy for targeting miRNAs.

In the following sub-sections, the focus is placed on contemporary strategies utilized to identify novel small molecules that influence miRNA function. This includes exploring the development, hypothesized mechanisms of action, and preliminary assessment of small molecule regulators of disease-associated miRNAs. The fundamental principles guiding the design and potential challenges associated with the methodologies for discovering small molecules targeting miRNAs are also elucidated.

Small molecule inhibitors of specific miRNA biogenesis identified through biochemical assays.

The development of *in vitro* biochemical assays to observe miRNA maturation has facilitated the discovery of small molecule inhibitors that can hinder miRNA activity. Biochemical assays offer several benefits, including a strong read-out, adaptability for high-throughput screening, and a reduced number of components compared to cell-based screening assays. Various *in vitro* tests have been published, with some designed to investigate the direct interaction between small molecules and primary or precursor miRNAs, as well as other proteins involved in miRNA biogenesis. Another set of assays has been developed to observe the enzymatic function of the machinery responsible for miRNA biogenesis. Collectively, these efforts have resulted in the creation of microarray platform assays, fluorescence-guided assays, and, more recently, catalytic chemiluminescence-based assays. The following sub-section provides an in-depth study of the design and utilization of these diverse technologies, along with a critical review of each method's advantages and limitations. Microarray technology has emerged as an effective method for the high-throughput screening of specific interactions between ligands and RNA. In a microarray procedure, a library of ligands is covalently attached to a glass slide, followed by incubation with a fluorescently marked RNA molecule. After subsequent washing stages, the compounds that have successfully bound and immobilized the labeled RNA are detected through fluorescence imaging techniques[79].

In a study conducted by Schneekloth's laboratory, a high-throughput screening (HTS) method was developed using a small molecule microarray (SMM) to identify inhibitors

of miR-21. The researchers screened a library of 20,000 compounds and identified 19 potential inhibitors of miR-21 biogenesis[80]. Of these, 11 were further analyzed using a differential scanning fluorimetry (DSF) assay measuring the change in the melting temperature of the miR, which indicated the compound's interaction and stabilization of the stem-loop structure. Compounds **1.01** and **1.02** (***Figure 7***) exhibited the most significant change in T_m, suggesting their binding to the hairpin structure. Two orthogonal fluorescence assays were employed to measure the binding affinity: one using a 2-aminopurine labeled pre-miR-21 and the other a fluorescence intensity assay using a Cy5-labeled pre-miR-21. Both assays confirmed that compound **1.01** had a K_D of 2.3-3.2 μM and compound **1.02** had a K_D of 700-800 nM.

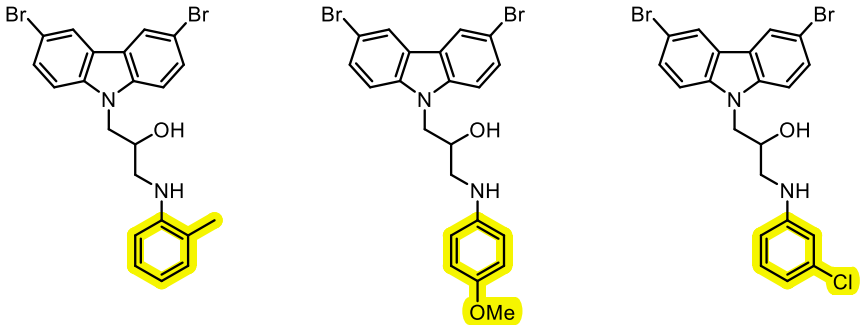

Figure 7 *- Compounds identified by Schneekloth lab as pre-miR-21 inhibitors using an original SMM.*

Further modifications to compounds **1.01** and **1.02** were made through a structure-activity relationships (SAR) study, including changes to the aniline-containing core, the aromatic substitution patterns, the carbazole moiety, and the linker structure and length. The study found that the dibromocarbazole moiety was crucial for interaction with pre-miR-21, while modifications to the linker regions and aniline substituents had minimal impact on binding. They concluded that compounds **1.02** and **1.03** (***Figure 7***), with K_D's between 0.8 and 2.0 μM, were the most effective in the series. Further investigation revealed that these compounds bound directly to or near the apical loop of pre-miR-21, thereby inhibiting Dicer processing. It is worth mentioning that the impact of compounds **1.01** to **1.03** on other pre-miRs remains uninvestigated, and their cellular activity has not been validated.

The Disney laboratory introduced a two-dimensional combinatorial screening (2-DCS) approach, utilizing microarray technology to probe RNA motifs (loops and bulges) and chemical interactions simultaneously (***Figure 8***)[81,82]. This method allows screening thousands of RNA motifs against ligands to identify selective interactions. More specifically, azide-bearing small molecules are immobilized on an alkyne-modified agarose microarray slide and probed with a ^{32}P-labeled RNA library. Specific competitor oligonucleotides are

included to ensure RNA-specific interactions. After imaging with a phosphorimager, bound

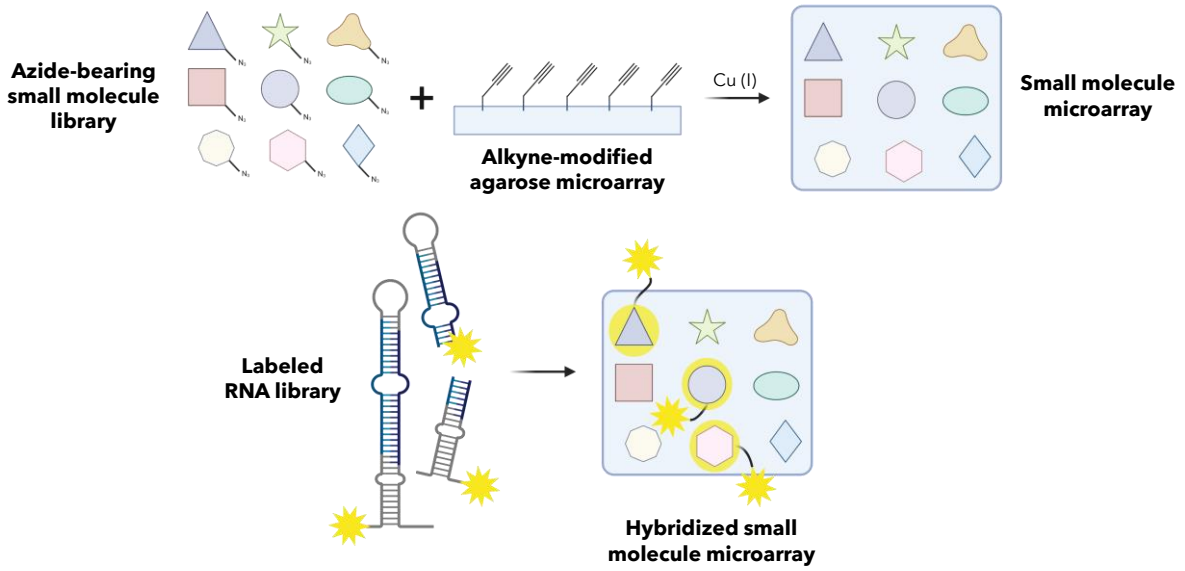

Figure 8 *– 2-Dimensional Combinatorial Screening (2-DCS) method. An azide-bearing small molecule library is immobilized on agarose-coated microarrays. These arrays are then exposed to a labeled RNA library containing distinct structural components and to competitor oligonucleotides sharing common structures. RNAs binding to the surface are extracted, and RNA sequencing (RNA-seq) identifies them. Subsequent statistical evaluation of the RNA-seq data highlights significant RNA fold-small molecule interactions, guiding the creation of new specific small molecule.*

RNAs are identified, amplified, and sequenced. The original study applied this approach to four aminoglycosides, revealing distinct RNA-binding preferences[81]. For instance, neomycin favored GA pairs, while tobramycin preferred GG pairs. This proof-of-concept study showcased the robustness and high-throughput capabilities of 2DCS, leading to the generation of substantial RNA–ligand interaction data. 2-DCS identified guanidilated neomycin (Compound **1.04**, ***Figure 9***) as a binder of the internal loop located in the pre-miR-10b, with guanidinium groups playing a key role in the binding[83].

A notable constraint of the small molecule microarray technologies is the need for the compounds to be fixed to the slides through a covalent tag. This can considerably limit the diversity and accessibility of the library. Additionally, there exists a risk that the covalent alteration of the small molecule might render it ineffective. To address the limitation of requiring covalent tagging in microarray technology, Disney's lab introduced an approach called 'AbsorbArray'[84]. This method enables unmodified compound libraries to be non-covalently adhered to microarray plates, allowing for probing with RNA libraries using 2DCS[84]. Small molecules were found to be successfully absorbed onto hydrated agarose-coated surfaces and retained after washing. To assess this new technique, the screening of about 700 pharmacologically active compounds identified three topoisomerase inhibitors binding to the pre-miR-21 hairpin, with K_D values between 24 and 58 nM. The most potent

hit, compound **1.05** (***Figure 9***), also bound the uracil bulge adjacent to the Dicer site with

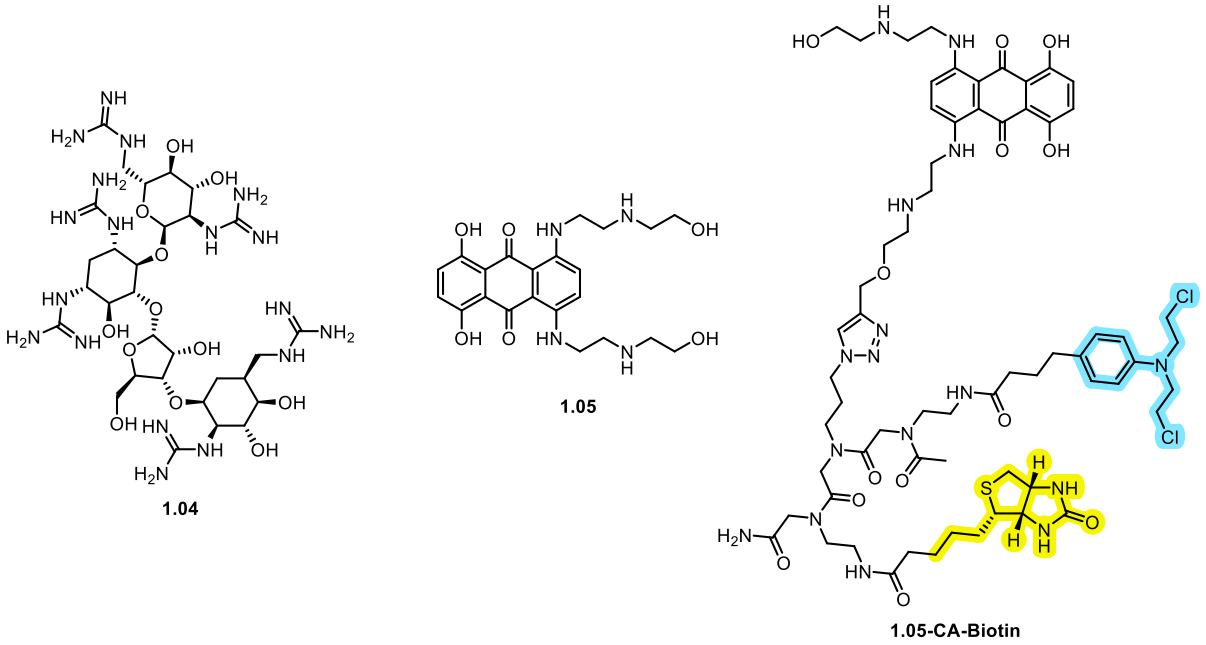

Figure 9 *– Chemical structures of* ***1.04***, ***1.05***. *Structure of* ***1.05-CA-Biotin*** *which is made of the RNA-binding structure* ***1.05***, *a biotin purification module (in yellow) and a cross-linking chlorambucil (CA) module (in blue).*

a K_D of 46 nM and inhibited mature miR-21 biogenesis in breast cancer cells. Hence, the selectivity of compound **1.05** was further explored, showing a significant decrease only in miR-21 levels among nine additional miRNAs. A Chemical Cross-Linking and Isolation by Pull-Down (Chem-CLIP) approach confirmed the direct interaction of compound **1.05** with miR-21 in cells. Chem-CLIP offers a powerful means to facilitate target identification and validation, providing researchers with invaluable insights into the interactions between ligands and their intended targets. Chem-CLIP uses a unique approach where an RNA-binding small molecule is modified with a chemical cross-linker (such as a nitrogen mustard or a diazirine moiety) and a biotin purification tag (see **1.05-CA-Biotin**, ***Figure 9***). When the small molecule binds to an RNA molecule, the cross-linker is brought into close proximity and reacts with high efficiency. This proximity-based reaction forms covalent adducts, which can be isolated and purified from cells using biotin. This purification method allows for the identification of cellular targets of the small molecule.

The Chem-CLIP probe, comprising parent compound **1.05** modified with biotin and chlorambucil crosslinking moiety, was designed to modify cellular RNA targets covalently (**1.05-CA-Biotin**, ***Figure 9***). Upon treating cells with this probe, the resulting conjugates were isolated and analyzed by RT-qPCR, successfully enriching pre-miR-21 by over 10-fold. This confirmed the direct interaction of compound **1.05** with miR-21 in cells. These findings underscore the potential of microarray-based screens in discovering novel small molecule modulators of miRNA function. Microarray-based screenings, while advantageous in monitoring ligand–RNA interactions, have key limitations, such as not assessing the

compounds' ability to inhibit miRNA maturation or function. Despite identifying ligands with high affinity to RNA, many were found incapable of inhibiting function, indicating a need for more complex approaches to simultaneously monitor both binding and functional inhibition.

In this context, the Garner laboratory developed an innovative method to identify miRNA inhibitors, referred to as the catalytic enzyme-linked click chemistry assay (cat-ELCCA), shown in ***Figure 10A***[85]. In this assay, pre-miRs labeled with biotin and containing a click chemistry handle (such as trans-cyclooctene) within the loop region are anchored onto microtiter plates coated with streptavidin. To pinpoint inhibitors of Dicer processing, these pre-miRs are exposed to Dicer in the presence of a compound library. The covalent labeling with a conjugate of horseradish peroxidase (HRP) and tetrazine facilitates a straightforward readout through catalytic HRP-based chemiluminescence. The assay here presented presents distinct features: first, an enhancement in sensitivity and signal-to-noise ratios through signal amplification; second, the elimination of compound fluorescence interference by employing a luminescence read-out; and third, a functional read-out that identifies only those ligands that inhibit Dicer processing of pre-miRs. Using this new approach, the Garner lab conducted a 2D screening to identify inhibitors of pre-miR-21 and pre-let-7d Dicer processing, testing 50,000 small molecules and 33,000 natural products[86,87]. The results yielded 170 and 47 confirmed hits from small molecules and natural products, respectively. An examination of the selectivity revealed that most small molecule hits showed no preference between pre-miR-21 and pre-let-7d, while some natural extracts demonstrated significant selectivity towards pre-miR-21.

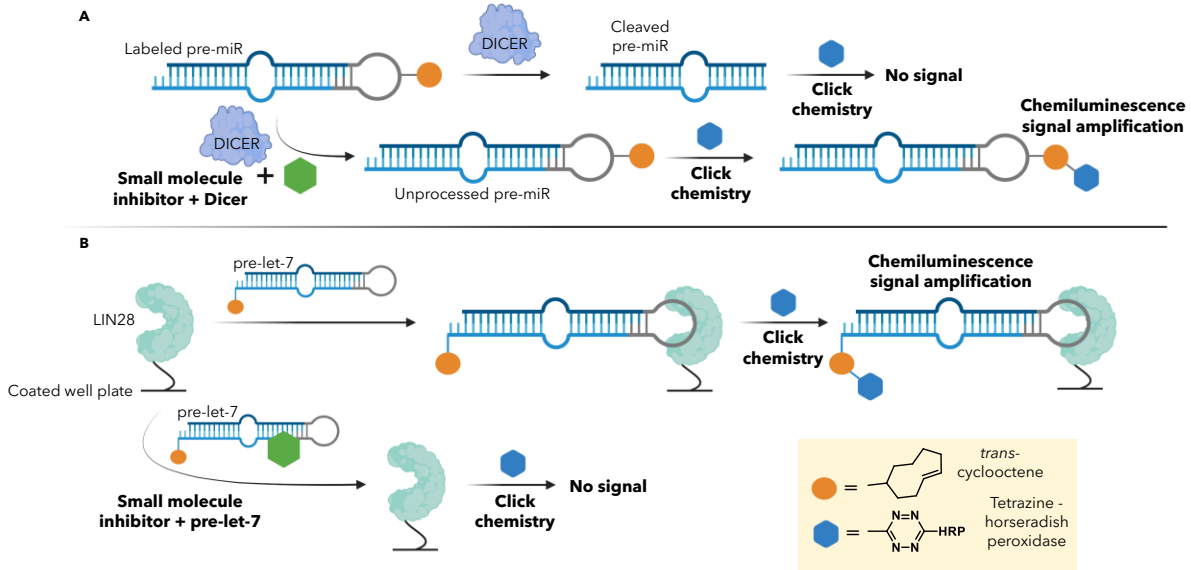

Figure 10 *– The two different catalytic enzyme-linked click chemistry assays (cat-ELCCA) for HTS developed by Garner's lab. a) cat-ELCCA used to identify DICER-mediated pre-miR processing inhibitors. b) cat-ELCCA used to identify LIN28-pre-let7d interaction modulators.*

Furthermore, Lorenz *et al.* adapted the cat-ELCCA method to detect small molecule inhibitors of the LIN28–pre-let-7d RNA/protein interaction, identifying analogs with a dibenzenesulfonamide scaffold that could inhibit this interaction (***Figure 10B***)[87]. They amplified the chemiluminescent signal through protein-miR binding, and any inhibition of this binding interaction suppresses the chemiluminescent signal. Using cat-ELCCA, the team conducted an HTS of more than 120,000 small molecules that identified **1.06** and **1.07** (***Figure 11***) as inhibitors of the Lin28-pre-let-7 interaction. These compounds had IC_{50} values of 8.3 and 10.3 μM, respectively, as confirmed by electrophoretic mobility shift assay (EMSA). After that, SAR studies showed that chloro- and methyl- substitutions on the outer phenyl rings maintained the inhibitory activity. However, the bis-sulfonamide in the 1,2-configuration on the central benzene ring was essential for the inhibitory activity. However, the application of these compounds in cellular contexts and their selectivity towards other precursor miRNAs has not been examined. Overall, the application of cat-ELCCA in identifying novel miRNA inhibitors is seen as promising, offering several advantages over existing assay methodologies.

The employment of biochemical *in vitro* assays for identifying miRNA inhibitors has been demonstrated to be effective through various methodologies. Although advantageous in their high-throughput capabilities, direct binding assays may lead to the recognition of ligands that bind without inhibiting miRNA activity or maturation. Conversely, assays focusing on direct function monitoring are more likely to yield active inhibitors, but achieving high substrate specificity is complex. Future *in vitro* screening platforms might integrate elements of both direct binding and functional inhibition assays to pinpoint more potent hits characterized by both efficacy and substrate specificity. Noteworthy, inhibitors discerned through *in vitro* assays may not necessarily translate to biological activity within a cellular context. Factors such as cell permeability, toxicity, stability, and other pharmacological limitations must be assessed independently, highlighting the complexity of the miRNA-targeted small molecule field.

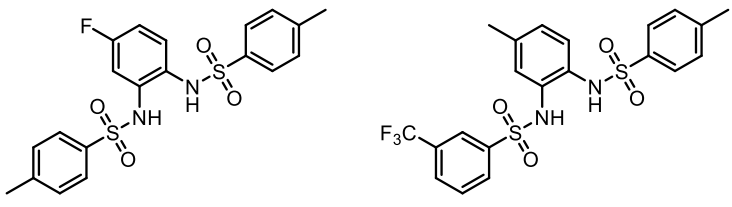

1.06 **1.07**

Figure 11 *– Chemical structures of* ***1.06*** *and* ***1.07****, both identified using cat-ELCCA assays.*

Small molecule inhibitors of specific miRNA biogenesis identified through in cellulo assays.

In cellulo assays exploring small molecule modulators of miRNA function and biogenesis present specific advantages over biochemical screening methods. Cellular assays can account for these variables, unlike *in vivo* assays, which may overlook the abovementioned factors. Moreover, cellular assays are not confined to known targets and can facilitate uncovering new biological targets and pathways. In the conventional approach, the miRNA target sequence is cloned on the 3'-UTR of a reporter gene like luciferase or GFP, thereby controlling the expression of the reporter (***Figure 12A***). However, several other techniques of cell-based reporter assay exist and are shown in *Figures 12B* and *12C*.

One of the first screening methods using cellular assays to highlight oncogene inhibitors was developed by the group of Deiters in 2008[88,89]. The test involved a reporter system, where the target miRNA controls the expression of a reporter gene (i.e., luciferase). If a compound can inhibit the target miRNA maturation, it will increase reporter gene expression and a bioluminescent signal can be measured. The higher the luciferase bioluminescence, the more effective the inhibitor is at blocking miRNA biogenesis. For instance, the authors first focused on miR-21, a well-documented oncogene pivotal in various cancers, such as antiapoptotic properties for tumoral cells. The group screened more than a thousand compounds from different libraries. They could highlight a promising azobenzene-based small molecule (Structure **1.08**, ***Figure 13***) as a transcriptional blocker of the host gene of miR-21, with an EC_{50} = 2 μM[88]. Hence, compound **1.08** was found to reduce by 78% mature miR-21 levels.

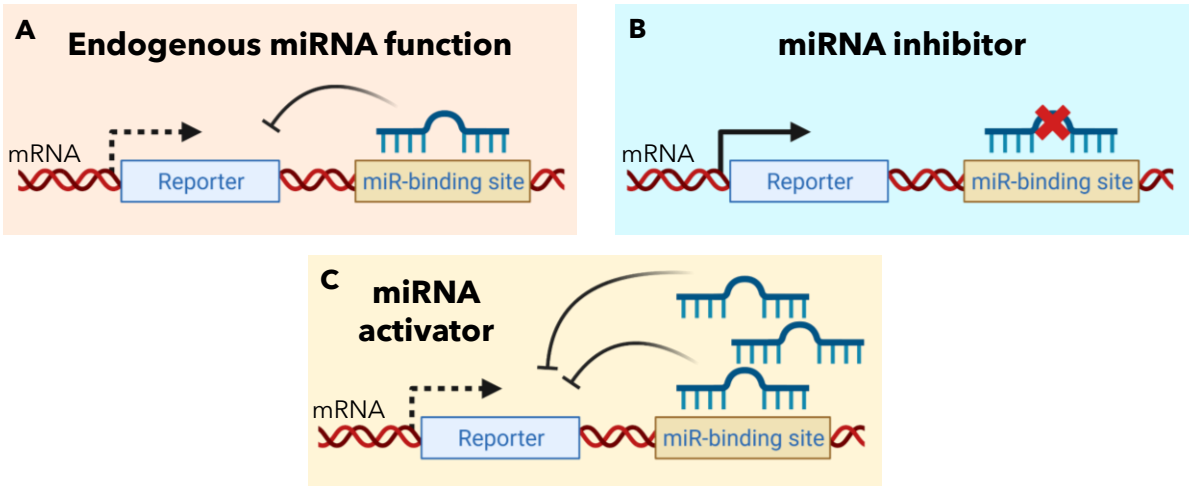

Figure 12 *- Cell-based reporter assays. A) Endogenous miRNA binding to the target site, thus repressing reporter expression. B) Use of a small molecule that inhibits miRNA function enhances reporter expression. C) Increasing miRNA expression or stabilizing its function results in a decreased reporter expression.*

Another HTS of around 300,000 compounds also led to the development of oxadiazole **1.09** (***Figure 13***), a specific inhibitor for miR-21. The compound showed a 60% increase in activity compared to hit compounds and did not affect other miRNAs in a HeLa cell-based assay. Surprisingly, it inhibited miRNA function rather than biogenesis since no effect was observed on pri- or mature miR-21 levels and demonstrated potential activity in various cancer cell lines (U87, A172, MCF7, and HCT-116)[90]. A year later, the same research group used the same approach to identify a new ether-amide molecule (compound **1.10**, ***Figure 13***), this time with a transcriptional inhibition activity on miR-21[91].

Differently, the Hwang lab directly monitored miRNA expression levels through RT-qPCR after treatment with small molecules rather than using a reporter system to observe changes in miRNA function[92]. The study initially focused on eight miRNAs targeting B-cell lymphoma 2 (BCL2)/adenovirus E1B 19 kDa protein-interacting protein 3 (BNIP3), a key regulator of cardiac cell death, in hypoxic cardiomyocytes. Among these, miR-182 was found to be most effective in reducing the expression of the target protein when treated with a miRNA mimic. The lab screened compounds from an in-house library to discover potential small molecules that could induce miR-182 expression and further explore this interaction. The screening was performed in hypoxic cardiomyocytes, followed by RT-qPCR analysis to detect changes in miR-182 levels. Among the screened small molecules, the GSK3β inhibitor **1.11** (***Figure 13***) was identified to induce miR-182 expression by 2-fold, inhibiting BNIP3 expression.

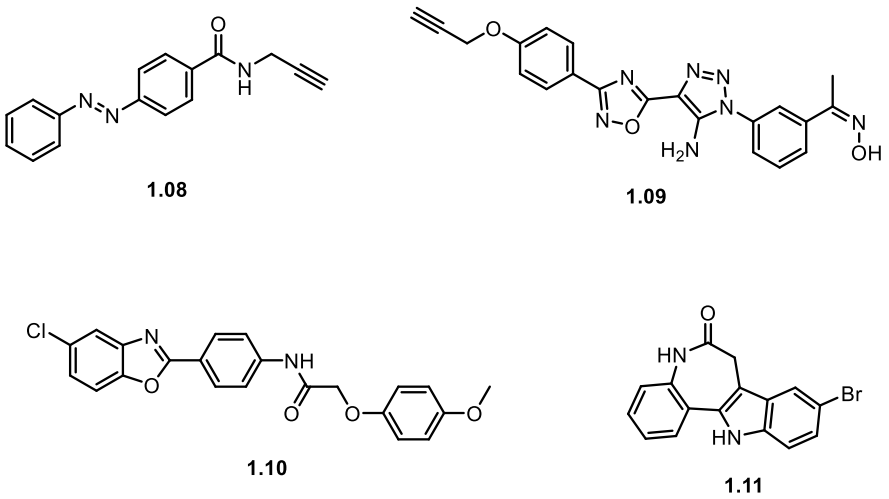

Figure 13 *- Chemical structures of* ***1.08***, ***1.09***, ***1.10***, *and* ***1.11***. *Small molecules identified by Deiters and Hwang lab through in cellulo assays.*

In summary, *in cellulo* methodologies have enabled the identification of small molecule modulators of miRNAs across various compound classes that might not have been achievable through biochemical techniques alone, as the complete miRNA biogenesis pathway, including upstream regulatory mechanisms, was essential. However, one limitation of cellular assays is that they only provide indirect measurements of changes in miRNA function. Thus, minor alterations in activity might be skipped, leading to missed potential hit compounds. This challenge is particularly pronounced in HTS conditions, where compounds are often tested at a single concentration. Nevertheless, the current cell-based reporter assay approach offers high sensitivity and a positive readout (increase in luminescence), minimizing false positive results.

Small molecule inhibitors of specific miRNA biogenesis identified through rational and de-novo computational design approaches.

Unlike conventional methods of small molecule discovery, which rely on empirical screening of chemical substances, rational drug design adopts a different approach. Herein, the development of small molecules is directed toward targets, for which the functional roles in cellular processes and 3D-structural information are understood[77,82]. The capacity to accurately predict RNA secondary and tertiary motifs from sequences through computational means offers a more rapid pathway to small molecule design[93]. However, this method is constrained since the structures of many disease-relevant RNAs are yet to be determined. Still, newly developed structural approaches might provide detailed insights into the 3D structures of miRNA targets and their interactions with small molecule inhibitors. Techniques such as X-ray crystallography, nuclear magnetic resonance (NMR) spectroscopy, and cryo-electron microscopy (cryo-EM) enabled the determination of high-resolution structures, illustrating the binding modes and molecular interactions between miRNA and small molecules. Integrating screening techniques and structural methods provides a comprehensive framework for designing and developing small molecule inhibitors targeting miRNA maturation.

Consequently, since classical HTS suffered from slow hit rates for new pre-miRNA binders, Disney's lab worked on a new method integrating computational and experimental techniques to predict the affinity of RNA motif-ligand pairs identified through 2-DCS (*See above*). This technique, named Structure-Activity Relationships Through Sequencing (StARTS), uses the sequences of RNA motifs chosen for ligand binding[94,95]. Statistical analysis then selects specific RNA motifs that appear with a confidence level of ≥95%. Given

that 2DCS facilitates the swift exploration of both chemical and RNA domains, potentially identifying numerous RNA motif-ligand pairs, assessing the affinities of each interaction becomes challenging. However, the combined computational and experimental strategy (StARTS) introduced in this study offers an efficient method for annotating an expanding database of RNA-ligand interactions.[95]

Starting from 2-DCS and StARTS, Disney's team developed a platform called "*InfoRNA*" to rapidly identify specific binders targeting a structured region (loop or bulge) of a biologically relevant RNA (***Figure 14***). First, 2-DCS allows for the identification of compounds targeting a specific RNA site, as described above. Once it is combined with StARTS, adding a scoring function allows for compound classification. Mining this classification against the entire miRnome directly identifies compounds that could specifically interact with the desired pri- or pre-miR. (***Figure 14***)[96,97].

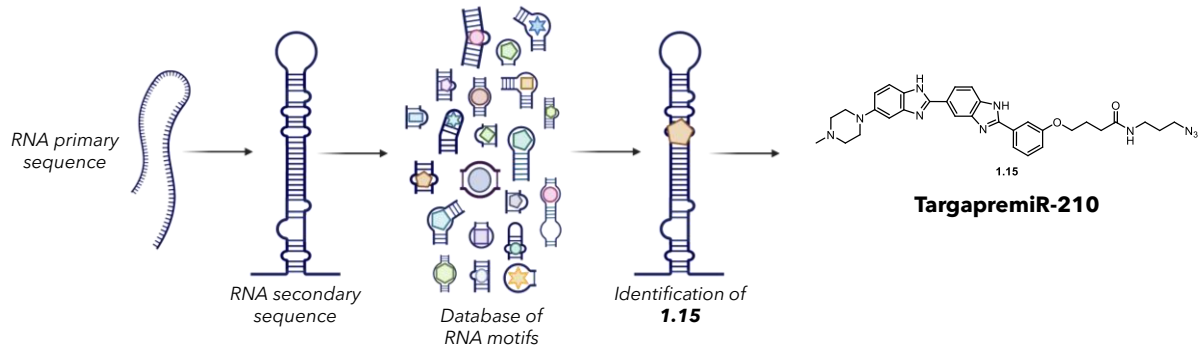

Figure 14 – *The InfoRNA platform and the identification of* ***1.15.***

In the end, Disney's group combined the sequence information of all the pri- and pre-miRNA found on miRbase with data on previously described secondary structure RNA-binder interaction[97–99]. Thus, they could screen over a thousand pre-miR sequences against more than 700 known RNA binding-small molecules. After narrowing their discovery to lead compounds binding to only Dicer and Drosha cleavage sites, they identified 26 compounds, and only 11 of them were reducing the maturation of their target miRNA *in cellulo*. InfoRNA gave the best "score" for binding interactions to compound **1.13** (***Figure 15A***) towards the hairpin loop of pre-miR-96. The InfoRNA platform led to the discovery of a series of compounds known as TargapremiR or TargaprimiR, the name being assigned depending on the target[100]. Take, for example, one of the first that was identified, targaprimir-96 (Targets pri-miR-96), resulting from the combination of compound **1.13** (***Figure 15A***) and another *bis*-benzimidazole scaffold recovered from InfoRNA, to have a dual binding mode on the pri-miR-96 sequence (shown in ***Figure 15B***). Targaprimir-96 (Compound **1.14**, ***Figure 15B***) was tested in triple-negative breast cancer cells (MDA-MB-231) and

significantly reduced mature miR-96 levels with an IC_{50} of 50 nM and a Kd value of 85 nM towards its target[101]. Another typical example of such compounds is targapremir-210 (**1.15**, ***Figure 14***), identified through the Inforna pipeline as a pre-miR-210 hairpin binder, which will be reviewed later in this work[102]. As a last example, targapremir-200c was designed using two scaffolds identified by the Informa platform. First, compound **1.16** (***Figure 15C***) was highlighted as a binder of the internal loop of pre-miR-200c. Then, compound **1.17** (***Figure 15C***) was identified as binding the adjacent AU base pair. Assembling the two monomers led to targapremir-200c (compound **1.18**, ***Figure 15C***), a highly specific compound that inhibits the biogenesis of miR-200c, whose overexpression is responsible for β-cells apoptosis in type 2 diabetes[103]. Interestingly, this compound is not only specific for pre-miR-200c across the miRnome but also for pre-miR-200c with respect to pre-miR-200a and pre-miR-200b, which bear a very similar structure and share the same biogenesis pathway.

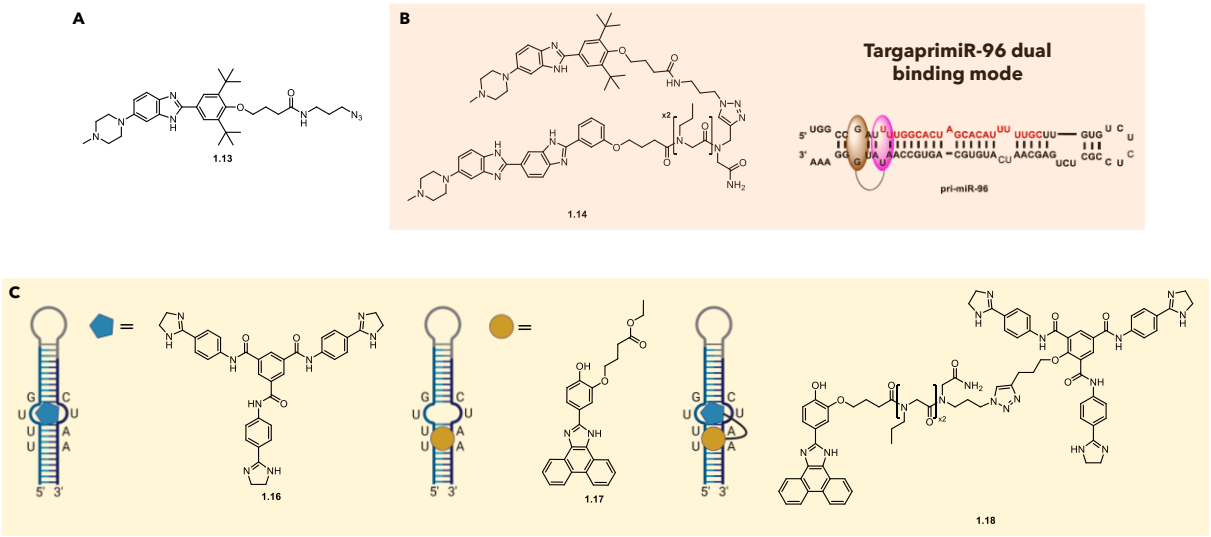

Figure 15 *– Chemical structures of several targapri- or targapremiR compounds. A) Chemical structure of* ***1.13****. B) Chemical structure of* ***1.14*** *and its dual binding mode towards pri-miR-96 upon combining two different RNA-binding structures. C) Combination of* ***1.16*** *and* ***1.17*** *to reach targaprimiR-200c (****1.18****)*

Another recent example of rational design of miRNA inhibitors is the fragment-based method, based on screening small fragments. Fragment-based drug design (FBDD) is a classical medicinal chemistry methodology employed to identify compounds bearing a low molecular weight (<300) and a low number of interaction functions (<3 H-bonds donors and acceptors). Starting from these compounds that are expected to have a modest affinity for the target, fragment growing and/or fragment linking are performed to improve binding. These are performed upon understanding the binding mode through techniques such as nuclear magnetic resonance (NMR), X-ray crystallography, and mass spectrometry (MS) that allow an understanding of how to modify the fragments for better affinity. NMR has been

largely applied in FBDD and the frame of RNA-binding compounds[104]. One of the approaches is based on ^{19}F-NMR fragment screening to identify small molecule compounds that bind to RNA structures[105]. Parallely, Varani lab designed a scalable NMR screening method to identify small molecule fragments that bind to miRNA precursor structures, tested explicitly on the pre-miR-21 stem-loop[106]. From a library of 420 compounds, four fragments (***Figure 16***) were identified *via* NMR-based triage methods. They applied their 1D ^{1}H line broadening technique to distinguish binding fragments from mixtures, an approach previously used towards viral RNA targets[107]. This method can identify fragments with an affinity K_D ranging from approximately 10 µM to 1 mM. Notably, the technique is target-independent and requires no modifications or optimizations for different targets. Subsequent 2D NOESY NMR experiments allowed the team to identify **1.19** (***Figure 16***) as the best fragment by confirming its specific binding near the DICER cleavage site onto the pre-miR-21 sequence[106]. The same research group recently described an example of a successful FBDD, still focused on the oncomiR miR-21 overexpression[108]. The best fragments highlighted in this study (**1.23** and **1.24**, ***Figure 16***) demonstrate a potent and specific affinity to pre-miR-21. The two fragments induce distinct structural and dynamic alterations in pre-miR-21 at the Dicer cleavage site, leading to inefficient RNA processing. As a result, **1.24** exhibits a reduction in Dicer processing in both *in vitro* and in cellular environments. This effect is specific, without impacting other miRs or cellular RNAs. Hence, a notable decrease in mature miR-21 levels in gastric and pancreatic cancer cell lines post-compound treatment is observed[108].

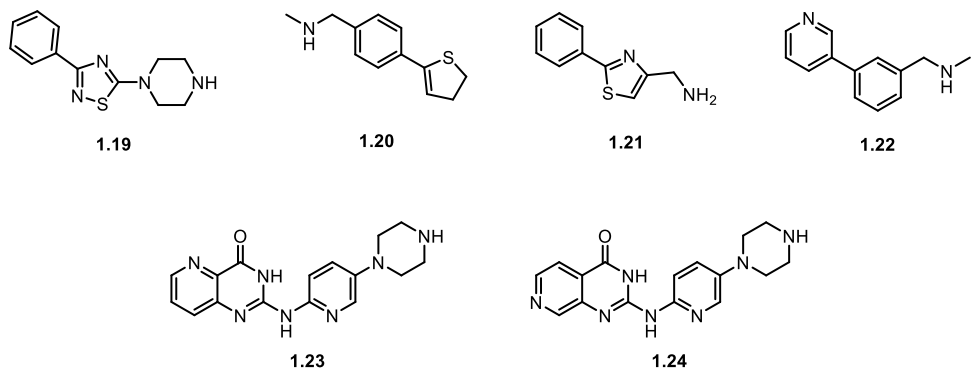

Figure 16 *- Chemical structures of* ***1.19***, ***1.20***, ***1.21***, ***1.22***, ***1.23*** *and* ***1.24***, *identified by the Varani lab through NMR fragment-based method (NMR-FBDD).*

Exploring novel approaches has recently paved the way for discovering ligands with enhanced capabilities. This exploration initially started following the necessity to identify and validate targets for the newly identified small molecule ligands. With this new goal in mind, the Chem-CLIP technique was also directed toward an FBDD technique. In addition

to its applications in target engagement experiments, Chem-CLIP has also been employed to screen and map the binding sites of low molecular weight fragments that target the oncogene pre-miR-21 (***Figure 17A***)[109]. Chem-CLIP fragment mapping (Chem-CLIP-Frag-Map) was utilized to identify fragments from a pool of 460 diazirine-containing compounds. These fragments were found to have the ability to form covalent bonds with RNA when exposed to irradiation. The most promising fragments were combined with a pre-miR-21 binder to create a highly potent bioactive compound **1.25** (***Figure 17A***). In subsequent experiments, this compound was shown to effectively inhibit the processing of pre-miR-21 and consequently reduce the levels of mature miR-21, along with associated gene expression observed in breast cancer cells[109]. More and more successful combinations of precise chemical modifications with biochemical, biophysical, and biological assays will result in identifying specific ligands that possess additional functionalities and can effectively interact with the desired target within cells and induce a biological effect without toxicity.

Developing new specific discovery methodologies is crucial to designing chemical tools that can precisely target RNA. Even if at their premises in the design of pre-miRNA binders, several new techniques widely used to target other RNA motifs are gaining attention. One suitable technique to be cited is SHAPE, a selective 2'-hydroxyl acylation analyzed by primer extension. This method allows the determination of RNA structure by identifying unpaired and paired bases[110], helping discover new structures that future ligands could target. Of course, other structural biology techniques can be employed to understand the 3D nature of the target RNA. Cryo-EM and crystallography are the most widely reviewed in the literature. A combination of innovative approaches, especially artificial intelligence (AI), with more classical ones described earlier, aims at identifying specific ligands for functional structures toward a relevant biological effect.

Another example of new modalities towards RNA targeting is bleomycin-induced cleavage, a compound recognized for its ability to cleave DNA and RNA (***Figure 17B***). Clinically used as an anticancer agent, its multifaceted mechanism of action includes topoisomerase inhibition. Thus, its application to RNA cleavage has been studied, particularly highlighting its favored cleavage site within the precursors of miR-10b (***Figure 17B***)[111]. The cleavage site is proximate to the Drosha and Dicer cleavage sites, and both *in vitro* and cellular studies have indicated a reduction in the maturation of oncogenic miR-10b. Further advancements led to the conjugation of bleomycin with specific RNA target binders, such as targapremiR-96 (**1.14** in ***Figure 15***)[112].

Ribonuclease targeting chimeras or RIBOTACs has also emerged as a novel promising new modality. This approach involves covalently linking a specific RNA ligand to

a molecule capable of recruiting and activating RNase L, an enzyme responsible for RNA degradation (***Figure 17C***)[113,114]. The initial introduction of a RIBOTAC was associated with the degradation of pri-miR-96, resulting in lower levels of the mature miR[113]. In a subsequent study, Costales *et al.* presented TGP210-RL, a RIBOTAC designed for the selective degradation of pre-miR-210[115]. This compound is an evolution of targapremiR-210 (TGP-210, **1.15**, ***Figure 14***), a molecule discussed above that binds to the pre-miR-210[102]. The fusion of TGP-210 with tetra-adenylate led to the creation of the RIBOTAC.

In the field of RIBOTAC, a recent outstanding work has been published by Tong, Disney, and colleagues illustrating that unsuccessful RNA-binding small molecules can be transformed into bioactive degraders (i.e., RIBOTAC)[116]. They revealed compounds such as pre-miR-155-RIBOTAC (**1.26**, ***Figure 17C***) by changing a previously identified compound, which was known to bind pre-miR-155 without any significant effect on the maturation of miR-155, with a new RNase-L-recruiting moiety. **1.26** decreased miR levels across various cell lines, both *in vitro* and *in vivo*. This reduction impacted cellular functions and proliferation influenced by miR-155. Additionally, this method was applied to two other biologically relevant targets, *JUN* and *MYC* mRNAs, resulting in the degradation of these

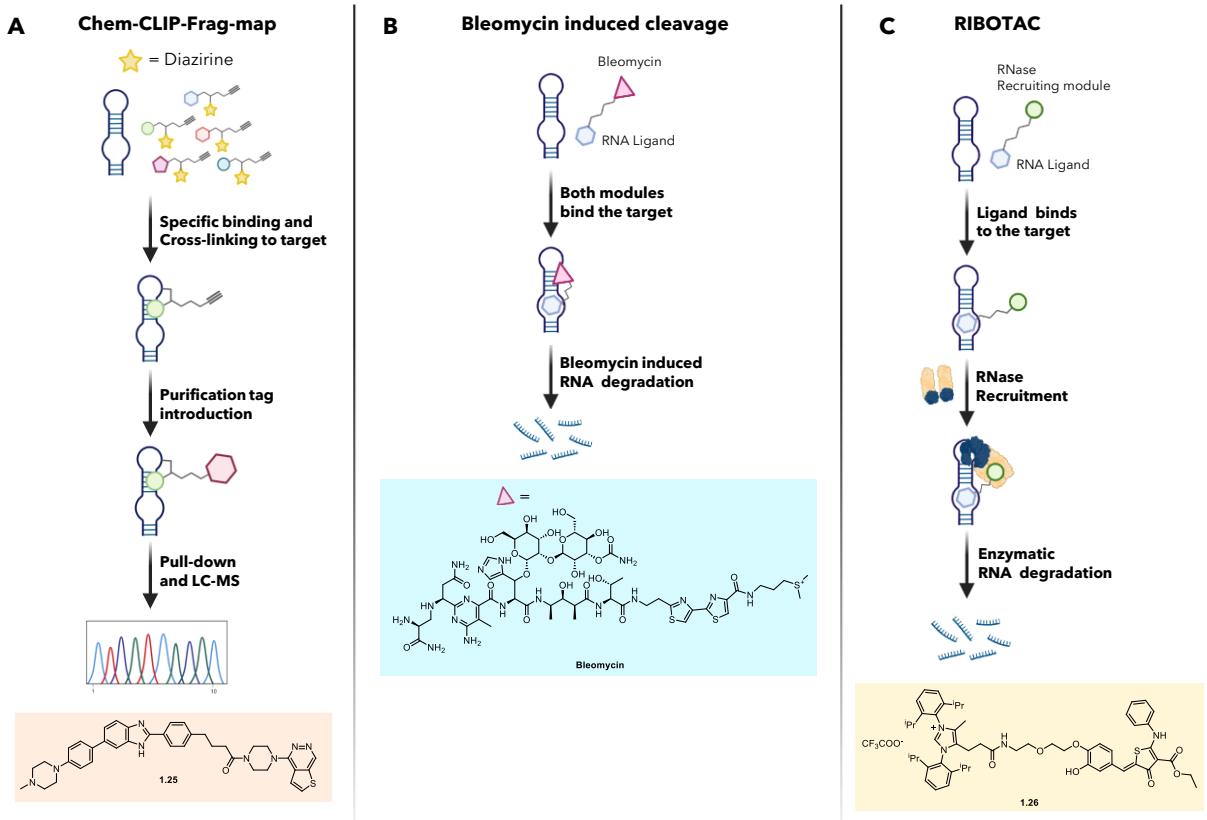

Figure 17 *– Small molecules RNA binding discovered via new techniques. A) Chem-CLIP-Frag-map identification of* ***1.25*** *via target engagement and binding site mapping. B) Conjugating bleomycin with potent RNA ligands results in RNA target cleavage (see compound* ***1.14****, Figure 15). C) Ribonuclease targeting chimeras (RIBOTACs) working as small molecules recruiting RNases for RNA cleavage.* ***1.26*** *is an example of RIBOTAC directed towards the degradation of pre-miR-155.*

targets and disruption of their associated oncogenic processes[116]. Historically, most bioactive molecules targeting miRs have been observed to bind near RNAse III functional sites, representing only a fraction of human miRs. The RIBOTAC strategy offers a broader approach, especially for miRs with less-defined functional sites.

In this context, our research group developed an innovative method for the design of oncogenic miRNA inhibitors. The first miRNA of interest for the group was miR-372, which acts as an oncogene in various cancers[117,118]. The design approach used in the team is based on the combination of different RNA binding domains, bringing both affinity and selectivity to act in a cooperative manner during the interaction. In a first attempt to design such ligands, the aminoglycoside neomycin was conjugated to artificial nucleobases, compounds able to form specific hydrogen bonds with DNA and RNA base pairs [119]. The conjugation of neomycin with nucleobase S (highlighted in yellow in ***Figure 18***) led to compound **1.27** (***Figure 18***)[120], which bears nanomolar affinity for pre-miR-372 *in vitro* and micromolar inhibition activity against its processing by Dicer. These results were confirmed in gastric cancer cells overexpressing the targeted miR-372. The proliferation of these cells was indeed reduced, which was linked to the dose-dependent inhibition of the production of miR-372 and the restoration of one of its target proteins, LATS2. Interestingly, the observed inhibition of proliferation was highly specific for cells overexpressing miR-372, and no effect was observed on other cell lines[119,121]. Further structural studies about these compounds' interaction sites led to adding a third binding domain represented by amino acids[120]. This led to improving the biological activity, further validating the strategy. After the various published works on miR-372, and in a complementary way, our group focused on the well-known oncomiR miR-21. A third RNA binding motif was added to the neomycin-artificial nucleobase conjugates presented above[122]. Amino acids were chosen for their known interaction with RNA since they are the main constituents of peptides, famous natural RNA binders. Compound **1.27** showed inhibition of miR-21 biogenesis and was thus used as a starting scaffold for designing a new series of pre-miR-21 binders. Two compounds, **1.28** and **1.29** (***Figure 18***), were identified as new potent binders. The work confirmed that the three domains act cooperatively (aminoglycoside in orange, artificial nucleobase in yellow, and amino acid in blue, ***Figure 18***), with the binding site located in the stem part of pre-miR-21. Those findings validate the hypothesis that both affinity and specific binding sites are crucial for the inhibitory efficacy of an RNA binder.

These previous studies recently led to a new series of compounds based on 2-deoxystreptamine, a part of neomycin known to be essential for RNA binding ability[123], and coupled with nucleobases. One compound (**1.30**, ***Figure 18***) showed a low micromolar IC_{50} value on Dicer cleavage and a good selectivity for a small set of pre-miRNAs[124], showing

that it is possible to reduce the size of the ligands while maintaining the desired activity. The exploration for additional RNA binding domains led our team to focus on bleomycins. These anticancer glycopeptides have a metal-binding domain and a C-terminal substituted bithiazole, known for RNA binding properties[125]. In recent work, Angelbello *et al.* highlighted bleomycins' properties in RNA binding and cleavage[111], making them suitable for designing innovative small molecules as modulators of miRNA biogenesis or function. A total of 24 compounds were synthesized across three series, employing amide, carbamate, and amines as linkers[126]. These were examined for their affinity, selectivity, and inhibitory activity against four oncogenic miRNAs: miR-21, miR-18a, miR-148a, and miR-373. The results revealed that compounds containing a sulfonamide or a secondary amine as a linker for the bleomycin A5 C-terminal chain were the most potent binders of pre-miR-21. Specifically, compounds **1.31** and **1.32** (***Figure 18***) emerged as the most potent binders and inhibitors. Molecular docking studies suggested that the likely binding site is situated at the Dicer cleavage site. Though not specific to a single RNA structure, these compounds displayed selectivity for pre-miRNAs and demonstrated activity in inhibiting oncomiRs levels. Further evaluation of the biological activity on glioblastoma U87 cells, which overexpress miR-21, miR-18a, and miR-148a, revealed significant antiproliferative effects. Compounds **1.31** and **1.32** were particularly noteworthy, as they exhibited this activity without toxicity toward healthy cells.

The multimodal approach described above yielded promising results but suffered from complex and time-consuming synthetic pathways. Additionally, most compounds produced had high molecular weight and exhibited physicochemical properties unsuitable for future applications. Therefore, our group described a *de novo* design of new RNA modulators in response to these limitations. The focus has been placed on developing miR-21 inhibitors that possess good affinity and selectivity and exhibit drug-like properties and synthetic accessibility[127]. 2-amino-dihydropyrrolopyridine has been chosen as an unexplored scaffold for preparing these new ligands, keeping in mind the two most important interactions required for suitable RNA binders, H-bonds and π-stacking. A new synthetic scheme was developed, with the critical step being a ruthenium-catalyzed [2+2+2]-cycloaddition, affording 30 unique and original compounds. Compound **1.33** (***Figure 18***) showed *in*-vitro affinity and activity towards the pre-miR-21 sequence in the low micromolar range. Molecular modeling and enzymatic footprinting confirmed the mechanism of action, and saturation-transfer difference (STD) NMR highlighted the chemical moieties involved in RNA-binder interactions.

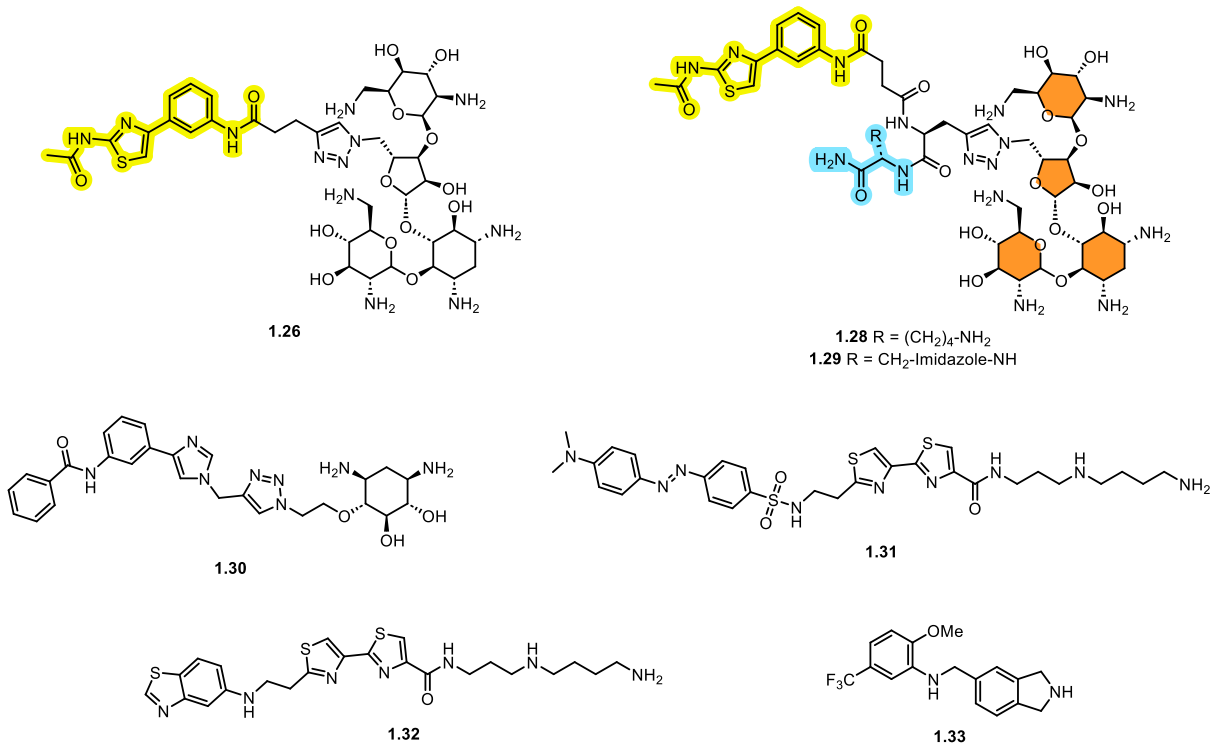

Figure 18 *- Chemical structures of* ***1.26*** *to* ***1.33****. All are small molecules identified by our group through rational de novo method.*

1.1.4 Conclusions and Outlook

The ongoing discovery of small molecules that selectively inhibit miRNA biogenesis or function holds significant promise for understanding miRNA biology and developing new therapeutic strategies for miRNA-related diseases, as shown by the success stories summarized here. In various studies, some of these small molecules have demonstrated superior potency and selectivity compared to ASOs, positioning them as potential drug candidates, especially against structured RNAs that ASOs cannot access. Many miRNA-targeting small molecules require high concentrations to elicit a biological response, potentially leading to unintended effects within *in cellulo* environments.

Rational design approaches commonly utilize aminoglycoside and benzimidazole scaffold structural features that facilitate interactions with RNA targets. Nevertheless, the discovery of novel scaffolds and pharmacophores that target miRNAs with high specificity remains an area requiring sustained effort. The diverse applications of *in vitro*, cell-based, and computational methodologies have each contributed to the success of discovering novel small molecules, with each approach offering unique strengths and weaknesses. More innovative work has begun integrating various aspects of each method, aiming to build on successes and overcome individual limitations. This trend will likely persist in future studies,

reflecting a concerted effort to address the existing challenges in targeting miRNAs with small molecules.

Furthermore, ongoing investments by biotech and pharmaceutical companies are expected to yield new drugs shortly, expanding the potential clinical applications of RNA ligands[128]. Overall, this field continues to evolve with continuous innovation, paving the way for exciting discoveries and therapeutic advancements. To that extent, the idea of developing miR-210 inhibitors gained interest recently; this oncomiR and why to inhibit its maturation will be extensively reviewed in the following section.

I.2 The hypoxamir: microRNA-210

I.2.1 Introduction

In molecular biology, a microRNA known as miR-210 has recently generated significant attention. As mentioned before, miRNAs play a crucial role in the intricate regulation of gene expression by employing various mechanisms. MiR-210 has been strongly associated with the hypoxia pathway, a biological process characterized by reduced cell oxygen levels. Specifically, when cells are exposed to low oxygen conditions, specific regulatory proteins called Hypoxia-inducible factors (HIFs) are activated, leading to the upregulation of miR-210[129]. This upregulation of miR-210 is an essential regulatory mechanism in cells experiencing oxygen deprivation.

miR-210 is derived from the *MIR210* gene located on chromosome 11p15.5. Noteworthy, the stem-loop structure of this microRNA is found within an intron of the AK123483 noncoding RNA[129]. After the first article that provided evidence of the functional association between hypoxia and the expression of specific hypoxia-regulated miRNAs (HRMs), resulting in the identification of key HRMs involved in cell survival under low oxygen conditions[130], subsequent studies have continued to uncover additional HRMs[131–135]. While variations exist in the HRMs identified by different research groups, the consistent up-regulation of miR-210 in response to hypoxia has been observed across multiple published studies in normal and transformed cells, indicating its crucial role in cellular adaptation to hypoxic environments[135–137]. Furthermore, miR-210's correlation with hypoxia has been established in *in-vitro* investigations and confirmed in *in-vivo* studies. Specifically, in tumor tissues such as breast, head, and neck cancers, the expression levels of miR-210 have been

found to correlate with hypoxia gene signatures, highlighting a direct association between miR-210 expression and hypoxia[137,138].

Hypoxic conditions lead to modifications in the expression of various genes, involving a key transcription factor called hypoxia-inducible factor (HIF-1), which is a heterodimer formed by an alpha (HIF-1α) and a beta (HIF-1β) subunit. When oxygen is available, HIF-α molecules go through prolyl hydroxylation mediated by three similar enzymes known as PHD1, PHD2, and PHD3, which rely on 2-oxoglutarate as a cofactor[139]. Upon regulation, the von Hippel-Lindau (VHL) protein binds to specific hydroxyprolyl residues in HIF-1α. This binding triggers the ubiquitination process, leading to the rapid degradation of HIF through the proteasome. Noteworthy, the HIF regulatory system has been directly implicated in the responses of tumor cells to hypoxia, and many tumors are now characterized by increased HIF levels[140,141]. Recent studies have shown that miR-210 expression is regulated by HIF-1α, highlighting again HIF-1 role in gene expression. First, Kulshreshtha *et al.* revealed miR-210 induction by hypoxia and regulation by HIF-1α, and then Camps *et al.* connected it with cancer development[130,138]. In 2011, Kelly *et al.* further investigated the regulation of miR-210 expression and completed the pathway that leads to its overexpression under hypoxia. In normoxic conditions, a low amount of miR-210 triggers high levels of GPD1L protein that will enhance prolyl hydroxylase domain enzymes (PHDs)

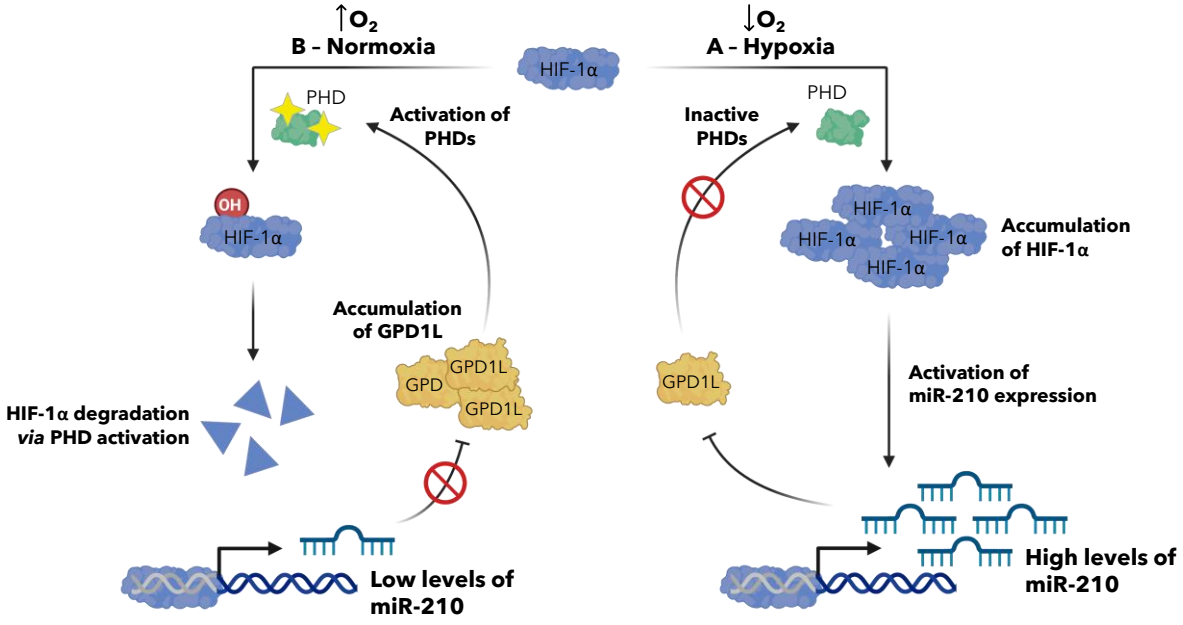

Figure 19 *– miR-210 effects on HIF-1α protein levels. Under normal oxygen conditions, HIF-1α is maintained at low levels through proline hydroxylation, which leads to its degradation via the proteasome. When HIF-1α protein levels are low, levels of GPD1L are high due to low levels of miR-210, which directly regulates GPD1L by binding to a specific site in its mRNA's 3'UTR. GPD1L, in turn, enhances the activity of the PHDs, triggering effective proline hydroxylation of HIF-1α. Under hypoxic conditions, an increase in HIF-1α protein levels and its transcriptional activity enhances the expression of miR-210. High miR-210 levels lead to decreased levels of GPD1L protein, resulting in the absence of activation of the activity of the PHDs. Consequently, this results in increased stabilization and accumulation of HIF-1α protein. This process establishes a positive feedback loop where miR-210 reinforces and sustains the levels of HIF-1α protein.*

activity. This results in decreased HIF-1α levels (***Figure 19***). However, with low oxygen levels (or other stimuli), overexpression of miR-210 leads to a decrease in GPD1L protein levels and no more activation of the PHDs. This inhibition, in turn, leads to increased stability of the HIF-1α protein and its transcriptional activity (***Figure 19***). According to the data collected by Kelly *et al.*, miR-210 initiates a positive feedback loop where HIF-1α drives the expression of miR-210, which further enhances the stability of HIF-1α protein[142,143].

Numerous studies have associated miR-210 with functionally essential targets involved in cancer and other human disorders. Its aberrant expression has been broadly reviewed, and a growing body of studies highlights its clinical relevance[143–145]. Additionally, the involvement of miR-210 has been investigated in several non-malignant conditions, ranging from artery diseases to sclerosis. Moreover, like other miRNAs regulating signaling pathways, miR-210 can have contrasting effects depending on the cell line or its intrinsic cellular position.

I.2.2 A multifaceted miRNA

Although miR-210 has been extensively studied in the context of cancer, it is also implicated in several physiological and pathological conditions[143,144]. This microRNA is known for its remarkable stability and ability to respond to different cellular stresses, making it a crucial player in cellular adaptation and homeostasis. Here, the critical roles of miR-210 will be explored, excluding its involvement in cancer, which will be the subject of the next sub-chapter.

In response to low oxygen levels, cells activate genes essential for endothelial cells to form new blood vessels, ensuring survival under hypoxic conditions. While much research has focused on the regulation of vascular endothelial growth factor (VEGF), a potent pro-angiogenic factor that supports the sprouting of endothelial cells, recent advances in miRNA biology have provided insights into the role of miR-210 in regulating angiogenesis under hypoxic conditions. Fasanaro *et al.* were among the first to report that miR-210, induced by hypoxia, contributes to the angiogenic response in endothelial cells[146]. MiR-210 has been shown to enhance VEGF-mediated cell migration and the formation of capillary-like structures. This effect is achieved through the suppression of ephrin-A3, a ligand for receptor tyrosine kinase, thus promoting angiogenesis[147]. The pro-angiogenic role of miR-210 has been studied in the context of myocardial infarction, where its delivery to the heart has been shown to improve endothelial cell survival, suggesting its potential therapeutic benefits[148]. Similarly, miR-210 regulates angiogenesis in ischemic

renal ischemia/reperfusion (I/R) injury. Here, miR-210 induction is crucial for promoting the expression of VEGF in endothelial cells, facilitating angiogenesis[149]. These findings highlight the importance of miR-210 in driving angiogenic responses and promoting microcirculation under both physiological and pathophysiological conditions.

Inflammation is another crucial response that occurs in the body when there is an infection or injury, and where miR-210 has its role to play. Inflammation serves the purpose of eliminating pathogens and damaged tissue while initiating the healing process. One characteristic of inflamed cells and tissues is the presence of low oxygen levels. This is caused by the damage to local blood vessels and the increased oxygen consumption by pathogens and specific immune cells[150]. Recent studies have highlighted the significant role of miR-210 in regulating the inflammatory response under highly stressful conditions[151-153]. Wang *et al.* have observed that miR-210 appears to have an essential regulatory function in the differentiation and activation of T-cells, particularly in the Th17 cell line[154]. This regulation occurs specifically under hypoxic conditions. Hence, miR-210 expression is upregulated in Th17 cells and controlled by the T-cell receptor and the CD28 coreceptor. Interestingly, lower levels of miR-210 promote the differentiation of Th17 cells under hypoxic conditions. This differentiation process is mediated by a feedback loop in which miR-210 inhibits the expression of HIF-1α. Through this feedback, miR-210 contributes to the regulation of Th17 cell differentiation. Another notable finding from Noman *et al.* revealed that miR-210 enhances the suppressive effects of myeloid-derived suppressor cells on T-cells. This enhancement occurs by increasing nitric oxide production and the activity of an enzyme called arginase[155]. In summary, miR-210 has emerged as a critical regulator of the inflammatory response under stressful conditions. Its upregulation in Th17 cells under hypoxia influences the differentiation and activation of these immune cells. Additionally, miR-210 enhances the suppressive activity of myeloid-derived suppressor cells on T-cells, ultimately impacting tumor growth.

A study by Chan *et al.* showed that miR-210 also plays a regulatory role in mitochondrial metabolism during hypoxic conditions[156]. Under hypoxia, the cellular metabolic process shifts from oxidative phosphorylation to glycolysis. Several proteins induced by hypoxia, such as lactate dehydrogenase A, cytochrome c oxidase, pyruvate dehydrogenase kinase, and mitochondrial protease LON, contribute to this metabolic change[157]. The upregulation of HIF-1α under hypoxia leads to increased expression of glycolytic enzymes and pyruvate dehydrogenase kinase while downregulating mitochondrial respiration[158]. MiR-210 downregulates the activity of the Krebs cycle enzymes. It affects mitochondrial function by targeting iron-sulfur cluster assembly proteins, resulting in increased generation of free radicals, enhanced cell endurance under hypoxic

conditions, and improved iron intake required for various cellular functions[159]. Specific targets of miR-210 include iron-sulfur cluster assembly proteins ½ and proteins involved in mitochondrial metabolic processes, such as aconitase and complex I, leading to reduced oxidative phosphorylation[156]. However, the role of miR-210 in modulating reactive oxygen species (ROS) levels in mitochondria is still not fully understood, and further research is thus needed. Given the diverse regulatory functions of miR-210 under hypoxia, additional roles in regulating mitochondrial function have been studied recently[160–162].

Based on the experimental evidence summarized herein, miR-210 has emerged as one of the most extensively studied miRNAs to date. In addition to its intricate involvement in regulating various biological processes, miR-210 has been linked to the development of numerous human diseases, particularly as a key player in hypoxic conditions. Recent research has shed light on the biological functions of miR-210 and its role in pathological states, as detailed above, for some human diseases. Other reviewed roles of miR-210 in non-cancerous disorders can be found in the non-exhaustive ***Table 3***.

Disease	Target	Function	Reference
Endometriosis	STAT3	STAT3 activation by miR-210 leads to cell proliferation and resistance to apoptosis	Okamoto *et al.*[163]
Myelodysplastic syndromes	SHIP-1	Hypoxia overexpresses miR-210 in the bone marrow, increasing cell survival	Lee *et al.*[164]
Hypertrophic Scar	STAT5A	miR-210 reduces STAT5 expression, promoting the differentiation of human dermal fibroblasts	Wei *et al.*[165]
Psoriasis	STAT6/LYN	miR-210 induces an immune imbalance in psoriasis	Wu *et al.*[166]
Acute Cerebral Infarction (ACI)	BDNF	miR-210 downregulation in ACI patients can be used as a diagnosis tool	Tian *et al.*[167]
Graves' Disease (GD)	FOXP3	High levels of miR-210 in GD patients can be used as a marker for this disease	Zheng *et al.*[168]

Table 3 *- miR-210 involvements in non-cancerous diseases.*

In brief, miR-210 and its regulatory activity clearly indicate its potential as a valuable target for therapeutic development. Although most studies are currently preliminary, it is anticipated that miR-210 will be a promising target for drug development in the future. However, it is essential to remember that miR-210's long list of effects on multiple systems can be challenging when considering it as a therapeutic target. The specific targeting of miR-210 may lead to unintended consequences or disruptions in other physiological

functions. Therefore, when developing therapeutic approaches targeting miR-210, careful consideration is required to address potential off-target effects. Further research and understanding of miR-210's regulatory network will be necessary to optimize its therapeutic potential and minimize possible limitations or unintended consequences in clinical applications.

I.2.3 MiR-210 and cancer

Considering the consistent and significant up-regulation of miR-210 in hypoxic cells and the prominent presence of hypoxia in solid tumors, it is logical to investigate the functions of miR-210 in tumorigenesis. Advances in bioinformatic tools for predicting miRNA targets, along with improvements in experimental techniques, have led to the identification of numerous targets of miR-210. These findings have revealed an important role of miR-210 in the initiation and progression of tumors[169]. ***Table 4*** provides a non-exhaustive compilation of the identified targets of miR-210, demonstrating its oncogenic potential and underscoring its involvement in tumor-related processes.

Cell type	Target	Function	Reference
Lung carcinoma	ALDHSA1	Mitochondrial metabolism	Bertero *et al.*[170]
Breast cancer	TfR	Mitochondrial metabolism	Yoshioka *et al.*[171]
Breast cancer	RAD52	Cell cycle / DNA damage	Crosby *et al.*[172]
Endothelial	GPD1L	Apoptosis	Fasanaro *et al.*[173]
Pancreatic cancer	HOXA1	Development	Huang *et al.*[174]

Table 4 *– Validated cancer-related targets of miR-210 targets.*

Hypoxic cancer cells are known for their resistance to conventional chemotherapy and radiotherapy. The association between miR-210 and apoptosis, as well as cell survival, has been extensively investigated. Its antiapoptotic and cytoprotective effects have been demonstrated in numerous studies involving cancer cells[175–178], as well as normal cells such as human pulmonary artery smooth muscle cells (HPASMC)[179] and neural progenitor cells[180]. Several functional targets of miR-210 associated with apoptosis have been identified; for example, it downregulates the expression of caspase-8-associated protein-2 (CASP8AP2), promoting the survival of stem cells[181]. In cells where miR-210 downregulated the activity of CASP8AP2, apoptosis was effectively suppressed even under conditions that would typically induce it, such as lethal anoxia and irradiation. Another example is E2F3, a transcription factor and a well-known cell cycle regulator. It is a direct target of miR-210 in

hypoxic HPASMC. Its downregulation contributes to the antiapoptotic effect of miR-210. Knocking down miR-210 in hypoxic HPASMC leads to the upregulation of E2F3 and induces apoptosis, indicating the antiapoptotic effect of miR-210 in HPASMC cells under hypoxic stress[179].

The cytoprotective effect of miR-210 against radiotherapy has also been investigated. Overexpression of miR-210 in the A549 cell line (lung carcinoma cells) under normoxic conditions can safeguard them from radiation[182]. In the study of Grosso *et al*., it was found that A549 cells expressing miR-210 under normal oxygen conditions showed a similar level of resistance to radiation as A549 cells expressing a control miRNA under hypoxic conditions. Moreover, the resistance to radiation was further enhanced in cells exposed to hypoxia. While the exact mechanisms underlying this radioresistance were not thoroughly investigated, it was proposed that cells expressing miR-210 exhibit accelerated repair of DNA double-strand breaks (DSBs), which could contribute to their increased resistance to radiation[182]. Mir-210 has also been reported to act as a protecting agent, playing a role in DNA repair mechanisms. Under normal metabolic conditions and certain environmental factors like UV and radiation, DNA damage occurs in most cases as a DSB[183]. Such damage leads to daily lesions in each cell, triggering cell senescence and the development of tumors[184]. It is vital to ensure that an organism's genetic material remains intact throughout its lifetime, and DNA repair is a crucial factor in accomplishing this goal. Recent research has revealed that miR-210 can inhibit the DNA repair system by targeting an enzyme called RAD52[185]. RAD52 is responsible for repairing DNA double-strand breaks (DSBs) by filling in single-stranded DNA gaps. MiR-210 binds directly to the 3′UTR region of RAD52, leading to translational repression. The downregulation of RAD52 under hypoxic conditions, which occurs due to miR-210 overexpression, is reversed by anti-miR-210 treatment[185]. This suggests that RAD52 is downregulated via a miR-210-dependent mechanism under hypoxia. The shutdown of DNA repair under low oxygen conditions may be crucial for conserving ATP and preserving cell viability during acute hypoxia, often called the "hang in there" response. Overall, hypoxia leads to high levels of miR-210, significantly impairing the DNA repair mechanism and promoting genetic instability. Consequently, this can result in either cell senescence or the acquisition of a mutational phenotype during tumor development.

Despite the numerous studies cited above demonstrating miR-210's role as an oncogene, a significant body of research suggests that miR-210 can also function as a tumor suppressor, effectively inhibiting tumor initiation. ***Table 5*** presents an overview of the identified targets of miR-210, supporting the notion of its potential involvement as a tumor suppressor.

Target	Function	Cell type	Reference
PTPN2	Regulates cell proliferation	ASC	Kim *et al.*[186]
PIK1	Regulates mitosis	CNE, Hela	He *et al.*[187]
Cdc25B	Regulates mitosis	CNE, Hela	He *et al.*[187]
Fam83D	Regulates mitosis	CNE, Hela	He *et al.*[187]
Bub1B	Regulates mitosis	CNE, Hela	He *et al.*[187]

Table 5 *- Tumor suppressor miR-210's targets.*

Giannakakis *et al.* observed that miR-210 was frequently deleted in ovarian cancer cell lines and samples, suggesting its potential role as a tumor suppressor gene[188]. They identified E2F3 as one of the targets of miR-210. Interestingly, E2F3, known for its pro-apoptotic effect in hypoxic HPASMC cells, promotes cell proliferation in this context. Overexpression of miR-210 reduced E2F3 expression, indicating that down-regulation of miR-210 in hypoxia may increase E2F3 expression, contributing to tumorigenesis. However, since both forms of E2F3, E2F3a, and E2F3b are targeted by miR-210, further experiments are needed to fully understand this interaction[188].

Tsuchiya *et al.* also showed the anti-proliferative role of miR-210 in esophageal squamous cell carcinoma (ESCC). They observed the down-regulation of miR-210 in ESCC cell lines and demonstrated that this led to cell cycle arrest and cell death. Fibroblast growth factor receptor-like 1 (FGFRL1) was identified as a direct target of miR-210 in this context[189]. Moreover, in addition to its previously shown ability to inhibit apoptosis, miR-210 mediated hypoxia-induced apoptosis in neuroblastoma cells, as Chio *et al.* highlighted[190]. They showed that overexpression of miR-210 in neuroblastoma cells under oxygen/glucose deprivation increased apoptosis by targeting the anti-apoptotic gene Bcl-2, reducing Bcl-2 levels at both mRNA and protein levels[190].

Furthermore, these findings regarding the anti-proliferative and apoptosis-inducing effects of miR-210 in various cancer cells shed light on its potential as a biomarker for early detection and prognostic evaluation in cancer. Understanding the role of miR-210 in these contexts is particularly relevant, considering the recognized significance of abnormal miRNA expression profiles in cancer and the potential of specific miRNA signatures to guide personalized treatment strategies. However, the conflicting results from numerous studies investigating miR-210's involvement in cancer diagnosis and prognosis necessitate further investigation and clarification. Compared to normal cells, abnormal expression profiles of miRNAs in cancer cells have been widely recognized. Specific miRNA signatures have diagnostic potential and can also classify cancer patients into subgroups with distinct prognoses, enabling personalized treatment approaches. Numerous studies have explored

the role of miR-210 in cancer diagnosis and prognosis[191]; however, these investigations have yielded conflicting findings. Most of the evidence indicates that miR-210 is up-regulated in various solid tumors, including breast cancer[138,192–195], head and neck cancer[196,197], pancreatic cancer[198,199], lung cancer[200–203], renal cancer[204–207], osteosarcoma[208–210], esophageal cancer[211], and ovarian cancer[212,213]. However, as seen before, inconsistent reports suggest miR-210 deletion in certain cases of ovarian cancer and down-regulation in some cases of esophageal cancer[188,189]. These contradictory results highlight the complex and heterogeneous nature of cancer.

In conclusion, miR-210 is a crucial biomolecule involved in the biological responses of cancer cells to low oxygen levels (hypoxia). It regulates various cellular processes such as metabolism, cell cycle, survival, differentiation, DNA repair, and immune response. Noteworthy, miR-210 can have contradictory functions in cancer development; it can act as both an oncogene and a tumor suppressor, depending on the specific conditions and duration of hypoxia. As expected, the effects of miR-210 in different cells rely on the target genes it interacts with. While several target genes have been identified, more research is needed to fully understand miR-210 functions and how it can be effectively targeted for cancer therapy. Regarding its diagnostic and prognostic value, miR-210 can be detected in both cancerous tissues and body fluids, making it helpful in distinguishing between cancer and non-cancerous conditions. However, using miR-210 alone as a prognostic factor requires further investigation to understand the reasons for inconsistencies in its up or down-regulation. Future research analyzing large groups of patients and integrating various genetic information could provide valuable insights into prognostic factors and the use of miR-210 for cancer therapy.

I.2.4 A regulator of circadian rhythm

Many biological processes follow a natural rhythm known as the circadian clock, which has an inherent period of approximately 24 hours[214,215]. The molecular mechanism that governs these circadian rhythms involves a series of interconnected feedback loops between transcription and translation, where specific factors inhibit the transcription of their own genes (***Figure 20***)[216]. The circadian clock is an intricate and finely tuned biological system that regulates various physiological processes in living organisms, including sleep-wake cycles, hormone secretion, metabolism, and cellular functions. It is an internal timekeeping mechanism that helps organisms anticipate and adapt to daily environmental changes. Disruptions to the circadian rhythm are associated with numerous health implications, including an increased risk of developing cancer[217,218].

More specifically, the circadian clock network consists of two transcriptional complexes that work oppositely to regulate the expression of clock-controlled genes (CCGs). On the one hand, the proteins BMAL1 and CLOCK form a clock activator complex that promotes the transcription of CCGs by recognizing specific protein-binding sites called E-box[219]. On the other hand, the association of CRY and PER proteins creates a transcriptional repressor complex that reduces the transcriptional activity driven by BMAL1/CLOCK[220,221]. However, additional negative regulators, such as REV-ERB nuclear receptors, also play a crucial role in maintaining a proper circadian rhythm[222]. This periodic competition between the clock activator and repressor complexes determines the circadian expression of approximately 5%–10% of the mammalian transcriptome[223].

MYC protein has been reported to be implicated in disrupting the circadian clock in cancer cells[224–226]. MYC is a transcription factor that plays a crucial role in regulating cell growth, proliferation, and metabolism. Studies have revealed that MYC can directly or indirectly affect several components of the circadian clock machinery, but the correct mechanism of repression is still highly debated. It can modulate the expression of the BMAL1 clock gene by binding to its promoter and altering its transcriptional activity[224,227]. This disruption in circadian clock genes and proteins by MYC can lead to perturbations in the timing of critical physiological processes in cancer cells, including cell growth and apoptosis. Hence, MYC, as a transcription factor, has different roles highly dependent on the interacting protein partner. Repression activity on the circadian machinery relies upon the heterodimerization of MYC with MAX protein (MYC-associated X-factor)[225]. They work

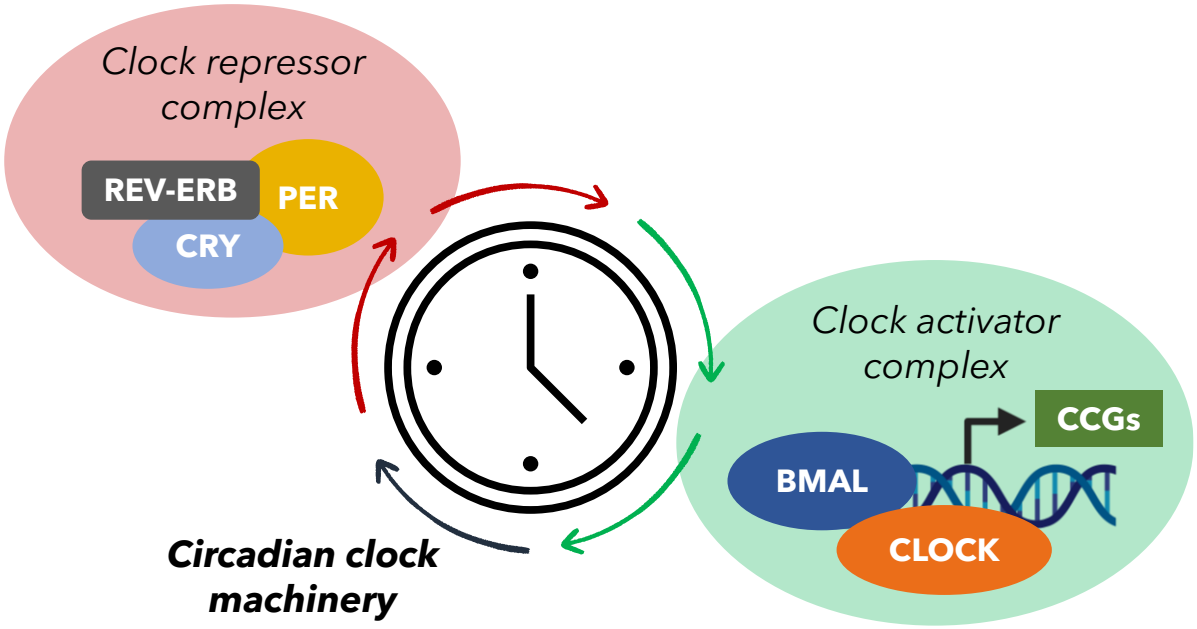

Figure 20 *– At the molecular level, the circadian clock machinery can be schematized as two transcriptional complexes regulating each other's activity. Proteins BMAL and CLOCK are transcriptional activators triggering CGGs' expression. These proteins also induce the expression of CRY and PER repressor proteins. The balance between activator and repressor proteins leads to a rhythmic expression of several genes.*

together to regulate gene expression by binding to specific DNA regions, controlling whether certain genes are turned on or off. MAX acts as a regulatory partner for MYC, stabilizing the MYC/MAX complex and modulating MYC's oncogenic activity[228]. In detail, our team at the Italian Institute of Technology (IIT) reported the role of MNT protein as a partner in MAX-mediated circadian regulation[225]. MNT is recruited to the promoters of clock core genes in a MAX-dependent manner and plays a crucial role in repressing the molecular clock. Knocking down MNT in MDA-MB-231 cells disrupts circadian oscillation, and similar effects were observed in MCF10A cells. Hence, the dysregulation of circadian rhythms due to MYC overexpression is linked to the MAX/MNT complex disruption, as MYC can compete with MNT for MAX binding. The collected data also suggest that the disruption of the MAX transcriptional network may play a role in circadian dysfunctions observed in various pathological conditions. For example, a recent study has proposed that the reduced expression of MNT is a significant functional event in response to hypoxia in different types of injuries and diseases[229]. Indeed, hypoxia can have severe consequences and disrupt circadian rhythms[230]. While proteins like HIF-1α and mTOR are known to affect the regulation of clock genes under low oxygen conditions, our findings suggest that disturbance of MAX/MNT complexes may also be a crucial factor contributing to this kind of disruption induced by hypoxia.

Additionally, recent studies conducted by various research groups have uncovered the involvement of microRNAs in the regulation of clock physiology. They can modulate the expression of key circadian clock genes, thereby affecting the overall functionality of the circadian system[231,232]. Besides, dysregulation of miRNA expression patterns has been observed in various types of cancer, where miRNAs can act as either tumor suppressors or oncogenes, influencing the development and progression of the disease. Understanding the relationship between circadian rhythm, cancer, and miRNAs can have significant implications for anticancer therapeutics research, and elucidating the biological molecular mechanisms underlying miRNA-mediated circadian regulation aims to find potential new strategies for cancer treatment. In this context, miR-210 has been reported to be a key modulator in the circadian clock/cancer relationship.

An interesting mechanism involves the downregulation of MNT through miR-210 upon binding to the 3'-UTR of MNT mRNA, leading to a decrease in both MNT mRNA and protein levels[233]. Zhang *et al.* confirmed that miR-210 is a direct target of the hypoxia-inducible factor HIF-1α and can downregulate MNT levels through gene expression analysis and RNA interference experiments. As MNT is known to counteract MYC, they investigated further to assess the mechanism of miR-210-mediated repression. MYC's ability to promote cell proliferation depends on its dimerization partner, MAX. The balance between

MYC/MAX and MNT/MAX is crucial for cell cycle entry, and loss of MNT can leave more space for MYC overexpression in cells and promote tumorigenesis. Although HIF-1α and HIF-2α have opposite effects on MYC-dependent proliferation, both HIFs induce miR-210 to ultimately activate MYC, suggesting complex regulation of MYC in different cellular contexts[233]. In summary, Zhang *et al.* findings demonstrate that miR-210 targets MNT to indirectly activate MYC, thus promoting cancer cell proliferation.

Another more recent study highlighted the role of miR-210 in downregulating MNT in idiopathic pulmonary fibrosis (IPF) fibroblasts[234]. The study reveals that MNT expression is suppressed in fibroblasts from individuals with IPF when exposed to hypoxic conditions. By reducing the levels of miR-210, they decreased the proliferation of IPF fibroblasts in response to hypoxia, and this decrease was linked to an increase in MNT expression. Noteworthy, when they knocked down MNT and miR-210, they observed a partial restoration of the proliferative response to hypoxia. Furthermore, overexpressing MNT in IPF fibroblasts attenuated hypoxia-induced proliferation, indicating the ability of miR-210 to enhance IPF fibroblast proliferation through MNT repression[233].

Based on these findings, targeting miR-210 holds an excellent chance to be an effective anticancer strategy by repressing MYC activity. The circadian clock, a crucial biological system, can be disrupted by MYC, leading to uncontrolled cancer cell proliferation. Understanding the intricate interactions among the circadian clock, miR-210, and MYC signaling pathways provides valuable insights into circadian regulation in cancer and other disorders. Further research must explore the therapeutic implications and develop targeted interventions for circadian-related conditions.

In conclusion, this initial literature review chapter underscores and confirms the significance of considering miRNAs (and their precursors) as viable biological targets. The examples presented at the beginning of this chapter shed light on the potential for designing novel RNA binders with exceptional selectivity, both *in vitro* and *in vivo*. As previously discussed, the captivating field of miRNA inhibitors is getting more and more attention owing to innovative design techniques and chemical ingenuity from both the private and academic sectors. Once deemed "undruggable", miRNAs now represent valuable targets in numerous diseases, particularly cancer. Extensive research has been conducted on various miRNAs, including miR-210, referred to as the "hypoxamir" due to its strong association with hypoxia-related human disorders. The preceding subsection highlighted the compelling reasons for targeting miR-210 as an intriguing and innovative anticancer strategy. Although the field may still be in its infancy, it holds great promise, which serves as the starting point for the current project, to be presented in the following section. It is worth mentioning that previously published works on small-molecule targeting

of specific miRNAs have inspired this project, which aims to inhibit the biogenesis of the oncogenic miR-210.

Aims of the project

Aims of the project

This PhD project, at the interface of medicinal chemistry and chemical biology, focuses on preparing new bioactive small molecules capable of inhibiting the maturation of a specific miRNA known as miR-210. The molecules designed and synthesized during this project should be prepared in order to be efficient and selective inhibitors of miR-210 maturation. The main goal is the reduction of miR-210 levels in tumor cells by impeding the Dicer processing of its hairpin precursor pre-miR-210 to repress any oncogenic downstream role this miRNA plays.

In the Preface and Chapter I, our team's focus on RNA targeting was outlined, specifically how we address oncogenic miRNAs, viral RNAs like HIV-1's TAR RNA, bacterial targets such as the prokaryotic ribosome's A-site or type I toxin-antitoxin systems[76,124,126,127,235]. Correlating our team's accumulated knowledge and expertise with published works, we have conceived a rational approach to design new and innovative ligands that should show high affinity and good selectivity towards the intended RNA target (i.e., pre-miR-210). Thus, we decided to use this approach to modify a known inhibitor or miR-210, referred to as targapremiR-210 (**1.15**), to prepare new efficient ligands (***Figure 21A***). Firstly, we employed the core structure of **1.15**, published by Costales *et al.*[102], and optimize the right part of it by introducing several other motifs capable of binding to RNA secondary structures to identify interesting motifs for good affinity toward the RNA target. Therefore, a first series of analogs will be based on the optimization of compound **1.15**. In this context, we prepared new analogs by modifying the core structure of this bis-benzimidazole molecule (highlighted in blue, ***Figure 21A***) and by changing the phenyl group's functionalization (highlighted in orange, ***Figure 21A***). This first SAR study conducted *in vitro* allowed us to identify the most promising compounds based on affinity (K_D measurements), selectivity (in the presence of other nucleic acid sequences), and inhibition activity toward the maturation of miR-210 (IC_{50} values assessing the potential of a compound to block the Dicer-mediated cleavage of miR-210 precursor). A preliminary evaluation in cellular contexts was also performed and allowed selecting the most suitable biological system for further studies on the compounds' mechanism of action. This first part of the work will be detailed in Chapter II.

Subsequently, with the idea of preparing original miR-210 inhibitors, we envisaged a second series of compounds featuring innovative and, to the best of our knowledge, unpublished chemical structures. The inspiration for this series originates from bleomycin A5 (also known as pingyangmycin), a natural glycopeptide widely employed as an anticancer drug due to its ability to interact with various nucleic acids. We hypothesize that

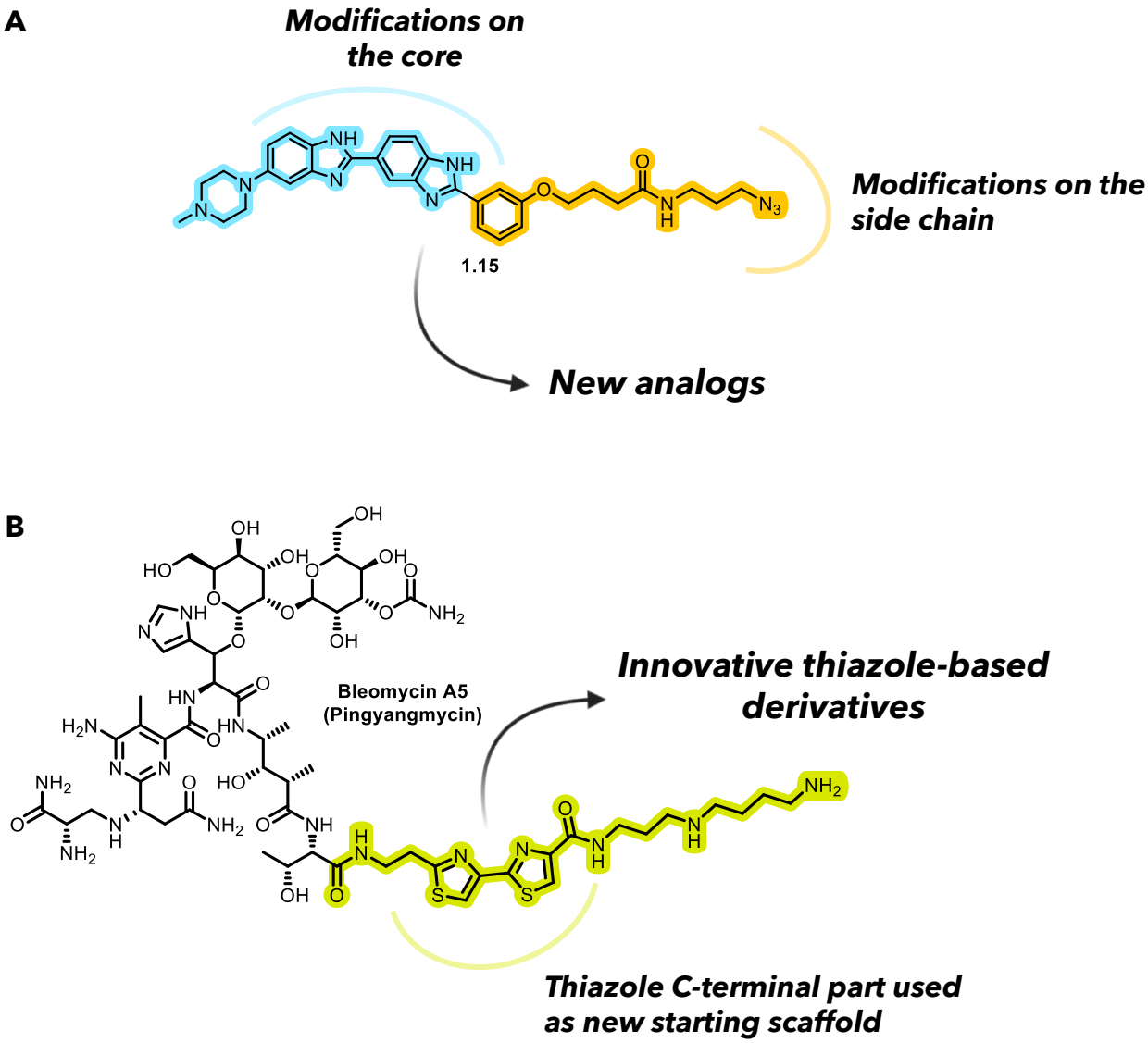

Figure 21 *– A) Compound* ***1.15*** *and the modifications that we envisage. B) Bleomycin A5 structure and its C-terminal part with the bis-thiazole scaffold, which will be used for the design of new and innovative derivatives.*

the C-terminal thiazole part of bleomycin A5 (***Figure 21B***) could replace the bis-benzimidazole core of **1.15** to generate new RNA binders[126]. Thus, we prepared several series of analogs containing either bis- or tris-thiazole scaffold as well as other motifs identified in the first SAR study or different moieties known to interact with the negatively charged RNA backbone or the RNA nucleobases.

The overarching aim of this project is to design and identify new miR-210 inhibitors and to study their biological activity *in vitro* and in cancer cells. As described in Chapter I, miR-210 overexpression in tumors is correlated with low oxygen levels, so we studied how these hypoxic conditions could be induced in several cancer cells. Once suitable conditions were found, we investigated the toxicity profile of our analogs based on the hypothesis that too-high toxicity would block the in-depth evaluation of the compounds' mechanism of action.

Subsequently, we used molecular biology techniques such as Western Blot or RT-qPCR to understand precisely how the best compounds could effectively reduce miR-210 levels in cancer cells and reduce the adaptive response toward hypoxic conditions of these cells. The downstream targets of miR-210 reviewed in Section I.2 (Chapter I) served as indicators of our compounds' efficacy. The design, synthesis, and evaluation of this new series of RNA binders will be detailed in Chapter III.

Chapter II

Synthesis and biological evaluation of novel benzimidazole derivatives

Chapter II | Synthesis and biological evaluation of novel benzimidazole derivatives

II.1 Introduction

As outlined in Chapter I, the primary objective of this PhD project was to initially synthesize benzimidazole-based derivatives, taking advantage of a previously published compound known to inhibit the maturation of miR-210. This compound (**1.15** or TGP-210) was chemically modified, and the obtained small library of analogs was tested *in vitro* for its affinity, selectivity, and inhibitory activity toward the pre-miR-210 target. Then, a preliminary *in cellulo* study led us to validate a correct cellular system, where miR-210 is overexpressed upon triggering hypoxic conditions in cancer cell lines. Moreover, a first assessment of the toxicity of the new derivates was performed, both in cancer and healthy cells.

As mentioned in Chapter I, some miRNAs are overexpressed in cancer cells and inhibit the synthesis of tumor suppressor proteins, classifying them as oncogenic microRNAs (*See Section I.1.1, Chapter I*). Herein, we focused on miR-210 for its implications in various diseases, including cancer. Modulating its maturation process could potentially restore normal tumor suppressor protein levels and inhibit cancer cell proliferation. Thus, we decided to hinder the biogenesis of miR-210 by blocking the transition step from pre-miR (sequence in ***Figure 22B***) to the miR duplex by preventing Dicer-mediated cleavage (***Figure***

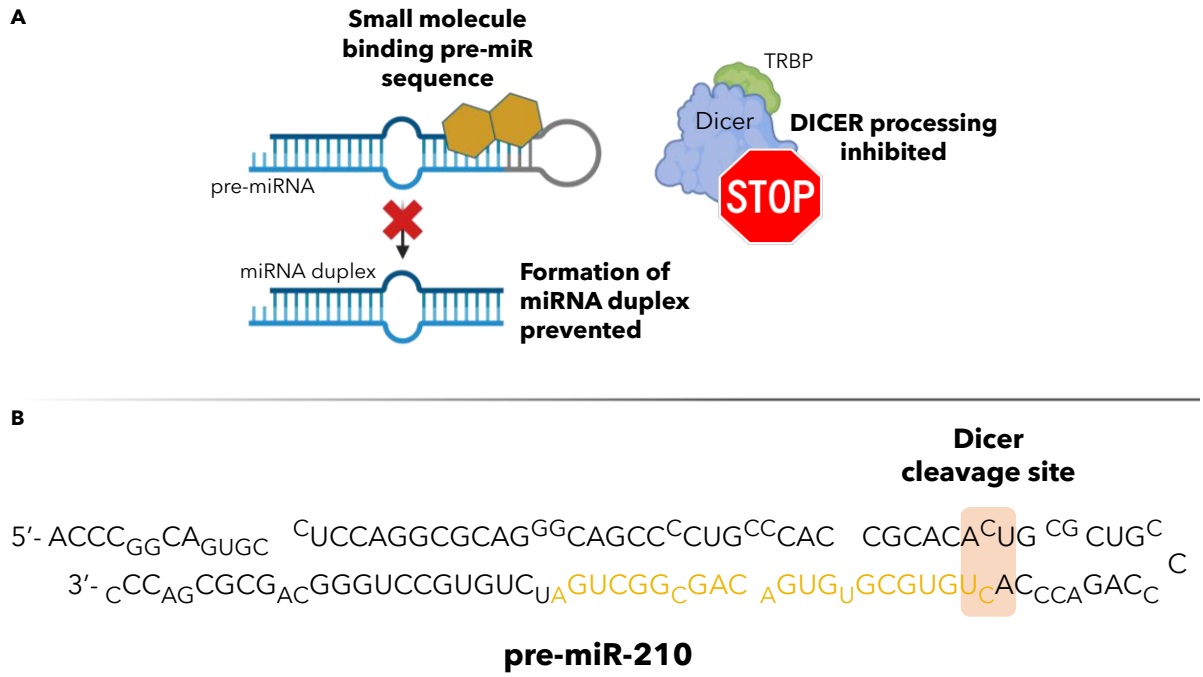

Figure 22 *– A) Inhibition of miRNA biogenesis by blocking Dicer-mediated cleavage via small molecule. B) Pre-miR-210 sequence with the Dicer cleavage site, and mature miR-210 sequence written in orange.*

22A). To avoid Dicer-cleavage, the proposed approach involves small RNA-binding molecules that interact with a specific region of pre-miR-210 (outlined in ***Figure 22B***), which is crucial for Dicer's optimal function. Consequently, Dicer's cleavage activity would be inhibited, stopping biogenesis and reducing the levels of miR-210 *in cellulo* (***Figure 22A***). In this context, the following sections will go through an introduction to the history of benzimidazole chemistry and their known biological activity, and finally, on the design, synthesis, and biochemical assessment of novel heterocyclic small molecules.

II.1.1 Benzimidazoles and their related biological activities. Essential motifs in drug discovery

Benzimidazoles, a well-known chemical moiety, were initially synthesized by Hoebrecker in 1872[236]. Subsequently, Ladenburg[237] and Wundt[238] also contributed to their synthesis. These compounds now belong to a diverse family of bioactive compounds with various medicinal uses. The extensive range of therapeutic applications has led to a significant interest in this benzimidazole scaffold, as evidenced by numerous studies and syntheses reported in the literature. All are underscoring the benzimidazole scaffold's importance and potential in medicinal chemistry.

This bicyclic heteroaromatic compound was first prepared from the reduction of 2-nitro-4-methylacetanilide (***Scheme 1A***) by Hoebrecker[236], affording 2,5 or 2,6-dimethylbenzimidazole. Some years later, the same compound was afforded by refluxing 3,4-diaminotoluene with acetic acid (***Scheme 1A***) by Ladenburg[237]. Such traditional methodologies presented several limitations, especially in the yield of the desired product and occasional requirements for elevated temperatures[239]. The benzimidazole synthesis was then performed with the condensation of *o*-phenylenediamine with carboxylic acids, esters, or aldehydes[239]. However, for cyclization to happen, strong acidic conditions or oxidative reagents were required. If yields were increased, some challenges remained, with excessive amounts of oxidative catalyst leading to potential metal contamination of the final product or highly complex workup procedures. Recently, several synthetic roads to benzimidazole were published, mainly all based on metal-catalyzed reactions between *o*-phenylenediamine and aromatic aldehydes or acids[240]. Besides, it must be noted that benzimidazoles exhibit prototropic tautomerism properties with the hydrogen atom attached to N-1 (***Scheme 1B***), leading to isomerization in derived compounds.

The distinct properties of benzimidazole-based compounds, such as their biological activity, photophysical properties, and self-assembly behavior, have contributed to their widespread use in various scientific disciplines. One of the remarkable aspects of

benzimidazole derivatives is their biological activity, which has been the focus of research since 1944[241]. Studies have shown that benzimidazoles exhibit properties similar to purines, leading to optimal biological responses. Notably, Brink *et al.* discovered that 5,6-dimethylbenzimidazole, a degradation product of vitamin B12, and its derivatives possess vitamin B12-like activity[242]. This finding led to further investigate the diverse range of activities associated with the benzimidazole heterocyclic scaffold[243]. These include anticonvulsants, antiparasitics, analgesics, antihistaminics, antihypertensives, antivirals, anticancer, antifungals, anti-inflammatory agents, proton pump inhibitors, and anticoagulants[244-250]. Several recent drugs based on benzimidazoles have shown remarkable clinical potential; some are highlighted in ***Scheme 1C*** as examples.

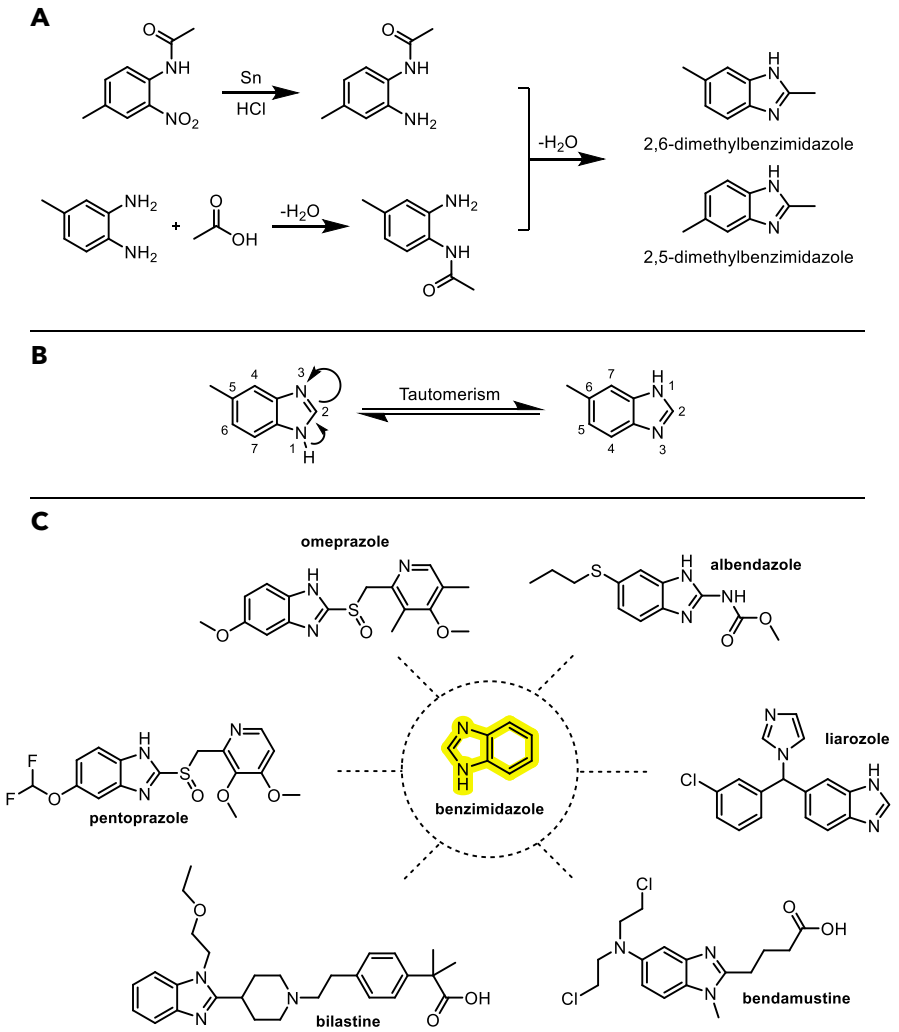

Scheme 1 *– A) First syntheses of benzimidazole heterocycles; b) Annular tautomerism of benzimidazole; C) Different examples of benzimidazole-based accepted drugs. Omeprazole and pantoprazole are widely used proton pump inhibitors (PPIs). Albendazole is an anthelmintic and antiprotozoal agent. Liarozole is a retinoic acid metabolism blocking agent (RAMBA). Bendamustine is a chemotherapy medication used in the treatment of chronic lymphocytic leukemia. Bilastine is an antihistamine medication.*

II.1.2 The use of benzimidazole derivatives to target nucleic acid sequences

Benzimidazole chemistry played a significant role in developing and synthesizing Hoechst compounds, a class of fluorescent dyes widely used in various biological applications[251,252]. Benzimidazole provides a core scaffold for creating diverse Hoechst derivatives, allowing for the fine-tuning of their properties, such as fluorescence intensity and spectral characteristics. Through strategic modifications of the benzimidazole moiety, researchers have successfully designed Hoechst compounds with improved solubility, enhanced cell permeability, and specific binding affinity to DNA. These advancements in benzimidazole chemistry have contributed significantly to the continuous improvement and innovation of Hoechst compounds, enabling their widespread use in fluorescence microscopy, DNA staining, and cell imaging techniques. Such stains bind to the minor groove of DNA, especially to A- and T-rich sequences that enhance fluorescence considerably[253]. Their chemical structure is based on a methyl-piperazine motif and two head-to-head benzimidazole rings, followed by a phenyl ring (***Figure 23***). The functionalization of the phenyl differentiates the three Hoechst stains from one another. Hoechst compounds can bind to all nucleic acids; indeed, the Hoechst 33258 can bind specifically to an RNA stem-loop structure, as noted by Cho *et al*. [254]. This makes them suitable starting points for new RNA ligands. Building on the widespread utility and adaptability of Hoechst compounds and other known RNA-binding motifs, the Disney lab used their 2DCS-based Inforna platform to design a new era of RNA-targeted therapeutics. As described in Chapter I, the family of compounds known as targapremiR or targaprimiR obtained using the Inforna platform are chemical structures made of different known RNA targeting moieties, including, for the majority of them, the bis-benzimidazole motif. This rational design of new mature miR inhibitors, outlined by Disney and colleagues, has thus highlighted several compounds with structural similarities with Hoechst stains as selective RNA ligands.

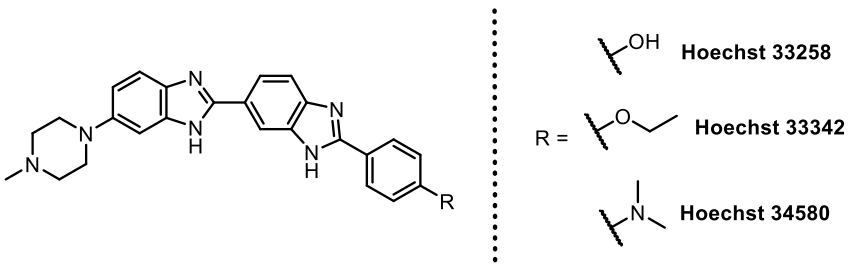

Figure 23 *– Different chemical structures of Hoechst dyes.*

TargapremiR-210

Chapter I details how Inforna's algorithm uses a method that connects RNA internal secondary structures with small molecules that can bind to them. Among the compounds investigated by Disney's lab, targapremiR-210 (**1.15** or TGP-210, ***Figure 24A***) has gained particular attention. TargapremiR-210 is a benzimidazole-based small molecule that selectively binds to the miRNA-210 hairpin precursor, inhibiting its processing and reducing mature miRNA-210 levels. It was first published in 2011, and the initial investigation in 2017 aimed to inhibit the Dicer-mediated cleavage of pre-miR-210 *in vitro*[102,255]. The insights provided in ***Figure 24B*** show that targapremir-210 can effectively block the enzymatic breakdown of pre-miR-210, even at nanomolar concentrations[255]. This correlates closely with its affinity towards the pre-miR-210 Dicer recognition site, precisely the 5'ACU3'/3'UCA5' sequence (with a reported K_D of 200 nM, see ***Figure 24C***). Interestingly, the researchers noted that targapremir-210 showed no binding interaction with a modified

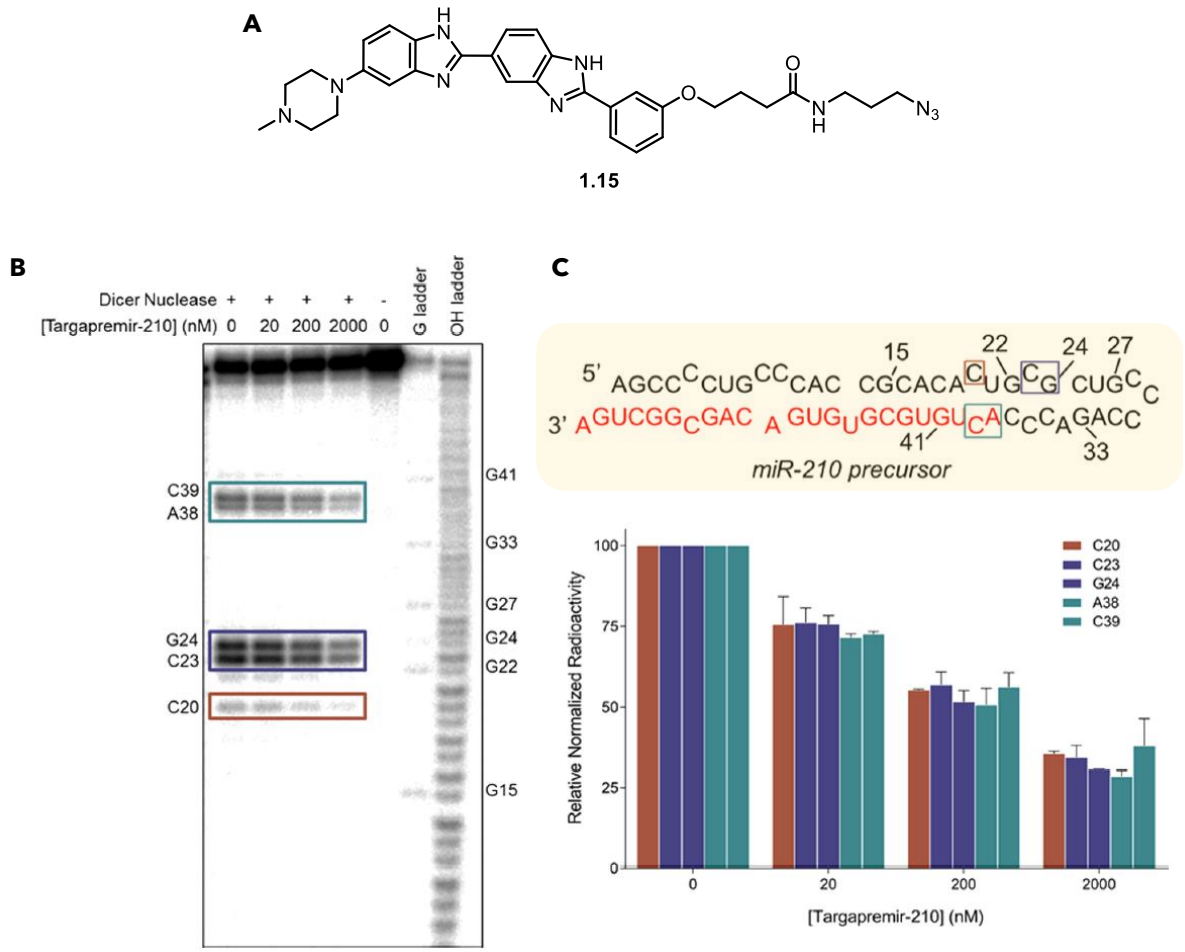

Figure 24 *- (A) TargapremiR-210 chemical structure. (B) Gel image illustrating how Dicer's processing of pre-miR-210 is impeded as the concentration of Targapremir-210 is increased. The portions of nucleotides safeguarded from Dicer cleavage are found in the boxes and pointed out in the secondary structure of miR-210 on the right. (C) This part of the figure shows the secondary structure of pre-miR-210 and the measurement of the degree of protection from Dicer's cleavage. Adapted from Costales et al*[102].

RNA where the Dicer recognition site was intentionally eliminated. In conclusion, the study indicates that targapremir-210 has a strong and specific affinity towards pre-miR-210, and this interaction is potent enough to impede its processing *in vitro*. Such results highlight the potential of this compound for developing novel therapeutics targeting diseases in which miRNA-210 dysregulation is implicated, such as various cancers and cardiovascular disorders.

Design of new targapremiR-210 analogs

In the context of this PhD work aimed at targeting miR-210 maturation, we first chose to explore the synthesis and characterization of **1.15** and novel bis-benzimidazole derivatives based on this chemical structure. To do this, a comprehensive approach has been employed, synthesizing various benzimidazole derivatives of **1.15** with diverse substituents at different positions (***Figure 25***). Compound **1.15** molecule features several groups on which it is possible to vary functions or add chemical groups, aiming to strengthen the interaction with the biological target and enhance the biological activity of this molecule. Modifications of **1.15** were primarily made to the side chain (highlighted in orange in ***Figure 25A***), as all Hoechst compounds that bind to nucleic acids share the bis-benzimidazole moiety (highlighted in blue in ***Figure 25A***). Consequently, it seemed logical to maintain the fixed blue portion initially. However, mono- and tris-benzimidazole compounds were also prepared to serve as controls and assess the importance of the bis-benzimidazole motif.

To increase affinity and selectivity for the target, our initial step involved identifying the extent of modification that could be tolerated on the orange side of the molecule (***Figure 25B***). The lateral chain underwent a two-step modification process: firstly, we reduced its size by removing the azide linker; then, we eliminated it, resulting in smaller intermediates. These new analogs were tested *in vitro* to determine how substantially the molecule could be altered without negatively impacting its effectiveness. Subsequently, our focus shifted to the phenyl group, specifically exploring the impact of introducing either a naphthalene or a quinoline moiety. Both moieties are well-known for their ability to form π-stacking interactions with DNA and RNA nucleotides, as we showed in the context of HIV-1 Tat-TAR interaction inhibitors[76]. Introducing these groups can increase interactions with the target, potentially improving the molecule's binding affinity.

Following our work on the phenyl-side chain motif, our synthesis efforts pivoted to the core of **1.15**. We focused specifically on the two benzimidazole groups, which form the essential structural backbone of the molecule. Our objective was to evaluate the

consequences of reducing or increasing the number of these benzimidazole units in the overall structure (***Figure 25C***). The mono- and tris-benzimidazole compounds were thus envisaged for SAR study. We hypothesized that a reduction in benzimidazole groups might increase the drug-like properties of the molecule, potentially enhancing its binding properties. However, we also recognized that these modifications could conversely lead to a loss of affinity, given the key role these groups play in the molecule's interaction with its target.

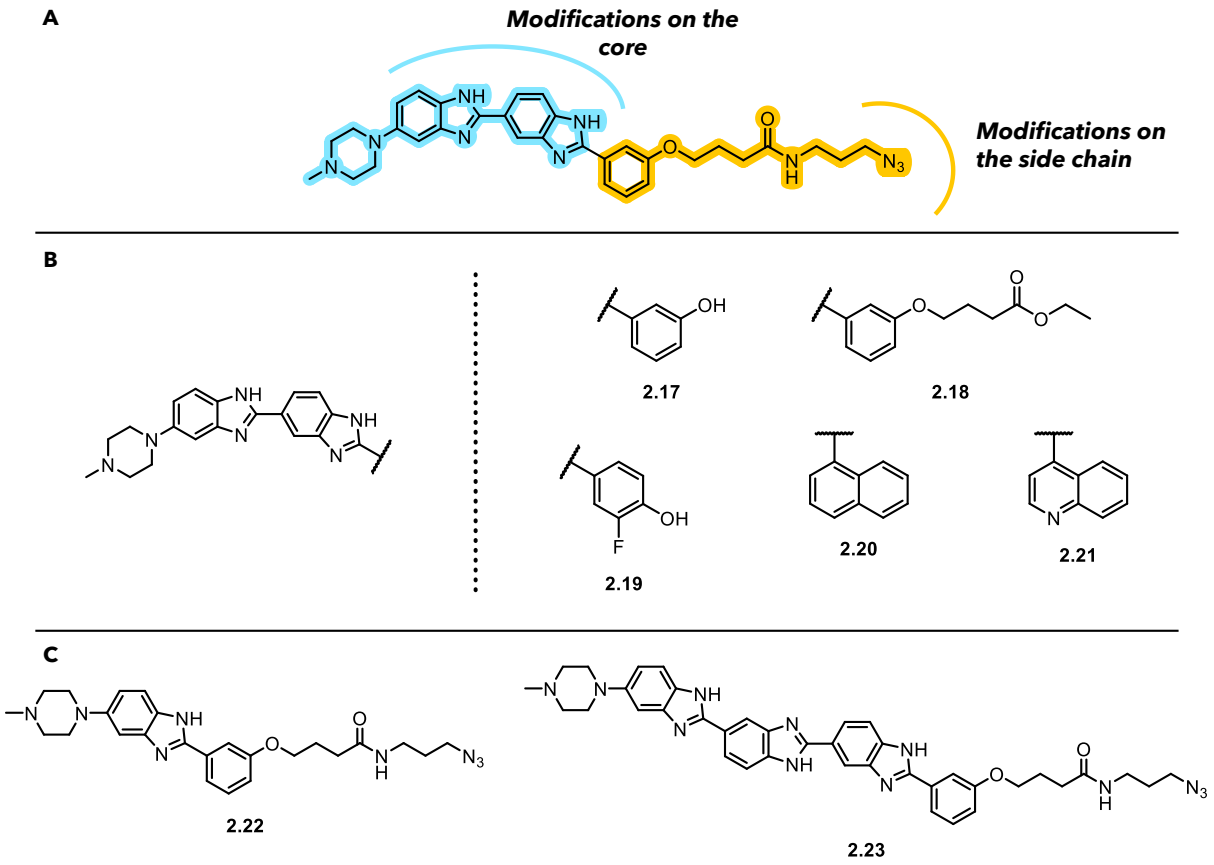

Figure 25 *– Chemical structures of* ***1.15*** *and of the envisaged analogs.*

After thorough structural characterization, the newly generated compounds have been assessed *in vitro* for their binding affinity to the miRNA-210 hairpin precursor through fluorescence-based biochemical assays. A back-and-forth strategy between organic synthesis and biochemical tests allowed for a small SAR analysis that provided valuable insights into the impact of different structural modifications on the compounds' interaction with the target pre-miRNA. Further assays to test the inhibition activity on the Dicer

processing of pre-miR-210 and intracellular evaluation allowed for an overall assessment of targapremiR-210 analogs in our specific biological setup.

II.2 Results and Discussion

II.2.1 Introduction

Initially, we focused our effort on synthesizing targapremiR-210 (**1.15**), but a clearly detailed synthesis of **1.15** has never been published. Looking at the literature[102,255], we

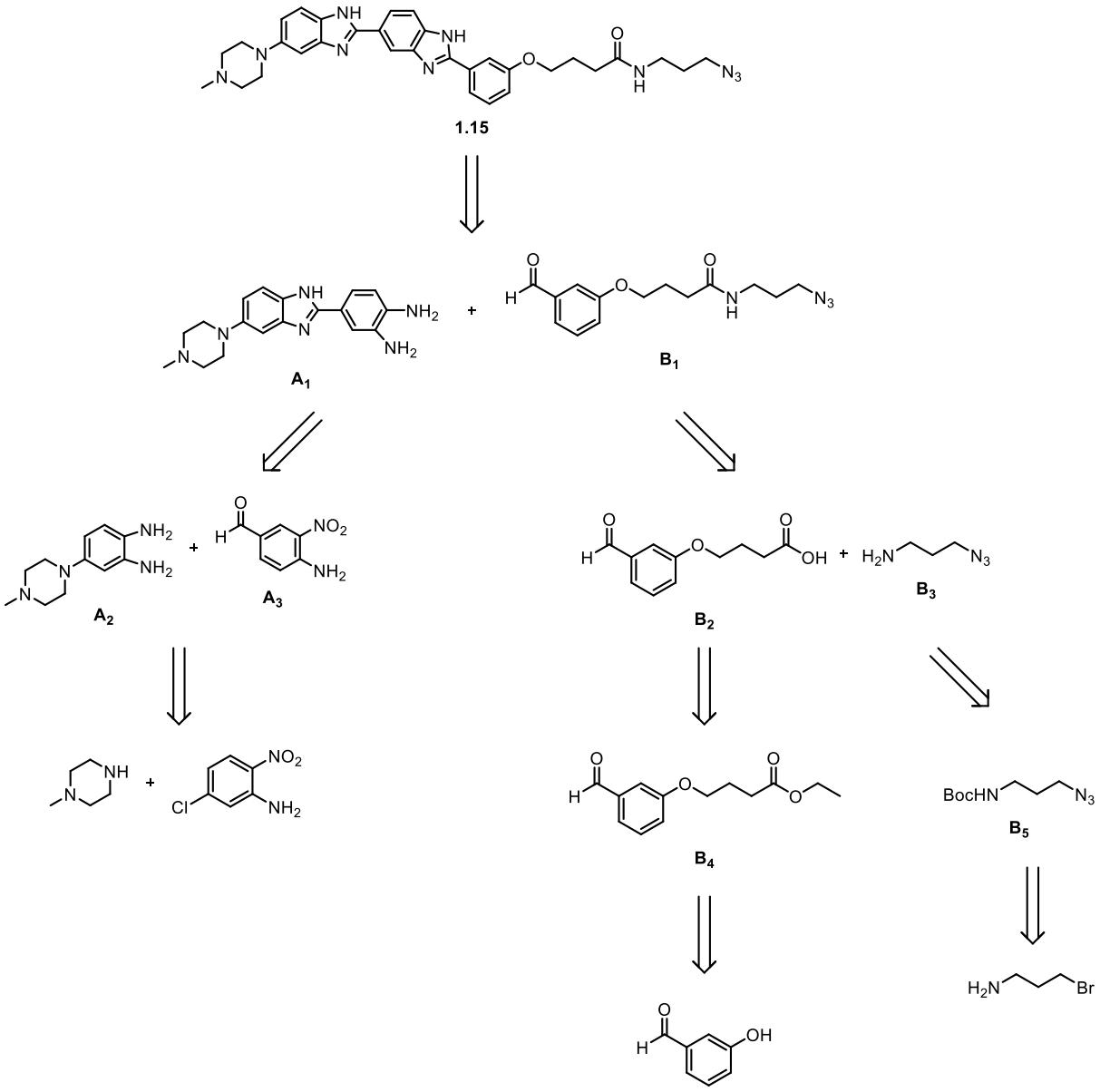

Scheme 2 *– Retrosynthetic approach for the synthesis of* ***1.15****.*

reached the retrosynthetic pathway shown in ***Scheme 2*** based on Disney and colleagues' work. This latter is based on two building blocks: $\mathbf{A_1}$ and $\mathbf{B_1}$. Both are combined through the second benzimidazole ring formation. Each of them is prepared from several other intermediates. Whereas $\mathbf{A_1}$ relies on the combination of $\mathbf{A_2}$ and $\mathbf{A_3}$ through a first benzimidazole motif formation, the $\mathbf{B_1}$ chemical structure has never been published. Its synthesis is based on a straightforward coupling between $\mathbf{B_2}$ and $\mathbf{B_3}$.

Our next idea was to use this very interesting retrosynthetic pathway to establish a robust and efficient pathway that would enable a straightforward production of new analogs. This led us to focus on the chemical conditions used to prepare **1.15**. In a first paper in 2011, Velagapudi *et al.* described the starting point for synthesizing bis-benzimidazole Hoechst derivatives, including **1.15**[255]. They used *o*-phenylenediamine building blocks coupled with the corresponding aldehyde using nitrobenzene at 140°C for 36 to 48h, depending on the substrates (***Scheme 3A***). Then, the desired lateral chain was coupled with the residual carboxylic acid using PyBOB coupling reagent. However, the quite harsh conditions of the benzimidazole forming step and the moderate yields obtained (around 50%) led us to evaluate other ways for our synthetic plan.

A literature review revealed that all synthetic procedures resulting in head-to-head bis-benzimidazole compounds rely on Hoechst derivatives synthesis. Therefore, we started looking at how such DNA stain derivatives are prepared. One of the first approaches for their synthesis is based on the condensation of *o*-phenylenediamines and imino-ethers. King *et al.* first highlighted this strategy in 1949[256], thus leading to several works published using this method. As a remarkable example, Argentini *et al.* proposed the synthesis of an *o*-carboranyl derivative of Hoechst 33258 (***Scheme 3B***)[257]. For synthesizing the first benzimidazole moiety, they condensed a diamine motif with a freshly prepared imino-ether derivative in the presence of acetic acid (AcOH) under reflux. They then tried to form the second heterocycle with the same procedure, with this time the imino-ether derivative being the phenyl bearing the lateral chain of the Hoechst derivative, but this condensation never worked. To solve the problem, they completely changed their synthetic plan. They went from a convergent synthesis to a linear one, starting "backward" from the phenyl group and building the bis-benzimidazole on it[257]. We looked at other published reactions to keep a convergent strategy for synthesizing some derivatives. We focused our attention on the aldehyde bisulfite adducts-based synthesis of benzimidazole. The formation of benzimidazole *via* aldehyde bisulfite adducts was first described by Ridley *et al*. to prepare some benzimidazoles and aza-analogs[258]. More recently, Eren *et al.* proposed a mechanism (***Scheme 3C***) for this coupling[259], starting from the nucleophilic attack of the amine onto the carbon atom of the aldehyde bisulfite adduct, leading to transition state 1 and the removal

of one water molecule. The remaining free amino group reacts with the alkyl sulfonate through transition state 2, losing a sodium bisulfite molecule. The newly formed dihydroimidazole intermediate undergoes aromatization, affording the formation of

the benzimidazole core[259]. This last step afforded the bis-benzimidazole molecules in yields ranging from 60 to 98%, depending on the structure of the aldehyde moiety. As a source of sodium bisulfite ions in solution for adduct formation, sodium metabisulfite ($Na_2S_2O_5$) is preferred instead of sodium bisulfite because it gives more sulfite ions upon solubilization. Several works led to synthesizing bis-benzimidazole Hoechst derivatives using $Na_2S_2O_5$[260-262]. More recently, Maji *et al.* reported the synthesis of a new bis-benzimidazole-carbazole derivative, mixing the two strategies mentioned above[263]. They first performed the first condensation between a small imino-ether building block and a diamine motif. Then, they used this first mono-benzimidazole intermediate and condensed it with another intermediate bearing an aldehyde function with the help of $Na_2S_2O_5$ in EtOH. They obtained a bis-benzimidazole derivative with a correct yield of 51%[263]. As a result, our primary goal was first to prepare **1.15** and some analogs; thus, we decided to adapt the synthetic pathway proposed by Maji *et al.* to end up with a convergent strategy that could be used for

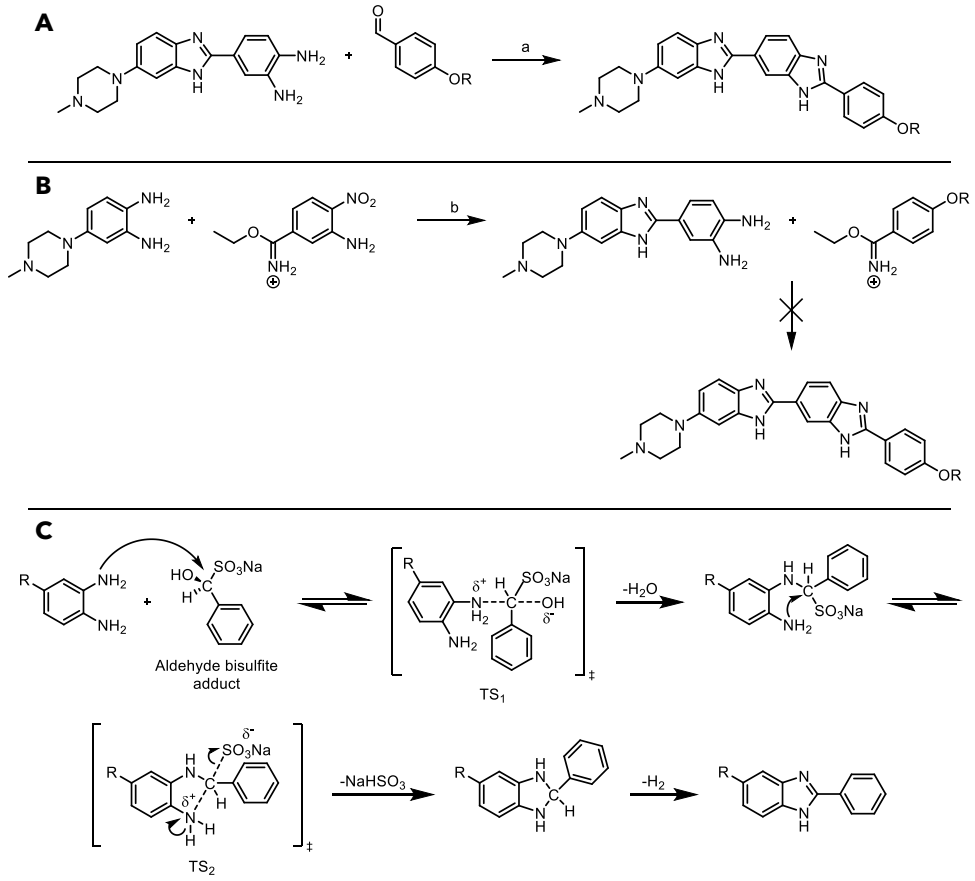

Scheme 3 *– Different synthetic approaches towards bis-benzimidazole derivatives. A) Synthesis described by Velagapudi et al. (a) Nitrobenzene, 140°C, 36 to 48h; b) Synthesis described by Argentini et al. (c) AcOH, reflux, 2h; D) Proposed mechanism for the synthesis of benzimidazole using $Na_2S_2O_5$.*

the rapid development of further analogs, only relying on one condensation step and not on a more extended linear synthesis.

II.2.2 Synthesis and functionalization of **1.15**

To afford **1.15**, we set up a successful strategy based on five straightforward steps. This convergent synthesis starts from 4 commercial compounds, as shown in the retrosynthetic scheme (***Scheme 4***): 1-methylpiperazine, 3-hydroxybenzaldehyde, 5-chloro-2-nitroaniline and ethyl 4-bromobutanoate. On one side, we synthesized the *o*–phenylenediamine intermediate (**A_1**) bearing the 1-methylpiperazine motif; parallelly, the phenyl intermediate (**B_1**) bearing the azide lateral chain was synthesized.

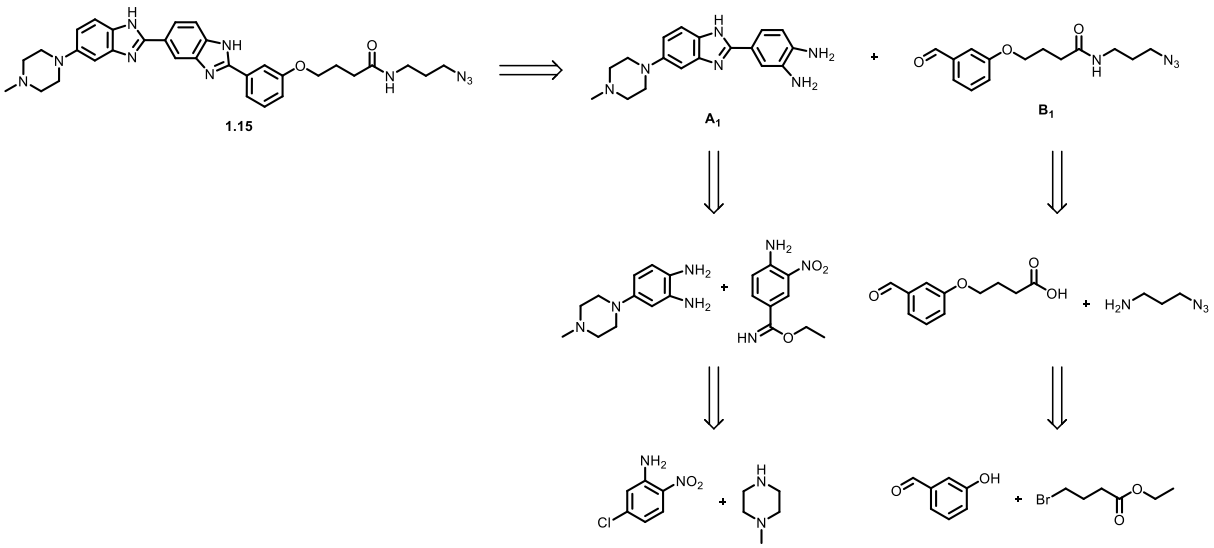

Scheme 4 – *Retrosynthetic scheme selected for **1.15** (TGP-210).*

Synthesis of building block 2.29 (B_1 intermediate)

The synthesis of the phenyl intermediate started with the protection of commercial 3-aminopropyl bromide with Boc_2O to reach compound **2.24**, which was further used without any purification. Then, NaN_3 was used to substitute the bromine with an azide group, leading to compound **2.25**, which was directly Boc-deprotected using a solution of MeOH and HCl. Finally, compound **2.26** was obtained with an overall yield of 73% over three steps (***Scheme 5A***). Parallelly, the alkylation of 3-hydroxybenzaldehyde using ethyl 4-bromobutanoate and potassium carbonate (K_2CO_3) resulted in compound **2.27** with a 93%

yield[255]. Saponification of the newly formed ester was then required, and the reaction was carried out following the Hall *et al.* patented procedure[264], using a 1M aqueous solution of NaOH and THF to allow the solubilization of the starting material. The corresponding acid (**2.28**) precipitate was collected with a 68% yield upon acidification. At this stage, compound **2.28** was coupled with the newly generated azide lateral chain (**2.26**) using the EDC- and HOSu-mediated coupling reaction to reach the desired aldehyde (**2.29**) with a 77% yield (***Scheme 5B***). To the best of our knowledge, this is the first fully detailed synthesis of aromatic aldehyde **2.29**. Given its easily modifiable lateral chain, this compound was required to prepare **1.15** and offers the potential for synthesizing further analogs.

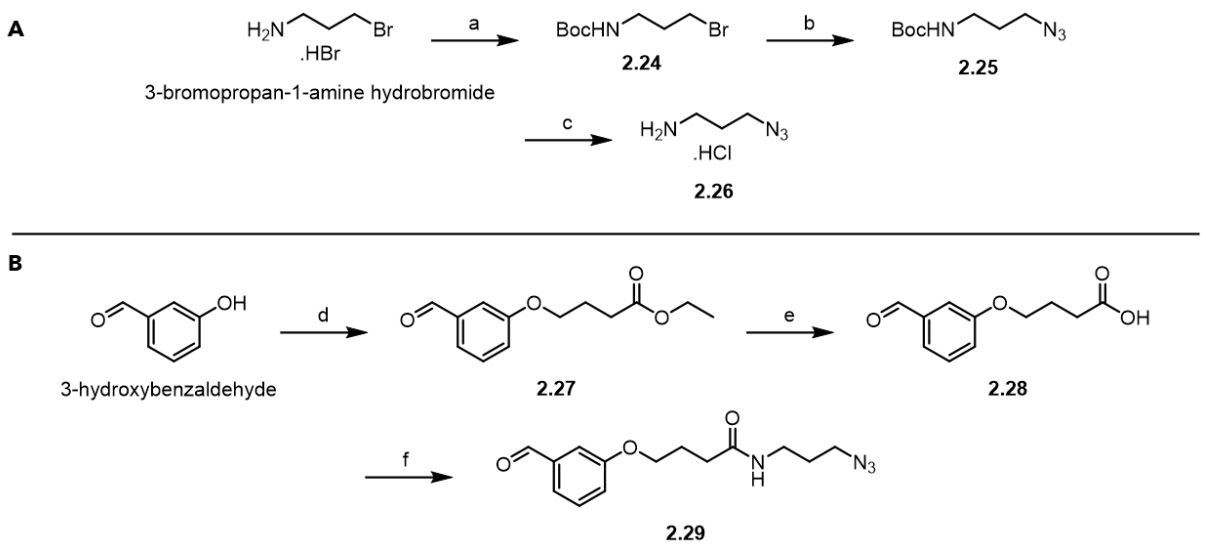

***Scheme 5**– Reagents, conditions and yields: A) (a) Boc_2O, Et_3N, DCM, rt, 12h; (b) NaN_3, H_2O-1,4-dioxane (1:1), 95°C to rt, 24h; (c) HCl (3M), MeOH, rt, 12h, 73% (over the 3 steps); B) (d) ethyl 4-bromobutanoate, K_2CO_3, DMF anh, 80°C, 12h, 93%; (e) NaOH (1M), THF, rt, 68%; (f) 3-azidopropan-1-amine hydrochloride (**2.34**), EDC, HOSu, Et_3N, DMF, rt, 12h, 77%.*

Synthesis of building block 2.35 (A_1 intermediate)

The synthesis continued with substituting 5-chloro-2-nitroaniline with 1-methylpiperazine using K_2CO_3 as the base and DMF as solvent (***Scheme 6B***)[265]. The resulting piperazinyl-2-nitroaniline (**2.32**), obtained with a 73% yield after 48h, was then catalytically hydrogenated with H_2 and palladium on activated charcoal (Pd/C). This step yielded compound **2.33** with 95% yield, affording the first intermediate suitable for forming the first benzimidazole moiety. In parallel, 4-amino-3-nitrobenzonitrile (**2.30**) was solubilized in dry ethanol, and HCl was bubbled through the mixture for 1h (***Scheme 6A***). Then, quite surprisingly, the reaction required 7 days of stirring at room temperature (rt), fully sealed, for completion. This reaction yielded the corresponding imino-ether

hydrochloride (**2.31**) with a 93% yield. The freshly obtained diamine (**2.33**) could now be condensed with the imino-ether intermediate (**2.31**). The reaction was performed using refluxing ethanol and glacial acetic acid in a 2:1 ratio as the solvent to afford the nitro amino benzimidazole derivative (**2.34**) with a yield of 84%[263,266]. After this step, compound **2.34** underwent another catalytic hydrogenation process, generating quantitatively the corresponding diamine (**2.35**). This intermediate was used for the next step without isolation due to the high instability of the two amino groups.

Lastly, the coupling between **2.35** and the previously synthesized aldehyde-containing intermediate (**2.29**) was accomplished using $Na_2S_2O_5$ in EtOH. The second benzimidazole ring formation led us to **1.15** (TGP-210), in 81% yield. Therefore, we built a synthetic approach for **1.15** in 5 steps (not counting the intermediate synthesis steps), with an overall 50% yield.

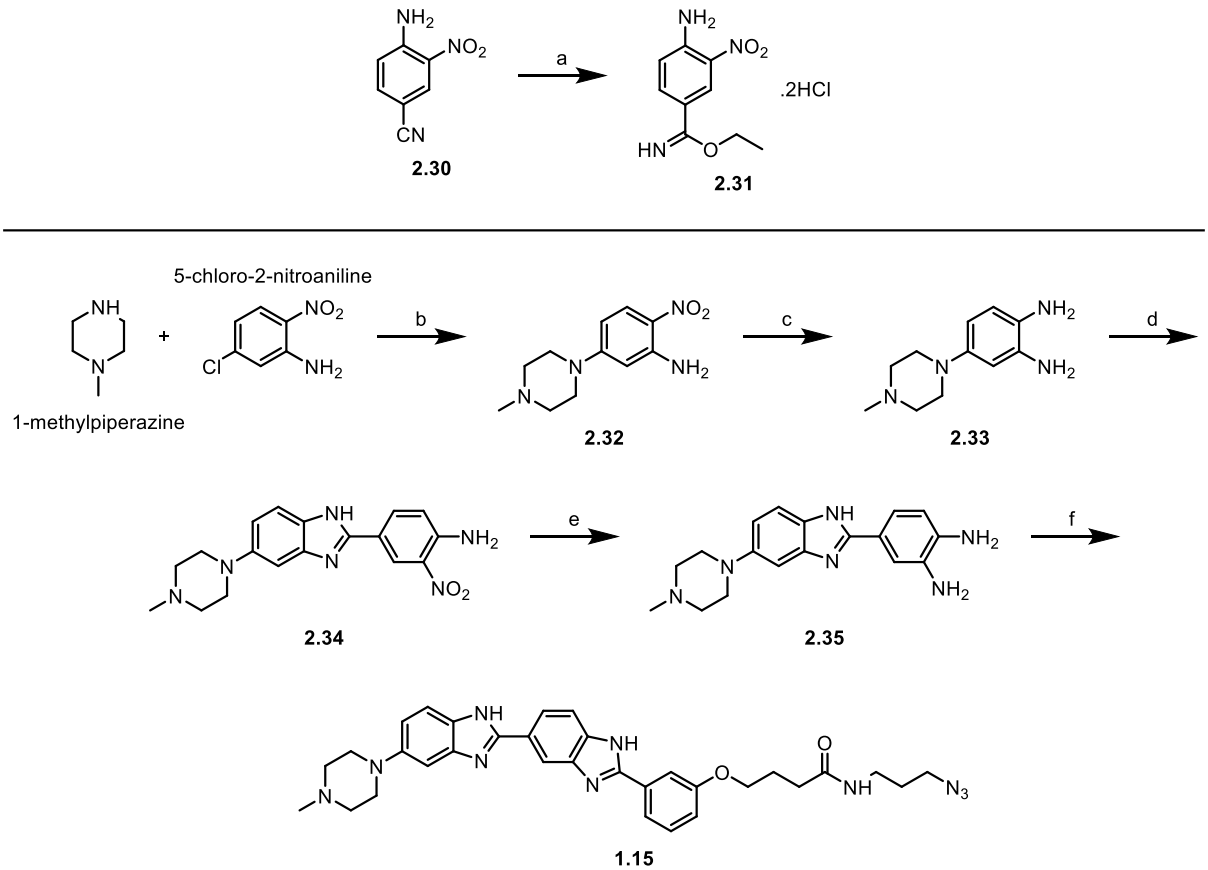

Scheme 6 *- Reagents, conditions, and yields: A) (a) $HCl_{(g)}$, EtOH, rt, 7d, 93%; B) (b) K_2CO_3, DMF anh, 120°C, 48h, 73%; (c) H_2, Pd/C, EtOH, rt, 4h, 95%; (d) Ethyl-4-amino-3-nitrobenzene carboximidate dihydrochloride (**2.31**), EtOH:AcOH (2:1), reflux, 24h, 90% ; (e) H_2, Pd/C, EtOH, rt, 12h, quantitative; (f) N-(3-azidopropyl)-4-(3-formylphenoxy)butanamide (**2.37**), $Na_2S_2O_5$, EtOH, 80 °C, 12 h, 81%.*

Synthesis of new 1.15 bis-benzimidazole analogs

Our synthetic strategy for synthesizing **1.15** allowed us to easily modify the lateral chain on the phenyl group once a sufficient stock of **2.35** was obtained. As mentioned in Section II.1.2, we first focused on different intermediates to be combined with **2.35** upon the formation of a second benzimidazole ring. Then, we envisaged changing the core structure of the bis-benzimidazole scaffold. Our synthetic plan was thus applied to the synthesis of a small set of analogs (***Scheme 7***) to have a clearer picture of the essential parts of the hit molecule (**1.15**) involved in binding and biological functions.

Firstly, the right-hand lateral chain was simplified to understand if the azide function was crucial for activity. Thus, compounds **2.17**, **2.18**, and **2.19** were synthesized using different lateral chain versions. In **2.17**, we removed it entirely using commercially available 3-hydroxybenzaldehyde to form the second benzimidazole motif with an 89% yield. Then, we prepared an analog of **1.15** under its ester form, thus adding an H-bond acceptor by combining **2.35** and **2.27**. This led to compound **2.18**, in 90% yield. Hence, **2.19** was synthesized, with a 90% yield, using commercial 3-fluoro-4-hydroxybenzaldehyde to understand if introducing fluorine in the compound could increase binding or inhibition activity. Afterward, **2.20** and **2.21** were synthesized after condensation of **2.35** with commercially available 1-naphtaldehyde and 4-quinolinecarboxaldehyde, with the idea of introducing two different aromatic moieties known to form π-stacking with RNA nucleobases. **2.20** was obtained quantitatively, while **2.21** was afforded with a moderate yield of 48%.

Parallelly, the decision was made to modify the core of the bis-benzimidazole scaffold. We first decided to reduce the number of benzimidazole moieties, affording **2.22**, the mono-benzimidazole version of **1.15**. This smaller version was obtained by directly condensing **2.29** with the diamine intermediate **2.33**. Then, an attempt was made to synthesize the tris-benzimidazole version by condensing the imino-ether intermediate **2.31** with the diamine **2.35**. This reaction led to **2.36** with a 99% yield. With this intermediate in our hands, we performed the catalytic hydrogenation of the nitro group with Pd/C and directly used the freshly obtained diamine intermediate for the condensation with **2.29**, using $Na_2S_2O_5$. Unfortunately, this third ring closure reaction did not work, probably due to a very high instability of the diamine intermediate. It must be noted that this reaction was attempted twice, and no further effort was put into synthesizing the tris-benzimidazole scaffold since we prioritized the first *in vitro* evaluation. Nevertheless, we decided to keep the intermediate **2.36** before hydrogenation as a new analog to be assessed for affinity towards pre-miR-210 too. Noteworthy, during the characterization of our new bis-

benzimidazole derivatives, we observed that some quaternary carbon signals in ^{13}C NMR spectra (see Material & Methods section) of the benzimidazole rings were not observable, probably due to tautomerism. Such observation has been previously noted by Boggu *et al.* in 2017[267].

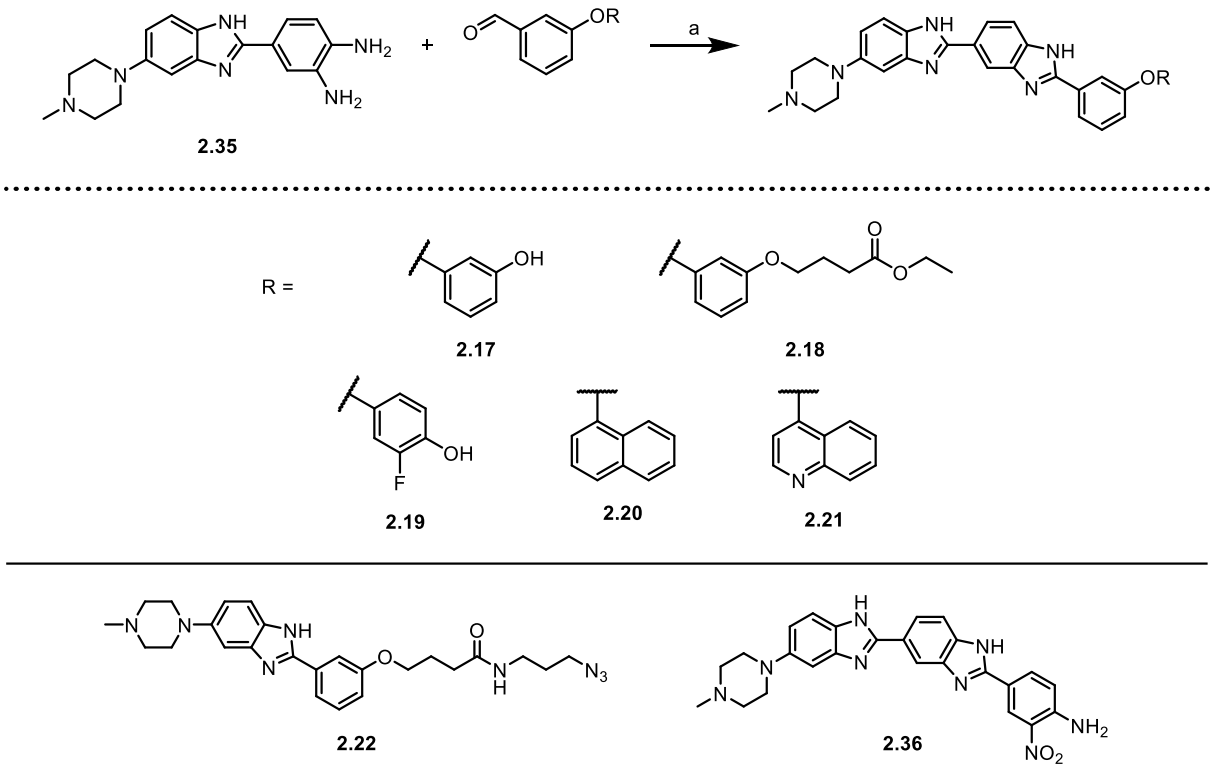

***Scheme 7**- Reagents and conditions: (a) Aldehyde, $Na_2S_2O_5$, EtOH, 80 °C, 12h. Yields: 89% (**2.17**), 90% (**2.18**), 90% (**2.19**), quantitative (**2.20**), 48% (**2.21**), 60% (**2.22**), 99% (**2.36**).*

II.2.2 *In vitro* characterization of the newly generated compounds

Upon synthesis of the molecules, *in vitro* biochemical evaluations were conducted on the target pre-miR-210 but also on other classical oncomiRs targets in the idea of a selectivity assay (e.g., pre-miR-21, pre-miR-148, and pre-miR-373). Each target pre-miRNA needed was modified with a fluorophore attached to its 5'-end and for specific experiments with a fluorescence quencher at its 3'-end.

Three fluorescence-based experiments have been developed in our laboratory to study the affinity, selectivity, and inhibitory activity of novel small molecules towards a pri- or pre-miR sequences (***Figure 26***). Here, we first used these assays to obtain the K_D values for each new compound and assess the binding affinity (***Figure 26A***). Indeed, the RNA's conformation changes upon ligand binding to the target, influencing its fluorescence

emission[268]. As a result, each RNA is exposed to increasing ligand concentrations, and the fluorescence variation is measured at the wavelength corresponding to the fluorophore. From the obtained values, linear regression yields a sigmoidal curve, allowing for the determination of the K_D values. Unless otherwise specified, all measurements are conducted in duplicate using automated methods. At least three independent experiments are performed to ensure repeatability and afford average K_D values and relative standard deviation.

To assess the selectivity of the best binders towards the target, *in vitro* competition assays were performed (***Figure 26B***). We determined K_D' and K_D'' values, representing the ligand's affinity in the presence of an excess (100 equivalents) of tRNA or DNA, respectively. These conditions simulate the cellular environment where the targeted RNAs are not predominant compared to other nucleic acids (such as DNA or tRNA). K_D values were compared to these new dissociation constants by measuring these ratios: K_D'/K_D and K_D''/K_D. The closer the value of these ratios is to 1, the better the corresponding compound's selectivity for the target RNA. Conversely, a ratio greater than 1 indicates the ligand's affinity for a nucleic acid other than the RNA under study.

Following a different fluorescence-based approach, the *in vitro* IC_{50} values were measured after these affinity assays. In this FRET-based assay (***Figure 26C***), the target pre-miRNAs are labeled at their 5'-end with the same fluorophore used for binding evaluation and at their 3'-end with a quencher (Eclipse Dark Quencher, EDQ). Both fluorophore and

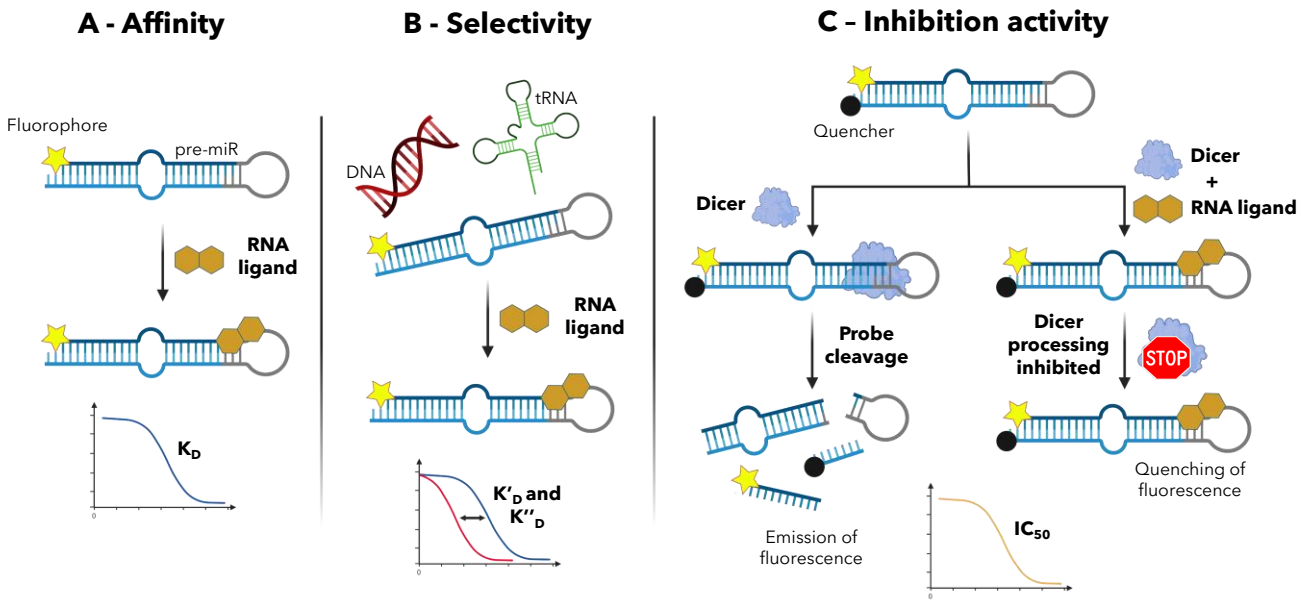

Figure 26 *– In-house fluorescence-based biochemical assays. A) affinity assay to determine the K_D binding constant; B) selectivity assay to assess the evolution of the K_D values in the presence of competitors (i.e., tRNA or DNA); C) FRET-based assay to establish an in vitro IC_{50} for each compound, thus revealing their inhibitory activity.*

quencher find themselves close together upon structuration, leading to fluorescence extinction. When treated with the Dicer enzyme, the RNA sequence is cleaved, and fluorescence emission increases since the fluorophore is no longer attached to the quencher. Whereas, if one of our ligands can bind the Dicer cleavage site of the target, the Dicer function is inhibited, and the sequence is no longer cleaved, leading to quenching of fluorescence. Consequently, target pre-miRNA is exposed to increasing ligand concentrations and fixed Dicer concentrations; then, fluorescence variation is measured at the wavelength corresponding to the fluorophore. From the obtained values, linear regression yields a sigmoidal curve, allowing for the determination of the IC_{50} values. IC_{50} represents the concentration where the binder inhibits half of the Dicer activity. This test allows us to identify, among the most affine ligands, the best inhibitors of Dicer-mediated miRNA biogenesis. It should be noted that the above-mentioned FRET test, used to assess the compounds' ability to inhibit pre-miRNA cleavage by Dicer, does not specify whether the tested molecules are RNA ligands or Dicer inhibitors. Therefore, it is essential to correlate inhibitory activity with dissociation constants to gain insight into the exact mechanism of action of the small molecules. Complementarily, studying the interaction site is also crucial, as even with similar K_D values, past observations have shown IC_{50} differences resulting from ligands interacting with sites that are more or less functional for Dicer cleavage.

As widely discussed in Chapter I, our target in this work was pre-miR-210, a very long RNA sequence composed of 110 nucleotides (see ***Figure 22B***). However, with modifications, such a long oligo is quite tricky to find commercially available since producers of RNA oligonucleotides tend to stop their synthesis offer to more or less 70 nt. In a first attempt to obtain the intact sequence, we decided to proceed with an in-house synthesis of the required RNA sequence *via* a ligation method using a specific enzyme (i.e., T4 ligase). We ordered the two required oligonucleotides (two 39-mer sequences detailed in the experimental part) that needed to be assembled, one with ATTO 647N fluorophore at 5′-position (Oligo A) and the other with a quencher (Black Hole Quencher, BHQ) at its 3′-end (Oligo B). Oligos A and B were ligated together upon the formation of a 3′ → 5′ phosphodiester bond between the 3′-OH and 5′-Phosphate groups of RNA molecules (see Material & Methods Section for detailed protocol). A first attempt was made by using previous conditions used by our group for this ligation reaction. In this protocol, the two oligos were first assembled in a microcentrifuge tube with T4 RNA ligase and RNAse inhibitors; then, the reaction was incubated at 37°C for 18h. The reaction outcome was observed following a denaturing polyacrylamide electrophoresis gel (***Figure 27A***). The reference strand (Oligo A) is observed on the left part of the gel (Lane 1); the other strand (Oligo B) has also been used in this gel (Lane 2), but as expected, no fluorescence is observed. On the right part of the same gel (Lane 3), the newly synthesized pre-miR-210 is

observed while quite a significant amount of starting oligo A is still present. As a result, an optimization process was needed to reach a more suitable experimental protocol. This optimization is highlighted in the second gel (***Figure 27B***). The result of several optimization steps is shown; we first tried to increase the duration of the reaction or to increase the amount of T4 ligase without any significant improvements. In the end, the introduction of a refolding step of the two oligos together (2 min at 90°C, 10 min at 4°C, and 25 min at 25°C) before adding the ligase and the inhibitors, and the increase of the incubation time, were the keys to the successful synthesis of the required RNA sequence with a proper yield. The folding steps were followed by the addition of the correct amount of T4 ligase and RNAse inhibitors, and then the reaction mixture was incubated for 48H at 37°C. The outcome of the optimized ligation reaction conditions is shown in Lane 3 *(**Figure 27B**)*, where we see an improvement in the conversion, with only remaining traces of Oligo A. Once finished, the reaction mixtures were purified by semi-preparative HPLC in Buffer B on a C8 column. Pure aliquots were lyophilized and solubilized again in a fixed volume of RNAse-free water. The RNA concentration was then determined by measuring absorbance at 260 nm on a spectrofluorometer. This protocol was applied to the preparation of the modified pre-miR-210 for affinity studies (5'ATTO-pre-miR-210) and the one for the inhibition FRET-based assays (5'ATTO-pre-miR-210-3'BHQ).

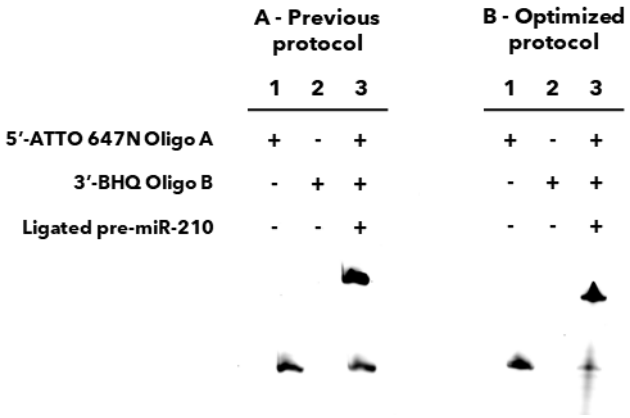

Figure 27 *– Denaturing polyacrylamide gel electrophoresis of two oligonucleotide ligation reactions. A) Ligation performed with our previous protocol. Lane 1 shows the reference Oligo A, Lane 2 shows the non-fluorescent Oligo B, and Lane 3 shows the ligated RNA sequence with some starting material left. B) Ligation performed with the newly optimized protocol. Lane 1 shows the reference Oligo A, Lane 2 shows the non-fluorescent Oligo B, and Lane 3 shows the ligated RNA sequence with only traces of starting material left.*

The first experiments for the determination of the affinity (measured as dissociation constants or K_D) and inhibition (quantified using IC_{50} values) were performed using the synthesized corresponding modified pre-miR-210 sequences. However, the first results were not satisfying since no fluorescence extinction was obtained in the FRET-based assays, and unusual curves were acquired in K_D experiment. In fact, at a high compound

concentration where normal DICER function should be inhibited, no absence of fluorescence was observed, which led us to the conclusion that another source of fluorescence was present in the mixture. We first performed a different affinity assay where an equimolar solution of ATTO-647 fluorophore replaced the pre-miR sequence. This first assessment allowed us to understand if any compound could bind to the fluorophore instead of the target RNA. Herein, no binding was observed with the fluorophore. We consequently decided to evaluate the synthesized compounds' absorption and fluorescence to understand if any conflict could come from an intrinsically fluorescent compound. To do so, a simple assay on a 96-well plate using a spectrofluorometer was performed; the compounds were solubilized in buffer A (see Material & Methods for specification) at 1 mM concentration, in a total volume of 100 µL. In the first assay, the absorption spectrum to obtain the maximum lambda (nm) for each compound was assessed, referring to the point where the absorbance is maximum. This gave us a first clue about the presence or not of possible conflict with several fluorophores; for instance, if we look at the spectrum of a widely used fluorophore called ATTO 647N, there is a peak at 647 nm. This value is the classical wavelength that needs to be used for ATTO 647N to exhibit its maximum fluorescence; therefore, if a compound shows the same or similar absorbance maximum, a modification of the fluorophore is probably mandatory. A second assay, more

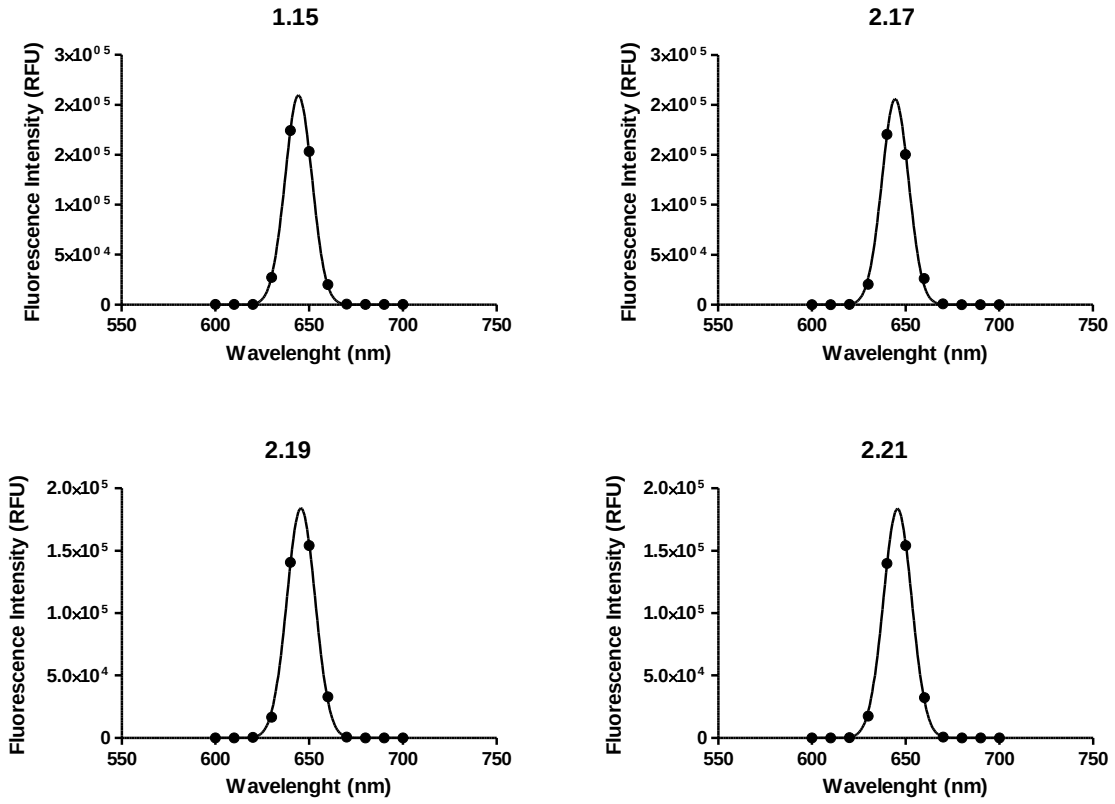

Figure 28 *– Fluorescence spectra of compounds* ***1.15***, ***2.17***, ***2.19***, *and* ***2.21*** *after light-excitation at 647 nm. The data are shown in relative fluorescence units (RFU) compared to non-fluorescent reaction buffer.*

accurate, for confirming the presence of any conflict was used. Here, the compounds were exposed to the same light excitation as the fluorophore. We excited all the compounds at 647 nm, most of which showed a fluorescent pattern for this wavelength. Examples of these excitation spectra can be found in ***Figure 28***, confirming the impossibility of using the ATTO 6647N fluorophore to evaluate the inhibition activity of this series of compounds since the four compounds emit when excited at the same wavelength as the fluorophore.

After seeing these results, the decision was made to switch to fluorescein as fluorophore (FAM), and this time, we were lucky to find a supplier able to synthesize such a long pre-miR sequence both in its 5' only modification or its FRET version with a quencher (i.e., Eclipse® Dark Quencher). The results presented hereafter were collected using these two commercial pre-miR-210 sequences. Considering the above introduction to the *in vitro* assays developed in our laboratory, we measured the dissociation constants of compounds **2.17** to **2.23** towards pre-miR-210 and other RNA (pre-miR-21, pre-miR-148, and A-site RNA) to have a first idea of the selectivity of these analogs. The K_D values obtained are compiled in ***Table 1*** and compared to those of the starting scaffold (i.e., targapremiR-210 or **1.15**). All compounds exhibit dissociation constants in the low micromolar range, from 0.45 to 5.91 µM.

Compound **1.15** bears one of the best dissociation constants, with a K_D of 0.54 µM, thus serving as a reliable reference for subsequent analog evaluations. In a previous study, Disney *et al.* reported a K_D value similar to ours, 0.66 µM, for the targapremiR-210 with *in vitro* transcribed pre-miR-210 [102]; variations in K_D values might be attributed to the different buffers employed in the respective assays.

Compounds	K_D (µM) - pre-miR-210	K_D (µM) - pre-miR-21	K_D (µM) - pre-miR-148
1.15	0.54 ± 0.02	1.72 ± 1.26	1.04*
2.17	2.30 ± 0.68	4.38 ± 3.11	3.15*
2.18	0.45 ± 0.01	0.71 ± 0.16	1.33*
2.19	1.13 ± 0.35	3.93 ± 2.74	1.46*
2.20	0.52 ± 0.12	1.20 ± 0.72	0.61*
2.21	0.56 ± 0.19	0.71 ± 0.17	Not Tested
2.22	5.91 ± 1.08	0.60 ± 0.25	1.83*
2.36	1.62 ± 0.25	4.61 ± 5.55	0.21*

Table 6 *– K_D values of **1.15** and analogs towards various pre-miR sequences. * Tested only once; error bar considered ± 10%.*

Three analogs showed K_D values similar to those of **1.15**, compounds **2.18**, **2.20**, and **2.21**. The elimination of the azide lateral chain resulted in compound **2.18**, which exhibited a slightly enhanced affinity (0.45 µM), suggesting the non-essential role of the azide function for binding. However, its utility in biotin-click chemistry experiments is acknowledged. Compound **2.17**, lacking the lateral chain, displayed reduced affinity (2.30 µM), highlighting the importance of the chain's initial segment. Hence, introducing fluorine to the phenyl group yielded compound **2.19**, which led to a 2-fold reduction in affinity (1.13 µM). Subsequent modifications involved replacing the phenyl group with two bigger aromatic moieties, naphthalene, and quinoline, resulting in compounds **2.20** and **2.21**, maintaining comparable affinity to **1.15** with K_D values of 0.52 and 0.56 µM, respectively. Altering the core structure, like in **2.22**, exhibited a significant reduction in affinity (K_D of 5.91 µM), likely due to decreased RNA interactions. Hence, compound **2.36**, a reaction intermediate, displayed a K_D of 1.62 µM.

These first affinity results led us to a preliminary conclusion that it is possible to modify the right part of the hit molecule **1.15** and that the affinity for the target relies on the methyl-piperazine bis-benzimidazole motif. This observation was confirmed by the K_D value of **2.22**, which showed a 10-fold decrease in affinity for pre-miR-210. Hence, introducing hydrophobic motifs seemed to favor the interaction with the target. Indeed, compounds **2.18**, **2.20**, and **2.21** showed good affinity, while **2.17**, **2.19**, and **2.36** obtained higher K_D values.

Regarding selectivity, all compounds show no selectivity toward pre-miR-210 compared to other pre-miR sequences. Compound **1.15**, for instance, displayed a reduced affinity for two other pre-miRNAs. For other miR precursors, the most affine compound for pre-miR-210, **2.18**, exhibited a diminished affinity for pre-miR-148 but maintained a comparable affinity for pre-miR-21 (K_D = 0.71 µM). Conversely, despite structural similarities, compounds **2.20** and **2.21** displayed divergent binding patterns for pre-miR-21, with **2.20** showing a decrease in affinity and vice-versa for **2.21**. Interestingly, intermediate **2.36** showed a low nanomolar K_D for pre-miR-148 (210 nM), suggesting potential for further exploration with this pre-miRNA.

Overall, all the compounds are suitable RNA binders with excellent K_D values toward a selection of RNA sequences. These results outlined the absence of selectivity for pre-miR-210 for all the derivatives, including **1.15**[102]. Such observation differs from previously published results from Disney and colleagues, who showed an *in cellulo* specificity of targapremiR-210 (**1.15**) for the pre-miR-210 sequence. However, the *in vitro* conditions we used to assess compounds' selectivity are particularly strict, while in cells, the levels of expression of miRNAs differ and contribute to the selectivity of the compounds, as shown

by the previously reported results about **1.15**. For our new analogs, the selectivity studies seemed to show that the methyl-piperazine benzimidazole aromatic group sequence is sufficient to induce a good affinity for RNA sequences. However, **2.22** results also indicate that the bis-benzimidazole motif is not strictly necessary. Indeed, the specificity for one pre-miR sequence might not be crucial since a small pool of miR is overexpressed in specific cancer cells, and the overexpression of such miRs could induce a number specificity rather than being linked to affinity. However, the newly generated compounds must have good selectivity in the presence of other nucleic acid sequences present in high amounts in a cellular context. Parallelly, the same K_D assay was repeated in the presence of the target pre-miR-210 and an excess of tRNA (measurement of K'_D) or DNA (measurement of K''_D). The results are shown in ***Table 7*** and are reported as a ratio between K'_D over K_D and K''_D over K_D. A result below or equal to 1 shows selectivity for pre-miR-210, whereas a result over 1 shows a loss of selectivity linked to the presence of the two nucleic acids competitors. The results show a clear selectivity for the target of compounds **1.15**, **2.17**, **2.18**, **2.19**, and **2.20** in the presence of tRNA. On the other hand, compound **2.18** shows a slight loss of selectivity in the presence of DNA. Compounds **2.20** and **2.21**, as expected, lose their affinity towards pre-miR-210 in the presence of an excess of DNA due to the introduction of bigger heteroaromatic moieties in their structures. Such chemical modification probably leads to DNA intercalation, the cause for this loss of affinity. However, the only difference between **2.20** and **2.21**, which is a nitrogen atom, resulted in the complete loss of selectivity for **2.20** since the two ratios are well above 1. The ratios of compound **2.17**, compared to **1.15** and **2.18**, did not confirm the importance of the lateral chain for selectivity. Hence, the reaction intermediate **2.36** kept the selectivity for pre-miR-210 in the presence of tRNA and lost it towards DNA.

Compounds	K_D (µM) - pre-miR-210	K'_D / K_D	K''_D / K_D
1.15	0.54 ± 0.02	0.7	1.7
2.17	2.30 ± 0.68	0.4	0.9
2.18	0.45 ± 0.01	1	3
2.19	1.13 ± 0.35	0.8	1.4
2.20	0.52 ± 0.12	2	2.4
2.21	0.56 ± 0.19	0.8	2.3
2.22	5.91 ± 1.08	Not Tested	Not Tested
2.36	1.62 ± 0.25	1.1	2.1

Table 7 *- K_D ratios in the presence of an excess of tRNA and DNA for **1.15** and analogs.*

After these binding assays, the analogs underwent FRET-based inhibition assay evaluations. The resulting IC_{50} values are compiled in ***Table 8***. All the compounds showed IC_{50} values in the same range, going from 1.71 to 11.6 μM, except for **2.22**, which showed no inhibition activity. Reference compound **1.15** displayed an IC_{50} value of 2.91 μM. Notably, compound **2.18**, which demonstrated the highest affinity, also exhibited excellent Dicer-cleavage inhibition with an IC_{50} of 1.70 μM. This shows the correlation between RNA binding ability and inhibition activity, positioning **2.18** as a notable derivative of **1.15** for subsequent investigations. While compounds **2.20** and **2.21** emerged as potential derivatives in terms of affinity, their binding sites appear somewhat distanced from the Dicer-cleavage site, as indicated by their respective IC_{50} values of 6.37 and 6.39 μM. The significance of the phenyl-lateral chain motif was confirmed, given that **2.17** registered a high micromolar IC_{50} of 8.68 μM. Incorporating fluorine (compound **2.19**) into the structure resulted in a compound with moderate inhibition, reflected by an IC_{50} of 8.53 μM. Mono-benzimidazole **2.22** displayed no inhibitory activity at the highest concentration tested (10 μM), and **2.36** obtained a moderately elevated IC_{50} of 4.51 μM.

Compounds	K_D (μM)	IC_{50} (μM)
1.15	0.54 ± 0.02	2.91 ± 0.48
2.17	2.30 ± 0.68	8.68 ± 2.92
2.18	0.45 ± 0.01	1.70 ± 0.20
2.19	1.13 ± 0.35	8.53 ± 1.07
2.20	0.52 ± 0.12	6.37 ± 0.48
2.21	0.56 ± 0.19	6.39 ± 0.49
2.22	5.91 ± 1.08	No inhibition
2.36	1.62 ± 0.25	4.51 ± 0.56

Table 8 *– K_D and IC_{50} values of **1.15** and analogs towards pre-miR-210.*

The good results obtained in these inhibition assays indicate that the bis-benzimidazole motif is required to properly position the ligands in Dicer-processing sites. The IC_{50} values correlate with the previously obtained K_D values, with compounds **1.15** and **2.18** to **2.21** showing good affinity and inhibition activity. On the other hand, **2.17** and **2.22,** which showed lower affinity, obtained very low or no inhibition activity toward pre-miR-210.

In conclusion, a small set of analogs of the previously reported ligand **1.15** was synthesized and assessed *in vitro* for their affinity and inhibitory activity toward the target

pre-miR-210. Compound **1.15**, with a K_D of 0.54 µM for pre-miR-210, served as a benchmark. The collected data revealed that structural alterations of the lateral chain did not deeply impact the affinity for pre-miR-210. However, the removal of the azide lateral chain, as in compound **2.18**, slightly enhanced affinity, while the complete removal of the lateral chain, as in **2.17**, led to a significant loss (6-fold) of affinity. Similarly, introducing fluorine (**2.19**) while removing the lateral chain led to a lower binding affinity. Hence, replacing the phenyl group with more extensive aromatic moieties in compounds **2.20** and **2.21** resulted in comparable affinities to **1.15**. However, core modifications (removal of one benzimidazole moiety), as seen in **2.22**, reduced affinity by a factor of 10. Selectivity assays with other pre-miRs indicated a consistent trend for most analogs, with an increased affinity for the A-site ribosomal RNA. The exception was compound **2.17**. Furthermore, when exposed to nucleic acid competitors (tRNA or DNA), compounds **2.20** and **2.21** showed the most significant loss of selectivity for the target. Regarding Dicer-cleavage inhibition, the results from the assays showed a perfect correlation between binding affinity and inhibition, with the most affine compounds exhibiting enhanced inhibitory activity. However, for compounds **2.20** and **2.21**, we can conclude that their binding site is not perfectly fit to the Dicer-cleavage site since they obtained higher IC_{50}s.

Compound **2.18** emerged as the most promising candidate, with the best balance between affinity and inhibitory activity, with a K_D of 0.45 µM and an IC_{50} of 1.70 µM. Overall, these preliminary *in vitro* assays allowed us to draw first conclusions on possible modifications of the hit molecule (**1.15**). The azide lateral chain is clearly not essential for the affinity and inhibition of miR-210 since the binding relies on the methyl-piperazine benzimidazole motif, leaving the phenyl part open for diversification. The introduction of apolar motifs seemed to increase affinity while using more polar functions decreased the K_D values. Lastly, the reduction of the length of the molecule appeared not to be a good idea, with compound **2.22** losing affinity and having no inhibitory activity at all. These findings emphasize the relationship between molecular structure, binding affinity, and inhibitory activity while giving us the first clues on how the hit molecule can be modified to generate lead ones. Nevertheless, to gain a deeper understanding of these analogs' potential, *in cellulo* assays were required to better understand their toxicity pattern towards several cancer cell lines.

II.2.3 Preliminary *in cellulo* evaluation

In vitro experiments offer a controlled environment, enabling precise manipulation of variables such as target abundance and salt concentrations while facilitating the study of compound specificity against quantified off-targets. However, transitioning to biologically relevant conditions, including *in vivo* settings, introduces complexities due to the high number of interacting variables. While cell culture experiments are not classified as *in vivo*, they can be seen as a bridge, offering insights into the potential behavior of small molecules within a biological environment. A crucial aspect of these studies is determining the toxicity threshold. Before assessing the biological impact of a compound on cellular processes, it is imperative to delineate the maximum concentration that cells can tolerate without significant cytotoxic repercussions.

All the assays used in this project are based on staining techniques highlighting specific cellular features. These techniques relied on light-based detection, either through fluorescence microscopy or plate reader measurements, to evaluate the level of luminescence or fluorescence emitted from the cells. CyQUANT Cell Proliferation Assay kit (Invitrogen, Life Technologies) was used to quantify the number of viable cells after treatment; this kit contains a dye that stains the nucleus of live cells. The cell lines chosen for this investigation were MDA-MB-231, BT474, and U2OS. The first cancer line is a highly aggressive, invasive, and poorly differentiated triple-negative breast cancer (TNBC) cell line as it lacks estrogen receptor (ER) and progesterone receptor (PR) expression, as well as HER2 (human epidermal growth factor receptor 2) amplification[269]. We also decided to use this cell line as a comparison with Disney's work on TargapremiR-210 to understand if our compound **1.15** could be used as a positive control. Nonetheless, we also used two other cancer cell lines, the breast cancer cell line BT474 and an osteosarcoma tumor cell line called U2OS. These cells were exposed to varying concentrations of our compounds under controlled conditions. The following sections detail the methodology and results of these assays.

As detailed in Chapter I, our focus was directed towards oncomiR-210, a microRNA known for its overexpression under hypoxic conditions. With these cellular assays, we aimed to assess the cytotoxicity of our compounds towards MDA-MB-231 cells. This cell line is known to overexpress miR-210 under hypoxic conditions, as widely mentioned in Section I.2 (Chapter I). However, we also used BT474 and U2OS cell lines for comparison. Our primary objective was to identify the toxicity of our compounds for further evaluation; ideally, our new analogs should show a toxicity profile under hypoxic conditions (high levels of miR-210) and no toxicity in normoxia. It is worth noting that miR-210 is also expressed in

tiny amounts in normal oxygen conditions; thus, toxicity in these conditions might result from possible activity correlated with this small quantity of miR-210 or an off-target effect. Nevertheless, an alternative approach to mimic hypoxic conditions was necessary due to several constraints in accessing a dedicated hypoxia chamber. A standard method in the scientific community involves the chemical induction of hypoxia using cobalt chloride ($CoCl_2$). This compound inhibits hypoxia-inducible factors (HIFs) degradation even in normoxic conditions [270,271]. As explained in Chapter I, stabilizing these transcription factors is crucial in activating the transcription of genes associated with hypoxic responses. An extensive review of the literature, particularly studies employing analogous cell lines, led us to use $CoCl_2$ at a concentration of 200 µM in the cell culture media. It is worth noting that $CoCl_2$ is non-toxic at this concentration, with potential cytotoxic effects only emerging at significantly elevated concentrations, typically exceeding 500 µM.

Building on this, we moved on with the first experiments of cytotoxicity. We treated the three cancer cell lines mentioned above with 10 µM of each compound for 72H. Both normoxic and chemically mimicked hypoxic conditions were considered. The cell viability results are shown in ***Figure 29***, only for the compounds that showed some activity below or around 10 µM. We decided to keep this concentration as a threshold for considering promising compounds for in-depth studies. A closer look at compound **1.15** reveals its negligible anti-proliferative effect on the U2OS cell line. However, a modest decline in cell survival was observed in BT474 and MDA-MB-231 cells, with pronounced activity under normoxic conditions. Contrarily, compound **2.18**, despite its promising *in vitro* performance, exhibited no significant activity in the breast cancer cell lines (not tested towards U2OS cells), independently from the oxygen conditions. Among all synthesized compounds, only **2.20** and **2.21** inhibited the proliferation of all the different types of cancer cells, probably related to their DNA intercalation off-target effect. If we focus on the difference in activity compared to hypoxia or normoxia, we can see that in MDA-MB-231 cells, both compounds are slightly more active in normoxia, whereas they have a different inhibition pattern in the other two cell lines. **2.20** exhibits a higher anti-proliferative activity under hypoxic conditions in U2OS cells. For technical reasons, it was not tested in hypoxia in BT474 cells, where it still has a strong activity in normal conditions. Hence, **2.21**, used against U2OS cells, kills almost all of them after 72H under normoxia, and this inhibition is slightly decreased in hypoxic conditions. Against BT474 cells, **2.21** has a reversed pattern of inhibition than on U2OS cells; it has a strong activity in normal conditions and a complete anti-proliferative activity under hypoxia. Their activity varied between normoxic and hypoxic conditions, suggesting a nuanced mechanism of action that is probably unrelated to a miRNA that plays a role only under hypoxic conditions. If we focus on compound **2.17**, which lacks the lateral chain on the phenyl group, it has a very slight

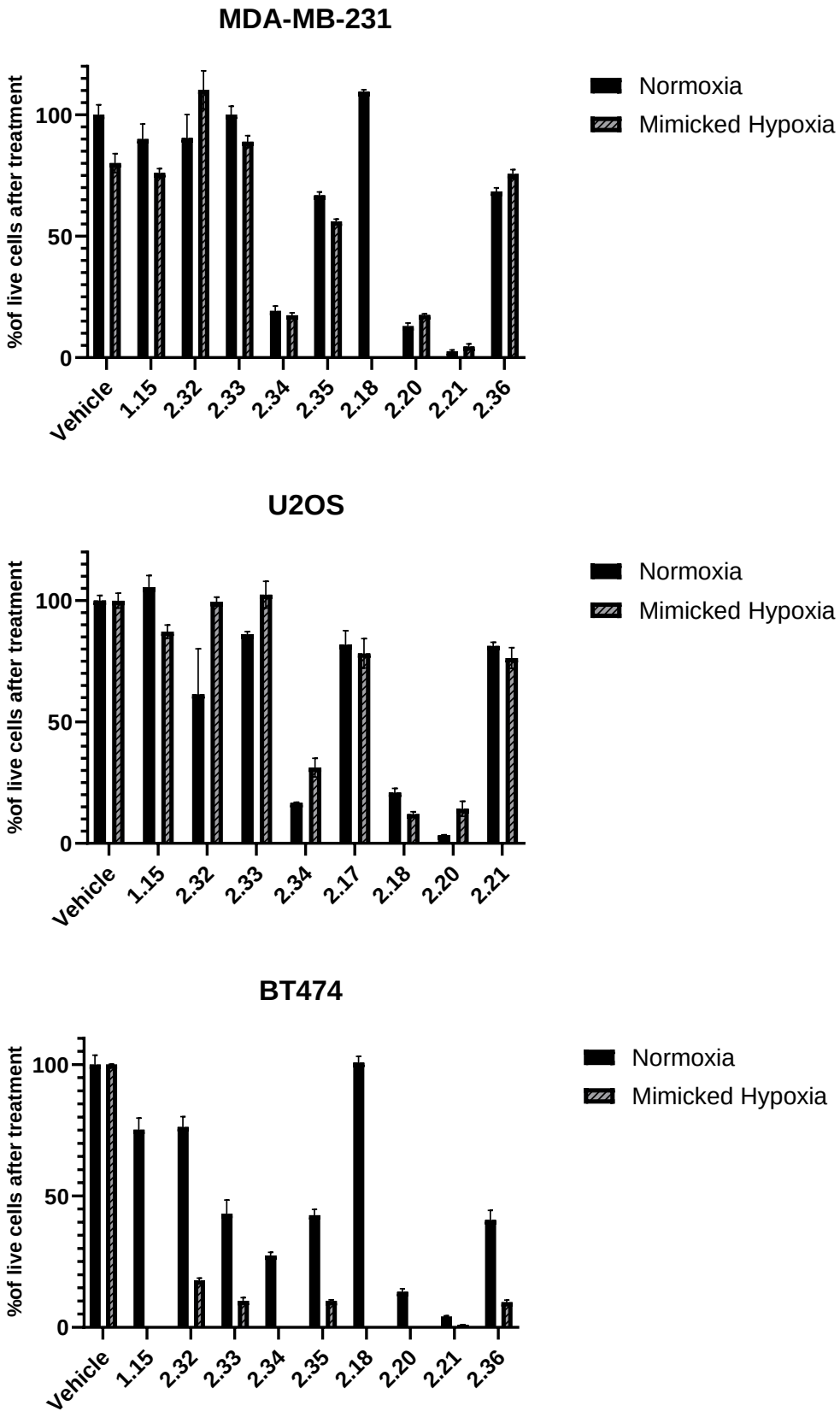

Figure 29 *– Toxicity of* ***1.15*** *and analogs towards different cancer cell lines. MDA-MB-231, U2OS, and BT474 cells were treated for 72h with DMSO (vehicle) or 10 µM of compound. Percentage of live cells after treatment has been determined with CyQUANT proliferation assay. Data are reported as mean ± SEM, n≥3.*

activity on U2OS cells, with 85% of living cells after 72H. Instead, in MDA-MB-231 cells, the anti-proliferative activity reaches 65% of living cells after 72H. No significative differences were observed under hypoxia on those two cell lines. In BT474 cells, **2.17** leaves only 45% of living cells after 72H under normoxia and only 10% under normoxia, highlighting a very interesting inhibition pattern for this compound.

Subsequently, we decided to explore the potential of reaction intermediates **2.32**, **2.33**, **2.34**, and **2.36**, all coming from the synthesis of the bis-benzimidazole scaffold. The rationale behind this was to ascertain if larger compounds, upon metabolism within cells, yielded these intermediates, which might then be the actual active agents. For the ones containing a nitro group (**2.32**, **2.33**, and **2.36**), we expected high toxicity triggered by this motif, which is known to be a toxicophore[272]. **2.34** shows a high proliferation inhibition activity towards the three cell lines. Under hypoxic conditions, it has the same activity in MDA-MB-231 cells but loses 2-fold of activity in U2OS. The small compound **2.32** showed only interesting toxicity towards U2OS cells under normal conditions, with only 50% of living cells after 72H, and a high anti-proliferative activity under hypoxia towards BT474 cells. For the reaction intermediate that should have led to the tris-benzimidazole compound, **2.36**, a reduction by half of the population of living cells is observed in BT474 cells under normal conditions, and this number goes down to 10% under normoxic conditions. Hence, **2.33,** the hydrogenation product of **2.32**, showed the same pattern of **2.36** towards BT474 cells with moderate activity in normal oxygen conditions and a very interesting one in hypoxic conditions. Nothing significant was observed in the two other cell lines. These are preliminary results to understand whether or not the compounds have an anti-proliferative activity towards different cancer cell lines. Noteworthy, the objective isn't merely to identify the most cytotoxic compound. A compound with excessive cytotoxicity could potentially lead to adverse side effects, and without other experiments, we cannot link this activity with the biological pathway of interest (i.e., miR-210).

Under hypoxic conditions, an *in cellulo* IC_{50} assay was performed in the different cell lines for the most interesting compounds. The results are compiled in ***Table 9***. Synthetic compounds tend to have better activity *in vitro* due to the lack of cellular constraints; however, if we look at compounds such as **2.20** and **2.21** that have *in vitro* IC_{50} values around 6 µM, this value goes down to approximately 2 µM *in cellulo*. These results highlight the potential off-targeting role of those compounds. Nevertheless, the best *in vitro* candidate, **2.18**, shows no significant toxicity on MDA-MB-231 cells below 10 µM. A result that needs to be kept in mind for further evaluation of the potential effect of the analog on the targeted biological pathway.

Compounds	IC_{50} (µM) – *In vitro*	IC_{50} (µM) – MDA-MB-231 cells	IC_{50} (µM) – BT474 cells
1.15	2.91 ± 0.48	0.94	Not measured
2.17	8.68 ± 2.92	2.69	Not measured
2.18	1.70 ± 0.20	> 10*	Not measured
2.20	6.37 ± 0.48	1.56	4.13
2.21	6.39 ± 0.49	1.63	2.55
2.22	No inhibition	> 10*	Not measured
2.36	4.51 ± 0.56	1.14	Not measured

***Table 9** – IC_{50} values of **1.15** and analogs in vitro and in cellulo. *Compounds showed no significant activity at the maximum dose tested (10 µM).*

In the last cytotoxicity assay, we focused on the potential impact of the synthesized compounds on healthy cells, referred to as primary mammary epithelial cells (hMEC). The results of this evaluation are illustrated in ***Figure 30A***. Regrettably, several compounds that previously demonstrated promising results, such as **2.15**, **2.18**, **2.20**, and **2.21**, exhibited pronounced toxicity towards these healthy cells. Post 72-hour treatment, the viability of these cells decreased, with remaining live cell percentages ranging from 40% to a mere 15%. Hence, the reference compound **1.15** shows a reduction of 2-fold of the percentage of living cells after 72H, considered moderate toxicity. **2.17** and **2.36** show the same toxicity pattern as compound **1.15**. **2.32** and **2.33** obtained the best score by only reducing the population of healthy cells by 5% after 72H.

After these cytotoxicity assays, we started to evaluate more in-depth biological activity of some compounds, aiming to discover any potential association with the targeted pathway. The first biological tool we used was the western blot analysis of HIF-1α levels, the transcription factor involved in the hypoxic response. Such molecular biology technique is based on separating proteins after having extracted them from cell culture and then can highlight the variation of protein levels. Given the established overexpression of HIF-1α under hypoxic conditions, our dual objectives were to validate this upregulation under $CoCl_2$-induced hypoxia and to employ **1.15** as a positive control, given its published role as a hypoxic response inhibitor. **1.15** was tested at a single concentration to see if it could reverse an eventual HIF-1α overexpression. ***Figure 30B*** distinctly highlights the upregulation of HIF-1α levels after 24h of $CoCl_2$ (300 µM) treatment in MDA-MB-231 cells.

Subsequent treatments with 10 μM of **1.15**, in the absence of $CoCl_2$, yielded no significant change in HIF-1α levels, aligned with expectations. However, with a co-treatment of $CoCl_2$ and **1.15,** a significative downregulation of HIF-1α levels. These findings collectively suggest that $CoCl_2$ correctly mimics hypoxic conditions in MDA-MD-231 cells and that **1.15** can reverse the cell response to hypoxia by downregulating HIF-1α levels.

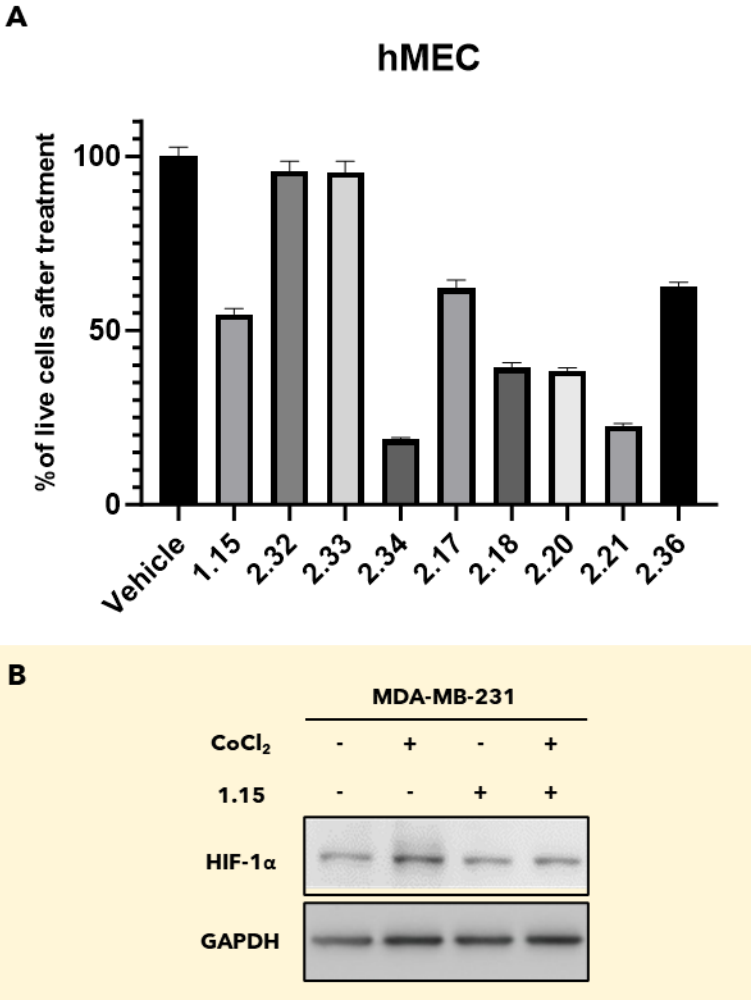

Figure 30 *– A) Effects of the different analogs and reaction intermediate (10 μM, 72H) on the proliferation of hMEC cells. Data are reported as the percentage of live cells after treatment ± SEM, n≥3. B) Western blot analysis of HIF1α and GAPDH (control) expression in MDA-MB-231 cells after 24 h of $CoCl_2$ and* ***1.15*** *treatment compared to untreated control.*

II.3 Conclusion

Reflecting on the entirety of the biochemical and cellular biology investigations, the *in vitro* assays provided an initial glimpse into the potential of the synthesized compounds. Compound **2.18** emerged as a standout in these assays, demonstrating superior affinity and

inhibitory activity towards the target pre-miR-210 sequence. This promising *in vitro* performance of **2.18** set the stage for subsequent evaluations and anticipated an eventual performance in cellular contexts.

In conclusion, the cytotoxicity assays conducted on the synthesized compounds have provided interesting insights into their potential in-depth evaluation. The three cancer cell lines—U2OS, BT474, and MDA-MB-231—contributed to elucidating the differential anti-proliferative activities of the compounds under varying oxygen conditions. Specifically, compounds **2.20** and **2.21** stood out for inhibiting proliferation across all tested cancer cell lines. However, when assessing toxicity towards primary mammary epithelial cells (hMEC), compounds **1.15**, **2.18**, **2.20**, and **2.21** displayed pronounced toxicity, while **2.32** and **2.33** demonstrated a more favorable toxicity profile.

The preliminary western blot analysis further enriched our understanding, particularly concerning the HIF-1α protein levels. The upregulation of HIF-1α post-$CoCl_2$ treatment in MDA-MB-231 cells reaffirmed the established model of HIF-1α overexpression under hypoxic conditions. Moreover, compound **1.15,** used as a control, validated the $CoCl_2$-induced hypoxia model and solidified its position as a reliable reference for hypoxic response inhibition.

An essential aspect of the first part of this PhD work was the synthesis of analogs of **1.15** to explore the relationship between chemical structure, *in vitro* activity, and *in cellulo* toxicity. Despite similarities in their core structures, the varied responses of different compounds reflect the profound influence of even minor structural modifications on biological activity. For instance, the removal of the azide function in **1.15** leading to **2.18** can be envisaged since *in vitro* activity was increased, and toxicity towards healthy cells remained at the same level. In **2.17**, the complete removal of the lateral chain led to an interesting result in BT474 cancer cell line while showing moderate toxicity in hMEC cells. The substitution of the phenyl group by a bigger aromatic compound led to too high toxicity towards both cancer and healthy cells, highlighting possible off-target effects. This interplay between structure and function necessitates a deeper dive into structure-activity relationships (SAR) to optimize *in vitro* and *in cellulo* efficacy while minimizing adverse effects. This could be done in the future by keeping the interesting results of this first preliminary study while changing the chemical parts of **1.15** left untouched here.

In summary, while several synthesized compounds showed promising *in vitro* results, with **2.18** being particularly remarkable, two pivotal *in cellulo* achievements can be cited: the successful induction of hypoxia using $CoCl_2$ and the validation of compound **1.15** as a reference compound for *in cellulo* hypoxic response inhibition. The insights obtained from

the small SAR study highlighted a strict link between chemical structure and biological outcomes that will undoubtedly drive the trajectory of subsequent analog synthesis.

Chapter III

Hit to lead optimization of novel miR-210 inhibitors:

Design, synthesis, and biological evaluation of tris-thiazole derivatives

Chapter III | Hit to lead optimization of novel miR-210 inhibitors: design, synthesis, and biological evaluation of tris-thiazole derivatives

III.1 Introduction

The preliminary work described and discussed in Chapter II facilitated a deeper understanding of the biological behavior of reference compound **1.15**, which represents the only positive control reported in the literature. Once this compound in hand, we observed that its biological activity in the biological system under study was not ideal. We thus decided to search for new original compounds to inhibit miR-210 biogenesis. Based on the findings from Chapter II and recent results obtained by our team[126], we started the rational design of novel compounds, which will be detailed in the following sections. These compounds' structures were inspired by the C-terminal moiety of the bleomycin natural products and several motifs that interact with the secondary structures of ncRNA. After chemical synthesis, the new compounds were fully characterized *in vitro* for their affinity, selectivity, and activity toward the target pre-miR-210. Then, a complete cellular biology study allowed us to obtain the toxicity profile *in cellulo* of the newly synthesized derivatives and to understand their mechanism of action. In short, the compounds were assessed for their ability to inhibit Dicer-cleavage of pre-miR-210, as explained in ***Figure 22*** in Section II.1 (Chapter II).

III.1.1 Previous work from our research group

Bleomycins are a class of antitumor glycopeptides first isolated by Umezawa *et al.* from the bacterium *Streptomyces verticellus*[273]. Employed as anticancer agents in combination with other antineoplastic agents, bleomycins are used to treat testicular, ovarian, cervical, head and neck, and esophageal cancers, along with thyroid carcinomas or lymphomas. Indeed, a therapeutic combination of bleomycin, etoposide, and cisplatin has shown efficacy in curing 90% of testicular cancer patients[274]. The bleomycins family comprises several members, the most extensively studied being: bleomycin A2, B2, and A5 (also known as pingyangmycin). Bleomycin is recognized on the World Health Organization's list of essential medicines, highlighting its role in basic health systems. Bleomycins A2 and B2 have been used together since their American Food and Drug Administration (FDA) approval in 1973 in the chemotherapy injection called Blenoxane, for example. Bleomycin A5 received approval in 1978 by the Chinese Food and Drug

Administration (SFDA) and remains the least used in Western countries. The chemical structures of A2, B2, and A5 are depicted in ***Figure 31***. While these three compounds share a common chemical scaffold, they differ in their respective positively charged R groups, as illustrated in ***Figure 31***. While they have different lateral positively charged chains, their similar structure is based on four different domains[275,276]: the disaccharide moiety (in yellow, ***Figure 31***), which is essential for cancer cell uptake *via* glucose transport[277–279]. The N-terminal part (in green, ***Figure 31***), combining a pyrimidine, an acetyl chain, and a β-aminoalanine, is responsible for chelating metal ions and causing DNA damage. The C-terminal domain (in blue, ***Figure 31***), which includes a bis-thiazole group and a side chain distinguishing the various bleomycins, is known to bind DNA by intercalating or minor groove interaction[275,276,280]. The positively charged lateral chain allows the electrostatic interaction with DNA. Lastly, the linker region connects three other moieties with a structure made of L-threonine and valerate subunits.

The anticancer activity of bleomycins relies on an oxidoreduction cycle that leads to an activated form of bleomycin responsible for DNA strand scission and topoisomerase inhibition[276]. Moreover, activated bleomycin is also known to induce the degradation of several other cellular components, including proteins[281], lipids[282], tRNA[283], and ncRNAs[111]. Notably, if we focus on the chemical structure of bleomycin, the different bis-thiazole side chains that carry positive charges in physiological conditions enhance interactions with the negatively charged backbone of DNA and RNA through electrostatic bonds. It seems, therefore, that the bis-thiazole moiety indicated in blue in ***Figure 31*** represents a scaffold of choice for interaction with nucleic acids. That is why we decided to employ this C-terminal part of bleomycins to design novel ligands, resulting in the development of innovative molecules.

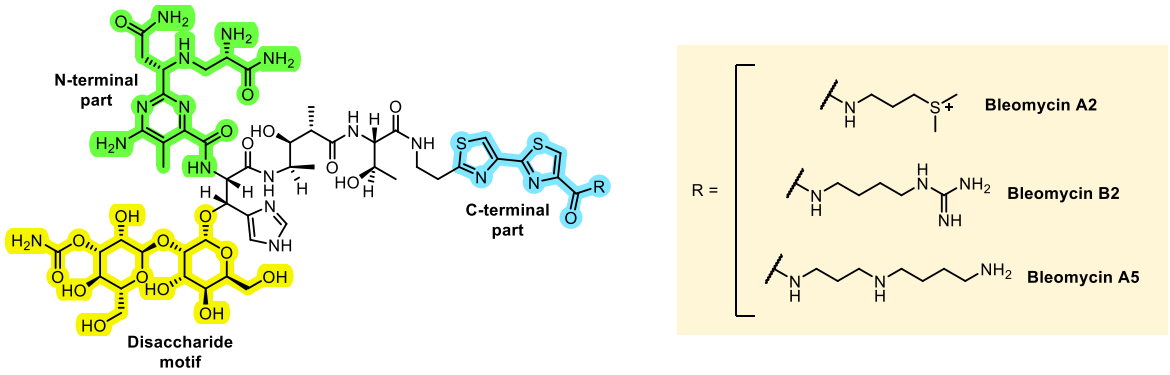

Figure 31 – *Chemical structures of bleomycins.*

Recently, our team devoted attention to the side chain of bleomycins and, more specifically, to the bis-thiazole-spermidine chain of bleomycin A5. Thus, compound **3.01** (***Figure 32A***) was prepared as a new RNA binder with several interactions formed with RNA nucleobases and phosphate groups, as highlighted in ***Figure 32B***. This compound was studied for its ability to inhibit the biogenesis of miR-21, a common and well-studied oncogenic miRNA[284,285]. **3.01** showed a moderate affinity (4.49 µM) but no inhibition activity.

This led Chloé Maucort *et al.*, from our group, to synthesize new and original compounds based on **3.01**[126]. In this project, innovative **3.01** analogs were designed and synthesized as new RNA ligands by conjugating the bis-thiazole scaffold of **3.01** to different chemical structures known for RNA interaction, aiming to inhibit oncogenic miR-21 biogenesis. Out of 24 compounds synthesized and tested against pre-miR-210, compounds **1.31** and **1.32** emerged as the most potent (***Figure 32A***, see also Section I.1.4, Chapter I), binding strongly to pre-miR-21, with K_D values of 76 and 250 nM, respectively. Both compounds effectively inhibited miR-21 maturation, likely by interacting with Dicer's cleavage site, with IC_{50} values *in vitro* in the low micromolar range of 1.62 µM for **1.31** and 3.74 µM for **1.32**. Even if not selective for one specific pre-miR, these compounds demonstrated high selectivity for pre-miRNA sequences compared to other nucleic acids. Hence, notable antiproliferative activity against glioblastoma U87 cells, which overexpresses miR-21, was observed. Both also showed activity against patient-derived cancer stem cells

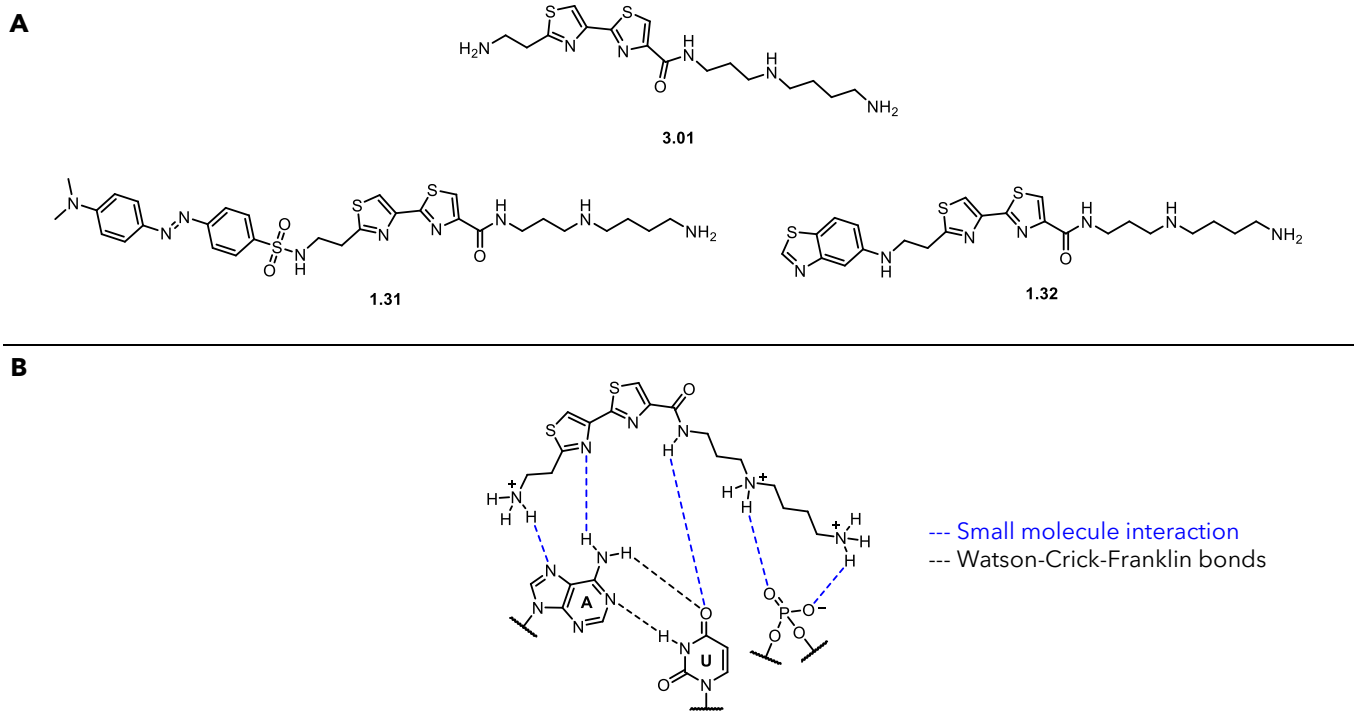

Figure 32 *– New compounds identified by Maucort et al. A) Chemical structures of* ***3.01***, ***1.31***, *and* ***1.32***. *B) Interactions possibly formed between* ***3.01*** *and RNA nucleobases or phosphate groups.*

(CSCs) without harming healthy cells. The synthesized compounds' efficacy in targeting cancer cells and their ability to inhibit the oncogenic miR-21 maturation positioned them as potential candidates, with an innovative mode of action, for subsequent research work. From these observations, it was clear that the aminoethyl-bis-thiazole scaffold would hold excellent promise as a starting scaffold for the design of more innovative pre-miR binders.

III.1.2 From compound **1.15** towards a new and original class of miR-210 inhibitors

Drawing from the results presented in Chapter II, compound **1.15** (TGP-210) is a very good binder for pre-miR-210, but its *in cellulo* activity needs to be amplified in our biological model. Modifications of the lateral chains carried out previously in Chapter II only allowed us to improve *in vitro* results, but no significant effect was observed on cellular studies. Therefore, based on the promising results obtained with **3.01**, **1.31**, and **1.32** *in cellulo*, we decided to explore the insertion of the aminoethyl-bis-thiazole moiety. For this purpose, we realized a computational structural alignment study between the core of **1.15** and the aminoethyl-bis-thiazole scaffold to devise a new and original series of compounds. Structural alignment is an approach that seeks to determine the correspondence between residues across two or more macromolecular chemical structures, focusing on the best overlap of their 3D conformation and overall shape. Such structural alignment was performed using LS-align software, where conformations with minimum energy were calculated, and the superposition result was obtained[286]. We decided to use compound **1.15** analog without the lateral chain (compound **2.17**, ***Scheme 7***) while keeping the methyl piperazine motif to focus on the essential part highlighted in our previous study. The alignment is shown in ***Figure 32***, **2.17** is highlighted in light green, and the best compound in terms of structural alignment is in orange.

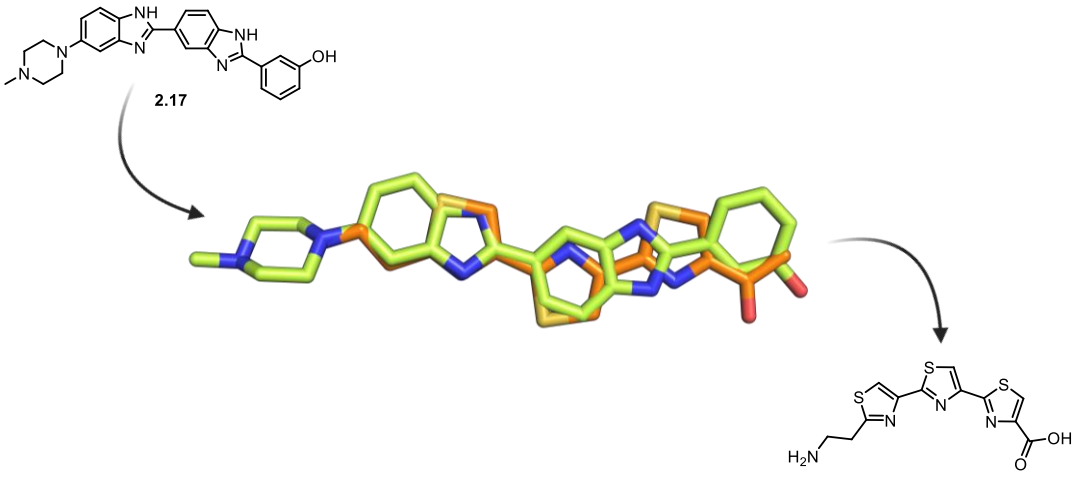

Figure 33 *– Alignment of molecules with the lowest energy conformations.* ***2.17*** *is shown in light green and the tris-thiazole scaffold in orange.*

A tris-thiazole motif (shown in orange, ***Figure 32***) was required to reach the best alignment since the bis-thiazole was found to be too short for perfect layering. A three-thiazole heterocycles scaffold was thus identified, paving the way for the design of new ligands based on this structure. This selection correlates perfectly with the known pharmacophore role of thiazole heterocycles, with their extensively studied presence in marketed drugs, including penicillin, bleomycins, abafungin, myxothiazol, amoxicillin, and epothilones, used for addressing several diseases[287-289].

To the best of our knowledge, it is the first time that the tris-thiazole scaffold has been used in the design of small molecule RNA ligands. Regarding how the selected scaffold will interact with the pre-miR RNA sequence, we hypothesized that the tris-thiazole will bind RNA base pairs *via* H-bonds (***Figure 35A***). This tris-thiazole scaffold allowed us to select several substituents for both right- and left-side functionalization (***Figure 34***). To introduce functional groups that might increase both affinity and selectivity for targeting pre-miR-210, several moieties identified from the literature as capable of forming specific interactions with structured RNAs were selected. It was first hypothesized that the two best motifs previously identified by Maucort *et al.*[126] (***Figure 32***) in the results mentioned above would be suitable for good affinity toward the pre-miR sequence. Therefore, a spermidine polyamine motif was selected, which plays several roles in various cellular processes such as cell growth or membrane stability[290]. Such polyamines exist as polycations at physiological pH, easily interacting with DNA and RNA phosphate backbone, as previously shown in ***Figure 32***. Then, we also introduced the diazobenzene motif, the second

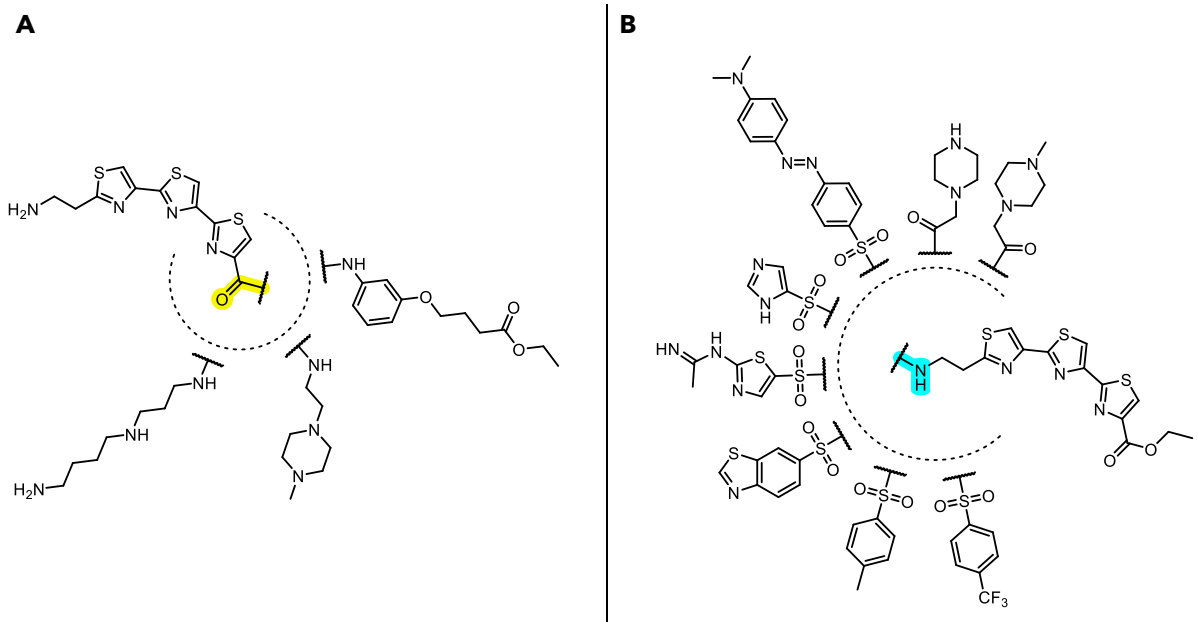

Figure 34 *– Chemical structure of the envisaged monosubstituted tris-thiazole analogs. A) Functionalization on the right side of the hit scaffold; b) Functionalization on the left side of the hit scaffold.*

promising motif outlined by our previous work. Following this first selection, we also kept the best motifs highlighted by our first SAR study (see compound **2.18**, Chapter II), which is to say, the phenyl motif with the ester lateral chain and the methylpiperazine. Hence, both substituted and unsubstituted piperazine were identified for their role in inhibitors of miRs[291]. Subsequently, heterocyclic motifs, such as imidazole, thiazole, and benzothiazole, were considered.

These various heteroaromatic rings were used to assess the influence of different heteroatoms. Indeed, these motifs are found in numerous active compounds and interact with nucleic acids through intercalation or a network of electrostatic and non-electrostatic bonds (***Figure 35B***). More precisely, the imidazole ring is found in the histidine amino acid, which is known to interact with RNA as other amino acids. Then, benzothiazole was selected for its similarity with the benzimidazole motif, which was widely reported in RNA binders[255].

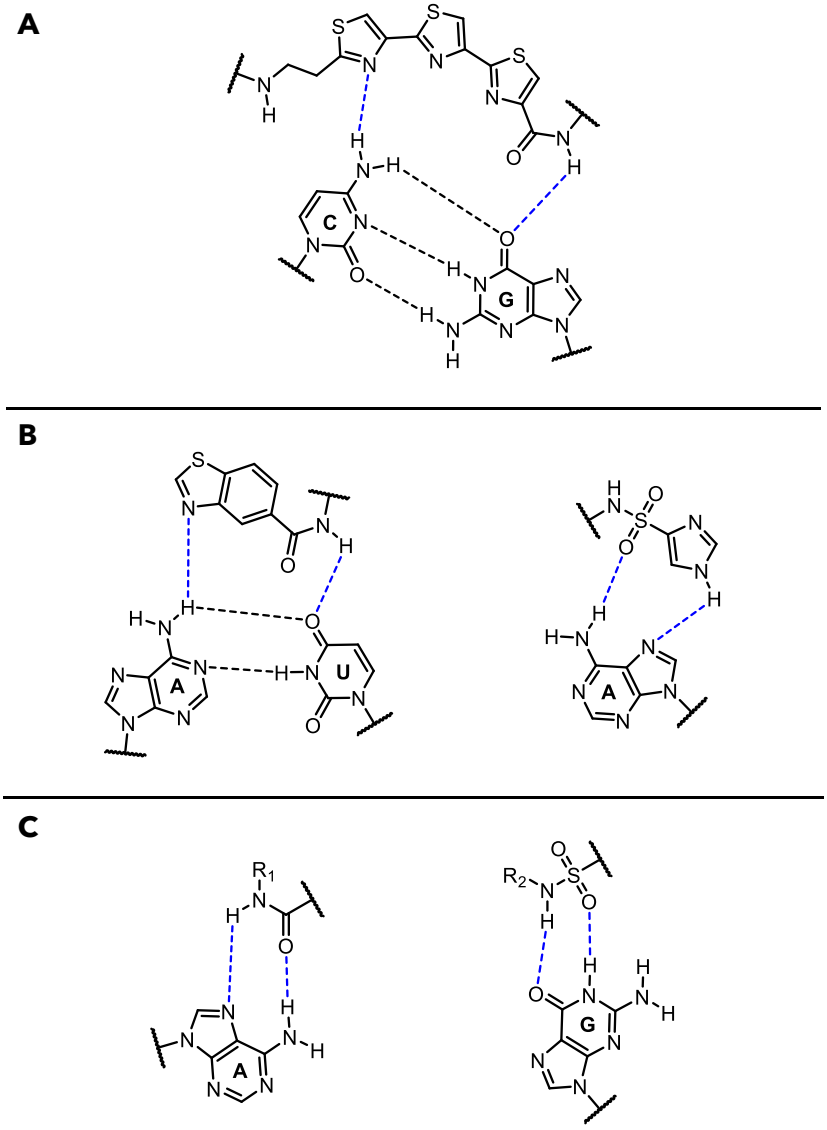

Figure 35 *– Possible interactions between nucleobases and: A) the tris-thiazole motif, B) benzothiazole and imidazole heteroaromatic motifs, C) amide and sulfonamide linkage functions.*

Additionally, aromatic motifs like toluene or trifluoromethyl substituted phenyl were explored to assess the influence and type of additional interactions these substituents might introduce. Notably, such compounds can interact with RNA through π-stacking interactions or hydrogen bonds facilitated by fluorine atoms. The methods to introduce these modifications will be detailed in the following sections. We functionalized the amino ethyl tris-thiazole scaffold with different linkage functions, going from a more classical amide to a sulfonamide bond. Such bonds might also introduce new interactions with the target, especially hydrogen bond-type interactions (***Figure 35C***). The choice of sulfonamides lies in their essential role in developing bioactive compounds, thanks to their high chemical and metabolic stability[292,293].

Therefore, our first idea was to keep the methylpiperazine motif to mimic the structure of targapremiR-210 (**1.15**), along with its known role in several pre-miR binders. However, it must be noted that its positively charged structure likely interacts non-specifically with the negatively charged backbone of the nucleic acid, which led us to the design of other derivatives. Overall, the substituents we decided to introduce on the tris-thiazole scaffold led to the design of analogs able to engage in interactions with unpaired bases and base pairs, forming triplets (***Figure 35B***). Such interactions occur at the single-strand/double-strand junctions of stem-loop structures found in miR-210 precursor. As previously outlined, the objective of the selected approach for the design of a novel chemical structure is to selectively target the oncogenic pre-miR-210 without interfering with other intracellular RNA and DNA sequences. This strategy has demonstrated efficacy in prior studies conducted by the team, and we aimed to apply it to a new series of compounds with suitable drug-like properties. *In vitro* evaluation of the new compounds led to a SAR study, highlighting the most interesting motifs that were combined in a second series of compounds.

III.2 Synthesis of a new series of tris-thiazole derivatives

As mentioned above, we began synthesizing new monosubstituted tris-thiazole compounds by inserting several modifications on the left or right part of the initial motif. To reach such analogs, it was decided to follow the retrosynthetic scheme below (***Scheme 8***). To functionalize the right part of the initial scaffold, we decided to perform coupling between the amines bearing the above-mentioned motifs and the aminoethyl tris-thiazole carboxylic acid (***Scheme 8A***). Different conditions were used to form the required amide

bond; we used mild coupling reagents, EDC and DECP, for most of the substrates. However, the stronger and more expensive HATU reagent was used for the poorly reactive amines. For the left-part functionalization, we focused on forming sulfonamide bonds with the corresponding sulfonyl chloride derivative and the free terminal amine of the tris-thiazole motif (***Scheme 8B***). Hence, carboxylic acids formed amide bonds upon coupling with the previously mentioned reagents (***Scheme 8B***). This retrosynthetic scheme made it clear that a common tris-thiazole precursor could be prepared to reach new analogs more efficiently and rapidly.

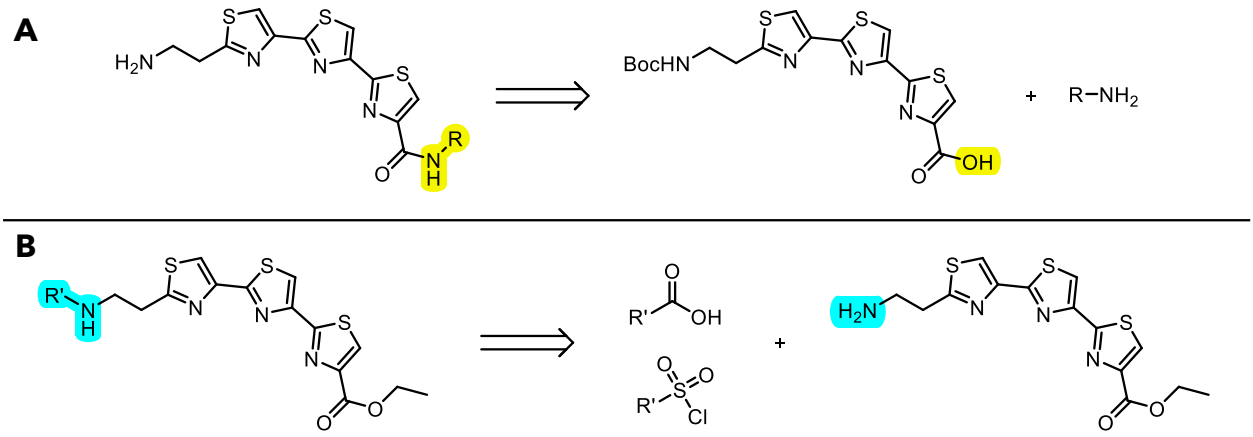

Scheme 8 – *Retrosynthetic approach for the synthesis of monosubstituted tris-thiazole derivatives.*

III.2.1 Synthesis of the tris-thiazole precursors

The synthetic strategy started with preparing a large stock of tris-thiazole precursors needed for further functionalization. Then, several substituents were introduced one by one while assessing their *in vitro* potential through affinity and inhibition activity assays.

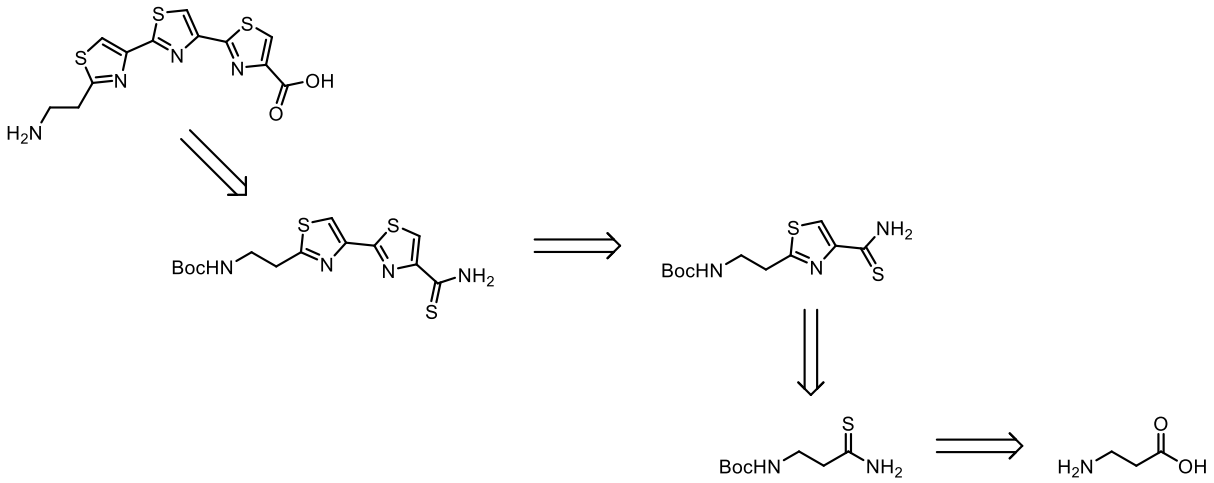

Scheme 9 – *Retrosynthesis approach for the preparation of the tris-thiazole scaffold.*

Following the retrosynthetic ***Scheme 9***, we prepared the common precursors bearing suitable chemical functions for further modifications.

We first prepared a stock of common precursors bearing suitable chemical functions for further modifications, following the retrosynthetic scheme below (***Scheme 9***). The literature offers several approaches for thiazole synthesis; however, we only reviewed the synthesis of 2,4-disubstituted-1,3-thiazoles. The first synthesis of a thiazole was by Hantzsch in 1887[294], involving the condensation of a thioamide with an α-haloketone (***Scheme 10B***). While being the oldest method for their synthesis, it remains the most reliable and efficient and relies on the high nucleophilicity of the sulfur atom in thioamides. Nevertheless, this synthetic approach releases a halogenic acid that might lead to unwanted side reactions such as epimerization or acid-catalyzed protecting group cleavage. To overcome such problems, other synthetic techniques exist, including condensation of thioamides with epoxides (Reaction B, ***Scheme 10A***)[295] or propargylic alcohols (Reaction C, ***Scheme 10A***)[296]. Another approach developed by Tang *et al.* involves a copper-catalyzed [3+3+1]-

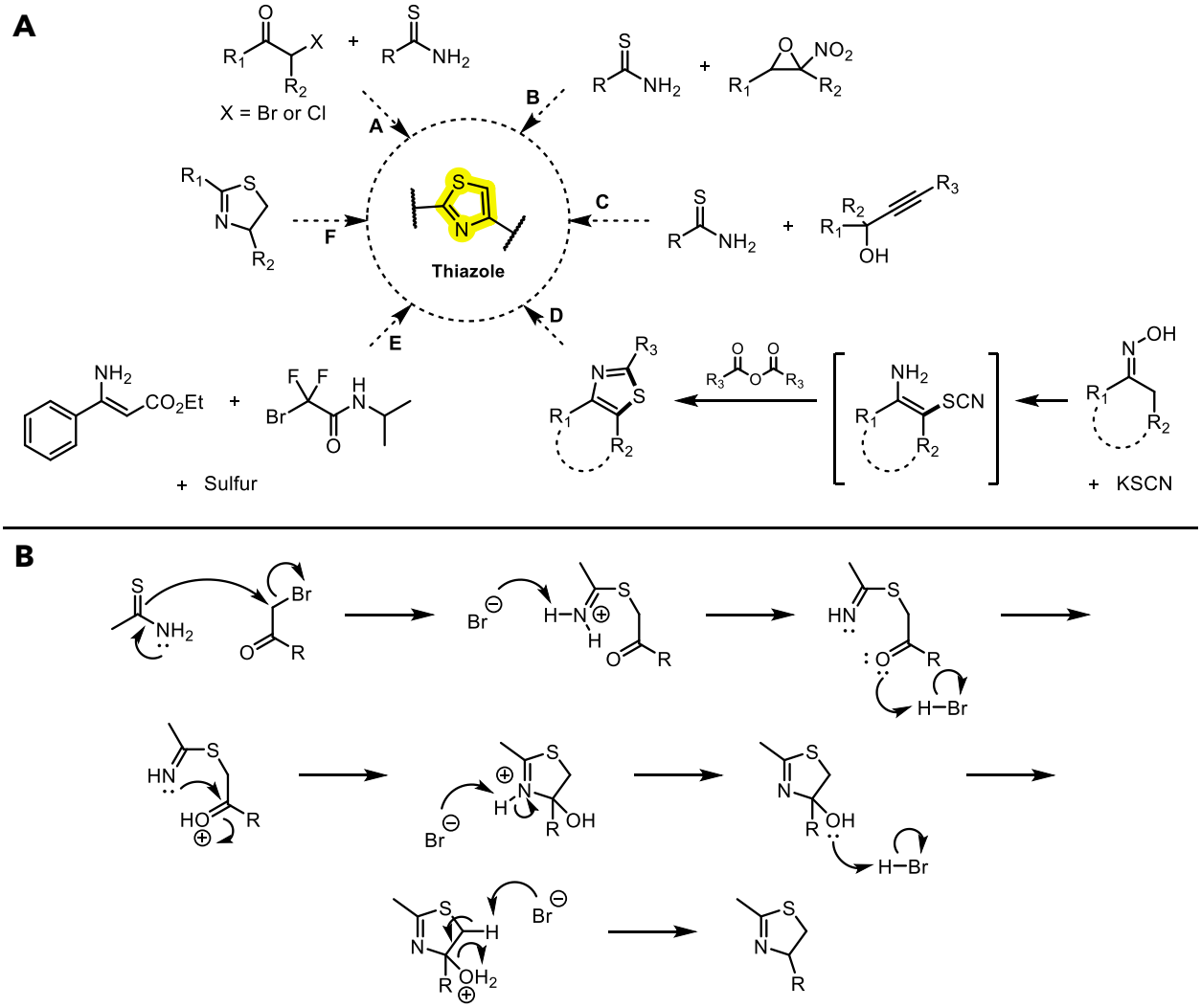

Scheme 10 *- Different synthetic strategies for the design of 2,4-disubstituted-1,3-thiazole.*

type condensation of an oxime, an anhydride, and a potassium thiocyanate (Reaction D, ***Scheme 10A***)[297]. Recently, Ma *et al.* proposed a multicomponent reaction for the synthesis of thiazoles from enaminoesters, sulfur, and bromodifluoroacetamides. This new approach can lead to the formation of thiazoles or isothiazoles upon two C-F bond cleavages and the formation of new C-S, C-N, and N-S bonds (Reaction E, ***Scheme 10A***)[298]. A last very straightforward approach that must be cited is the oxidation of thiazolines with DDQ, highlighted by Alom *et al.* (Reaction F, ***Scheme 10A***)[299].

In this work, we selected the Hantzsch cyclization to form the tris-thiazole precursors since it seemed the most appropriate way to reach common precursors for further modifications. The synthetic pathway (***Scheme 11***) started from two affordable starting materials, β-alanine (**3.02**) and thionyl chloride. Once HCl was formed *in situ,* the acid-catalyzed esterification led to ethyl 3-aminopropanoate (**3.03**), with an excellent yield of 97%. **3.04** was obtained after amino group protection with Boc_2O, in 96% yield. The ester function was then transformed into the corresponding amide (**3.05**) *via* ammonolysis using liquid ammonia[300]. Subsequently, **3.05** was converted into its thioamide version using Lawesson's reagent *via* the homonymous reaction, affording *tert*-butyl-*N*-(3-amino-3-thioxopropyl)carbamate (**3.06**) in 70% yield. Then, **3.06** underwent the first Hantzsch cyclization with ethyl bromopyruvate. As mentioned, HBr molecules are released during the mechanism, leading to Boc protecting group cleavage. After cyclization, this side reaction triggered the need to re-protect the amino group to afford **3.07** in two steps with an overall yield of 88%.

At this stage, the first thiazole cycle was formed, and the following steps were consecutively repeated twice to reach the three thiazole cycles required. Our choice to repeat the same reactions was inspired by the work of Quada *et al.*, which described the synthesis of novel thiazole derivatives using the same subsequent reactions[301]. Therefore, **3.07** underwent ammonolysis using liquid ammonia, affording **3.08** in 90% yield. Lawesson's reaction allowed us to obtain the corresponding thioamide of **3.08**, referred to as **3.09**, and obtained with 85% yield. This reaction required modifications from classical reported conditions to make it more suitable and yield consistent for our synthesis. Starting material **3.08** was first completely solubilized in a mixture of THF and toluene (2:1 ratio) at 100°C, then Lawesson's reagent was added, and the reaction mixture was stirred for 20 min. Noteworthy, reagents needed to be well stored under Ar due to the high risk of degradation; the reaction was also carried under Ar atmosphere. Following this reaction, **3.09** went through the second Hantzsch reaction with ethyl bromopyruvate to reach **3.10** in 95% yield. Another amino group protection was required and afforded **3.11** in a quantitative reaction.

At this point, the three-reaction cycle was carried out again; first, ammonolysis of **3.11** afforded **3.12** in quantitative amount. Then, Lawesson's reaction transformed the amide group of **3.12** into the corresponding thioamide (**3.13**), with 92% yield. A last Hantzsch reaction, between **3.13** and ethyl bromopyruvate, afforded the tris-thiazole derivate. Without any intermediate characterization, the free amino group was protected again with Boc_2O, allowing for the formation of **3.14** with a 92% yield over two steps. A last saponification step of the ester was required to reach the desired precursor, ready to be modified with different substituents on the right side. LiOH in a mixture of H_2O and THF (2:1 ratio) was used for the saponification of **3.14**, and a last acidification step afforded **3.15a** in

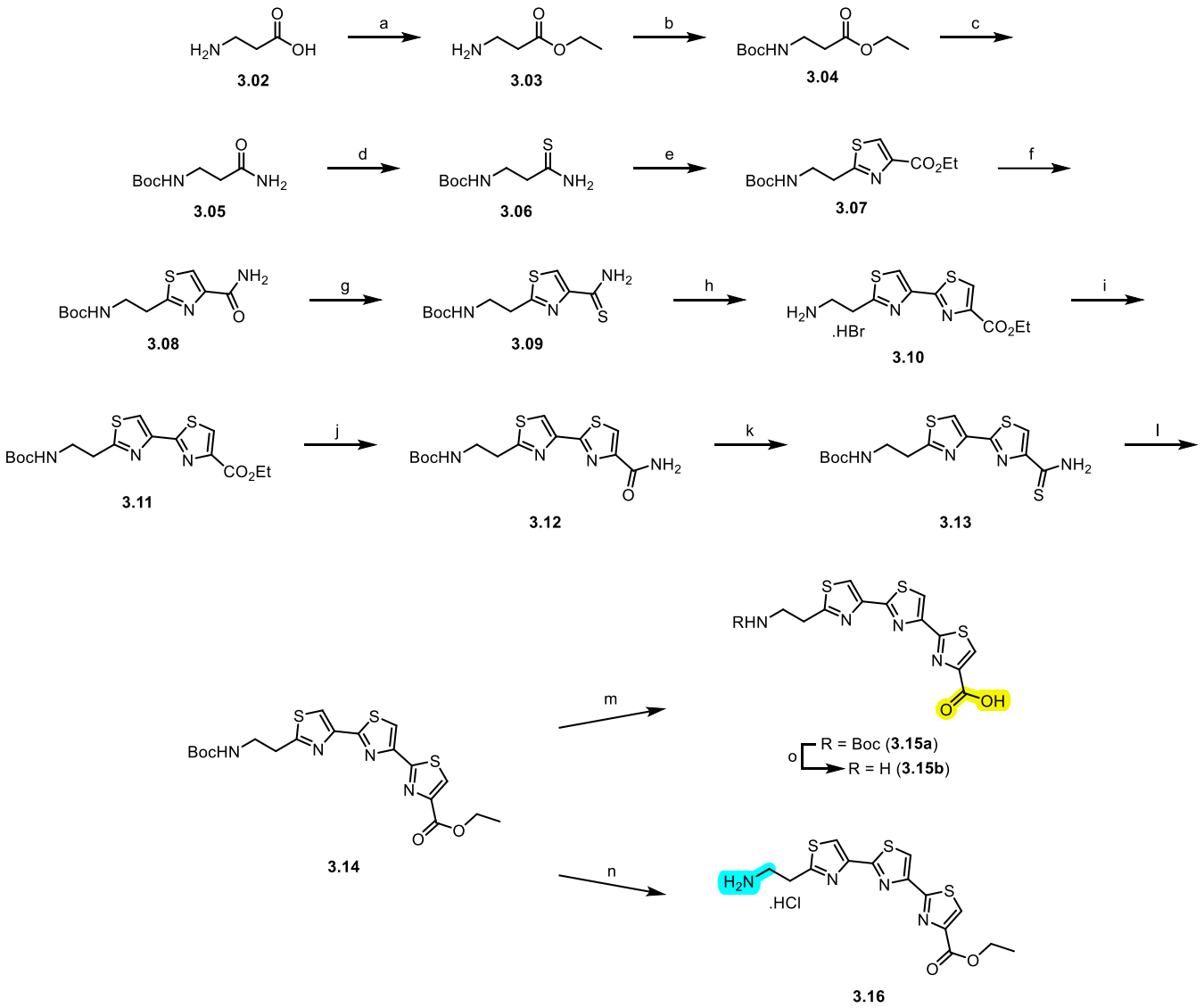

Scheme 11 *- Reagents, conditions, and yields: (a) $SoCl_2$, EtOH, O°C to 70°C, 3h, 97%; (b) Boc_2O, Et_3N, DCM, O°C to r.t., 16h, 96%; (c) NH_4OH, 70°C, 16h, 87%; (d) Lawesson's reagent, THF, 24h, 70%; (e) 1) Ethyl bromopyruvate, EtOH, 60°C, 1h30; 2) Boc_2O, Et_3N, DCM, O°C to r.t., 16h, 88% over two steps; (f) NH_4OH, EtOH, 70°C, 2h, 90%; (g) Lawesson's reagent, THF-Toluene (2:1), 20min, 85%; (h) Ethyl bromopyruvate, EtOH, 60°C, 16h, 95%; (i) Boc_2O, H_2O-1,4-diocane (1:1), O°C to r.t., 16h, quantitative; (j) NH_4OH, EtOH, 70°C, 3h, quantitative; (k) Lawesson's reagent, THF-Toluene (2:1), 30min, 92%; (l) 1) Ethyl bromopyruvate, EtOH, 80°C, 16h; 2) Boc_2O, Et_3N, H_2O-1,4-dioxane (1:1), O°C to r.t., 4h, 92% over two steps; (m) LiOH, H_2O-THF (2:1), 4h, 99%; (n) 4M HCl in 1,4-dioxane, 30min, quantitative; (o) 4M HCl in 1,4-dioxane, 30min, quantitative.*

99% yield. Cleavage of the Boc protecting group with a 4M HCl solution in 1,4-dioxane allowed us to reach **3.15b** in quantitative yield. A 0.5M aqueous solution of potassium bisulfate ($KHSO_4$) was used to acidify the mixture without Boc-protecting group removal. Hence, the cleavage of the Boc group of **3.14**, with a 4M HCl solution in 1,4-dioxane, led to the precursor **3.16**. This latter was used for further functionalization on the left part of the tris-thiazole motif. The following sections will detail how we used precursors **3.15a** and **3.16** to reach innovative monosubstituted tris-thiazole derivatives.

III.2.2 Synthesis of mono-substituted tris-thiazole compounds – Functionalization of **3.15a**

Based on the knowledge acquired by the team during the synthesis and evaluation of a library of bis-thiazole derivatives, we focused here on the preparation of novel tris-thiazole analogs. The first modifications were performed on the carboxylic acid function of **3.15a** to reach a first set of mono-substituted derivatives upon coupling with amines (***Scheme 12C***). Three different motifs were selected for the functionalization of the carboxylic acid function, one being the aliphatic spermidine known as the N^4,N^8-di-*tert*-butoxycarbonylspermidine, and the 4-(3-aminophenoxy)butanoate motif. These two intermediates had to be prepared with the required amino groups for coupling with **3.15a** (***Scheme 12A*** *and* ***12B***). As a non-symmetric, linear polyamine, the synthesis of the spermidine motif in compound **3.20** required selective protection. The synthetic strategy selected is based on Pittelkow *et al.*'s work, starting from commercial *N*-Boc-1,4-butanediamine (**3.17**)[302]. This mono-protected diamine was alkylated *via* a Michael addition of acrylonitrile, affording **3.18** in 97% yield. Thus, the resulting secondary amine was Boc-protected to reach **3.19** quantitatively. The final nitrile function reduction using $LiALH_4$ yielded N^4,N^8-di-*tert*-butoxycarbonylspermidine (**3.20**) with a 55% yield, essential for the subsequent convergent synthesis. Parallelly, 4-(3-aminophenoxy)butanoate (**3.23**) was prepared following a straightforward synthesis starting from the alkylation of commercially available 3-nitrophenol (**3.21**), following Nguyen *et al.*'s work[303]. This Williamson ether formation yielded **3.22** in 99% yield. Lastly, reduction of the nitro group was performed using H_2 and palladium on activated carbon (Pd/C), affording **3.23** with a 95% yield.

Following the preparation of the two free amino-containing intermediates, coupling between **3.15a** and the terminal primary amines of commercial 1-(2-aminoethyl)-4-methylpiperazine, **3.20** and **3.23** was carried out. A last Boc cleavage was then performed using a 4M HCl solution in 1,4-dioxane. For the formation of **3.24a** and **3.25a**, we selected a mild coupling reagent such as EDC (carbodiimide activation). This procedure goes

through the formation of a reactive *O*-acylisourea that needs to be transformed into a succinimide ester to avoid any side reactions, such as the cyclization of itself to form an oxazolone or the formation of *N*-acylurea derivatives (***Scheme 13A***)[304]. Such side products would not only diminish the overall yield of the process but also complicate the work-up and isolation of the desired product. To minimize these side effects, additives like HOSu were added to react directly with the freshly obtained *O*-acylisourea, forming the mildest activated ester form[305]. After forming the activated ester, which can be observed by thin-layer chromatography (TLC), the free amine can be added to finalize the coupling, leading to the corresponding amide (***Scheme 13A***). Therefore, for **3.24a** and **3.25a** preparation, couplings were performed with a mixture of *N*-hydroxysuccinimide (HOSu) and 1-ethyl-3-(3-dimethylaminopropyl)carbodiimide (EDC). Compound **3.24a** was obtained in 47% yield over the 2 steps. On the other side, compound **3.25a** was obtained with a 65% yield. A last cleavage of the Boc-protecting groups yielded **3.24b** and **3.25b** with respective yields of

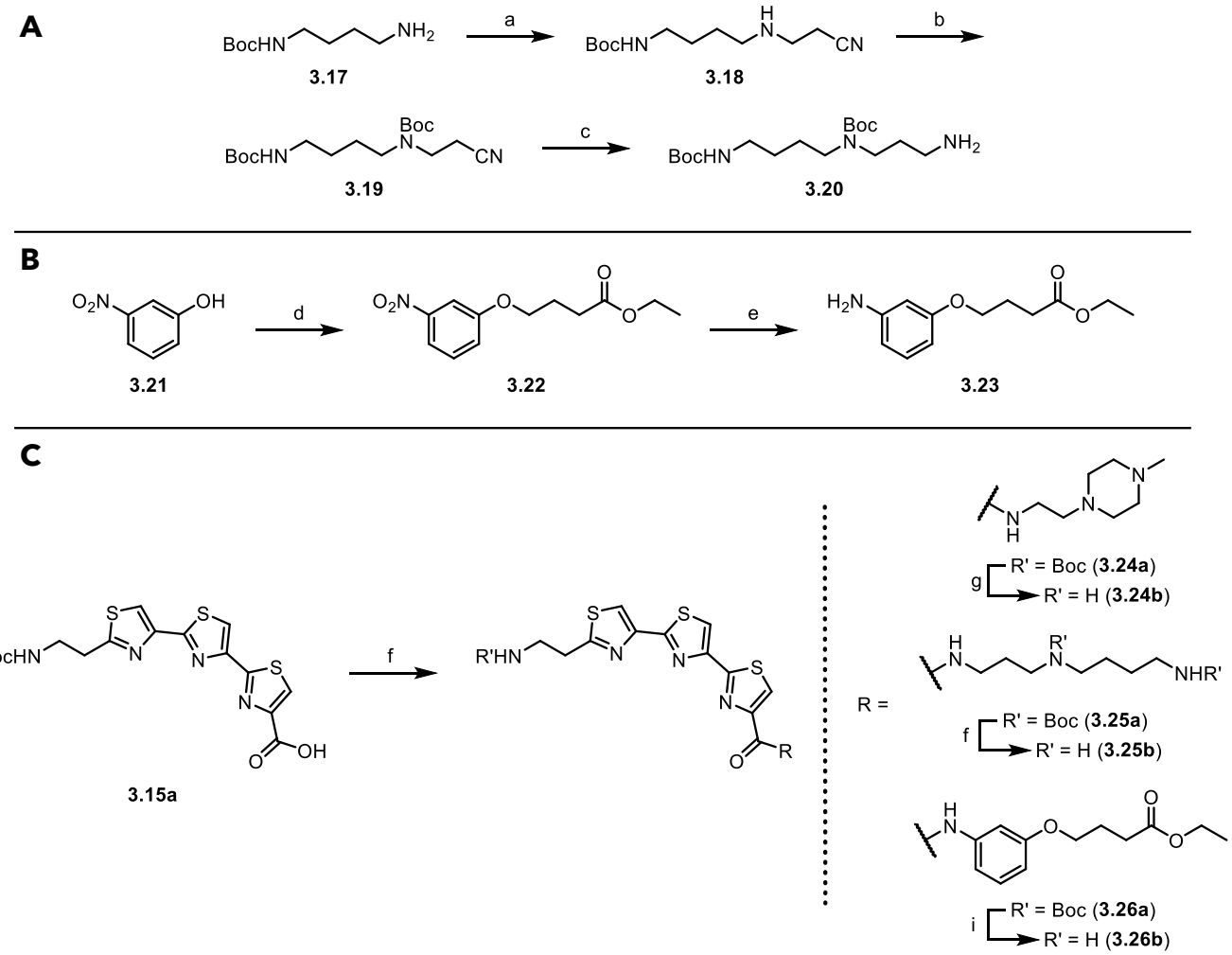

Scheme 12 *- Reagents, conditions, and yields: (a) acrylonitrile, MeOH, rt, 16h, 97%; (b) Boc_2O, DCM, rt, 16h; (c) $LiAlH_4$, Et_2O, -10°C, 55%; (d) ethyl 4-bromobutyrate, K_2CO_3, DMF, 90°C, 16h, 99%; (e) H_2, Pd/C, EtOH, rt, 16h, 95%; (f) amine, HOSu, EDC, DIPEA, DCM, rt, until completion, 47% (**3.24a**) 65% (**3.25a**) or amine, HATU, DIPEA, DMF, rt, until completion, 83% (**3.26a**); (g), (h), and (i) 4M HCl in 1,4-dioxane, rt, 30min, 94% (**3.24b**) / 91% (**3.25b**) / 97% (**3.26b**).*

94% and 91%. The last coupling involved the introduction of the intermediate **3.23**. A first coupling was performed between **3.23** and **3.15a** using EDC/HOSu; unfortunately, the electron-deficient amine never reacted with the activated ester.

We thus decided to change the conditions and use a stronger, yet more expensive, coupling reagent, the Hexafluorophosphate Azabenzotriazole Tetramethyl Uronium (HATU). In this case, the deprotonated acid reacts first with the electron-deficient carbon of the uronium salt derivate (***Scheme 13B***). Then, the resulting HOAt anion reacts with the newly formed activated carboxylic acid to form the OAt-active ester. Finally, the amine adds to the Oat-ester, forming the corresponding amide (***Scheme 13B***)[305]. HATU is a very efficient coupling reagent and is now the reference reagent for poorly reactive substrates; this high efficiency leading to higher yields has been connected to a neighboring effect coming from the nitrogen atom that stabilizes the incoming amine through a 7-membered ring transition state (***Scheme 13B***)[306]. This new procedure allowed us to reach compound **3.26a** with a yield of 83%, directly followed by Boc group cleavage to obtain **3.26b** in 97% yield.

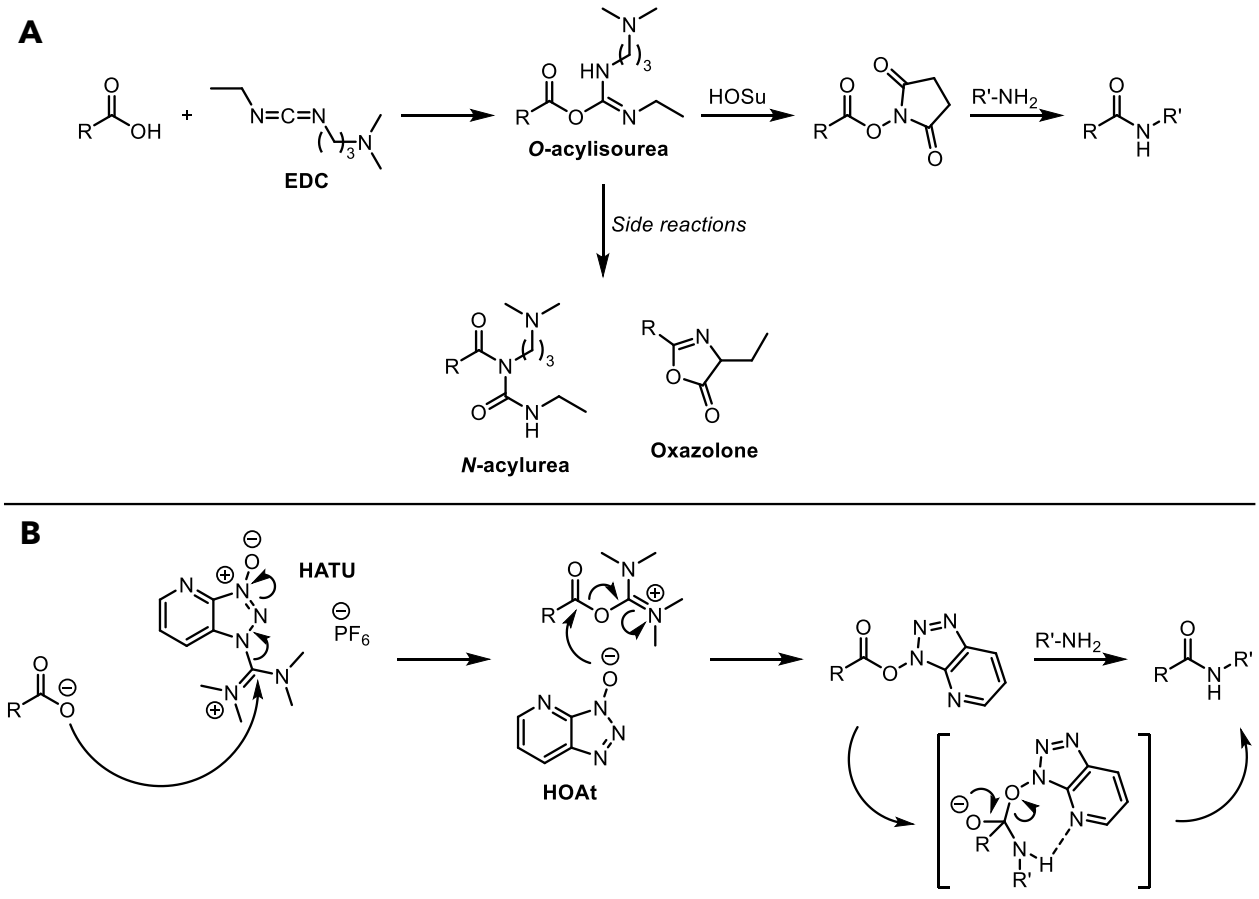

Scheme 13 – *Coupling mechanism with A) EDC/HOSu or B) HATU.*

III.2.3 Synthesis of mono-substituted tris-thiazole compounds – Functionalization of **3.16**

In this section, we describe the modifications inserted *via* the free amine function on the left side of compound **3.16**. Whereas substituents were introduced on the left, the ester function on the right was untouched. As anticipated in the previous section, two ways were chosen to form new analogs, one with coupling conditions and the other upon the creation of sulfonamide bonds.

The conventional approach for the synthesis of sulfonamides involves the reaction between an amine and a sulfonyl chloride in the presence of a base. Given the commercial availability of a wide array of sulfonyl chlorides and the simplicity of the synthetic pathway, the reaction was conducted between several sulfonyl chlorides and the free amino group of **3.16** in the presence of Et_3N and DMF as solvent. This led to the formation of sulfonamides, resulting in compounds **3.27** to **3.33**, with yields ranging from 20% to 66% (***Scheme 14***). 4-methylbenzensulfonyl chloride and 4-(trifluoromethyl)benzenesulfonyl chloride afforded compounds **3.27** and **3.28**, with respective yields of 66 and 34%. Then, three heterocyclic sulfonyl chlorides were used: benzo[*d*]thiazole-6-sulfonyl chloride afforded **3.29** in 42% yield, 2-acetamidamidothiazole-5-sulfonyl chloride led to **3.30** with 20% yield. These relatively low yields result from complex purification processes, which required dry loading

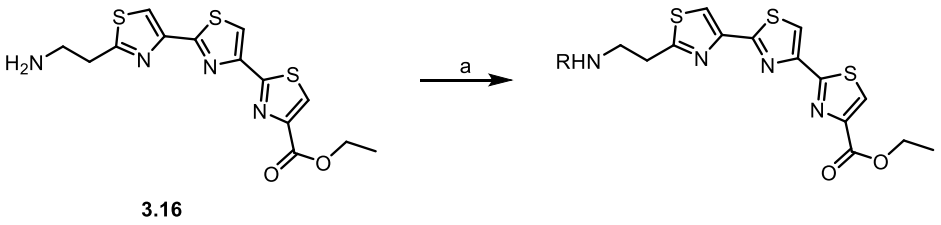

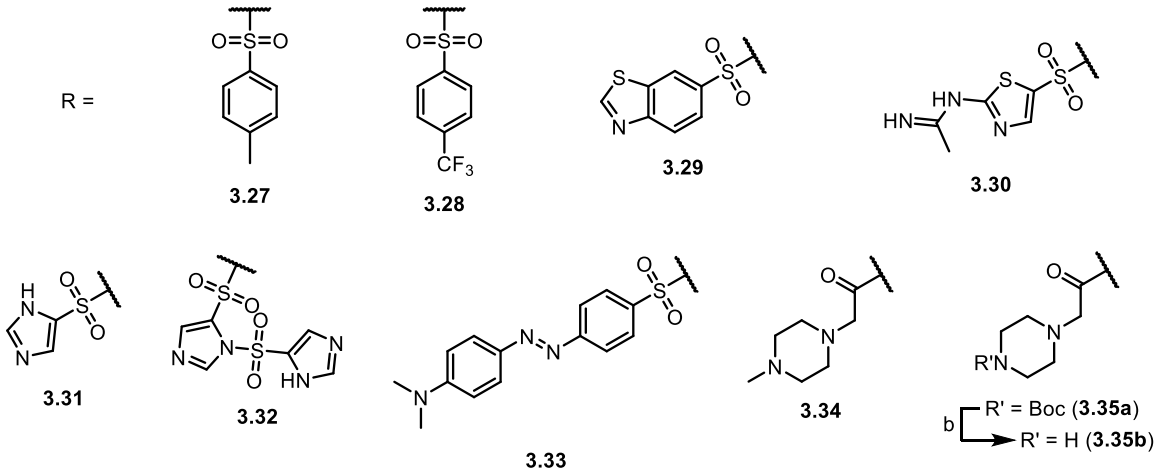

Scheme 14 *- Reagents, conditions, and yields: (a) sulfonyl chloride derivatives, Et_3N, DMF, rt, until completion, 66% (**3.27**) / 34% (**3.28**) / 42% (**3.29**) / 20% (**3.30**) / 51% (**3.31** and **3.32**) or 2-(4-methylpiperazin-1-yl)acetic acid, $POCl(EtO)_2$, Et_3N, THF, rt, 40% (**3.34**) or 4-(tert-butoxycarbonyl)piperazine-1-carboxylic acid, HATU, DIPEA, DMF, rt, 49% (**3.35a**); (b) 4M HCl in 1,4-dioxane, rt, 30min, 98% (**3.35b**).*

of the samples because of low solubility with the eluent. However, even in these conditions, part of the product crystallized in the solid deposit and required more polar solvents to elute, leading to poor separation.

For the last heteroaromatic sulfonyl chloride, we used 1*H*-imidazole-4-sulfonyl chloride, and two compounds were obtained after a complicated purification. TLC did not allow us to observe the two different chemicals, but flash chromatography afforded **3.31** and **3.32**. Compound **3.32** resulted from the sulfonyl chloride's second reaction with the free secondary amine of imidazole. Unfortunately, only **3.32** has been kept for further studies since we have yet to manage to remove all traces of it in the compound **3.31** batch. For compound **3.33**, the formation of the compound was observed in TLC. Still, its apolar structure led to an analog impossible to purify and solubilize in the ordinary solvents available in the lab, even in dimethyl sulfoxide (DMSO). This problem of solubilization forced us to abandon its synthesis.

For the last two compounds, coupling conditions were used to reach **3.34** and **3.35a**, with 2-(4-methylpiperazin-1-yl)acetic acid and 4-(tert-butoxycarbonyl)piperazine-1-carboxylic acid as respective acid substrate. Several attempts were made using classical EDC/HOSu conditions, but the tris-thiazole amine (**3.16**) was not reacting with the activated ester. We thus decided to try another coupling agent known as diethyl chlorophosphate (DECP) with Et_3N and THF as the solvent, based on the work of Lee *et al.,* who identified this coupling reagent in the field of thiazole-based cephalosporines[307]. The reaction forms a highly reactive acyloxy diethyl enol phosphate before the reaction with the appropriate amine (***Scheme 15***). However, in our case, this coupling formed **3.34** with a moderate 40% yield. This moderate yield is probably due to the impossible isolation of the activated ester, like in Lee's work, thus leaving high amounts of DECP reagent in the mixture that will react primarily with the amine *via* a simple substitution reaction. Therefore, to form **3.34a**, we used the procedure with HATU, but still, a moderate yield was obtained (49%). Subsequent quantitative cleavage of the Boc protecting group led to the final compound **3.35b**.

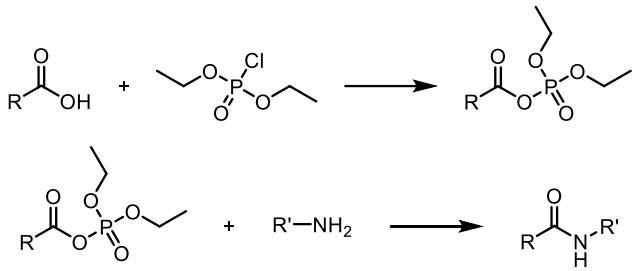

Scheme 15 *- Coupling mechanism with DECP.*

III.3 *In vitro* biochemical evaluation of the first series of compounds and SAR study

Following the synthesis of the first series of novel molecules, *in vitro* assays were conducted, beginning with evaluating the dissociation constants (K_D) of the synthesized molecules against pre-miR-210. Subsequent inhibitory activity of Dicer function evaluation was performed to reach IC_{50} values for the most promising compounds. Such fluorescence-based biochemical assays were performed, as explained in Section II.2.2, Chapter II.

The affinity of these analogs towards pre-miR-210 was also compared to the reference molecule **1.15** and their unsubstituted precursors **3.12b** and **3.16**. To verify our alignment study that suggested focusing on tris-thiazole derivatives, we also decided to introduce some bis-thiazole products previously prepared in our group (see Section III.1.1). We selected six derivatives from the *in-house* library that displayed a good affinity towards another oncogenic miR (i.e., miR-21), their structures are shown in ***Figure 36***. All of them were still available in the lab, except for **3.41**, which had to be resynthesized as described in the experimental procedures section.

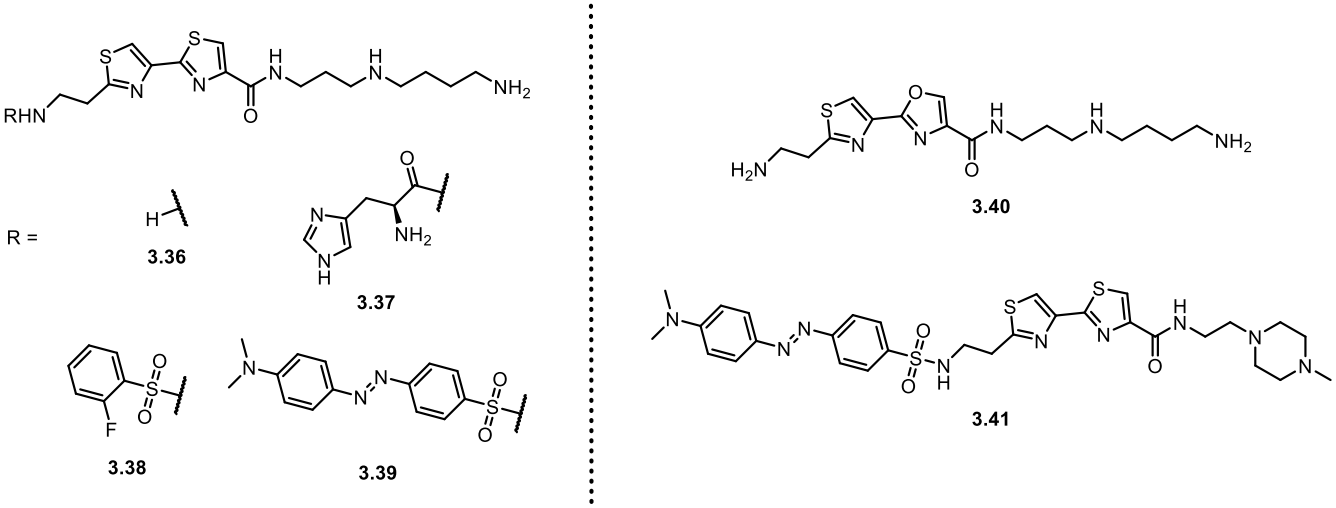

Figure 36 *- Chemical structure of bis-thiazole derivatives (**3.36** to **3.41**).*

The results of this *in vitro* evaluation are compiled in ***Table 10***.

Groups	Compounds	K_D (μM) – pre-miR-210	K'_D / K_D	K''_D / K_D
TGP-210	**1.15**	0.54 ± 0.02	0.8	1.6
Starting materials	**3.15b**	No binding	-	-
	3.16	2.46 ± 0.16	2.1	4.1
Bis-thiazole derivatives	**3.36**	2.21 ± 0.14	0.9	1.2
	3.37	0.93 ± 0.38	0.8	2.1
	3.38	2.45 ± 0.36	3.0	5.4
	3.39	0.38 ± 0.35	1.4	> 10
	3.40	0.31*	> 10	> 10
	3.41	0.31 ± 0.13	6.4	5.3
Tris-thiazole analogs of 3.15a	**3.24b**	1.58 ± 0.54	1.9	4.1
	3.25b	0.17 ± 0.01	2.6	7.3
	3.26b	0.12 ± 0.07	1.2	6
Tris-thiazole analogs of 3.16	**3.27**	3.78 ± 0.37	2.2	Not Tested
	3.28	No binding	-	-
	3.29	5.94 ± 0.15	1.5	0.6
	3.30	6.29 ± 2.15	0.9	3.4
	3.32	No binding	-	-
	3.34	5.28 ± 1.56	0.6	3
	3.35b	4.53 ± 1.85	0.5	1.8

Table 10 *- K_D values and K_D ratios in the presence of an excess of tRNA and DNA of **3.15b**, **3.16**, and analogs towards various pre-miR sequences. * Tested only once; error bar considered ± 10%.*

In the employed conditions, TargapremiR-210 **1.15** showed a submicromolar affinity of 0.54 μM. Starting material **3.15b** containing a free carboxylic acid showed no binding affinity, while the same compound bearing an ethyl ester moiety as in **3.16** showed a K_D of 2.46 μM. This suggests that small variations in the right part of the compounds could induce major differences in binding affinity. Most of the synthesized derivatives showed good binding affinity, with K_D values ranging from 120.0 nM to 6.29 μM. Bis-thiazole compound **3.36**, bearing the spermidine side chain on the right part and a free amine on the left part, showed a K_D of 2.21 μM similar to the one it had for pre-miR-21. The introduction of histidine on the left part, as in **3.37**, led to an increase in affinity with a K_D of 0.93 μM, while introducing a fluorobenzene aromatic ring, as in **3.38**, did not significantly impact affinity with a K_D value

similar to reference compounds. The addition of the diazobenzene motif, as in **3.39**, afforded one of the strongest ligands with an approximately 6-fold increase in affinity compared to the reference compounds **3.16** and **3.36**. A similar result was obtained with the oxazole-thiazole derivative **3.40**, which showed a very interesting affinity with a K_D of 0.31 µM, if confirmed by replication. The hybrid compound **3.41**, with the diazobenzene motif on the left part and the methyl piperazine motif on the right part instead of the spermidine chain, showed a very good K_D of 0.31 µM.

Among the tris-thiazole derivatives **3.24b-3.35b**, **3.25b** and **3.26b** showed the best results with submicromolar affinities of 0.17 and 0.12 µM, respectively. Given the similarity of these values, the spermidine side chain of **3.25b** clearly does not add relevant interactions compared to the phenyl-ester chain of **3.26b**, which is more straightforward to prepare. Compounds **3.24b**, **3.27**, **3.29**, **3.30**, **3.34**, and **3.35b** show similar results with K_D values in the low micromolar range (1.58 µM – 6.29 µM), except for two sulfonamide derivatives **3.28** and **3.32** that are not able to bind the target. This illustrates that the introduced modifications on the right part of the compound did not bring a better affinity and that the sulfonamide linker used for conjugation is not favorable for affinity. This was contrary to initial expectations, as the sulfonamide linkage was hypothesized to enhance binding for the target sequence. Similarly, incorporating an additional thiazole ring led to a loss of affinity compared to the reference compound **3.16**, with a K_D going from 2.46 µM for **3.16** to 6.29 µM for **3.30**. Among the analogs of **3.15a** studied, the most affine was compound **3.27**, which features a toluene motif, and those with a piperazine motif (**3.34** and **3.35b**). Removing the methyl group from the piperazine structure, as in compound **3.35b**, was not essential for maintaining affinity.

As detailed in Section II.2.2 (Chapter II), selectivity assays were also performed in the presence of an excess of tRNA (K'_D) or DNA (K''_D), with ratios of K_D values above 1 showing a loss of selectivity for the target pre-miR-210. Interestingly, compound **1.15** showed excellent selectivity in both tRNA and DNA presence. Most of the tested compounds showed reasonable selectivity in the presence of tRNA (ratio of K_D values with and without tRNA below 5) except the oxazole-thiazole derivative **3.40**, which lost affinity in this competitor's presence. Selectivity values were less favorable in the presence of DNA. Indeed, the good binders, **3.39** and **3.40**, lost their affinity in the presence of DNA, together with **3.41** which decreased the affinity by 20-fold. The other bis-thiazole derivatives bearing moderate affinity showed good selectivity. Hence, compound **3.34** retained its selectivity in the presence of tRNA but lost it when DNA was introduced in the assay. However, removing the methyl group, yielding **3.35b**, restored this lost selectivity. It was also observed that all

compounds maintained this pattern by keeping their selectivity in the presence of tRNA but losing it when DNA was added with the pre-miR-210 sequence.

Overall, the results obtained with these bis-thiazole and tris-thiazole derivatives confirm that the benzimidazole ring of **1.15** can be replaced with thiazole heterocycles, leading to strong RNA ligands of pre-mir-210. However, while **1.15** showed good affinity and selectivity, the best binders, **3.39**, **3.40**, **3.41**, **3.25b**, and **3.26b** are not selective in the presence of DNA.

The extremely promising submicromolar affinities of some of the compounds led us to conduct inhibition studies on pre-miR-210 processing. As illustrated in ***Table 11***, the ability of each compound to block the Dicer-processing of pre-miR-210 has been studied.

Groups	Compounds	K_D (μM) – pre-miR-210	IC_{50} (μM)
TGP-210	**1.15**	0.54 ± 0.02	2.91 ± 0.48
Starting material	**3.16**	2.46 ± 0.16	No inhibition
Bis-thiazole derivatives	**3.36**	2.21 ± 0.14	No inhibition
	3.37	0.93 ± 0.38	No inhibition
	3.38	2.45 ± 0.36	No inhibition
	3.39	0.38 ± 0.35	2.69 ± 0.61
	3.40	0.31*	16.6*
	3.41	0.31 ± 0.13	15.7*
Tris-thiazole analogs of 3.15a	**3.24b**	1.58 ± 0.54	No inhibition
	3.25b	0.17 ± 0.01	23.5 ± 6.05
	3.26b	0.12 ± 0.07	3.31 ± 0.95
Tris-thiazole analogs of 3.16	**3.34**	5.28 ± 1.56	3.03*
	3.35b	4.53 ± 1.85	No inhibition

Table 11 *- K_D and IC_{50} values of **3.16** and analogs towards various pre-miR sequences. * Tested only once; error bar considered ± 10%.*

As a first result, the reference common precursor **3.16** showed no inhibition of the Dicer function. Compounds **3.36**, **3.37**, and **3.38** were found to be inactive, thereby suggesting that the bis-thiazole motif is not the appropriate scaffold for inhibiting miR-210 maturation. Among the bis-thiazole tested compounds, only **3.39** demonstrated significant activity with an IC_{50} of 2.69 μM. Along with **3.39**, the best binders of pre-miR-210 **3.40**, **3.41**, **3.25b** and **3.26b** were also the best inhibitors bearing IC_{50} values of 16.6, 15.7, 23.5 and

3.31 µM, respectively. Differences in the binding site, that can be more or less favorable for inhibition, could account for the observed differences in the inhibition activity of compounds bearing similar affinity. Comparing the IC_{50} values of compounds **3.24b**, bearing the piperazine on the right side, and **3.34**, bearing the piperazine on the left side, revealed that the presence of the methylpiperazine motif on the left side resulted in an excellent IC_{50} value of around 3 µM. At the same time, no inhibition was observed when put on the right side. Indeed, the result obtained with **3.35b** showed that the absence of the methyl group on the piperazine led to an unexpected activity loss. This outlined the importance of the methylpiperazine moiety for activity, together with its left-side position. Conversely, compound **3.25b** exhibited a relatively high IC_{50} value of 23.5 µM, suggesting that the spermidine moiety is not the most suitable motif for pre-miR-210 processing inhibition. Overall, these results showed that **3.26b** bearing the tris-thiazole moiety and the phenyl-ester chain on the right part of the conjugate bears the best affinity and inhibition activity similar to the ones of **1.15**. Furthermore, **3.34**, bearing the tris-thiazole coupled on the left side with methylpiperazine via an amide bond, showed one of the best inhibition activities while having a higher K_D value.

These results have provided essential insights into the structure-activity relationships of small molecules as binders of pre-miR-210. Indeed, **3.26b** and **3.34** were the best compounds in terms of affinity and activity, highlighting the importance of the methylpiperazine motif positioned at the left side of the molecule and of the phenyl-ester lateral chain previously identified in the results presented in Chapter II. Compounds with better affinity than the first hit **1.15** were designed, and IC_{50}s in the same range were obtained. While some compounds showed promising activity, there were clear limitations in selectivity and functional group suitability. The collected data also highlighted the complexity of designing small molecules that are both active and selective, and the best ligands and inhibitors appear to lack selectivity. The following work focused on optimizing these compounds, considering the nuanced effects of different moieties and functional groups on affinity and activity, together with combining the best motifs outlined.

III.4 Synthesis of the second series of compounds

The previous section provided an *in vitro* analysis of the first series of novel mono-substituted tris-thiazole small molecules designed to bind pre-miR-210 and the comparison with bis-thiazole compounds. This initial assessment revealed quite complex structure-

activity relationships, where small changes in the structures led to significant variations in K_D or IC_{50} values, together with variations in selectivity. Among the compounds evaluated, compound **3.26b** stood out for its promising results, showing a favorable IC_{50} value of 3.31 μM that correlated well with a high affinity for the pre-miR-210, with a K_D of 120 nM and we thus chose this compound as the starting hit to be optimized.

Given these encouraging findings, our next step was clear: we focused on hit compound **3.26b** and further functionalized it with several motifs on the free amine, as shown in ***Figure 37***. Concentrating on compound **3.26b** and its new derivatives, we aimed to build on what we have learned so far and take a significant step toward developing a more effective molecule for inhibiting miR-210 maturation. It was first decided to take advantage of our previous results, which highlighted the methylpiperazine as an adequate motif of pre-miR-210, and then to add several other heterocycles. In this context, we selected some heteroaromatic motifs from the first series and new ones, such as benzothiazole, naphthyridine, quinoxaline, methylpyrazine, pyridine, and thiophene motifs, all of which were previously identified in other selective RNA ligands.

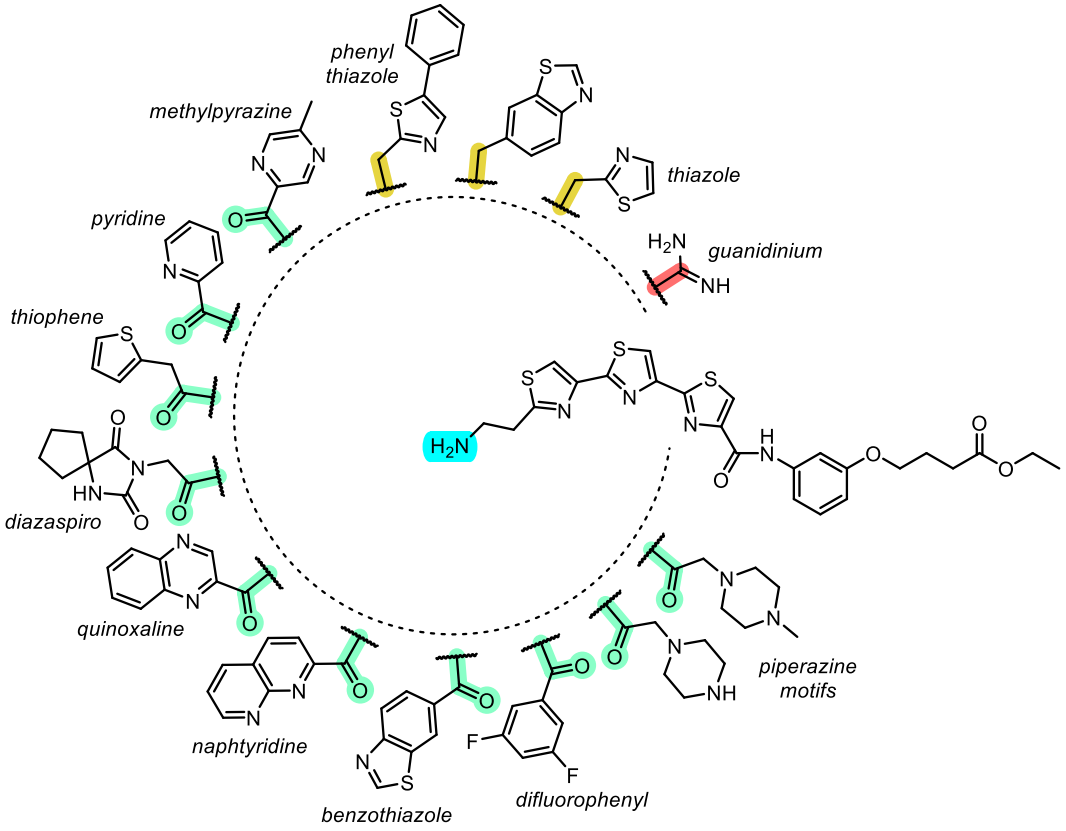

Figure 37 *- Chemical structure of the new disubstituted tris-thiazole analogs.*

The naphthyridine motif has been described for its ability to selectively interact with guanines *via* hydrogen bonds (see ***Figure 38A***) [308]. Then, a quinoxaline ring was selected after its recent discovery as an RNA sequence binder[309]. Hence, the pyridine ring was chosen for its recently highlighted role in RNA nucleobase recognition in double-stranded RNA[310]. The other rings were selected for the presence of heteroatoms that might form H-bonds with RNA sequences. Hence, two more different substituents were introduced, the diazaspiro[4.4]nonane-2,4-dione and the difluorobenzene. The first was selected to build a non-planar compound while forming new hydrophobic interactions with the target pre-miR sequence. Then, the difluorobenzene motif was chosen for the known role of fluorine in forming interactions with RNA nucleobases. Furthermore, more polar functions, such as the addition of a guanidinium group, were chosen to enhance affinity through strong electrostatic interactions or more specific interactions with unpaired bases (see ***Figure 38A***)[120,122,126,311]. The introduction of this very polar motif was also correlated with its renowned role in forming interactions with RNA sequences[312,313]. These motifs were all introduced using classical coupling conditions (in green, ***Figure 37***) but started to lead to compounds with solubility and purification problems. As a result, we decided to switch from the amide linkage function to a secondary amine upon reductive amination reaction (in orange, ***Figure 37***).

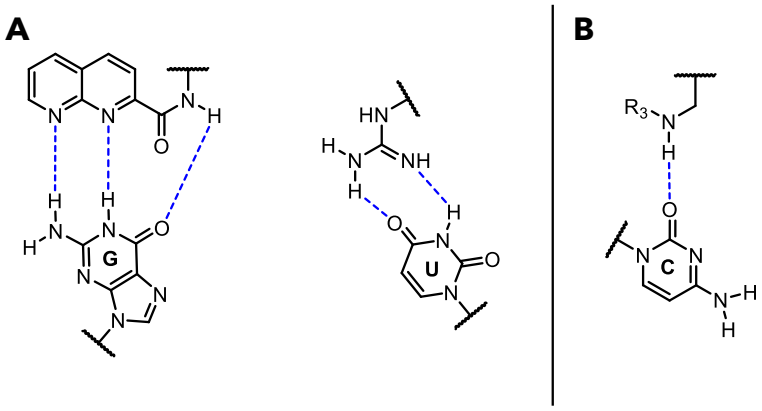

Figure 38 *– Possible interactions between nucleobases and: A) naphthyridine and guanidine motifs, B) amine linkage functions.*

The reductive amination reaction forms a C-N bond, resulting in secondary or tertiary amines. These amines are of interest for forming non-covalent bonds with biological targets, are favorable for solubility, and are particularly useful for interactions with RNA nucleobases (see ***Figure 38B***). The small set of selected motifs was chosen to understand if another thiazole could trigger more affinity. Also, introducing a thiazole allowed us to evaluate the benefit of using benzo-heterocycles instead of simple heterocycles. Therefore, we decided to follow the retrosynthetic approach shown in ***Scheme 16*** to prepare these new analogs of

3.26b. The previously mentioned conditions, using HATU as the coupling reagent, were used to form the required amide bond. For the reductive amination products, the selected aldehydes were used to react with the terminal amine of **3.26b**, followed by a reduction step using trichlorosilane. Lastly, for the guanylation of the terminal amine, a protected triflate derivative of guanidine was used. The following sections will describe extensively the reaction conditions, and the *in vitro* assessment of the newly generated analogs will also be detailed.

III.4.1 Synthesis of 2,4-disubstituted analogs of **3.26b** – Amide linkage series

Building on the promising results obtained with compound **3.26b**, the next synthetic plan was directed toward its optimization. Specifically, we focused on preparing derivatives of **3.26b** by functionalizing its left part. The modification strategy chosen involved incorporating different motifs upon amide bond formation. Compound **3.26b** was used as a common precursor to prepare new derivatives. The synthesis of this compound, described in the previous section, was repeated on the gram scale (≈ 6g) to afford the precursor in a large amount for further functionalization. With a stock of **3.26b** in our hand, we performed couplings with several commercially available carboxylic acids. Given the good yields for coupling reactions obtained previously with HATU, we chose this coupling reagent for this series. As a result, 10 new and original compounds were synthesized, with yields ranging from 40 to 96% (***Scheme 17***). Firstly, 2-(4-methylpiperazin-1-yl)acetic acid was used to prepare **3.42** with an excellent 96% yield. Then, 4-(tert-butoxycarbonyl)piperazine-1-carboxylic acid was used to reach compound **3.43a** with a 45% yield. Problems with the purification process, which requested a highly polar solvent mixture of DCM and EtOH to obtain the pure fraction, led to this moderate yield of 45%, the rest being impure fractions. A cleavage step using a 4M HCl solution in 1,4-dioxane was required to reach **3.43b** in quantitative yield. In a second choice, various chemical motifs containing heteroaromatic rings were coupled to **3.26b**. Compound **3.44** bearing the benzothiazole ring was prepared with benzo[*d*]thiazole-6-carboxylic acid in 40% yield. Then **3.45** was afforded using 1,8-naphthyridine-2-carboxylic acid in 71%. The quinoxaline ring compound **3.46** was

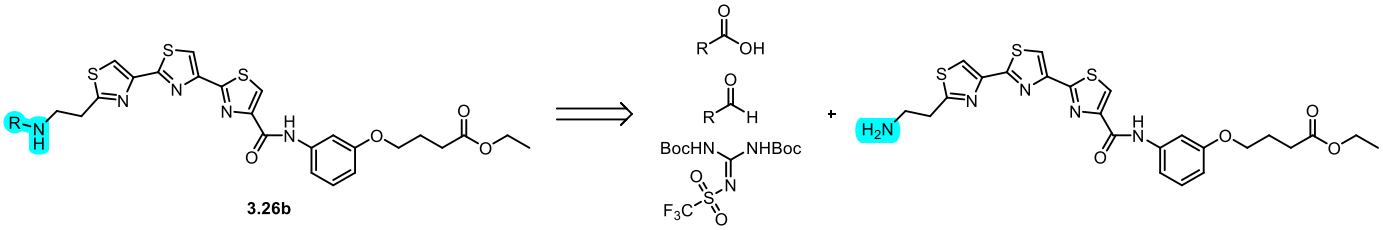

Scheme 16 – *Retrosynthetic approach for the design of new analogs of* ***3.26b***.

obtained with a 45% after coupling with quinoxaline-2-carboxylic acid, and **3.47** with the methylpyrazine ring was afforded in 70% yield, using 5-methylpyrazine-2-carboxylic acid. Picolinic acid and 2-(thiophen-2-yl)acetic acid ring led to compounds **3.48** and **3.49** in 48% and 66% yield, respectively. The same purification issues encountered in the synthesis of **3.43a** are also responsible for the slightly low yields obtained in this series.

Two other carboxylic acids were also selected for further functionalization, one being the 2-(2,4-Dioxo-1,3-diazaspiro[4.4]nonan-3-yl)acetic acid, affording **3.50** in 80% yield. The other one was 3,5-difluorobenzoic acid, which led to **3.51** in 71% yield.

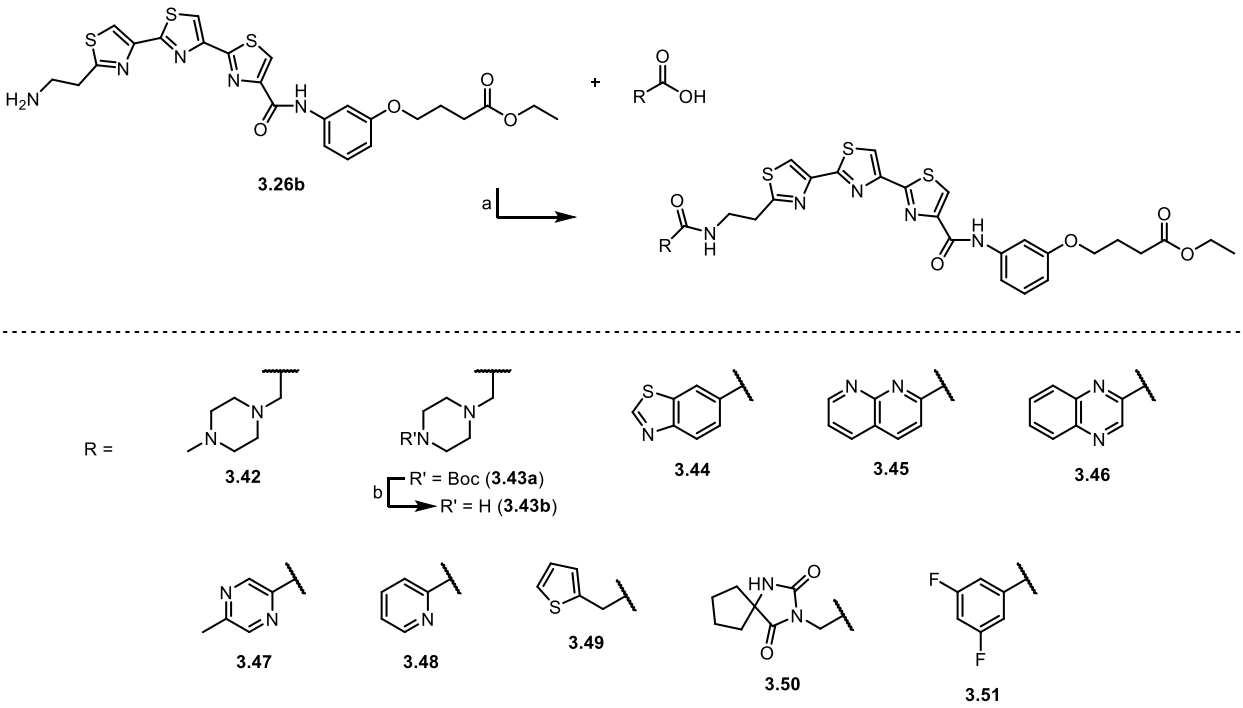

Scheme 17 *- Reagents, conditions, and yields: (a) carboxylic acid, HATU, DIPEA, DMF, rt, until completion, 96% (**3.42**) / 45% (**3.43a**) / 40% (**3.44**) / 71% (**3.45**) / 45% (**3.46**) / 70% (**3.47**) / 48% (**3.48**) / 66% (**3.49**) / 80% (**3.50**) / 71% (**3.51**); (b) 4M HCl in 1,4-dioxane, rt, 30min, quantitative (**3.43b**).*

III.4.2 Synthesis of 2,4-disubstituted analogs of **3.26b** – Amine linkage series

After synthesizing a series of derivatives based on the coupling between **3.26b** and various carboxylic acids, the synthesis of the secondary amine products is described in the following section. Multiple reactions are described in the literature to form a C-N bond from a primary or secondary amine. Besides classic nucleophilic substitution, the Aza-Michael reaction can be cited as an example. This reaction allows the addition of a Michael acceptor-type group, which are α-β unsaturated compounds with electron-withdrawing groups to an amine (Reaction A, ***Scheme 18***). Although effective, these reactions could lead to polysubstitution if primary amines are used. Mannich and Petasis' multicomponent reactions

are also options for functionalizing primary or secondary amines (Reaction B and C, ***Scheme 18***). The Mannich reaction allows the condensation of a non-enolizable aldehyde (usually formaldehyde), an amine, and a carbonyl compound in an acidic environment, resulting in β-aminoketones and β-aminoaldehydes. The Petasis reaction is a boronic version of the Mannich reaction involving an amine, a carbonyl, and a vinyl or aryl boronic acid.

Lastly, reductive amination also allows the substitution of primary or secondary amines in two steps (Reaction D, ***Scheme 18***). First, the reaction with a carbonyl compound (aldehyde or ketone) in an acidic environment forms an imine or iminium ion. Then, reducing this function leads to the formation of the secondary or tertiary amine. It's worth noting that the reduction of the imine or iminium function is much faster than the reduction of ketones or aldehydes, allowing this reaction to be carried out in a one-pot manner. In the field of synthetic organic chemistry, the process of reductive amination is a crucial process for creating secondary and tertiary amines. This method has become very popular in the synthesis of natural substances, essential drug components, and a variety of pharmaceuticals and agricultural chemicals[314,315]. Among all the reductive agents required to reduce imines, hydride-donor reagents such as sodium cyanoborohydride ($NaBH_3CN$) or sodium triacetoxyborohydride ($NaHB(OAc)_3$) remain the most widely used[316,317]. However, they both present two significant issues: sensitivity to protic solvents leading to an excess of reagents to be used and a reactivity with several functional groups that may be present in the molecule. Moreover, $NaBH_3CN$ is not acceptable in green chemistry because of the residual cyanide possibly present. To avoid such problems, Kobayashi *et* al. published the

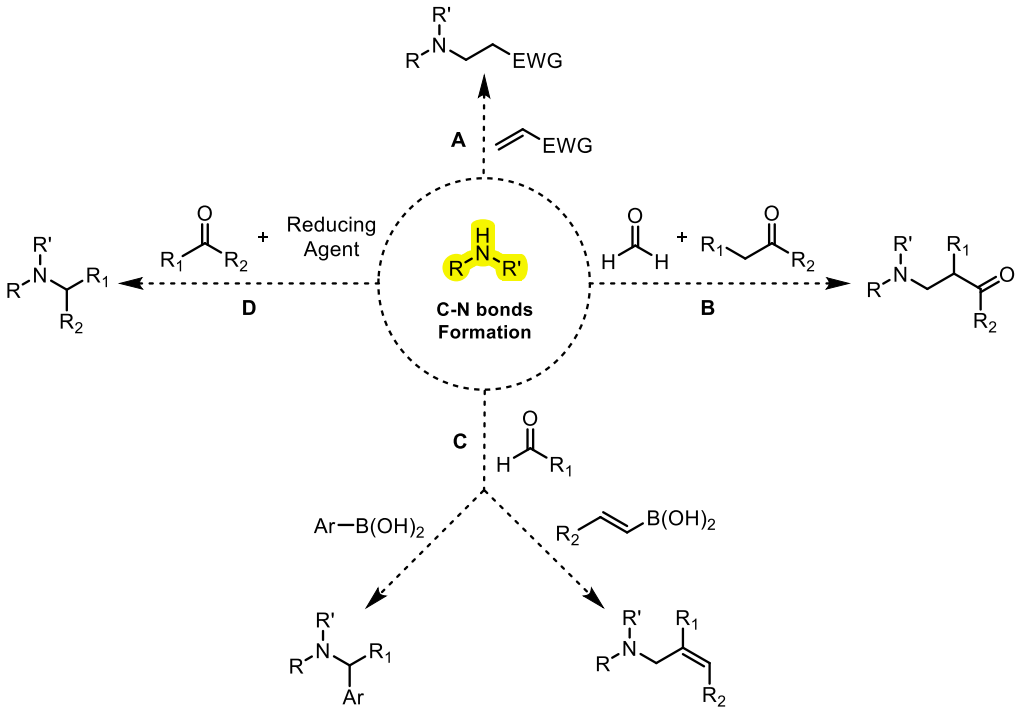

Scheme 18 *- Different synthetic strategies for the formation of C-N bonds.*

use of trichlorosilane to reduce aldehydes and imines[318]. Trichlorosilane is a cost-effective, widely available chemical often used as a raw material in the production of silicon chips. In their paper, Kobayashi and colleagues showed that a Lewis base is needed to activate the reagent for the reaction, probably acting as a catalyst. Thus, they used dimethylformamide (DMF), a low-cost solvent, to fulfill this role. Inspired by this work, Popov *et al.* showed how this method can perform reductive amination of aldehydes with amines using trichlorosilane catalyzed by DMF in toluene or DCM[319]. They produced compounds bearing potentially reducible functional groups such as ester, ketone, amide, nitro groups, nitriles, azide, double and triple bonds, and sulfonamides. All these motifs remained intact under these conditions.

Among all these options, we introduced functional groups *via* reductive amination based on Popov *et al.* work[319], thus relying on trichlorosilane as a reducing agent. The reaction between three commercially available aldehydes and **3.26b** was performed, affording compounds **3.52** to **3.54** with yields ranging from 32 to 52% (***Scheme 19***). Regarding the chosen groups, we opted for heteroaromatic motifs with benzothiazole, phenyl-thiazole, and thiazole. Benzo[*d*]thiazole-5-carbaldehyde allowed the formation of compound **3.52** in 52% yield. The 5-phenylthiazole-2-carbaldehyde afforded the derivative **3.53** in 38% yield. Lastly, **3.54** was obtained using thiazole-2-carbaldehyde, with a 32% yield.

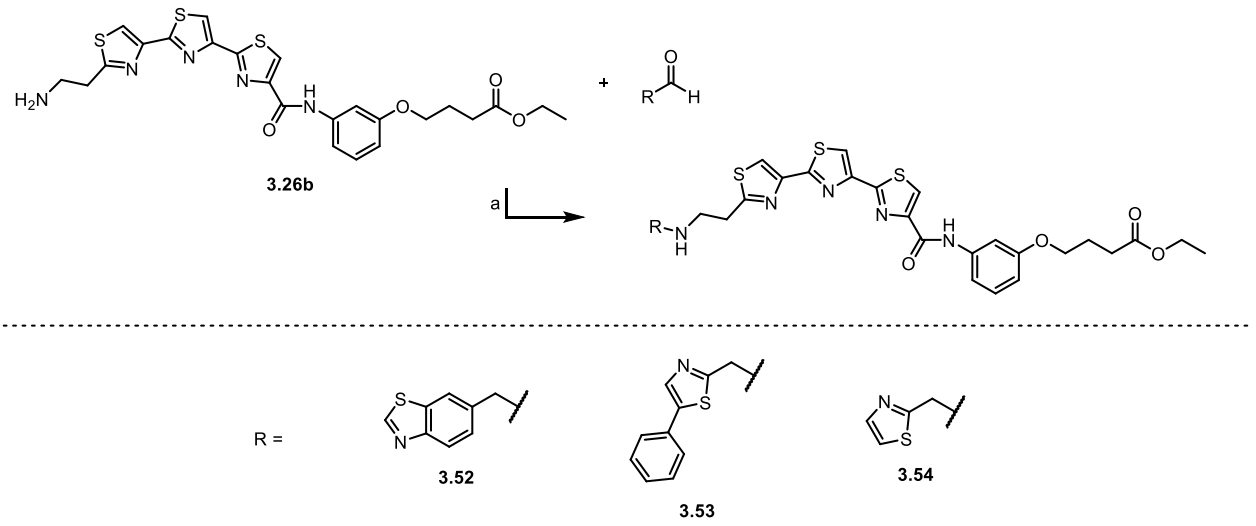

Scheme 19 *- Reagents, conditions, and yields: (a) aldehyde, $HSiCl_3$, molecular sieves 4Å, DMF, rt, until completion, 53% (**3.52**) / 38% (**3.53**) / 32% (**3.54**).*

III.4.3 Synthesis of 2,4-disubstituted analogs of **3.26b** – Guanylation

As the next functionalization step, we prepared compound **3.55b** (***Scheme 20***). To guanylate **3.26b**, commercial *N*,*N*'-di-Boc-guanidine triflate, in the presence of Et_3N, was

used to obtain molecule **3.55a** with a 97% yield[320]. This compound was then deprotected in the presence of HCl, resulting in compound **3.55b** with a 95% yield.

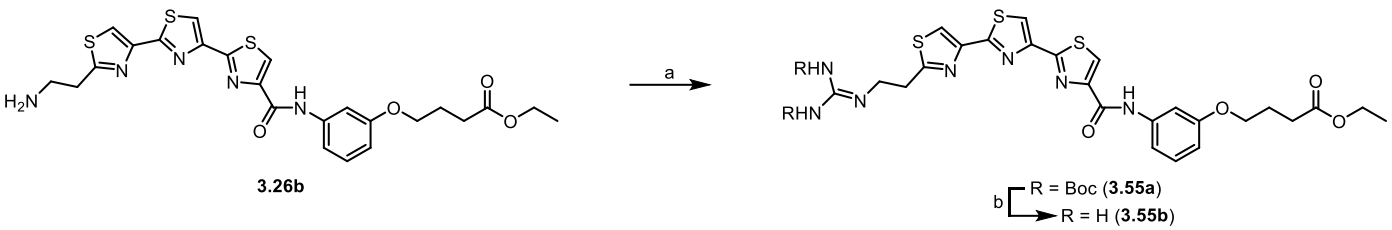

Scheme 20 *- Reagents, conditions, and yields: (a) 1,3-Di-Boc-2-(trifluoromethylsulfonyl)guanidine, Et_3N, DMF, rt, 16h, 97%; (b) 4M HCl in 1,4-dioxane, rt, 30min, 95%.*

III.5 In vitro biochemical evaluation of the second series of compounds and SAR study

Once this new molecule series was synthesized, *in vitro* analyses were conducted again. This involved evaluating the affinity constant (K_D) of the new analogs with pre-miR-210 and assessing their selectivity in the presence of nucleic acid competitors for the most affine binders. Subsequent IC_{50} studies were carried out for the molecules identified as the most promising in terms of affinity. The results are compiled in ***Table 12*** below.

Groups	Compounds	K_D (µM) - pre-miR-210	K'_D / K_D	K''_D / K_D
TGP-210	**1.15**	0.54 ± 0.02	0.8	1.6
Starting material	**3.26b**	0.12 ± 0.07	1.2	6
Amide-linker series	**3.42**	0.94 ± 0.17	0.6	0.8
	3.43b	0.71 ± 0.07	0.9	0.8
	3.44	> 1 mM	-	-
	3.45	11.7 ± 2.00	1.3	1.5
	3.46	> 1 mM	-	-
	3.47	> 1 mM	-	-
	3.48	> 1 mM	-	-
	3.49	> 1 mM	-	-
	3.50	> 1 mM	-	-
	3.51	> 1 mM	-	-

Table 12 *- K_D and K_D ratios in the presence of tRNA and DNA of **3.26** and analogs towards various pre-miR sequences.*

For this new series of **3.26b** analogs, only 3 compounds showed a K_D value below the maximum dose tested (1 mM). Compounds **3.42**, **3.43b**, and **3.45** exhibited K_D values ranging from 0.71 to 11.7 µM. Compounds **3.42** and **3.43b** showed an affinity slightly higher than their precursor **3.26b** (0.12 µM) with K_Ds of 0.94 and 0.71, respectively. However, **3.26b** lacked selectivity when used in the presence of an excess of tRNA and DNA, while both compounds **3.42** and **3.43b** restored it. Then, if we compare the two analogs, removing the methyl group on the piperazine motif seemed to moderately increase the affinity without affecting selectivity. The result of compound **3.45**, with a K_D of 11.7 µM, indicated that adding more heteroaromatic rings did not lead to a more affine analog. For the other analogs, an unexpected absence of affinity for pre-miR-210 was observed, at least not below 1 mM. Noteworthy, all the compounds were first solubilized in DMSO for the affinity assays, but then the serial dilutions of each of them were performed in Buffer A. Such dilutions could have led to precipitation or crystallization, not visible to the naked eye. This led us to look closely at the Log P values of the newly generated compounds to verify if any solubility issues could have increased K_D values due to less compound available for binding pre-miR-210 sequence. Indeed, compounds **3.44** to **3.51** showed very high calculated Log P values (using SwissADME models); thus, the higher the Log P, the lower the solubility in water. All the analogs, except **3.42** and **3.43b**, obtained Log P values ranging from 5 to 6.92. Even if showing a K_D below 1 mM, compound **3.45** solubility issues could have lowered its affinity.

We then switched to the *in vitro* testing of the analogs formed upon reductive amination and the guanylated analog. The results are shown in ***Table 13*** below.

Groups	Compounds	K_D (µM) – pre-miR-210	K'_D / K_D	K''_D / K_D
TGP-210	**1.15**	0.54 ± 0.02	0.8	1.6
Starting material	**3.26b**	0.12 ± 0.07	1.2	6
Amine-linker series	**3.52**	0.56*	0.8	1.5
	3.53	> 1 mM	-	-
	3.54	> 1 mM	-	-
Guanylated analog	**3.55b**	0.20 ± 0.05	1	1.6

Table 13 *- K_D and K_D ratios in the presence of tRNA and DNA of* ***3.26b*** *and analogs towards various pre-miR sequences. * Tested only once; error bar considered ± 10%.*

Herein, two compounds showed interesting results with a K_D of 0.56 µM for **3.52** and 202 nM for **3.55b**. The other two, **3.53** and **3.54**, did not exhibit any K_D values below the maximum dose tested of 1 mM. As expected, the results obtained with compounds **3.52** and **3.55b** suggested that introducing more polar motifs increased affinity. Compound **3.52**'s result, compared to **3.44**, with the amide linkage function, showed that reductive amination products can increase affinity while helping with solubility issues for big aromatic rings. Also, benzothiazole derivative **3.44** showed good selectivity towards pre-miR-210, while **3.55b** lost some when DNA was added to the assay. Still, compound **3.55b** showed the best result in terms of K_D for this second series of analogs, highlighting the importance of polar motifs for binding pre-miR-210. Compounds **3.53** and **3.54** showed an unexpected affinity profile, with no response observed even at 1 mM. Such data could have resulted from the aforementioned solubility issues or the confirmation that a fused phenyl-thiazole ring is needed for good interaction with the pre-miR-210 sequence.

After assessing the binding characteristics of the newly generated analogs, we explored their possible role as Dicer-processing inhibitors. Consequently, the compounds with the highest affinity, identified from the previously mentioned affinity and selectivity tests, were selected for IC_{50} studies. Results are compiled in ***Table 14***.

Groups	Compounds	K_D (µM) – pre-miR-210	IC_{50} (µM)
TGP-210	**1.15**	0.54 ± 0.02	2.91 ± 0.48
Starting material	**3.26b**	0.12 ± 0.07	3.31 ± 0.95
Amide-linker series	**3.42**	0.94 ± 0.17	2.25 ± 0.49
	3.43b	0.71 ± 0.07	3.01 ± 0.44
	3.45	11.7 ± 2.00	No inhibition
	3.46	> 1 mM	No inhibition
Amine-linker series	**3.52**	0.56*	No inhibition
	3.54	> 1 mM	No inhibition
Guanylated analog	**3.55b**	0.20 ± 0.05	2.31 ± 0.12

Table 14 *- K_D and IC_{50} values of **3.26b** and analogs towards various pre-miR sequences.*

In the evaluation of *in vitro* inhibition of miR-210 maturation, several significant observations were made. The reference compound **3.26b** already exhibited interesting inhibitory properties. However, testing of the three most affine compounds revealed them to be even more potent inhibitors, with IC_{50} values ranging from 2.25 to 3.01 µM. The

comparison between compounds **3.42** and **3.43b** showed that the removal of the methyl group from the piperazine motif did not substantially affect the activity, indicating a small level of flexibility in this part compared to our first series in which using unsubstituted piperazine translated into a loss of activity. Parallelly, the guanylation of the terminal amine of **3.26b** led to the synthesis of compound **3.55b**. This compound emerged as an excellent inhibitor, with an IC_{50} of 2.31 µM, further broadening the series of potentially effective inhibitors.

These findings have successfully highlighted three promising candidates for further *in cellulo* assays. The consistent inhibitory activity, correlated with good affinity and selectivity patterns, displayed by these compounds marked them as significant for further exploration of their role in a cellular context.

III.6 Preliminary conclusions

The collected data provided a comprehensive overview of the evaluation and analysis of various compounds for their affinity for pre-miR-210 and their inhibitory activity against miR-210 maturation. Firstly, a series based on a small set of mono-derivatized tris-thiazole compounds of the precursors **3.15a** and **3.16** was prepared. *In vitro* evaluation towards pre-miR-210 revealed **3.26b** and **3.34** as the best analogs in terms of affinity and activity, outlining the significance of the left-positioned methyl piperazine motif and the phenyl-ester lateral chain (identified in Chapter II) for good interaction with the target. Despite designing compounds with enhanced affinity compared to the initial hit **1.15**, and achieving comparable IC_{50}s, challenges in selectivity and functional group suitability remained yet to be solved. Testing these first series of compounds showed that **3.26b** was the most active analog and thus led to the synthesis of new analogs of this latter.

Three affine compounds have been identified among the newly synthesized **3.26b** analogs: **3.42**, **3.43b**, and **3.55b**. They exhibited potent inhibitory activity with IC_{50} values ranging from 2.25 to 3.01 µM. This highlighted their potential as effective inhibitors of miR-210 maturation. The key chemical modifications that contributed to the activity include the guanylation of the terminal amine. At the same time, removing the methyl from the piperazine motif was found to be non-essential for maintaining activity. These insights into the compounds' affinity, selectivity, and activity served as a solid foundation for the following stages of the project. The identified compounds will undergo further in-depth analysis and testing, focusing on their toxicity towards different cancer cell lines and the actual *in cellulo*

inhibition of miR-210 to ascertain their true potential as therapeutic agents regulating miR-210 maturation.

III.7 Biological evaluation of miR-210 inhibition

The literature review found in Chapter I has made it clear that miR-210 and its precursors are important biological targets. The results described in Chapter II and above show the possibility of creating new pre-miR-210 binders with great *in vitro* affinity and selectivity. The following section will focus on assessing the newly synthesized analogs in a cellular context. First, a suitable biological system for testing the compounds will be set up. Then, molecular biology techniques will allow us to evaluate the role of our compounds on the expression of miR-210 and its related target genes.

III.7.1 Overexpression of miR-210: mimicking hypoxic conditions

As widely detailed in Chapter I, the microRNA-210 is also called the *hypoxamiR* outlining its role in hypoxic-related diseases. Before examining a compound's ability to functionally affect a cellular system, it is necessary to set up a suitable cellular model. Herein, we had to find good conditions to trigger hypoxia in our cancer cell lines. As mentioned in Section II.2.3 of Chapter II, we were able to induce hypoxic conditions in triple-negative breast cancer cell lines MDA-MB-231 by using $CoCl_2$, a renowned compound used to mimic the low levels of oxygen in cell culture by inhibiting hypoxia-inducible factors (HIFs) degradation thus activating the transcription of hypoxia-related genes. Our preliminary Western Blot analysis, presented in Chapter II, showed that $CoCl_2$ effectively upregulated HIF-1α in MDA-MB-231 cells, leading to the first conclusion that it could be used for further analysis. HIF-1α, after being upregulated by hypoxic conditions, has different roles (***Figure 39A***). One is inducing the expression of several genes (e.g., *CA9*, *BNIP3*), and another is enhancing miR-210 expression. Then, miR-210 initiates a positive feedback loop where indirect HIF-1α stabilization increases its expression (***Figure 39A***).

To have a clearer picture of the efficacy of $CoCl_2$, we decided to perform real-time quantitative polymerase chain reaction (RT-qPCR) analyses to check the levels of a renowned hypoxia marker: the carbonic anhydrase 9 (CA9). HIF-1α regulates several gene expressions by binding to their promoters; in this context, one of its best-characterized targets is CA9.

Accordingly, HIF-1α and CA9 are the most consistently upregulated molecules in hypoxia-related diseases, and their role as biomarkers has been extensively reviewed in the literature[321–325]. Even if mentioned in several published works[326–328], we decided to verify that using $CoCl_2$ in our cellular model would trigger an upregulation of *CA9* mRNA (*CA9*) levels. Two cancer cell lines were chosen: the triple-breast cancer MDA-MB-231 line and the melanoma A375 cell line. The first one had already been confirmed as suitable in our previous study (Section II.2.3, Chapter II), and the second was selected to have a control cell line. Both cells were treated with 200 µM of $CoCl_2$ using a freshly prepared solution in water. After 24 hours, total RNA was extracted with miRNeasy Mini™ kit and reverse-transcribed using SuperScript™ VILO Master Mix following the manufacturer's instructions. The results, shown in ***Figure 39C*** and ***39D***, clearly indicated that treating both cell lines with $CoCl_2$ led to an increase in *CA9* levels. However, in MDA-MB-231 cells, *CA9* level is increased by 3-fold (***Figure 39C***), while in A375, the levels of the gene are increased by more than 20-fold (***Figure 39D***). These data indicated a significant response to hypoxic conditions from the melanoma cells (A375) compared to cancer cells (MDA-MB-231).

Thanks to the results of our collaborators in the United Kingdom (Dr. Francesco Crea), we could perform a comparison analysis between A375 cells grown in a hypoxia chamber, an incubator for cell culture with only 1% of O_2, and A375 cells where hypoxic conditions are mimicked with $CoCl_2$ (***Figure 39B***). As a result, we could highlight that the hypoxia chamber and $CoCl_2$ triggered the same effect on levels of *CA9*, with a 20-fold increase in expression compared to vehicle. However, $CoCl_2$ only requested 24h to obtain the same level of *CA9* expression compared to 48h in the hypoxia chamber. Indeed, our cellular model where hypoxic conditions were mimicked with $CoCl_2$ was thus well established and ready for further analysis of our newly generated compounds.

As a result, we had two suitable cancer cell lines for our study in our hands. We thus decided to perform RT-qPCR analysis to assess the levels of miR-210 and its precursors in both cell lines in normoxic or hypoxic conditions. To achieve such a study, cells were treated with 200 µM of $CoCl_2$ for 24 hours. RNA was extracted following the abovementioned conditions, except for evaluating mature miR levels. Because of their tiny size, detecting miRs by PCR remains a technical challenge and cannot be reached with classical conditions. A precise and sensitive approach has been developed by Lunn *et al.* called the miRCURY™ LNA microRNA PCR system[329]. This new system allows for the polyadenylation of miRs together with reverse transcription affording cDNA, and then PCR reaction is carried out with the help of locked nucleic acids (LNA™). LNAs increase the affinity of oligonucleotides towards their complementary cDNA target. From the results shown in ***Figure 40***, we deduced that all the precursors and miR-210 were overexpressed in both cell lines under

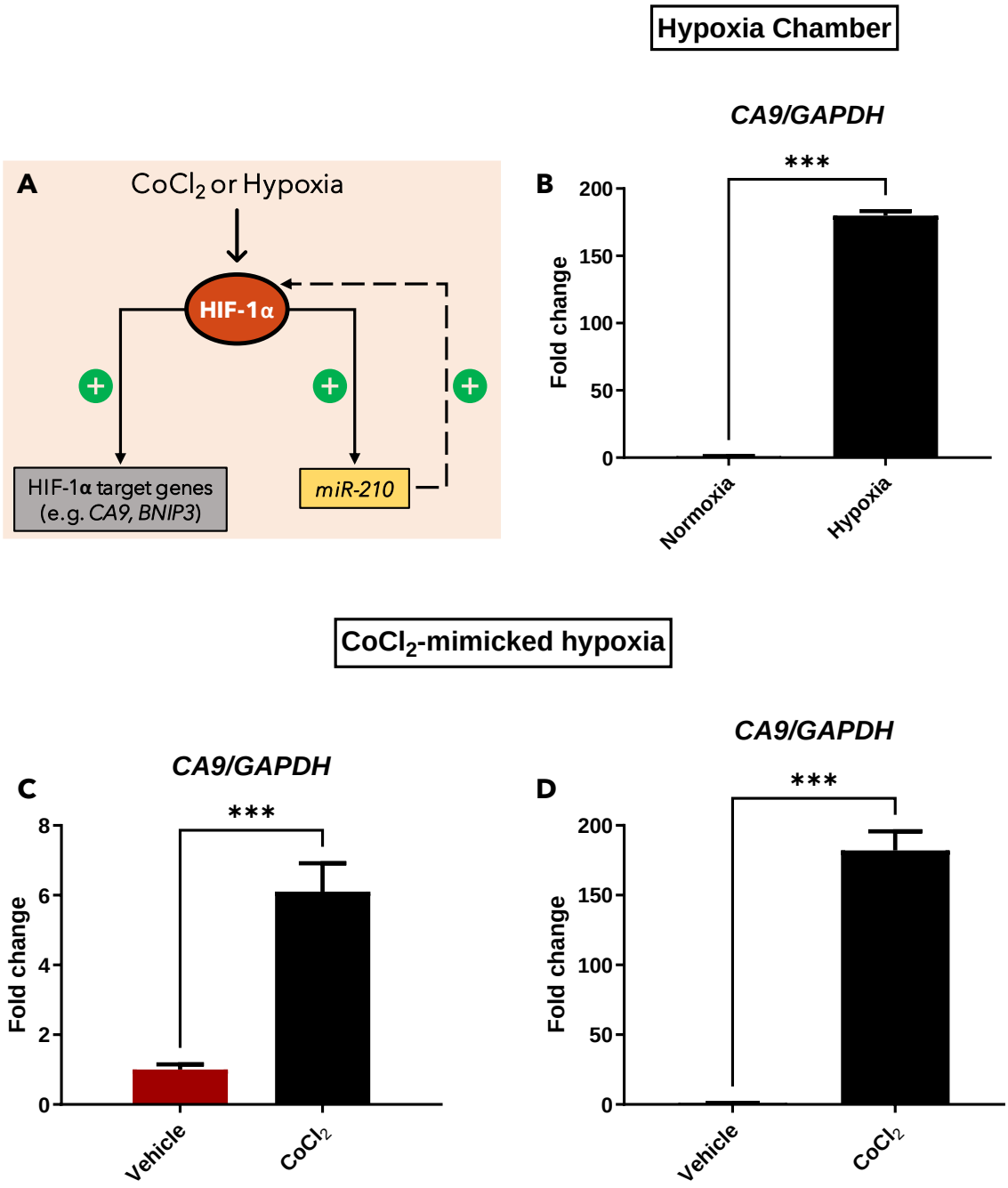

Figure 39 *– (A) Schematic of miR-210 feedback on HIF-1α under hypoxic conditions. (B) The expression of the hypoxia-inducible gene, CA9, was evaluated by RT-qPCR in A375 cancer cells grown in normal conditions or in hypoxia chamber for 48h. GAPDH was used for normalization. The expression of CA9 in normal condition was set to 1. Shown as mean ± SD, n≥2. ***p<0.001 hypoxia vs. normal condition, determined by a two-tails Student t-test. (C) MDA-MB-231 and (D) A375 cancer cells were treated for 24h with water (vehicle) or 200 µM of $CoCl_2$. Then, CA9 mRNA levels were evaluated by RT-qPCR using GAPDH for normalization. The value of water (vehicle) was set to 1. Data are reported as mean ± SD, n≥2.***p<0.001 $CoCl_2$ vs. vehicle, determined by a two-tails Student t-test.*

hypoxia. Then, if we focus first on pri-miR-210 (***Figure 40A***), the precursor of miR-210 in the nucleus, its levels were quite in the same range for both cell lines with approximately a 6-fold increase compared to vehicle. On the other hand, pre-miR-210 levels were evaluated (***Figure 40B***). In MDA-MB-231 cells, an increase of 10-fold was observed, while in A375 cells, this growth stopped at 3-fold. However, it must be noted that pre-miR levels study remains

complicated due to this precursor's very low transcriptional level, leading to low repeatability.

Mature miR-210 levels were also assessed. Pre-miR processing affords two arms of miR; however, only one usually leads to the functional mature miR. Herein, the 3p arm of miR-210 was studied due to its widely studied role in several diseases, including cancer, thus confirming its functional role[195,202,203,330]. In ***Figure 40C***, an evident overexpression of miR-210 has been observed under hypoxia in both cell lines. In A375, an increase in miR-210 by 7-fold could be observed, even if not significant, due to a low number of replicates. Whereas, in MDA-MB-231 cells, a moderate increase, by 2.8-fold, has been obtained. Collectively, these data again highlighted the potential of both cell lines for further study of new miR-210 inhibitors, with A375 cells that seemingly showed a higher response to hypoxic conditions regarding miR-210 and precursor expression. Also, we decided to do a literature review to see which of the two cell lines had already been studied in the context of miR-210.

Recently, Evangelista *et al.* identified miR-210 as a regulatory miR in different types of cancer while showing its specific role in MDA-MB-231 cells[331]. Many studies correlated miR-210 with MDA-MB-231 cancer cells[331–334], suggesting its essential role in the proliferation of this cell line. Increased levels of miR-210 and HIF-1α have also been previously observed in other breast cancer cell lines and tissues[335,336]. Hence, Disney and colleagues described the biological activity of their targapremiR-210 (**1.15**), which served as a benchmark compound for this study in the MDA-MB-231 cancer cell line[102]. For the A375 cell line, only one recent work by Spakova *et al.* evaluated miR-210 levels by showing that its silencing led to apoptosis[337], thus confirming the use of miR-210 inhibitors as innovative anticancer agents.

Our first PCR analysis and the literature review highlighted the MDA-MB-231 as an appropriate cellular model to study miR-210 inhibition by small molecules under hypoxic conditions. The large number of published works will thus be used as references for our study, and compound **1.15** will serve as a positive control (see Section II.2.3, Chapter II).

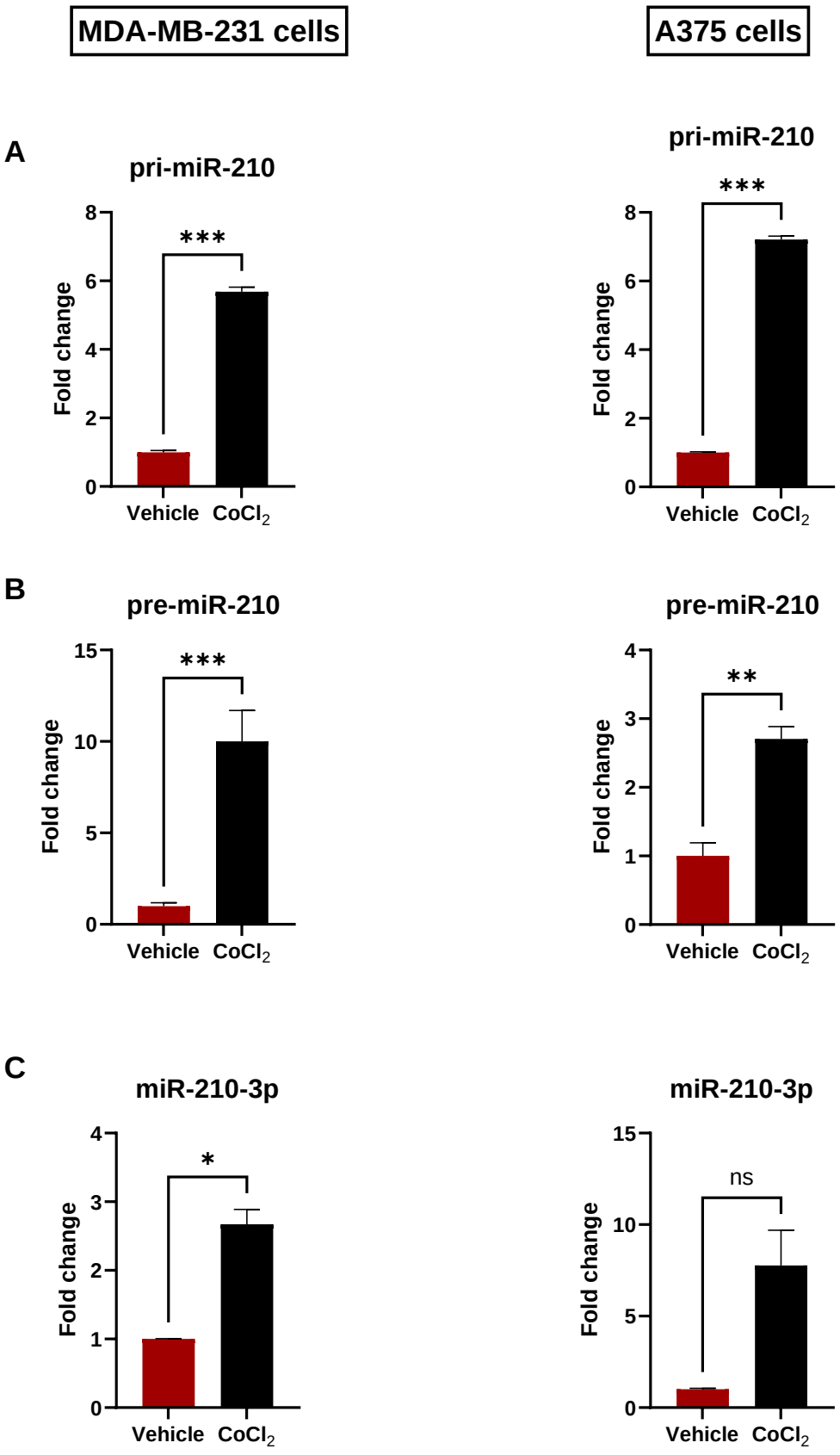

Figure 40 *- MDA-MB-231 and A375 cancer cells were treated for 24h with water (vehicle) or 200 µM of CoCl2. Then, pri-, pre-, and miR-210 levels were determined by RT-qPCR using GAPDH for normalization. The value of water (vehicle) was set to 1. Data are reported as mean ± SEM, n≥2. *p<0.05; **p<0.01;***p<0.001, $CoCl_2$ vs. vehicle, determined by a two-tails Student t-test.*

III.7.2 Toxicity profile of the lead compounds

In agreement with our *in vitro* results, we evaluated the biological activity of the best newly generated compounds. Firstly, we decided to assess the toxicity of our best analogs, including the most active ones (**3.42**, **3.43b**, and **3.55b**) *in vitro* and their common precursor, **3.26b**, towards MDA-MB-231 cells. The compounds were screened at 30 µM and 10 µM. The idea was to exclude any too-highly toxic compounds since too-high toxicity would probably mean targeting biological off-targets and antiproliferative activity towards healthy cells. By looking at ***Figure 41A***, the non-antiproliferative activity of compounds **1.15**, **3.26b**, and **3.55b** at 10 µM could be assessed. Then, **3.42** showed very little antiproliferative activity both in normoxia or hypoxia, with a percentage of living cells after treatment of around 85%. The most toxic compound was **3.43b**, which exhibited a reduction in the rate of living cells by 33% in normoxia and 52% in hypoxic conditions. Hence, only **3.43b** showed a statistically significant higher anti-proliferative activity under hypoxic conditions. This data suggested the correlation between **3.43b** biological function and the hypoxic circuit. ***Figure 41B*** shows the results after 48h of 30 µM treatment. Compound **1.15** started to have an antiproliferative activity, with a reduction of 13% of live cells in normoxia and 30% under hypoxia. This activity seemed to be linked with the hypoxic response of MDA-MB-231 cells since it increased in co-treatment with $CoCl_2$. **3.26b** and **3.55b** kept their very little toxicity, with 80% of cells still alive after 48h; surprisingly, **3.55b** showed even greater activity in normal conditions. On the other hand, compounds **3.42** and **3.43b** exhibited extremely high toxicity by killing all the population of cancer cells after 48h. These results confirmed that the best *in vitro* inhibitors would have to be used at 10 µM and not at higher concentrations due to high toxicity profiles, except for **3.55b**. However, even if the

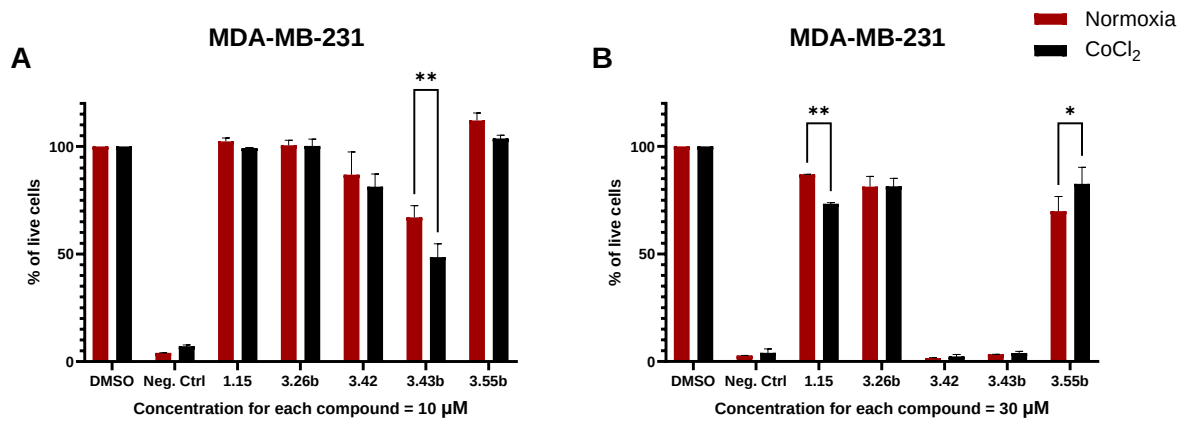

Figure 41 *– MDA-MB-231 Cell viability assay. Cells were treated with 10 µM (A) or 30 µM (B) of the indicated compounds or vehicle (DMSO) in presence of $CoCl_2$ ($CoCl_2$) or DMSO (Normoxia) Percentage of live cells after treatment has been determined with CyQUANT proliferation assay. Data are reported as mean ± SD, n≥2. *p<0.05; **p<0.01, $CoCl_2$ vs. normoxia, determined by two-way ANOVA with Šídák post hoc test.*

desired target, miR-210, is technically only overexpressed under hypoxic conditions, no clear link between toxicity and hypoxia could be deduced.

As a result, a suitable cellular model was validated, with MDA-MB-231 cancer cells treated with 200 µM of $CoCl_2$ to mimic hypoxic conditions perfectly. Also, we identified the maximum dose at which the small molecules might be tested to avoid off-targeting, which is to say 10 µM. We also decided to pursue the evaluation with **3.42** and **3.55b** since **3.43b** was already showing a high antiproliferative activity at 10 µM.

III.7.3 Cellular responses of the lead compounds

Given the abovementioned results, we studied the cellular mechanisms affected by our two lead analogs, **3.42** and **3.55b**. Reference hit compound **1.15** was also used as a positive control. Our first study was directed at assessing the effect of those compounds on *CA9* levels to evaluate their role in reverting $CoCl_2$-mediated HIF-1α transcriptional activity in MDA-MB-231 cancer cells. The results have been compiled in ***Figure 42A***; compound **3.42** significantly reduced (2-fold) the overexpression of *CA9* after 24h, showing a reversion of the hypoxic response in MDA-MB-231 cells. Hence, reference compound **1.15** did not

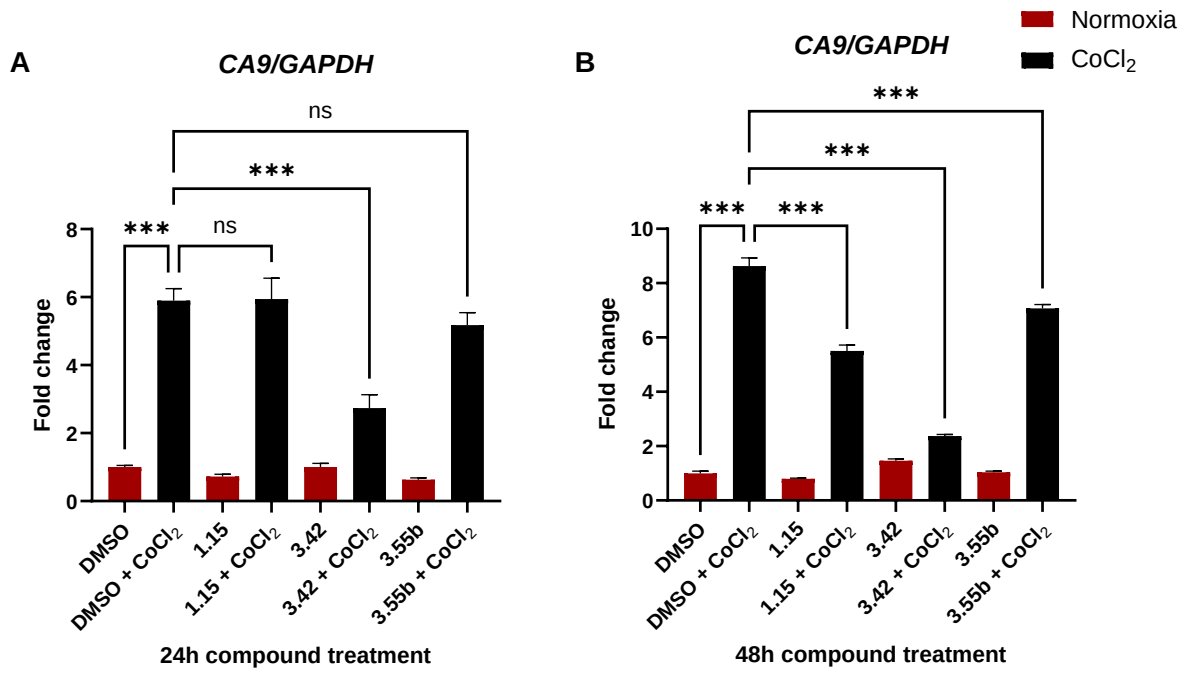

Figure 42 *– CA9 levels evaluation after 24 or 48 hours of treatment. (A) MDA-MB-231 cancer cells were treated for 24h with 10 µM of compounds or vehicle (DMSO) in presence of 200 µM of $CoCl_2$ ($CoCl_2$) or DMSO (normoxia). (B) MDA-MB-231 cancer cells were treated first for 24h with DMSO (vehicle) or 10 µM of compounds, then for another 24h with 10 µM of compounds or vehicle (DMSO) in presence of 200 µM of $CoCl_2$ or DMSO (normoxia). CA9 mRNA levels were determined by RT-qPCR using GAPDH for normalization. The value of DMSO (vehicle) in normoxia was set to 1. Data are reported as mean ± SEM, n≥2. ***p<0.001, determined by one-way ANOVA with Tukey post hoc test.*

affect *CA9* levels, and **3.55b** started to exhibit a reversion pattern yet insignificant. These first exciting results confirmed the role of **3.42** in the hypoxic circuit in breast cancer cells. However, to further validate the function of our analog, we wanted to observe an effect from **1.15** to compare their efficacy. To reach this goal, we decided to go from 24 hours of treatment to 48 hours while conserving 24 hours of $CoCl_2$ treatment. Cells were thus pre-treated with 24h of compound solution only. Then, for the next 24 hours, both the compound and $CoCl_2$ solution were inserted into the cell medium. We hypothesized that this pre-treatment would give the required time for the compound to reach and bind its target, while $CoCl_2$ activity had already been shown to be effective after only 24 hours (see Section III.3.1, Chapter III). As demonstrated in ***Figure 42B***, pre-treatment led to a reversion activity of all three compounds. **3.26b** conserved its excellent ability to revert *CA9* expression with a 4-fold reduction this time. Hence, **1.15** showed a statistically significant 1.6-fold reduction in hypoxia-induced *CA9* levels, and **3.55b** a 1.2-fold reduction. As a result, the three compounds tested showed a reversion activity on breast cancer cells' hypoxic response, **3.26b** being the most active compound. These promising results led us to further characterize compound **3.26b** activity towards mature miR-210 and other downstream cellular targets, together with evaluating the levels of upstream precursors of miR-210.

Consequently, we evaluated by RT-qPCR the pri- and pre-miR-210 expression levels, together with mature miR-210-3p levels. To find a second downstream gene to look at, we decided to assess the levels of the hypoxia-induced *BNIP3* (Bcl-2 19 kDa Interacting Protein) gene. Its expression can be induced by hypoxic conditions through transcriptional control by HIF-1α; several works have correlated the overexpression of BNIP3 protein in tumors with a pro-apoptotic activity[338–340]. The expression of BNIP3 was found to be increased in the areas close to necrosis, commonly observed in solid tumors[341]. These observations were consistent with an up-regulation of the HIF-1α complex transcriptional pathway. However, this was somewhat surprising as this protein typically promotes apoptosis and fights against tumor activities[339]. It is now being considered that the early increase of BNIP3 in low-oxygen conditions may choose clones within the hypoxic region that resist apoptosis[342]. This could lead to the development of more aggressive cancer types in later stages[342]. We thus selected *BNIP3* as a good marker of the hypoxic response in MDA-MB-231 cancer cells, as also outlined by Bando *et al*[343].

This new round of PCR results is shown in ***Figure 43***, where **3.42** significantly reverted the overexpression of pri- and pre-miR-210 (***Figure 43A*** and ***43B***) under $CoCl_2$-induced hypoxic conditions. Hence, levels of mature miR-210 were evaluated, and its maturation was inhibited with a 2.5-fold reversion in miR expression (***Figure 43C***). In

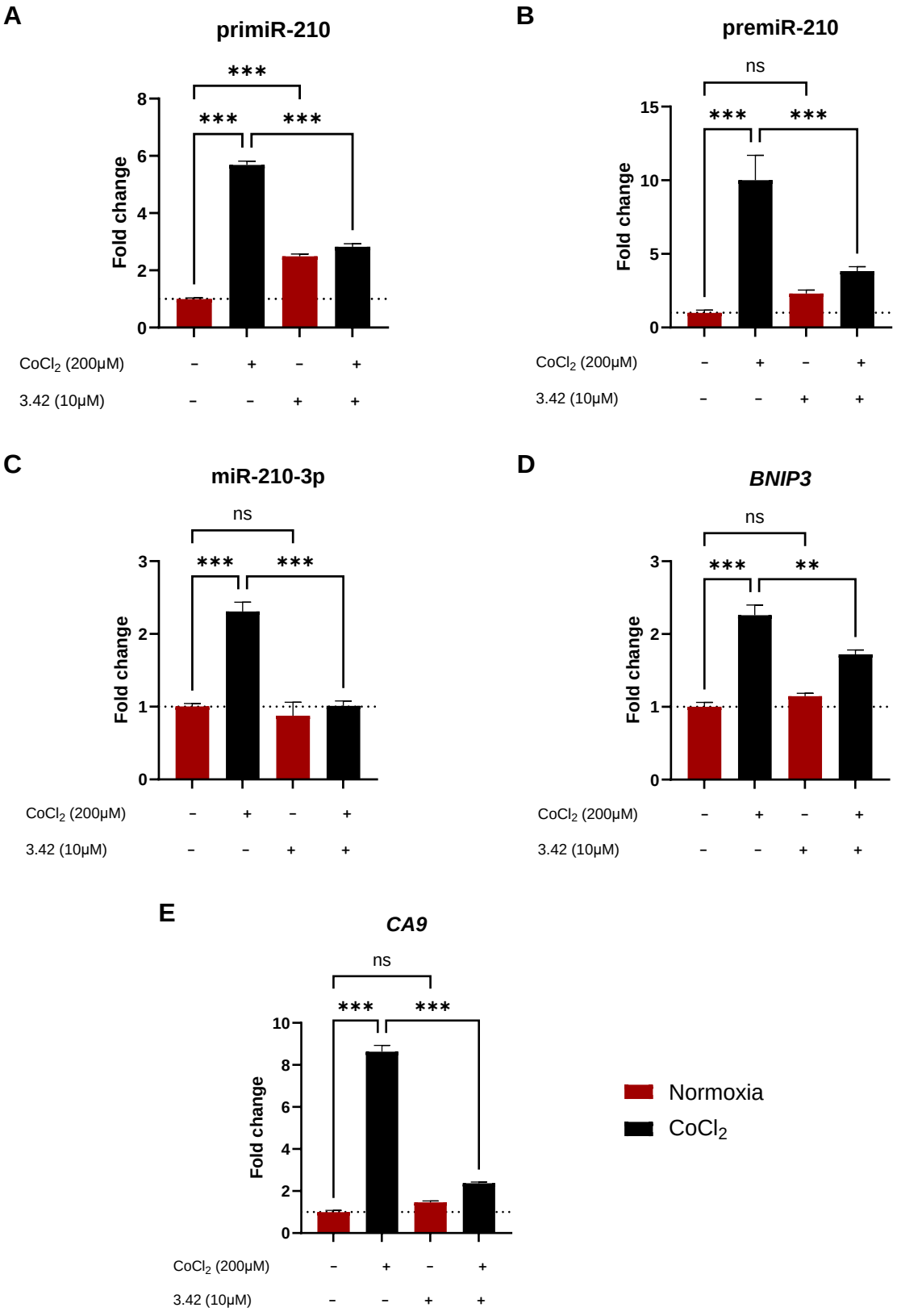

Figure 43 *– miR-210 inhibitor,* ***3.42****, reverts $CoCl_2$-mediated HIF-1α transcriptional activity in breast cancer cells. (A-E) MDA-MB-231 cancer cells were treated first for 24h with DMSO (vehicle) or 10 µM of compounds, then for another 24h with 10 µM of compounds or vehicle (DMSO) in presence of 200 µM of $CoCl_2$ ($CoCl_2$) or DMSO (normoxia). Pri-, pre-, miR-210, BNIP3, and CA9 levels were determined by RT-qPCR using GAPDH for normalization. The value of DMSO (vehicle) in normoxia was set to 1. Data are reported as mean ± SEM, n≥2. **p<0.01;***p<0.001, determined by one-way ANOVA with Tukey post hoc test.*

agreement with the scheme shown in ***Figure 39A***, a reduction in miR-210 expression may induce a negative feedback on its own precursors (pr-miR-210 and pre-miR-210) and could lead to an indirect transcriptional silencing effect on pri- and thus on pre-miR-210 levels. These results proved that **3.42**'s mode of action is inhibition of miR-210 biogenesis. Noteworthy, in normal oxygen levels, **3.42** slightly reduced the maturation levels of miR-210 while inducing an unexpectedly small induction of pri- and pre-miR-210, probably due to the accumulation of these latter since no transcriptional feedback from mature miR-210 is happening under normoxia.

In ***Figure 43D*** and ***43E***, the downstream effects of the reversion of the hypoxic response from **3.42** are shown. **3.42** reduced significantly *CA9* and *BNIP3 levels* by 4-fold and 1.5-fold, respectively. This regulation happened without any interference in normoxia, further confirming the reversion of the hypoxic response of MD-MB-231 cancer cells.

With these excellent results, we decided to perform a dose-response PCR analysis to correlate an increasing concentration of **3.42** with an increasing reversion in the abovementioned markers. The results are compiled in ***Figure 44***; we decided to evaluate the levels of pri-miR-210 and mature miR-210 levels, together with *CA9* assessment. This time, cells were pre-treated with an increasing concentration of **3.42** for 24 hours, from 2.5 to 10 µM. Then, for another 24 hours, the cells were exposed to the same range of concentrations of **3.42** and 200 µM of $CoCl_2$. In ***Figure 44A*** and ***44C***, the results on pri- and miR-210 are shown, and a statistically significant decrease in their levels was linked to an increasing concentration of **3.42**. However, pri-miR-210 levels are significantly reduced with only 2.5 µM of the compound, while mature miR-210 needed 10 µM to reach complete maturation reversion. The same trend was observed with *CA9* levels (***Figure 44B***), with a reversion effect of **3.42** already significant at 2.5 µM. These results confirmed the inhibitory activity of **3.42** towards mature miR-210 levels and the reversion of its downstream targets. The results on miR-210 fold change were then fitted on a graph, and a dose-response curve allowed us to obtain an *in cellulo* IC_{50} value of 4.04 µM (***Figure 44D***). This value was compared to the previously obtained *in-vitro* IC_{50} value of 2.25 µM, and an expected slight increase in its value was observed since cellular contexts are more complex and the probability for the compound to reach its target efficiently is lower than *in vitro*. Hence, following this array of experiments, we focused our attention on immunoblot assays to first confirm the post-translational effects of **3.42** on HIF-1α protein levels and then to verify its connection to the MYC/MAX pathway, as explained in Section I.2.4, Chapter I.

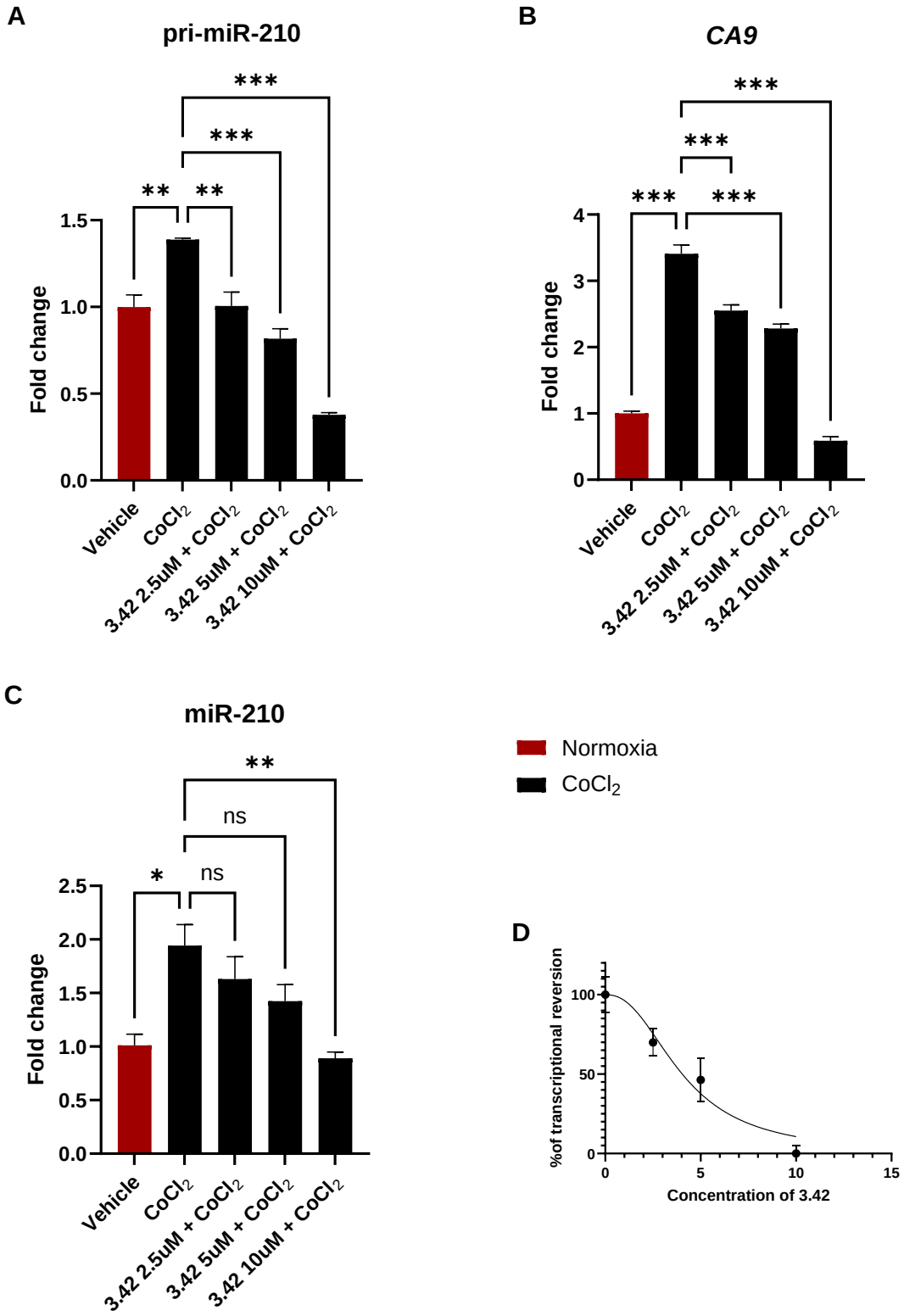

Figure 44 *– Dose-response effects of* ***3.42*** *in breast cancer cells. (A-C) MDA-MB-231 cancer cells were treated first for 24h with DMSO (vehicle) or 2.5, 5, and 10 μM of compound, then for another 24h with 2.5, 5, and 10 μM of compounds or vehicle (DMSO) in presence of 200 μM of $CoCl_2$ ($CoCl_2$) or DMSO (normoxia). Pri-, miR-210, and CA9 levels were determined by RT-qPCR using GAPDH for normalization. The value of DMSO (vehicle) in normoxia was set to 1. Data are reported as mean ± SEM, n≥3. *p<0.05; **p<0.01;***p<0.001, determined by one-way ANOVA with Tukey post hoc test. (D) Dose-response curve showing the inhibitory effect of* ***3.42*** *on the maturation of miR-210. IC_{50} was estimated from the sigmoidal dose-response curve analysis using the proper constraints. Normalized percentages of miR-210 fold change are reported as mean ± SEM. Mean of $CoCl_2$ ($CoCl_2$) was set to 100%.*

For these last assays, immunoblot experiments were performed on MDA-MB-231 cells. By reducing the levels of mature miR-210 in cells, **3.42** should also reduce the overexpression of the HIF-1α transcription factor through the pathway detailed in ***Figure 45***, in which an accumulation of GPD1L protein leads to prolyl hydroxylase enzymes activation (PHDs) and thus HIF-1α degradation *via* hydroxylation. Based on these observations, we looked at HIF-1α protein levels under hypoxic conditions. As shown in ***Figure 46***, compound **3.42** could reverse the up-regulation of HIF-1α observed when only $CoCl_2$ is used to treat the cell line. Such results further confirmed that **3.42** indirectly decreases HIF-1α levels by blocking miR-210, thus leading to higher HIF-1α degradation.

In a second time, we decided to assess the levels of MNT protein in breast cancer cells after treatment with **3.42**. As detailed in Section I.2.4 of Chapter I, Zhang *et al.* showed how high levels of miR-210 could revert MNT levels, thereby increasing the activity of the widely studied oncoprotein MYC[233]. We thus decided to perform another immunoblot experiment to assess the MNT protein levels. The result is shown in ***Figure 46***, and no effect was observed on MNT up-regulation. This unfortunate result probably relies on the fact that

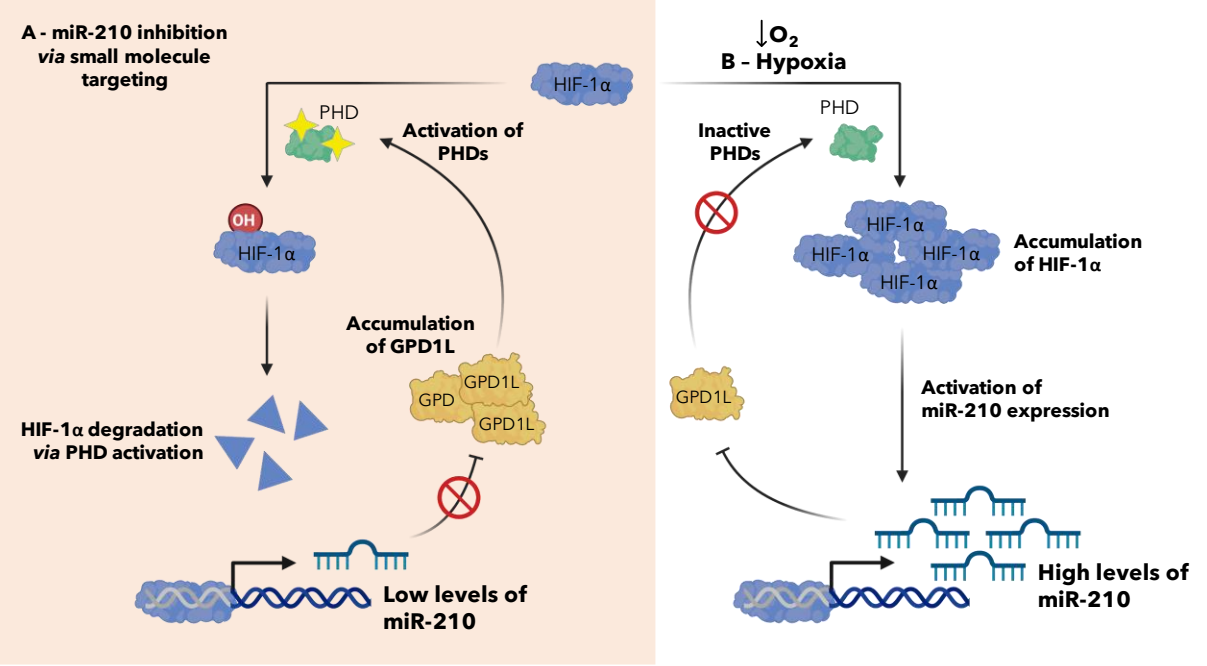

Figure 45 *- miR-210 inhibition effects on HIF-1α protein levels. A) Small molecule inhibitor of miR-210 represses the hypoxic response of cancer cells, thus HIF-1α is maintained at low levels through proline hydroxylation, which leads to its degradation via the proteasome. When HIF-1α protein levels are low, levels of GPD1L are high due to low levels of miR-210, which directly regulates GPD1L by binding to a specific site in its mRNA's 3'UTR. GPD1L, in turn, enhances the activity of the PHDs, triggering effective proline hydroxylation of HIF-1α. B) miR-210 signaling pathway under hypoxic conditions, an increase in HIF-1α protein levels and its transcriptional activity enhances the expression of miR-210. High miR-210 levels lead to decreased levels of GPD1L protein, resulting in the absence of activation of the activity of the PHDs. Consequently, this results in increased stabilization and accumulation of HIF-1α protein. This process establishes a positive feedback loop where miR-210 reinforces and sustains the levels of HIF-1α protein.*

we never obtained the reversion of MNT expression under hypoxic conditions, in which high levels of miR-210 should have reverted it, as shown in Zhang *et al.* work[233]. As mentioned at the end of Section I.2.4 (Chapter I), our team has highlighted a close connection between MNT regulation and circadian clock disruption. However, no MNT variations were observed, so no further efforts were made on this aspect, as we prioritized the confirmation of the inhibition of miR-210, thus leaving the door open for future investigation on the connection between miR-210 and the circadian clock.

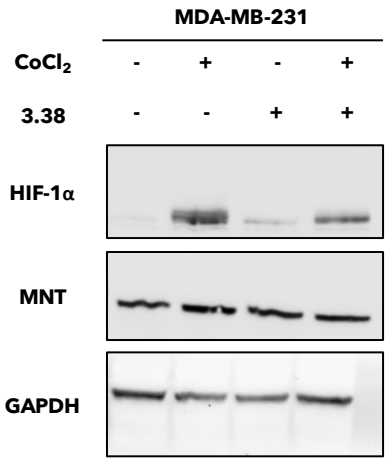

Figure 46 *– Compound* ***3.26b*** *post-translation effects as assessed by immunoblotting. Total protein extracts from MDA-MB-231 cells upon the indicated treatments were assessed by immunoblot analysis with specific anti-MNT and anti-HIF-1α antibodies. GAPDH was used as a loading control.*

III.8 Conclusion

Considering all the biochemical and cell biology results detailed in this Chapter, two different series of innovative tris-thiazole derivatives were synthesized, and *in vitro* tests offered preliminary insights into the potential effectiveness of these compounds. Specifically, three affine compounds have been identified among the newly synthesized **3.26b** analogs: **3.42**, **3.43b**, and **3.55b**. They exhibited potent inhibitory activity toward miR-210 levels with IC_{50} values ranging from 2.25 to 2.31 µM. This highlighted their potential as effective inhibitors of miR-210 maturation. These encouraging *in vitro* results laid good conditions for further assessments and hinted at potential efficacy in cellular environments.

Overall, the cellular biology results demonstrated the ability of the synthesized lead compound **3.42** to reduce the levels of miR-210 within cellular environments effectively. The

observed decrease in miR-210 maturation was also correlated with an expected reduction in its precursor levels, pri- and pre-miR-210. Hence, **3.42** also reverted the hypoxia response of breast cancer cells MDA-MB-210, as shown by the significant reduction in HIF-1α protein levels and relative target genes mRNA levels, such as *CA9* and *BNIP3*. A clear dose-response pattern was also observed, with increasing concentrations of **3.42** linked to increasing reversion of *CA9* gene expression or mature miR-210 levels. To the best of our knowledge, these data clearly represent the first time that a small heterocyclic compound has been shown to revert the hypoxic response of breast cancer cells through the blockage of the Dicer-processing of pre-miR-210. The observed decrease in miR-210 levels highlights the potential of this compound as a promising candidate for further development and investigation.

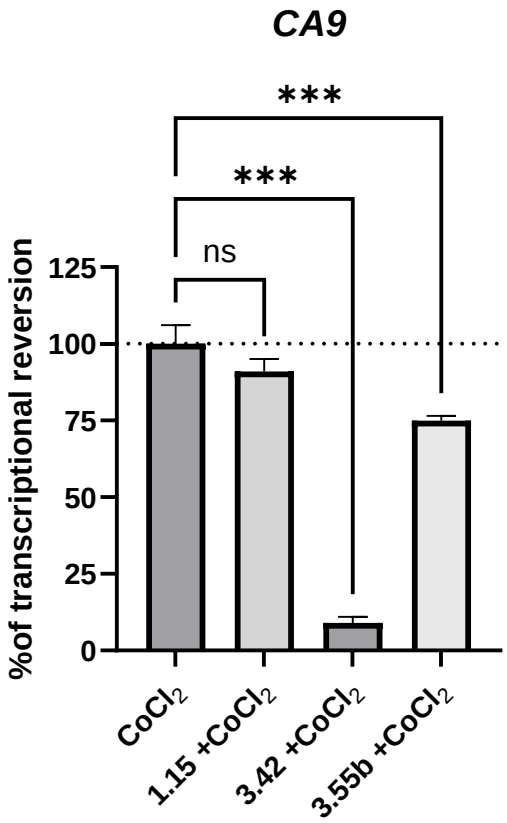

Figure 47 *- miR-210 inhibitors,* ***3.42*** *and* ***3.55b****, reverts $CoCl_2$-mediated HIF-1α transcriptional activity in breast cancer cells. Two of the newly synthesized compounds revert the expression of CA9.* ***1.15*** *(TGP-210) reverts this expression by only 10%, while* ***3.42*** *and* ***3.55b*** *revert the expression by 30% and 90%, respectively. The value of DMSO+$CoCl_2$ (vehicle) was set to 100%. Data are reported as percentage of transcriptional reversion.*

Nevertheless, **3.42** was not the only compound highlighted by our *in vitro* assays. Compound **3.55b** was also tested, and both **3.42** and **3.55b** reversed the expression of the *CA9* gene (***Figure 47***). At 10 μM, they could significantly reverse the hypoxic response of breast cancer cells, while our reference compound **1.15** never showed any activity in our conditions. In ***Figure 47***, **1.15** only showed 10% of *CA9* transcriptional reversion, whereas

3.55b showed a 30% reversion, and **3.42** reverted the expression by 90%. The following steps will thoroughly evaluate the best compound's safety, specificity, and efficacy in future *in vivo* models to further ascertain its potential as a novel therapeutic agent for targeting miR-210 in cancer therapy. Noteworthy, we focused only on the best *in vitro* compound, **3.42**. Still, an in-depth cellular study of **3.55b**'s mechanism of action would pave the way for identifying a possible new miR-210 inhibitor.

Chapter IV

Conclusions and Outlook

Chapter IV | Conclusions and Outlook

In recent years, RNA has emerged as a significant biological target, offering new ways for therapeutic intervention and advancing our understanding of complex cellular processes. The interest in targeting nucleic acids, especially RNA, for therapeutic purposes is well established today and no longer needs to be demonstrated. A large number of coding and non-coding RNAs have now been proven to be directly linked to a wide range of diseases. The recent development of RNA vaccines, for example, which has helped address a global health crisis, proves the effectiveness of mRNA for treating viral infections like COVID-19. Additionally, this led to the launch of Phase I clinical trials in the United States for an RNA vaccine for the treatment of HIV-1. RNA emerged as a solution where classical biological tools have failed. In particular, non-coding RNAs are increasingly attracting the attention of researchers in medicinal chemistry. Targeting proteins has shown some limits, and considering ncRNAs, whether human, viral, or bacterial, allows for the development of new and innovative therapeutic applications. This transformation in the scientific landscape set the stage for the research detailed in this PhD thesis, focusing on the design and evaluation of small molecules as inhibitors of a specific ncRNA.

The known strategies for targeting RNA are based on one hand on the use of antisense oligonucleotides capable of specifically recognizing a specific linear sequence and, on the other hand, on the use of small molecule binders that can selectively bind to the highly structured region of a target RNA. In the presented work, new inhibitors targeting the scientifically and therapeutically important miRNA (miR) class of ncRNA were designed using this second approach. MiRNAs are involved in regulating gene expression, and their overexpression has been directly linked to many diseases, including tumors. More specifically, a specific oncogenic miR known as miR-210 has been widely studied and correlated with low oxygen conditions (hypoxia) in several cancer cells. Indeed, the up-regulation of this miRNA has been correlated with an elevated rate of proliferation of cancer cells and transcriptional regulation of several target genes. Therefore, we have designed, synthesized, and biologically studied an innovative series of compounds capable of interfering with the biogenesis of miR-210. The main goal was to prepare a series of compounds that bind to the stem-loop precursor of miR-210 (pre-miR-210) to impede its cleavage by the Dicer enzyme. The main milestones reached in this project are highlighted hereafter.

I began this manuscript by addressing the need for novel scaffolds and diversifiable moieties within the field of miRNA inhibitors small molecules to expand the scope of chemical probes of miR functions and potential miR-targeted therapeutics. Consequently,

we began this work with a comprehensive optimization study based on a known binder of miR-210 precursor. This bis-benzimidazole compound (**1.15** or targapremiR-210) was discovered first by Velagapudi *et al.* in 2011 *via* a two-dimensional combinatorial screening (2DCS) and described as an inhibitor of miR-210 maturation in 2017 by the same research group[102,255]. We first decided to synthesize several benzimidazole-based analogs of **1.15** to explore the connections between chemical structure, *in vitro* activity, and *in cellulo* toxicity. Thus, **7 new and original analogs** were prepared and tested *in vitro* for their affinity and inhibitory activity towards pre-miR-210. Hence, a preliminary *in cellulo* study was performed to assess their toxicity and eventual reversion of miR-210 levels. Despite similarities in their core structures, the varied responses of the different analogs reflected the profound influence of even minor structural modifications on biological activity. One promising analog (**2.18**), without the terminal azide-containing lateral chain, was highlighted with **high *in vitro* affinity and activity** compared to **1.15**, with IC_{50} values going from 2.91 to 1.70 µM. The summary of this preliminary SAR study is shown in ***Figure 48***.

Subsequently, evaluations were made in a cellular context, and no toxicity was exhibited from the best *in vitro* compounds in three cancer cell lines. In contrast, moderate toxicity was observed in healthy cells. Together with promising *in vitro* results, two essentials *in cellulo* achievements were reached: the **successful induction of hypoxic conditions** required to observe an overexpression of miR-210 and the validation of **1.15** as a positive

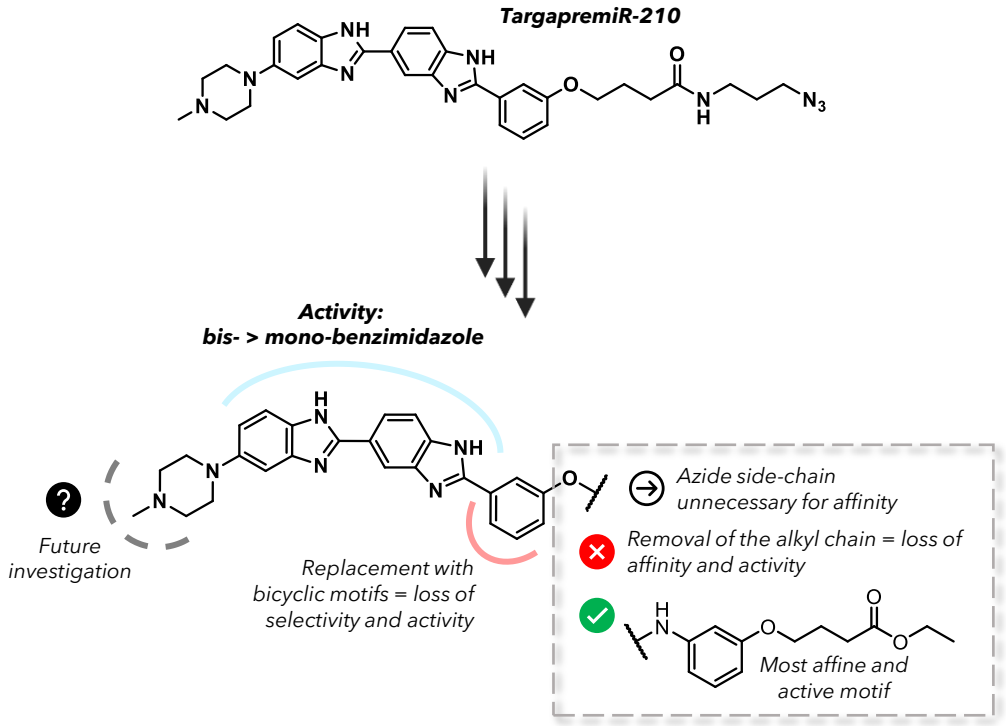

Figure 48 *– Summary of SAR analysis on the optimization of targapremiR-210 (**1.15**). In this project, the functionalization of the phenyl was extensively studied with suitable modifications outlined, the piperazine motif was left untouched, making it available for future chemical optimizations.*

control. The insights obtained from the SAR study and the first *in cellulo* assays outlined a strict link between chemical structure and biological effects that undoubtedly drove the trajectory of our subsequent analog synthesis.

With the idea to rationally design innovative small molecule inhibitors of miR-210 and synthesize original compounds, we combined previous results from our team with our first SAR analysis. In recent studies, the C-terminal part of the anticancer agent bleomycin A5 was identified as a suitable RNA binder. Recently, our team used its bis-thiazole chain to prepare inhibitors of another overexpressed and widely studied oncomiR (i.e., miR-21). Drawing from the results from our first SAR study on analogs of **1.15** and from the recent validation of the thiazole heterocycles as a promising RNA ligand, we performed an *in silico* 3D structural alignment, which confirmed the possibility of replacing the bis-benzimidazole core of **1.15** with a tris-thiazole motif. This led us to design a new series of compounds using the tris-thiazole motif as a central scaffold, suitable for further functionalization. As shown in ***Figure 49A***, we first decided to prepare mono-substituted compounds by inserting motifs identified in the first SAR study or different moieties known to interact with the negatively charged RNA backbone or the RNA nucleobases. Such motifs were inserted upon the formation of amide or sulfonamide bonds, thus allowing us to assess which linkage function was the most suitable for affinity and inhibition activity toward the target miRNA. Indeed, a continuous back-and-forth from organic synthesis to biochemical evaluation, i.e., K_D and IC_{50} measurements, led to the identification of **17 new and interesting hit compounds**. The summary of the SAR analysis of the first series of mono-substituted tris-thiazole derivatives is shown in ***Figure 49A***. This SAR study revealed the critical role of the piperazine motif (**3.34** and **3.35b**) and the phenyl-ester lateral chain (**3.26b**) in enhancing binding affinity and selectivity. For example, the phenyl-ester analog **3.26b** showed a K_D value of 120 nM, whereas reference **1.15** showed a K_D of 540 nM.

Building on these promising results, we decided to use **3.26b** as a new scaffold for further hit-to-lead optimization by introducing motifs highlighted as very promising for increasing affinity toward pre-miR-210. To link such motifs, we also tried to change the linkage function by inserting reductive amination products in the series. This second series of compounds afforded **14 new disubstituted tris-thiazole compounds.** Three affine lead compounds were identified among the newly synthesized **3.26b** analogs. Compounds **3.42** and **3.43b** highlighted again the suitability of the piperazine (substituted or not) motif for good affinity. Hence, analog **3.55b** bearing a guanidine group showed interesting results, outlining the importance of polar groups for better affinity. They also exhibited potent inhibitory activity with IC_{50} values ranging from 2.25 to 2.31 µM, thus validating their potential as effective inhibitors of miR-210 maturation. On the other hand, inserting

heteroaromatic cycles was unsuitable for targeting pre-miR-210, with an overall high increase in the K_D values of these analogs. The summary of the SAR analysis of the first series of mono-substituted tris-thiazole derivatives is shown in ***Figure 49B***.

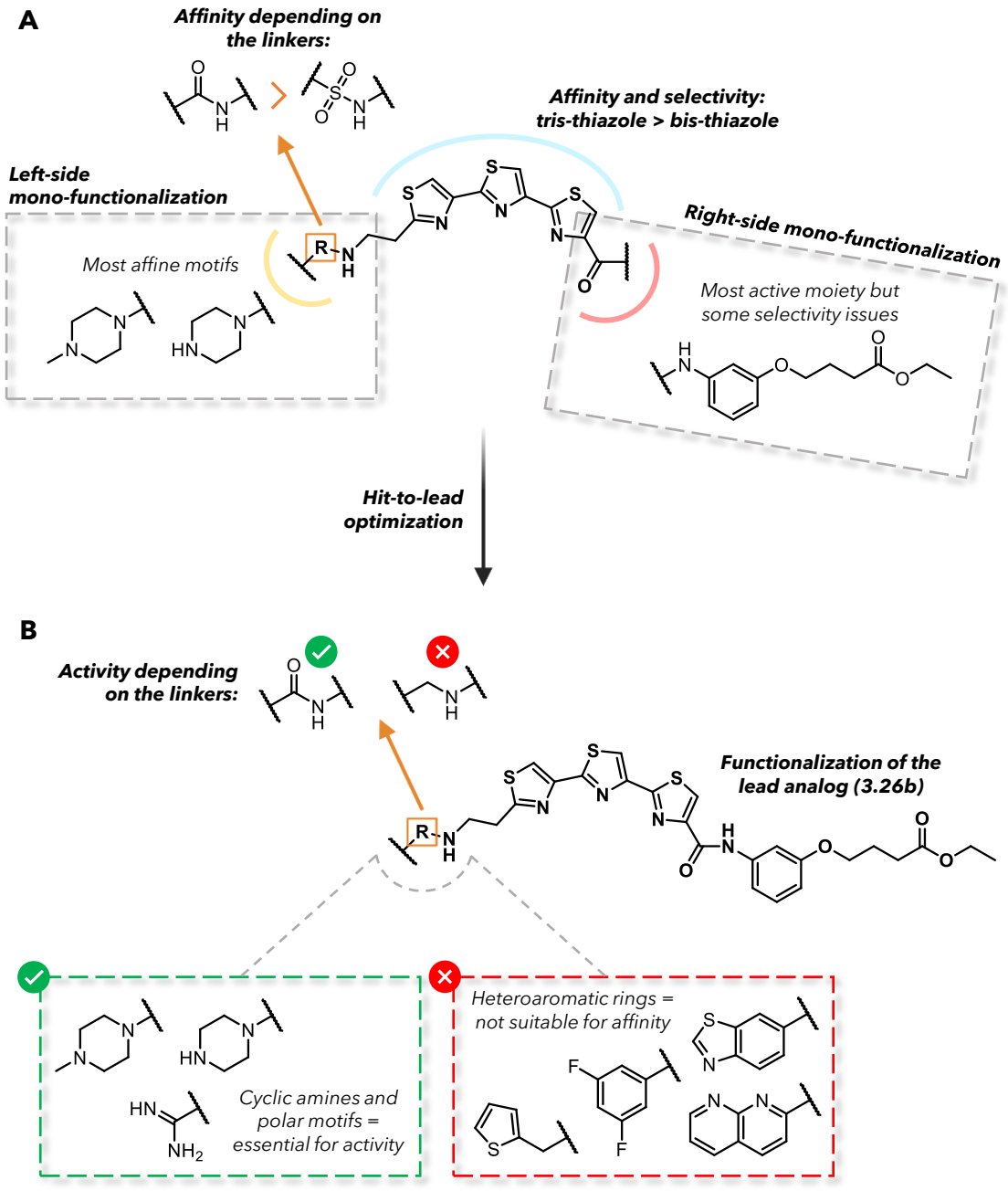

Figure 49 *– Summary of SAR analysis on A) the first series of mono-substituted tris-thiazole derivatives, and B) the second series of di-substituted tris-thiazole derivatives.*

Following the biochemical identification of promising *in vitro* miR-210 inhibitors, the subsequent phase involved an in-depth *in cellulo* testing of these compounds to evaluate

their ability to block miR-210 maturation in a cellular context. Firstly, suitable conditions had to be identified, such as finding the right cancer cell line and the conditions to mimic hypoxic conditions, thus leading to miR-210 overexpression. As a result, we identified two suitable cancer cell lines, the MDA-MB-231 breast cancer cell line and the A375 melanoma cell line. Both cell lines were treated with $CoCl_2$, and overexpression of miR-210 was assessed and confirmed by RT-qPCR. On the other hand, the cytotoxicity patterns of the newly generated derivatives were measured, leading us to use each compound at 10 μM concentration, at which any toxicity was absent. Overall, the experimental data showed the lead compound's (analog bearing the methyl-piperazine motif, **3.42**) effectiveness in **lowering mature miR-210 levels within cells**. This reduction also significantly decreased the upstream precursors of miR-210 levels (i.e., pri-miR-210 and pre-miR-210).

Parallelly, the reversion of the adaptive hypoxic response of breast cancer cells was observed. Indeed, the reversion of the hypoxia marker HIF-1α levels and related miR-210 target gene levels, such as *CA9* and *BNIP3*, was confirmed. A distinct dose-response pattern was also noted, linking increased concentrations of **3.42** to enhanced reversion of *CA9* gene expression or mature miR-210 levels. These data confirmed **3.42**'s potential as a significant candidate for **inhibiting miR-210 biogenesis** of pre-miR-210 **and reverting the hypoxic response** in breast cancer cells. To the best of our knowledge, this is one of the first works describing how a small heterocyclic compound can successfully reverse the hypoxic response in breast cancer cells by blocking miR-210 maturation. The proven reduction in miR-210 levels emphasizes the potential of this compound for further study and development. Upcoming steps should focus on target engagement assays and on meticulously evaluating the safety and effectiveness of this compound for potential *in vivo* studies, thus validating its potential role in targeting miR-210 in cancer treatment. It is now widely recognized that tumor hypoxia is a crucial impediment to effective cancer therapy; therefore, finding a compound that reverts the hypoxic response in cancer cells might lead to more effective therapies[344–346]. Hence, although the focus has been placed on **3.42**, an extensive cellular study of **3.55b** might also reveal another promising miR-210 inhibitor, leaving the door open for future *in cellulo* investigation.

In conclusion, this PhD represents a substantial contribution to the field of miR-targeting small molecules, more generally in the field of ncRNAs. The findings detailed in this manuscript increase the understanding of the dynamics of small molecule interactions with ncRNAs and pave the way for the continued development and optimization of such compounds. This manuscript presents an example of hit-to-lead development of specific RNA ligands, and it represents an innovative example of the rational design of small molecules. Consequently, this optimistic view of the RNA-targeting field led us to publish a

review entitled "Navigating the rapidly changing landscape of small-molecule RNA targeting" in ***Nature Reviews Chemistry*** (See Annex 1) earlier this year. This review aims to invite chemists to enter the field of RNA by detailing the most recent approaches for future developments and innovations. Two scientific articles presenting the results described in Chapters II and III, respectively, are currently in preparation.

As a conclusive remark, it must be noted that in these three years of PhD, the aims of the project have been successfully met with the identification of compounds effectively inhibiting miR-210 levels in a cellular context and able to reverse the adaptive hypoxic response in breast cancer cells. With an organic chemistry background, this project allowed me to explore the fields of cellular biology and molecular medicine, alternating between organic synthesis, *in vitro* biochemical evaluations, and cellular biology assays. This manuscript is not meant to be an exhaustive list of the achievements and side projects I was involved in; however, it should be noted that during these three years, I had the chance to take part in another RNA-targeting project in collaboration with the laboratory of Dr. Tiziano Bandiera from the Italian Institute of Technology. A summary of the results obtained can be found in Annex 2. On a different note, I also had the great chance to supervise a Master 2 intern for six months (i.e., Malik Zerguine), alongside my decision to be a teaching assistant over these three years of PhD, thus participating in teaching organic chemistry to undergraduate students. The opportunity to co-host preventive interventions on the topic of AIDS for middle school audiences was also given to me earlier this year.

Lastly, I had the opportunity to present the project at different international conferences, which led to the **Best Poster Communication Award** at the *Mediterranean Young Researchers Days* in 2022 and to be one of the awardees of the **Excellence Prize of the Université Côte d'Azur** for excellent communications at international conferences.

Annexes

Annex 1 | ***Nature Reviews Chemistry*** – Accepted Manuscript

Navigating the rapidly changing landscape of small-molecule RNA targeting

Sandra Kovachka,[1,¥] **Marc Panosetti**,[1,2,¥] Benedetto Grimaldi,[2] Stéphane Azoulay,[1] Audrey Di Giorgio,[1] Maria Duca[1,*]

[1] Université Côte d'Azur, CNRS, Institute of Chemistry of Nice, 28 avenue Valrose, Nice, France

[2] Molecular Medicine Research Line, Istituto Italiano di Tecnologia (IIT), Via Morego 30, 16163, Genoa, Italy

[¥] **These authors contributed equally to the manuscript**

* Corresponding author: maria.duca@univ-cotedazur.fr

Abstract

RNA targeting using small molecules represents one of the major challenges of current medicinal chemistry and the development of innovative methodologies to identify RNA binders has attracted enormous attention in chemical biology and drug discovery during recent years. Although various classes of antibiotics targeting bacterial ribosomal RNA have been on the market for many decades, the renewed interest in RNA targeting is due to the need to better understand complex intracellular processes involving RNA. In this context, small molecules are privileged tools to explore the biological functions of RNAs, to validate RNA as therapeutic targets and eventually to become new drugs. This is perfectly illustrated by the recent FDA approval of risdiplam, a mRNA splicing modifier for the treatment of spinal muscular atrophy. Despite recent progresses, the rational design of specific RNA binders calls for a better understanding of the interactions which have to be formed with the RNA target to reach the desired biological response. In this review, we will focus on the main challenges that need to be addressed by chemists to approach this original and underexplored chemical space, together with the most up-to-date strategies developed to bind, interact and affect biologically relevant RNAs.

Accepted Manuscript

Introduction

The paradigm of RNA targeting with both oligonucleotides and small molecules has existed in chemical and biological sciences for many years.[1] The recognition of the essential roles played by RNAs in living systems grew incessantly in the last decades until the discovery of many new classes of RNAs involved not only in transcription and translation, but also in the regulation of gene expression. While oligonucleotides recognize RNAs by sequence complementarity thanks to the formation of Watson-Crick-Franklin hydrogen bonds with single-stranded RNAs, small molecules target specific sites in structured RNAs where the association of single-stranded and double-stranded regions leads to the formation of specific tridimensional structures.[1] This structure-recognition depends on the formation of binding pockets similar to the ones found in proteins. Oligonucleotides are important tools both for the fundamental study of RNAs functions and for their potential therapeutic applications. Still, their use remains limited due pharmacokinetic and pharmacodynamic drawbacks.[2] Furthermore, since biologically relevant RNAs are highly structured, oligonucleotides cannot access and interact efficiently with these structures. While some of these limitations have been addressed,[3] a complementary approach based on the use of small molecules has been developed and holds great potential for chemical intervention on RNA functions.[1,4-6]

The history of RNA ligands begins with the discovery of the first RNA binders in the early forties. Different classes of natural products were identified as antibiotics with streptomycin being the first aminoglycoside example (FIG. 1).[7] Their binding to prokaryotic ribosomal RNA induces the impairment of protein synthesis in bacteria leading to their antimicrobial activity.[8] Aminoglycosides are constituted by positively charged aminooligosaccharides that can easily interact with the negatively charged RNA backbone.[9] Also, their three-dimensional shape allows them to interact selectively with the A-site region of prokaryotic ribosomal RNA.

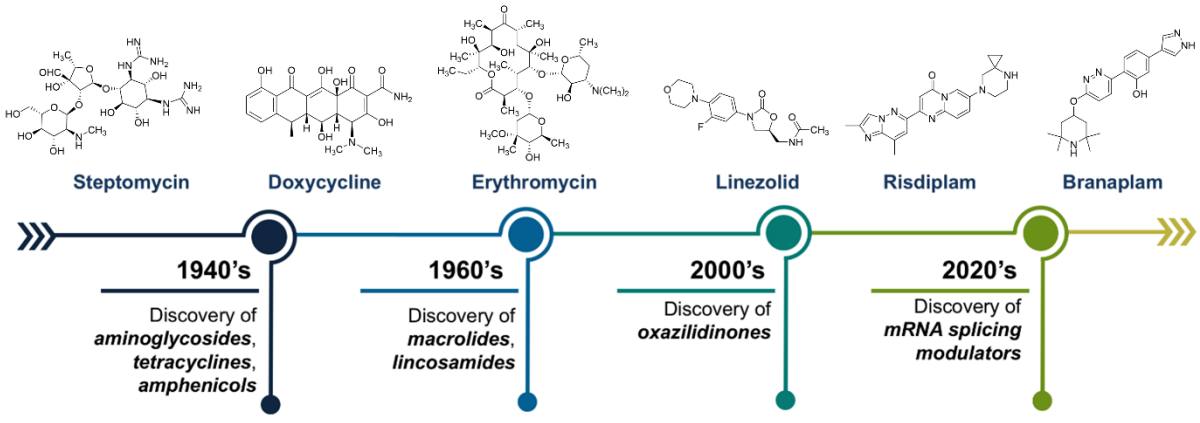

Fig. 1. | **Historical view of RNA ligands as marketed drugs.** Chronological timeline illustrating the main landmarks in the RNA targeting by small molecules field with examples of marketed drugs.

Subsequently, other natural compounds with varied chemical structures were identified as ribosome binders with antimicrobial properties. These include tetracyclines (e.g., doxycycline), macrolides (e.g.,

ted Manuscript

erythromycin), and oxazolidinones (e.g., linezolid). .[8] The therapeutic potential of RNA-targeting was also recently highlighted by the FDA approval of risdiplam for spinal muscular atrophy (SMA) treatment.[10] Concomitantly, numerous compounds have been documented as RNA binders, serving both therapeutic and research purposes, thereby enhancing understanding of small-molecule RNA targeting strategies.[1]

In this review, we aim to illustrate the chemical structures of reported RNA binders together with the interactions they form with the RNA target and discuss the important molecular features for binding, selectivity and biological activity. The recent modalities adding new functions to specific RNA binders will then be detailed. Finally, the gaps needing to be filled to bring the field toward a further level of applications in chemical biology and in clinics will be presented. Since the methodologies employed have been reviewed and detailed elsewhere, they will be described only briefly.[1] This manuscript will focus on the challenges that have been recently overcome and the ones that yet remain to be met by chemists toward the design of new chemical tools for RNA targeting and the strategies that have been put in place toward this goal. Altogether, this review aims at inviting medicinal chemists and chemical biologists to enter the field and have keys to approach it for future developments and innovations.

Molecular features and selective interactions driving RNA binding and subsequent biological activity Challenges in identifying RNA binders are primarily due to RNA's inherent structure (See BOX 1). A first obstacle is the RNA's highly negatively charged backbone restricting compatible chemical structures and favoring interactions with positively charged compounds. .[11] Also, RNA has only four bases compared to proteins' 20 amino acids. Recent studies indicate that selecting appropriate chemical scaffolds can help design ligands suitable for RNA's chemical space.[4] Finally, unlike most protein targets, biologically relevant RNAs exist in a dynamic ensemble of various structures based on base pairing..[12] While some structures are prevalent, others are minimal. Factors like salt concentration, intracellular interactions or mutations influence this balance. Altering this dynamic ensemble may impact the RNA's function, but determining the biologically active RNA conformation *in vivo* remains challenging. The lack of knowledge about the actual isoform the compound will bind to and how this will affect RNA function represents thus the third major drawback. Fortunately, structural biologists have now a range of techniques in addition to X-ray, such as advanced NMR and cryo-EM, that should lead to important developments in the near future.[1]

Given these premises, the design of selective RNA binders as potential drugs or as chemical probes cannot be performed as usually done for protein targeting. Indeed, small molecule/RNA interactions are dominated by hydrogen bonding and π-stacking interactions that constitute more than half of the identified interactions so far.[13] These are followed by hydrophobic interactions and weak hydrogen bonds. Conversely, compounds that target proteins mainly form hydrophobic contacts that constitute almost half of the formed interactions followed by hydrogen bonding and π-stacking. The compounds reported since the discovery of the first RNA binders, until the identification of specific and drug-like

Accepted Manuscript

molecules acting on bacterial riboswitches[14] or modifying RNA splicing,[10] show that the above-mentioned challenges are about to be overcome paving the way for major discoveries in the next years. However, as detailed below, it is still difficult to perform a rational design of ligands specific for a particular RNA target. In this context, the future of the field is still uncertain, and more efforts is needed to assess whether RNA targeting with small molecules will actually open new avenues to answer important biological questions and discover new drugs.

In the upcoming sections, we provide an exploration of the obstacles and limitations that have been tackled in the quest to efficiently target RNA with small molecules. We indeed believe that a better understanding of the formed interactions upon the study of RNA binders is key to the development of improved ligands.

Beyond the phosphate backbone: how to reach selectivity with positively charged ligands. RNA's negative charge creates a substantial negative surface associated with paired and unpaired nucleobases. The resulting 3D structure differs from double-helical DNA, being more similar to proteins. The phosphate backbone calls for the use of compounds containing chemical groups protonated at physiological pH, as seen in aminoglycosides, that favor electrostatic interactions with phosphates and specific hydrogen bonds, particularly with unpaired bases.[7] Aminoglycosides predominantly bind to RNA regions with internal loops and bulges that distort the double helix.[15] For instance, plazomicin (compound **1**), the latest approved aminoglycoside, interacts with the ribosomal A-site through π-stacking and hydrogen bond interactions with nucleobases as revealed by X-ray (FIG. 2a).[16] Additionally, plazomicin's hydroxy-aminobutyric acid (HABA) tail forms a H-bond with an uracil base. Altogether, this leads to a strong and selective interaction even if electrostatic interactions are also formed, reinforcing binding but hampering aminoglycoside specificity. To overcome this issue, aminoglycosides have been conjugated with moieties able to establish more selective interactions with the target.[17] One important strategy toward the improvement of aminoglycoside selectivity is their conjugation with nucleobases.[18] A relevant example is a modified neomycin designed to selectively target HIV-1 dimerization initiation site (DIS), a highly conserved RNA stem-loop structure located in the 5'-non-coding region of the viral genome.[19] Its dimerization is a key step in HIV replication and its inhibition has been considered for potential antiviral therapies. The structural study of neomycin in complex with DIS and with A-site rRNA fragment shows high similarities to DIS, highlighting an adenine base involved in a key interaction with ring I of neomycin in DIS, but not in the ribosomal A-site.[19] Indeed, ring I was replaced by a thymine leading to neomycin derivative **2** (FIG. 2b) able to bind DIS with an improved specificity compared to neomycin. This example illustrates how the appropriate addition of H-bonds donors and acceptors based on the structure of the RNA target and on knowledge about base complementarity could increase selectivity for the desired target.

Accepted Manuscript

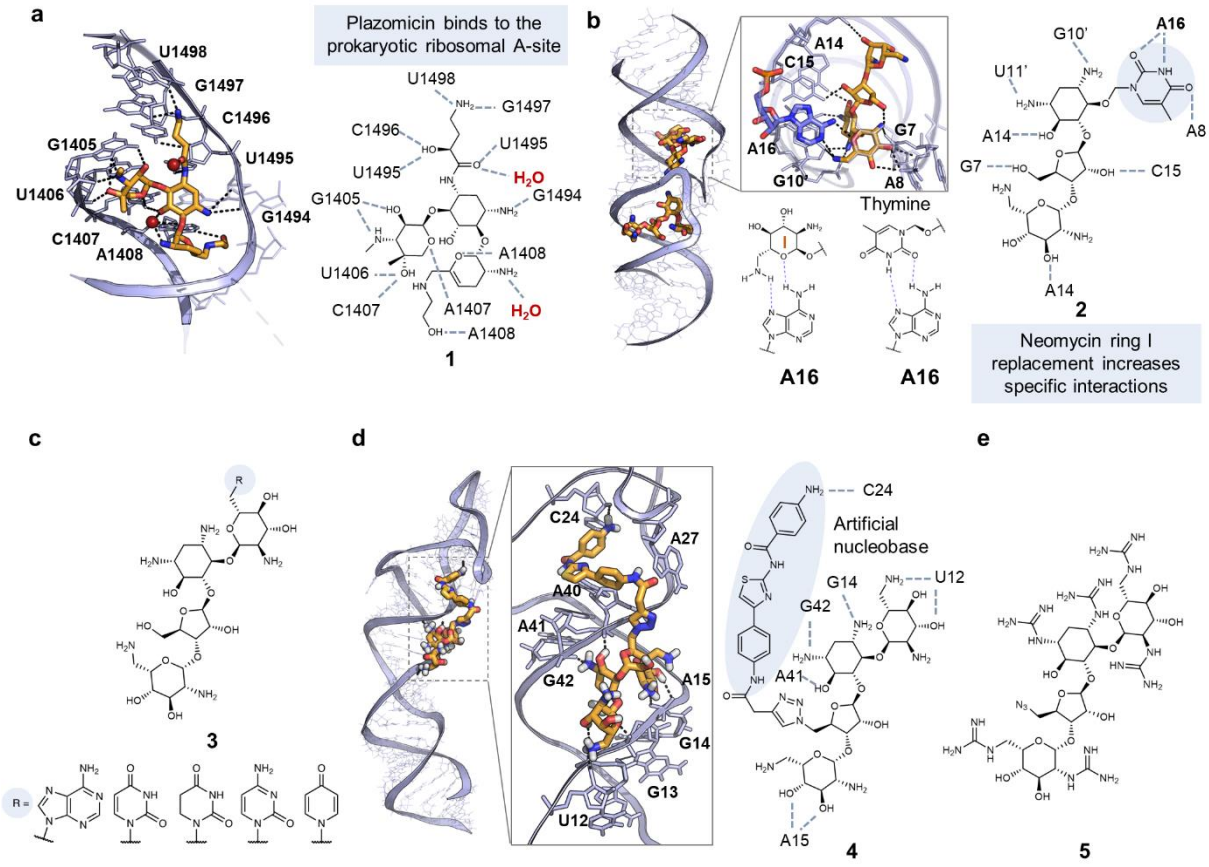

Fig. 2 | **Examples of RNA binders based on aminoglycoside structure. a |** On the left, crystal structure of plazomicin **1** within its A-site binding site. The ligand is shown in orange sticks white contact residues are shown in light blue sticks, H-bonds are shown as black dashes (PDB ID: 71H5). On the right 2D representation of plazomicin and the contact nucleotides in the binding site. **b |** On the left, crystal structure of-neomycin within the DIS kissing complex, target residue for specific interaction A16 is shown as blue sticks (PDB ID: 2FCY). Comparison between the H-bond A16-Neomycin-ring I and A16-Neomycin-thymine is shown below. On the right 2D representation of Neomycin-Thymine conjugate **2** and the contact nucleotides in the binding site. **c |** Neomycin-nucleobase conjugates **3**; **d |** Neomycin-artificial nucleobase conjugate **4** and its binding to stem-loop structured precursor of oncogenic miR-372 as confirmed by footprinting and molecular docking. **4** interacts predominantly at the stem region (U12–G14 and A40-G42) close to the site of cleavage by Dicer. **e |** Guanidilated neomycin **5** identified upon 2-DCS as a specific binder of the internal loop of pre-miR-10b.

In a similar way, neomycin and paromomycin were conjugated with nucleobases as in **3** (FIG. 2c) to obtain ligands with an improved affinity for HIV-1 TAR RNA over A-site.[20] This result was however difficult to predict, and rational drug design remains challenging even in the presence of structural information, most likely due to the intrinsic dynamic of the RNA systems. Furthermore, in these last examples, no biological activity was reported, suggesting a lack of specificity in cells. Other types of heteroaromatic compounds have been applied to prepare aminoglycoside conjugates targeting the biogenesis of oncogenic microRNAs (miRNAs or miR) that are essential regulators of gene expression.[21] To design selective ligands of stem-loop-structured precursors of oncogenic miRNAs and inhibit miRNAs biogenesis, neomycin was conjugated to artificial nucleobases,[22-25] that are heteroaromatic compounds able to form specific hydrogen bonds with DNA and RNA base pairs thus

Accepted M.

inducing the formation of base triplets.[26] This led to compounds, such as **4** (FIG. 2d), that selectively inhibits the biogenesis of a small set of overexpressed oncogenic miRNAs in cancer cells.[25] Notably, the incorporation of the phenyl-thiazole heteroaromatic component directed neomycin to the stem-loop precursor of oncogenic miR-372, pre-miR-372, inhibiting Dicer cleavage and miRNA maturation. This resulted in effective miR-372 inhibition *in vitro* and specific proliferation inhibition in cancer cells overexpressing miR-372 without toxicity. Footprinting and molecular docking analyses suggested that a third RNA binding domain might enhance affinity and selectivity. Consequently, amino acids, natural RNA binders, were added thus improving binding and inhibitory activity due to additional interactions.[23] Noteworthy, despite their selectivity for pre-miRNAs over tRNA and DNA, these ligands bind also to a small set of other pre-miRNAs. The specificity of biological activity for cells overexpressing miR-372, corroborated by other studies, indicates that selectivity strongly depends on intracellular target expression levels as well as on binding RNA in a functional site to effectively inhibit its function or processing. Strong binding to non-functional off-target sites may not result in any activity nor toxicity. Therefore, associating binding with function is crucial in designing biologically active, selective RNA binders and evaluating potential off-target implications.

In a complementary approach, a two-dimensional combinatorial screening (2-DCS) was developed where a large set of compounds were immobilized on microarrays and screened against thousands of RNA motifs, such as bulges or internal loops.[27] 2-DCS enabled for example the identification of guanidilated aminoglycosides as specific binders of RNA internal loops. Guanidilated neomycin (compound **5**, FIG. 2e) was found to bind a 5'-AUACC/3'-UAAGG internal loop that was specifically found in the precursor of oncogenic miR-10b and inhibited its production in cells with micromolar activity. Compound **5** was thus a specific ligand of pre-miR10b, the guanidinium groups probably playing an important role in RNA binding.[28]

It is thus possible to approach the negatively charged backbone with positively charged compounds in a selective manner giving electrostatic interactions an important role.[29] However, the association of these kind of compounds with moieties chosen for their ability to form specific hydrogen bonds and hydrophobic interactions clearly increases selectivity. The search for ligands whose main binding mode is not driven by the formation of electrostatic interactions led to the discovery of more drug-like and specific binders as it will be highlighted in the following sections.

Encompassing nucleobases interactions: how to target RNA secondary and tertiary structures. The second challenge in the discovery of RNA binders is the particular chemical space of the target when compared to proteins This calls for a new paradigm to design selective ligands and the strategies employed to face this challenge could be broadly divided into two categories: (i) the design of binders based on the structure of the target and the potential interactions to be formed with it and (ii) the use of high-throughput methodologies combining screening with bioinformatics and biophysics to identify new scaffolds. The success of these strategies relies heavily on a thorough understanding of the

Accepted Manuscript

secondary and tertiary structures of the target, which play a critical role in determining potential binding pockets for ligands.

In this context, a relevant example is represented by dimethylamiloride (DMA, compound **6** in FIG. 3a) that compared with aminoglycosides showed lower affinity but promising selectivity.[30] Iterative modifications at C(5)- and C(6)-positions allowed the establishment of strong interactions with the bulge regions of HIV-1 TAR RNA. Derivative **7** (FIG. 3a) demonstrated a 100-fold increase in activity over the parent compound **6** in Tat peptide displacement assays against TAR.[30] The same scaffold was modified to direct the ligands against other viral RNAs.[31-33] Some DMA analogs, such as compound **8** (FIG. 3a) showed promising antiviral activity by reducing SARS-CoV-2 virus titer in infected cells. These amiloride compounds bind to bulges and/or loop residues of 5'-UTR domains of SARS-CoV-2 RNA genome thanks to the interaction with specific binding sites.[33] Amilorides could thus represent promising chemical probes to understand SARS-CoV-2 pathology, even if they generally show modest selectivity as they are also able to bind other RNAs or viral proteins.[34]

Similar interactions were found for the triaminotriazine moiety that has been employed in the design of various DNA and RNA ligands and is responsible for the recognition of T-T and U-U mismatches. The two edges of the triazine heterocycle can form a full set of Janus-wedge hydrogen bonds with poorly paired uracil and thymine residues (FIG. 3b) or can bind one of the two nucleobases and displace the other one out of the helix. The addition of bisamidinium groove-binding linkers, as in compounds **9-11** (FIG. 3b) allowed to prepare multimeric compounds to target DNA and RNA triplet repeat expansions but also to add electrostatic interactions with the phosphate backbone in the major groove of double helix.[35,36] These compounds were specific for the CUG expanded triplet repeats, r(CUG)^{exp}, found in the 3′-untranslated region of the dystrophia myotonica protein kinase (DMPK) gene causing the myotonic dystrophy type 1 (DM1).[37] The pathology is due to splicing errors caused by these repeated RNA triplets whose targeting has been proposed for the discovery of DM1 treatments.[38] The biological evaluation of compound **9** resulted in efficient inhibition of MBNL1-r(CUG)^{exp} interaction with micromolar activities *in vitro* and in cells and opened the way to the synthesis of oligomers of compound **9** to increase the potency by binding to multiple repeats.[39,40]

Accepted Manuscript

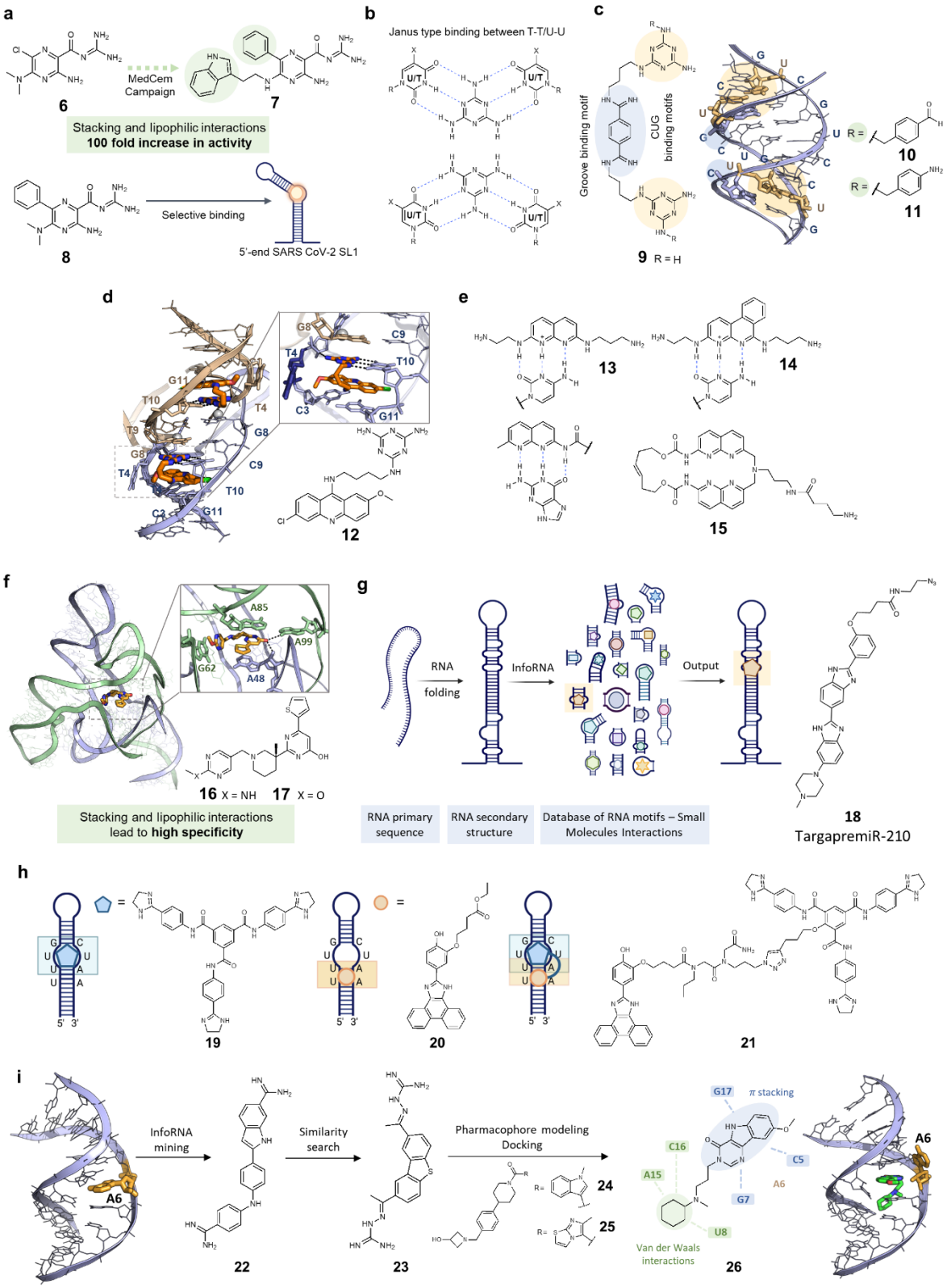

Fig. 3. | **Examples of RNA binders targeting secondary structures. a |** Compound **6** optimization led to **7** and **8**; **b |** Janus-wedge hydrogen bonds formed by the triaminotriazine moiety; **c |** Cartoon representation of a CUG repeat (PDB ID: 3GM7) with highlighted the binding residues for compounds **9-11** in sticks; **d |** Compound **12** binding to DNA CTG repeats: the triaminotriazine forms H-bonds with T10 inducing a displacement of T4 (represented in dark blue sticks) while the acridine intercalates between T10 and C3-G11 pair (PDB ID: 6M4T); **e |** Naphthyridines **13-15** forming H-bonds with C and G; **f |** Ribocil (**16**) and Ribocil-D (**17**) chemical structures and binding mode in FMN riboswitch (PDB ID: 5KX9). **g |** InfoRNA

pipeline led to Targapremir-210 (**18**); **h |** Discovery of compound **21** starting from **19** binding to the U-U internal loop, and **20** binding to the adjacent U-A pair; **i |** Structure-based drug design of **26**. The apo NMR structure bearing the A bulge (highlighted in light orange) is shown on the left (PDB ID: 6VA1). The complex between **22** and the RNA results in A6 displacement and in the design of **26** whose binding mode is shown on the left (PDB ID 6VA4).

The conjugation of the acridine intercalator with the triaminotriazine scaffold led to compound **12** (FIG. 3d).[41] While the triazine heterocycle forms hydrogen bonds with poorly paired uracil residues, both acridine and triaminotriazine moieties form important π-stacking interactions with paired bases, eventually increasing affinity and selectivity, as illustrated by the crystal structure of CTG DNA repeat expansion in complex with **12** (FIG. 3d).[42] It is however clear that these compounds are selective for $r(CUG)^{exp}$ and $r(CTG)^{exp}$ but cannot distinguish between DNA and RNA which could limit their biological applications.[35,36]

Similarly, naphthyridine scaffold has been employed in compounds used as DNA and RNA molecular glues.[43] This compound can form specific hydrogen bonds with unpaired guanine and cytosine bases (FIG. 3e) and dimers have been prepared to control hybridization events between two single-stranded DNAs and higher order RNA structures.[44,45] For instance, compounds **13** and **14** (FIG. 3e) are able to bind to the loop residues inducing the dimerization of two pre-miRNAs structures. This tridimensional assembly prevents Dicer processing and represents an original mechanism of inhibition.[46] Other types of naphthyridine derivatives, such as cyclic mismatch binding ligands (CMBLs), were recently reported as rationally designed ligands to target CGG repeats in RNA.[47] In a remarkable work, a strategy integrating high-throughput sequencing with conventional SELEX followed by bioinformatic analysis was employed to identify hairpin loop sequences of pre-miRNA showing high binding affinity and specificity for a water-soluble cyclic mismatch binding ligand **15** (FIG. 3e).[48] Binding was observed for both endogenous pre-miR33a and pre-miR24-2 comprising characteristic binding motifs. Dose-dependent decrease in the cleaved products formation was also observed in the presence of **15** for the *in vitro* Dicer cleavage reaction of pre-miR33a thus confirming the potential of such an approach, but no intracellular activity was reported.

While distinct from aminoglycosides, these guanidilated and protonated compounds maintain interactions based on electrostatic forces, which can compromise selectivity. In this context, ribocil (compound **16**, FIG. 3f) marks a significant shift towards specific RNA binders with drug-like properties.[14] Identified as an inhibitor of the flavin mononucleotide (FMN) riboswitch, ribocil targets these conserved prokaryotic RNAs that adjust gene expression upon binding to specific endogenous ligands. The FMN riboswitch regulates riboflavin concentrations and controls genes related to its biosynthesis and transport. A high-throughput screening highlighted the S enantiomer of ribocil as an effective inhibitor, reducing riboflavin levels in *E. coli*. Various analogs, including ribocil D (compound **17**, FIG. 3f), have been explored, revealing π-stacking interactions and crucial H-bonds between the carbonyl, the 2'-OH of adenosine 48, and the exocyclic NH_2 of adenosine 99.[49] This suggests that RNA

Accepted Manuscript

binding does not strictly require protonated groups if hydrogen bonds are established. Additional drug-like compounds, such as those binding to Xist, which plays a role in X chromosome inactivation, further exemplify this trend.[50,51] From the examples above, it is clear that both screening and the design based on the potential formed interactions are efficient strategies for the discovery of selective ligands. The more information is gathered about the RNA structure, the best the design and understanding of the interactions will be. A combination of all these approaches would thus be ideal for the discovery of efficient RNA binders.

The closest approach to this ideal goal is represented by InfoRNA methodology that belongs to a series of recently developed new platforms.[52] While most of these approaches, such as dynamic combinatorial chemistry (DCC) or DNA-encoded libraries (DEL) are still being validated (see BOX 2), InfoRNA played a crucial role in the discovery of new binders that have been validated *in vitro*, in cells and *in vivo*. InfoRNA methodology is based on the 2-DCS approach described above, combined with structure–activity relationships through sequencing (StARTS) process that is a statistical method allowing for anticipating the affinity and selectivity of RNA library's compounds thus scoring binding interactions.[53] This leads to the identification of the RNA motifs that are the most suitable targets of a particular small-molecule binder. Finally, the obtained database is mined against folded RNA structures within the human transcriptome to identify potentially druggable RNA targets from sequence and the corresponding specific ligand.[54] The benzimidazole scaffold at the core of Hoechst derivatives was found in many of the RNA binders identified by Inforna.[55] A typical example is compound **18** (FIG. 3g) that was identified as a specific binder of miR-210 hairpin precursor. MiR-210 regulates hypoxia inducible factors (HIFs) that play critical roles in cancer maintenance since a hypoxic state is critical to the metastatic and invasive features of most solid cancers.[56] Compound **18** was able to bind to pre-miR-210 and inhibit its processing toward mature miRNA through a specific interaction with 5'-ACU-3'/3'-UCA-5' internal loop that represents its Dicer-cleavage site. This also induced a decrease of HIF-1α and apoptosis of triple negative breast cancer.[56] This highly specific effect shows that Hoechst intercalators can be modified to specifically recognize a RNA region (sequence and structure) and to avoid off-target effects. In another remarkable example, compound **19** (FIG. 3h) was discovered with InfoRNA, as able to specifically interact with a 1 x 1 UU internal loop located in the cleavage site of Dicer on pre-miR-200c, while compound **20** interacts with adjacent AU base pair.[57] MiR-200c belongs to the miR-200 family including five different members associated with type 2 diabetes (T2D). Overexpression of miR-200c alone is sufficient to induce β cell apoptosis *in vivo*. Assembling the two ligands, led to compound **21** that is remarkably specific for miR-200c with respect to the other members of the family. Binding of this small molecule inhibits the biogenesis of miR-200c in a cellular model of T2D thus reducing the amount of the miRNA as well as β cell apoptosis. Compound **21** has no other targets across the miRnome, the transcriptome or the proteome showing that conjugation of two ligands specific for two different RNA sites could direct binding on a unique region where these two sites are close and distinguish between similar pre-miRNAs sequences. Importantly, this compound is targeting

Accepted Manuscript

specifically pre-miR-200c that could not be targeted using an oligonucleotide, this latter needing more extended single-stranded regions to bind. Using multiple methodologies, specific compounds were identified to correct Tau pre-mRNA splicing linked to many neurodegenerative diseases.[58] InfoRNA led to compound **22** (FIG. 3i), and a chemical similarity search, to analog **23**. NMR and fluorescence assays built a pharmacophore model, leading to hit expansion and optimized compounds **24** and **25**. Compound **26** was finally obtained through molecular docking, and bears micromolar activity *in vitro*, in cells, and *in vivo*. This example highlights the importance of combining different techniques to optimize RNA ligands and understand the underlying molecular mechanism. InfoRNA clearly represents a suitable approach to identify RNA binders bearing a high and specific biological activity that has been directly related to the RNA target upon target engagement experiments and confirmed *in vivo*.

In summary, the design of ligands tailored for the formation of strong interactions with the RNA target can be very efficient but bears a high risk to lead to binders with low specificity. Integrated approaches, such as Selex or InfoRNA as well as other methodologies described in Box 2, despite possible increased failure rates, present a higher potential for the discovery of specific ligands. Nucleobase targeting by small molecules predominantly relies on a structure-based approach over a sequence-based one. Successful interactions depend on the target's three-dimensional environment and the potential for RNA to adapt conformationally, creating specific binding sites.[59] Therefore, understanding the relevant 3D structure is essential for the discovery of new ligands, as discussed in the next section.

Targeting the dynamic 3D structure of biologically relevant RNAs. The understanding of the secondary and tertiary structures of the targeted RNAs and of the pairing interactions that play a major role in the formation of binding pockets, is strongly connected with the examples of RNA binders shown in the sections above for the overall recognition of the target. A further level of complexity is added by the fact that in most cases the RNA target bears more than one possible conformation and that the conformations adopted in solution or in complex with the intracellular partners are of major importance for its function.[12] While the identification of strong (at least nanomolar) RNA binders is accessible, the determination of the biologically relevant RNA structure is essential for the design of selective binders. Noteworthy, ligand binding to an RNA target can induce a conformational change, as demonstrated by the benzimidazole ligands of the IRES IIa domain in the HCV RNA genome or by naphthyridine carbamate dimers (NCD) against r(UGGAA)exp repeats in spinocerebellar ataxia type 31.[59,60] Binding could thus involve induced fit but also conformational selection mechanisms and this complexifies the understanding of the interactions as well as the design of ligands appropriate for a specific target.[61-63] Structural biology, biochemistry, biophysics and molecular modeling are thus essential fields contributing to the design of efficient binders. Even if algorithms are available to predict the RNA base pairing and the resulting structure, experimental validation is essential to assess their reliability.

NMR has been and still is a privileged technique to assess RNA structure and ligand binding.[64] In this context, NMR approaches, mainly based on the observation of either the target or ligand ^{1}H nuclei, have

Accepted Manuscript

been developed to study RNA dynamics (detection of dynamic sub-states) as well as RNA–ligand interactions.[65,66] Thus, NMR studies allowed for the elucidation of Risdiplam's mode of action, the first splicing modifier approved for clinical use in 2020 for the treatment of SMA and initially identified through phenotypic screening.[67] The binding mode of SMN-C5, risdiplam's analog, is shown in FIG. 4a. Further to its ability to bind RNA through H-bonding and π-stacking interactions, risdiplam and its analogs stabilize the interaction between the 5' splice site and the U1 small nuclear ribonucleoprotein (snRNP) of the spliceosome, acting as a molecular glue between protein and RNA. ^{1}H NMR experiments can be difficult to interpret when studying larger strands of RNA and in this case, it is possible to use ^{19}F nucleus to follow conformational changes and/or binding events. As an example, it has been shown that chiral fluorinated diaminocyclopentanes (general structure **27**, FIG. 4b) could bind to different structured RNAs leading to distinct ^{19}F NMR signal splittings.[68] Therefore, fluorinated ligands can be exploited as sensitive NMR probes to investigate dynamic RNA structures, delivering a topological footprint of the RNA. These small fluorinated reporters were also used for monitoring the binding of unlabeled RNA with unlabeled ligands and to qualitatively rank different binders for a structured RNA.[44]

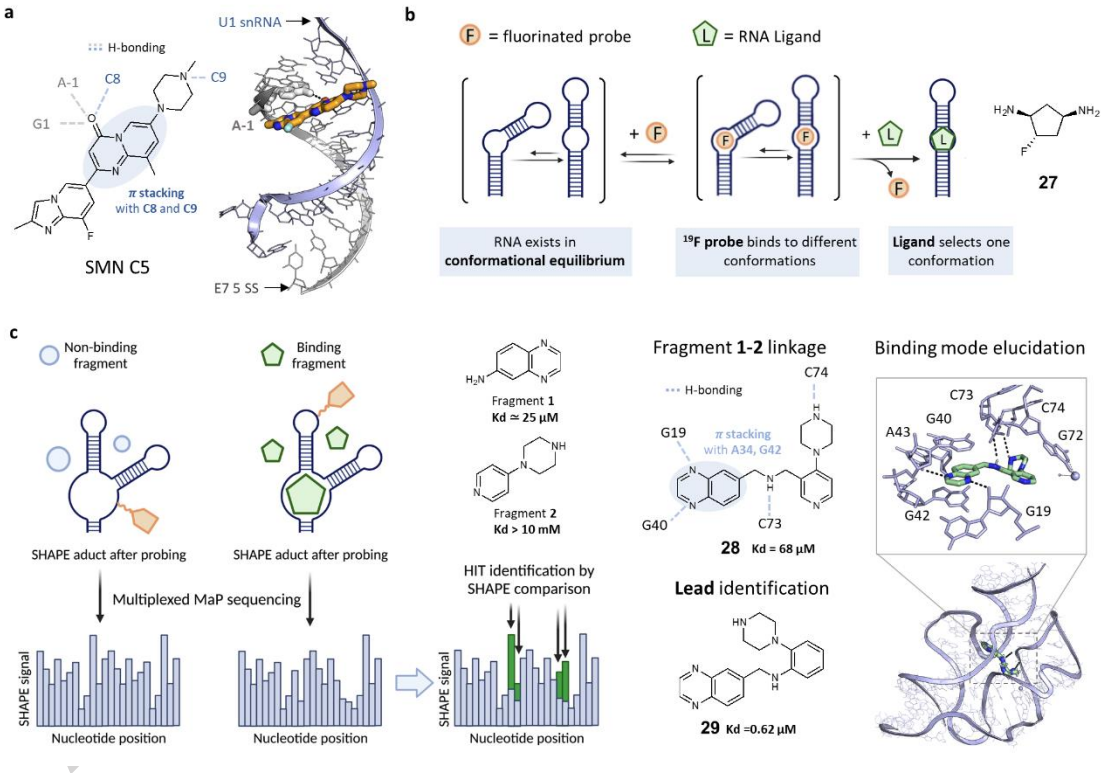

Fig. 4. | **NMR and SHAPE methodologies for RNA structure determination. a** | **SMN C5** molecular glue between U1 snRNA (represented in light blue) and E7 5' SS (represented in white) by stabilizing a bulged A (white sticks) inside the duplex. Binding mode determined by NMR (PDB ID:6HMO); **b** | Fluorinated probe **27** binds to different RNA conformations existing in solution and thus the conformational ensemble can be studied by ^{19}F NMR. Upon binding of the unmarked ligand, the selection of the bound conformation and the perturbation of the equilibrium can be monitored by ^{19}F NMR; **c** | Cartoon representation of SHAPE-MaP methodology. Binding events perturb SHAPE signal and the comparison between bound and unbound structure leads to identification of the binding nucleotides (indicated in green). Binding fragments **1** and **2** are next linked together to improve binding affinity, leading to compound **28**. Binding mode elucidation of **28** by X-ray inside the TPP

riboswitch (PDB ID: 7TZU, ligand **28** represented with green sticks, key contact nucleotides are shown) and subsequent structure based molecular modeling led to the design of optimized compound **29**.

Among the most relevant techniques available to access RNA secondary and tertiary structures, selective 2'-hydroxyl acylation analyzed by primer extension (SHAPE) is largely applied to accurately identify paired and unpaired bases on RNA sequences as well as transcriptome-wide.[69,70] Mutational profiling (SHAPE-MaP) makes possible the *de novo* and large-scale identification of RNA functional motifs.[71] This helped in the understanding of actual structures that can be found *in vivo* and that can represent the target of ligands even if the dynamics of RNA and of ligand binding events make the design of compounds appropriate for the desired biological activity very difficult.[72] Recently, SHAPE chemical probing of RNA and fragment-based ligand discovery were both combined to discover small fragments binding an RNA structure of interest, the thiamine pyrophosphate (TPP) riboswitch, and to identify the individual sites of binding at roughly nucleotide resolution.[73] The fragments were identified through a particularly clever workflow including a modular RNA screening construct containing two target motifs that allowed the assessment of affinity and specificity during the screening. The authors then linked fragments interacting with two different sites on the targeted RNA to efficiently obtain optimized compounds, such as compounds **28** and **29** (FIG. 4c). Without resemblance to the native ligand, they are not only druglike and with high ligand efficiency, but also able to modulate RNA conformation during co-transcriptional folding.

A combination of artificial intelligence (AI)-augmented molecular simulations with experimental techniques such as SHAPE-MaP, microscale thermophoresis (MST) or fluorescence intensity assays (FIA) was also recently employed to evaluate the predictability of RNA dynamics and ligand binding events.[74].[12] It was shown for cognate and synthetic ligands of PreQ1 riboswitch that unbiased molecular dynamics (MD) simulations with classical all-atom force-fields for RNA and water can provide the same flexibility profile as measured in SHAPE experiments. Since the time scales for ligand dissociation are far slower than MD, an AI-augmented MD method, called RAVE, was developed and revealed to be able to reproduce relative binding affinity measurements obtained from experimental results. Furthermore, this methodology was able to highlight which nucleotides are essential for ligand dissociation in a reliable way. These interactions would have been difficult to identify otherwise since they are distant from the binding site and do not interact directly with the studied ligands.

Other structural biology approaches, especially crystallography and cryo-EM, can be employed to better understand the three-dimensional structure of the target together with its dynamic, but can rarely account for the entire conformational landscape of a particular RNA alone. It is thus clear that a combination of multiple innovative approaches will achieve the goal of identifying specific ligands for functional structures toward a relevant biological output.

New modalities achieving RNA binding with additional functionalities

Accepted Manuscript

Recent strategies have enabled the design of ligands with enhanced features, primarily driven by the need for target identification and validation. An efficient method in this regard is chemical cross-linking and isolation by pull-down (Chem-CLIP).[75] In this technique, an RNA-binding molecule is equipped with a chemical cross-linker, like nitrogen mustard or diazirine, and a biotin purification tag (FIG. 5a).[76] Upon RNA binding, the cross linker is brought into high concentration and undergoes a proximity-based reaction. Resulting covalent adducts, purified *via* biotin, reveal the molecule's cellular targets. Chem-CLIP was employed to map binding sites against oncogenic pre-miR-21, leading to the identification of fragments from 460 diazirine compounds that bind RNA upon irradiation. Notably, combining promising fragments with a pre-miR-21 binder produced compound **30** (FIG. 5e), which inhibited pre-miR-21 processing in breast cancer cells. Covalent RNA ligand binding offers a promising approach for ligand discovery and intracellular RNA target validation. Combined transcriptome-wide analyses can further elucidate intracellular targets, as evidenced by studies on PreQ1 riboswitch and QSOX1 mRNA 5'-UTR binders.[77,78] Such research shows the feasibility of studying small molecule/RNA interactions in intact biological systems. and demonstrate that it is possible to study small molecule/RNA interactions in an unbiased way and in intact biological systems.

The introduction of cleavage activity and RNA binding is another modality that showed excellent results. Inspiration for this came from RNases enzymes that can cleave RNA thanks to the presence of one or two histidine residues in their catalytic site. These two residues act as acidic and basic imidazolium and imidazole units coordinating the phosphorous intermediate during the transition state together with other protonated side chains such as lysine (FIG. 5b) inducing the cleavage of the phosphodiester bond. Adding one or more histidine or imidazole residues to RNA ligands such as intercalators,[79] peptides,[80] or aminoglycosides[81] has thus been applied as a strategy to induce RNA cleavage more or less specifically depending on the selectivity of the RNA binder.

A known compound able to induce DNA and RNA cleavage is bleomycin, a natural product extracted from *Streptomyces* and used in clinics as an anticancer agent with a complex mechanism of action including topoisomerase inhibition.[82] Bleomycin was thus also applied to RNA cleavage by studying its preferential cleavage site and identifying it in the precursors of miR-10b (FIG. 5c).[83] Cleavage occurred close to the Drosha and Dicer cleavage site and it was demonstrated *in vitro* and in cells to reduce the production of oncogenic miR-10b. Bleomycin was then conjugated to binders specific for a particular RNA target such as targaprimiR-96 (compound **31**, FIG. 5e)[84] or ligand of r(CUG)^{exp} to induce a specific cleavage and degradation of the target.[85]

Accepted Manuscript

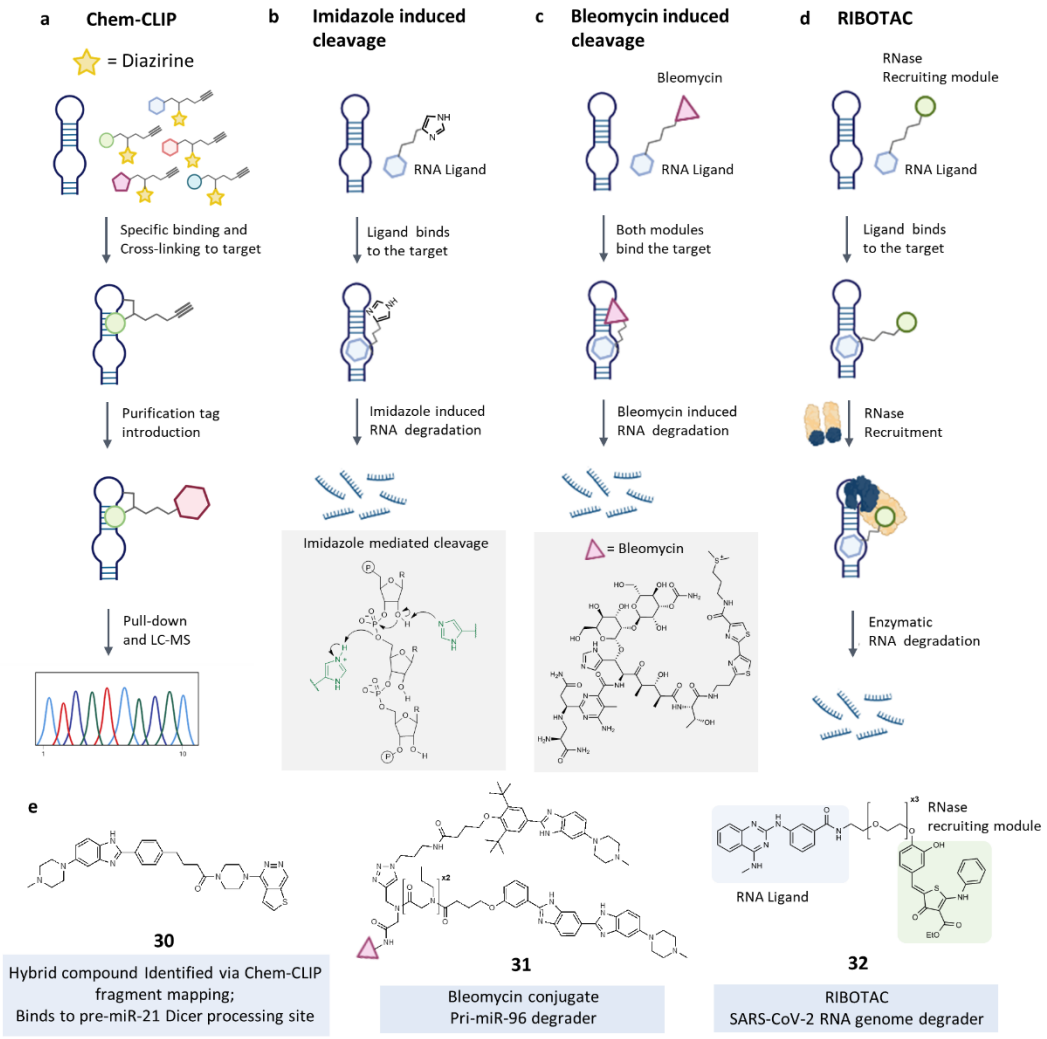

Fig. 5 | **Achieving RNA binding with additional functionalities. a |** Chem-CLIP methodology for target engagement or binding site mapping through covalent binding; **b |** RNA ligands conjugated with imidazole are able to induce RNA cleavage, the mechanism is shown in the grey box; **c |** Bleomycin conjugated to efficient RNA ligands induces cleavage of the RNA target; **d |** Ribonuclease targeting chimeras (RIBOTACs) are bivalent compounds able to recruit RNases and induce RNA cleavage**; e |** Chemical structures of pre-miR-21 binder **30** identified via Chem-CLIP-Frag-Map, Bleomycin conjugate of targapri-miR96 **31** and RIBOTAC **32** against the SARS-CoV-2 RNA genome.

Altogether, these examples based on the conjugation of a covalent or cleavage moiety to an RNA ligand illustrate that these methodologies can be useful not only in target validation studies, but also to increase the actual biological effect when the selectivity is not affected.

A recent innovation in RNA targeting is the development of ribonuclease targeting chimeras, or RIBOTACs.[86] These involve covalently linking a specific RNA ligand to a molecule that activates RNase L, an RNA-degrading enzyme (FIG. 5d). This approach has been applied to various RNA binders, including targapremir-210 (**18**) and targapremir-96, and has been explored for targeting the RNA genome of SARS-CoV2, highlighting its potential in RNA therapeutics.[87] Using InfoRNA, a binder was identified for the SARS-CoV-2 frameshifting element RNA, that bears a 1x1 nucleotide UU internal loop crucial for frameshifting function.[87] Subsequent detailed *in vitro* and *in cellulo* analysis led

Accepted

to the discovery of compound **32** (FIG. 5e), a ligand with nanomolar affinity that stabilizes the RNA's hairpin structure and inhibits frameshifting. Chem-CLIP was employed to ascertain the intracellular target of **32**, upon conjugation to a nitrogen mustard. Additionally, **32** was modified to create RIBOTAC **32** (FIG. 5e), which induces targeted RNA cleavage, similar to how PROTACs target proteins This compound effectively degraded the entire SARS-CoV construct. Optimization of the RIBOTAC strategy enhanced the compound's bioactivity, as evidenced by intracellular luciferase reporter assays. This methodological combination of chemical modification and various assays facilitated the identification of specific ligands that effectively target cells without inducing toxicity. The question of the applicability of these complex tools *in vivo* remains open, but the numerous examples reported so far hold the promise for further developments in the near future analogously to what happened for PROTACs.[88] The combination of RNA binding and selectivity properties of a ligand with a chemical tool with covalent and/or cleavage properties certainly represents an interesting approach for chemical biology and medicinal chemistry applications. This leads to compounds that move away from the commonly accepted drug-like properties but many recent developments in drug discovery show that these criteria need to remain flexible to leave the way open to new modalities toward major therapeutic discoveries.

Shaping Future Medicinal and Synthetic Chemistry of small molecules targeting RNA

As shown in this overview of design strategies and chemical approaches that have been used in recent years to approach RNA as a biological target, the general knowledge about RNA binders is continuously growing and major improvements are in progress thanks to innovation and inventiveness in this particular and yet fascinating field. RNA that was once considered undruggable and almost impossible to be targeted specifically is now considered a valuable target with the potential to become more and more exploited in the discovery of chemical probes to better understand its numerous and still unknown functions. Many efforts have been engaged by the academic and private sector to expand the field of RNA targeting by small molecules. Despite the numerous developments that have been performed during the last decades and even if the contribution for a better understanding of complex biological processes is undeniable , it remains hard to predict if RNA binders will fulfillall expectations and open new avenues for therapy. The analysis of the RNA binders reported so far allows for the identification of some common features, such as the presence of protonated groups, the introduction of nitrogen-containing heteroaromatic moieties or nucleobases and often the use of sp3-rich compounds corresponding to the tendency in medicinal chemistry to escape from flatland. Drug-likeness has been achieved successfully, but it is essential to leave the field open to new modalities bearing originaloutside common drug-like landscape. The most important question that remains open concerns a standard methodology to obtain of the desired and specific biological effect with such RNA-targeting small molecules. Despite relevant *in vivo* studies and a few clinical successes, many reported ligands lack in cells and *in vivo* proof of specificity and correlation between the observed biological effect and the

Accepted Manuscript

specific targeting of the desired RNA. Further studies are thus needed especially concerning target validation experiments, structural biology regarding the actual conformation and structure of the target and *in vivo* validation of the biological activity. Also, it is somehow hard to distinguish between biological activity induced by pure RNA binders, by RNA-protein inhibitors or RNA-protein glues in a biological context where a lot of off targets could reduce the biological activity even without inducing toxic effects. This is of course true for all bioactive molecules, but somehow it became evident mainly in the RNA-targeting field. A deep study of the site(s) of interaction and the accurate choice of these sites that must be functional to lead to activity, is an essential parameter to reach the desired activity. The tools presented here, including chemical strategies for the targeting of RNA primary, secondary and tertiary structures and innovative approaches to understand RNA binding, function and biological outcome represent the main basis and guidelines for what should be the next step: rational design of ligands specific for the desired target and bearing efficient and potent biological activity thus creating new ways to answer complex biological questions and opening new avenues for therapy. The upcoming years will be decisive to confirm (or not) this optimistic view of the field.

Accepted Manuscript

Box 1 – Primary, secondary and tertiary structures of RNA explained.

Ribonucleic acids (RNAs) are multifaceted molecules accomplishing various tasks in living cells by acquiring complex and unique 3D structures. These latter are formed through different levels of organization, including primary, secondary, tertiary, and quaternary structures and provide resourceful sites for selective and specific identification by proteins or small molecules. The primary structure of RNA consists of a linear sequence of nucleotides, each comprising a nucleobase, a ribose sugar, and a phosphate group that links the sugars through phosphodiester bonds. The four nucleobases: guanine (G), adenine (A), cytosine (C), and uracil (U), attach to the backbone with, respectively, their N9 for purines (A and G) and their N1 for pyrimidines (C and U) and the ribose sugars.[89]

RNA secondary structures result from hydrogen bonds between nucleobases, forming various folding patterns. The most common secondary structure is the Watson-Crick-Franklin canonical base pairing between A-U and C-G base pairs, resulting in RNA double helices with an A-form, instead of the B-form found in DNA due to a hydroxyl group at the 2' position of the sugar. Other secondary structures such as internal loops, hairpin loops, and bulges are formed by single-stranded sections of nucleotides.[90] Overall, secondary structures are behind the formation of 3D arrangements of RNA, called tertiary structures.[91,92]

RNA tertiary structures arise from connections between secondary structures, leading to specific tridimensional arrangements. The stacking of bases increases the likelihood of these interactions, leading to complex structures such as pseudoknots and kissing loop complexes.[93] G-quadruplexes, riboswitches and triple helices are also part of RNA tertiary structures. RNA quaternary structures occur when RNA interacts with other biomolecules to carry out its biological function.

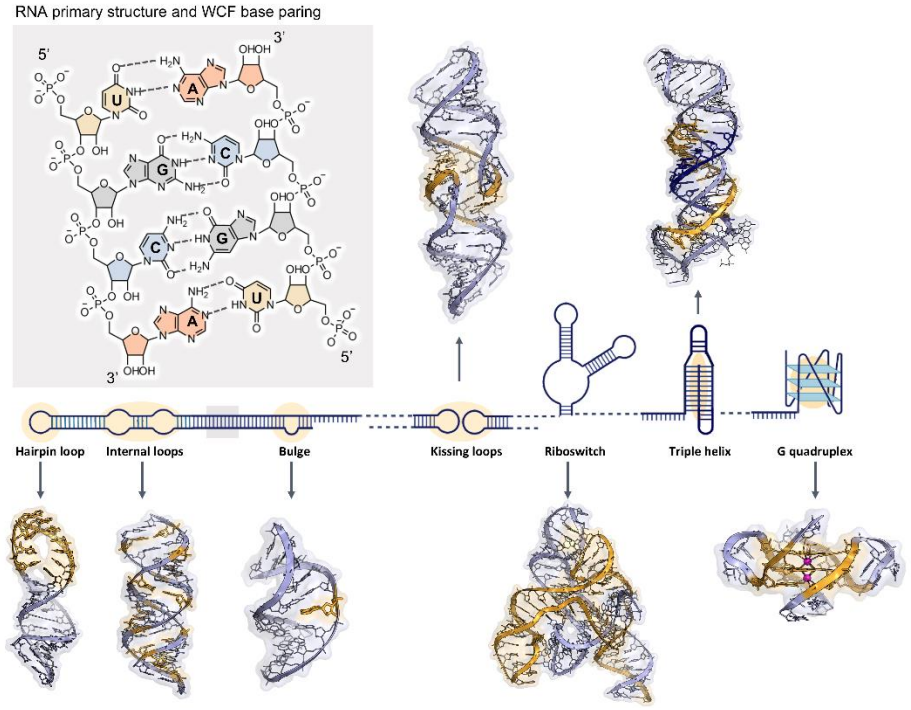

Accepted Manuscript

Box 2 - Integrated technologies for the discovery of RNA ligands

Beside the development of predictive approaches and chemoinformatic tools to describe the main features for RNA targeting, such as R-BIND (RNA-targeted BIoactive LigaNd Database), innovative screening methodologies have been developed for the discovery of RNA binders and have been integrated to the methodologies described in this manuscript.[94-96] Fragment-based drug discovery (FBDD),[97] coupled to Chem-CLIP or SHAPE, has been particularly useful for the discovery of original chemical scaffolds.[73,76] Dynamic combinatorial chemistry (DCC, a) was shown as a powerful strategy to identify specific bioactive compounds. Compounds able to assembly and form a dynamic library *via* a reversible reaction are put in the presence of the biological target to favor the formation of the strongest binder(s).[98] *In situ* approaches have also led to informative results. Potent modulators of RNA function could indeed be assembled *in cellulo* by using cells as a reaction vessel and a disease-causing RNA as a catalyst.[99]

Also, the use of DNA-encoded libraries (DEL, b) has been applied to the search for RNA binders. In a relevant example, a screen of a DNA-encoded library against a library of RNA structures in order to evaluate 300 million interactions in total, allowed for the identification of numerous ligand/target pairs.[100]

High-throughput screenings have been also largely applied to the discovery of RNA binders. Beside phenotypic screenings, various recent innovative methodologies have been reported. Among them, Automated Ligand Detection System (ALIS, c), an indirect affinity-selection mass spectrometry (AS-MS) has been employed for the high-throughput screening of unbiased libraries of small molecules for ncRNAs interactions.[101].[51] Also, catalytic enzyme-linked click chemistry assay (cat-ELCCA) was applied to the screening for compounds able to inhibit pre-let7/Lin28 interactions. The main advantages of these assays are the robustness, the high sensitivity due to catalytic signal amplification and negligible compound interference compared to other fluorescence-based assays.

Accepted Manuscript

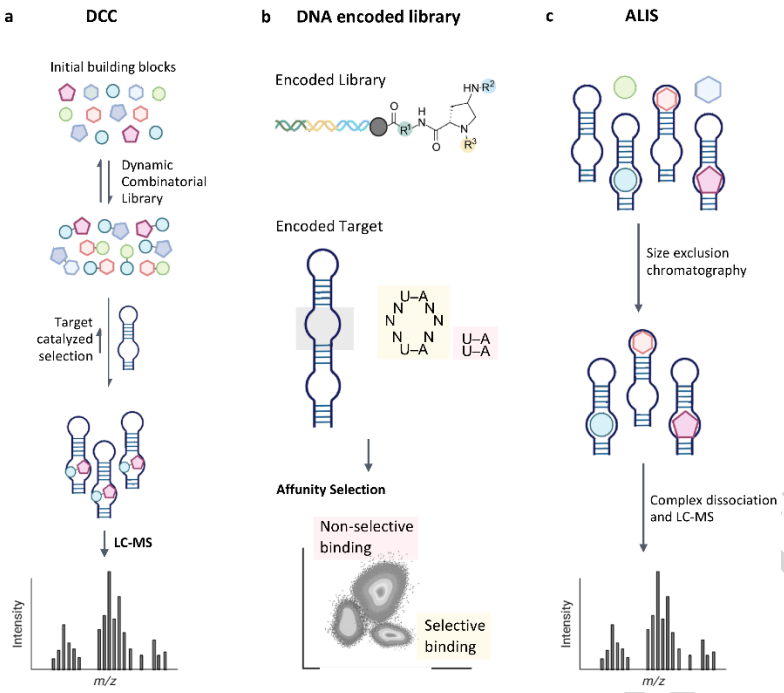

Accepted Manuscript

Acknowledgments

The authors thank the Italian Institute of Technology (IIT) and Université Côte d'Azur for financial support to M.P. as PhD fellowship, respectively. The authors also thank BoostUrCareer COFUND project with Région PACA and European Union's Horizon 2020 research and innovation program under grant agreement no. 847581 for PhD fellowship to S.K.

Competing Interests

The authors declare no competing interests.

Accepted Manuscript

References

1 Childs-Disney, J. L. *et al.* Targeting RNA structures with small molecules. *Nat. Rev. Drug Discov.* **21**, 736-762 (2022).

2 Crooke, S. T., Baker, B. F., Crooke, R. M. & Liang, X. H. Antisense technology: an overview and prospectus. *Nat. Rev. Drug Discov.* **20**, 427-453 (2021).

3 Roberts, T. C., Langer, R. & Wood, M. J. A. Advances in oligonucleotide drug delivery. *Nat. Rev. Drug Discov.* **19**, 673-694 (2020).

4 Falese, J. P., Donlic, A. & Hargrove, A. E. Targeting RNA with small molecules: from fundamental principles towards the clinic. *Chem. Soc. Rev.* **50**, 2224-2243 (2021).

5 Warner, K. D., Hajdin, C. E. & Weeks, K. M. Principles for targeting RNA with drug-like small molecules. *Nat. Rev. Drug Discov.* **17**, 547-558 (2018).

6 Zamani, F. & Suzuki, T. Synthetic RNA Modulators in Drug Discovery. *J. Med. Chem.* **64**, 7110-7155 (2021).

7 Magnet, S. & Blanchard, J. S. Molecular insights into aminoglycoside action and resistance. *Chem. Rev.* **105**, 477-498 (2005).

8 Wilson, D. N. Ribosome-targeting antibiotics and mechanisms of bacterial resistance. *Nat. Rev. Microbiol.* **12**, 35-48 (2014).

9 Thomas, J. R. & Hergenrother, P. J. Targeting RNA with small molecules. *Chem. Rev.* **108**, 1171-1224 (2008).

10 Ratni, H., Scalco, R. S. & Stephan, A. H. Risdiplam, the First Approved Small Molecule Splicing Modifier Drug as a Blueprint for Future Transformative Medicines. *ACS Med. Chem. Lett.* **12**, 874-877 (2021).

11 Di Giorgio, A. & Duca, M. Synthetic small-molecule RNA ligands: future prospects as therapeutic agents. *MedChemComm* **10**, 1242-1255 (2019).

12 Ganser, L. R. *et al.* High-performance virtual screening by targeting a high-resolution RNA dynamic ensemble. *Nat. Struct. Mol. Biol.* **25**, 425-434 (2018).

13 Padroni, G., Patwardhan, N. N., Schapira, M. & Hargrove, A. E. Systematic analysis of the interactions driving small molecule-RNA recognition. *RSC Med. Chem.* **11**, 802-813 (2020).

14 Howe, J. A. *et al.* Selective small-molecule inhibition of an RNA structural element. *Nature* **526**, 672-677 (2015).

15 Wang, S., Huber, P. W., Cui, M., Czarnik, A. W. & Mei, H. Y. Binding of neomycin to the TAR element of HIV-1 RNA induces dissociation of Tat protein by an allosteric mechanism. *Biochemistry* **37**, 5549-5557 (1998).

16 Golkar, T. *et al.* Structural basis for plazomicin antibiotic action and resistance. *Commun. Biol.* **4**, 729 (2021).

17 Aradi, K., Di Giorgio, A. & Duca, M. Aminoglycoside Conjugation for RNA Targeting: Antimicrobials and Beyond. *Chem. Eur. J.* **26**, 12273-12309 (2020).

18 Bera, S., Mondal, D., Palit, S. & Schweizer, F. Structural modifications of the neomycin class of aminoglycosides. *MedChemComm*, 1499 (2016).

19 Ennifar, E. *et al.* Structure-guided discovery of a novel aminoglycoside conjugate targeting HIV-1 RNA viral genome. *ACS Chem. Biol.* **8**, 2509-2517 (2013).

20 Blount, K. F. & Tor, Y. A tale of two targets: differential RNA selectivity of nucleobase-aminoglycoside conjugates. *ChemBioChem* **7**, 1612-1621 (2006).

21 Gebert, L. F. R. & MacRae, I. J. Regulation of microRNA function in animals. *Nat. Rev. Mol. Cell. Biol.* **20**, 21-37 (2019).

22 Maucort, C. *et al.* Design and Implementation of Synthetic RNA Binders for the Inhibition of miR-21 Biogenesis. *ACS Med. Chem. Lett.* **12**, 899-906 (2021).

23 Vo, D. D. *et al.* Building of neomycin-nucleobase-amino acid conjugates for the inhibition of oncogenic miRNAs biogenesis. *Org. Biomol. Chem.* **16**, 6262-6274 (2018).

24 Vo, D. D. *et al.* Targeting the production of oncogenic microRNAs with multimodal synthetic small molecules. *ACS Chem. Biol.* **9**, 711-721 (2014).

Accepted Manuscript

25 Vo, D. D. *et al.* Oncogenic MicroRNAs Biogenesis as a Drug Target: Structure-Activity Relationship Studies on New Aminoglycoside Conjugates. *Chem. Eur. J.* **22**, 5350-5362 (2016).

26 Malnuit, V., Duca, M. & Benhida, R. Targeting DNA base pair mismatch with artificial nucleobases. Advances and perspectives in triple helix strategy. *Org. Biomol. Chem.* **9**, 326-336 (2011).

27 Disney, M. D. *et al.* Two-dimensional combinatorial screening identifies specific aminoglycoside-RNA internal loop partners. *J. Am. Chem. Soc.* **130**, 11185-11194 (2008).

28 Velagapudi, S. P. & Disney, M. D. Two-dimensional combinatorial screening enables the bottom-up design of a microRNA-10b inhibitor. *Chem. Commun. (Camb)* **50**, 3027-3029 (2014).

29 Davis, B. *et al.* Rational design of inhibitors of HIV-1 TAR RNA through the stabilisation of electrostatic "hot spots". *J. Mol. Biol.* **336**, 343-356 (2004).

30 Patwardhan, N. N. *et al.* Amiloride as a new RNA-binding scaffold with activity against HIV-1 TAR. *MedChemComm* **8**, 1022-1036 (2017).

31 Davila-Calderon, J. *et al.* IRES-targeting small molecule inhibits enterovirus 71 replication via allosteric stabilization of a ternary complex. *Nat. Commun.* **11**, 4775 (2020).

32 Patwardhan, N. N., Cai, Z., Newson, C. N. & Hargrove, A. E. Fluorescent peptide displacement as a general assay for screening small molecule libraries against RNA. *Org. Biomol. Chem.* **17**, 1778-1786 (2019).

33 Zafferani, M. *et al.* Amilorides inhibit SARS-CoV-2 replication in vitro by targeting RNA structures. *Sci. Adv.* **7**, eabl6096 (2021).

34 Wilson, L., Gage, P. & Ewart, G. Hexamethylene amiloride blocks E protein ion channels and inhibits coronavirus replication. *Virology* **353**, 294-306 (2006).

35 Hagler, L. D. *et al.* Versatile Target-Guided Screen for Discovering Bidirectional Transcription Inhibitors of a Trinucleotide Repeat Disease. *ACS Med. Chem. Lett.* **12**, 935-940 (2021).

36 Hagler, L. D. *et al.* Expanded DNA and RNA Trinucleotide Repeats in Myotonic Dystrophy Type 1 Select Their Own Multitarget, Sequence-Selective Inhibitors. *Biochemistry* **59**, 3463-3472 (2020).

37 Mirkin, S. M. Expandable DNA repeats and human disease. *Nature* **447**, 932-940 (2007).

38 Wong, C. H. *et al.* Targeting toxic RNAs that cause myotonic dystrophy type 1 (DM1) with a bisamidinium inhibitor. *J. Am. Chem. Soc.* **136**, 6355-6361 (2014).

39 Krueger, S. B., Lanzendorf, A. N., Jeon, H. H. & Zimmerman, S. C. Selective and Reversible Ligand Assembly on the DNA and RNA Repeat Sequences in Myotonic Dystrophy. *ChemBioChem* **23**, e202200260 (2022).

40 Pushechnikov, A. *et al.* Rational design of ligands targeting triplet repeating transcripts that cause RNA dominant disease: application to myotonic muscular dystrophy type 1 and spinocerebellar ataxia type 3. *J. Am. Chem. Soc.* **131**, 9767-9779 (2009).

41 Jahromi, A. H. *et al.* A novel CUG(exp).MBNL1 inhibitor with therapeutic potential for myotonic dystrophy type 1. *ACS Chem. Biol.* **8**, 1037-1043 (2013).

42 Chien, C. M. *et al.* Structural Basis for Targeting T:T Mismatch with Triaminotriazine-Acridine Conjugate Induces a U-Shaped Head-to-Head Four-Way Junction in CTG Repeat DNA. *J. Am. Chem. Soc.* **142**, 11165-11172 (2020).

43 Murata, A., Otabe, T., Zhang, J. & Nakatani, K. BzDANP, a Small-Molecule Modulator of Pre-miR-29a Maturation by Dicer. *ACS Chem. Biol.* **11**, 2790-2796 (2016).

44 Lombes, T. *et al.* Investigation of RNA-ligand interactions by 19F NMR spectroscopy using fluorinated probes. *Angew. Chem. Int. Ed. Engl.* **51**, 9530-9534 (2012).

45 Murata, A., Nakamori, M. & Nakatani, K. Modulating RNA secondary and tertiary structures by mismatch binding ligands. *Methods* **167**, 78-91 (2019).

46 Murata, A. *et al.* Small Molecule-Induced Dimerization of Hairpin RNA Interfered with the Dicer Cleavage Reaction. *Biochemistry* **60**, 245-249 (2021).

47 Konieczny, P. *et al.* Cyclic mismatch binding ligands interact with disease-associated CGG trinucleotide repeats in RNA and suppress their translation. *Nucleic Acids Res.* **49**, 9479-9495 (2021).

Accepted Manuscript

48 Mukherjee, S. *et al.* HT-SELEX-based identification of binding pre-miRNA hairpin-motif for small molecules. *Mol. Ther. Nucleic Acids* **27**, 165-174 (2022).

49 Howe, J. A. *et al.* Atomic resolution mechanistic studies of ribocil: A highly selective unnatural ligand mimic of the E. coli FMN riboswitch. *RNA Biol.* **13**, 946-954 (2016).

50 Aguilar, R. *et al.* Targeting Xist with compounds that disrupt RNA structure and X inactivation. *Nature* **604**, 160-166 (2022).

51 Carrette, L. L. G. *et al.* A mixed modality approach towards Xi reactivation for Rett syndrome and other X-linked disorders. *Proc. Natl. Acad. Sci. USA* **115**, E668-E675 (2018).

52 Ursu, A. *et al.* Design of small molecules targeting RNA structure from sequence. *Chem Soc Rev* **49**, 7252-7270 (2020).

53 Velagapudi, S. P., Seedhouse, S. J. & Disney, M. D. Structure-activity relationships through sequencing (StARTS) defines optimal and suboptimal RNA motif targets for small molecules. *Angew. Chem. Int. Ed. Engl.* **49**, 3816-3818 (2010).

54 Disney, M. D. *et al.* Inforna 2.0: A Platform for the Sequence-Based Design of Small Molecules Targeting Structured RNAs. *ACS Chem. Biol.* **11**, 1720-1728 (2016).

55 Velagapudi, S. P., Gallo, S. M. & Disney, M. D. Sequence-based design of bioactive small molecules that target precursor microRNAs. *Nat. Chem. Biol.* **10**, 291-297 (2014).

56 Costales, M. G. *et al.* Small Molecule Inhibition of microRNA-210 Reprograms an Oncogenic Hypoxic Circuit. *J Am Chem Soc* **139**, 3446-3455 (2017).

57 Haniff, H. S. *et al.* A structure-specific small molecule inhibits a miRNA-200 family member precursor and reverses a type 2 diabetes phenotype. *Cell Chem. Biol.* **29**, 300-311 e310 (2022).

58 Chen, J. L. *et al.* Design, Optimization, and Study of Small Molecules That Target Tau Pre-mRNA and Affect Splicing. *J. Am. Chem. Soc.* **142**, 8706-8727 (2020).

59 Dibrov, S. M. *et al.* Structure of a hepatitis C virus RNA domain in complex with a translation inhibitor reveals a binding mode reminiscent of riboswitches. *Proc. Natl. Acad. Sci. USA* **109**, 5223-5228 (2012).

60 Shibata, T. *et al.* Small molecule targeting r(UGGAA)(n) disrupts RNA foci and alleviates disease phenotype in Drosophila model. *Nat. Commun.* **12**, 236 (2021).

61 Boehr, D. D., Nussinov, R. & Wright, P. E. The role of dynamic conformational ensembles in biomolecular recognition. *Nat. Chem. Biol.* **5**, 789-796 (2009).

62 Nakatani, K. Possibilities and challenges of small molecule organic compounds for the treatment of repeat diseases. *Proc. Jpn. Acad. Ser. B Phys. Biol. Sci.* **98**, 30-48 (2022).

63 Vogt, A. D. & Di Cera, E. Conformational selection or induced fit? A critical appraisal of the kinetic mechanism. *Biochemistry* **51**, 5894-5902 (2012).

64 Bailor, M. H., Mustoe, A. M., Brooks, C. L., 3rd & Al-Hashimi, H. M. Topological constraints: using RNA secondary structure to model 3D conformation, folding pathways, and dynamic adaptation. *Curr. Opin. Struct. Biol.* **21**, 296-305 (2011).

65 Marusic, M., Toplishek, M. & Plavec, J. NMR of RNA - Structure and interactions. *Curr. Opin. Struct. Biol.* **79**, 102532 (2023).

66 Shortridge, M. D. *et al.* Drug-Like Small Molecules That Inhibit Expression of the Oncogenic MicroRNA-21. *ACS Chem Biol* **18**, 237-250 (2023).

67 Campagne, S. *et al.* Structural basis of a small molecule targeting RNA for a specific splicing correction. *Nat. Chem. Biol.* **15**, 1191-1198 (2019).

68 Moumne, R. *et al.* Fluorinated diaminocyclopentanes as chiral sensitive NMR probes of RNA structure. *J. Am. Chem. Soc.* **132**, 13111-13113 (2010).

69 Bevilacqua, P. C., Ritchey, L. E., Su, Z. & Assmann, S. M. Genome-Wide Analysis of RNA Secondary Structure. *Annu. Rev. Genet.* **50**, 235-266 (2016).

70 Deigan, K. E., Li, T. W., Mathews, D. H. & Weeks, K. M. Accurate SHAPE-directed RNA structure determination. *Proc. Natl. Acad. Sci. USA* **106**, 97-102 (2009).

71 Siegfried, N. A., Busan, S., Rice, G. M., Nelson, J. A. & Weeks, K. M. RNA motif discovery by SHAPE and mutational profiling (SHAPE-MaP). *Nat. Methods* **11**, 959-965 (2014).

Accepted Manuscript

72 Weeks, K. M. SHAPE Directed Discovery of New Functions in Large RNAs. *Acc. Chem. Res.* **54**, 2502-2517 (2021).

73 Zeller, M. J. *et al.* SHAPE-enabled fragment-based ligand discovery for RNA. *Proc. Natl. Acad. Sci. USA* **119**, e2122660119 (2022).

74 Wang, Y., Parmar, S., Schneekloth, J. S. & Tiwary, P. Interrogating RNA-Small Molecule Interactions with Structure Probing and Artificial Intelligence-Augmented Molecular Simulations. *ACS Cent. Sci.* **8**, 741-748 (2022).

75 Velagapudi, S. P., Li, Y. & Disney, M. D. A cross-linking approach to map small molecule-RNA binding sites in cells. *Bioorg Med Chem Lett* **29**, 1532-1536 (2019).

76 Suresh, B. M. *et al.* A general fragment-based approach to identify and optimize bioactive ligands targeting RNA. *Proc. Natl. Acad. Sci. USA* **117**, 33197-33203 (2020).

77 Balaratnam, S. *et al.* A chemical probe based on the PreQ(1) metabolite enables transcriptome-wide mapping of binding sites. *Nat Commun* **12**, 5856 (2021).

78 Tong, Y. *et al.* Transcriptome-Wide Mapping of Small-Molecule RNA-Binding Sites in Cells Informs an Isoform-Specific Degrader of QSOX1 mRNA. *J Am Chem Soc* **144**, 11620-11625 (2022).

79 Vlassov, V. V., Zuber, G., Felden, B., Behr, J. P. & Giege, R. Cleavage of tRNA with imidazole and spermine imidazole constructs: a new approach for probing RNA structure. *Nucleic Acids Res.* **23**, 3161-3167 (1995).

80 Tamkovich, N. *et al.* Design, RNA cleavage and antiviral activity of new artificial ribonucleases derived from mono-, di- and tripeptides connected by linkers of different hydrophobicity. *Bioorg. Med. Chem.* **24**, 1346-1355 (2016).

81 Martin, C. *et al.* Design, Synthesis, and Evaluation of Neomycin-Imidazole Conjugates for RNA Cleavage. *ChemPlusChem* **87**, e202200250 (2022).

82 Hecht, S. M. Bleomycin: new perspectives on the mechanism of action. *J Nat Prod* **63**, 158-168 (2000).

83 Angelbello, A. J. & Disney, M. D. Bleomycin Can Cleave an Oncogenic Noncoding RNA. *ChemBioChem* **19**, 43-47 (2018).

84 Li, Y. & Disney, M. D. Precise Small Molecule Degradation of a Noncoding RNA Identifies Cellular Binding Sites and Modulates an Oncogenic Phenotype. *ACS Chem. Biol.* **13**, 3065-3071 (2018).

85 Angelbello, A. J. *et al.* Precise small-molecule cleavage of an r(CUG) repeat expansion in a myotonic dystrophy mouse model. *Proc. Natl. Acad. Sci. USA* **116**, 7799-7804 (2019).

86 Liu, X. *et al.* Targeted Degradation of the Oncogenic MicroRNA 17-92 Cluster by Structure-Targeting Ligands. *J. Am. Chem. Soc.* **142**, 6970-6982 (2020).

87 Haniff, H. S. *et al.* Targeting the SARS-CoV-2 RNA Genome with Small Molecule Binders and Ribonuclease Targeting Chimera (RIBOTAC) Degraders. *ACS Cent. Sci.* **6**, 1713-1721 (2020).

88 Li, K. & Crews, C. M. PROTACs: past, present and future. *Chem Soc Rev* **51**, 5214-5236 (2022).

89 Morgan, B. S. & Hargrove, A. E. Synthetic Receptors for Biomolecules: Design Principles and Applications. *The Royal Society of Chemistry*, 253-325 (2015).

90 Kenyon, J., Prestwood, L. & Lever, A. Current perspectives on RNA secondary structure probing. *Biochem Soc Trans* **42**, 1251-1255 (2014).

91 Batey, R. T., Rambo, R. P. & Doudna, J. A. Tertiary Motifs in RNA Structure and Folding. *Angew Chem Int Ed Engl* **38**, 2326-2343 (1999).

92 Butcher, S. E. & Pyle, A. M. The molecular interactions that stabilize RNA tertiary structure: RNA motifs, patterns, and networks. *Acc. Chem. Res.* **44**, 1302-1311 (2011).

93 Jones, C. P. & R., F.-D. A. A. RNA quaternary structure and global symmetry. *Trends in Biochemical Sciences* **40**, 211-220 (2015).

94 Donlic, A. *et al.* R-BIND 2.0: An Updated Database of Bioactive RNA-Targeting Small Molecules and Associated RNA Secondary Structures. *ACS Chem. Biol.* **17**, 1556-1566 (2022).

Accepted Manuscript

95 Morgan, B. S., Forte, J. E., Culver, R. N., Zhang, Y. & Hargrove, A. E. Discovery of Key Physicochemical, Structural, and Spatial Properties of RNA-Targeted Bioactive Ligands. *Angew. Chem. Int. Ed. Engl.* **56**, 13498-13502 (2017).

96 Xie, J. & Frank, A. T. Mining for Ligandable Cavities in RNA. *ACS Med. Chem. Lett.* **12**, 928-934 (2021).

97 Murray, C. W. & Rees, D. C. The rise of fragment-based drug discovery. *Nat. Chem.* **1**, 187-192 (2009).

98 Umuhire Juru, A., Cai, Z., Jan, A. & Hargrove, A. E. Template-guided selection of RNA ligands using imine-based dynamic combinatorial chemistry. *Chem. Commun. (Camb)* **56**, 3555-3558 (2020).

99 Rzuczek, S. G., Park, H. & Disney, M. D. A toxic RNA catalyzes the in cellulo synthesis of its own inhibitor. *Angew. Chem. Int. Ed. Engl.* **53**, 10956-10959 (2014).

100 Benhamou, R. I. *et al.* DNA-encoded library versus RNA-encoded library selection enables design of an oncogenic noncoding RNA inhibitor. *Proc. Natl. Acad. Sci. USA* **119** (2022).

101 Rizvi, N. F. *et al.* Discovery of Selective RNA-Binding Small Molecules by Affinity-Selection Mass Spectrometry. *ACS Chem. Biol.* **13**, 820-831 (2018).

Accepted Manuscript

Annex 2 | Side-project: Discovery of small molecule inhibitors of miR-21 biogenesis

Alongside the main PhD project, I contributed to another ongoing project in collaboration with the laboratory of Dr. Tiziano Bandiera from the Italian Institute of Technology (IIT). The laboratory of Dr. Tiziano Bandiera has extensive experience in running drug discovery projects and it was decided to combine the large libraries of compounds of IIT with our experience in the field to discover new and efficient miR-21 inhibitors.

More specifically, the oncogenic miR-21 is one of the most extensively studied miRNAs since it is upregulated in nearly all cancers, acting as an inhibitor of tumor suppressor proteins[347]. Therefore, its downregulation represents a potential therapeutic approach for treating many tumors. Promising approaches for downregulating miR-21 production include antisense oligonucleotides (ASOs), miR sponges, CRISP/Cas9 genome editing, and small molecules[18,127]. This last approach offers an important alternative to the others, which suffer from well-known administration and pharmacokinetic limitations. Therefore, this project aims to discover new, drug-like small molecule modulators of the miR-21 biogenesis. In the search for new chemotypes capable of selectively interacting with the secondary structure of RNA targets, two well-known approaches were used to reach rapid results: Fragment-Based Drug Discovery (FBDD) and High-Throughput-Screening (HTS).

By applying a ^{19}F-NMR-based FBDD[348,349], we screened a small library of about 600 fluorinated fragments, allowing us to easily discriminate binders from non-binders of pre-miR-21. The selected fragments can be further optimized to enhance affinity and selectivity through merging, linking, or fragment growing.

To find new chemotypes capable of decreasing the levels of miR-21 in cells, a ^{19}F-NMR Fragment-based Lead Discovery approach was used against pre-miR-21[348,349].

A small library (LEF, Local Environment of Fluorine) of fluorinated fragments was screened in mixtures of 20-25 compounds each in the absence or presence of pre-miR-21[350]. Compounds that bind to the target show a line broadening of their ^{19}F NMR signal and are easily identified[351]. Fluorescent Polarization binding assays further validated the hits identified through NMR. The compounds able to bind the pre-miR-21 using both approaches required to be tested for their ability to inhibit Dicer cleavage *in vitro*. Thanks to our collaboration, the team of Dr. Bandiera in IIT sent us the newly identified binders, and we tested them with our FRET-based inhibition assay, following the protocol detailed in Section II.2.2, Chapter II. This workflow enabled the identification of small molecules as an

interesting starting point for novel miR-21 modulators, which could be further developed for use in cancer therapy.

Moreover, through a HTS of about 4000 compounds from our library, we could identify new chemotypes with good affinities to pre-miR-21 in preliminary in vitro assays. This workflow has led us to discover new small molecules that represent a good starting point for developing novel miR-21 modulators with excellent potential in cancer therapy.

Altogether, the biochemical assays performed in ICN allowed for the identification of promising pre-miR-21 binders that are currently under evaluation for their biological activity in cancer cells.

Materials & Methods

Materials & Methods

Cellular and Molecular Biology

Cell Lines

Human skin cancer A375 (CRL-1619), BT-474 (HTB-20), and human breast cancer MDA-MB-231 (CRL-HTB-26) cell lines were acquired from the American Type Culture Collection (ATCC). Human mammary epithelial cells hMEC (A10565) were acquired from Thermo Fischer Scientific.

A375, BT-474, and MDA MB 231 cells were grown in Dulbecco's Modified Eagle's Medium High Glucose, 4.5 g/l D-glucose (DMEM), supplemented with 4 mM L-glutamine, 10% fetal bovine serum (FBS) and 1X penicillin/streptomycin solution. hMEC cells were grown in HuMEC Ready Medium.

Chemicals

Cobalt chloride hexahydrate ($CoCl_2$, catalog#C8661) was acquired from Sigma-Aldrich.

Cytotoxicity assays

Cells were seeded in 96-well plates at 2000 cells/100 µL/well in culture medium and incubated overnight. For cytotoxicity assays, at 72 h post-treatment, the relative percentage of cell number was evaluated with the CyQUANT kit (Invitrogen, Carlsbad, CA, USA), setting vehicle-treated sample as 100%. Seven 3-fold serial dilutions of a 100 µM concentration of compounds were used to obtain log(inhibitor) versus response curves using GraphPad Prism 10 software (San Diego, CA, USA). IC_{50} values deriving from at least three independent experiments were used to obtain mean IC_{50} ± SEM values.

Reverse transcription quantitative polymerase chain reaction (RT-qPCR)

Total RNA was extracted using TRIzol™ Reagent (Life Technologies, catalog#15596018) or miRNeasy Mini™ kit (Qiagen, catalog#217004). Then RNA was reverse-transcribed using SuperScript™ VILO™ Master Mix (Life Technologies, catalog#117552ABI50) or miRCURY

LNA RT kit (Qiagen, catalog#339340) following manufacturer's instructions. The RNA extracted was quantified using the ND-1000 spectrophotometer (Nanodrop, Wilmington, DE).

Quantitative real-time PCR reactions were performed on a magnetic induction (Mic) qPCR cycler (Bio Molecular Systems, Upper Coomera, Australia), and the amplifications were done using the iTap^{M} Universal SYBR® Green Supermix (Bio-Rad, catalog#1725125). The thermal cycling conditions were composed of 50°C for 2 minutes followed by an initial denaturation step at 95°C for 10 minutes, 40 cycles at 95°C for 15 seconds, 60°C for 1 minute, and a last melting curve stage at 95°C for 15 seconds, 60°C for 1 minute and 95°C for 15 seconds. For specific miRNA amplification, miRCURY LNA SYBR® Green PCR Kit (Qiagen, catalog#339345) and miRCURY LNA miRNA PCR Assays (Qiagen, catalog#339306). For individual assays, a PCR primer mix was used for each of the differentially expressed miRNAs. The cycling conditions were 95°C for 2 minutes for heat inactivation, followed by 40 cycles at 95°C for 60 seconds and 56°C for 1 minute. The relative quantification in gene expression was determined using the 2^(-ΔCt) method. *GAPDH* transcript was used for normalization. Primer sequences are listed in ***Table 16***.

Human Target	Forward primer (5′ – 3′)	Reverse primer (5′ – 3′)
GAPDH	AAGGTGAAGGTCGGAGTCAA	AATGAAGGGGTCATTGATGG
CA9	GTCCAGCTGAATTCCTGCCT	CCTTCTGTGCTGCCTTCTCA
BNIP3	CAGGGCTCCTGGGTAGAACT	CCCTGTTGGTATCTTGTGGTGT
MNT	CCCCACTGACTGTCATCCCTA	GGCAGGCTCCTTAATGCTGAG
pri-miR-210	GACTGGCCTTTGGAAGCTCC	ACAGCCTTTCTCAGGTGCAG
pre-miR-210	GCAGCCCCTGCCCACCGCACACT	CCGCTGTCACACGCACAG
hsa-miR-210-3p	CUGUGCGUGUGACAGCGGCUGA	-
hsa-miR-210-5p	AGCCCCUGCCCACCGCACACUG	-

Table 15 *– List of forward and reverse primers used in qRT-PCR analysis of this study.*

Immunoblotting

Cells were lysed, and protein samples extracted in RIPA buffer (150 mM Sodium chloride, 1% Triton X-100, 0.5% Sodium deoxycholate, 0.1% Sodium dodecyl sulfate, 50 mM TRIS-HCl, PH 7.4 and protease inhibitors).

Cell proteins (20 µg) were electrophoresed using 8%-15% polyacrylamide gels at 130V in non-reducing conditions. Proteins were transferred to a nitrocellulose membrane

(GeHealthcare Life Science, catalog#10600001) and activated with 20% methanol at 100V. Membranes were blocked with 5% non-fat dry milk in Tris-buffered saline (TBS) with 0.1% Tween 20 (TBST) at room temperature. HIF-1α, MNT, and GAPDH levels were analyzed with rabbit anti-HIF-1α (Novus, catalog#NB100-449), rabbit anti-MNT (BethylLab, catalog#A303-626), and mouse anti-GAPDH (Invitrogen, catalog#398600) specific antibodies. Membranes were incubated with specific antibodies diluted in TBST buffer containing 5% bovine serum albumin (BSA). Anti-HIF-1α and anti-MNT antibodies were diluted at 1:1000. Anti-GAPDH antibody was diluted at 1:100.000.

Immunoblot signals were visualized by the chemiluminescent ECL Star substrate (Euroclone, catalog#EMP001005) using the ChemiDocTM MP Imaging System (Bio-Rad, Hercules, CA, USA). Densitometry analysis was performed with ImageJ software (Wayne Rasband, USA).

Statistical Analysis

For RT–qPCR and cell proliferation analyses, statistical significance between groups was calculated by two-way ANOVA associated with Tukey post-tests and two-tails Student's *t*-test. These statistical analyses were performed using GraphPad Prism 10 (San Diego, CA, USA) software package. Significance values were $p < 0.05$ (*), $p < 0.01$ (**), and $p < 0.001$ (***).

Biochemistry

All reagents and solvents were purchased from Sigma Aldrich (St Louis, MO, U.S.A.). Tris·HCl, PBS and all inorganic salts for buffers were purchased from Merck (molecular biology grade). All buffers and solutions employed in fluorescence-based assays were filtered through 0.22 µm Millipore filters (GP ExpressPLUS® membrane). Tris·HCl 20 mM, pH 7.2 containing 12 mM NaCl, 3 mM $MgCl_2$, and 1 mM DTT (**Buffer A**) was used for FRET assays and K_D determination.

RNA and DNA oligonucleotides were purchased from Eurofins Genomics (Ebersberg, Germany) or Eurogentec (Liege, Belgium). For competition experiments in the presence of tRNA, a mixture of pre- and mature yeast tRNAs (from Escherichia coli, Sigma-Aldrich) was added to buffer A to obtain a 100-fold nucleotide excess compared to pre-miRNAs. For

competition experiments in the presence of a dsDNA, a 15-mer sequence (5'-CGTTTTTATTTTTGC-3') and its complementary oligonucleotide, annealed beforehand, were added to buffer A to obtain a 100-fold nucleotide excess compared to pre-miRNAs. Ambion™ RNase III for inhibition FRET-based assays was purchased from Invitrogen (Carlsbad, CA, USA). Oligonucleotide used in this study sequences are listed in ***Table 17***.

Name	Sequence (5' – 3')
pre-miR-210 for K_D assays	[FAM] (ACC CAG GGC AGC CCC UGC CCA CCG CAC ACU GCG CUG CCC CAG ACC CAC UGU GCG UGU GAC AGC GGC UGA UCU GC)
pre-miR-210 for IC_{50} assays	[FAM] (ACC CAG GGC AGC CCC UGC CCA CCG CAC ACU GCG CUG CCC CAG ACC CAC UGU GCG UGU GAC AGC GGC UGA UCU GC) [EDQ]
pre-miR-148a for K_D assays	[FAM] (GAG GCA AAG UUC UGA GAC ACU CCG ACU CUG AGU AUG AUA GAA GUC AGU GCA CUA CAG AAC UUU GUC UC)
pre-miR-21 for K_D assays	[FAM] (UGU CGG GUA GCU UAU CAG ACU GAU GUU GAC UGU UGA AUC UCA UGG CAA CAC CAG UCG AUG GGC UGU CUG ACA)
A site for K_D assays	[FAM] (GGC GUC ACA CCU UCG GCU GAA CUC GCC)

Table 16 *- List of oligonucleotide sequences used in fluorescence-based assays of this study.*

Affinity assays

Compound solutions were prepared as serial dilutions in buffer A at a concentration four times higher than the desired final concentration to allow for the subsequent dilution while adding the RNA solution. Binding experiments were performed in 384-well plates (Greiner bio-one, catalog#781076) in a final volume of 60 µL using an epMotion® automated pipetting system (Eppendorf, catalog#5070). Each experiment was performed in duplicate and repeated three times. Refolding of the RNA was performed using a ThermoStat Plus thermocycler (Eppendorf, catalog#5352) as follow: the RNA, diluted in 1 mL of buffer A, was first denatured by heating to 90°C for 2 min, then cooled to 4°C for 10 min followed by incubation at 25°C for 15 min. After refolding, the RNA was diluted to a working concentration of 10 nM. 30 µL of pre-miRNA beacon solution was added in each well containing 30 µL of each desired compound concentration (final volume 60 µL). Fluorescence was measured after incubating the plate at 4°C overnight. The fluorescence was then measured at various temperatures from 5°C to 35°C on a SpectraMax® M5e

spectrofluorometer (Molecular Devices) with an excitation filter of 485 nm and emission filter of 535 nm corresponding to the FAM wavelengths. Fluorescence intensity values were normalized to the maximum fluorescence intensity (RNA without compound). For competition experiments, the diluted RNA solution was first mixed with 100 eq. of tRNA or random DNA.

FRET-based inhibition assay

Compound solutions were prepared as serial dilutions in buffer A at a concentration eight times higher than the desired final concentration to allow for the subsequent dilution while adding the RNA solution. Inhibition experiments were performed in 384-well plates (Greiner bio-one) in a final volume of 40 µL using an epMotion® automated pipetting system (Eppendorf, catalog#5070). Each experiment was performed in duplicate and repeated three times. Refolding of the RNA was performed using a ThermoStat Plus thermocycler (Eppendorf, catalog#5352) as follow: the RNA, diluted in 1 mL of buffer A, was first denatured by heating to 90°C for 2 min, then cooled to 4°C for 10 min followed by incubation at 25°C for 15 min. After refolding, the RNA was diluted to a working concentration of 100 nM. 20 µL of pre-miRNA beacon solution was added in each well containing 10 µL of each desired compound concentration. These pre-treatment mixtures were incubated at room temperature for 30 min. 0.25 U of Ambion™ RNase III in 10 µL of buffer A were then added to each well. Fluorescence was measured, on a SpectraMax® M5e spectrofluorometer (Molecular Devices), after 1 to 2h incubation at 37°C, with an excitation filter of 485 nm and emission filter of 535 nm corresponding to the FAM wavelengths. Fluorescence intensity values were normalized to the maximum fluorescence intensity (RNA without compound).

Data Analysis

Binding and activity data were analyzed using log(inhibitor) versus response nonlinear regression curve, using GraphPad Prism 10 software. This nonlinear regression being based on the following equation:

$$y = \min + \frac{(max - min)}{(1 + 10^{(\log(A-x) \times hill\ slope)}}$$

With *min* = minimal value for *y*, *max* = maximal value for *y*, and *A* = K_D or IC_{50} depending on the assay. Binding profiles were modeled using a simple model assuming a one-to-one stoichiometry.

Ligation reaction

T4 RNA ligase (10 U/µL) and Reaction buffer (10X) were purchased from Thermo Scientific (San Jose, CA, USA). RNAse Inhibitors RNAsin® (40 U/µL) were purchased from Promega (Madison, WI, USA). Oligonucleotides were purchased from Eurogentec (Liege, Belgium). Oligonucleotides (listed in ***Table 17***) were diluted in 100 µL of 1X Reaction buffer to reach a final concentration of 0.1 nmol/µL.

The two selected oligonucleotides were refolded together following the previously detailed protocol (2 min at 90°C, 10 min at 4°C, and 25 min at 25°C). The two oligonucleotides were assembled in a sterile microcentrifuge tube with the following composition for ligation: refolded oligonucleotide solution (200 µL), RNAse inhibitors RNAsin® (5 µL), Reaction buffer 1X (14 µL) and T4 ligase (20 µL). The reaction mixture was incubated at 37°C for 48h. Purification was performed by semi-preparative HPLC on an HPLC chromatographic system (Water Alliance 2695) equipped with a reverse phase (RP) analytical column Discovery® BIO Wide Pore C_8 (4.6 x 250 mm, 5 µM). 50 µL of the reaction mixture was injected without any further dilution; the analyses were run at room temperature with a flow of 1 µL/min. The mobile phase consisted of Triethylammonium acetate (0.1M) pH 7.4 (**Buffer B**) (eluent A) and acetonitrile (eluent B). Elution method: the ratio of eluents A and B changed linearly from 0% B to 98% B over 15 min, followed by 5 min elution at 90% eluent B, and then 5 min in equilibration elution to reset the starting conditions.

Name	Sequence (5′ – 3′)
39-mer-5′-Phosphate	[Phosphate] (CCA GAC CCA CUG UGC GUG UGA CAG CGG CUG AUC UGU GCC)
39-mer-5′-FAM	[FAM] (GGC GCA GGG CAG CCC CUG CCC ACC GCA CAC UGC GCU GCC)
39-mer–5′-Phosphate-3′-EDQ	[Phosphate] (CCA GAC CCA CUG UGC GUG UGA CAG CGG CUG AUC UGU GCC) [EDQ]

Table 17 *- List of oligonucleotide sequences used in ligation reactions.*

Polyacrylamide gel electrophoresis (PAGE)

Samples were resuspended in 95% formamide and heated at 90°C for 2min before being loaded onto a denaturing 20% polyacrylamide (19:1 acrylamide/bisacrylamide) containing 7.5M Urea in 1X TBA Buffer (50 mM Tris base, 55mM boric acid, 1mM EDTA). Gels were canned with a Versadoc (Bio-Rad, Hercules, CA, USA) at 480 nm.

Chemical Structures of **1.15** (TargapremiR-210) and analogs

TargapremiR-210

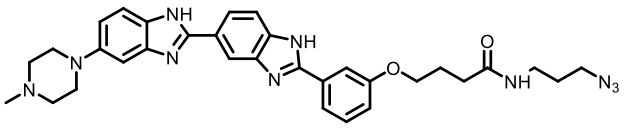

1.15

Reactive Intermediates used in cellular assays

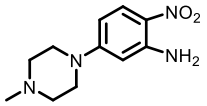

2.32

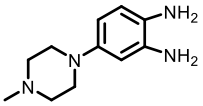

2.33

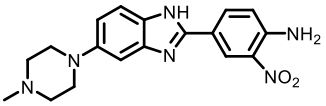

2.34

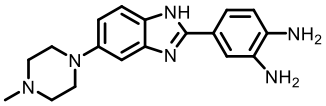

2.35

Prepared Analogs of 1.15

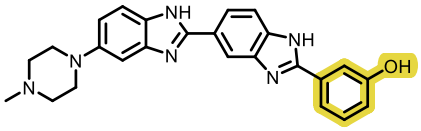

2.17

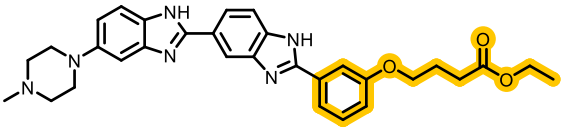

2.18

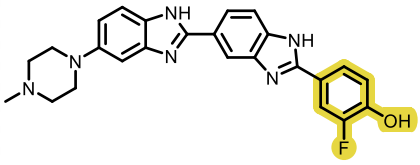

2.19

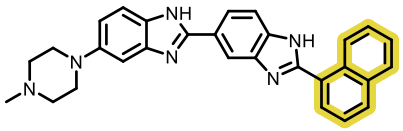

2.20

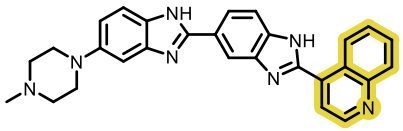

2.21

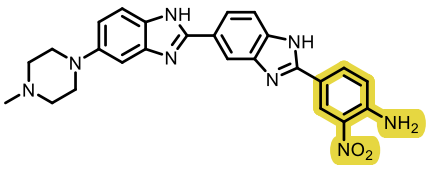

2.36

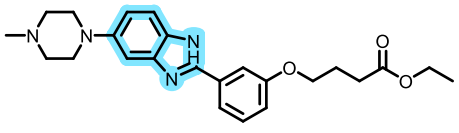

2.22

Chemical Structures of mono-substituted tris-thiazole and bis-thiazole

Reference compounds

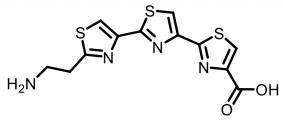
3.15b

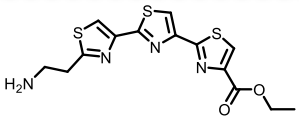
3.16

Analogs of 3.15b

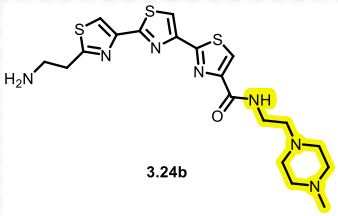
3.24b

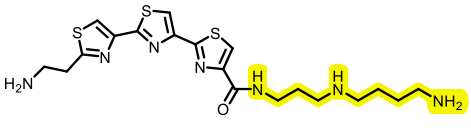
3.25b

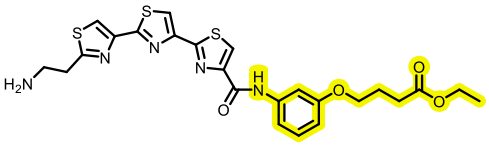
3.26b

Analogs of 3.16

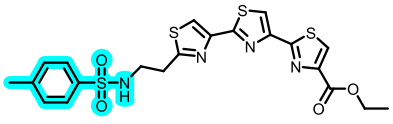
3.27

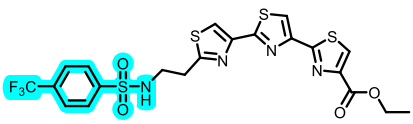
3.28

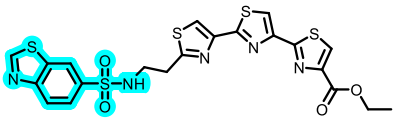
3.29

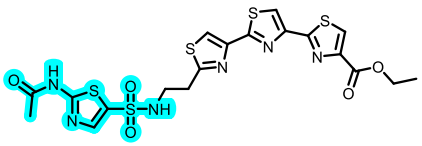
3.30

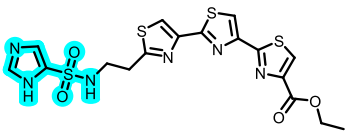
3.31

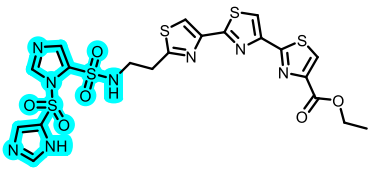
3.32

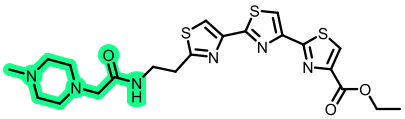
3.34

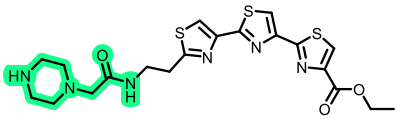
3.35b

Bis-thiazole derivatives used in biochemical assays

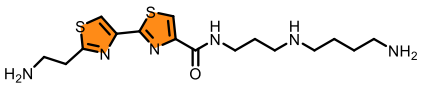
3.36

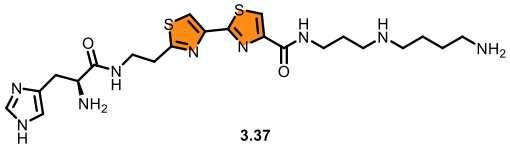
3.37

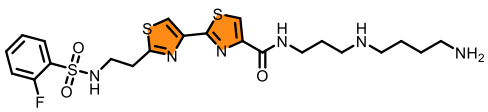
3.38

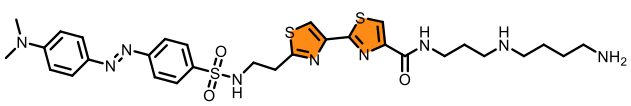
3.39

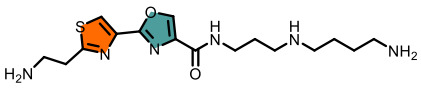
3.40

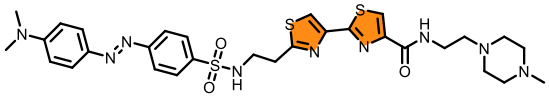
3.41

Chemical structures of 2,4-disubstituted analogs of **3.26b**

Analogs of 3.26b

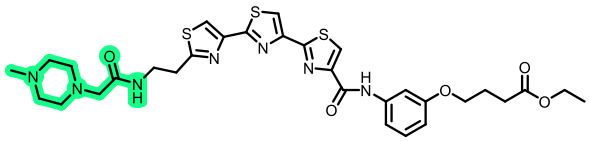
3.42

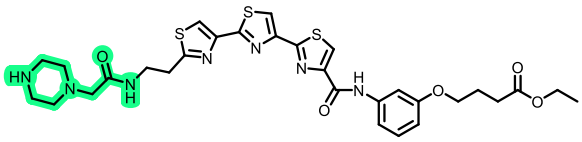
3.43b

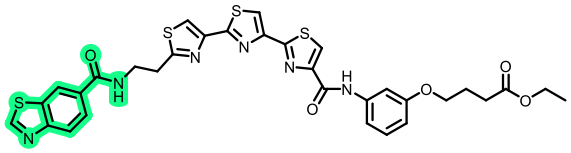
3.44

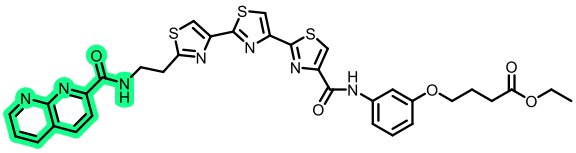
3.45

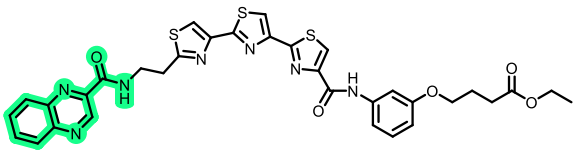
3.46

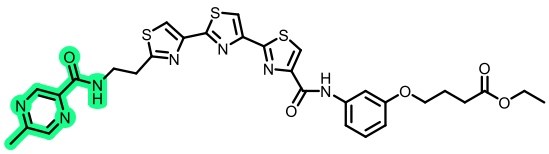
3.47

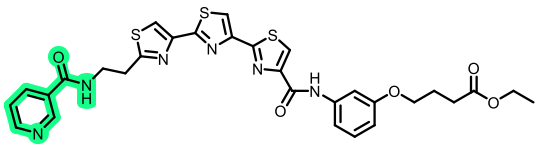
3.48

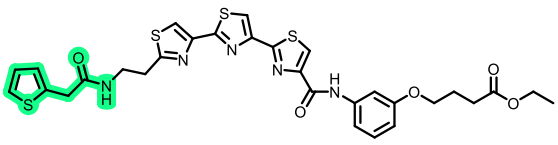
3.49

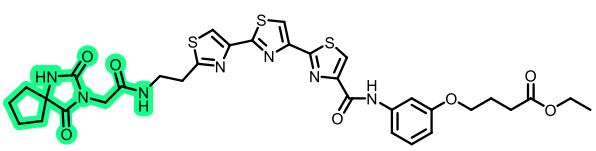
3.50

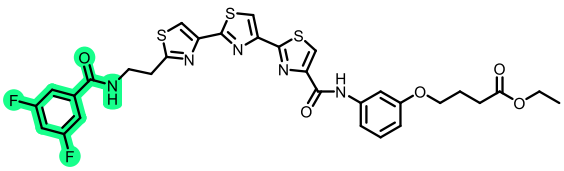
3.51

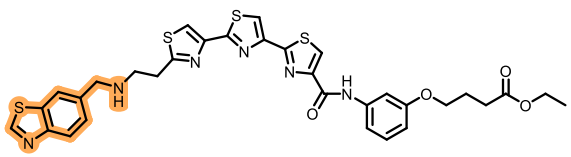
3.52

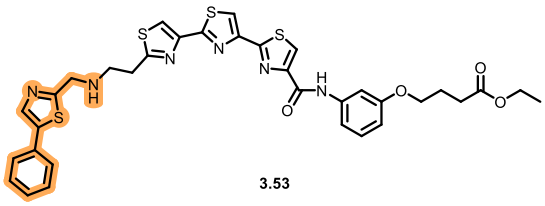
3.53

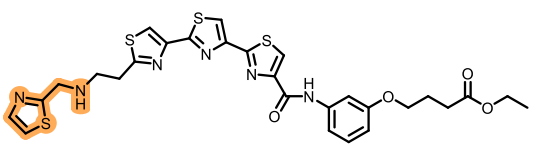
3.54

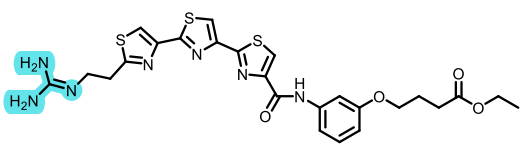
3.55b

Chemistry

Reagents and solvents were purchased from Aldrich, BLDPharm, ABCR, Carlo Erba and used without further purification. Flash columns chromatography were carried out on silica gel columns (Interchim Puriflash silica HP 15 to 50 µM) on a Puriflash® instrument (Interchim, catalog #XS420). Analytical thin-layer chromatography (TLC) was conducted on Sigma-Aldrich precoated silica gel and compounds were visualized by irradiation (254 nm) and/or by staining with appropriate revelators.

Purity was checked using two different HPLC analytical method. **Method A**: Purity was checked on a HPLC chromatographic system (Acquity Waters) equipped with a reverse phase (RP) analytical column Phenomenex® Synergi™ Fusion-RP 80 Å C_{18} (4.6 x 250 mm, 4 µM particle size) (Waters, Milford, MA, USA). Compounds were dissolved in acetonitrile or methanol; the analyses were run at room temperature with a flow of 1 µL/min. The mobile phase consisted of water containing 0.1% trifluoroacetic acid (eluent A) and acetonitrile containing 0.1% trifluoroacetic acid (eluent B). Elution method: the ratio of eluents A and B changed linearly from 5% B to 60% B over 20 min, followed by 10 min isocratic elution at 100% eluent B and then 5 min in equilibration elution to reset the starting conditions. The purity of the final compounds was at least 95%. The column effluent was monitored at 254 and 214 nm. **Method B**: Purity was checked on a UHPLC chromatographic system (Acquity Waters) equipped with a reverse phase (RP) analytical column Cortecs® 90 Å C_{18}+ (4.6 x 100 mm, 2.7 µM particle size) (Waters, Milford, MA, USA). Compounds were dissolved in acetonitrile or methanol; the analyses were run at room temperature with a flow of 1.5 µL/min. The mobile phase consisted of water containing 0.1% trifluoroacetic acid (eluent A) and acetonitrile containing 0.1% trifluoroacetic acid (eluent B). Elution method: the ratio of eluents A and B changed linearly from 5% B to 100% B over 6 min, followed by 2 min isocratic elution at 100% eluent B and then 4 min in equilibration elution to reset the starting conditions. The purity of the final compounds was at least 95%. The column effluent was monitored at 254 and 214 nm.

^{1}H and ^{13}C NMR spectra were recorded on Bruker AC400 and 500 MHz spectrometers. Chemical shifts are reported in parts per million (ppm, δ) referenced to the residual ^{1}H resonance of the solvent (D_2O, δ 4.79; $CDCl_3$, δ 7.26; CD_3OD, δ 3.31, DMF-d_7, δ 2.75, 2.92, 8.03; acetone-d_6, δ 2.05 and DMSO-d_6, δ 2.50) and referenced to the residual ^{13}C resonance of the solvent ($CDCl_3$, δ 77.2; CD_3OD, δ 49.0 DMF-d_7, δ 29.8, 34.9, 163.1; acetone-d_6, δ 29.8, 206.3 and DMSO-d_6, δ 39.52). Splitting patterns are designed as follows: s (singlet), d (doublet), t (triplet), q (quadruplet) p (pentuplet), m (multiplet), and br (broad). Coupling constants (J) are listed in hertz (Hz). For reading convenience of NMR analysis, each atom's

number attribution does not follow IUPAC rules but is based on the different fragments used during synthesis. However, IUPAC rules have been followed for naming all compounds.

Low-resolution mass spectra (MS) were obtained with a Bruker Daltonics Esquire 3000+ electrospray spectrometer equipped with API ionization source. High-resolution mass spectrometry (HRMS) was carried out on a LTQ Orbitrap hybrid mass spectrometer with an electrospray ionization probe (ThermoScientific, San Jose, CA) by direct infusion from a pump syringe to confirm the correct molar mass and high purity of the compounds.

General procedures

General procedure A – Boc cleavage The Boc-protected product (1 eq) was solubilized in HCl/1,4-dioxane (4 M, 2 mL for 0.1 mmol of protected product) and stirred at room temperature until completion, which was TLC monitored. The mixture was carefully concentrated under reduced pressure and then triturated with Et_2O. The resulting white precipitate was collected by filtration and then washed with Et_2O. Drying under reduced pressure afforded the desired product.

General procedure B – Sulfonamide formation Et_3N (3 eq) was added to a solution of the appropriate amine (1 eq) in DMF. The mixture was stirred at room temperature for 10 min. Then, the sulfonyl chloride derivative (1.2 eq) was added, and the mixture was stirred at room temperature until completion, monitored by TLC. The mixture was concentrated under vacuum, a solution of $KHSO_4$ (0.5 M) was added, and the aqueous phase was extracted with DCM. The organic phase was dried over $MgSO_4$ and concentrated under reduced pressure. The crude residue was purified by flash chromatography using whether a mixture of DCM and MeOH or cHex and EtOAc as eluent.

General procedure C – Coupling using HATU HATU (1.3 eq) was added to a 0°C solution of the appropriate acid (1.2 eq) and DIPEA (1.5 eq) in DMF. The mixture was stirred at 0°C, under Ar, for 10 min. The selected amine (1 eq) and DIPEA (1.1 eq), solubilized in DMF, were then added to the 0°C solution, and the reaction mixture was allowed to warm up to room temperature and stirred at room temperature until completion, which was TLC monitored. The mixture was concentrated under vacuum, a solution of $KHSO_4$ (0.5 M) was added, and the aqueous phase was extracted with DCM. The organic phase was dried over $MgSO_4$ and concentrated under reduced pressure. The crude residue was purified by flash chromatography using whether a mixture of DCM and MeOH or DCM and EtOH as eluent.

General procedure D – Coupling using EDC/HOSu EDC.HCl (1.2 eq) and HOSu (1.2 eq) were added to a solution of the appropriate acid (1 eq) in DMF. The mixture was stirred at room temperature, under Ar, for 2h. The selected amine (1.1 eq) and Et_3N (1.2 eq), solubilized in DMF, were then added to the solution, and the reaction mixture was stirred at room temperature until completion, which was TLC monitored. The mixture was concentrated under vacuum, a solution of $KHSO_4$ (0.5 M) was added, and the aqueous phase was extracted with DCM. The organic phase was dried over $MgSO_4$ and concentrated under reduced pressure. The crude residue was purified by flash chromatography using a mixture of DCM and MeOH as eluent.

General procedure E – Coupling using diethyl chlorophosphate (DECP) Diethyl chlorophosphate (5 eq) was added to a solution of the appropriate acid (1 eq) and Et_3N (2 eq) in THF. The mixture was stirred at room temperature, under Ar, for 1h. The selected amine (1 eq) was then added to the solution, and the reaction mixture was stirred at room temperature until completion, which was TLC monitored. The mixture was concentrated under vacuum, a solution of $KHSO_4$ (0.5 M) was added, and the aqueous phase was extracted with DCM. The organic phase was dried over $MgSO_4$ and concentrated under reduced pressure. The crude residue was purified by flash chromatography using whether a mixture of DCM and MeOH or cHex and EtOAc as eluent.

General procedure F – Reductive amination The appropriate aldehyde (1.2 eq) was added to a solution of the amine (1 eq) and activated molecular sieves 4 Å in DMF. The mixture was stirred at room temperature under Ar, until complete formation of the imine intermediate, which was TLC monitored. Reaction mixture was poured into a new flask *via* a syringe, then it was cooled down to 0°C. Then, trichlorosilane (2 eq) was added dropwise and the reaction was stirred at room temperature, under Ar, for 16h. The mixture was concentrated under vacuum, a solution of $NaHCO_3$ (sat.) was added, and the aqueous phase was extracted with DCM. The organic phase was dried over $MgSO_4$ and concentrated under reduced pressure. The crude residue was purified by flash chromatography using whether a mixture of DCM and EtOH or cHex and EtOAc as eluent.

Synthesis of TargapremiR-210 (1.15) and analogs

Synthesis of *tert*-butyl (3-bromopropyl)carbamate (2.24)

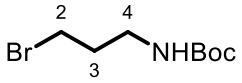

Chemical Formula: $C_8H_{16}BrNO_2$
Exact Mass: 237,04
Molecular Weight: 238,13

Et_3N (3.82 mL, 27.4 mmol, 2 eq) was added to a 0°C solution of 3-aminopropyl bromide hydrobromide (3 g, 13.7 mmol, 1 eq) in DCM (25 mL). Di-*tert*-butyl dicarbonate (3.59 g, 16.4 mmol, 1.2 eq), solubilized in DCM (15 mL), was then added dropwise to the 0°C solution, and the reaction mixture was allowed to warm up to room temperature and was stirred until completion. The mixture was concentrated under reduced pressure, water was added, and the aqueous phase was extracted with DCM. The organic phase was washed with brine, dried over $MgSO_4$ and concentrated under reduced pressure. The crude residue **2.24** (3.2 g) was used directly, without further purification, for the next reaction.

$\mathbf{R_f}$ = 0.45 (cHex/EtOAc 80:20).

Synthesis of *tert*-butyl (3-azidopropyl)carbamate (2.25)

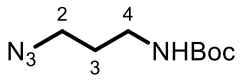

Chemical Formula: $C_8H_{16}N_4O_2$
Exact Mass: 200,13
Molecular Weight: 200,24

A solution of **2.24** (3.2 g, 13.4 mmol, 1 eq) and sodium azide (1.75 g, 26.8 mmol, 2 eq), in H_2O/1,4-dioxane (1:1, 30 mL), was stirred at 95°C for 2 h. Then, the reaction mixture was allowed to cool down to room temperature and was stirred for 24h. The mixture was concentrated under reduced pressure, water was added, and the aqueous phase was extracted with DCM. The organic phase was washed with brine, dried over $MgSO_4$ and concentrated under reduced pressure. The crude residue **2.25** (2.2g, 82%) was used directly, without further purification, for the next reaction.

R_f = 0.52 (cHex/EtOAc 80:20).

^{1}H NMR (200 MHz, $CDCl_3$) δ (ppm) 4.63 (br, 1H, NH), 3.36 (t, J = 6.7 Hz, 2H, H_2), 3.20 (t, J = 6.7 Hz, 2H, H_4), 1.76 (m, J = 6.7 Hz, 2H, H_3), 1.44 (s, 9H, H_{Boc}).

^{13}C NMR (50 MHz, $CDCl_3$) δ (ppm) 156.1 (1C, C_{Boc}), 79.6 (1C, $C_{IV.Boc}$), 67.2 (1C, C_2), 49.2 (1C, C_4), 29.4 (1C, C_3), 28.5 (3C, $3CH_{3.Boc}$).

MS (ESI) *m/z* 222.9 $(M+Na)^+$ (Theoretical 223.1).

Synthesis of 3-azidopropan-1-amine hydrochloride (2.26)

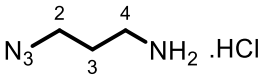

Chemical Formula: $C_3H_9ClN_4$
Exact Mass: 136,05
Molecular Weight: 136,58

A solution of **2.25** (2.2 g, 11 mmol, 1 eq) in MeOH/HCl (3M, 24:6, 20 mL), was stirred at room temperature until completion. The mixture was concentrated under reduced pressure, followed by co-evaporation with toluene, to afford compound **2.26** (1.1 g, 73%) as a white solid.

R_f = 0.32 (DCM/MeOH [10% NH_4OH] 90:10)

^{1}H NMR (400 MHz, DMSO-d_6) δ (ppm) 8.29 (s, 1H), 3.44 (t, J = 6.6 Hz, 1H), 2.78 (m, 1H), 1.82 (m, 1H).

^{13}C NMR (101 MHz, DMSO-d_6) δ (ppm) 47.9 (1C, C_2), 36.4 (1C, C_4), 26.4 (1C, C_3).

Synthesis of ethyl 10 -(1-formylphenoxy)butanoate (2.27)

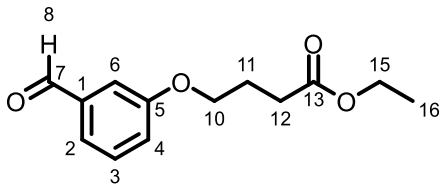

Chemical Formula: $C_{13}H_{16}O_4$
Exact Mass: 236,10
Molecular Weight: 236,27

To a solution of 3-hydroxybenzaldehyde (2 g, 16.4 mmol, 1 eq) in anhydrous DMF (55 mL), K_2CO_3 (6.8 g, 49.1 mmol, 3 eq) was added. The mixture was stirred at 80°C, under Ar, for 10 min. Then, ethyl 4-bromoethanoate (3.83 g, 19.6 mmol, 1.2 eq) was added and the mixture was stirred at 80°C, under Ar, for 16h. The mixture was concentrated under vacuum, water was added, and the aqueous phase was extracted with EtOAc. The organic phase was washed with brine, dried over $MgSO_4$ and concentrated under reduced pressure. The crude residue was purified by flash chromatography (cHex/EtOAc gradient 90:10 to 70:30, v/v) to provide **2.27** (3.6 g, 93%) as a colorless oil.

R_f = 0.68 (cHex/EtOAc 70:30).

^{1}H NMR (400 MHz, $CDCl_3$) δ (ppm) 9.93 (s, 1H, H_8), 7.45 – 7.37 (m, 2H, H_2 and H_6), 7.36 – 7.32 (m, 1H, H_3), 7.16 – 7.10 (m, 1H, H_4), 4.16 – 4.09 (m, 2H, H_{15}), 4.04 (t, J = 7.3 Hz, 2H, H_{10}), 2.49 (t, J = 7.3 Hz, 2H, H_{12}), 2.11 (p, J = 7.3 Hz, 2H, H_{11}), 1.23 (t, J = 7.1 Hz, 3H, H_{16}).

^{13}C NMR (101 MHz, $CDCl_3$) δ (ppm) 192.1 (1C, C_7), 173.1 (1C, C_{13}), 159.5 (1C, C_5), 137.9 (1C, C_1), 130.1, 123.5 (2C, C_2 and C_6), 121.9 (1C, C_4), 112.9 (1C, C_3), 67.1 (1C, C_{10}), 60.5 (1C, C_{15}), 30.8 (1C, C_{12}), 24.6 (1C, C_{11}), 14.3 (1C, C_{16}).

MS (ESI) *m/z* 237.1 $(M+H)^+$ (Theoretical 237.1).

HPLC-RP rt = 23.25 min (Method A).

Synthesis of 10-(1-formylphenoxy)butanoic acid (2.28)

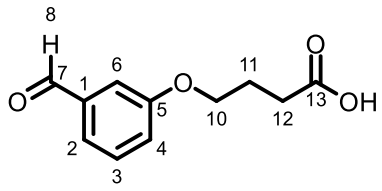

Chemical Formula: $C_{11}H_{12}O_4$
Exact Mass: 208,07
Molecular Weight: 208,21

To a solution of compound **2.27** (200 mg, 0.85 mmol, 1 eq) in THF (1 mL), LiOH (1M, 1.69 mmol, 2 eq) was added. The mixture was stirred at room temperature until completion, which was TLC monitored. Then, the solution was acidified with HCl (1M). The mixture was concentrated under reduced pressure, water was added, and the aqueous phase was extracted with EtOAc. The organic phases were washed with brine, dried over $MgSO_4$ and concentrated under reduced pressure. The crude residue was purified by preparative TLC with development by cHex/EtOAc (gradient 60:40, v/v) to provide **2.28** (120 mg, 68%) as a white solid.

R_f = 0.32 (cHex/EtOAc 70:30).

^{1}H NMR (400 MHz, Acetone-d_6) δ (ppm) 10.00 (s, 1H, H_8), 7.54 – 7.48 (m, 2H, H_2 and H_6), 7.47 – 7.42 (m, 1H, H_3), 7.31 – 7.23 (m, 1H, H_4), 4.15 (t, J = 6.4 Hz, 2H, H_{10}), 2.53 (t, J = 7.3 Hz, 2H, H_{12}), 2.14 – 2.06 (m, 2H, H_{11}).

^{13}C NMR (101 MHz, Acetone-d_6) δ (ppm) 192.8 (1C, C_7), 174.3 (1C, C_{13}), 160.5 (1C, C_5), 139.2 (1C, C_1), 131.1, 123.3 (2C, C_2 and C_6), 122.1 (1C, C_4), 114.4 (1C, C_3), 68.0 (1C, C_{10}), 30.5 (1C, C_{12}), 25.3 (1C, C_{11}).

MS (ESI) *m/z* 207.3 $(M-H)^+$ (Theoretical 207.1).

HPLC-RP rt = 16.20 min (Method A).

Synthesis of *N*-(17-azidopropyl)-10-(1-formylphenoxy)butanamide (2.29)

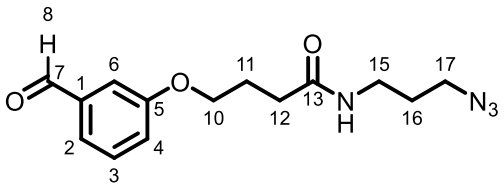

Chemical Formula: $C_{14}H_{18}N_4O_3$
Exact Mass: 290,14
Molecular Weight: 290,32

Coupling between **2.28** (350 mg, 1.68 mmol, 1 eq) and **2.26** (252 mg, 1.85 mmol, 1.1 eq) was performed following general procedure D with EDC (386 mg, 2.0 mmol, 1.2 eq) and HOSu (232 mg, 2.0 mmol, 1.2 eq) using DMF (6 mL) as solvent. The crude residue was purified by flash chromatography (DCM/MeOH gradient 100:0 to 98:2, v/v) to provide **2.29** (380 mg, 77%) as pale green oil.

R_f = 0.45 (DCM/MeOH 98:2).

^{1}H NMR (400 MHz, CD_3OD) δ (ppm) 9.94 (s, 1H, H_8), 7.53 – 7.47 (m, 2H, H_2 and H_6), 7.44 – 7.41 (m, 1H, H_3), 7.28 – 7.20 (m, 1H, H_4), 4.08 (t, J = 6.1 Hz, 2H, H_{10}), 3.37 – 3.30 (m, 2H, H_{17}), 3.25 (t, J = 6.8 Hz, 2H, H_{15}), 2.40 (t, J = 6.1 Hz, 2H, H_{12}), 2.15 – 2.06 (m, 2H, H_{11}), 1.74 (p, J = 6.8 Hz, 2H, H_{16}).

^{13}C NMR (101 MHz, CD_3OD) δ (ppm) 194.0 (1C, C_7), 175.5 (1C, C_{13}), 161.0 (1C, C_5), 139.4 (1C, C_1), 131.3, 124.0 (2C, C_2 and C_6), 122.6 (1C, C_4), 114.5 (1C, C_3), 68.5 (1C, C_{10}), 50.0 (1C, C_{17}), 37.7 (1C, C_{15}), 33.5 (1C, C_{12}), 29.7 (1C, C_{11}), 26.5 (1C, C_{16}).

MS (ESI) *m/z* 291.6 $(M+H)^+$ (Theoretical 291.1).

Synthesis of ethyl 6-amino-5-nitrobenzimidate dihydrochloride (2.31)

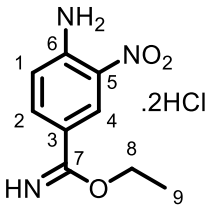

Chemical Formula: $C_9H_{13}Cl_2N_3O_3$
Exact Mass: 281,03
Molecular Weight: 282,12

A suspension of 4-amino-3-nitrobenzonitrile (1 g, 6.13 mmol, 1 eq) in absolute ethanol (100 mL) was cooled over an ice bath. Then, anhydrous HCl gas was bubbled rapidly through the mixture for 30 min. The thick suspension was stirred for 7 days. The mixture was concentrated under reduced pressure and then triturated with Et_2O. Filtration followed by drying under reduced pressure afforded the pure product **2.31** (1.6 g, 93%) as a yellow solid.

R_f = 0.33 (DCM/MeOH 98:2).

^{1}H NMR (200 MHz, DMSO-d_6) δ (ppm) 11.43 (br, 2H, NH_2), 8.80 (d, J = 2.2 Hz, 1H, H_4), 8.37 (br, 1H, NH), 8.09 (dd, J = 9.1, 2.2 Hz, 1H, H_2), 7.17 (d, J = 9.1 Hz, 1H, H_1), 4.57 (q, J = 7.0 Hz, 1H, H_8), 1.46 (t, J = 7.0 Hz, 2H, H_9).

^{13}C NMR (101 MHz, CD_3OD) δ (ppm) 168.7 (1C, C_7), 149.9 (1C, C_{Ar}), 133.8 (1C, C_{Ar}), 129.2 (1C, C_{Ar}), 119.7 (1C, C_{Ar}), 111.1 (1C, C_{Ar}), 69.2 (1C, C_8), 13.5 (1C, C_9).

MS (ESI) *m/z* 210.1 $(M+H)^+$ (Theoretical 210.2).

Synthesis of 2-(4-methylpiperazin-1-yl)-5-nitroaniline (2.32)

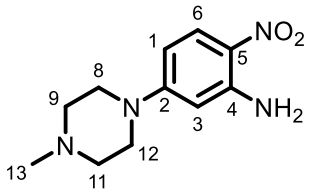

Chemical Formula: $C_{11}H_{16}N_4O_2$
Exact Mass: 236,13
Molecular Weight: 236,28

To a solution of 1-methylpiperazine (1.1 mL, 10 mmol, 1 eq) in anhydrous DMF (15 mL), K_2CO_3 (1.68 g, 12 mmol, 1.2 eq) was added. The mixture was stirred at 120°C, under Ar, for 10 min. Then, 5-chloro-2-nitroaniline (1.72 mg, 10 mmol, 1 eq) was added and the mixture was stirred at 120°C, under Ar, for 48h. The mixture was concentrated under vacuum, water was added, and the aqueous phase was extracted with DCM. The organic phase was then dried over $MgSO_4$ and concentrated under reduced pressure. The crude residue was purified by flash chromatography (DCM/MeOH gradient 100:0 to 96:4, v/v) to provide **2.32** (1.73 g, 73%) as a bright yellow solid.

R_f = 0.33 (DCM/MeOH 95:5).

^{1}H NMR (400 MHz, $CDCl_3$) δ (ppm) 8.01 (d, J = 9.7 Hz, 1H, H_6), 6.28 (dd, J = 9.7, 2.6 Hz, 1H, H_1), 6.14 (br, 2H, NH_2), 5.94 (d, J = 2.6 Hz, 1H, H_3), 3.40 – 3.34 (m, 4H, H_8 and H_{12}), 2.54 – 2.49 (m, 4H, H_9 and H_{11}), 2.34 (s, 3H, H_{13}).

^{13}C NMR (101 MHz, $CDCl_3$) δ (ppm) 155.6 (1C, C_2), 147.2 (1C, C_4), 128.4 (1C, C_6), 124.9 (1C, C_5), 105.8 (1C C_1), 98.5 (1C, C_3), 54.7 (2C, C_9 and C_{11}), 46.9 (2C, C_8 and C_{12}), 46.2 (1C, C_{13}).

MS (ESI) *m/z* 237.1 $(M+H)^+$ (Theoretical 237.1).

Synthesis of 4-(4-methylpiperazin-1-yl)benzene-4,5-diamine (2.33)

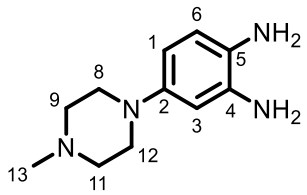

Chemical Formula: $C_{11}H_{18}N_4$
Exact Mass: 206,15
Molecular Weight: 206,29

To a suspension of **2.32** (300 mg, 1.27 mmol, 1 eq) in absolute EtOH (15 mL), 10% Pd/C (30 mg) was added. The mixture was degassed three times (vacuum/Ar), then stirred at room temperature under H_2 for 4h. The mixture was filtered through a pad of Celite®, the flask and the pad were washed with EtOH. The filtrate was concentrated under reduced pressure, affording the orange-brown colored diamine **2.33** (250 mg, 95%). **2.33** was used directly for the following reaction, as the diamine product was found to be unstable.

R_f = 0.27 (DCM/MeOH [10% NH_4OH] 90:10).

^{1}H NMR (400 MHz, CD_3OD) δ (ppm) 6.66 (d, J = 8.4 Hz, 1H, H_6), 6.48 (d, J = 2.6 Hz, 1H, H_3), 6.32 (dd, J = 8.4, 2.6 Hz, 1H, H_1), 3.09 – 3.01 (m, 4H, H_8 and H_{12}), 2.63 – 2.59 (m, 4H, H_9 and H_{11}), 2.34 (s, 3H, H_{13}).

^{13}C NMR (101 MHz, CD_3OD) δ (ppm) 146.6 (1C, C_2), 137.4 (1C, C_4), 129.7 (1C, C_5), 118.9 (1C, C_6), 109.8 (1C, C_1), 107.8 (1C, C_3), 56.0 (2C, C_9 and C_{11}), 51.8 (2C, C_8 and C_{12}), 46.1 (1C, C_{13}).

MS (ESI) *m/z* 207.1 $(M+H)^+$ (Theoretical 207.1).

Synthesis of 17-[2-(10-methylpiperazin-7-yl)benzimidazol-15-yl]-19-nitroaniline (2.34)

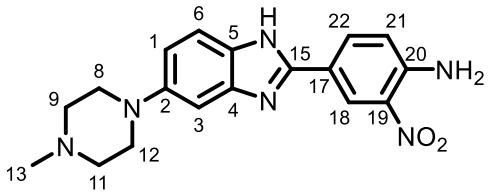

Chemical Formula: $C_{18}H_{20}N_6O_2$
Exact Mass: 352,16
Molecular Weight: 352,40

A solution of compound **2.31** (573 mg, 2.03 mmol, 1 eq) and freshly prepared compound **2.33** (420 mg, 2.03 mmol, 1 eq), in absolute ethanol/glacial acetic acid (2:1 (v/v), 36 mL), was stirred at 80°C, under Ar, for 24h. The mixture was concentrated under reduced pressure, the pasty residue was then solubilized in water and aqueous ammonia solution (36%). The suspension was allowed to stand overnight. The resulting brick-red precipitate was collected by filtration and then washed with water. The solid was solubilized in methanol/glacial acetic acid (9:1, v/v), then made alkaline with aqueous ammonia solution (36%). The suspension was allowed to stand overnight. The orange precipitate was collected by filtration and then washed with water and acetone. Drying under reduced pressure afforded the pure product **2.34** (640 mg, 90%) as an ochre solid.

R_f = 0.25 (DCM/MeOH 85:15).

^{1}H NMR (400 MHz, CD_3OD) δ (ppm) 8.79 (d, J = 2.1 Hz, 1H, H_{18}), 8.07 (dd, J = 8.9, 2.1 Hz, 1H, H_{22}), 7.48 (d, J = 8.8 Hz, 1H, H_6), 7.13 (m, 2H, H_{21} and H_3), 7.05 (dd, J = 8.8, 2.1 Hz, 1H, H_1), 3.27 – 3.19 (m, 4H, H_8 and H_{12}), 2.73 – 2.65 (m, 4H, H_9 and H_{11}), 2.39 (s, 3H, H_{13}).

^{13}C NMR (101 MHz, CD_3OD) δ (ppm) 149.6 (1C, C_{15}), 148.3 (2C, C_2 and C_{20}), 134.2, 132.3 (2C, C_{19} and C_{22}), 124.9 (1C, C_{18}), 120.9 (1C, C_{21}), 118.9 (1C, C_{17}), 116.5, 116.4 (2C, C_1 and C_6), 103.6 (1C, C_3), 56.1 (2C, C_9 and C_{11}), 51.7 (2C, C_8 and C_{12}), 46.0 (1C, C_{13}).

MS (ESI) *m/z* 353.5 $(M+H)^+$ (Theoretical 353.2).

Synthesis of 17-[2-(10-methylpiperazin-7-yl)benzimidazol-15-yl]-19,20-benzenediamine (2.35)

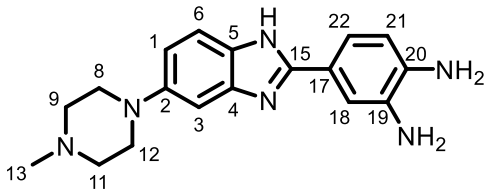

Chemical Formula: $C_{18}H_{22}N_6$
Exact Mass: 322,19
Molecular Weight: 322,42

To a suspension of **2.34** (213 mg, 0.6 mmol, 1 eq) in absolute EtOH (8 mL), 10% Pd/C (22 mg) was added. The mixture was degassed three times (vacuum/Ar), then stirred at room temperature under H_2 overnight. The mixture was filtered through a pad of Celite®, then flask and pad were washed with EtOH. The filtrate was concentrated under reduced pressure, affording the very unstable, orange-colored diamine **2.35** (192 mg, quantitative).

R_f = 0.40 (DCM/MeOH [10% NH_4OH] 85:15).

^{1}H NMR (400 MHz, CD_3OD) δ (ppm) 7.42 (d, J = 8.8 Hz, 1H, H_6), 7.37 (d, J = 2.0 Hz, 1H, H_{18}), 7.29 (dd, J = 8.1, 2.0 Hz, 1H, H_{22}), 7.09 (d, J = 2.3 Hz, 1H, H_3), 6.98 (dd, J = 8.8, 2.3 Hz, 1H, H_1), 6.78 (d, J = 8.1 Hz, 1H, H_{21}), 3.23 – 3.16 (m, 4H, H_8 and H_{12}), 2.69 – 2.65 (m, 4H, H_9 and H_{11}), 2.37 (s, 3H, H_{13}).

^{13}C NMR (100 MHz, CD_3OD) δ (ppm) 154.5 (1C, C_{15}), 149.2 (1C, C_2), 140.2, 139.2 (2C, C_5 and C_{20}), 135.9, 135.8 (2C, C_4 and C_{19}), 121.3 (1C, C_{17}), 119.4 (1C, C_{22}), 116.7 (1C, C_{21}), 116.1, 115.9 (2C, C_1 and C_6), 115.3 (1C, C_{18}), 102.4 (1C, C_3), 56.1 (2C, C_9 and C_{11}), 52.0 (2C, C_8 and C_{12}), 46.0 (1C, C_{13}).

MS (ESI) *m/z* 323.5 $(M+H)^+$ (Theoretical 323.2).

Synthesis of TargapremiR-210 or *N*-(3-Azidopropyl)-4-[3-[6-(4-methyl-1-piperazinyl)[2,6'-bi-1*H*-benzimidazol]-2'-yl]phenoxy]butanamide (1.15)

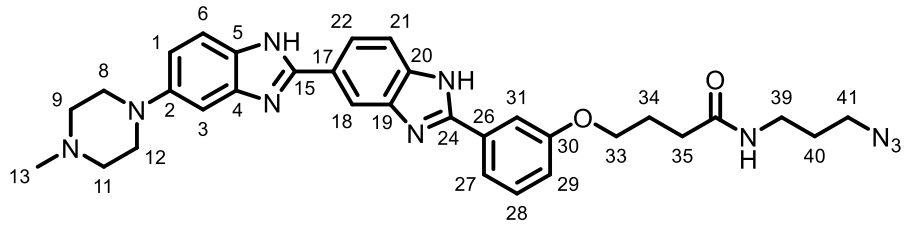

Chemical Formula: $C_{32}H_{36}N_{10}O_2$
Exact Mass: 592,30
Molecular Weight: 592,71

A solution of freshly prepared compound **2.35** (90 mg, 0.28 mmol, 1 eq), compound **2.29** (162 mg, 0.56 mmol, 2 eq) and $Na_2S_2O_5$ (64 mg, 0.33 mmol, 1.2 eq) in absolute ethanol (10 mL), was stirred at 80°C, under Ar, for 16h. The mixture was concentrated under reduced pressure. The crude residue was purified by flash chromatography (DCM/MeOH gradient 100:0 to 80:20, v/v) to provide **1.15** (134 mg, 81%) as a pale-yellow solid.

R_f = 0.20 (DCM/MeOH 80:20).

^{1}H NMR (400 MHz, CD_3OD) δ (ppm) 8.26 (s, 1H, H_{18}), 7.95 (d, J = 8.4 Hz, 1H, H_{22}), 7.71 – 7.63 (m, 3H, H_{21}, H_{27} and H_{31}), 7.48 (d, J = 8.8 Hz, 1H, H_6), 7.41 (t, J = 8.0 Hz, 1H, H_{28}), 7.12 – 7.09 (m, 1H, H_3), 7.06 – 6.99 (m, 2H, H_1 and H_{29}), 4.08 (t, J = 6.1 Hz, 2H, H_{33}), 3.33 – 3.29 (m, 2H, H_{41}), 3.26 (t, J = 6.8 Hz, 2H, H_{39}), 3.23 – 3.17 (m, 4H, H_8 and H_{12}), 2.70 – 2.64 (m, 4H, H_9 and H_{11}), 2.42 (t, J = 7.4 Hz, 2H, H_{35}), 2.37 (s, 3H, H_{13}), 2.16 – 2.07 (m, 2H, H_{34}), 1.73 (p, J = 6.8 Hz, 2H, H_{40}).

^{13}C NMR (101 MHz, CD_3OD) δ (ppm) 175.5 (1C, C_{36}), 160.9 (1C, C_{30}), 155.0 (1C, C_{24}), 153.6 (1C, C_{15}), 149.5 (1C, C_2), 144.4 (1C, C_{IV}), 131.8 (1C, C_{26}), 131.3 (1C, C_{28}), 126.0 (1C, C_{17}), 122.8 (1C, C_{22}), 120.3 (1C, C_{21}), 118.3 (1C, C_{29}), 116.4 (2C, C_1 and C_6), 113.5 (2C, C_{27} and C_{31}), 105.3 (1C, C_3), 68.4 (1C, C_{33}), 56.1 (2C, C_9 and C_{11}), 51.7 (2C, C_8 and C_{12}), 50.1 (1C, C_{38}), 46.0 (1C, C_{13}), 37.8 (1C, C_{40}), 33.5 (1C, C_{35}), 29.7 (1C, C_{39}), 26.6 (1C, C_{34}).

HRMS (ESI) *m/z* 593.30975 $(M+H)^+$ (Theoretical 593.30955).

HPLC-RP rt = 13.53 min (Method A).

Synthesis of 3-(5-(4-methylpiperazin-1-yl)-1H,1'H-[2,5'-bibenzo[d]imidazol]-2'-yl)phenol (2.17)

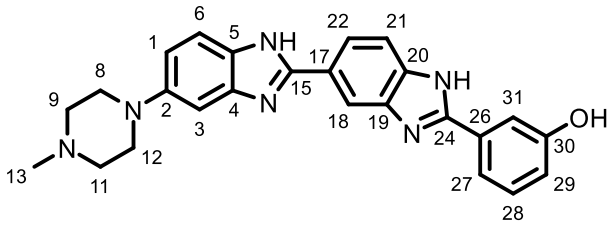

Chemical Formula: $C_{25}H_{24}N_6O$
Exact Mass: 424,20
Molecular Weight: 424,51

A solution of freshly prepared compound **2.35** (50 mg, 0.15 mmol, 1 eq), compound 3-hydroxybenzaldehyde (38 mg, 0.30 mmol, 2 eq) and $Na_2S_2O_5$ (35 mg, 0.18 mmol, 1.2 eq) in absolute ethanol (5 mL), was stirred at 80°C, under Ar, for 16h. The mixture was concentrated under reduced pressure. The crude residue was purified by flash chromatography (DCM/MeOH gradient 100:0 to 80:20, v/v) to provide **2.17** (52 mg, 80%) as a grey solid.

R_f = 0.34 (DCM/MeOH 70:30).

^{1}H NMR (400 MHz, CD_3OD) δ (ppm) 8.28 (d, J = 1.7 Hz, 1H, H_{18}), 7.97 (dd, J = 8.5, 1.7 Hz, 1H, H_{22}), 7.71 (d, J = 8.5 Hz, 1H, H_{21}), 7.61 – 7.54 (m, 2H, H_{27} and H_{31}), 7.51 (d, J = 8.8 Hz, 1H, H_6), 7.36 (t, J = 8.2 Hz, 1H, H_{28}), 7.15 (d, J = 2.2 Hz, 1H, H_3), 7.04 (dd, J = 8.8, 2.2 Hz, 1H, H_1), 6.99 – 6.92 (m, 1H, H_{29}), 3.38 – 3.17 (m, 4H, H_8 and H_{12}), 2.93 – 2.86 (m, 4H, H_9 and H_{11}), 2.54 (s, 3H, H_{13}).

^{13}C NMR (101 MHz, CD_3OD) δ (ppm) 157.8 (1C, C_{30}), 147.3 (1C, C_2), 131.1, 130.0 (2C, C_{19} and C_{22}), 117.4, 117.2 (2C, C_1 and C_{29}), 113.5 (1C, C_6), 109.1 (1C, C_3), 53.9 (2C, C_9 and C_{11}), 49.1 (2C, C_8 and C_{12}), 44.2 (1C, C_{13}).

HRMS (ESI) *m/z* 425.20844 $(M+H)^+$ (Theoretical 425.20837).

HPLC-RP rt = 2.7 min (Method B).

Synthesis of ethyl 4-(3-(5-(4-methylpiperazin-1-yl)-1H,1'H-[2,5'-bibenzo[*d*]imidazol]-2'-yl)phenoxy)butanoate (2.18)

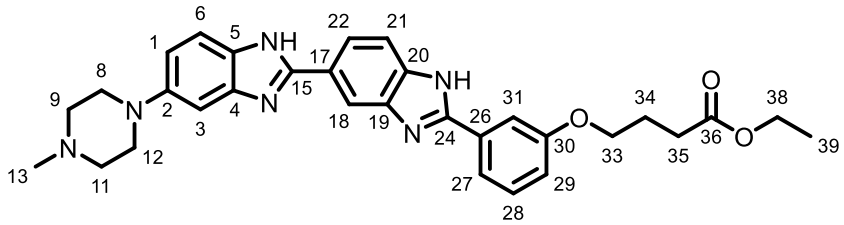

Chemical Formula: $C_{31}H_{34}N_6O_3$
Exact Mass: 538,27
Molecular Weight: 538,65

A solution of freshly prepared compound **2.35** (100 mg, 0.31 mmol, 1 eq), compound **2.27** (183 mg, 0.77 mmol, 2.5 eq) and $Na_2S_2O_5$ (71 mg, 0.37 mmol, 1.2 eq) in absolute ethanol (11 mL), was stirred at 80°C, under Ar, for 16h. The mixture was concentrated under reduced pressure. The crude residue was purified by flash chromatography (DCM/MeOH gradient 100:0 to 80:20, v/v) to provide **2.18** (150 mg, 90%) as an orange solid.

R_f = 0.23 (DCM/MeOH 95:05).

^{1}H NMR (400 MHz, CD_3OD) *δ* (ppm) 8.27 (s, 1H, H_{18}), 7.96 (d, *J* = 8.5 Hz, 1H, H_{22}), 7.74 – 7.65 (m, 3H, H_{21}, H_{27} and H_{31}), 7.50 (d, *J* = 8.8 Hz, 1H, H_6), 7.44 (t, *J* = 8.2 Hz, 1H, H_{28}), 7.13 (d, *J* = 1.9 Hz, 1H, H_3), 7.11 – 7.00 (m, 2H, H_1 and H_{29}), 4.19 – 4.09 (m, 4H, H_{33} and H_{38}), 3.26 – 3.21 (m, 4H, H_8 and H_{12}), 2.77 – 2.70 (m, 4H, H_9 and H_{11}), 2.55 (t, *J* = 7.2 Hz, 2H, H_{35}), 2.42 (s, 3H, H_{13}), 2.12 (p, *J* = 7.2 Hz, 2H, H_{34}), 1.25 (t, *J* = 7.1 Hz, 3H, H_{39}).

^{13}C NMR (101 MHz, CD_3OD) *δ* (ppm) 175.0 (1C, C_{36}), 160.9 (1C, C_{30}), 155.0 (1C, C_{24}), 153.7 (1C, C_{15}), 149.5 (1C, C_2), 131.8 (1C, C_{26}), 131.3 (1C, C_{28}), 126.0 (1C, C_{17}),122.8 (1C, C_{22}), 120.3 (1C, C_{21}), 118.3 (1C, C_{29}), 116.5 (2C, C_1 and C_6), 113.6 (2C, C_{27} and C_{31}), 102.4 (1C, C_3), 68.2 (1C, C_{33}), 61.6 (1C, C_{38}), 56.0 (2C, C_9 and C_{11}), 51.6 (2C, C_8 and C_{12}), 45.8 (1C, C_{13}), 31.7 (1C, C_{35}), 25.8 (1C, C_{34}), 14.5 (1C, C_{39}).

HRMS (ESI) *m/z* 539.27618 $(M+H)^+$ (Theoretical 539.27706).

HPLC-RP rt = 14.95 min (Method A).

Synthesis of 2-fluoro-4-(5-(4-methylpiperazin-1-yl)-1H,1'H-[2,5'-bibenzo[d]imidazol]-2'-yl)phenol (2.19)

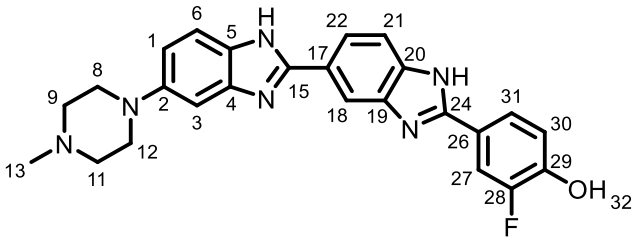

Chemical Formula: $C_{25}H_{23}FN_6O$
Exact Mass: 442,19
Molecular Weight: 442,50

A solution of freshly prepared compound **2.35** (60 mg, 0.19 mmol, 1 eq), 3-fluoro-4-hydroxybenzaldehyde (52 mg, 0.37 mmol, 2 eq) and $Na_2S_2O_5$ (45 mg, 0.23 mmol, 1.2 eq) in absolute ethanol (6 mL), was stirred at 80°C, under Ar, for 16h. The mixture was concentrated under reduced pressure. The crude residue was purified by flash chromatography (DCM/MeOH gradient 100:0 to 90:10, v/v) to provide **2.19** (73 mg, 90%) as a grey solid.

R_f = 0.36 (DCM/MeOH 92:8)

^{1}H NMR (400 MHz, CD_3OD) δ (ppm) 8.26 (d, J = 1.6 Hz, 1H, H_{18}), 7.96 (dd, J = 8.5, 1.6 Hz, 1H, H_{22}), 7.85 (dd, J = 12.0, 2.1 Hz, 1H, H_{31}), 7.82 – 7.75 (m, 1H, H_{27}), 7.69 (d, J = 8.5 Hz, 1H, H_{21}), 7.51 (d, J = 8.8 Hz, 1H, H_6), 7.17 – 7.12 (m, 1H, H_3), 7.12 – 7.01 (m, 2H, H_1 and H_{30}), 3.28 – 3.18 (m, 4H, H_8 and H_{12}), 2.78 – 2.71 (m, 4H, H_9 and H_{11}), 2.43 (s, 3H, H_{13}).

^{13}C NMR (101 MHz, CD_3OD) δ (ppm) 150.7, 150.5 (2C, C_{24} and C_{28}), 148.1, 147.8, 147.7 (3C, C_2, C_{15} and C_{29}), 123.3 (1C, C_{27}), 121.2, 120.9 (2C, C_{22} and C_{26}), 118.0, 115.1 (2C, C_1 and C_{30}), 114.4, 114.2 (2C, C_{18} and C_{31}), 101.1 (1C, C_3), 54.7 (2C, C_9 and C_{11}), 50.3 (2C, C_8 and C_{12}), 44.5 (1C, C_{13}).

HRMS (ESI) *m/z* 443.19937 $(M+H)^+$ (Theoretical 443.19901).

HPLC-RP rt = 2.7 min (Method B).

Synthesis of 5-(4-methylpiperazin-1-yl)-2'-(naphthalen-1-yl)-1H,1'H-2,5'-bibenzo[d]imidazole (2.20)

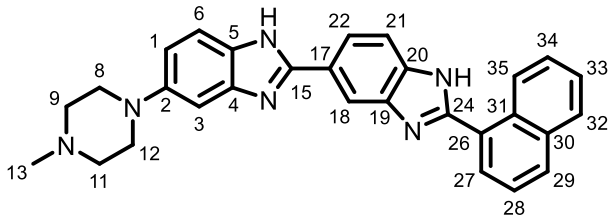

Chemical Formula: $C_{29}H_{26}N_6$
Exact Mass: 458,22
Molecular Weight: 458,57

A solution of freshly prepared compound **2.35** (60 mg, 0.18 mmol, 1 eq), 1-naphtaldehyde (58 mg, 0.36 mmol, 2 eq) and $Na_2S_2O_5$ (42 mg, 0.22 mmol, 1.2 eq) in absolute ethanol (6 mL), was stirred at 80°C, under Ar, for 16h. The mixture was concentrated under reduced pressure. The crude residue was purified by flash chromatography (DCM/MeOH gradient 100:0 to 85:15, v/v) to provide **2.20** (82 mg, quantitative) as a yellow solid.

R_f = 0.21 (DCM/MeOH 85:15).

^{1}H NMR (400 MHz, CD_3OD) δ (ppm) 8.57 – 8.48 (m, 1H, H_{Napht}), 8.38 (d, J = 1.6 Hz, 1H, H_{18}), 8.13 – 8.03 (m, 2H, H_{22} and H_{Napht}), 8.02 – 7.96 (m, 1H, H_{Napht}), 7.91 (dd, J = 7.2, 1.2 Hz, 1H, H_{Napht}), 7.81 (d, J = 8.5 Hz, 1H, H_{Napht}), 7.71 – 7.56 (m, 3H, H_{21} and 2H_{Napht}), 7.53 (d, J = 8.8 Hz, 1H, H_6), 7.16 (m, 1H, H_3), 7.05 (dd, J = 8.8, 2.2 Hz, 1H, H_1), 3.30 – 3.23 (m, 4H, H_8 and H_{12}), 2.84 – 2.77 (m, 4H, H_9 and H_{11}), 2.48 (s, 3H, H_{13}).

^{13}C NMR (101 MHz, CD_3OD) δ (ppm) 155.2 (1C, C_{24}), 153.8 (1C, C_{15}), 149.4 (1C, C_2), 135.4 (1C, C_{IV}), 132.4, 132.0, 129.6, 129.5, 128.8, 128.4 (6C, 6CH_{Napht}), 127.6 (1C, C_{IV}), 126.6 (1C, CH_{Napht}), 126.2, 126.0 (2C, 2C_{IV}), 122.8 (1C, C_{22}), 116.5 (2C, C_1 and C_6), 56.0 (2C, C_9 and C_{11}), 51.5 (2C, C_8 and C_{12}), 45.7 (1C, C_{13}).

HRMS (ESI) *m/z* 459.22940 $(M+H)^+$ (Theoretical 459.22972).

HPLC-RP rt = 3.2 min (Method B).

Synthesis of 5-(4-methylpiperazin-1-yl)-2'-(quinolin-4-yl)-1H,1'H-2,5'-bibenzo[d]imidazole (2.21)

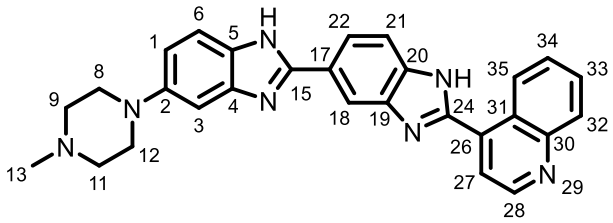

Chemical Formula: $C_{28}H_{25}N_7$
Exact Mass: 459,22
Molecular Weight: 459,56

A solution of freshly prepared compound **2.35** (74 mg, 0.23 mmol, 1 eq), 4-quinolinecarboxaldehyde (72 mg, 0.46 mmol, 2 eq) and $Na_2S_2O_5$ (53 mg, 0.28 mmol, 1.2 eq) in absolute ethanol (8 mL), was stirred at 80°C, under Ar, for 16h. The mixture was concentrated under reduced pressure. The crude residue was purified by flash chromatography (DCM/MeOH gradient 100:0 to 80:20, v/v) to provide **2.21** (51 mg, 48%) as an orange solid.

R_f = 0.25 (DCM/MeOH 80:20).

^{1}H NMR (400 MHz, CD_3OD) δ (ppm) 8.99 (d, J = 4.5 Hz, 1H, H_{28}), 8.86 – 8.77 (m, 1H, H_{35}), 8.39 (s, 1H, H_{18}), 8.15 (d, J = 8.2 Hz, 1H, H_{22}), 8.06 (dd, J = 8.5, 1.5 Hz, 1H, H_{32}), 7.91 – 7.79 (m, 3H, H_{21}, H_{27} and H_{33}), 7.74 (ddd, J = 8.3, 6.9, 1.2 Hz, 1H, H_{34}), 7.51 (d, J = 8.8 Hz, 1H, H_6), 7.12 (m, 1H, H_3), 7.04 (dd, J = 8.8, 2.2 Hz, 1H, H_1), 3.25 – 3.18 (m, 4H, H_8 and H_{12}), 2.70 – 2.62 (m, 4H, H_9 and H_{11}), 2.37 (s, 3H, H_{13}).

^{13}C NMR (101 MHz, CD_3OD) δ (ppm) 153.4 (1C, C_{24}), 152.0 (1C, C_{15}), 150.8 (1C, C_{28}), 149.7, 149.6 (2C, C_2 and C_{30}), 137.4 (1C, C_{IV}), 131.6 (1C, C_{33}), 129.9 (1C, C_{22}), 129.2 (1C, C_{34}), 127.4 (1C, C_{35}), 126.8, 126.7 (2C, $2C_{IV}$), 123.4 (1C, C_{32}), 122.7 (2C, C_{21} and C_{27}), 116.5 (2C, C_1 and C_6), 56.1 (2C, C_9 and C_{11}), 51.7 (2C, C_8 and C_{12}), 46.0 (1C, C_{13}).

HRMS (ESI) *m/z* 460.22467 $(M+H)^+$ (Theoretical 460.22497).

HPLC-RP rt = 3.1 min (Method B).

Synthesis of N-(3-azidopropyl)-4-(3-(5-(4-methylpiperazin-1-yl)-1H-benzo[d]imidazol-2-yl)phenoxy)butanamide (2.22)

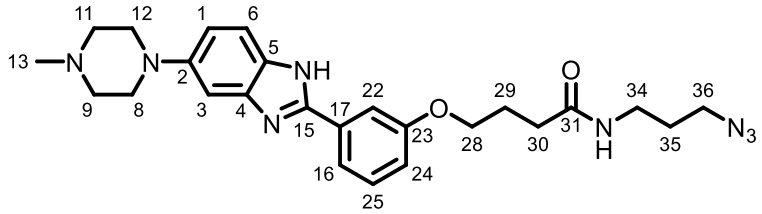

Chemical Formula: $C_{25}H_{32}N_8O_2$
Exact Mass: 476,26
Molecular Weight: 476,58

A solution of freshly prepared compound **2.33** (60 mg, 0.3 mmol, 1 eq), compound **2.29** (174 mg, 0.6 mmol, 2 eq) and $Na_2S_2O_5$ (68 mg, 0.36 mmol, 1.2 eq) in absolute ethanol (10 mL), was stirred at 80°C, under Ar, for 16h. The mixture was concentrated under reduced pressure. The crude residue was purified by flash chromatography (DCM/MeOH gradient 100:0 to 90:10, v/v) to provide **2.22** (83 mg, 60%) as a red solid.

R_f = 0.44 (DCM/MeOH 90:10).

^{1}H NMR (400 MHz, (CD_3OD) δ (ppm) 7.66 – 7.57 (m, 2H, H_{26} and H_{22}), 7.50 (d, J = 8.8 Hz, 1H, H_6), 7.41 (t, J = 8.0 Hz, 1H, H_{25}), 7.15 – 7.10 (m, 1H, H_3), 7.10 – 6.99 (m, 2H, H_1 and H_{24}), 4.10 (t, J = 6.2 Hz, 2H, H_{28}), 3.35 – 3.27 (m, 2H, H_{36}), 3.26 – 3.23 (m, 6H, H_8, H_{12} and H_{34}), 2.80 – 2.69 (m, 4H, H_9 and H_{11}), 2.47 – 2.38 (m, 5H, H_{30} and H_{13}), 2.19 – 2.06 (m, 2H, H_{29}), 1.73 (p, J = 6.8 Hz, 2H, H_{35}).

^{13}C NMR (101 MHz, CD_3OD) δ (ppm) 175.7 (1C, C_{31}), 161.1 (1C, C_{23}), 153.0 (1C, C_{15}), 149.8 (1C, C_2), 132.5 (1C, C_{17}), 131.4 (1C, C_{25}), 120.0 (1C, C_{26}), 117.8 (2C, C_1 and C_{24}), 116.9 (1C, C_6), 113.4 (1C, C_{22}), 68.5 (1C, C_{28}), 56.2 (2C, C_9 and C_{11}), 51.6 (2C, C_8 and C_{12}), 50.2 (1C, C_{34}), 45.9 (1C, C_{13}), 37.9 (1C, C_{36}), 33.7 (1C, C_{30}), 29.9 (1C, C_{35}), 26.7 (1C, C_{29}).

HRMS (ESI) *m/z* 477.27261 $(M+H)^+$ (Theoretical 477.27265).

HPLC-RP rt = 3.1 min (Method B).

Synthesis of 4-(5-(4-methylpiperazin-1-yl)-1H,1'H-[2,5'-bibenzo[d]imidazol]-2'-yl)-2-nitroaniline (2.36)

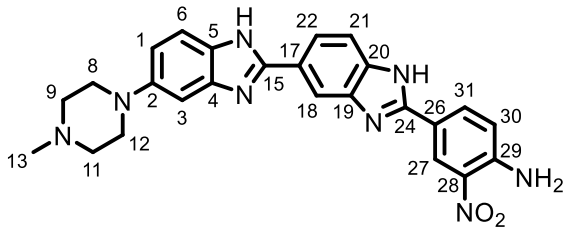

Chemical Formula: $C_{25}H_{24}N_8O_2$
Exact Mass: 468,20
Molecular Weight: 468,52

A solution of compound **2.31** (80 mg, 0.28 mmol, 1 eq) and freshly prepared compound **2.35** (90 mg, 0.28 mmol, 1 eq), in absolute ethanol/glacial acetic acid (2:1 (v/v), 8 mL), was stirred at 80°C, under Ar, for 24h. The mixture was concentrated under reduced pressure. The crude residue was purified by flash chromatography (DCM/MeOH gradient 100:0 to 80:20, v/v) to provide **2.36** (130 mg, 99%) as a grey solid.

R_f = 0.35 (DCM/MeOH 85:15).

^{1}H NMR (400 MHz, (CD_3OD) δ (ppm) 8.78 (d, J = 2.1 Hz, 1H, H_{27}), 8.16 – 8.11 (m, 1H, H_{18}), 8.04 (dd, J = 8.9, 2.1 Hz, 1H, H_{31}), 7.87 (dd, J = 8.5, 1.6 Hz, 1H, H_{22}), 7.61 (d, J = 8.5 Hz, 1H, H_{21}), 7.46 (d, J = 8.8 Hz, 1H, H_6), 7.09 (d, J = 2.2 Hz, 1H, H_3), 7.06 (d, J = 8.9 Hz, 1H, H_{30}), 7.00 (dd, J = 8.8, 2.2 Hz, 1H, H_1), 3.32 – 3.26 (m, 4H, H_8 and H_{12}), 3.00 – 2.93 (m, 4H, H_9 and H_{11}), 2.59 (s, 3H, H_{13}).

^{13}C NMR (101 MHz, CD_3OD) δ (ppm) 153.9, 153.7 (2C, C_{15} and C_{24}), 149.0 (1C, C_2), 148.6 (1C, C_{29}), 141.9 (1C, C_{20}), 140.1 (1C, C_4), 136.0 (1C, C_{19}), 134.2 (1C, C_{31}), 132.3 (1C, C_5), 125.7 (1C, C_{17}), 125.4 (1C, C_{27}), 122.5 (1C, C_{22}), 120.8 (1C, C_{30}), 118.1 (1C, C_{26}), 116.6 (1C, C_6), 116.5 (1C, C_1), 116.4 (1C, C_{21}), 113.7 (1C, C_{18}), 102.5 (1C, C_3), 55.6 (2C, C_9 and C_{11}), 50.9 (2C, C_8 and C_{12}), 45.1 (1C, C_{13}).

HRMS (ESI) *m/z* 469.21011 $(M+H)^+$ (Theoretical 469.21005).

Synthesis of thiazole derivatives

Synthesis of ethyl 3-aminopropanoate (3.03)

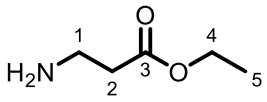

Chemical Formula: $C_5H_{11}NO_2$
Exact Mass: 117,08
Molecular Weight: 117,15

A solution of β-Alanine (2 g, 22.4 mmol, 1 eq) in absolute EtOH (20 mL) was cooled down to 0°C. Then $SOCl_2$ (2 ml, 28.1 mmol, 1.2 eq) was added dropwise and the mixture was stirred at 70°C, for 2h30. The mixture was concentrated under reduced pressure and then triturated with Et_2O. The resulting precipitate was collected by filtration and then washed with Et_2O. Drying under reduced pressure afforded the pure product **3.03** (3.37 g, 97%) as a white powder.

R_f = 0.57 (DCM/MeOH 80:20).

^{1}H NMR (400 MHz, CD_3OD) δ (ppm) 4.20 (q, J = 7.1 Hz, 2H, H_4), 3.21 (t, J = 6.5 Hz, 2H, H_1), 2.76 (t, J = 6.5 Hz, 2H, H_2), 1.28 (t, J = 7.1 Hz, 3H, H_5).

^{13}C NMR (101 MHz, CD_3OD) δ (ppm) 179.7 (1C, C_3), 60.2 (1C, C_4), 37.5 (1C, C_1), 36.9 (1C, C_2), 13.4 (1C, C_5).

MS (ESI) *m/z* 118.5 $(M+H)^+$ (Theoretical 118.1).

Synthesis of ethyl 3-((*tert*-butoxycarbonyl)amino)propanoate (3.04)

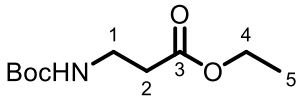

Chemical Formula: $C_{10}H_{19}NO_4$
Exact Mass: 217,13
Molecular Weight: 217,27

Et_3N (1.1 mL, 7.8 mmol, 1.2 eq) was added to a 0°C solution of **3.03** (1 g, 6.5 mmol, 1 eq) in DCM (40 mL). Di-*tert*-butyl dicarbonate (1.7 g, 7.8 mmol, 1.2 eq), solubilized in DCM (20 mL), was then added dropwise to the 0°C solution, and the reaction mixture was allowed to warm up to room temperature and stirred for 16h. A solution of $KHSO_4$ (0.5 M) was added, and the aqueous phase was extracted with DCM. The organic phase was dried over $MgSO_4$ and concentrated under reduced pressure. Drying under reduced pressure afforded the pure product **3.04** (1.36 g, 96%), as a grey solid.

R_f = 0.85 (DCM/MeOH 95:5).

^{1}H NMR (400 MHz, $CDCl_3$) δ (ppm) 5.00 (br, 1H, NH), 4.15 (q, J = 7.1 Hz, 2H, H_4), 3.39 (q, J = 6.0 Hz, 2H, H_1), 2.51 (t, J = 6.0 Hz, 2H, H_2), 1.43 (t, J = 7.1 Hz, 3H, H_5), 1.26 (s, 9H, H_{Boc}).

^{13}C NMR (101 MHz, $CDCl_3$) δ (ppm) 171.9 (1C, C_3), 155.4 (1C, C_{Boc}), 78.7 (1C, $C_{IV.Boc}$), 60.1 (1C, C_4), 35.7 (1C, C_1), 34.2 (1C, C_2), 27.9 (3C, $CH_{3.Boc}$), 13.7 (1C, C_5).

MS (ESI) *m/z* 218.5 $(M+H)^+$ (Theoretical 218.1).

Synthesis of *tert*-butyl (3-amino-3-oxopropyl)carbamate (3.05)

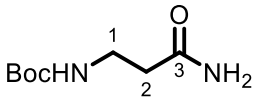

Chemical Formula: $C_8H_{16}N_2O_3$
Exact Mass: 188,12
Molecular Weight: 188,23

A solution of **3.04** (1.4 g, 6.2 mmol, 1 eq) in an aqueous ammonia solution (36%, 15 mL) and ethanol (5 mL) was stirred at room temperature, for 16h. The mixture was carefully concentrated under vacuum and then triturated with Et_2O. The resulting white precipitate was collected by filtration and then washed with Et_2O. Drying under reduced pressure afforded the pure product **3.05** (1.03 g, 87%) as a white solid.

R_f = 0.28 (DCM/MeOH 95:5).

^{1}H NMR (400 MHz, $CDCl_3$) δ (ppm) 5.83 (br, 2H, NH_2), 5.16 (br, 1H, NH), 3.40 (q, J = 6.0 Hz, 2H, H_1), 2.45 (t, J = 6.0 Hz, 2H, H_2), 1.43 (s, 9H, H_{Boc}).

^{13}C NMR (101 MHz, $CDCl_3$) δ (ppm) 174.2 (1C, C_3), 156.0 (1C, C_{Boc}), 79.3 (1C, $C_{IV.Boc}$), 36.2 (1C, C_1), 35.5 (1C, C_2), 28.2 (3C, $CH_{3.Boc}$).

MS (ESI) *m/z* 189.5 $(M+H)^+$ (Theoretical 189.1).

Synthesis of *tert*-butyl (3-amino-3-thioxopropyl)carbamate (3.06)

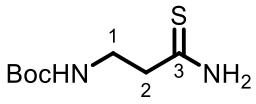

Chemical Formula: $C_8H_{16}N_2O_2S$
Exact Mass: 204,09
Molecular Weight: 204,29

A solution of **3.05** (3.4 g, 18 mmol, 1 eq) and Lawesson's reagent (4.4 g, 10.1 mmol, 0.6 eq) in THF (120 mL) was stirred at room temperature for 24h. The mixture was concentrated under reduced pressure, a solution of $NaHCO_3$ (sat.) was added, and the aqueous phase was extracted with DCM. The organic phase was washed with brine, dried over $MgSO_4$ and concentrated under reduced pressure. The crude residue was purified by flash chromatography (cHex/EtOAc gradient 90:10 to 40:60, v/v) to provide **3.06** (2.57 g, 70%) as a yellow solid.

R_f = 0.65 (cHex/EtOAc 3:7).

^{1}H NMR (400 MHz, $CDCl_3$) δ (ppm) 7.66 (br, 2H, NH_2), 5.14 (br, 1H, NH), 3.54 (q, J = 6.0 Hz, 2H, H_1), 2.85 (t, J = 6.0 Hz, 2H, H_2), 1.42 (s, 9H, $H_{3.Boc}$).

^{13}C NMR (101 MHz, $CDCl_3$) δ (ppm) 207.8 (1C, C_3), 156.5 (1C, C_{Boc}), 80.0 (1C, $C_{IV.Boc}$), 44.9 (1C, C_2), 39.2 (1C, C_1), 28.5 (3C, $CH_{3.Boc}$).

MS (ESI) *m/z* 227.2 $(M+Na)^+$ (Theoretical 227.1).

Synthesis of ethyl 2-(2-((*tert*-butoxycarbonyl)amino)ethyl)thiazole-4-carboxylate (3.07)

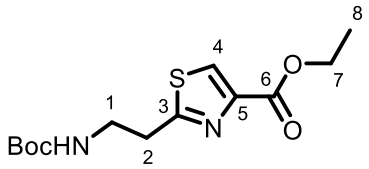

Chemical Formula: $C_{13}H_{20}N_2O_4S$
Exact Mass: 300,11
Molecular Weight: 300,37

A solution of **3.06** (8.8 g, 43 mmol, 1 eq) in absolute ethanol (45 mL) was stirred at 60°C, under Ar, until complete solubilization of the starting material. Then, ethyl bromopyruvate (1.6 mL, 56 mmol, 1.3 eq) was added and the mixture was stirred at 80°C, under Ar, for 1h30. The mixture was concentrated under reduced pressure and then triturated with Et_2O [R_f = 0.66 (DCM/MeOH 90:10)]. Precipitate was directly solubilized in DCM (60 mL) and Et_3N (16.3 mL, 117 mmol, 4 eq), then cooled down to 0°C. Di-*tert*-butyl dicarbonate (9.6 g, 43.9 mmol, 1.5 eq), solubilized in DCM (20 mL), was then added dropwise to the 0°C solution, and the reaction mixture was allowed to warm up to room temperature and stirred for 4h. A solution of $KHSO_4$ (0.5 M) was added, and the aqueous phase was extracted with DCM. The organic phase was dried over $MgSO_4$ and concentrated under reduced pressure. Drying under reduced pressure afforded the pure product **3.07** (8.6 g, 98%), as a grey solid, which was used without further purification.

R_f = 0.33 (cHex/EtOAc 6:4).

^{1}H NMR (400 MHz, $CDCl_3$) δ (ppm) 8.07 (s, 1H, H_4), 4.93 (br, 1H, NH), 4.41 (q, J = 7.1 Hz, 2H, H_7), 3.57 (q, J = 6.5 Hz, 2H, H_1), 3.25 (t, J = 6.5 Hz, 2H, H_2), 1.42 (s, 9H, H_{Boc}), 1.40 (t, J = 7.1 Hz, 3H, H_8).

^{13}C NMR (101 MHz, $CDCl_3$) δ (ppm) 168.9 (1C, C_6), 161.5 (1C, C_3), 156.0 (1C, C_{Boc}), 147.2 (1C, C_5), 127.6 (1C, C_4), 79.8 (1C, $C_{IV.Boc}$), 61.6 (1C, C_7), 40.1 (1C, C_1), 34.0 (1C, C_2), 28.5 (3C, $CH_{3.Boc}$), 14.5 (1C, C_8).

MS (ESI) *m/z* 323.1 $(M+Na)^+$ (Theoretical 323.1).

Synthesis of *tert*-butyl (2-(4-carbamoylthiazol-2-yl)ethyl)carbamate (3.08)

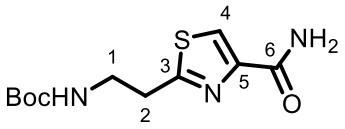

Chemical Formula: $C_{11}H_{17}N_3O_3S$
Exact Mass: 271,10
Molecular Weight: 271,34

A solution of **3.07** (8.6 g, 28.6 mmol, 1 eq) in an aqueous ammonia solution (36%, 120 mL) and ethanol (25 mL) was stirred at 70°C, for 2h. The mixture was carefully concentrated under vacuum and then triturated with Et_2O. The suspension was allowed to stand overnight. The resulting pale-yellow precipitate was collected by filtration and then washed with Et_2O. Drying under reduced pressure afforded the pure product **3.08** (7.8 g, 90%) as a pale-yellow solid.

R_f = 0.21 (cHex/EtOAc 3:7).

^{1}H NMR (400 MHz, $CDCl_3$) δ (ppm) 8.04 (s, 1H, H_4), 7.15 (br, 1H, NH_2), 5.83 (br, 1H, NH_2), 4.90 (br, 1H, NH), 3.58 (m, 2H, H_1), 3.19 (t, J = 6.4 Hz, 2H, H_2), 1.44 (s, 9H, H_{Boc}).

^{13}C NMR (101 MHz, $CDCl_3$) δ (ppm) 168.3 (1C, C_6), 163.3 (1C, C_3), 156.0 (1C, C_{Boc}), 149.5 (1C, C_5), 124.4 (1C, C_4), 79.9 (1C, $C_{IV.Boc}$), 39.9 (1C, C_1), 33.7 (1C, C_2), 28.6 (3C, $CH_{3.Boc}$).

MS (ESI) *m/z* 294.3 $(M+Na)^+$ (Theoretical 294.1).

Synthesis of *tert*-butyl (2-(4-carbamothioylthiazol-2-yl)ethyl)carbamate (3.09)

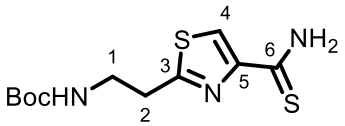

Chemical Formula: $C_{11}H_{17}N_3O_2S_2$
Exact Mass: 287,08
Molecular Weight: 287,40

A solution of **3.08** (2 g, 7.37 mmol, 1 eq) in THF/Toluene (2:1, 30 mL) was stirred at 100°C, under Ar, until complete solubilization of the starting material. Then, Lawesson's reagent (1.49 g, 3.69 mmol, 0.5 eq) was added and the mixture was stirred at 100°C, under Ar, for 20 min. The mixture was concentrated under reduced pressure, a solution of $NaHCO_3$ (sat.) was added, and the aqueous phase was extracted with EtOAc. The organic phase was washed with brine, dried over $MgSO_4$ and concentrated under reduced pressure. The crude residue was purified by flash chromatography (cHex/EtOAc gradient 80:20 to 10:90, v/v) to provide **3.09** (1.8 g, 85%) as a yellow solid.

R_f = 0.48 (cHex/EtOAc 6:4).

^{1}H NMR (400 MHz, $CDCl_3$) δ (ppm) 8.63 (br, 1H, NH_2), 8.34 (s, 1H, H_4), 7.60 (br, 1H; NH_2), 4.80 (br, 1H, NH), 3.58 (m, 2H, H_1), 3.19 (t, J = 6.2 Hz, 2H, H_2), 1.43 (s, 9H, H_{Boc}).

^{13}C NMR (101 MHz, $CDCl_3$) δ (ppm) 190.8 (1C, C_6), 167.9 (1C, C_3), 156.0 (1C, C_{Boc}), 153.1 (1C, C_5), 127.5 (1C, C_4), 80.0 (1C, $C_{IV.Boc}$), 39.8 (1C, C_1), 33.9 (1C, C_2), 28.6 (3C, $CH_{3.Boc}$).

MS (ESI) *m/z* 288.4 $(M+H)^+$ (Theoretical 288.1).

Synthesis of ethyl 2'-(2-aminoethyl)-[2,4'-bithiazole]-4-carboxylate hydrobromide (3.10)

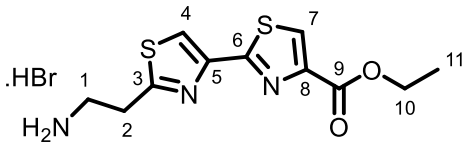

Chemical Formula: $C_{11}H_{13}N_3O_2S_2$
Exact Mass: 283,04
Molecular Weight: 283,36

A solution of **3.09** (4.1 g, 14.3 mmol, 1 eq) in absolute ethanol (40 mL) was stirred at 60°C, under Ar, until complete solubilization of the starting material. Then, ethyl bromopyruvate (2.33 mL, 18.5 mmol, 1.3 eq) was added and the mixture was stirred at 60°C, under Ar, for 16h. The mixture was concentrated under reduced pressure and then triturated with Et_2O. Filtration followed by drying under reduced pressure afforded the pure product **3.10** (4.95 g, 95%) as a grey solid.

R_f = 0.55 (DCM/MeOH 8:2).

^{1}H NMR (400 MHz, CD_3OD) δ (ppm) 8.44 (s, 1H, H_7), 8.32 (s, 1H, H_4), 4.45 (q, J = 7.1 Hz, 2H, H_{10}), 3.54 – 3.45 (m, 2H, H_1), 3.34 (m, 2H, H_2), 1.44 (t, J = 7.1 Hz, 3H, H_{11}).

^{13}C NMR (101 MHz, CD_3OD) δ (ppm) 168.5 (1C, C_9), 164.6 (1C, C_6), 162.6 (1C, C_3), 149.2 (1C, C_8), 148.6 (1C, C_5), 129.6 (1C, C_7), 119.8 (1C, C_4), 62.6 (1C, C_{10}), 39.5 (1C, C_1), 31.1 (1C, C_2), 14.6 (1C, C_{11}).

MS (ESI) *m/z* 284.4 $(M+H)^+$ (Theoretical 284.0).

Synthesis of ethyl 2'-(2-((*tert*-butoxycarbonyl)amino)ethyl)-[2,4'-bithiazole]-4-carboxylate (3.11)

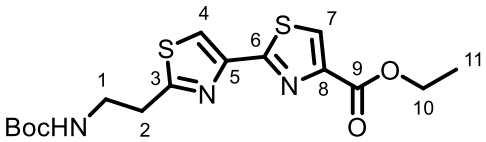

Chemical Formula: $C_{16}H_{21}N_3O_4S_2$
Exact Mass: 383,10
Molecular Weight: 383,48

Et_3N (3.64 mL, 26.1 mmol, 2 eq) was added to a 0°C solution of **3.10** (4.75 g, 13.1 mmol, 1 eq) in H_2O/1,4-Dioxane (1:1, 100 mL). Di-*tert*-butyl dicarbonate (3.1 g, 14.3 mmol, 1.1 eq), dissolved in H_2O/1,4-Dioxane (1:1, 20 mL), was then added dropwise to the 0°C solution, and the reaction mixture was allowed to warm up to room temperature and stirred for 16h. The mixture was concentrated under reduced pressure, a solution of $KHSO_4$ (0.5 M) was added, and the aqueous phase was extracted with DCM. The organic phase was dried over $MgSO_4$ and concentrated under reduced pressure. The crude residue was purified by flash chromatography (DCM/MeOH gradient 100:0 to 95:5, v/v) to provide **3.11** (5 g, quantitative) as a white solid.

R_f = 0.46 (DCM/MeOH 98:2).

^{1}H NMR (400 MHz, CD_3OD) δ (ppm) 8.38 (s, 1H, H_7), 8.21 (s, 1H, H_4), 4.42 (q, J = 7.1 Hz, 2H, H_{10}), 3.49 (t, J = 6.7 Hz, 2H, H_1), 3.22 (t, J = 6.7 Hz, 2H, H_2), 1.45 – 1.37 (m, 16H, H_{11} and H_{Boc}).

^{13}C NMR (101 MHz, CD_3OD) δ (ppm) 168.7 (1C, C_9), 163.3 (1C, C_6), 161.4 (1C, C_3), 155.8 (1C, C_{Boc}), 148.1 (1C, C_8), 147.9 (1C, C_5), 127.7 (1C, C_7), 117.1 (1C, C_4), 79.6 (1C, $C_{IV.Boc}$), 61.5 (1C, C_{10}), 39.7 (1C, C_1), 33.4 (1C, C_2), 28.4 (3C, $CH_{3.Boc}$), 14.3 (1C, C_{11}).

MS (ESI) *m/z* 384.3 $(M+H)^+$ (Theoretical 384.1).

Synthesis of *tert*-butyl (2-(4-carbamoyl-[2,4'-bithiazol]-2'-yl)ethyl)carbamate (3.12)

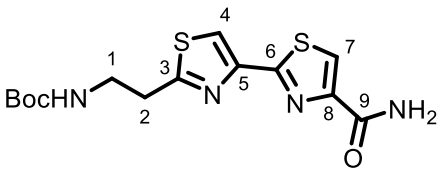

Chemical Formula: $C_{14}H_{18}N_4O_3S_2$
Exact Mass: 354,08
Molecular Weight: 354,44

A solution of **3.11** (5 g, 13.1 mmol, 1 eq) in an aqueous ammonia solution (36%, 325 mL) and ethanol (45 mL) was stirred at 70°C, for 3h. The mixture was carefully concentrated under vacuum and then triturated with Et_2O. The suspension was allowed to stand overnight. The resulting off-white precipitate was collected by filtration and then washed with Et_2O. Drying under reduced pressure afforded the pure product **3.12** (4.6 g, quantitative) as an off-white solid.

R_f = 0.33 (DCM/MeOH 96:4).

^{1}H NMR (400 MHz, $CDCl_3$) δ (ppm) 8.16 (s, 1H, H_7), 7.86 (s, 1H, H_4), 7.23 (br, 1H, NH_2), 5.69 (br, 1H, NH_2), 5.04 (br, 1H, NH), 3.67 – 3.57 (m, 2H, H_1), 3.25 (t, J = 6.4 Hz, 2H, H_2), 1.45 (s, 9H, H_{Boc}).

^{13}C NMR (101 MHz, CD_3OD) δ (ppm) 170.9 (1C, C_9), 165.6 (1C, C_6), 164.1 (1C, C_3), 158.3 (1C, C_{Boc}), 151.6 (1C, C_8), 149.4 (1C, C_5), 125.6 (1C, C_7), 118.5 (1C, C_4), 80.2 (1C, $C_{IV.Boc}$), 41.1 (1C, C_1), 34.3 (1C, C_2), 28.7 (3C, $CH_{3.Boc}$).

MS (ESI) *m/z* 355.2 $(M+H)^+$ (Theoretical 355.1).

Synthesis of *tert*-butyl (2-(4-carbamothioyl-[2,4'-bithiazol]-2'-yl)ethyl)carbamate (3.13)

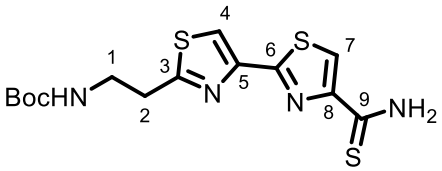

Chemical Formula: $C_{14}H_{18}N_4O_2S_3$
Exact Mass: 370,06
Molecular Weight: 370,50

A solution of **3.12** (2.45 g, 6.91 mmol, 1 eq) in THF/Toluene (2:1, 100 mL) was stirred at 100°C, under Ar, until complete solubilization of the starting material. Then, Lawesson's reagent (1.4 g, 3.46 mmol, 0.5 eq) was added and the mixture was stirred at 100°C, under Ar, for 30 min. The mixture was concentrated under reduced pressure, a solution of $NaHCO_3$ (sat.) was added, and the aqueous phase was extracted with EtOAc. The organic phase was washed with brine, dried over $MgSO_4$ and concentrated under reduced pressure. The crude residue was purified by flash chromatography (cHex/EtOAc gradient 90:10 to 20:80, v/v) to provide **3.13** (2.35 g, 92%) as a yellow solid.

R_f = 0.5 (cHex/EtOAc 4:5).

^{1}H NMR (400 MHz, $CDCl_3$) δ (ppm) 8.70 (br, 1H, NH_2), 8.47 (s, 1H,H_7), 7.85 (s, 1H, H_4), 7.64 (br, 1H, NH_2), 5.03 (br, 1H, NH), 3.62 (dd, 6.2 Hz, 2H, H_1), 3.24 (t, J = 6.2 Hz, 2H, H_2), 1.44 (s, 9H, H_{Boc}).

^{13}C NMR (101 MHz, $CDCl_3$) δ (ppm) 190.3 (1C, C_9), 169.4 (1C, C_6), 162.0 (1C, C_3), 156.3 (1C, C_{Boc}), 153.8 (1C, C_8), 148.0 (1C, C_5), 127.7 (1C, C_7), 117.0 (1C, C_4), 79.7 (1C, $C_{IV.Boc}$), 39.6 (1C, C_1), 33.3 (1C, C_2), 28.2 (3C, $CH_{3.Boc}$).

MS (ESI) *m/z* 371.4 $(M+H)^+$ (Theoretical 371.1).

Synthesis of ethyl 2''-(2-((*tert*-butoxycarbonyl)amino)ethyl)-[2,4':2',4''-terthiazole]-4-carboxylate (3.14)

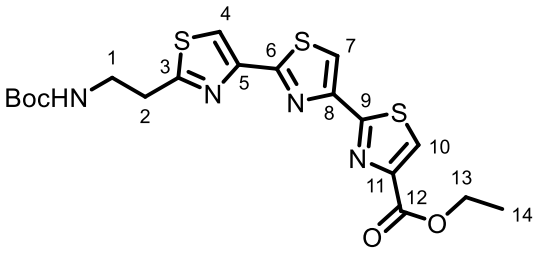

Chemical Formula: $C_{19}H_{22}N_4O_4S_3$
Exact Mass: 466,08
Molecular Weight: 466,59

A solution of **3.13** (2.40 g, 6.48 mmol, 1 eq) in absolute ethanol (130 mL) was stirred at 60°C, under Ar, until complete solubilization of the starting material. Then, ethyl bromopyruvate (1.1 mL, 8.42 mmol, 1.3 eq) was added and the mixture was stirred at 80°C, under Ar, for 16h. The mixture was concentrated under reduced pressure and then triturated with Et_2O. Precipitate was directly solubilized in H_2O/1,4-Dioxane (1:1, 80 mL) and Et_3N (1.71 mL, 12.3 mmol, 2 eq), then cooled down to 0°C. Di-*tert*-butyl dicarbonate (1.48 g, 6.78 mmol, 1.2 eq), dissolved in H_2O/1,4-Dioxane (1:1, 20 mL), was then added dropwise to the 0°C solution, and the reaction mixture was allowed to warm up to room temperature and stirred for 4h. The mixture was concentrated under reduced pressure, a solution of $KHSO_4$ (0.5 M) was added, and the aqueous phase was extracted with DCM. The organic phase was dried over $MgSO_4$ and concentrated under reduced pressure. The crude residue was purified by flash chromatography (cHex/EtOAc gradient 100:0 to 50:50, v/v) to provide **3.14** (2.75 g, 92%) as a white solid.

R_f = 0.58 (cHex/EtOAc 5:5).

^{1}H NMR (400 MHz, $CDCl_3$) δ (ppm) 8.20 (s, 1H, H_{10}), 8.17 (s, 1H, H_7), 7.97 (s, 1H, H_4), 5.06 (br, 1H, NH), 4.46 (q, J = 7.1 Hz, 2H, H_{13}), 3.62 (dd, J = 6.4 Hz, 2H, H_1), 3.25 (t, J = 6.4 Hz, 2H, H_2), 1.48 – 1.40 (m, 16h, H_{14} and H_{Boc}).

^{13}C NMR (101 MHz, $CDCl_3$) δ (ppm) 163.6 (1C, C_{12}), 163.2 (1C, C_9), 161.7 (1C, C_6), 156.1 (1C, C_3), 149.4 (1C, C_{11}), 148.6 (1C, C_8), 148.2 (1C, C_5), 128.0 (1C, C_{10}), 118.1 (1C, C_7), 116.8 (1C, C_4), 79.8 (1C, $C_{IV.Boc}$), 61.8 (1C, C_{13}), 39.9 (1C, C_1), 33.7 (1C, C_2), 28.6 (3C, $CH_{3.Boc}$), 14.6 (1C, C_{14}).

MS (ESI) *m/z* 367.3 $([M\text{-Boc}]+H)^+$ (Theoretical 367.0).

Synthesis of 2''-(2-((*tert*-butoxycarbonyl)amino)ethyl)-[2,4':2',4''-*ter*thiazole]-4-carboxylic acid (3.15a)

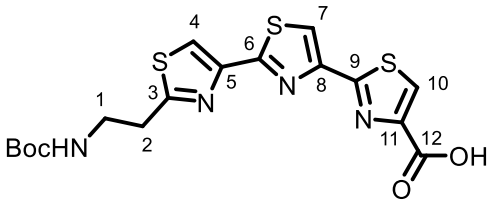

Chemical Formula: $C_{17}H_{18}N_4O_4S_3$
Exact Mass: 438,05
Molecular Weight: 438,54

A solution of **3.14** (700 mg, 1.50 mmol, 1 eq) in H_2O/THF (2:1, 22 mL) was stirred at room temperature, until complete solubilization of the starting material. Then, LiOH (180 mg, 7.50 mmol, 5 eq) was added and the mixture was stirred at room temperature for 4h. The mixture was concentrated under reduced pressure. Precipitation of the compound was performed by adding a solution of $KHSO_4$ (0.5M) until pH 2. Lyophilization afforded the pure product **3.15a** (655 mg, 99%) as a white solid.

R_f = 0.3 (DCM/MeOH 9:1).

^{1}H NMR (400 MHz, DMF-d_7) δ (ppm) 8.59 (s, 1H, H_{10}), 8.46 (s, 1H, H_7), 8.34 (s, 1H, H_4), 7.00 (br, NH), 3.52 (dd, J = 6.8 Hz, 2H, H_1), 3.29 (t, J = 6.8 Hz, 2H, H_2), 1.41 (s, 9H, H_{Boc}).

^{13}C NMR (101 MHz, DMF-d_7) δ (ppm) 170.9 (1C, C_{12}), 164.7 (1C, C_9), 163.6 (1C, C_6), 163.3 (1C, C_3), 157.1 (1C, C_{Boc}), 150.3 (1C, C_{11}), 149.9 (1C, C_8), 148.8 (1C, C_5), 129.9 (1C, C_{10}), 119.3 (1C, C_7), 118.8 (1C, C_4), 79.0 (1C, $C_{IV.Boc}$), 41.3 (1C, C_1), 34.4 (1C, C_2), 28.9 (3C, $CH_{3.Boc}$).

MS (ESI) *m/z* 339.3 $([M\text{-Boc}]+H)^+$ (Theoretical 339.0).

Synthesis of 2''-(2-aminoethyl)-[2,4':2',4''-*ter*thiazole]-4-carboxylic acid (3.15b)

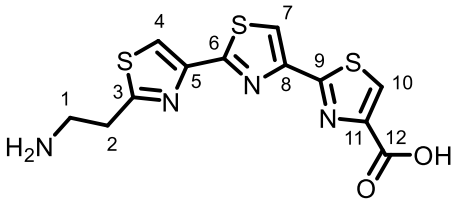

Chemical Formula: $C_{12}H_{10}N_4O_2S_3$
Exact Mass: 338,00
Molecular Weight: 338,42

Deprotection of compound **3.15a** (50 mg, 0.11 mmol, 1 eq) was performed using TFA (440 µL, 5.70 mmol, 50 eq.) in DCM (2 mL). The mixture was concentrated under reduced pressure and then triturated with Et_2O. Filtration followed by drying under reduced pressure afforded the pure product **3.15b** (34 mg, 66%) as a white solid.

^{1}H NMR (400 MHz, DMSO-d_6) δ (ppm) 8.42 (s, 1H, H_{10}), 8.36 (s, 1H, H_7), 8.33 (s, 1H, H_4), 3.64 – 2.89 (m, 4H, H_1 and H_2).

^{13}C NMR (101 MHz, DMSO-d_6) δ (ppm) 167.5 (1C, C_{12}), 162.8 (1C, C_9), 161.6 (1C, C_6), 161.4 (1C, C_3), 148.7 (1C, C_{11}), 147.1 (2C, C_5 and C_8), 128.1 (1C, C_{10}), 118.6 (1C, C_7), 118.5 (1C, C_4), 38.2 (1C, C_1), 30.5 (1C, C_2).

HRMS (ESI) *m/z* 339.00409 $(M+H)^+$ (Theoretical 339.00386).

HPLC-RP rt = 2.9 min (Method B).

Synthesis of ethyl 2''-(2-aminoethyl)-[2,4':2',4''-terthiazole]-4-carboxylate hydrochloride (3.16)

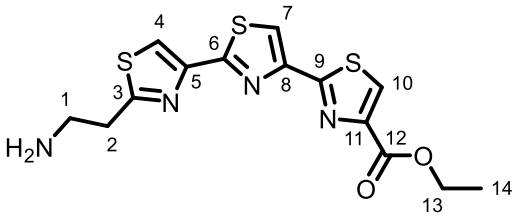

Chemical Formula: $C_{14}H_{14}N_4O_2S_3$
Exact Mass: 366,03
Molecular Weight: 366,47

Deprotection of compound **3.14** (400 mg, 0.86 mmol, 1 eq) was performed following general procedure A with HCl/1,4-dioxane (4M, 9 mL). After purification compound **3.16** (320 mg, 93%) was obtained as a white solid.

R_f = 0.4 (DCM/MeOH [10% NH_4OH] 9:1).

^{1}H NMR (400 MHz, DMSO-d_6) δ (ppm) 8.59 (s, 1H, H_{10}), 8.43 (s, 1H, H_7), 8.34 (s, 1H, H_4), 8.25 (br, 2H, NH_2), 4.35 (q, J = 7.1 Hz, 2H, H_{13}), 3.48 – 3.39 (m, 2H, H_1), 3.31 – 3.25 (m, 2H, H_2), 1.33 (t, J = 7.1 Hz, 3H, H_{14}).

^{13}C NMR (101 MHz, DMSO-d_6) δ (ppm) 167.5 (1C, C_{12}), 162.9 (1C, C_9), 162.2 (1C, C_6), 160.6 (1C, C_3), 148.4 (1C, C_{11}), 147.0 (2C, C_5 and C_8), 129.7 (1C, C_{10}), 119.0 (1C, C_7), 118.7 (1C, C_4), 60.9 (1C, C_{13}), 38.0 (1C, C_1), 30.3 (1C, C_2), 14.2 (1C, C_{14}).

HRMS (ESI) *m/z* 367.03516 $(M+H)^+$ (Theoretical 367.03516).

HPLC-RP rt = 3.7 min (Method B).

Synthesis of *tert*-butyl (4-((2-cyanoethyl)amino)butyl)carbamate (3.18)

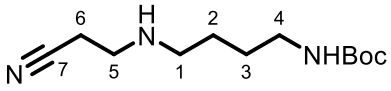

Chemical Formula: $C_{12}H_{23}N_3O_2$
Exact Mass: 241,18
Molecular Weight: 241,33

A solution of *N*-Boc-1,4-butanediamine (984 mg, 5.23 mmol, 1 eq) in MeOH (30 mL) was cooled down to 0°C. Then acrylonitrile (0.4 ml, 5.23 mmol, 1 eq) was added dropwise and the mixture was stirred at room temperature, for 16h. The mixture was concentrated under reduced pressure. The crude residue was purified by flash chromatography (DCM/MeOH gradient 100:0 to 95:5, v/v) to provide **3.18** (1.22 g, 97%) as a colorless oil.

R_f = 0.38 (DCM/MeOH 96:4).

^{1}H NMR (400 MHz, $CDCl_3$) δ (ppm) 4.72 (br, 1H, NH), 3.16 - 3.09 (m, 2H, H_4), 2.92 (t, J = 6.6 Hz, 2H, H_6), 2.65 (t, J = 6.6 Hz, 2H, H_5), 2.52 (t, J = 6.6 Hz, 2H, H_1), 1.56 - 1.49 (m, 4H, H_2 and H_3), 1.44 (s, 9H, H_{Boc}).

Synthesis of *tert*-butyl (4-((tert-butoxycarbonyl)amino)butyl)(2-cyanoethyl)carbamate (3.19)

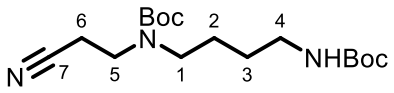

Chemical Formula: $C_{17}H_{31}N_3O_4$
Exact Mass: 341,23
Molecular Weight: 341,45

A solution of **3.18** (1.22 g, 5.1 mmol, 1 eq) in DCM (20 mL) was cooled down to 0°C. Di-*tert*-butyl dicarbonate (1.21 g, 5.6 mmol, 1.2 eq), solubilized in DCM (10 mL), was then added dropwise to the 0°C solution, and the reaction mixture was allowed to warm up to room temperature and stirred for 16h. Water was added, and the aqueous phase was extracted with DCM. The organic phase was dried over $MgSO_4$ and concentrated under reduced pressure. The mixture was concentrated under reduced pressure. The crude residue was purified by flash chromatography (cHex/EtOAc gradient 80:20 to 60:40, v/v) to provide **3.19** (1.72 g, quantitative) as a colorless oil.

R_f = 0.42 (cHex/EtOAc 70:30).

^{1}H NMR (400 MHz, $CDCl_3$) δ (ppm) 4.56 (br, 1H, NH), 3.46 (t, J = 6.7 Hz, 2H, H_5), 3.28 (t, J = 7.0 Hz, 2H, H_1), 3.13 (dd, J = 6.4 Hz, 12.5 Hz, 2H, H_4), 2.61 (m, 2H, H_6), 1.59 - 1.43 (m, 22H, H_2, H_3 and H_{Boc}).

MS (ESI) *m/z* 364.5 $(M+Na)^+$ (Theoretical 364.2).

Synthesis of *tert*-butyl (3-aminopropyl)(4-((tert-butoxycarbonyl)amino)butyl)carbamate (3.20)

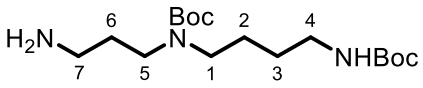

Chemical Formula: $C_{17}H_{35}N_3O_4$
Exact Mass: 345,26
Molecular Weight: 345,48

A solution of **3.19** (3.30 g, 9.7 mmol, 1 eq) in Et_2O (120 mL) was cooled down to -10°C. Then $LiAlH_4$ (1.47 g, 38.7 mmol, 4 eq) was added dropwise and the mixture was stirred at -10°C, for 30min. Then, the reaction mixture was allowed to warm up to room temperature and stirred for 2h. $LiAlH_4$ was neutralized with subsequent addition of: water (2 mL), a solution of 10% NaOH (2 mL), water (3 mL), and finally $MgSO_4$ was added to the mixture, which was then stirred for 15min. The mixture was filtered through a pad of Celite®, the flask and the pad were washed with Et_2O. The filtrate was concentrated under reduced pressure, affording the colorless oil compound **3.20** (1.85 g, 56%).

R_f = 0.29 (DCM/MeOH [10% NH_4OH] 9:1).

^{1}H NMR (400 MHz, $CDCl_3$) δ (ppm) 4.56 (br, 1H, NH), 3.26 (br, 2H, H_5), 3.16 - 3.07 (m, 4H, H_1 and H_4) 2.70 (t, J = 6.7 Hz, 2H, H_7), 1.66 (s, 2H, NH), 1.54 1.38 (m, 24H, H_2, H_3, H_6 and H_{Boc}).

MS (ESI) *m/z* 346.1 $(M+H)^+$ (Theoretical 346.2).

Synthesis of ethyl 4-(3-nitrophenoxy)butanoate (3.22)

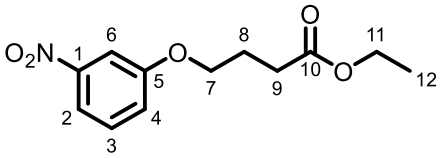

Chemical Formula: $C_{12}H_{15}NO_5$
Exact Mass: 253,10
Molecular Weight: 253,25

To a solution of 3-nitrophenol (1 g, 7.2 mmol, 1 eq) in anhydrous DMF (10 mL), K_2CO_3 (2 g, 14.4 mmol, 2 eq) was added. The mixture was stirred at 90°C, under Ar, for 10 min. Then, ethyl 4-bromoethanoate (1.68 g, 8.6 mmol, 1.2 eq) was added, and the mixture was stirred at 90°C, under Ar, for 16h. The mixture was concentrated under vacuum, water was added, and the aqueous phase was extracted with EtOAc. The organic phase was washed with brine, dried over $MgSO_4$, and concentrated under reduced pressure. The crude residue was purified by flash chromatography (cHex/EtOAc gradient 90:10 to 70:30, v/v) to provide **3.22** (1.8 g, 99%) as a yellow oil.

R_f = 0.5 (cHex/EtOAc 8:2).

^{1}H NMR (400 MHz, $CDCl_3$) δ (ppm) 7.82 (ddd, J = 8.1, 2.2, 0.8 Hz, 1H, H_2), 7.72 (t, J = 2.2 Hz, 1H, H_6), 7.42 (t, J = 8.1 Hz, 1H, H_3), 7.21 (ddd, J = 8.1, 2.2, 0.8 Hz, 1H, H_4), 4.16 (q, J = 7.1 Hz, 2H, H_{11}), 4.10 (t, J = 6.1 Hz, 2H, H_7), 2.53 (t, J = 7.2 Hz, 2H, H_9), 2.16 (m, 2H, H_8), 1.27 (t, J = 7.1 Hz, 3H, H_{12}).

MS (ESI) *m/z* 254.3 $(M+H)^+$ (Theoretical 254.1).

Synthesis of ethyl 4-(3-aminophenoxy)butanoate (3.23)

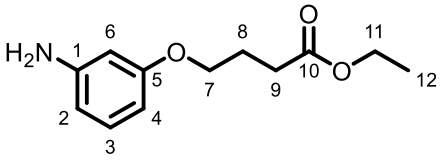

Chemical Formula: $C_{12}H_{17}NO_3$
Exact Mass: 223,12
Molecular Weight: 223,27

To a suspension of **3.22** (1.47 g, 5.8 mmol, 1 eq) in absolute EtOH (80 mL), 10% Pd/C (147 mg) was added. The mixture was degassed three times (vacuum/Ar), then stirred at room temperature under H_2 for 4h. The mixture was filtered through a pad of Celite®, the flask and the pad were washed with EtOH. The filtrate was concentrated under reduced pressure, affording a yellowish oil **3.23** (1.30 g, quantitative).

R_f = 0.3 (cHex/EtOAc 8:2).

^{1}H NMR (400 MHz, DMSO-d_6) δ (ppm) 6.87 (t, J = 8.0 Hz, 1H, H_2), 6.17 – 6.09 (m, 2H, H_3 and H_6), 6.08 – 6.02 (m, 1H, H_4), 5.00 (s, 2H, NH_2), 4.06 (q, J = 7.1 Hz, 2H, H_{11}), 3.86 (t, J = 6.3 Hz, 2H, H_7), 2.42 (t, J = 6.3 Hz, 2H, H_9), 1.97 – 1.87 (m, 2H, H_8), 1.18 (t, J = 7.1 Hz, 3H, H_{12}).

MS (ESI) *m/z* 224.4 $(M+H)^+$ (Theoretical 224.12).

Synthesis of *tert*-butyl (2-(4-((2-(4-methylpiperazin-1-yl)ethyl)carbamoyl)-[2,4':2',4''-terthiazol]-2''-yl)ethyl)carbamate (3.24a)

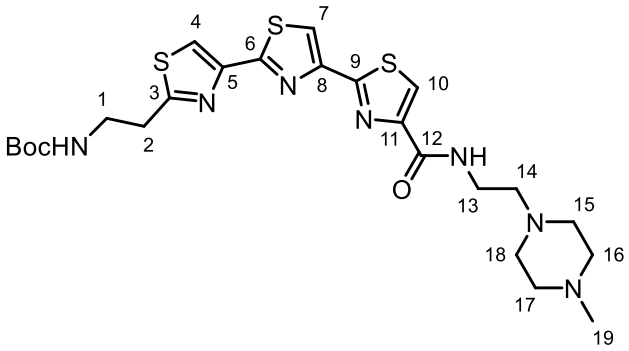

Chemical Formula: $C_{24}H_{33}N_7O_3S_3$
Exact Mass: 563,18
Molecular Weight: 563,75

Coupling between **3.15a** (100 mg, 0.23 mmol, 1 eq) and 2-(4-Methylpiperazin-1-yl)ethanamine (67.5 µL, 0.34 mmol, 1.5 eq) was performed following general procedure D with EDC (70 mg, 0.36 mmol, 1.6 eq) and HOSu (52.5 mg, 0.46 mmol, 2 eq) using DCM (2 mL) as solvent. The crude residue was purified by flash chromatography (DCM/MeOH gradient 100:0 to 85:15, v/v) to provide **3.24a** (60 mg, 47%) as a white solid.

R_f = 0.5 (DCM/MeOH 85:15).

^{1}H NMR (400 MHz, CD_3OD) δ (ppm) 8.21 (s, 1H, H_{10}), 8.20 (s, 1H, H_7), 8.12 (s, 1H, H_4), 3.59 (t, J = 6.5 Hz, 2H, H_{13}), 3.50 (t, J = 6.7 Hz, 2H, H_1), 3.23 (t, J = 6.7 Hz, 2H, H_2), 2.86 – 2.58 (m, 10H, H_{15}, H_{16}, H_{17}, H_{18} and H_{14}), 2.46 (s, 3H, H_{19}), 1.42 (s, 9H, H_{Boc}).

^{13}C NMR (101 MHz, CD_3OD) δ (ppm) 171.0 (1C, C_{12}), 165.1 (1C, C_9), 164.2 (1C, C_6), 163.6 (1C, C_3), 158.5 (1C, C_{Boc}), 151.8 (1C, C_{11}), 150.7 (1C, C_8), 149.4 (1C, C_5), 125.3 (1C, C_{10}), 119.1 (1C, C_7), 118.5 (1C, C_4), 80.4 (1C, $C_{IV.Boc}$), 58.0 (1C, C_{14}), 55.6 (2C, C_{15} and C_{18}), 53.1 (2C, C_{16} and C_{17}), 45.4 (1C, C_{19}), 41.3 (1C, C_1), 37.5 (1C, C_{13}), 34.5 (1C, C_2), 28.9 (3C, $CH_{3.Boc}$).

MS (ESI) *m/z* 564.6 $(M+H)^+$ (Theoretical 564.2).

Synthesis of 2''-(2-aminoethyl)-N-(2-(4-methylpiperazin-1-yl)ethyl)-[2,4':2',4''-terthiazole]-4-carboxamide (3.24b)

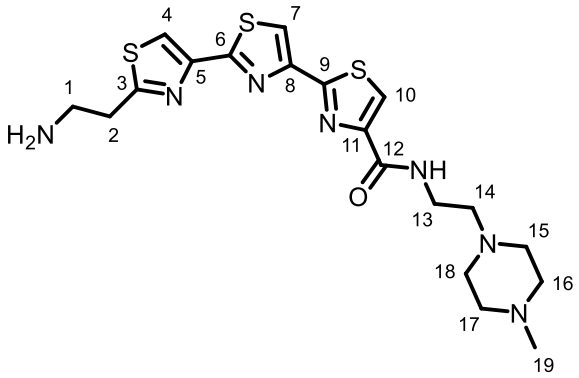

Chemical Formula: $C_{19}H_{25}N_7OS_3$
Exact Mass: 463,13
Molecular Weight: 463,64

Deprotection of compound **3.24b** (22 mg, 0.39 mmol, 1 eq) was performed following general procedure A with HCl/1,4-dioxane (4M, 1 mL). After purification compound **3.24b** (18 mg, 99%) was obtained as a white solid.

R_f = 0.42 (DCM/MeOH [10% NH_4OH] 9:1).

^{1}H NMR (400 MHz, D_2O) δ (ppm) 8.20 (s, 1H, H_{10}), 8.13 (s, 1H, H_7), 8.08 (s, 1H, H_4), 3.91 (t, J = 6.5 Hz, 2H, H_{13}), 3.87 – 3.67 (m, 8H, H_{15}, H_{16}, H_{17} and H_{18}), 3.63 (t, J = 6.7 Hz, 2H, H_1), 3.57 – 3.51 (m, 2H, H_{14}), 3.50 – 3.42 (m, J = 6.7 Hz, 2H, H_2), 3.09 (s, 3H, H_{19}).

^{13}C NMR (101 MHz, DMSO-d_6) δ (ppm) 167.5 (1C, C_{12}), 163.0 (1C, C_9), 161.5 (1C, C_6), 160.1 (1C, C_3), 150.30 (1C, C_{11}), 148.75 (1C, C_8), 147.01 (1C, C_5), 124.8 (1C, C_{10}), 118.7 (1C, C_7), 118.6 (1C, C_4), 40.1-38.9 (2C, C_1 and C_{19}), 38.0 (1C, C_{13}), 30.2 (1C, C_2).

MS (ESI) *m/z* $(M+H)^+$ (Theoretical 463.1).

Synthesis of ethyl 4-(3-(2''-(2-((*tert*-butoxycarbonyl)amino)ethyl)-[2,4':2',4''-terthiazole]-4-carboxamido)phenoxy)butanoate (3.26a)

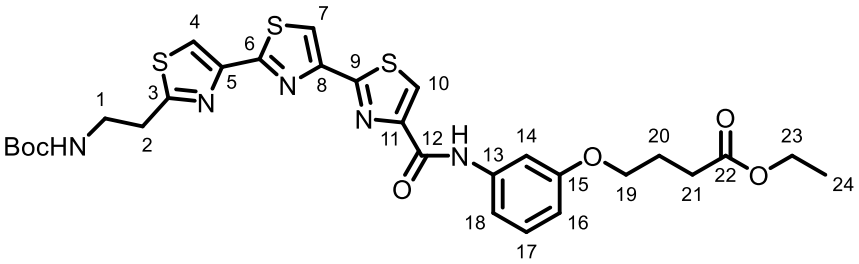

Chemical Formula: $C_{29}H_{33}N_5O_6S_3$
Exact Mass: 643,16
Molecular Weight: 643,79

Coupling between ethyl 4-(3-aminophenoxy)butanoate (572 mg, 2.56 mmol, 1.2 eq) and **3.15a** (937 mg, 2.14 mmol, 1 eq) was performed following general procedure C with HATU (1.06 g, 2.78 mmol, 1.3 eq) and DIPEA (560 µL, 3.20 mmol, 1.5 eq) using DMF (8.5 mL) as solvent. The crude residue was purified by flash chromatography (DCM/MeOH gradient 100:0 to 85:15, v/v) to provide **3.26a** (1.15 g, 83%) as a white solid.

R_f = 0.5 (DCM/MeOH 85:15).

^{1}H NMR (400 MHz, $CDCl_3$) δ (ppm) 9.22 (s, 1H, NH), 8.23 (s, 1H, H_{10}), 8.07 (s, 1H, H_7), 8.00 (s, 1H, H_4), 7.50 (t, J = 2.2 Hz, 1H, H_{18}), 7.30 – 7.24 (m, 1H, H_{14}), 7.23 – 7.17 (m, 1H, H_{17}), 6.74 – 6.66 (m, 1H, H_{16}), 5.06 (br, 1H, NH), 4.16 (q, J = 7.1 Hz, 2H, H_{23}), 4.06 (t, J = 6.1 Hz, 2H, H_{19}), 3.63 (dd, J = 6.2 Hz, 2H, H_1), 3.26 (t, J = 6.4 Hz, 2H, H_2), 2.53 (t, J = 7.3 Hz, 2H, H_{21}), 2.19 – 2.07 (m, 2H, H_{20}), 1.46 (s, 9H, H_{Boc}), 1.27 (t, J = 7.1 Hz, 3H, H_{24}).

^{13}C NMR (101 MHz, $CDCl_3$) δ (ppm) 173.5 (1C, C_{22}), 169.3 (1C, C_3), 163.7 (1C, C_6), 162.9 (1C, C_9), 159.7 (1C, C_{15}), 159.0 (1C, C_{12}), 156.0 (1C, C_{Boc}), 151.0 (1C, C_{11}), 149.4 (1C, C_8), 148.5 (1C, C_5), 139.1 (1C, C_{13}), 130.0 (1C, C_{14}), 124.7 (1C, C_{10}), 117.6 (1C, C_7), 117.1 (1C, C_4), 112.3 (1C, C_{17}), 111.2 (1C, C_{16}), 106.2 (1C, C_{18}), 79.8 (1C, $C_{IV.Boc}$), 67.1 (1C, C_{19}), 60.7 (1C, C_{23}), 40.0 (1C, C_1), 33.7 (1C, C_2), 31.1 (1C, C_{21}), 28.6 (3C, $CH_{3.Boc}$), 24.9 (1C, C_{20}), 14.5 (1C, C_{24}).

MS (ESI) *m/z* 644.4 $(M+H)^+$ (Theoretical 644.2).

Synthesis of ethyl 4-(3-(2''-(2-aminoethyl)-[2,4':2',4''-terthiazole]-4-carboxamido)phenoxy)butanoate hydrochloride (3.26b)

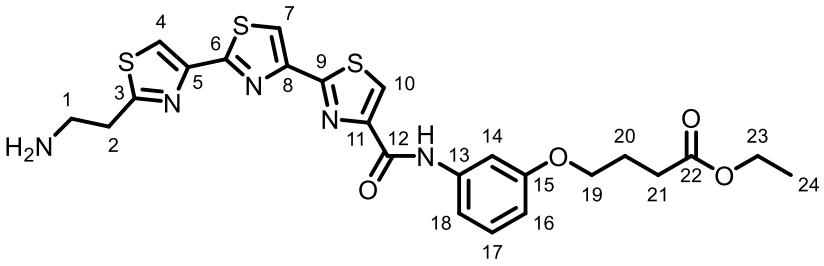

Chemical Formula: $C_{24}H_{25}N_5O_4S_3$
Exact Mass: 543,11
Molecular Weight: 543,68

Deprotection of compound **3.26a** (400 mg, 0.86 mmol, 1 eq) was performed following general procedure A with HCl/1,4-dioxane (4M, 3 mL). After purification compound **3.26b** (32 mg, 97%) was obtained as a white solid.

R_f = 0.43 (DCM/MeOH [10% NH_4OH] 9:1).

^{1}H NMR (400 MHz, DMSO-d_6) δ (ppm) 10.19 (s, 1H, NH), 8.55 (s, 1H, H_{10}), 8.51 (s, 1H, H_7), 8.36 (s, 1H, H_4), 8.16 (br, 2H, NH_2), 7.53 (t, J = 2.2 Hz, 1H, H_{14}), 7.45 (dd, J = 8.1, 2.2 Hz, 1H, H_{18}), 7.27 (t, J = 8.1 Hz, 1H, H_{17}), 6.71 (dd, J = 8.1, 2.2 Hz, 1H, H_{16}), 4.08 (q, J = 7.1 Hz, 2H, H_{23}), 4.00 (t, J = 6.8 Hz, 2H, H_{19}), 3.42 (m, 2H, H_1), 3.30 (m, 2H, H_2), 2.46 (t, J = 6.8 Hz, 2H, H_{21}), 2.00 (p, J = 6.8 Hz, 2H, H_{20}), 1.19 (t, J = 7.1 Hz, 3H, H_{24}).

^{13}C NMR (101 MHz, DMSO-d_6) δ (ppm) 172.5 (1C, C_{22}), 167.5 (1C, C_3), 163.0 (1C, C_6), 161.6 (1C, C_9), 158.9 (1C, C_{15}), 158.7 (1C, C_{12}), 150.5 (1C, C_{11}), 148.7 (1C, C_8), 147.0 (1C, C_5), 139.5 (1C, C_{13}), 129.5 (1C, C_{17}), 125.6 (1C, C_{10}), 119.2 (1C, C_7), 118.7 (1C, C_4), 112.6 (1C, C_{18}), 110.1 (1C, C_{16}), 106.5 (1C, C_{14}), 66.5 (1C, C_{19}), 59.9 (1C, C_{23}), 38.0 (1C, C_2), 30.3 (1C, C_1), 30.2 (1C, C_{21}), 24.3 (1C, C_{20}), 14.1 (1C, C_{24}).

HRMS (ESI) *m/z* 544.11523 $(M+H)^+$ (Theoretical 544.11414).

HPLC-RP rt = 5.1 min (Method B).

Synthesis of ethyl 2''-(2-((4-methylphenyl)sulfonamido)ethyl)-[2,4':2',4''-terthiazole]-4-carboxylate (3.27)

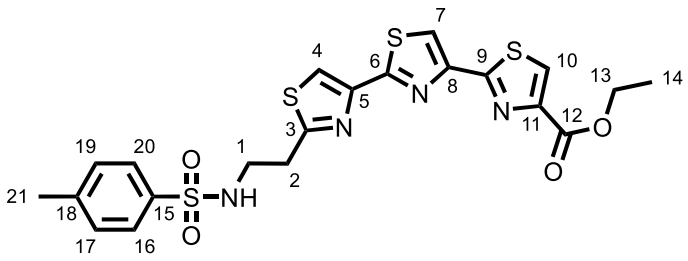

Chemical Formula: $C_{21}H_{20}N_4O_4S_4$
Exact Mass: 520,04
Molecular Weight: 520,66

Compound **3.27** was synthesized following general procedure B using **3.16** (50 mg, 0.11 mmol, 1 eq), 4-methylbenzenesulfonyl chloride (26 mg, 0.13 mmol, 1.2 eq) and Et_3N (47 µL, 0.33 mmol, 3 eq) in DMF (3 mL). The crude residue was purified by flash chromatography (cHex/EtOAc gradient 80:20 to 40:60, v/v) to provide **3.27** (38.7 mg, 66%) as a grey solid.

R_f = 0.55 (cHex/EtOAc 5:5).

^{1}H NMR (400 MHz, $CDCl_3$) δ (ppm) 8.20 (s, 1H, H_{10}), 8.18 (s, 1H, H_7), 7.94 (s, 1H, H_4), 7.77 (d, J = 8.2 Hz, 2H, H_{17} and H_{19}), 7.29 (d, J = 8.2 Hz, 2H, H_{16} and H_{20}), 4.46 (q, J = 7.1 Hz, 2H, H_{13}), 3.47 (t, J = 6.1 Hz, 2H, H_1), 3.20 (t, J = 6.1 Hz, 2H, H_2), 2.40 (s, 3H, H_{21}), 1.44 (t, J = 7.1 Hz, 2H, H_{14}).

^{13}C NMR (101 MHz, DMSO-d_6) δ (ppm) 168.9 (1C, C_{12}), 163.0 (1C, C_9), 162.3 (1C, C_6), 160.7 (1C, C_3), 148.3 (1C, C_{11}), 147.0 (1C, C_8), 146.8 (1C, C_5), 142.7 (1C, C_{18}), 137.3 (1C, C_{15}), 129.6 (3C, C_{10}, C_{16} and C_{20}), 126.5 (2C, C_{18} and C_{19}), 118.8 (1C, C_7) , 118.3 (1C, C_4), 60.9 (1C, C_{13}), 42.1 (1C, C_1), 32.7 (1C, C_2), 20.9 (1C, C_{21}), 14.2 (1C, C_{14}).

HRMS (ESI) *m/z* 521.04449 $(M+H)^+$ (Theoretical 521.04401).

HPLC-RP rt = 6.7 min (Method B).

Synthesis of ethyl 2''-(2-((4-(trifluoromethyl)phenyl)sulfonamido)ethyl)-[2,4':2',4''-terthiazole]-4-carboxylate (3.28)

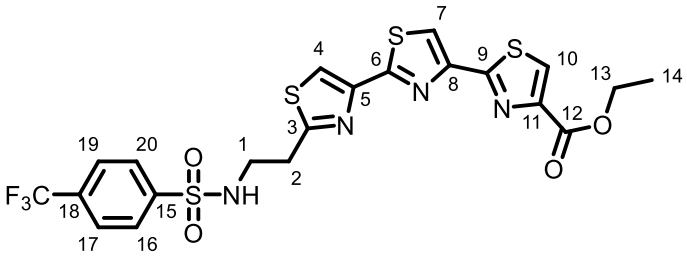

Chemical Formula: $C_{21}H_{17}F_3N_4O_4S_4$
Exact Mass: 574,01
Molecular Weight: 574,63

Compound **3.28** was synthesized following general procedure B using **3.16** (50 mg, 0.12 mmol, 1 eq), 4-(trifluoromethyl)benzensulfonyl chloride (36 mg, 0.15 mmol, 1.2 eq) and Et_3N (52 µL, 0.37mmol, 3 eq) in DMF (3 mL). The crude residue was purified by flash chromatography (cHex/EtOAc gradient 80:20 to 30:70, v/v) to provide **3.28** (24.1 mg, 34%) as a white solid.

R_f = 0.45 (cHex/EtOAc 5:5).

^{1}H NMR (400 MHz, DMSO-d_6) δ (ppm) 8.59 (s, 1H, H_{10}), 8.40 (s, 1H, H_7), 8.24 (s, 1H, H_4), 8.21 (br, 1H, NH), 7.98 (d, J = 8.4 Hz, 2H, H_{16} and H_{20}), 7.93 (d, J = 8.4 Hz, 2H, H_{17} and H_{19}), 4.35 (q, J = 7.1 Hz, 2H, H_{13}), 3.29 – 3.25 (m, 2H, H_1), 3.22 – 3.17 (m, 2H, H_2), 1.34 (t, J = 7.1 Hz, 3H, H_{14}).

^{13}C NMR (101 MHz, DMSO-d_6) δ (ppm) 168.7 (1C, C_{12}), 162.9 (1C, C_9), 162.3 (1C, C_6), 160.6 (1C, C_3), 148.4 (1C, C_{11}), 147.0 (1C, C_8), 146.8 (1C, C_5), 144.3 (1C, C_{18}), 132.2 (1C, C_{15}), 129.6 (1C, C_{10}), 127.4 (3C, C_{16}, C_{18} and C_{20}), 126.4 (2C, C_{17} and C_{19}), 118.8 (1C, C_7), 118.3 (1C, C_4), 60.9 (1C, C_{13}), 42.2 (1C, C_1), 32.8 (1C, C_2), 14.2 (1C, C_{14}).

HRMS (ESI) *m/z* 575.01587 $(M+H)^+$ (Theoretical 575.01575).

HPLC-RP rt = 6.9 min (Method B).

Synthesis of ethyl 2''-(2-(benzo[d]thiazole-6-sulfonamido)ethyl)-[2,4':2',4''-terthiazole]-4-carboxylate (3.29)

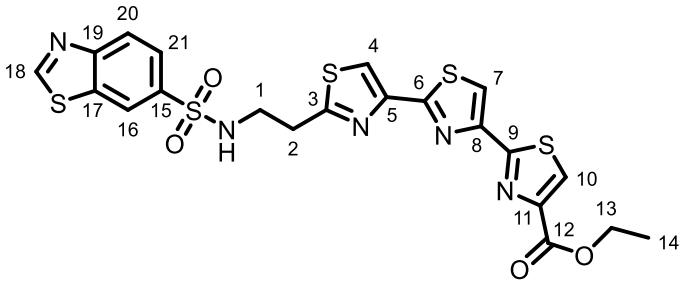

Chemical Formula: $C_{21}H_{17}N_5O_4S_5$
Exact Mass: 562,99
Molecular Weight: 563,70

Compound **3.29** was synthesized following general procedure B using **3.16** (50 mg, 0.12 mmol, 1 eq), benzo[d]thiazole-6-sulfonyl chloride (35 mg, 0.15 mmol, 1.2 eq) and Et_3N (52 µL, 0.37mmol, 3 eq) in DMF (3 mL). The crude residue was purified by flash chromatography (cHex/EtOAc gradient 80:20 to 30:70, v/v) to provide **3.29** (29.3 mg, 42%) as a grey solid.

R_f = 0.33 (cHex/EtOAc 4:6).

^{1}H NMR (400 MHz, DMSO-d_6) δ (ppm) 9.58 (s, 1H, H_{18}), 8.68 (d, J = 1.8 Hz, 1H, H_{16}), 8.59 (s, 1H, H_{10}), 8.38 (s, 1H, H_7), 8.27 – 8.21 (m, 2H, H_4 and H_{20}), 8.03 (br, 1H, NH), 7.90 (dd, J = 8.6, 1.8 Hz, 1H, H_{21}), 4.35 (q, J = 7.1 Hz, 2H, H_{13}), 3.28 – 3.22 (m, 2H, H_1), 3.22 – 3.14 (m, 2H, H_2), 1.34 (t, J = 7.1 Hz, 3H, H_{14}).

^{13}C NMR (101 MHz, DMSO-d_6) δ (ppm) 168.8 (1C, C_{12}), 162.9 (1C, C_9), 162.3 (1C, C_6), 160.7 (1C, C_3), 160.5 (1C, C_{19}), 155.0 (1C, C_{18}), 148.3 (1C, C_{11}), 147.0 (1C, C_8), 146.7 (1C, C_5), 137.1 (1C, C_{15}), 134.1 (1C, C_{17}), 129.6 (1C, C_{10}), 124.1 (1C, C_{21}), 123.7 (1C, C_{20}), 122.1 (1C, C_{16}), 118.8 (1C, C_7), 118.3 (1C, C_4), 60.9 (1C, C_{13}), 42.2 (1C, C_1), 32.8 (1C, C_2), 14.2 (1C, C_{14}).

HRMS (ESI) *m/z* 563.99567 $(M+H)^+$ (Theoretical 563.99568).

HPLC-RP rt = 6.1 min (Method B).

Synthesis of ethyl 2''-(2-((2-acetamidothiazole)-5-sulfonamido)ethyl)-[2,4':2',4''-terthiazole]-4-carboxylate (3.30)

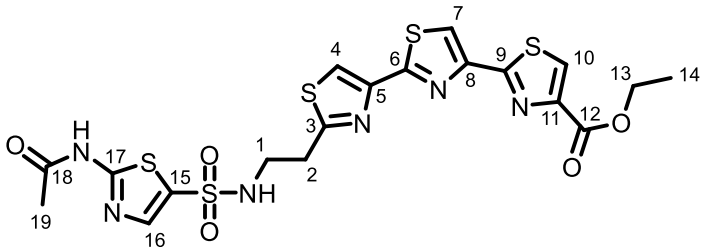

Chemical Formula: $C_{19}H_{18}N_6O_5S_5$
Exact Mass: 569,99
Molecular Weight: 570,69

Compound **3.30** was synthesized following general procedure B using **3.16** (39 mg, 0.10 mmol, 1 eq), 2-acetamidothiazole-5-sulfonyl chloride (25 mg, 0.10 mmol, 1.2 eq) and Et_3N (52 µL, 0.37mmol, 3 eq) in DMF (3 mL). The crude residue was purified by flash chromatography (cHex/EtOAc gradient 80:20 to 30:70, v/v) to provide **3.30** (11 mg, 18%) as a white solid.

R_f = 0.45 (cHex/EtOAc 5:5).

^{1}H NMR (400 MHz, DMSO-d_6) δ (ppm) 12.57 (s, 1H, NH), 8.59 (s, 1H, H_{16}), 8.40 (s, 1H, H_{10}), 8.25 (s, 1H, H_7), 8.12 (t, J = 5.6 Hz, NH), 7.89 (s, 1H, H_4), 4.35 (q, J = 7.1 Hz, 2H, H_{13}), 3.30 – 3.25 (m, 2H, H_1), 3.22 (t, J = 6.1 Hz, 2H, H_2), 2.15 (s, 3H, H_{19}), 1.34 (t, J = 7.1 Hz, 3H, H_{14}).

^{13}C NMR (101 MHz, DMSO-d_6) δ (ppm) 169.3 (1C, C_{18}), 168.8 (1C, C_{12}), 163.0 (1C, C_9), 162.3 (1C, C_6), 161.8 (1C, C_{17}), 160.7 (1C, C_3), 148.3 (1C, C_{11}), 147.0 (1C, C_8), 146.8 (1C, C_5), 142.5 (1C, C_{16}), 129.6 (1C, C_{10}), 128.6 (1C, C_{15}), 118.8 (1C, C_7), 118.3 (1C, C_4), 60.9 (1C, C_{13}), 42.2 (1C, C_1), 32.6 (1C, C_2), 22.3 (1C, C_{19}), 14.2 (1C, C_{14}).

HRMS (ESI) *m/z* 571.00195 $(M+H)^+$ (Theoretical 571.00150).

HPLC-RP rt = 5.5 min (Method B).

Synthesis of ethyl 2''-(2-((1-((1*H*-imidazol-5-yl)sulfonyl)-1*H*-imidazole)-5-sulfonamido)ethyl)-[2,4':2',4''-terthiazole]-4-carboxylate (3.32)

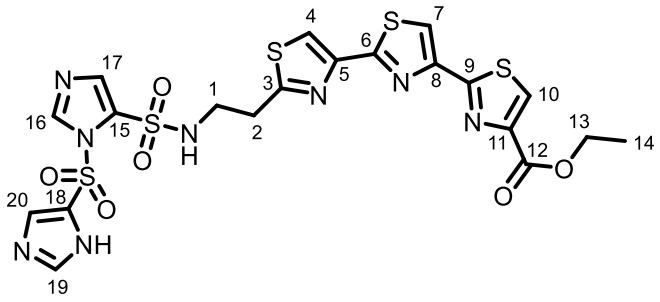

Chemical Formula: $C_{20}H_{18}N_8O_6S_5$
Exact Mass: 626,00
Molecular Weight: 626,71

Compound **3.32** was synthesized following general procedure B using **3.16** (50 mg, 0.12 mmol, 1 eq), 1H-imidazole-4-sulfonyl chloride (25 mg, 0.15 mmol, 1.2 eq) and Et_3N (52 µL, 0.37mmol, 3 eq) in DMF (3 mL). The crude residue was purified by flash chromatography (cHex/EtOAc gradient 80:20 to 30:70, v/v) to provide **3.32** (32 mg, 53%) as a white solid.

R_f = 0.55 (cHex/EtOAc 5:5).

^{1}H NMR (400 MHz, DMSO-d_6) δ (ppm) 13.38 (s, 1H, NH), 8.59 (s, 1H, H_{10}), 8.45 (d, J = 1.5 Hz, 1H, H_{17}), 8.41 (s, 1H, H_7), 8.37 (d, J = 1.5 Hz, 1H, H_{20}), 8.26 (s, 1H, H_4), 8.10 – 8.04 (m, 2H, H_{16} and H_{19}), 8.00 (br, 1H, NH), 4.35 (q, J = 7.1 Hz, 2H, H_{13}), 3.37 – 3.31 (m, 2H, H_1), 3.24 – 3.15 (m, 2H, H_2), 1.34 (t, J = 7.1 Hz, 3H, H_{14}).

^{13}C NMR (101 MHz, DMSO-d_6) δ (ppm) 168.8 (1C, C_{12}), 163.0 (1C, C_9), 162.3 (1C, C_6), 160.7 (1C, C_3), 148.3 (1C, C_{11}), 147.0 (1C, C_8), 146.8 (1C, C_5), 142.4 (1C, C_{16}), 139.5 (1C, C_{19}), 138.4 (1C, C_{18}), 134.5 (1C, C_{17}), 129.6 (1C, C_{10}), 126.0 (1C, C_{15}), 120.2 (1C, C_{20}), 118.9 (1C, C_7), 118.3 (1C, C_4), 60.9 (1C, C_{13}), 42.2 (1C, C_1), 32.9 (1C, C_2), 14.2 (1C, C_{14}).

HRMS (ESI) *m/z* 627.00269 $(M+H)^+$ (Theoretical 627.00256).

Synthesis of ethyl 2''-(2-(2-(4-methylpiperazin-1-yl)acetamido)ethyl)-[2,4':2',4''-terthiazole]-4-carboxylate (3.34)

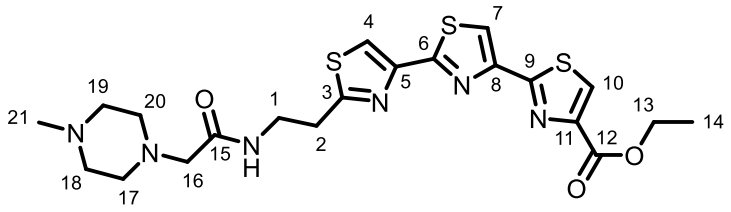

Chemical Formula: $C_{21}H_{26}N_6O_3S_3$
Exact Mass: 506,12
Molecular Weight: 506,66

Coupling between **3.16** (60 mg, 0.13 mmol, 1 eq) and 2-(4-methylpiperazin-1-yl)acetic acid (21.2 mg, 0.13 mmol, 1 eq) was performed following general procedure E with diethyl chlorophosphate (97 µL, 0.67 mmol, 5 eq) and Et_3N (48 µL, 0.27 mmol, 2 eq) using THF (2 mL) as solvent. The crude residue was purified by flash chromatography (DCM/MeOH gradient 100:0 to 85:15, v/v) to provide **3.34** (27 mg, 40%) as a white solid.

R_f = 0.45 (DCM/MeOH 9:1).

^{1}H NMR (400 MHz, $CDCl_3$) δ (ppm) 8.17 (s, 1H, H_{10}), 8.16 (s, 1H, H_7), 7.96 (s, 1H, H_4), 7.63 (m, 1H, NH), 4.42 (q, J = 7.1 Hz, 2H, H_{13}), 3.81 – 3.75 (m, 2H, H_1), 3.25 (t, J = 6.2 Hz, 2H, H_2), 2.96 (s, 2H, H_{16}), 2.45 (m, 4H, H_{17} and H_{20}), 2.38 – 2.19 (m, 4H, H_{18} and H_{19}), 2.11 (s, 3H, H_{21}), 1.40 (t, J = 7.1 Hz, 3H, H_{14}).

^{13}C NMR (101 MHz, $CDCl_3$) δ (ppm) 170.4 (1C, C_{12}), 169.1 (1C, C_{15}), 163.3 (1C, C_9), 162.9 (1C, C_6), 161.5 (1C, C_3), 149.4 (1C, C_{11}), 148.4 (1C, C_8), 148.1 (1C, C_5), 127.9 (1C, C_{10}), 117.9 (1C, C_7), 116.9 (1C, C_4), 61.6 (1C, C_{13}), 61.4 (1C, C_{16}), 54.9 (2C, C_{18} and C_{19}), 53.2 (2C, C_{17} and C_{20}), 37.7 (1C, C_1), 33.2 (1C, C_2), 30.7 (1C, C_{21}), 14.4 (1C, C_{14}).

HRMS (ESI) *m/z* 507.13016 $(M+H)^+$ (Theoretical 507.13013).

Synthesis of ethyl 2''-(2-(4-(*tert*-butoxycarbonyl)piperazine-1-carboxamido)ethyl)-[2,4':2',4''-terthiazole]-4-carboxylate (3.35a)

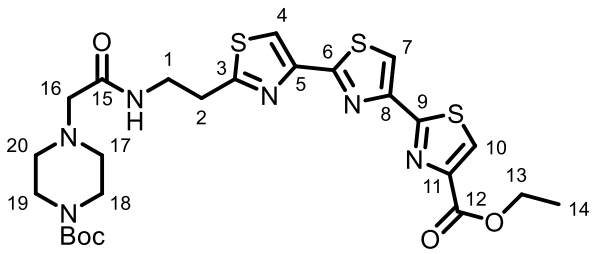

Chemical Formula: $C_{25}H_{32}N_6O_5S_3$
Exact Mass: 592,16
Molecular Weight: 592,75

Coupling between **3.16** (50 mg, 0.12 mmol, 1 eq) and 4-(*tert*-butoxycarbonyl)piperazine-1-carboxylic acid (32 mg, 0.37 mmol, 1.2 eq) was performed following general procedure C with HATU (56 mg, 0.15 mmol, 1.3 eq) and DIPEA (65 µL, 0.37 mmol, 1.5 eq) using DMF (2 mL) as solvent. The crude residue was purified by flash chromatography (DCM/MeOH gradient 100:0 to 85:15, v/v) to provide **3.35a** (35 mg, 49%) as a white solid.

R_f = 0.70 (DCM/MeOH 85:15).

^{1}H NMR (400 MHz, CD_3OD) δ (ppm) 8.42 (s, 1H, H_{10}), 8.34 (s, 1H, H_7), 8.17 (s, 1H, H_4), 4.43 (q, J = 7.1 Hz, 2H, H_{13}), 3.73 (t, J = 6.4 Hz, 2H, H_1), 3.32 (m, 2H, H_2), 3.00 (s, 2H, H_{16}), 2.38 (s, 4H, H_{17} and H_{20}), 1.46 – 1.40 (m, 2H, H_{14}), 1.37 (s, 9H, H_{Boc}).

MS (ESI) *m/z* 593.6 $(M+H)^+$ (Theoretical 593.2).

Synthesis of ethyl 2''-(2-(2-(piperazin-1-yl)acetamido)ethyl)-[2,4':2',4''-terthiazole]-4-carboxylate (3.35b)

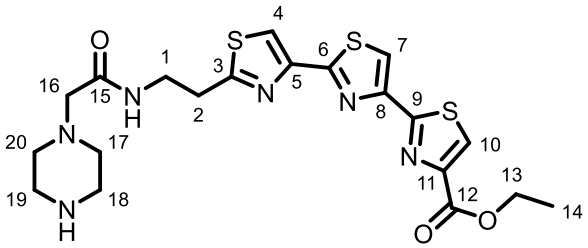

Chemical Formula: $C_{20}H_{24}N_6O_3S_3$
Exact Mass: 492,11
Molecular Weight: 492,63

Deprotection of compound **3.35a** (35 mg, 0.06 mmol, 1 eq) was performed following general procedure A with HCl/1,4-dioxane (4M, 2 mL). After purification compound **3.35b** (28.5 mg, 96%) was obtained as a grey solid.

R_f = 0.4 (DCM/MeOH 95:5).

^{1}H NMR (400 MHz, D_2O) *δ* (ppm) 8.21 (s, 1H, H_{10}), 7.95 (s, 1H, H_7), 7.89 (s, 1H, H_4), 4.27 (q, *J* = 7.1 Hz, 2H, H_{13}), 3.69 (s, 2H, H_{16}), 3.60 (t, *J* = 6.4 Hz, 2H, H_1), 3.43 – 3.34 (m, 4H, H_{17} and H_{20}), 3.27 – 3.20 (m, 4H, H_{18} and H_{19}), 3.17 (t, *J* = 6.4 Hz, 2H, H_2), 1.33 (t, *J* = 7.1 Hz, 3H, H_{14}).

^{13}C NMR (101 MHz, D_2O) *δ* (ppm) 147.6, 146.4, 146.1 (3C, C_5, C_8 and C_{11}), 129.4 (1C, C_{10}), 119.1, 119.1 (2C, C_4 and C_7), 62.6 (1C, C_{13}), 58. 3 (1C, C_{16}), 49.1 (2C, C_{18} and C_{19}), 41.7 (2C, C_{17} and C_{20}), 39.0 (1C, C_1), 32.0 (1C, C_2), 13.4 (1C, C_{14}).

HRMS (ESI) *m/z* 493.11398 $(M+H)^+$ (Theoretical 493.11448).

tert-butyl (2-(4-((2-(4-methylpiperazin-1-yl)ethyl)carbamoyl)-[2,4'-bithiazol]-2'-yl)ethyl)carbamate

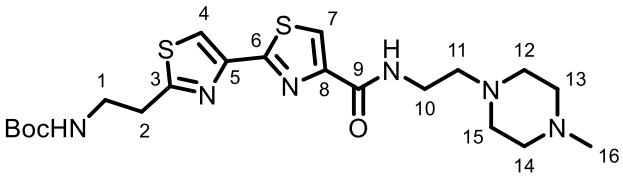

Chemical Formula: $C_{21}H_{32}N_6O_3S_2$
Exact Mass: 480,20
Molecular Weight: 480,65

Coupling between 2'-(2-((*tert*-butoxycarbonyl)amino)ethyl)-[2,4'-bithiazole]-4-carboxylic acid (60 mg, 0.17 mmol, 1 eq) and 2-(4-Methylpiperazin-1-yl)ethanamine (50 µL, 0.25 mmol, 1.5 eq) was performed following general procedure D with EDC (52 mg, 0.27 mmol, 1.6 eq) and HOSu (39 mg, 0.34 mmol, 2 eq) using DMF (2 mL) as solvent. The crude residue was purified by flash chromatography (DCM/MeOH gradient 100:0 to 85:15, v/v) to provide the pure compound (50.8 mg, 63%) as a grey solid.

R_f = 0.5 (DCM/MeOH 95:5).

^{1}H NMR (400 MHz, CD_3OD) δ (ppm) 8.16 (s, 1H, H_7), 8.09 (s, 1H, H_4), 3.57 (t, J = 6.7 Hz, 2H, H_{10}), 3.48 (t, J = 6.7 Hz, 2H, H_1), 3.22 (t, J = 6.7 Hz, 2H, H_2), 2.74-2.41 (m, 10H, H_{11}, H_{12}, H_{13}, H_{14} and H_{15}), 2.29 (s, 3H, H_{16}), 1.41 (s, 9H, H_{Boc}).

^{13}C NMR (101 MHz, CD_3OD) δ (ppm) 170.9 (1C, C_9), 164.1 (1C, C_6), 163.4 (1C, C_3), 158.3 (1C, C_{Boc}), 151.6 (1C, C_8), 149.4 (1C, C_5), 124.9 (1C, C_7), 118.3 (1C, C_4), 80.2 (1C, $C_{IV.Boc}$), 58.0 (1C, H_{11}), 55.7 (2C, C_{13} and C_{14}), 53.6 (2C, C_{12} and C_{15}), 46.0 (1C, C_{16}), 41.1 (1C, C_1), 37.4 (1C, C_{10}), 34.3 (1C, C_2), 28.7 (3C, $CH_{3.Boc}$).

MS (ESI) *m/z* 481.4 $(M+H)^+$ (Theoretical 481.2).

2'-(2-aminoethyl)-*N*-(2-(4-methylpiperazin-1-yl)ethyl)-[2,4'-bithiazole]-4-carboxamide

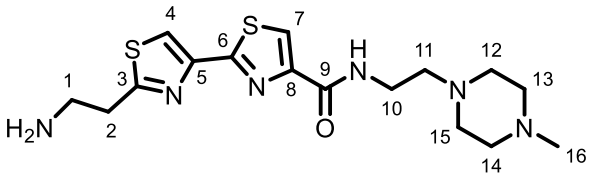

Chemical Formula: $C_{16}H_{24}N_6OS_2$
Exact Mass: 380,15
Molecular Weight: 380,53

Deprotection of *tert*-butyl (2-(4-((2-(4-methylpiperazin-1-yl)ethyl)carbamoyl)-[2,4'-bithiazol]-2'-yl)ethyl)carbamate (50.8 mg, 0.10 mmol, 1 eq) was performed following general procedure A with HCl/1,4-dioxane (4M, 2 mL). After purification the pure compound (51 mg, 98%) was obtained as a white solid.

R_f = 0.6 (DCM/MeOH [10% NH_4OH] 90:10)

^{1}H NMR (400 MHz, DMSO-d_6) δ (ppm) 9.15 (br, 1H, NH), 8.63 (br, 2H, NH_2), 8.52 (s, 1H, H_7), 8.48 (s, 1H, H_4), 3.98 – 3.43 (m, 16H, H_1, H_2, H_{10}, H_{11}, H_{12}, H_{13}, H_{14} and H_{15}), 3.03 (s, 3H, H_{16}).

(E)-2'-(2-((4-((4-(dimethylamino)phenyl)diazenyl)phenyl)sulfonamido)ethyl)-N-(2-(4-methylpiperazin-1-yl)ethyl)-[2,4'-bithiazole]-4-carboxamide (3.41)

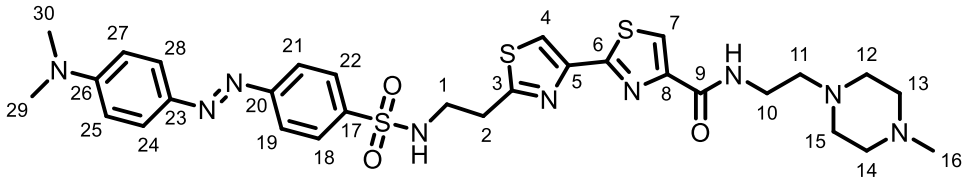

Chemical Formula: $C_{30}H_{37}N_9O_3S_3$
Exact Mass: 667,22
Molecular Weight: 667,87

Compound **3.41** was synthesized following general procedure B using 2'-(2-aminoethyl)-*N*-(2-(4-methylpiperazin-1-yl)ethyl)-[2,4'-bithiazole]-4-carboxamide (51.8 mg, 0.10 mmol, 1 eq), (E)-4-((4-(dimethylamino)phenyl)diazenyl)benzenesulfonyl chloride (41.1 mg, 0.13 mmol, 1.2 eq) and Et_3N (74 µL, 0.53 mmol, 5 eq) in DMF (2 mL). The crude residue was purified by flash chromatography (DCM/MeOH gradient 100:0 to 80:20, v/v) to provide **3.41** (70.6 mg, 78%) as a white solid.

R_f = 0.2 (DCM/MeOH 9:1).

^{1}H NMR (400 MHz, CD_3OD) δ (ppm) 8.12 (s, 1H, H_7), 8.02 (s, 1H, H_4), 7.90 – 7.77 (m, 6H, H_{18}, H_{19}, H_{21}, H_{22}, H_{24} and H_{28}), 6.85 (s, 1H, H_{27}), 6.83 (s, 1H, H_{25}), 3.51 (t, J = 6.5 Hz, 2H, H_{10}), 3.45 (t, J = 6.4 Hz, 2H, H_1), 3.22 (t, J = 6.4 Hz, 2H, H_2), 3.13 (s, 6H, H_{29} and H_{30}), 2.91 – 2.61 (m, 10H, H_{11}, H_{12}, H_{13}, H_{14} and H_{15}), 2.53 (s, 3H, H_{16}).

^{13}C NMR (101 MHz, CD_3OD) δ (ppm) 170.3 (1C, C_9), 163.5 (1C, C_6), 163.4 (1C, C_3), 156.6 (1C, C_{20}), 154.9 (1C, C_{26}), 152.7 (1C, C_8), 149.5 (1C, C_5), 144.8 (1C, C_{17}), 141.0 (1C, C_{23}), 129.0 (2C, C_{19} and C_{21}), 126.7 (2C, C_{18} and C_{22}), 125.0 (1C, C_7), 123.4 (2C, C_{24} and C_{28}), 118.5 (1C, C_4), 112.6 (2C, C_{25} and C_{27}), 57.7 (1C, C_{11}), 55.4 (2C, C_{13} and C_{14}), 52.6 (2C, C_{12} and C_{15}), 46.1 (1C, C_{16}), 43.5 (1C, C_1), 40.4 (2C, C_{29} and C_{30}), 37.3 (1C, C_{10}), 34.1 (1C, C_2).

HRMS (ESI) *m/z* 668.22620 $(M+H)^+$ (Theoretical 668.22542).

Synthesis of ethyl 4-(3-(2''-(2-(2-(4-methylpiperazin-1-yl)acetamido)ethyl)-[2,4':2',4''-terthiazole]-4-carboxamido)phenoxy)butanoate (3.42)

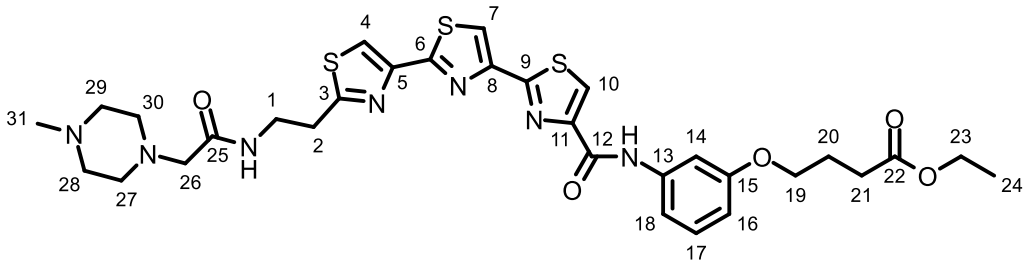

Chemical Formula: $C_{31}H_{37}N_7O_5S_3$
Exact Mass: 683,20
Molecular Weight: 683,86

Coupling between **3.26b** (80 mg, 0.14 mmol, 1 eq) and 2-(4-methylpiperazin-1-yl)acetic acid (26 mg, 0.16 mmol, 1.2 eq) was performed following general procedure C with HATU (68 mg, 0.18 mmol, 1.3 eq) and DIPEA (36 µL, 0.21 mmol, 1.5 eq) using DMF (1 mL) as solvent. The crude residue was purified by flash chromatography (DCM/MeOH gradient 100:0 to 85:15, v/v) to provide **3.42** (91.2 mg, 96%) as a white solid.

R_f = 0.3 (DCM/MeOH 85:15).

^{1}H NMR (400 MHz, DMSO-d_6) δ (ppm) 10.18 (s, 1H, NH), 8.53 (s, 1H, H_{10}), 8.49 (s, 1H, H_7), 8.31 (s, 1H, H_4), 7.88 (t, J = 6.5 Hz, 1H, NH), 7.52 (t, J = 2.2 Hz, 1H, H_{14}), 7.49 – 7.42 (m, 1H, H_{18}), 7.28 (t, J = 8.2 Hz, 1H, H_{17}), 6.75 – 6.68 (m, 1H, H_{16}), 4.09 (q, J = 7.1 Hz, 2H, H_{23}), 4.01 (t, J = 6.3 Hz, 2H, H_{19}), 3.56 (q, J = 6.5 Hz, 2H, H_1), 3.25 (t, J = 6.5 Hz, 2H, H_2), 2.88 (s, 2H, H_{26}), 2.49 – 2.43 (t, J = 6.3 Hz, 2H, H_{21}), 2.36 (s, 3H, H_{31}), 2.27 (s, 4H, H_{27} and H_{30}), 2.08 (s, 4H, H_{28} and H_{29}), 2.00 (p, J = 6.3 Hz, 2H, H_{20}), 1.19 (t, J = 7.1 Hz, 3H, H_{24}).

^{13}C NMR (101 MHz, DMSO-d_6) δ (ppm) 172.0 (1C, C_{22}), 169.2 (1C, C_{25}), 168.8 (1C, C_9), 162.7 (1C, C_6), 161.2 (1C, C_3), 158.4 (1C, C_{15}), 158.2 (1C, C_{12}), 150.0 (1C, C_{11}), 148.1 (1C, C_8), 146.3 (1C, C_5), 139.0 (1C, C_{13}), 129.0 (1C, C_{17}), 125.1 (1C, C_{10}), 118.5 (1C, C_7), 117.8 (1C, C_4), 112.0 (1C, C_{18}), 109.5 (1C, C_{16}), 106.0 (1C, C_{14}), 66.0 (1C, C_{19}), 60.7 (1C, C_{26}), 59.3 (1C, C_{23}), 53.9 (2C, C_{28} and C_{29}), 52.1 (2C, C_{27} and C_{30}), 45.0 (1C, C_{31}), 37.4 (1C, C_1), 32.1 (1C, C_2), 29.6 (1C, C_{21}), 23.7 (1C, C_{20}), 13.6 (1C, C_{24}).

HRMS (ESI) *m/z* 684.20929 $(M+H)^+$ (Theoretical 684.20911).

HPLC-RP rt = 5.1 min (Method B).

Synthesis of *tert*-butyl 4-(2-((2-(4-((3-(4-ethoxy-4-oxobutoxy)phenyl)carbamoyl)-[2,4':2',4''-terthiazol]-2''-yl)ethyl)amino)-2-oxoethyl)piperazine-1-carboxylate (3.43a)

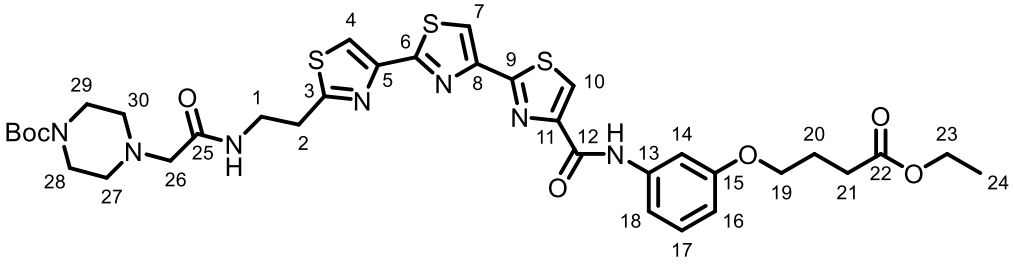

Chemical Formula: $C_{35}H_{43}N_7O_7S_3$
Exact Mass: 769,24
Molecular Weight: 769,95

Coupling between **3.26b** (35 mg, 0.06 mmol, 1 eq) and 2-(4-(*tert*-butoxycarbonyl)piperazin-1-yl)acetic acid (18 mg, 0.07 mmol, 1.2 eq) was performed following general procedure C with HATU (30 mg, 0.098 mmol, 1.3 eq) and DIPEA (16 µL, 0.09 mmol, 1.5 eq) using DMF (1 mL) as solvent. The crude residue was purified by flash chromatography (DCM/EtOH gradient 100:0 to 85:15, v/v) to provide **3.43a** (20.6 mg, 45%) as a white solid.

R_f = 0.44 (DCM/EtOH 98:2).

^{1}H NMR (400 MHz, DMSO-d_6) δ (ppm) 10.17 (s, 1H, NH), 8.52 (s, 1H, H_{10}), 8.49 (s, 1H, H_7), 8.32 (s, 1H, H_4), 7.97 (t, J = 6.4 Hz, 1H, NH), 7.52 (t, J = 2.2 Hz, 1H, H_{14}), 7.48 – 7.39 (m, 1H, H_{18}), 7.27 (t, J = 8.1 Hz, 1H, H_{17}), 6.71 (dd, J = 8.1, 2.2 Hz, 1H, H_{16}), 4.08 (q, J = 7.1 Hz, 2H, H_{23}), 4.01 (t, J = 6.3 Hz, 2H, H_{19}), 3.55 (q, J = 6.4 Hz, 2H, H_1), 3.30 – 3.28 (t, J = 6.4 Hz, 2H, H_2), 3.28 – 3.21 (m, 4H, H_{28} and H_{29}), 2.92 (s, 2H, H_{26}), 2.49 – 2.44 (m, 2H, H_{21}), 2.36 – 2.29 (m, 4H, H_{27} and H_{30}), 2.00 (p, J = 6.3 Hz, 2H, H_{20}), 1.34 (s, 9H, H_{Boc}), 1.19 (t, J = 7.1 Hz, 3H, H_{24}).

^{13}C NMR (101 MHz, DMSO-d_6) δ (ppm) 172.5 (1C, C_{22}), 169.7 (1C, C_{25}), 169.2 (1C, C_9), 163.2 (1C, C_6), 161.7 (1C, C_3), 158.9, 158.7 (2C, C_{12} and C_{15}), 153.7 (1C, C_{Boc}), 150.5 (1C, C_{11}), 148.7 (1C, C_8), 146.8 (1C, C_5), 139.5 (1C, C_{13}), 129.5 (1C, C_{17}), 125.6 (1C, C_{10}), 119.0 (1C, C_7), 118.4 (1C, C_4), 112.5 (1C, C_{18}), 110.1 (1C, C_{16}), 106.5 (1C, C_{14}), 78.7 (1C, $C_{IV.Boc}$), 66.5 (1C, C_{19}), 61.0 (1C, C_{26}), 59.9 (1C, C_{23}), 52.5 (2C, C_{27} and C_{30}), 39.5 (2C, C_{28} and C_{29}) 38.1 (1C, C_1), 32.6 (1C, C_2), 30.2 (1C, C_{21}), 28.0 (3C, $CH_{3.Boc}$), 24.2 (1C, C_{20}), 14.1 (1C, C_{24}).

MS (ESI) *m/z* 770.6 ($[M+H]^+$ (Theoretical 770.2).

Synthesis of ethyl 4-(3-(2''-(2-(2-(piperazin-1-yl)acetamido)ethyl)-[2,4':2',4''-terthiazole]-4-carboxamido)phenoxy)butanoate (3.43b)

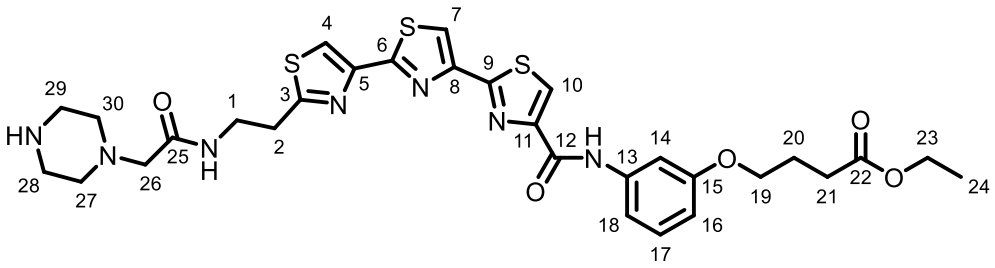

Chemical Formula: $C_{30}H_{35}N_7O_5S_3$
Exact Mass: 669,19
Molecular Weight: 669,83

Deprotection of compound **3.43a** (20.6 mg, 0.03 mmol, 1 eq) was performed following general procedure A with HCl/1,4-dioxane (4M, 2 mL). After purification compound **3.43b** (16.5 mg, 92%) was obtained as a white solid.

R_f = 0.4 (DCM/MeOH [10% NH_4OH] 9:1).

^{1}H NMR (400 MHz, DMSO-d_6) δ (ppm) 10.21 (s, 1H, NH), 9.96 (s, 1H, NH), 8.94 (t, J = 5.7 Hz, 1H, NH), 8.55 (s, 1H, H_{10}), 8.51 (s, 1H, H_7), 8.32 (s, 1H, H_4), 7.54 (t, J = 2.2 Hz, 1H, H_{14}), 7.51 – 7.41 (m, 1H, H_{18}), 7.27 (t, J = 8.1 Hz, 1H, H_{17}), 6.70 (dd, J = 8.1, 2.2 Hz, 1H, H_{16}), 4.08 (q, J = 7.1 Hz, 2H, H_{23}), 4.04 – 3.95 (m, 2H, H_{19}), 3.63 – 3.56 (m, 2H, H_1), 3.56 – 3.45 (br, 4H, H_{28} and H_{29}), 3.44 – 3.33 (br, 4H, H_{27} and H_{30}), 3.27 (t, J = 6.8 Hz, 2H, H_2), 2.49 – 2.44 (m, 2H, H_{21}), 1.99 (p, J = 6.8 Hz, 2H, H_{20}), 1.18 (t, J = 7.1 Hz, 3H, H_{24}).

^{13}C NMR (101 MHz, DMSO-d_6) δ (ppm) 172.5 (1C, C_{22}), 169.2 (2C, C_9 and C_{25}), 163.2 (1C, C_6), 161.7 (1C, C_3), 158.9, 158.7 (2C, C_{12} and C_{15}), 150.5 (1C, C_{11}), 148.6 (1C, C_8), 147.0 (1C, C_5), 139.5 (1C, C_{13}), 129.5 (1C, C_{17}), 125.6 (1C, C_{10}), 119.1 (1C, C_7), 118.3 (1C, C_4), 112.6 (1C, C_{18}), 110.0 (1C, C_{16}), 106.5 (1C, C_{14}), 66.5 (1C, C_{19}), 59.9 (1C, C_{23}), 48.6, 40.2 (4C, C_{27}, C_{28}, C_{29} and C_{30}), 38.4 (1C, C_1), 32.4 (1C, C_2), 30.2 (1C, C_{21}), 24.3 (1C, C_{20}), 14.1 (1C, C_{24}).

HRMS (ESI) *m/z* 670.19342 $(M+H)^+$ (Theoretical 670.19346).

HPLC-RP rt = 5.1 min (Method B).

Synthesis of ethyl 4-(3-(2''-(2-(benzo[d]thiazole-6-carboxamido)ethyl)-[2,4':2',4''-terthiazole]-4-carboxamido)phenoxy)butanoate (3.44)

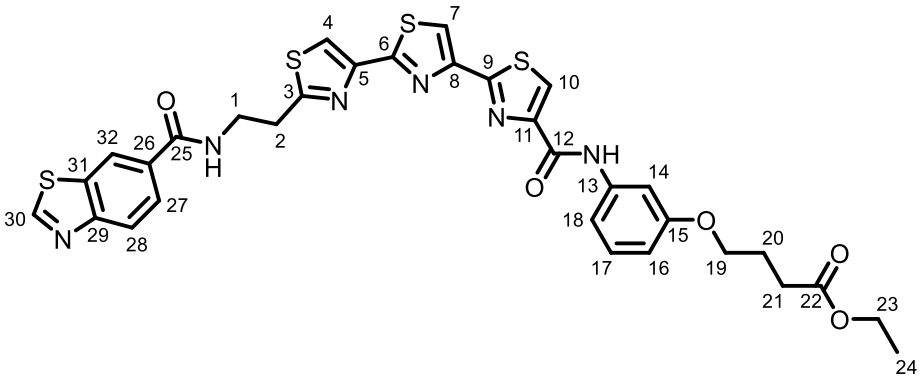

Chemical Formula: $C_{32}H_{28}N_6O_5S_4$
Exact Mass: 704,10
Molecular Weight: 704,85

Coupling between **3.26b** (50 mg, 0.09 mmol, 1 eq) and benzo[*d*]thiazole-6-carboxylic acid (18 mg, 0.11 mmol, 1.2 eq) was performed following general procedure C with HATU (43 mg, 0.11 mmol, 1.3 eq) and DIPEA (22 µL, 0.13 mmol, 1.5 eq) using DMF (1 mL) as solvent. The crude residue was purified by flash chromatography (DCM/MeOH gradient 100:0 to 85:15, v/v) to provide **3.44** (23.4 mg, 40%) as a white solid.

R_f = 0.55 (DCM/MeOH 85:15).

^{1}H NMR (400 MHz, DMSO-d_6) δ (ppm) 10.17 (s, 1H, NH), 9.53 (s, 1H, H_{30}), 8.86 (t, J = 5.6 Hz, 1H, NH), 8.64 (d, J = 1.4 Hz, 1H, H_{32}), 8.50 (s, 1H, H_{10}), 8.49 (s, 1H, H_7), 8.30 (s, 1H, H_4), 8.16 (d, J = 8.5 Hz, 1H, H_{28}), 8.00 (dd, J = 8.5, 1.4 Hz, 1H, H_{27}), 7.52 (t, J = 1.8 Hz, 1H, H_{14}), 7.47 – 7.42 (m, 1H, H_{18}), 7.27 (t, J = 8.2 Hz, 1H, H_{17}), 6.71 (dd, J = 8.2, 1.8 Hz, 1H, H_{16}), 4.08 (q, J = 7.1 Hz, 2H, H_{23}), 4.01 (t, J = 6.3 Hz, 2H, H_{19}), 3.74 (q, J = 6.6 Hz, 2H, H_1), 3.38 (t, J = 6.6 Hz, 2H, H_2), 2.49 – 2.44 (m, 2H, H_{21}), 2.00 (p, J = 6.3 Hz, 2H, H_{20}), 1.19 (t, J = 7.1 Hz, 3H, H_{24}).

^{13}C NMR (101 MHz, DMSO-d_6) δ (ppm) 172.0 (1C, C_{22}), 168.9 (1C, C_{25}), 165.5 (1C, C_9), 162.7 (1C, C_6), 161.2 (1C, C_3), 158.4, 158.3, 158.2 (3C, C_{12}, C_{15} and C_{29}), 154.1 (1C, C_{30}), 150.0 (1C, C_{11}), 148.1 (1C, C_8), 146.4 (1C, C_5), 139.0 (1C, C_{13}), 133.1 (1C, C_{31}), 131.1 (1C, C_{26}), 129.0 (1C, C_{17}), 125.1 (1C, C_{10}), 124.7 (1C, C_{27}), 122.2 (1C, C_{28}), 121.5 (1C, C_{32}), 118.5 (1C, C_7), 117.8 (1C, C_4), 112.0 (1C, C_{18}), 109.5 (1C, C_{16}), 106.0 (1C, C_{14}), 65.9 (1C, C_{19}), 59.3 (1C, C_{23}), 37.7 (1C, C_1), 31.9 (1C, C_2), 29.6 (1C, C_{21}), 23.7 (1C, C_{20}), 13.6 (1C, C_{24}).

HRMS (ESI) *m/z* 705.10760 $(M+H)^+$ (Theoretical 705.10768).

HPLC-RP rt = 7.2 min (Method B).

Synthesis of ethyl 4-(3-(2''-(2-(1,8-naphthyridine-2-carboxamido)ethyl)-[2,4':2',4''-terthiazole]-4-carboxamido)phenoxy)butanoate (3.45)

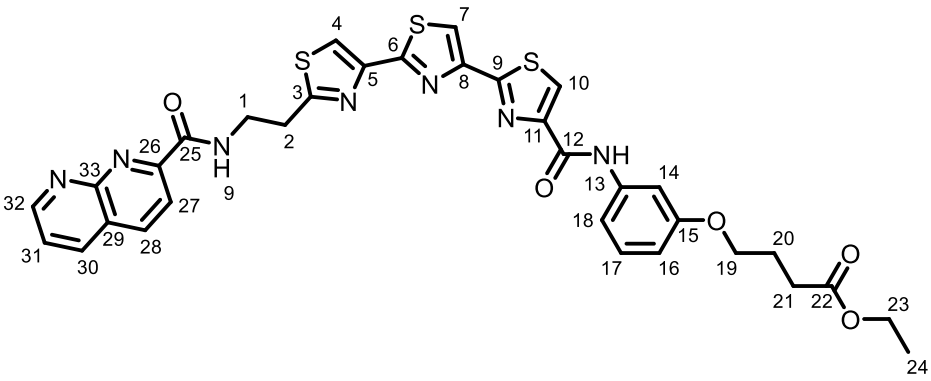

Chemical Formula: $C_{33}H_{29}N_7O_5S_3$
Exact Mass: 699,14
Molecular Weight: 699,82

Coupling between **3.26b** (50 mg, 0.09 mmol, 1 eq) and 1,8-naphthyridine-2-carboxylic acid (18 mg, 0.10 mmol, 1.2 eq) was performed following general procedure C with HATU (43 mg, 0.11 mmol, 1.3 eq) and DIPEA (22 µL, 0.13 mmol, 1.5 eq) using DMF (1 mL) as solvent. The crude residue was purified by flash chromatography (DCM/MeOH gradient 100:0 to 85:15, v/v) to provide **3.45** (45.5 mg, 76%) as a white solid.

R_f = 0.60 (DCM/MeOH 95:5).

^{1}H NMR (400 MHz, CD_3OD) δ (ppm) 10.17 (s, 1H, NH), 9.36 (t, *J* = 6.7 Hz, 1H, NH), 9.21 (dd, *J* = 4.2, 2.0 Hz, 1H, H_{32}), 8.68 (d, *J* = 8.4 Hz, 1H, H_{28}), 8.58 (dd, *J* = 8.2, 2.0 Hz, 1H, H_{30}), 8.49 (s, 1H, H_{10}, 8.48 (s, 1H, H_7), 8.29 – 8.25 (m, 2H, H_4 and H_{27}), 7.74 (dd, *J* = 8.2, 4.2 Hz, 1H, H_{31}), 7.52 (t, *J* = 2.0 Hz, 1H, H_{14}), 7.44 (ddd, *J* = 8.1, 2.0, 0.9 Hz, 1H, H_{18}), 7.27 (t, *J* = 8.1 Hz, 1H, H_{17}), 6.70 (ddd, *J* = 8.1, 2.0, 0.9 Hz, 1H, H_{16}), 4.08 (q, *J* = 7.1 Hz, 2H, H_{23}), 4.00 (t, *J* = 6.3 Hz, 2H, H_{19}), 3.84 (q, *J* = 6.7 Hz, 2H, H_1), 3.44 (t, *J* = 6.7 Hz, 2H, H_2), 2.49 – 2.44 (m, 2H, H_{21}), 2.05 – 1.94 (m, 2H, H_{20}), 1.19 (t, *J* = 7.1 Hz, 3H, H_{24}).

HRMS (ESI) *m/z* 700.14539 $(M+H)^+$ (Theoretical 700.14651).

HPLC-RP rt = 7.0 min (Method B).

Synthesis of ethyl 4-(3-(2''-(2-(quinoxaline-2-carboxamido)ethyl)-[2,4':2',4''-terthiazole]-4-carboxamido)phenoxy)butanoate (3.46)

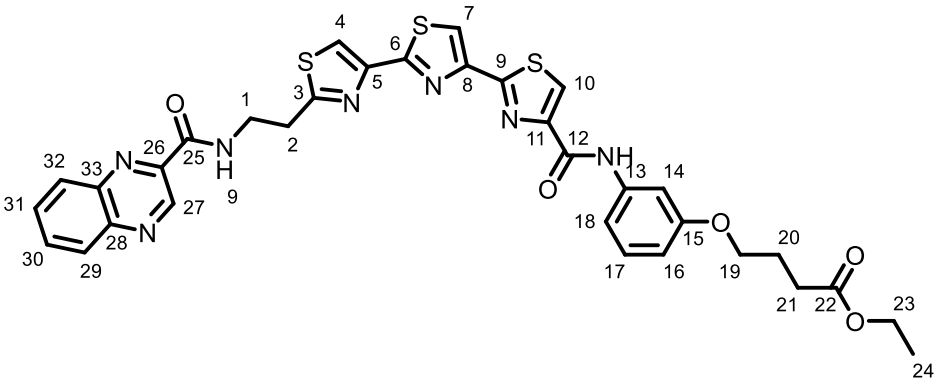

Chemical Formula: $C_{33}H_{29}N_7O_5S_3$
Exact Mass: 699,14
Molecular Weight: 699,82

Coupling between **3.26b** (35 mg, 0.06 mmol, 1 eq) and quinoxaline-2-carboxylic acid (13 mg, 0.07 mmol, 1.2 eq) was performed following general procedure C with HATU (30 mg, 0.098 mmol, 1.3 eq) and DIPEA (16 µL, 0.09 mmol, 1.5 eq) using DMF (1 mL) as solvent. The crude residue was purified by flash chromatography (DCM/EtOH gradient 100:0 to 85:15, v/v) to provide **3.46** (18.7 mg, 44%) as a white solid.

R_f = 0.55 (DCM/EtOH 95:5).

^{1}H NMR (400 MHz, DMSO-d_6) δ (ppm) 10.16 (s, 1H, NH), 9.47 (s, 1H, H_{27}), 9.33 (t, J = 6.6 Hz, 1H, NH), 8.49 (s, 1H, H_{10}), 8.48 (s, 1H, H_7), 8.29 (s, 1H, H_4), 8.23 – 8.17 (m, 2H, H_{29} and H_{32}), 8.05 – 7.89 (m, 2H, H_{30} and H_{31}), 7.52 (t, J = 2.2 Hz, 1H, H_{14}), 7.47 – 7.41 (m, 1H, H_{18}), 7.27 (t, J = 8.2 Hz, 1H, H_{17}), 6.70 (dd, J = 8.2, 2.2 Hz, 1H, H_{16}), 4.08 (q, J = 7.1 Hz, 2H, H_{23}), 4.00 (t, J = 6.3 Hz, 2H, H_{19}), 3.84 (q, J = 6.6 Hz, 2H, H_1), 3.43 (t, J = 6.6 Hz, 2H, H_2), 2.49 – 2.45 (t, J = 6.3 Hz, 2H, H_{21}), 2.01 (p, J = 6.3 Hz, 2H, H_{20}), 1.19 (t, J = 7.1 Hz, 3H, H_{24}).

^{13}C NMR (101 MHz, DMSO-d_6) δ (ppm) 172.5 (1C, C_{22}), 169.4 (1C, C_{25}), 163.2, 163.2 (2C, C_9 and C_6), 161.7 (1C, C_3), 158.9, 158.7 (2C, C_{12} and C_{15}), 150.5 (1C, C_{11}), 148.6 (1C, C_8), 146.9 (1C, C_5), 144.1 (1C, C_{27}), 143.7 (1C, C_{28}), 143.0 (1C, C_{26}), 139.8 (1C, C_{33}), 139.5 (1C, C_{13}), 131.9, 131.3 (2C, C_{30} and C_{31}), 129.5, 129.4, 129.1 (3C, C_{17}, C_{29} and C_{32}), 125.6 (1C, C_{10}), 119.0 (1C, C_7), 118.3 (1C, C_4), 112.5 (1C, C_{18}), 110.0 (1C, C_{16}), 106.5 (1C, C_{14}), 66.5 (1C, C_{19}), 59.9 (1C, C_{23}), 38.7 (1C, C_1), 32.4 (1C, C_2), 30.2 (1C, C_{21}), 24.3 (1C, C_{20}), 14.1 (1C, C_{24}).

HRMS (ESI) *m/z* 700.14679 $(M+H)^+$ (Theoretical 700.14651).

HPLC-RP rt = 7.8 min (Method B).

Synthesis of ethyl 4-(3-(2''-(2-(5-methylpyrazine-2-carboxamido)ethyl)-[2,4':2',4''-terthiazole]-4-carboxamido)phenoxy)butanoate (3.47)

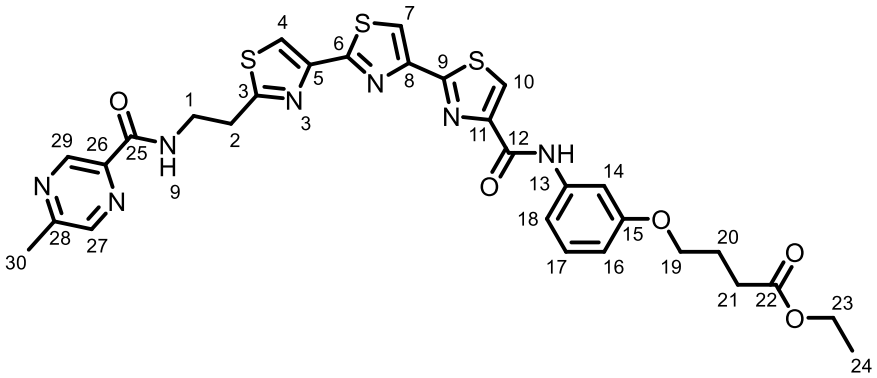

Chemical Formula: $C_{30}H_{29}N_7O_5S_3$
Exact Mass: 663,14
Molecular Weight: 663,79

Coupling between **3.26b** (40 mg, 0.07 mmol, 1 eq) and 5-methylpyrazine-2-carboxylic acid (11 mg, 0.83 mmol, 1.2 eq) was performed following general procedure C with HATU (34 mg, 0.09 mmol, 1.3 eq) and DIPEA (18 µL, 0.10 mmol, 1.5 eq) using DMF (1 mL) as solvent. The crude residue was purified by flash chromatography (DCM/EtOH gradient 100:0 to 85:15, v/v) to provide **3.47** (31.7 mg, 69%) as a white solid.

R_f = 0.26 (DCM/EtOH 95:5).

^{1}H NMR (400 MHz, DMSO-d_6) δ (ppm) 10.16 (s, 1H, NH), 9.13 (t, J = 6.6 Hz, 1H, NH), 9.06 – 9.02 (m, 1H, H_{29}), 8.64 – 8.60 (m, 1H, H_{27}), 8.50 (s, 1H, H_{10}), 8.48 (s, 1H, H_7), 8.26 (s, 1H, H_4), 7.52 (t, J = 1.9 Hz, 1H, H_{14}), 7.46 – 7.41 (m, 1H, H_{18}), 7.27 (t, J = 8.1 Hz, 1H, H_{17}), 6.70 (dd, J = 8.1, 1.9 Hz, 1H, H_{16}), 4.08 (q, J = 7.1 Hz, 2H, H_{23}), 4.00 (t, J = 6.3 Hz, 2H, H_{19}), 3.75 (q, J = 6.6 Hz, 2H, H_1), 3.36 (t, J = 6.6 Hz, 2H, H_2), 2.59 (s, 3H, H_{30}), 2.49 – 2.45 (t, J = 6.3 Hz, 2H, H_{21}), 2.00 (p, J = 6.3 Hz, 2H, H_{20}), 1.18 (t, J = 7.1 Hz, 3H, H_{24}).

^{13}C NMR (101 MHz, DMSO-d_6) δ (ppm) 172.5 (1C, C_{22}), 169.3 (1C, C_{25}), 163.2, 163.1 (2C, C_9 and C_6), 161.7 (1C, C_3), 158.9, 158.7 (2C, C_{12} and C_{15}), 157.0 (1C, C_{28}), 150.5 (1C, C_{11}), 148.6 (1C, C_8), 146.9 (1C, C_5), 142.9 (1C, C_{29}), 142.4 (1C, C_{27}), 141.9 (1C, C_{26}), 139.5 (1C, C_{13}), 129.5 (1C, C_{17}), 125.6 (1C, C_{10}), 119.1 (1C, C_7), 118.2 (1C, C_4), 112.5 (1C, C_{18}), 110.0 (1C, C_{16}), 106.5 (1C, C_{14}), 66.5 (1C, C_{19}), 59.9 (1C, C_{23}), 38.5 (1C, C_1), 32.3 (1C, C_2), 30.2 (1C, C_{21}), 24.3 (1C, C_{20}), 21.3 (1C, C_{30}), 14.1 (1C, C_{24}).

HRMS (ESI) *m/z* 664.14697 $(M+H)^+$ (Theoretical 664.14651).

HPLC-RP rt = 7.4 min (Method B).

Synthesis of ethyl 4-(3-(2''-(2-(picolinamido)ethyl)-[2,4':2',4''-terthiazole]-4-carboxamido)phenoxy)butanoate (3.48)

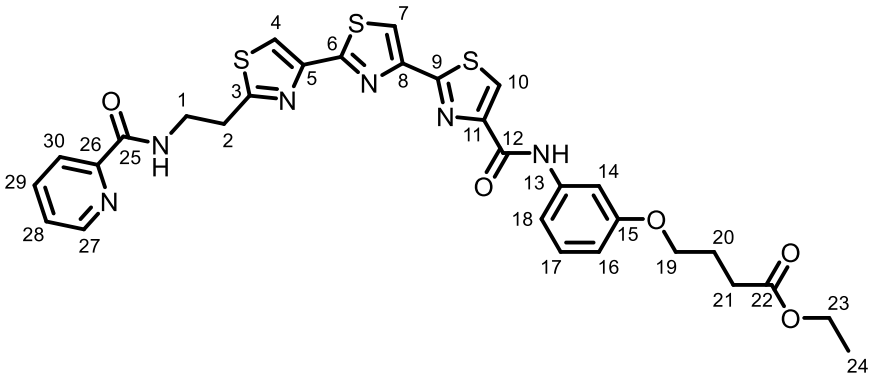

Chemical Formula: $C_{30}H_{28}N_6O_5S_3$
Exact Mass: 648,13
Molecular Weight: 648,77

Coupling between **3.26b** (35 mg, 0.06 mmol, 1 eq) and picolinic acid (9 mg, 0.07 mmol, 1.2 eq) was performed following general procedure C with HATU (30 mg, 0.098 mmol, 1.3 eq) and DIPEA (16 µL, 0.09 mmol, 1.5 eq) using DMF (1 mL) as solvent. The crude residue was purified by flash chromatography (DCM/EtOH gradient 100:0 to 85:15, v/v) to provide **3.48** (19 mg, 49%) as a white solid.

R_f = 0.25 (DCM/EtOH 98:2).

^{1}H NMR (400 MHz, $CDCl_3$) δ (ppm) 9.37 (s, 1H, NH), 8.87 (br, 1H, NH), 8.74 – 8.68 (m, 1H, H_{27}), 8.39 – 8.32 (m, 2H, H_7 and H_{30}), 8.23 (s, 1H, H_{10}), 8.15 (s, 1H, H_4), 8.00 (td, J = 7.5, 2.0 Hz, 1H, H_{29}), 7.64 (t, J = 2.0 Hz, 1H, H_{28}), 7.57 (m, 1H, H_{18}), 7.44 – 7.38 (m, 1H, H_{17}), 7.35 (m, 1H, H_{14}), 6.84 (ddd, J = 8.0, 1.4 Hz, 1H, H_{16}), 4.30 (q, J = 7.1 Hz, 1H, H_{23}), 4.20 (t, J = 6.3 Hz, 1H, H_{19}), 4.13 (q, J = 6.4 Hz, 1H, H_1), 3.54 (t, J = 6.4 Hz, 1H, H_2), 2.67 (t, J = 6.3 Hz, 1H, H_{21}), 2.34 – 2.19 (m, 1H, H_{20}), 1.41 (t, J = 7.1 Hz, 1H, H_{24}).

^{13}C NMR (101 MHz, CDCl3) δ (ppm) 173.4 (1C, C_{22}), 169.0 (1C, C_{25}), 164.6 (1C, C_3), 163.6 (1C, C_6), 162.8 (1C, C_9), 159.6 (1C, C_{15}), 159.0 (1C, C_{12}), 150.9 (1C, C_{26}), 149.9 (1C, C_{11}), 149.3 (1C, C_8), 148.5 (1C, C_5), 148.2 (1C, C_{27}), 139.0 (1C, C_{13}), 137.5 (1C, C_{29}), 130.0 (1C, C_{17}), 126.4 (1C, C_{18}), 124.6 (1C, C_{10}), 122.4 (1C, C_{30}), 117.6 (1C, C_7), 116.9 (1C, C_4), 112.2 (1C, C_{14}), 111.1 (1C, C_{16}), 106.1 (1C, C_{28}), 67.0 (1C, C_{19}), 60.6 (1C, C_{23}), 38.6 (1C, C_1), 33.1 (1C, C_2), 31.0 (1C, C_{21}), 24.8 (1C, C_{20}), 14.4 (1C, C_{24}).

HRMS (ESI) *m/z* 649.13599 $(M+H)^+$ (Theoretical 649.13561).

HPLC-RP rt = 6.2 min (Method B).

Synthesis of ethyl 4-(3-(2''-(2-(thiophene-2-carboxamido)ethyl)-[2,4':2',4''-terthiazole]-4-carboxamido)phenoxy)butanoate (3.49)

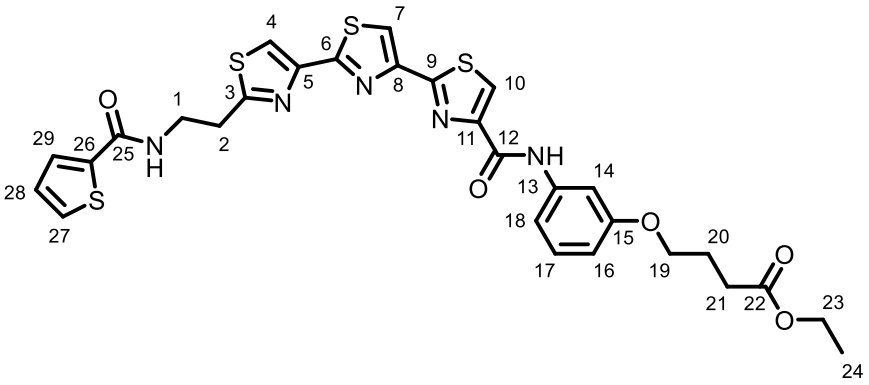

Chemical Formula: $C_{29}H_{27}N_5O_5S_4$
Exact Mass: 653,09
Molecular Weight: 653,80

Coupling between **3.26b** (35 mg, 0.06 mmol, 1 eq) and thiophene-2-carboxylic acid (9 mg, 0.07 mmol, 1.2 eq) was performed following general procedure C with HATU (30 mg, 0.098 mmol, 1.3 eq) and DIPEA (16 µL, 0.09 mmol, 1.5 eq) Using DMF (1 mL) as solvent. The crude residue was purified by flash chromatography (DCM/EtOH gradient 100:0 to 85:15, v/v) to provide **3.49** (25.9 mg, 66%) as a white solid.

R_f = 0.32 (DCM/EtOH 98:2).

^{1}H NMR (400 MHz, DMSO-d_6) δ (ppm) 10.17 (s, 1H, NH), 8.71 (t, J = 6.6 Hz, 1H, NH), 8.50 (s, 1H, H_{10}), 8.48 (s, 1H, H_7), 8.29 (s, 1H, H_4), 7.77 – 7.72 (m, 2H, H_{27} and H_{28}), 7.52 (t, J = 1.9 Hz, 1H, H_{14}), 7.46 – 7.42 (m, 1H, H_{18}), 7.27 (t, J = 8.2 Hz, 1H, H_{17}), 7.15 (dd, J = 4.9, 3.8 Hz, 1H, H_{29}), 6.70 (dd, J = 8.2, 1.9 Hz, 1H, H_{16}), 4.08 (q, J = 7.1 Hz, 2H, H_{23}), 4.00 (t, J = 6.3 Hz, 2H, H_{19}), 3.66 (q, J = 6.6 Hz, 2H, H_1), 3.36 – 3.33 (t, J = 6.6 Hz, 2H, H_2), 2.49 – 2.44 (m, 2H, H_{21}), 2.00 (p, J = 6.3 Hz, 2H, H_{20}), 1.19 (t, J = 7.1 Hz, 3H, H_{24}).

^{13}C NMR (101 MHz, DMSO-d_6) δ (ppm) 172.5 (1C, C_{22}), 169.3 (1C, C_{25}), 163.2 (1C, C_9), 161.7 (1C, C_6), 161.3 (1C, C_3), 158.9, 158.7 (2C, C_{12} and C_{15}), 150.5 (1C, C_{11}), 148.6 (1C, C_8), 146.9 (1C, C_5), 139.7 (1C, C_{26}), 139.5 (1C, C_{13}), 130.8 (1C, C_{28}), 129.5 (1C, C_{17}), 128.1 (1C, C_{27}), 127.9 (1C, C_{29}), 125.6 (1C, C_{10}), 119.0 (1C, C_7), 118.3 (1C, C_4), 112.5 (1C, C_{18}), 110.0 (1C, C_{16}), 106.5 (1C, C_{14}), 66.5 (1C, C_{19}), 59.9 (1C, C_{23}), 39.5 (1C, C_1), 32.5 (1C, C_2), 30.2 (1C, C_{21}), 24.3 (1C, C_{20}), 14.1 (1C, C_{24}).

HRMS (ESI) *m/z* 654.09741 $(M+H)^+$ (Theoretical 654.08951).

HPLC-RP rt = 7.3 min (Method B).

Synthesis of ethyl 4-(3-(2''-(2-(2-(2,4-dioxo-1,3-diazaspiro[4.4]nonan-3-yl)acetamido)ethyl)-[2,4':2',4''-terthiazole]-4-carboxamido)phenoxy)butanoate

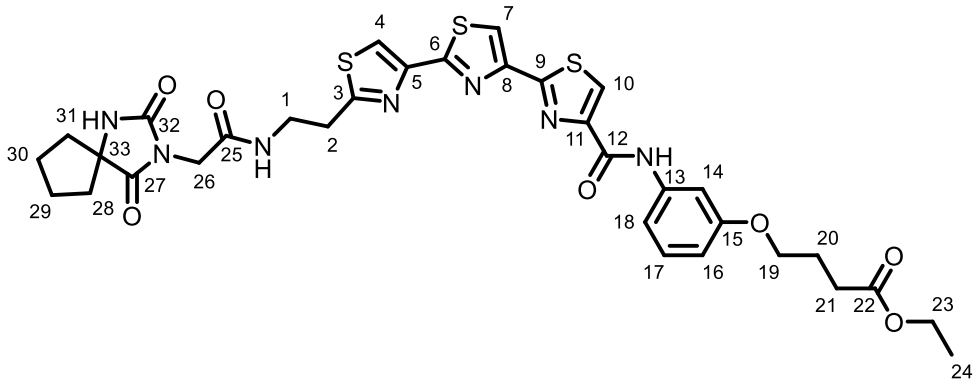

Chemical Formula: $C_{33}H_{35}N_7O_7S_3$
Exact Mass: 737,18
Molecular Weight: 737,87

Coupling between **3.26b** (50 mg, 0.09 mmol, 1 eq) and (2,4-Dioxo-1,3-diaza-spiro[4,4]non-3-yl)-acetic acid (22 mg, 0.10 mmol, 1.2 eq) was performed following general procedure C with HATU (43 mg, 0.11 mmol, 1.3 eq) and DIPEA (22 µL, 0.13 mmol, 1.5 eq) using DMF (1 mL) as solvent. The crude residue was purified by flash chromatography (DCM/MeOH gradient 100:0 to 85:15, v/v) to provide **3.50** (50 mg, 80%) as a white solid.

R_f = 0.45 (DCM/MeOH 95:5).

^{1}H NMR (400 MHz, DMSO-d_6) δ (ppm) 10.18 (s, 1H, NH), 8.52 (s, 1H, H_7), 8.49 (s, 1H, H_{10}), 8.48 (s, 1H, NH), 8.35 (m, 1H, NH), 8.31 (s, 1H, H_4), 7.52 (t, J = 2.0 Hz, 1H, H_{14}), 7.44 (m, 1H, H_{18}), 7.27 (t, J = 8.2 Hz, 1H, H_{17}), 6.71 (dd, J = 8.2, 2.0 Hz, 1H, H_{16}), 4.08 (q, J = 7.1 Hz, 2H, H_{23}), 4.01 (t, J = 6.3 Hz, 2H, H_{19}), 3.95 (s, 2H, H_{26}), 3.51 (dd, J = 12.6, 6.5 Hz, 2H, H_1), 3.21 (t, J = 6.5 Hz, 2H, H_2), 2.49 – 2.44 (m, 2H, H_{21}), 2.05 – 1.90 (m, 4H, H_{20} and H_{31}), 1.79 – 1.65 (m, 6H, H_{28}, H_{29} and H_{30}), 1.19 (t, J = 7.1 Hz, 3H, H_{24}).

^{13}C NMR (101 MHz, DMSO-d_6) δ (ppm) 177.4 (1C, C_{32}), 172.5 (1C, C_{22}), 169.2 (1C, C_{25}), 166.2 (1C, C_9), 163.2 (1C, C_6), 161.7 (1C, C_3), 158.9 (1C, C_{12}), 158.7 (1C, C_{15}), 155.3 (1C, C_{22}), 150.5 (1C, C_{11}), 148.6 (1C, C_8), 146.9 (1C, C_5), 139.5 (1C, C_{13}), 129.5 (1C, C_{17}), 125.6 (1C, C_{10}), 119.0 (1C, C_7), 118.2 (1C, C_4), 112.5 (1C, C_{18}), 110.0 (1C, C_{16}), 106.5 (1C, C_{14}), 67.3 (1C, C_{33}), 66.5 (1C, C_{19}), 59.9 (1C, C_{32}), 39.5 (3C, $C_{26,}$ C_{28} and C_{31}), 37.1 (1C, C_1), 32.5 (1C, C_2), 30.1 (1C, C_{21}), 24.6 (1C, C_{20}), 24.2 (2C, C_{29} and C_{30}), 14.1 (1C, C_{24}).

HRMS (ESI) *m/z* 738.18311 $(M+H)^+$ (Theoretical 738.18328).

HPLC-RP rt = 6.7 min (Method B).

Synthesis of ethyl 4-(3-(2''-(2-(3,5-difluorobenzamido)ethyl)-[2,4':2',4''-terthiazole]-4-carboxamido)phenoxy)butanoate (3.51)

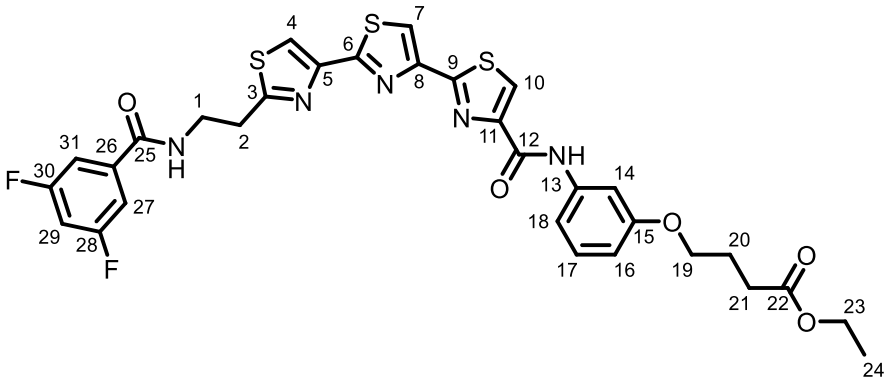

Chemical Formula: $C_{31}H_{27}F_2N_5O_5S_3$
Exact Mass: 683,11
Molecular Weight: 683,76

Coupling between **3.26b** (40 mg, 0.07 mmol, 1 eq) and 3,5-difluorobenzoic acid (13 mg, 0.83 mmol, 1.2 eq) was performed following general procedure C with HATU (34 mg, 0.09 mmol, 1.3 eq) and DIPEA (18 µL, 0.10 mmol, 1.5 eq) using DMF (1 mL) as solvent. The crude residue was purified by flash chromatography (DCM/EtOH gradient 100:0 to 85:15, v/v) to provide **3.51** (33.5 mg, 71%) as a white solid.

R_f = 0.44 (DCM/EtOH 95:5).

^{1}H NMR (400 MHz, DMSO-d_6) δ (ppm) 10.16 (s, 1H, NH), 8.87 (t, J = 6.3 Hz, 1H, NH), 8.50 (s, 1H, H_{10}), 8.48 (s, 1H, H_7), 8.28 (s, 1H, H_4), 7.57 – 7.49 (m, 3H, H_{14}, H_{27} and H_{31}), 7.48 – 7.41 (m, 2H, H_{18} and H_{29}), 7.27 (t, J = 8.1 Hz, 1H, H_{17}), 6.74 – 6.67 (m, 1H, H_{16}), 4.08 (q, J = 7.1 Hz, 2H, H_{23}), 4.00 (t, J = 6.2 Hz, 2H, H_{19}), 3.69 (q, J = 6.3 Hz, 2H, H_1), 3.39 – 3.33 (m, 2H, H_2), 2.49 – 2.42 (m, 2H, H_{21}), 2.00 (p, J = 6.2 Hz, 2H, H_{20}), 1.19 (t, J = 7.1 Hz, 3H, H_{24}).

^{13}C NMR (101 MHz, DMSO-d_6) δ (ppm) 172.5 (1C, C_{22}), 169.2 (1C, C_3), 163.8 (1C, C_{25}), 163.4 (d, $J_{C\text{-}F}$ = 12.7 Hz, 1C, $C_{IV.CF}$), 163.2 (1C, C_2), 161.7 (1C, C_3), 160.9 (d, $J_{C\text{-}F}$ = 12.7 Hz, 1C, $C_{IV.CF}$), 158.9 (1C, C_{15}), 158.7 (1C, C_{12}), 150.5 (1C, C_{11}), 148.6 (1C, C_8), 146.9 (1C, C_5), 139.5 (1C, C_{13}), 137.8 (t, $J_{C\text{-}F}$ = 8.3 Hz, 1C, C_{26}), 129.5 (1C, C_{17}), 125.6 (1C, C_{10}), 119.0 (1C, C_7), 118.3 (1C, C_4), 112.5 (1C, C_{18}), 110.6, 110.6 (d, $J_{C\text{-}F}$ = 7.3 Hz, 1C, $C_{IV.Aromatic}$) , 110.4 (d, $J_{C\text{-}F}$ = 7.3 Hz, 1C, $C_{IV.Aromatic}$), 110.0 (1C, C_{16}), 106.7 (1C, C_{29}), 106.5 (1C, C_{14}), 66.5 (1C, C_{19}), 59.9 (1C, C_{23}), 39.5 (1C, C_1), 32.2 (1C, C_2), 30.1 (1C, C_{21}), 24.2 (1C, C_{20}), 14.1 (1C, C_{24}).

HRMS (ESI) *m/z* 684.12097 $(M+H)^+$ (Theoretical 684.12151).

HPLC-RP rt = 7.5 min (Method B).

Synthesis of ethyl 4-(3-(2''-(2-((benzo[d]thiazol-5-ylmethyl)amino)ethyl)-[2,4':2',4''-terthiazole]-4-carboxamido)phenoxy)butanoate (3.52)

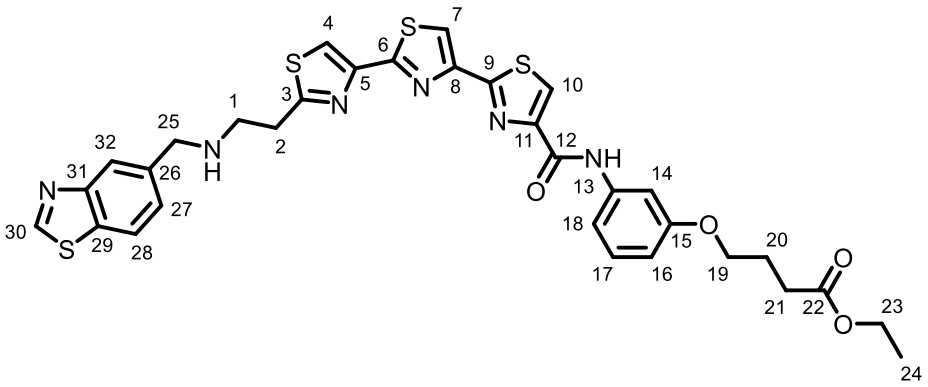

Chemical Formula: $C_{32}H_{30}N_6O_4S_4$
Exact Mass: 690,12
Molecular Weight: 690,87

Reaction between **3.26b** (40 mg, 0.067 mmol, 1 eq) and benzo[*d*]thiazole-5-carbaldehyde (14 mg, 0.07 mmol, 1.2 eq) was performed following general procedure F with molecular sieves 4 Å (150 mg) and $SiHCl_3$ (15 µL, 0.15 mmol, 2 eq) using DMF (1.5 mL) as solvent. The crude residue was purified by flash chromatography (DCM/EtOH gradient 100:0 to 85:15, v/v) to provide **3.52** (26 mg, 52%) as a white solid.

R_f = 0.57 (DCM/EtOH 95:5).

^{1}H NMR (400 MHz, $CDCl_3$) δ (ppm) 9.21 (s, 1H, NH), 9.02 (s, 1H, H_{30}), 8.22 (s, 1H, H_{10}), 8.20 (s, 1H, H_{32}), 8.03 (s, 1H, H_7), 8.00 - 7.95 (s, 2H, H_{28} and H_4), 7.62 (d, J = 8.2 Hz, 1H, H_{27}), 7.50 (t, J = 2.2 Hz, 1H, H_{14}), 7.31 – 7.25 (m, 1H, H_{17}), 7.24 – 7.18 (m, 1H, H_{18}), 6.70 (dd, J = 8.2, 2.2 Hz, 1H, H_{16}), 4.22 (s, 2H, H_{25}), 4.16 (q, J = 7.1 Hz, 2H, H_{23}), 4.06 (t, J = 6.8 Hz, 2H, H_{19}), 3.48 – 3.39 (m, 2H, H_1), 3.37 – 3.30 (m, 2H, H_2), 2.53 (t, J = 6.8 Hz, 2H, H_{21}), 2.19 – 2.08 (m, 2H, H_{20}), 1.27 (t, J = 7.1 Hz, 3H, H_{24}).

^{13}C NMR (101 MHz, $CDCl_3$) δ (ppm) 173.4 (1C, C_{22}), 168.8 (1C, C_9), 163.2 (1C, C_6), 162.7 (1C, C_3), 159.7, 158.9 (2C, C_{12} and C_{15}), 155.0, 153.7 (2C, C_{30} and C_{31}), 151.0 (1C, C_{11}), 149.4 (1C, C_8), 148.1 (1C, C_5), 139.0 (1C, C_{13}), 133.8 (2C, C_{26} and C_{29}), 129.9 (1C, C_{27}), 126.7, 124.7 (C, C_{10} and C_{32}), 124.1 (1C, C_{28}), 122.6 (1C, C_4), 117.5 (1C, C_7), 117.3 (1C, C_4), 112.3 (1C, C_{18}), 111.1 (1C, C_{16}), 106.2 (1C, C_{14}), 67.0 (1C, C_{19}), 60.6 (1C, C_{23}), 52.7 (1C, C_{25}), 47.0 (1C, C_2), 31.7 (1C, C_1), 31.0 (1C, C_{21}), 24.8 (1C, C_{20}), 14.4 (1C, C_{24}).

HRMS (ESI) *m/z* 691.12817 $(M+H)^+$ (Theoretical 691.12841).

HPLC-RP rt = 5.9 min (Method B).

Synthesis of ethyl 4-(3-(2''-(2-(((5-phenylthiazol-2-yl)methyl)amino)ethyl)-[2,4':2',4''-terthiazole]-4-carboxamido)phenoxy)butanoate (3.53)

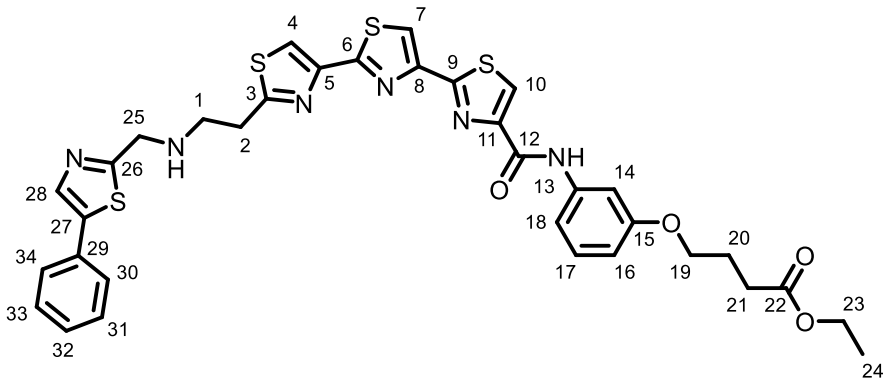

Chemical Formula: $C_{34}H_{32}N_6O_4S_4$
Exact Mass: 716,14
Molecular Weight: 716,91

Reaction between **3.26b** (40 mg, 0.067 mmol, 1 eq) and 5-phenylthiazole-2-carbaldehyde (17 mg, 0.09 mmol, 1.2 eq) was performed following general procedure F with molecular sieves 4 Å (150 mg) and $SiHCl_3$ (15 µL, 0.15 mmol, 2 eq) using DMF (1.5 mL) as solvent. The crude residue was purified by flash chromatography (DCM/EtOH gradient 100:0 to 85:15, v/v) to provide **3.53** (20 mg, 38%) as a white solid.

R_f = 0.5 (DCM/EtOH 95:5).

^{1}H NMR (400 MHz, DMSO-d_6) δ (ppm) 10.17 (s, 1H, NH), 8.49 (s, 1H, NH), 8.47 (s, 1H, H_{10}), 8.29 (s, 1H, H_7), 8.05 (s, 1H, H_4), 7.60 – 7.54 (m, 2H, H_{Aryl}), 7.54 – 7.50 (m, 1H, H_{14}), 7.47 – 7.42 (m, 1H, H_{18}), 7.41 – 7.33 (m, 2H, H_{17} and H_{Aryl}), 7.33 – 7.24 (m, 2H, H_{Aryl}), 6.71 (dd, J = 8.2, 2.5 Hz, 1H, H_{16}), 4.12 – 4.05 (m, 4H, H_{23} and H_{25}), 4.00 (t, J = 6.3 Hz, 2H, H_{19}), 3.24 (t, J = 6.5 Hz, 2H, H_1), 3.06 (t, J = 6.5 Hz, 2H, H_2), 2.49 – 2.44 (t, J = 6.6 Hz, 2H, H_{21}), 2.01 (p, J = 6.6 Hz, 2H, H_{20}), 1.19 (t, J = 7.1 Hz, 3H, H_{24}).

^{13}C NMR (101 MHz, DMSO-d_6) δ (ppm) 172.5 (1C, C_{22}), 170.7 (2C, C_9 and C_{26}), 163.4 (1C, C_6), 161.7 (1C, C_3), 159.0, 158.7 (2C, C_{12} and C_{15}), 150.5 (1C, C_{11}), 148.6 (1C, C_8), 146.6 (1C, C_5), 139.5 (1C, C_{13}), 138.2, 138.0 (3C, C_{27}, C_{28} and C_{29}), 131.3, 129.5, 129.2, 128.0, 126.2, 126.1, 125.6 (7C, C_{10}, C_{17}, C_{30}, C_{31}, C_{32}, C_{33} and C_{34}), 118.9 (1C, C_7), 118.2 (1C, C_4), 112.6 (1C, C_{18}), 110.1 (1C, C_{16}), 106.5 (1C, C_{14}), 66.5 (1C, C_{19}), 59.9 (1C, C_{23}), 50.2 (1C, C_{25}), 48.3 (1C, C_2), 33.2 (1C, C_1), 30.2 (1C, C_{21}), 24.3 (1C, C_{20}), 14.1 (1C, C_{24}).

HRMS (ESI) *m/z* 717.14429 $(M+H)^+$ (Theoretical 717.14406).

HPLC-RP rt = 6.5 min (Method B).

Synthesis of ethyl 4-(3-(2''-(2-((thiazol-2-ylmethyl)amino)ethyl)-[2,4':2',4''-terthiazole]-4-carboxamido)phenoxy)butanoate (3.54)

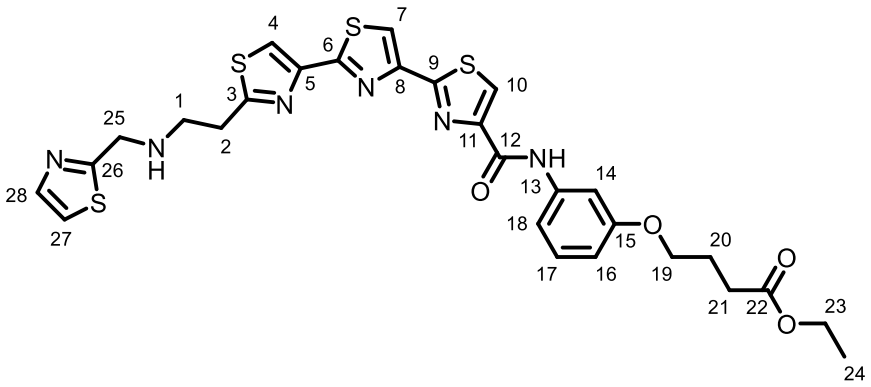

Chemical Formula: $C_{28}H_{28}N_6O_4S_4$
Exact Mass: 640,11
Molecular Weight: 640,81

Reaction between **3.26b** (40 mg, 0.067 mmol, 1 eq) and thiazole-2-carbaldehyde (8 µL, 0.09 mmol, 1.2 eq) was performed following general procedure F with molecular sieves 4 Å (150 mg) and $SiHCl_3$ (15 µL, 0.15 mmol, 2 eq) using DMF (1.5 mL) as solvent. The crude residue was purified by flash chromatography (DCM/EtOH gradient 100:0 to 85:15, v/v) to provide **3.54** (15 mg, 32%) as a white solid.

R_f = 0.6 (DCM/EtOH 95:5).

^{1}H NMR (400 MHz, DMSO-d_6) δ (ppm) 10.17 (s, 1H, NH), 8.49 (s, 1H, H_{10}), 8.49 (s, 1H, H_7), 8.27 (s, 1H, H_4), 7.71 (d, J = 3.3 Hz, 1H, H_{28}), 7.59 (d, J = 3.3 Hz, 1H, H_{27}), 7.52 (t, J = 2.2 Hz, 1H, H_{14}), 7.46 – 7.42 (m, 1H, H_{18}), 7.27 (t, J = 8.2 Hz, 1H, H_{17}), 6.70 (dd, J = 8.2, 2.2 Hz, 1H, H_{16}), 4.12 – 4.04 (m, 4H, H_{23} and H_{25}), 4.00 (t, J = 6.3 Hz, 2H, H_{19}), 3.23 (t, J = 6.4 Hz, 2H, H_1), 3.03 (t, J = 6.4 Hz, 2H, H_2), 2.46 (t, J = 6.3 Hz, 2H, H_{21}), 2.01 (p, J = 6.3 Hz, 2H, H_{20}), 1.19 (t, J = 7.1 Hz, 3H, H_{24}).

^{13}C NMR (101 MHz, DMSO-d_6) δ (ppm) 172.5 (1C, C_{22}), 170.6 (1C, C_{26}), 169.2 (1C, C_9), 163.4 (1C, C_6), 161.7 (1C, C_3), 158.9, 158.7 (2C, C_{12} and C_{15}), 150.5 (1C, C_{11}), 148.6 (1C, C_8), 146.5 (1C, C_5), 142.2 (1C, C_{28}), 139.5 (1C, C_{13}), 129.5 (1C, C_{17}), 125.6 (1C, C_{10}), 119.7 (1C, C_{27}), 118.9 (1C, C_7), 118.2 (1C, C_4), 112.5 (1C, C_{18}), 110.0 (1C, C_{16}), 106.5 (1C, C_{14}), 66.5 (1C, C_{19}), 59.9 (1C, C_{23}), 50.0 (1C, C_{25}), 48.1 (1C, C_2), 33.2 (1C, C_1), 30.2 (1C, C_{21}), 24.3 (1C, C_{20}), 14.1 (1C, C_{24}).

HRMS (ESI) *m/z* 641.11304 $(M+H)^+$ (Theoretical 641.11276).

HPLC-RP rt = 5.7 min (Method B).

Synthesis of ethyl 4-(3-(2''-(2-((2,2,10,10-tetramethyl-4,8-dioxo-3,9-dioxa-5,7-diazaundecan-6-ylidene)amino)ethyl)-[2,4':2',4''-terthiazole]-4-carboxamido)phenoxy)butanoate (3.55a)

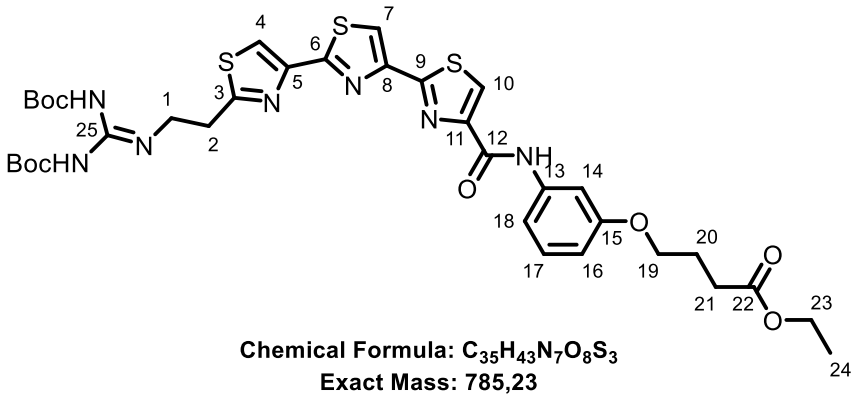

Chemical Formula: $C_{35}H_{43}N_7O_8S_3$
Exact Mass: 785,23
Molecular Weight: 785,95

A solution of **3.26b** (50 mg, 0.09 mmol, 1eq) and Et_3N (24 µL, 0.17 mmol, 2 eq) in DMF (2 mL) was stirred at room temperature, until complete solubilization of the starting material. Then, 1,3-di-Boc-2-(trifluoromethylsulfonyl)guanidine (67 mg, 0.17 mmol, 2 eq) was added and the mixture was stirred at room temperature for 16h. The mixture was concentrated under reduced pressure, a solution of $KHSO_4$ (0.5 M) was added, and the aqueous phase was extracted with DCM. The organic phase was dried over $MgSO_4$ and concentrated under reduced pressure. The crude residue was purified by flash chromatography (DCM/MeOH gradient 100:0 to 90:10, v/v) to provide **3.55a** (66 mg, 97%) as a white solid.

R_f = 0.6 (DCM/MeOH 95:5).

^{1}H NMR (400 MHz, $CDCl_3$) δ (ppm) 11.50 (s, 1H, NH), 9.22 (s, 1H, NH), 8.91 (s, 1H, NH), 8.23 (s, 1H, H_{10}), 8.07 (s, 1H, H_7), 8.02 (s, 1H, H_4), 7.50 (t, J = 2.2 Hz, 1H, H_{14}), 7.28 – 7.25 (m, 1H, H_{17}), 7.23 – 7.19 (m, 1H, H_{18}), 6.74 – 6.67 (m, 1H, H_{16}), 4.16 (q, J = 7.1 Hz, 2H, H_{23}), 4.06 (t, J = 6.1 Hz, 2H, H_{19}), 4.00 – 3.94 (m, 2H, H_1), 3.38 – 3.30 (m, 2H, H_2), 2.53 (t, J = 7.3 Hz, 2H, H_{21}), 2.19 – 2.08 (m, 2H, H_{20}), 1.52 (s, 9H, H_{Boc}), 1.48 (s, 9H, H_{Boc}), 1.27 (t, J = 7.1 Hz, 3H, H_{24}).

^{13}C NMR (101 MHz, $CDCl_3$) δ (ppm) 173.4 (1C, C_{22}), 168.7 (1C, C_9), 163.6 (1C, C_6), 162.9 (1C, C_3), 159.7 (2C, C_{15} and C_{Boc}), 159.0 (2C, C_{12} and C_{Boc}), 153.1 (1C, C_{25}), 151.0 (1C, C_{11}), 149.3 (1C, C_8), 148.6 (1C, C_5), 139.0 (1C, C_{13}), 129.9 (1C, C_{17}), 124.6 (1C, C_{10}), 117.6 (1C, C_7), 117.0 (1C, C_4), 112.2 (1C, C_{18}), 111.1 (1C, C_{16}), 106.2 (1C, C_{14}), 77.4 (2C, $C_{IV.Boc}$), 67.0 (1C, C_{19}), 60.6 (1C, C_{23}), 40.1 (1C, C_1), 32.9 (1C, C_2), 31.0 (1C, C_{21}), 28.4 (3C, $CH_{3.Boc}$), 28.2 (3C, $CH_{3.Boc}$), 24.8 (1C, C_{20}), 14.4 (1C, C_{24}).

MS (ESI) *m/z* 786.3 $(M+H)^+$ (Theoretical 786.2)

Synthesis of ethyl 4-(3-(2''-(2-((diaminomethylene)amino)ethyl)-[2,4':2',4''-terthiazole]-4-carboxamido)phenoxy)butanoate (3.55b)

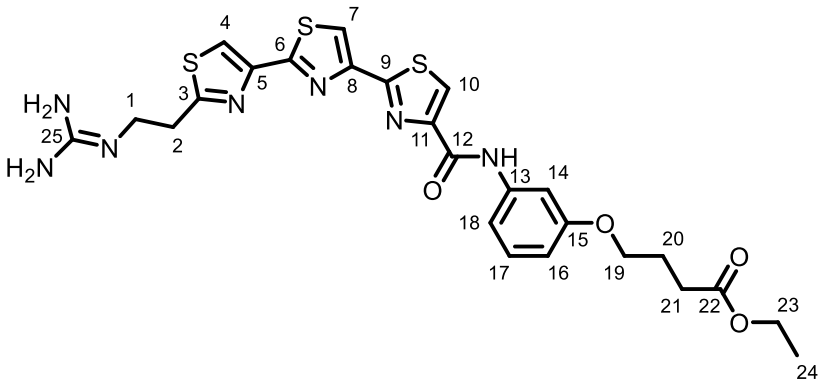

Chemical Formula: $C_{25}H_{27}N_7O_4S_3$
Exact Mass: 585,13
Molecular Weight: 585,72

Deprotection of compound **3.55a** (66 mg, 0.08 mmol, 1 eq) was performed following general procedure A with HCl/1,4-dioxane (4M, 4 mL). After purification compound **3.55b** (60 mg, 98%) was obtained as a white solid.

^{1}H NMR (400 MHz, DMSO-d_6) δ (ppm) 10.23 (s, 1H, NH), 8.49 (s, 1H, H_{10}), 8.42 (s, 1H, H_7), 8.28 (s, 1H, H_4), 7.58 (t, J = 2.2 Hz, 1H, H_{14}), 7.45 (s, 1H, NH), 7.38 – 7.32 (m, 1H, H_{17}), 7.32 – 7.23 (m, 1H, H_{18}), 6.76 – 6.65 (m, 1H, H_{16}), 4.04 (q, J = 7.1 Hz, 2H, H_{23}), 3.98 (t, J = 7.0 Hz, 2H, H_{19}), 3.64 – 3.56 (m, 2H, H_1), 3.31 – 3.24 (m, 2H, H_2), 2.43 (t, J = 7.0 Hz, 2H, H_{21}), 2.02 – 1.91 (m, 2H, H_{20}), 1.15 (t, J = 7.1 Hz, 3H, H_{24}).

^{13}C NMR (101 MHz, DMSO-d_6) δ (ppm) 172.4 (1C, C_{22}), 168.5 (1C, C_3), 163.0 (1C, C_6), 161.6 (1C, C_9), 158.9 (1C, C_{15}), 158.6 (1C, C_{12}), 156.9 (1C, C_{25}), 150.4 (1C, C_{11}), 148.6 (1C, C_8), 146.8 (1C, C_5), 139.4 (1C, C_{13}), 129.4 (1C, C_{17}), 125.6 (1C, C_{10}), 119.1 (1C, C_7), 118.5 (1C, C_4), 112.5 (1C, C_{18}), 110.1 (1C, C_{16}), 106.5 (1C, C_{14}), 66.4 (1C, C_{19}), 59.8 (1C, C_{23}), 39.5 (1C, C_1), 32.1 (1C, C_2), 30.1 (1C, C_{21}), 24.2 (1C, C_{20}), 14.0 (1C, C_{24}).

References

References

[1] Pina, A. S.; Hussain, A.; *et al.* An Historical Overview of Drug Discovery. In *Methods in Molecular Biology*; Humana Press Inc., 2009; Vol. 572, pp 3–12.

[2] Kiriiri, G. K.; Njogu, P. M.; *et al.* Exploring Different Approaches to Improve the Success of Drug Discovery and Development Projects: A Review. *Futur J Pharm Sci* **2020**, *6* (1).

[3] Clamp, M.; Fry, B.; *et al.* Distinguishing Protein-Coding and Noncoding Genes in the Human Genome. *Proc Natl Acad Sci U S A* **2007**, *104* (49).

[4] Santos, R.; Ursu, O.; *et al.* A Comprehensive Map of Molecular Drug Targets. *Nat Rev Drug Discov* **2016**, *16* (1), 19.

[5] Hoagland, M. B.; Sthephenson, M. L.; *et al.* A Soluble Ribonucleic Acid Intermediate in Protein Synthesis. *J Biol Chem* **1958**, *231* (1), 241.

[6] Müller, A.; MacCallum, R. M.; *et al.* Structural Characterization of the Human Proteome. *Genome Res* **2002**, *12* (11), 1625.

[7] Nurk, S.; Koren, S.; *et al.* The Complete Sequence of a Human Genome. *Science (1979)* **2022**, *376* (6588), 44.

[8] Wery, M.; Kwapisz, M.; *et al.* Noncoding RNAs in Gene Regulation. *WIREs: Systems Biology and Medicine* **2011**, *3* (6), 728.

[9] Doudna, J. A.; Lorsch, J. R. Ribozyme Catalysis: Not Different, Just Worse. *Nat Struct Mol Biol* **2005**, *12* (5), 395.

[10] Engreitz, J. M.; Haines, J. E.; *et al.* Local Regulation of Gene Expression by LncRNA Promoters, Transcription and Splicing. *Nature* **2016**, *539* (7629), 452.

[11] Goodall, G. J.; Wickramasinghe, V. O. RNA in Cancer. *Nat Rev Cancer* **2021**, *21* (1), 22.

[12] Cooper, T. A.; Wan, L.; *et al.* RNA and Disease. *Cell* **2009**, *136* (4), 777.

[13] Poltronieri, P.; Sun, B.; *et al.* RNA Viruses: RNA Roles in Pathogenesis, Coreplication and Viral Load. *Curr Genomics* **2015**, *16*, 327.

[14] Esteller, M. Non-Coding RNAs in Human Disease. *Nat Rev Genet* **2011**, *12* (12), 861.

[15] Crooke, S. T.; Baker, B. F.; *et al.* Antisense Technology: An Overview and Prospectus. *Nat Rev Drug Discov* **2021**, *20* (6), 427.

[16] Roberts, T. C.; Langer, R.; *et al.* Advances in Oligonucleotide Drug Delivery. *Nat Rev Drug Discov* **2020**, *19* (10), 673.

[17] Zamani, F.; Suzuki, T. Synthetic RNA Modulators in Drug Discovery. *J Med Chem* **2021**, *64* (11), 7110.

[18] Childs-Disney, J. L.; Yang, X.; *et al.* Targeting RNA Structures with Small Molecules. *Nat Rev Drug Discov* **2022**, *21* (10), 736.

[19] Kovachka, S.; Panosetti, M.; *et al.* Navigating the Rapidly Changing Landscape of Small-Molecule RNA Targeting. *Nat Rev Chem* **2023**.

[20] Falese, J. P.; Donlic, A.; *et al.* Targeting RNA with Small Molecules: From Fundamental Principles towards the Clinic. *Chem Soc Rev* **2021**, *50* (4), 2224.

[21] Di Giorgio, A.; Duca, M. Synthetic Small-Molecule RNA Ligands: Future Prospects as Therapeutic Agents. *Med Chem Comm* **2019**, *10* (8), 1242.

[22] Thomas, J. R.; Hergenrother, P. J. Targeting RNA with Small Molecules. *Chem Rev* **2008**, *108* (4), 1171.

[23] Warner, K. D.; Hajdin, C. E.; *et al.* Principles for Targeting RNA with Drug-like Small Molecules. *Nat Rev Drug Discov* **2018**, *17* (8), 547.

[24] Magnet, S.; Blanchard, J. S. Molecular Insights into Aminoglycoside Action and Resistance. *Chem Rev* **2005**, *105* (2), 477.

[25] Wilson, D. N. Ribosome-Targeting Antibiotics and Mechanisms of Bacterial Resistance. *Nat Rev Microbiol* **2014**, *12* (1), 35.

[26] Ratni, H.; Ebeling, M.; *et al.* Discovery of Risdiplam, a Selective Survival of Motor Neuron-2 (SMN2) Gene Splicing Modifier for the Treatment of Spinal Muscular Atrophy (SMA). *J Med Chem* **2018**, *61* (15), 6501.

[27] Ratni, H.; Scalco, R. S.; *et al.* Risdiplam, the First Approved Small Molecule Splicing Modifier Drug as a Blueprint for Future Transformative Medicines. *ACS Med Chem Lett* **2021**, *12* (6), 874.

[28] Ambros, V. The Evolution of Our Thinking about MicroRNAs. *Nat Med* **2008**, *14* (10), 1036.

[29] Hanna, J.; Hossain, G. S.; *et al.* The Potential for MicroRNA Therapeutics and Clinical Research. *Front Genet* **2019**, *10*.

[30] Green, D.; Dalmay, T.; *et al.* Microguards and Micromessengers of the Genome. *Heredity (Edinb)* **2016**, *116* (2), 125.

[31] Lee, R. C.; Feinbaum, R. L.; *et al.* The C. Elegans Heterochronic Gene Lin-4 Encodes Small RNAs with Antisense Complementarity to Lin-14. *Cell* **1993**, *75*, 843.

[32] Bartel, D. P. MicroRNAs: Genomics, Biogenesis, Mechanism, and Function. *Cell* **2004**, *116*, 281.

[33] Kozomara, A.; Birgaoanu, M.; *et al.* MiRBase: From MicroRNA Sequences to Function. *Nucleic Acids Res* **2019**, *47* (D1), D155.

[34] Griffiths-Jones, S.; Grocock, R. J.; *et al.* MiRBase: MicroRNA Sequences, Targets and Gene Nomenclature. *Nucleic Acids Res* **2006**, *34* (Database issue).

[35] Wright, M. W.; Bruford, E. A. Naming "Junk": Human Non-Protein Coding RNA (NcRNA) Gene Nomenclature. *Hum Genomics* **2011**, *5* (2), 90.

[36] He, L.; Hannon, G. J. MicroRNAs: Small RNAs with a Big Role in Gene Regulation. *Nat Rev Genet* **2004**, *5* (7), 522.

[37] Wang, W. X.; Rajeev, B. W.; *et al.* The Expression of MicroRNA MiR-107 Decreases Early in Alzheimer's Disease and May Accelerate Disease Progression through Regulation of β-Site Amyloid Precursor Protein-Cleaving Enzyme 1. *Journal of Neuroscience* **2008**, *28* (5), 1213.

[38] Gehrke, S.; Imai, Y.; *et al.* Pathogenic LRRK2 Negatively Regulates MicroRNA-Mediated Translational Repression. *Nature* **2010**, *466* (7306), 637.

[39] Haramati, S.; Chapnik, E.; *et al.* MiRNA Malfunction Causes Spinal Motor Neuron Disease. *Proc Natl Acad Sci U S A* **2010**, *107* (29), 13111.

[40] Yang, B.; Lin, H.; *et al.* The Muscle-Specific MicroRNA MiR-1 Regulates Cardiac Arrhythmogenic Potential by Targeting GJA1 and KCNJ2. *Nat Med* **2007**, *13* (4), 486.

[41] Lewis, M. A.; Quint, E.; *et al.* An ENU-Induced Mutation of MiR-96 Associated with Progressive Hearing Loss in Mice. *Nat Genet* **2009**, *41* (5), 614.

[42] Thum, T.; Gross, C.; *et al.* MicroRNA-21 Contributes to Myocardial Disease by Stimulating MAP Kinase Signalling in Fibroblasts. *Nature* **2008**, *456* (7224), 980.

[43] Urdinguio, R. G.; Fernandez, A. F.; *et al.* Disrupted Microrna Expression Caused by Mecp2 Loss in a Mouse Model of Rett Syndrome. *Epigenetics* **2010**, *5* (7), 656.

[44] Hammond, S. M. MicroRNAs as Tumor Suppressors. *Nat Genet* **2007**, *39*, 582.

[45] Esquela-Kerscher, A.; Slack, F. J. Oncomirs - MicroRNAs with a Role in Cancer. *Nat Rev Cancer* **2006**, *6* (4), 259.

[46] Nicoloso, M. S. MicroRNAs — the Micro Steering of Tumour Metastases. *Nat Rev Cancer* **2009**, *9*, 293.

[47] Zhang, L.; Liao, Y.; *et al.* MicroRNA-34 Family: A Potential Tumor Suppressor and Therapeutic Candidate in Cancer. *Journal of Experimental and Clinical Cancer Research* **2019**, *38* (1).

[48] Kalfert, D.; Ludvikova, M.; *et al.* Multifunctional Roles of MiR-34a in Cancer: A Review with the Emphasis on Head and Neck Squamous Cell Carcinoma and Thyroid Cancer with Clinical Implications. *Diagnostics* **2020**, *10* (8), 563.

[49] Meng, F.; Henson, R.; *et al.* MicroRNA-21 Regulates Expression of the PTEN Tumor Suppressor Gene in Human Hepatocellular Cancer. *Gastroenterology* **2007**, *133* (2), 647.

[50] Asangani, I. A.; Rasheed, S. A. K.; *et al.* MicroRNA-21 (MiR-21) Post-Transcriptionally Downregulates Tumor Suppressor Pdcd4 and Stimulates Invasion, Intravasation and Metastasis in Colorectal Cancer. *Oncogene* **2008**, *27* (15), 2128.

[51] Calin, G. A.; Croce, C. M. MicroRNA Signatures in Human Cancers. *Nat Rev Cancer* **2006**, *6* (11), 857.

[52] Kim, V. N. MicroRNA Biogenesis: Coordinated Cropping and Dicing. *Nat Rev Mol Cell Biol* **2005**, *6* (5), 376.

[53] Winter, J.; Jung, S.; *et al.* Many Roads to Maturity: MicroRNA Biogenesis Pathways and Their Regulation. *Nat Cell Biol* **2009**, *11* (3).

[54] Denli, A. M.; Tops, B. B. J.; *et al.* Processing of Primary MicroRNAs by the Microprocessor Complex. *Nature* **2004**, *432*, 231.

[55] Han, J.; Lee, Y.; *et al.* The Drosha-DGCR8 Complex in Primary MicroRNA Processing. *Genes Dev* **2004**, *18* (24), 3016.

[56] Stillman, Bruce.; Stewart, D. J. (David J.; *et al. Regulatory RNAs*; Cold Spring Harbor Laboratory Press, 2006.

[57] Yoda, M.; Kawamata, T.; *et al.* ATP-Dependent Human RISC Assembly Pathways. *Nat Struct Mol Biol* **2010**, *17* (1), 17.

[58] Pratt, A. J.; MacRae, I. J. The RNA-Induced Silencing Complex: A Versatile Gene-Silencing Machine. *Journal of Biological Chemistry* **2009**, *284* (27), 17897.

[59] Huntzinger, E.; Izaurralde, E. Gene Silencing by MicroRNAs: Contributions of Translational Repression and MRNA Decay. *Nat Rev Genet* **2011**, *12* (2), 99.

[60] O'Brien, J.; Hayder, H.; *et al.* Overview of MicroRNA Biogenesis, Mechanisms of Actions, and Circulation. *Front Endocrinol (Lausanne)* **2018**, *9* (AUG).

[61] Yang, S.; Maurin, T.; *et al.* Conserved Vertebrate Mir-451 Provides a Platform for Dicer-Independent, Ago2-Mediated MicroRNA Biogenesis. *Proc Natl Acad Sci U S A* **2010**, *107* (34), 15163.

[62] Ruby, J. G.; Jan, C. H.; *et al.* Intronic MicroRNA Precursors That Bypass Drosha Processing. *Nature* **2007**, *448* (7149), 83.

[63] Morgan, B. S.; Hargrove, A. E. Synthetic Receptors for Oligonucleotides and Nucleic Acids. In *Monographs in Supramolecular Chemistry*; 2015; pp 253–325.

[64] Kenyon, J.; Prestwood, L.; *et al.* RNA UK 2014: Current Perspectives on RNA Secondary Structure Probing. *Biochem Soc Trans* **2014**, *42* (4), 1251.

[65] Rossor, A. M.; Reilly, M. M.; *et al.* Antisense Oligonucleotides and Other Genetic Therapies Made Simple. *Pract Neurol* **2018**, *18* (2), 126.

[66] Stenvang, J.; Petri, A.; *et al.* Inhibition of MicroRNA Function by AntimiR Oligonucleotides. *Silence* **2012**, *3* (1).

[67] Lima, J. F.; Cerqueira, L.; *et al.* Anti-MiRNA Oligonucleotides: A Comprehensive Guide for Design. *RNA Biol* **2018**, *15* (3), 338.

[68] Davis, S.; Lollo, B.; *et al.* Improved Targeting of MiRNA with Antisense Oligonucleotides. *Nucleic Acids Res* **2006**, *34* (8), 2294.

[69] Seto, A. G.; Beatty, X.; *et al.* Cobomarsen, an Oligonucleotide Inhibitor of MiR-155, Co-Ordinately Regulates Multiple Survival Pathways to Reduce Cellular Proliferation and Survival in Cutaneous T-Cell Lymphoma. *Br J Haematol* **2018**, *183* (3), 428.

[70] *RG-125(AZD4076), a microRNA Therapeutic Targeting microRNA-103/107 being Developed for the Treatment of NASH in Patients with Type 2 Diabetes/Pre-Diabetes, Enters Phase I Clinical Development*.

[71] Gebert, L. F. R.; Rebhan, M. A. E.; *et al.* Miravirsen (SPC3649) Can Inhibit the Biogenesis of MiR-122. *Nucleic Acids Res* **2014**, *42* (1), 609.

[72] Chioccioli, M.; Roy, S.; *et al.* A Lung Targeted MiR-29 Mimic as a Therapy for Pulmonary Fibrosis. *EBioMedicine* **2022**, *85*, 104304.

[73] Gomez, I. G.; MacKenna, D. A.; *et al.* Anti-MicroRNA-21 Oligonucleotides Prevent Alport Nephropathy Progression by Stimulating Metabolic Pathways. *Journal of Clinical Investigation* **2015**, *125* (1), 141.

[74] Hermann, T. Small Molecules Targeting Viral RNA. *Wiley Interdiscip Rev RNA* **2016**, *7* (6), 726.

[75] Wang, S.; Huber, P. W.; *et al.* Binding of Neomycin to the TAR Element of HIV-1 RNA Induces Dissociation of Tat Protein by an Allosteric Mechanism. *Biochemistry* **1998**, *37* (16), 5549.

[76] Martin, C.; De Piccoli, S.; *et al.* Unveiling RNA-Binding Properties of Verapamil and Preparation of New Derivatives as Inhibitors of HIV-1 Tat-TAR Interaction. *Chempluschem* **2020**, *85* (1), 207.

[77] Shortridge, M. D.; Varani, G. Structure Based Approaches for Targeting Non-Coding RNAs with Small Molecules. *Curr Opin Struct Biol* **2015**, *30*, 79.

[78] Velagapudi, S. P.; Vummidi, B. R.; *et al.* Small Molecule Chemical Probes of MicroRNA Function. *Curr Opin Chem Biol* **2015**, *24*, 97.

[79] Connelly, C. M.; Abulwerdi, F. A.; *et al.* Discovery of RNA Binding Small Molecules Using Small Molecule Microarrays. *Methods in Molecular Biology* **2017**, *1518*, 157.

[80] Connelly, C. M.; Boer, R. E.; *et al.* Discovery of Inhibitors of MicroRNA-21 Processing Using Small Molecule Microarrays. *ACS Chem Biol* **2017**, *12* (2), 435.

[81] Disney, M. D.; Labuda, L. P.; *et al.* Two-Dimensional Combinatorial Screening Identifies Specific Aminoglycoside-RNA Internal Loop Partners. *J Am Chem Soc* **2008**, *130* (33), 11185.

[82] Disney, M. D.; Angelbello, A. J. Rational Design of Small Molecules Targeting Oncogenic Noncoding RNAs from Sequence. *Acc Chem Res* **2016**, *49* (12), 2698.

[83] Velagapudi, S. P.; Disney, M. D. Two-Dimensional Combinatorial Screening Enables the Bottom-up Design of a MicroRNA-10b Inhibitor. *Chemical Communications* **2014**, *50* (23), 3027.

[84] Velagapudi, S. P.; Costales, M. G.; *et al.* Approved Anti-Cancer Drugs Target Oncogenic Non-Coding RNAs. *Cell Chem Biol* **2018**, *25* (9), 1086.

[85] Lorenz, D. A.; Song, J. M.; *et al.* High-Throughput Platform Assay Technology for the Discovery of Pre-Microrna-Selective Small Molecule Probes. *Bioconjug Chem* **2015**, *26* (1), 19.

[86] Lorenz, D. A.; Vander Roest, S.; *et al.* Development and Implementation of an HTS-Compatible Assay for the Discovery of Selective Small-Molecule Ligands for Pre-MicroRNAs. *SLAS Discovery* **2018**, *23* (1), 47.

[87] Lorenz, D. A.; Kaur, T.; *et al.* Expansion of Cat-ELCCA for the Discovery of Small Molecule Inhibitors of the Pre-Let-7-Lin28 RNA-Protein Interaction. *ACS Med Chem Lett* **2018**, *9* (6), 517.

[88] Gumireddy, K.; Young, D. D.; *et al.* Small-Molecule Inhibitors of MicroRNA MiR-21 Function. *Angewandte Chemie - International Edition* **2008**, *47* (39), 7482.

[89] Connelly, C. M.; Thomas, M.; *et al.* High-Throughput Luciferase Reporter Assay for Small-Molecule Inhibitors of MicroRNA Function. *J Biomol Screen* **2012**, *17* (6), 822.

[90] Naro, Y.; Ankenbruck, N.; *et al.* Small Molecule Inhibition of MicroRNA MiR-21 Rescues Chemosensitivity of Renal-Cell Carcinoma to Topotecan. *J Med Chem* **2018**, *61* (14), 5900.

[91] Ankenbruck, N.; Kumbhare, R.; *et al.* Small Molecule Inhibition of MicroRNA-21 Expression Reduces Cell Viability and Microtumor Formation. *Bioorg Med Chem* **2019**, *27* (16), 3735.

[92] Lee, S. Y.; Lee, S.; *et al.* Small Molecule-Mediated up-Regulation of MicroRNA Targeting a Key Cell Death Modulator BNIP3 Improves Cardiac Function Following Ischemic Injury. *Sci Rep* **2016**, *6* (1), 1.

[93] Mathews, D. H.; Disney, M. D.; *et al.* Incorporating Chemical Modification Constraints into a Dynamic Programming Algorithm for Prediction of RNA Secondary Structure. *Proc Natl Acad Sci U S A* **2004**, *101* (19), 7287.

[94] Paul, D. J.; Seedhouse, S. J.; *et al.* Two-Dimensional Combinatorial Screening and the RNA Privileged Space Predictor Program Efficiently Identify Aminoglycoside RNA Hairpin Loop Interactions. *Nucleic Acids Res* **2009**, *37* (17), 5894.

[95] Velagapudi, S. P.; Seedhouse, S. J.; *et al.* Structure-Activity Relationships through Sequencing (StARTS) Defines Optimal and Suboptimal RNA Motif Targets for Small Molecules. *Angewandte Chemie - International Edition* **2010**, *49* (22), 3816.

[96] Velagapudi, S. P.; Gallo, S. M.; *et al.* Sequence-Based Design of Bioactive Small Molecules That Target Precursor MicroRNAs. *Nat Chem Biol* **2014**, *10* (4), 291.

[97] Disney, M. D.; Winkelsas, A. M.; *et al.* Inforna 2.0: A Platform for the Sequence-Based Design of Small Molecules Targeting Structured RNAs. *ACS Chem Biol* **2016**, *11* (6), 1720.

[98] Disney, M. D.; Yildirim, I.; *et al.* Methods to Enable the Design of Bioactive Small Molecules Targeting RNA. *Org Biomol Chem* **2014**, *12* (7), 1029.

[99] Disney, M. D. Targeting RNA with Small Molecules To Capture Opportunities at the Intersection of Chemistry, Biology, and Medicine. *J Am Chem Soc* **2019**, *141* (17), 6776.

[100] Velagapudi, S. P.; Luo, Y.; *et al.* Defining RNA-Small Molecule Affinity Landscapes Enables Design of a Small Molecule Inhibitor of an Oncogenic Noncoding RNA. *ACS Cent Sci* **2017**, *3* (3), 205.

[101] Velagapudi, S. P.; Cameron, M. D.; *et al.* Design of a Small Molecule against an Oncogenic Noncoding RNA. *Proc Natl Acad Sci U S A* **2016**, *113* (21), 5898.

[102] Costales, M. G.; Haga, C. L.; *et al.* Small Molecule Inhibition of MicroRNA-210 Reprograms an Oncogenic Hypoxic Circuit. *J Am Chem Soc* **2017**, *139* (9), 3446.

[103] Haniff, H. S.; Liu, X.; *et al.* A Structure-Specific Small Molecule Inhibits a MiRNA-200 Family Member Precursor and Reverses a Type 2 Diabetes Phenotype. *Cell Chem Biol* **2022**, *29* (2), 300.

[104] Marušič, M.; Toplishek, M.; *et al.* NMR of RNA - Structure and Interactions. *Curr Opin Struct Biol* **2023**, *79*, 102532.

[105] Garavís, M.; López-Méndez, B.; *et al.* Discovery of Selective Ligands for Telomeric RNA G-Quadruplexes (TERRA) through 19F-NMR Based Fragment Screening. *ACS Chem Biol* **2014**, *9* (7), 1559.

[106] Shortridge, M. D.; Varani, G. Efficient NMR Screening Approach to Discover Small Molecule Fragments Binding Structured RNA. *ACS Med Chem Lett* **2021**, *12* (8), 1253.

[107] Abulwerdi, F. A.; Shortridge, M. D.; *et al.* Development of Small Molecules with a Noncanonical Binding Mode to HIV-1 Trans Activation Response (TAR) RNA. *J Med Chem* **2016**, *59* (24), 11148.

[108] Shortridge, M. D.; Chaubey, B.; *et al.* Drug-Like Small Molecules That Inhibit Expression of the Oncogenic MicroRNA-21. *ACS Chem Biol* **2023**, *18* (2), 237.

[109] Suresh, B. M.; Li, W.; *et al.* A General Fragment-Based Approach to Identify and Optimize Bioactive Ligands Targeting RNA. *Proc Natl Acad Sci U S A* **2020**, *117* (52), 33197.

[110] Deigan, K. E.; Li, T. W.; *et al.* Accurate SHAPE-Directed RNA Structure Determination. *Proc Natl Acad Sci U S A* **2009**, *106* (1), 97.

[111] Angelbello, A. J.; Disney, M. D. Bleomycin Can Cleave an Oncogenic Noncoding RNA. *ChemBioChem* **2018**, *19* (1), 43.

[112] Li, Y.; Disney, M. D. Precise Small Molecule Degradation of a Noncoding RNA Identifies Cellular Binding Sites and Modulates an Oncogenic Phenotype. *ACS Chem Biol* **2018**, *13* (11), 3065.

[113] Costales, M. G.; Matsumoto, Y.; *et al.* Small Molecule Targeted Recruitment of a Nuclease to RNA. *J Am Chem Soc* **2018**, *140* (22), 6741.

[114] Haj-Yahia, S.; Nandi, A.; *et al.* Targeted Degradation of Structured RNAs via Ribonuclease-Targeting Chimeras (RiboTacs). *Expert Opin Drug Discov* **2023**, *18* (8).

[115] Costales, M. G.; Suresh, B.; *et al.* Targeted Small Molecule Degradation of a Hypoxia-Associated Non-Coding RNA Enhances the Selectivity of an RNA Targeted Small Molecule. *Cell Chem Biol* **2019**, *26* (8), 1180.

[116] Tong, Y.; Lee, Y.; *et al.* Programming Inactive RNA-Binding Small Molecules into Bioactive Degraders. *Nature 2023 618:7963* **2023**, *618* (7963), 169.

[117] Shah, J. A.; Khattak, S.; *et al.* Potential Biomarkers of Mir-371–373 Gene Cluster in Tumorigenesis. *Life* **2021**, *11* (9).

[118] Tajik, F.; Alian, F.; *et al.* MicroRNA-372 Acts as a Double-Edged Sword in Human Cancers. *Heliyon* **2023**, *9* (5).

[119] Vo, D. D.; Staedel, C.; *et al.* Targeting the Production of Oncogenic MicroRNAs with Multimodal Synthetic Small Molecules. *ACS Chem Biol* **2014**, *9* (3), 711.

[120] Vo, D. D.; Becquart, C.; *et al.* Building of Neomycin-Nucleobase-Amino Acid Conjugates for the Inhibition of Oncogenic MiRNAs Biogenesis. *Org Biomol Chem* **2018**, *16* (34), 6262.

[121] Vo, D. D.; Tran, T. P. A.; *et al.* Oncogenic MicroRNAs Biogenesis as a Drug Target: Structure-Activity Relationship Studies on New Aminoglycoside Conjugates. *Chemistry - A European Journal* **2016**, *22* (15), 5350.

[122] Maucort, C.; Vo, D. D.; *et al.* Design and Implementation of Synthetic RNA Binders for the Inhibition of MiR-21 Biogenesis. *ACS Med Chem Lett* **2021**, *12* (6), 899.

[123] Yoshizawa, S.; Fourmy, D.; *et al.* Sequence-Specific Recognition of the Major Groove of RNA by Deoxystreptamine. *Biochemistry* **2002**, *41* (20), 6263.

[124] Tran, T. P. A.; Poulet, S.; *et al.* Development of 2-Deoxystreptamine–Nucleobase Conjugates for the Inhibition of Oncogenic MiRNA Production. *RSC Med Chem* **2022**, *13* (3), 311.

[125] Hecht, S. M. Bleomycin: New Perspectives on the Mechanism of Action. *J Nat Prod* **2000**, *63* (1), 158.

[126] Maucort, C.; Bonnet, M.; *et al.* Synthesis of Bleomycin-Inspired RNA Ligands Targeting the Biogenesis of Oncogenic MiRNAs. *J Med Chem* **2023**, *66* (15), 10639.

[127] Shcheholeva, I.; Fernández-Remacha, D.; *et al.* De Novo Design of Pre-miR-21 Maturation Inhibitors: Synthesis and Activity Assessment. *Chemistry – A European Journal* **2023**, *29* (40).

[128] Garber, K. Drugging RNA. *Nat Biotechnol* **2023**, *41*, 745.

[129] Huang, X.; Le, Q. T.; *et al.* MiR-210 - Micromanager of the Hypoxia Pathway. *Trends in Molecular Medicine*. May 2010, pp 230–237.

[130] Kulshreshtha, R.; Ferracin, M.; *et al.* A MicroRNA Signature of Hypoxia. *Mol Cell Biol* **2007**, *27* (5), 1859.

[131] Ivan, M.; Harris, A. L.; *et al.* Hypoxia Response and MicroRNAs: No Longer Two Separate Worlds. *J Cell Mol Med* **2008**, *12* (5a), 1426.

[132] Crosby, M.; Devlin, C.; *et al.* Emerging Roles of MicroRNAs in the Molecular Responses to Hypoxia. *Curr Pharm Des* **2009**, *15* (33), 3861.

[133] McCormick, R.; Buffa, F. M.; *et al.* The Role of Hypoxia Regulated MicroRNAs in Cancer. *Curr Top Microbiol Immunol* **2010**, *345*, 47.

[134] Nallamshetty, S.; Chan, S. Y.; *et al.* Hypoxia: A Master Regulator of MicroRNA Biogenesis and Activity. *Free Radic Biol Med* **2013**, *64*, 20.

[135] Gee, H. E.; Ivan, C.; *et al.* HypoxamiRs and Cancer: From Biology to Targeted Therapy. *Antioxid Redox Signal* **2014**, *21* (8), 1220.

[136] Chan, S. Y.; Loscalzo, J. MicroRNA-210: A Unique and Pleiotropic Hypoxamir. *Cell Cycle* **2010**, *9* (6), 1072.

[137] Ivan, M.; Huang, X. MiR-210: Fine-Tuning the Hypoxic Response. *Adv Exp Med Biol* **2014**, *772*, 205.

[138] Camps, C.; Buffa, F. M.; *et al.* Hsa-MiR-210 Is Induced by Hypoxia and Is an Independent Prognostic Factor in Breast Cancer. *Clin Cancer Res* **2008**, *14* (5), 1340.

[139] Semenza, G. L. Targeting HIF-1 for Cancer Therapy. *Nat Rev Cancer* **2003**, *3* (10), 721.

[140] Harris, A. L. Hypoxia - A Key Regulatory Factor in Tumour Growth. *Nat Rev Cancer* **2002**, *2* (1), 38.

[141] Semenza, G. L. HIF-1 and Tumor Progression: Pathophysiology and Therapeutics. *Trends Mol Med* **2002**, *8*.

[142] Kelly, T. J.; Souza, A. L.; *et al.* A Hypoxia-Induced Positive Feedback Loop Promotes Hypoxia-Inducible Factor 1α Stability through MiR-210 Suppression of Glycerol-3-Phosphate Dehydrogenase 1-Like. *Mol Cell Biol* **2011**, *31* (13), 2696.

[143] Hui, X.; Al-Ward, H.; *et al.* The Role of MiR-210 in the Biological System: A Current Overview. *Hum Hered* **2020**, *84* (6), 233.

[144] Khalilian, S.; Bijanvand, A.; *et al.* A Review on the Role of MiR-210 in Human Disorders. *Pathol Res Pract* **2023**, *241*, 154244.

[145] Zaccagnini, G.; Maimone, B.; *et al.* Overexpression of MiR-210 and Its Significance in Ischemic Tissue Damage. *Sci Rep* **2017**, *7* (1).

[146] Fasanaro, P.; D'Alessandra, Y.; *et al.* MicroRNA-210 Modulates Endothelial Cell Response to Hypoxia and Inhibits the Receptor Tyrosine Kinase Ligand Ephrin-A3. *J Biol Chem* **2008**, *283* (23), 15878.

[147] Pulkkinen, K.; Malm, T.; *et al.* Hypoxia Induces MicroRNA MiR-210 in Vitro and in Vivo Ephrin-A3 and Neuronal Pentraxin 1 Are Potentially Regulated by MiR-210. *FEBS Lett* **2008**, *582* (16), 2397.

[148] Hu, S.; Huang, M.; *et al.* MicroRNA-210 as a Novel Therapy for Treatment of Ischemic Heart Disease. *Circulation* **2010**, *122* (11 Suppl), S124.

[149] Liu, F.; Lou, Y. L.; *et al.* Upregulation of MicroRNA-210 Regulates Renal Angiogenesis Mediated by Activation of VEGF Signaling Pathway under Ischemia/Perfusion Injury in Vivo and in Vitro. *Kidney Blood Press Res* **2012**, *35* (3), 182.

[150] Bertero, T.; Rezzonico, R.; *et al.* Impact of MicroRNAs in the Cellular Response to Hypoxia. *Int Rev Cell Mol Biol* **2017**, *333*, 91.

[151] Taylor, C. T.; Doherty, G.; *et al.* Hypoxia-Dependent Regulation of Inflammatory Pathways in Immune Cells. *J Clin Invest* **2016**, *126* (10), 3716.

[152] Germana, Z.; Simona, G.; *et al.* Hypoxia-Induced MiR-210 Modulates the Inflammatory Response and Fibrosis upon Acute Ischemia. *Cell Death Dis* **2021**, *12* (5).

[153] Kieran, N. W.; Suresh, R.; *et al.* MicroRNA-210 Regulates the Metabolic and Inflammatory Status of Primary Human Astrocytes. *J Neuroinflammation* **2022**, *19* (1).

[154] Wang, H.; Flach, H.; *et al.* Negative Regulation of Hif1a Expression and TH17 Differentiation by the Hypoxia-Regulated MicroRNA MiR-210. *Nat Immunol* **2014**, *15* (4), 393.

[155] Noman, M. Z.; Janji, B.; *et al.* Tumor-Promoting Effects of Myeloid-Derived Suppressor Cells Are Potentiated by Hypoxia-Induced Expression of MiR-210. *Cancer Res* **2015**, *75* (18), 3771.

[156] Chan, S. Y.; Zhang, Y. Y.; *et al.* MicroRNA-210 Controls Mitochondrial Metabolism during Hypoxia by Repressing the Iron-Sulfur Cluster Assembly Proteins ISCU1/2. *Cell Metab* **2009**, *10* (4), 273.

[157] Tong, W. H.; Rouault, T. A. Functions of Mitochondrial ISCU and Cytosolic ISCU in Mammalian Iron-Sulfur Cluster Biogenesis and Iron Homeostasis. *Cell Metab* **2006**, *3* (3), 199.

[158] Denko, N. C. Hypoxia, HIF1 and Glucose Metabolism in the Solid Tumour. *Nat Rev Cancer* **2008**, *8* (9), 705.

[159] Favaro, E.; Ramachandran, A.; *et al.* MicroRNA-210 Regulates Mitochondrial Free Radical Response to Hypoxia and Krebs Cycle in Cancer Cells by Targeting Iron Sulfur Cluster Protein ISCU. *PLoS One* **2010**, *5* (4), 10345.

[160] Grosso, S.; Doyen, J.; *et al.* MiR-210 Promotes a Hypoxic Phenotype and Increases Radioresistance in Human Lung Cancer Cell Lines. *Cell Death Dis* **2013**, *4* (3).

[161] Song, R.; Dasgupta, C.; *et al.* MicroRNA-210 Controls Mitochondrial Metabolism and Protects Heart Function in Myocardial Infarction. *Circulation* **2022**, *145* (15), 1140.

[162] Ismaeel, A.; FLETCHER, E. M. M. A.; *et al.* Skeletal Muscle MiR-210 Expression Is Associated with Mitochondrial Function in Peripheral Artery Disease Patients. *Translational Research* **2022**, *246*, 66.

[163] Okamoto, M.; Nasu, K.; *et al.* Enhanced MiR-210 Expression Promotes the Pathogenesis of Endometriosis through Activation of Signal Transducer and Activator of Transcription 3. *Human Reproduction* **2015**, *30* (3), 632.

[164] Lee, D. W.; Futami, M.; *et al.* Loss of SHIP-1 Protein Expression in High-Risk Myelodysplastic Syndromes Is Associated with MiR-210 and MiR-155. *Oncogene* **2012**, *31* (37), 4085.

[165] Wei, S.; Qiu, Y. MiR-210-5p Regulates STAT3 Activation by Targeting STAT5A in the Differentiation of Dermal Fibroblasts. *3 Biotech* **2021**, *11* (5).

[166] Wu, R.; Zeng, J.; *et al.* MicroRNA-210 Overexpression Promotes Psoriasis-like Inflammation by Inducing Th1 and Th17 Cell Differentiation. *Journal of Clinical Investigation* **2018**, *128* (6), 2551.

[167] Tian, H.; Zhao, Y.; *et al.* Expression of MiR-210, MiR-137, and MiR-153 in Patients with Acute Cerebral Infarction. *Biomed Res Int* **2021**, *2021*.

[168] Zheng, L.; Zhuang, C.; *et al.* Serum MiR-146a, MiR-155, and MiR-210 as Potential Markers of Graves' Disease. *J Clin Lab Anal* **2018**, *32* (2).

[169] Bertero, T.; Robbe-Sermesant, K.; *et al.* MicroRNA Target Identification: Lessons from HypoxamiRs. *Antioxid Redox Signal* **2014**, *21* (8), 1249.

[170] Bertero, T.; Grosso, S.; *et al.* "Seed-Milarity" Confers to Hsa-MiR-210 and Hsa-MiR-147b Similar Functional Activity. *PLoS One* **2012**, *7* (9).

[171] Yoshioka, Y.; Kosaka, N.; *et al.* Micromanaging Iron Homeostasis: Hypoxia-Inducible Micro-RNA-210 Suppresses Iron Homeostasis-Related Proteins. *J Biol Chem* **2012**, *287* (41), 34110.

[172] Crosby, M. E.; Kulshreshtha, R.; *et al.* MicroRNA Regulation of DNA Repair Gene Expression in Hypoxic Stress. *Cancer Res* **2009**, *69* (3), 1221.

[173] Fasanaro, P.; Greco, S.; *et al.* An Integrated Approach for Experimental Target Identification of Hypoxia-Induced MiR-210. *J Biol Chem* **2009**, *284* (50), 35134.

[174] Huang, X.; Ding, L.; *et al.* Hypoxia Inducible Mir-210 Regulates Normoxic Gene Expression Involved in Tumor Initiation. *Mol Cell* **2009**, *35* (6), 856.

[175] Yang, W.; Sun, T.; *et al.* Downregulation of MiR-210 Expression Inhibits Proliferation, Induces Apoptosis and Enhances Radiosensitivity in Hypoxic Human Hepatoma Cells in Vitro. *Exp Cell Res* **2012**, *318* (8), 944.

[176] Fasanaro, P.; Romani, S.; *et al.* ROD1 Is a Seedless Target Gene of Hypoxia-Induced MiR-210. *PLoS One* **2012**, *7* (9), 44651.

[177] Liu, Y.; Han, Y.; *et al.* Synthetic MiRNA-Mowers Targeting MiR-183-96-182 Cluster or MiR-210 Inhibit Growth and Migration and Induce Apoptosis in Bladder Cancer Cells. *PLoS One* **2012**, *7* (12), 52280.

[178] Ren, J.; Li, X.; *et al.* MiR-210-3p Regulates the Proliferation and Apoptosis of Non-small Cell Lung Cancer Cells by Targeting SIN3A. *Exp Ther Med* **2019**, *18* (4), 2565.

[179] Gou, D.; Ramchandran, R.; *et al.* MiR-210 Has an Antiapoptotic Effect in Pulmonary Artery Smooth Muscle Cells during Hypoxia. *Am J Physiol Lung Cell Mol Physiol* **2012**, *303* (8), 682.

[180] Wang, F.; Xiong, L.; *et al.* MiR-210 Suppresses BNIP3 to Protect against the Apoptosis of Neural Progenitor Cells. *Stem Cell Res* **2013**, *11* (1), 657.

[181] Kim, H. W.; Haider, H. K.; *et al.* Ischemic Preconditioning Augments Survival of Stem Cells via MiR-210 Expression by Targeting Caspase-8-Associated Protein 2. *J Biol Chem* **2009**, *284* (48), 33161.

[182] Grosso, S.; Doyen, J.; *et al.* MiR-210 Promotes a Hypoxic Phenotype and Increases Radioresistance in Human Lung Cancer Cell Lines. *Cell Death Dis* **2013**, *4* (3).

[183] Cann, K. L.; Hicks, G. G. Regulation of the Cellular DNA Double-Strand Break Response. *Biochemistry and Cell Biology* **2007**, *85* (6), 663.

[184] Hanahan, D.; Weinberg, R. A. Hallmarks of Cancer: The next Generation. *Cell* **2011**, *144* (5), 646.

[185] Crosby, M. E.; Kulshreshtha, R.; *et al.* MicroRNA Regulation of DNA Repair Gene Expression in Hypoxic Stress. *Cancer Res* **2009**, *69* (3), 1221.

[186] Kim, J. H.; Park, S. G.; *et al.* Reactive Oxygen Species-Responsive MiR-210 Regulates Proliferation and Migration of Adipose-Derived Stem Cells via PTPN2. *Cell Death Dis* **2013**, *4* (4).

[187] He, J.; Wu, J.; *et al.* MiR-210 Disturbs Mitotic Progression through Regulating a Group of Mitosis-Related Genes. *Nucleic Acids Res* **2013**, *41* (1), 498.

[188] Giannakakis, A.; Sandaltzopoulos, R.; *et al.* MiR-210 Links Hypoxia with Cell Cycle Regulation and Is Deleted in Human Epithelial Ovarian Cancer. *Cancer Biol Ther* **2008**, *7* (2), 255.

[189] Tsuchiya, S.; Fujiwara, T.; *et al.* MicroRNA-210 Regulates Cancer Cell Proliferation through Targeting Fibroblast Growth Factor Receptor-like 1 (FGFRL1). *J Biol Chem* **2011**, *286* (1), 420.

[190] Chio, C. C.; Lin, J. W.; *et al.* MicroRNA-210 Targets Antiapoptotic Bcl-2 Expression and Mediates Hypoxia-Induced Apoptosis of Neuroblastoma Cells. *Arch Toxicol* **2013**, *87* (3), 459.

[191] Feng, S.; He, A.; *et al.* Diagnostic Significance of MiR-210 as a Potential Tumor Biomarker of Human Cancer Detection: An Updated Pooled Analysis of 30 Articles. *Onco Targets Ther* **2019**, *12*, 479.

[192] Rothé, F.; Ignatiadis, M.; *et al.* Global MicroRNA Expression Profiling Identifies MiR-210 Associated with Tumor Proliferation, Invasion and Poor Clinical Outcome in Breast Cancer. *PLoS One* **2011**, *6* (6), 20980.

[193] Toyama, T.; Kondo, N.; *et al.* High Expression of MicroRNA-210 Is an Independent Factor Indicating a Poor Prognosis in Japanese Triple-Negative Breast Cancer Patients. *Jpn J Clin Oncol* **2012**, *42* (4), 256.

[194] Pasculli, B.; Barbano, R.; *et al.* Hsa-MiR-210-3p Expression in Breast Cancer and Its Putative Association with Worse Outcome in Patients Treated with Docetaxel. *Sci Rep* **2019**, *9* (1), 1.

[195] Du, Y.; Wei, N.; *et al.* A MiR-210-3p Regulon That Controls the Warburg Effect by Modulating HIF-1α and P53 Activity in Triple-Negative Breast Cancer. *Cell Death Dis* **2020**, *11* (9), 1.

[196] Scapoli, L.; Palmieri, A.; *et al.* MicroRNA Expression Profiling of Oral Carcinoma Identifies New Markers of Tumor Progression. *Int J Immunopathol Pharmacol* **2010**, *23* (4), 1229.

[197] Gee, H. E.; Camps, C.; *et al.* Hsa-Mir-210 Is a Marker of Tumor Hypoxia and a Prognostic Factor in Head and Neck Cancer. *Cancer* **2010**, *116* (9), 2148.

[198] Greither, T.; Grochola, L. F.; *et al.* Elevated Expression of MicroRNAs 155, 203, 210 and 222 in Pancreatic Tumors Is Associated with Poorer Survival. *Int J Cancer* **2010**, *126* (1), 73.

[199] Sun, F.; Lyn, Y.; *et al.* MiR-210 Regulates Pancreatic Cancer Development. *Eur Rev Med Pharmacol Sci* **2018**, *22*.

[200] Miko, E.; Czimmerer, Z.; *et al.* Differentially Expressed Micrornas in Small Cell Lung Cancer. *Exp Lung Res* **2009**, *35* (8), 646.

[201] Puisségur, M. P.; Mazure, N. M.; *et al.* MiR-210 Is Overexpressed in Late Stages of Lung Cancer and Mediates Mitochondrial Alterations Associated with Modulation of HIF-1 Activity. *Cell Death Differ* **2011**, *18* (3), 465.

[202] Chen, Q.; Zhang, H.; *et al.* Mir-210-3p Promotes Lung Cancer Development and Progression by Modulating Usf1 and Pcgf3. *Onco Targets Ther* **2021**, *14*, 3687.

[203] Arora, L.; Patra, D.; *et al.* Hypoxia-Induced MiR-210-3p Expression in Lung Adenocarcinoma Potentiates Tumor Development by Regulating CCL2-Mediated Monocyte Infiltration. *Mol Oncol* **2023**.

[204] Neal, C. S.; Michael, M. Z.; *et al.* The VHL-Dependent Regulation of MicroRNAs in Renal Cancer. *BMC Med* **2010**, *8*.

[205] McCormick, R. I.; Blick, C.; *et al.* MiR-210 Is a Target of Hypoxia-Inducible Factors 1 and 2 in Renal Cancer, Regulates ISCU and Correlates with Good Prognosis. *Br J Cancer* **2013**, *108* (5), 1133.

[206] Wang, X.; Wang, T.; *et al.* Serum Exosomal MiR-210 as a Potential Biomarker for Clear Cell Renal Cell Carcinoma. *J Cell Biochem* **2019**, *120* (2), 1492.

[207] Petrozza, V.; Costantini, M.; *et al.* Emerging Role of Secreted MiR-210-3p as Potential Biomarker for Clear Cell Renal Cell Carcinoma Metastasis. *Cancer Biomarkers* **2020**, *27* (2), 181.

[208] Cai, H.; Lin, L.; *et al.* Prognostic Evaluation of MicroRNA-210 Expression in Pediatric Osteosarcoma. *Medical Oncology* **2013**, *30* (2).

[209] Liu, W.; Jiang, D.; *et al.* MiR-210-5p Promotes Epithelial–Mesenchymal Transition by Inhibiting PIK3R5 Thereby Activating Oncogenic Autophagy in Osteosarcoma Cells. *Cell Death Dis* **2020**, *11* (2).

[210] Zhang, J.; Chou, X.; *et al.* CircKMT2D Contributes to H2O2-Attenuated Osteosarcoma Progression via the MiR-210/Autophagy Pathway. *Exp Ther Med* **2020**, *20* (5), 1.

[211] Liu, S. G.; Qin, X. G.; *et al.* Differential Expression of MiRNAs in Esophageal Cancer Tissue. *Oncol Lett* **2013**, *5* (5), 1639.

[212] Vaksman, O.; Stavnes, H. T.; *et al.* MiRNA Profiling along Tumour Progression in Ovarian Carcinoma. *J Cell Mol Med* **2011**, *15* (7), 1593.

[213] Zhao, Y.; Liu, S.; *et al.* Effect of MicroRNA-210 on the Growth of Ovarian Cancer Cells and the Efficacy of Radiotherapy. *Gynecol Obstet Invest* **2021**, *86* (1–2), 71.

[214] Schibler, U.; Sassone-Corsi, P. A Web of Circadian Pacemakers. *Cell* **2002**, *111*, 919.

[215] Dibner, C.; Schibler, U.; *et al.* The Mammalian Circadian Timing System: Organization and Coordination of Central and Peripheral Clocks. *Annu Rev Physiol* **2010**, *72*, 517.

[216] Ko, C. H.; Takahashi, J. S. Molecular Components of the Mammalian Circadian Clock. *Hum Mol Genet* **2006**, *15*.

[217] Hastings, M. H.; Reddy, A. B.; *et al.* A Clockwork Web: Circadian Timing in Brain and Periphery, in Health and Disease. *Nat Rev Neurosci* **2003**, *4* (8), 649.

[218] Lee, Y. Roles of Circadian Clocks in Cancer Pathogenesis and Treatment. *Exp Mol Med* **2021**, *53* (10), 1529.

[219] Shearman, L. P.; Sriram, S.; *et al.* Interacting Molecular Loops in the Mammalian Circadian Clock. *Science (1979)* **2000**, *288*.

[220] Gijsbertus T. J., V. der H.; Manja, M.; *et al.* Mammalian Cry1 and Cry2 Are Essential for Maintenance of Circadian Rhythms. *Nature* **1999**, *398*, 627.

[221] Zheng, B.; Albrecht, U.; *et al.* Nonredundant Roles of the MPer1 and MPer2 Genes in the Mammalian Circadian Clock. *Cell* **2001**, *105*, 683.

[222] Cho, H.; Zhao, X.; *et al.* Regulation of Circadian Behaviour and Metabolism by REV-ERB-α and REV-ERB-β. *Nature* **2012**, *485* (7396), 123.

[223] Miller, B. H.; Mcdearmon, E. L.; *et al.* Circadian and CLOCK-Controlled Regulation of the Mouse Transcriptome and Cell Proliferation. *Proc Natl Acad Sci U S A* **2007**, *104*, 3342.

[224] Altman, B. J.; Hsieh, A. L.; *et al.* MYC Disrupts the Circadian Clock and Metabolism in Cancer Cells. *Cell Metab* **2015**, *22* (6), 1009.

[225] Blaževitš, O.; Bolshette, N.; *et al.* MYC-Associated Factor Max Is a Regulator of the Circadian Clock. *Int J Mol Sci* **2020**, *21* (7).

[226] Burchett, J. B.; Knudsen-Clark, A. M.; *et al.* MYC Ran Up the Clock: The Complex Interplay between MYC and the Molecular Circadian Clock in Cancer. *Int J Mol Sci* **2021**, *22* (14), 7761.

[227] Shostak, A.; Ruppert, B.; *et al.* MYC/MIZ1-Dependent Gene Repression Inversely Coordinates the Circadian Clock with Cell Cycle and Proliferation. *Nat Commun* **2016**, *7*.

[228] Grandori, C.; Cowley, S. M.; *et al.* The MYC/MAX/MAD Network and the Transcriptional Control of Cell Behavior. *Annu. Rev. Cell Dev. Biol* **2000**, *16*, 653.

[229] Yang, G.; Hurlin, P. J. MNT and Emerging Concepts of MNT-MYC Antagonism. *Genes (Basel)* **2017**, *8* (2).

[230] Yu, C.; Yang, S. L.; *et al.* Hypoxia Disrupts the Expression Levels of Circadian Rhythm Genes in Hepatocellular Carcinoma. *Mol Med Rep* **2015**, *11* (5), 4002.

[231] Cheng, H. Y. M.; Obrietan, K. Revealing a Role of MicroRNAs in the Regulation of the Biological Clock. *Cell Cycle* **2007**, *6* (24), 3034.

[232] Hansen, K. F.; Sakamoto, K.; *et al.* MicroRNAs: A Potential Interface between the Circadian Clock and Human Health. *Genome Med* **2011**, *3*.

[233] Zhang, Z.; Sun, H.; *et al.* MicroRNA MiR-210 Modulates Cellular Response to Hypoxia through the MYC Antagonist MNT. *Cell Cycle* **2009**, *8* (17), 2756.

[234] Bodempudi, V.; Hergert, P.; *et al.* MiR-210 Promotes IPF Fibroblast Proliferation in Response to Hypoxia. *Am J Physiol Lung Cell Mol Physiol* **2014**, *307*, 283.

[235] Tran, T. P. A.; Vo, D. D.; *et al.* Ribosome-Targeting Antibiotics as Inhibitors of Oncogenic MicroRNAs Biogenesis: Old Scaffolds for New Perspectives in RNA Targeting. *Bioorg Med Chem* **2015**, *23* (17), 5334.

[236] Hoebrecker, F. Benzimidazole. *Ber* **1872**, *5*.

[237] Ladenburg, A. Benzimidazole. *Ber* **1875**, *8*.

[238] Wundt. Derivate Der Phenylendiamine. *Ber* **1878**, *11*.

[239] Wright, J. B. The Chemistry of the Benzimidazoles. *Chem Rev* **1951**, *48*.

[240] Faheem, M.; Rathaur, A.; *et al.* A Review on the Modern Synthetic Approach of Benzimidazole Candidate. *ChemistrySelect* **2020**, *5* (13), 3981.

[241] Woolley, D. W. SOME BIOLOGICAL EFFECTS PRODUCED BY BENZIMIDAZOLE AND THEIR REVERSAL BY PURINES. *Journal of Biological Chemistry* **1944**, *152* (2), 225.

[242] Brink, N. G.; Flokers, K. Biochemistry of Vitamin B12 with 5,6-Dimethylbenzimidazole as the Degradation Product. *J. Am. Chem. Soc.* **1949**, *71*.

[243] Emerson, G.; Brink, N. G.; *et al.* The Detection of Reverse Mutations at the Mtr Locus in Neurospora and Evidence of Possible Intragenic (Second Site) Suppresor Mutations. *J. Am. Chem. Soc.* **1950**, *72*.

[244] Rossignol, J. F.; Maisonneuve, H. Benzimidazoles in the Treatment of Trichuriasis: A Review. *Ann Trop Med Parasitol* **1984**, *78* (2), 135.

[245] McKELLAR, Q. A.; SCOTT, E. W. The Benzimidazole Anthelmintic Agents--a Review. *J Vet Pharmacol Ther* **1990**, *13* (3), 223.

[246] Boiani, M.; Gonzalez, M. Imidazole and Benzimidazole Derivatives as Chemotherapeutic Agents. *Mini Rev Med Chem* **2005**, *5* (4), 409.

[247] Patil, A.; Ganguly, S.; *et al.* A Systematic Review of Benzimidazole Derivates as an Antiulcer Agent. *J. Chem.* **2008**, *1* (3), 447.

[248] Narasimhan, B.; Sharma, D.; *et al.* Benzimidazole: A Medicinally Important Heterocyclic Moiety. *Medicinal Chemistry Research* **2012**, *21* (3), 269.

[249] Jiménez-Juárez, R.; Cruz-Chávez, W.; *et al.* Synthesis and Antimycobacterial Activity of 2,5-Disubstituted and 1,2,5-Trisubstituted Benzimidazoles. *Front Chem* **2020**, *8*, 433.

[250] Banerjee, S.; Mukherjee, S.; *et al.* A Critical Review of Benzimidazole: Sky-High Objectives towards the Lead Molecule to Predict the Future in Medicinal Chemistry. *Results Chem* **2023**, *6*, 101013.

[251] Latt, S. A.; Stetten, G.; *et al.* RECENT DEVELOPMENTS IN THE DETECTION OF DEOXYRIBONUCLEIC ACID SYNTHESIS BY 33258 HOECHST FLUORESCENCE1'2. *Journal of Histochemistry & Cytochemistry* **1975**, *23* (7), 493.

[252] Latt, S. A.; Stetten', G. SPECTRAL STUDIES ON 33258 HOECHST AND RELATED BISBENZIMIDAZOLE DYES USEFUL FOR FLUORESCENT DETECTION OF DEOXYRIBONUCLEIC ACID SYNTHESIS. *Journal of Histochemistry & Cytochemistry* **1976**, *24* (1), 24.

[253] Bucevičius, J.; Lukinavičius, G.; *et al.* The Use of Hoechst Dyes for DNA Staining and Beyond. *Chemosensors* **2018**, *6* (2).

[254] Cho, J.; Rando, R. R. Specific Binding of Hoechst 33258 to Site 1 Thymidylate Synthase MRNA. *Nucleic Acids Res* **2000**, *28* (10), 2158.

[255] Velagapudi, S. P.; Seedhouse, S. J.; *et al.* Defining the RNA Internal Loops Preferred by Benzimidazole Derivatives via 2D Combinatorial Screening and Computational Analysis. *J Am Chem Soc* **2011**, *133* (26), 10111.

[256] King, F. E.; Acheson, R. M. 297. The Synthesis of Benziminazoles from Ortho-Phenylenediamines and Imino-Ethers. *J Chem Soc* **1949**, 1396.

[257] Argentini, M.; Dos Santos, D. F.; *et al.* Synthesis of an O-Carboranyl Derivative of 4-[5-(4-Methyl-1-Piperazinyl)-2,5'-Bi-1H-Benzimidazol-2'-Yl]Phenol. *Inorg Chem* **1998**, *37* (23), 6018.

[258] Ridley, H. F.; Spickett, R. G. W.; *et al.* A New Synthesis of Benzimidazoles and Aza-Analogs. *J Heterocycl Chem* **1965**, *2* (4), 453.

[259] Eren, B.; Bekdemir, Y. Simple, Mild, and Highly Efficient Synthesis of 2-Substituted Benzimidazoles and Bisbenzimidazoles. *Quim Nova* **2014**, *37* (4), 643.

[260] Singh, M.; Tandon, V. Synthesis and Biological Activity of Novel Inhibitors of Topoisomerase I: 2-Aryl-Substituted 2-Bis-1H-Benzimidazoles. *Eur J Med Chem* **2011**, *46* (2), 659.

[261] Yang, F.; Wang, C.; *et al.* Hoechst-Naphthalimide Dyad with Dual Emissions as Specific and Ratiometric Sensor for Nucleus DNA Damage. *Chinese Chemical Letters* **2017**, *28* (10), 2019.

[262] Özil, M.; Parlak, C.; *et al.* A Simple and Efficient Synthesis of Benzimidazoles Containing Piperazine or Morpholine Skeleton at C-6 Position as Glucosidase Inhibitors with Antioxidant Activity. *Bioorg Chem* **2018**, *76*, 468.

[263] Maji, B.; Kumar, K.; *et al.* Design and Synthesis of New Benzimidazole-Carbazole Conjugates for the Stabilization of Human Telomeric DNA, Telomerase Inhibition, and Their Selective Action on Cancer Cells. *J Med Chem* **2014**, *57* (16), 6973.

[264] Hall, M.; Kirkland, T.; *et al.* Cell Impermeable Coelenterazine Analogues. JP2020510617A, 2018.

[265] De La Fuente, T.; Martín-Fontecha, M.; *et al.* Benzimidazole Derivatives as New Serotonin 5-HT6 Receptor Antagonists. Molecular Mechanisms of Receptor Inactivation. *J Med Chem* **2010**, *53* (3), 1357.

[266] Kelly, D. P.; Stuart Bateman, B. A.; *et al.* DNA Binding Compounds. V. Synthesis and Characterization of Boron-Containing Bibenzimidazoles Related to the DNA Minor Groove Binder, Hoechst 33258. *Aust. J. Chem* **1994**, *47*, 247.

[267] Boggu, P. R.; Venkateswararao, E.; *et al.* Exploration of SAR for Novel 2-Benzylbenzimidazole Analogs as Inhibitor of Transcription Factor NF-KB. *Arch Pharm Res* **2017**, *40* (4), 469.

[268] Llano-Sotelo, B.; Chow, C. S. RNA-Aminoglycoside Antibiotic Interactions: Fluorescence Detection of Binding and Conformational Change. *Bioorg Med Chem Lett* **1999**, *9*, 213.

[269] Chavez, K. J.; Garimella, S. V.; *et al.* Triple Negative Breast Cancer Cell Lines: One Tool in the Search for Better Treatment of Triple Negative Breast Cancer. *Breast Dis* **2011**, *32* (1–2), 35.

[270] Hirsilä, M.; Koivunen, P.; *et al.* Effect of Desferrioxamine and Metals on the Hydroxylases in the Oxygen Sensing Pathway. *FASEB J* **2005**, *19* (10), 1308.

[271] Muñoz-Sánchez, J.; Chánez-Cárdenas, M. E. The Use of Cobalt Chloride as a Chemical Hypoxia Model. *Journal of Applied Toxicology* **2019**, *39* (4), 556.

[272] Nepali, K.; Lee, H. Y.; *et al.* Nitro-Group-Containing Drugs. *J Med Chem* **2019**, *62* (6), 2851.

[273] Umezawa, H.; Maeda, K.; *et al.* New Antibiotics, Bleomycin A and B. *J Antibiot (Tokyo)* **1966**, *19* (5).

[274] Einhorn, L. H. Curing Metastatic Testicular Cancer. *Proc Natl Acad Sci U S A* **2002**, *99* (7), 4592.

[275] Goodwin, K. D.; Lewis, M. A.; *et al.* Crystal Structure of DNA-Bound Co(III)·bleomycin B2: Insights on Intercalation and Minor Groove Binding. *Proc Natl Acad Sci U S A* **2008**, *105* (13), 5052.

[276] Chen, J.; Stubbe, J. A. Bleomycins: Towards Better Therapeutics. *Nat Rev Cancer* **2005**, *5* (2), 102.

[277] Yu, Z.; Schmaltz, R. M.; *et al.* Selective Tumor Cell Targeting by the Disaccharide Moiety of Bleomycin. *J Am Chem Soc* **2013**, *135* (8), 2883.

[278] Bhattacharya, C.; Yu, Z.; *et al.* The Carbamoylmannose Moiety of Bleomycin Mediates Selective Tumor Cell Targeting. *Biochemistry* **2014**, *53* (20), 3264.

[279] Schroeder, B. R.; Ghare, M. I.; *et al.* The Disaccharide Moiety of Bleomycin Facilitates Uptake by Cancer Cells. *J Am Chem Soc* **2014**, *136* (39), 13641.

[280] Kuwahara, J.; Sugiura, Y. Sequence-Specific Recognition and Cleavage of DNA by Metallobleomycin: Minor Groove Binding and Possible Interaction Mode. *Proc Natl Acad Sci U S A* **1988**, *85* (8), 2459.

[281] Rana, T. M.; Meares, C. F. Transfer of Oxygen from an Artificial Protease to Peptide Carbon during Proteolysis. *Proc Natl Acad Sci U S A* **1991**, *88* (23), 10578.

[282] Ekimoto, H.; Takahashi, K.; *et al.* Lipid Peroxidation by Bleomycin-Iron Complexes in Vitro. *J Antibiot (Tokyo)* **1985**, *38* (8), 1077.

[283] Magliozzo, R. S.; Peisach, J.; *et al.* Transfer RNA Is Cleaved by Activated Bleomycin. *Mol Pharmacol* **1989**, *35* (4).

[284] Huang, Y.; Yang, Y. B.; *et al.* MicroRNA-21 Gene and Cancer. *Medical Oncology* **2013**, *30* (1).

[285] Bautista-Sánchez, D.; Arriaga-Canon, C.; *et al.* The Promising Role of MiR-21 as a Cancer Biomarker and Its Importance in RNA-Based Therapeutics. *Mol Ther Nucleic Acids* **2020**, *20*, 409.

[286] Hu, J.; Liu, Z.; *et al.* LS-Align: An Atom-Level, Flexible Ligand Structural Alignment Algorithm for High-Throughput Virtual Screening. *Bioinformatics* **2018**, *34* (13), 2209.

[287] Mishra, I.; Mishra, R.; *et al.* A Retrospect on Antimicrobial Potential of Thiazole Scaffold. *J Heterocycl Chem* **2020**, *57* (6), 2304.

[288] Petrou, A.; Fesatidou, M.; *et al.* Thiazole Ring—a Biologically Active Scaffold. *Molecules* **2021**, *26* (11).

[289] Niu, Z. X.; Wang, Y. T.; *et al.* Application and Synthesis of Thiazole Ring in Clinically Approved Drugs. *Eur J Med Chem* **2023**, *250*.

[290] Thomas, T.; Thomas, T. J. Polyamines in Cell Growth and Cell Death: Molecular Mechanisms and Therapeutic Applications. *Cell Mol Life Sci* **2001**, *58* (2), 244.

[291] Van Meter, E. N.; Onyango, J. A.; *et al.* A Review of Currently Identified Small Molecule Modulators of MicroRNA Function. *European Journal of Medicinal Chemistry*. Elsevier Masson SAS February 15, 2020.

[292] Maren, T. H. Relations between Structure and Biological Activity of Sulfonamides. *Annu Rev Pharmacol Toxicol* **1976**, *16*.

[293] Adsmond, D. A.; Grant, D. J. W. Hydrogen Bonding in Sulfonamides. *J Pharm Sci* **2001**, *90* (12), 2058.

[294] Hantzsch, A.; Weber, J. H. Ueber Verbindungen Des Thiazols (Pyridins Der Thiophenreihe). *Berichte der deutschen chemischen Gesellschaft* **1887**, *20* (2), 3118.

[295] Weiß, K. M.; Wei, S.; *et al.* Novel One-Pot Process for the Synthesis of 1,3-Thiazolesvia Organocatalysed Epoxidation of Nitro-Olefins. *Org Biomol Chem* **2011**, *9* (9), 3457.

[296] Gao, X.; Pan, Y. M.; *et al.* Facile One-Pot Synthesis of Three Different Substituted Thiazoles from Propargylic Alcohols. *Org Biomol Chem* **2010**, *8* (14), 3259.

[297] Tang, X.; Yang, J.; *et al.* Access to Thiazole via Copper-Catalyzed [3+1+1]-Type Condensation Reaction under Redox-Neutral Conditions. *Journal of Organic Chemistry* **2016**, *81* (22), 11461.

[298] Ma, X.; Yu, X.; *et al.* Synthesis of Thiazoles and Isothiazoles via Three-Component Reaction of Enaminoesters, Sulfur, and Bromodifluoroacetamides/Esters. *Org Lett* **2020**, *22* (14), 5284.

[299] Alom, N. E.; Wu, F.; *et al.* One-Pot Strategy for Thiazoline Synthesis from Alkenes and Thioamides. *Org Lett* **2017**, *19* (4), 930.

[300] Griffin, J.; Atherton, J.; *et al.* The Ammonolysis of Esters in Liquid Ammonia. *J Phys Org Chem* **2013**, *26* (12), 1032.

[301] Quada, J. C.; Boturyn, D.; *et al.* Photoactivated DNA Cleavage by Compounds Structurally Related to the Bithiazole Moiety of Bleomycin. *Bioorg Med Chem* **2001**, *9* (9), 2303.

[302] Pittelkow, M.; Lewinsky, R.; *et al.* Selective Synthesis of Carbamate Protected Polyamines Using Alkyl Phenyl Carbonates. *Synthesis (Stuttg)* **2002**, *2002* (15), 2195.

[303] Nguyen, W.; Jacobson, J.; *et al.* Identification of 5-Substituted 2-Acylaminothiazoles That Activate Tat-Mediated Transcription in HIV-1 Latency Models. *J Med Chem* **2019**, *62* (10), 5148.

[304] Siengalewicz, P.; Mulzer, J.; *et al.* 6.09 Synthesis of Esters and Lactones. *Comprehensive Organic Synthesis: Second Edition* **2014**, *6*, 355.

[305] El-Faham, A.; Albericio, F. Peptide Coupling Reagents, More than a Letter Soup. *Chem Rev* **2011**, *111* (11), 6557.

[306] Carpino, L. A.; Imazumi, H.; *et al.* Comparison of the Effects of 5- and 6-HOAt on Model Peptide Coupling Reactions Relative to the Cases for the 4- and 7-Isomers. *Org Lett* **2000**, *2* (15), 2253.

[307] Lee, H. W.; Kang, T. W.; *et al.* Diethyl Chlorophosphate: An Effective and Convenient Coupling Reagent of Cephalosporin Derivatives. *Synth Commun* **1998**, *28* (1), 35.

[308] Nakatani, K.; Sando, S.; *et al.* Recognition of a Single Guanine Bulge by 2-Acylamino-1,8-Naphthyridine. *J Am Chem Soc* **2000**, *122* (10), 2172.

[309] Patra, D.; Banerjee, S.; *et al.* A Pyrimido-Quinoxaline Fused Heterocycle Lights Up Transfer RNA upon Binding at the Mg2+ Binding Site. *Chembiochem* **2021**, *22* (2), 359.

[310] Ryan, C. A.; Baskevics, V.; *et al.* 2-Guanidyl Pyridine PNA Nucleobase for Triple-Helical Hoogsteen Recognition of Cytosine in Double-Stranded RNA. *Chemical Communications* **2022**, *58* (51), 7148.

[311] Childs-Disney, J. L.; Yang, X.; *et al.* Targeting RNA Structures with Small Molecules. *Nat Rev Drug Discov* **2022**, *21* (10), 736.

[312] Blanco, F.; Kelly, B.; *et al.* Non-Covalent Interactions: Complexes of Guanidinium with DNA and RNA Nucleobases. *Journal of Physical Chemistry B* **2013**, *117* (39), 11608.

[313] Vušurović, J.; Schneeberger, E. M.; *et al.* Interactions of Protonated Guanidine and Guanidine Derivatives with Multiply Deprotonated RNA Probed by Electrospray Ionization and Collisionally Activated Dissociation. *ChemistryOpen* **2017**, *6* (6), 739.

[314] Roughley, S. D.; Jordan, A. M. The Medicinal Chemist's Toolbox: An Analysis of Reactions Used in the Pursuit of Drug Candidates. *J Med Chem* **2011**, *54* (10), 3451.

[315] Afanasyev, O. I.; Kuchuk, E.; *et al.* Reductive Amination in the Synthesis of Pharmaceuticals. *Chem Rev* **2019**, *119* (23), 11857.

[316] Borch, R. F.; Bernstein, M. D.; *et al.* The Cyanohydridoborate Anion as a Selective Reducing Agent. *J Am Chem Soc* **1971**, *93* (12), 2897.

[317] Abdel-Magid, A. F.; Maryanoff, C. A.; *et al.* Reductive Amination of Aldehydes and Ketones by Using Sodium Triacetoxyborohydride. *Tetrahedron Lett* **1990**, *31* (39), 5595.

[318] Kobayashi, S.; Yasuda, M.; *et al.* Trichlorosilane-Dimethylformamide (Cl3SiH-DMF) as an Efficient Reducing Agent. Reduction of Aldehydes and Imines and Reductive Amination of Aldehydes under Mild Conditions Using Hypervalent Hydridosilicates. *https://doi.org/10.1246/cl.1996.407* **2006**, No. 5, 407.

[319] Popov, K. K.; Campbell, J. L. P.; *et al.* Reductive Amination Revisited: Reduction of Aldimines with Trichlorosilane Catalyzed by Dimethylformamide–Functional Group Tolerance, Scope, and Limitations. *Journal of Organic Chemistry* **2022**, *87* (2), 920.

[320] Feichtinger, K.; Zapf, C.; *et al.* Diprotected Triflylguanidines: A New Class of Guanidinylation Reagents. *Journal of Organic Chemistry* **1998**, *63* (12), 3804.

[321] Vordermark, D.; Brown, J. M. Endogenous Markers of Tumor Hypoxia: Predictors of Clinical Radiation Resistance? *Strahlentherapie und Onkologie* **2003**, *179* (12), 801.

[322] Said, H. M.; Hagemann, C.; *et al.* Expression Patterns of the Hypoxia-Related Genes Osteopontin, CA9, Erythropoietin, VEGF and HIF-1α in Human Glioma in Vitro and in Vivo. *Radiotherapy and Oncology* **2007**, *83* (3), 398.

[323] Tanaka, N.; Kato, H.; *et al.* Expression of Carbonic Anhydrase 9, a Potential Intrinsic Marker of Hypoxia, Is Associated with Poor Prognosis in Oesophageal Squamous Cell Carcinoma. *Br J Cancer* **2008**, *99* (9), 1468.

[324] Erpolat, O. P.; Gocun, P. U.; *et al.* Hypoxia-Related Molecules HIF-1α, CA9, and Osteopontin: Predictors of Survival in Patients with High-Grade Glioma. *Strahlentherapie und Onkologie* **2013**, *189* (2), 147.

[325] Pastorekova, S.; Gillies, R. J. The Role of Carbonic Anhydrase IX in Cancer Development: Links to Hypoxia, Acidosis, and Beyond. *Cancer and Metastasis Reviews* **2019**, *38* (1–2), 65.

[326] Chu, C. Y.; Jin, Y. T.; *et al.* CA IX Is Upregulated in CoCl2-Induced Hypoxia and Associated with Cell Invasive Potential and a Poor Prognosis of Breast Cancer. *Int J Oncol* **2016**, *48* (1), 271.

[327] Hyuga, S.; Wada, H.; *et al.* Expression of Carbonic Anhydrase IX Is Associated with Poor Prognosis through Regulation of the Epithelial-Mesenchymal Transition in Hepatocellular Carcinoma. *Int J Oncol* **2017**, *51* (4), 1179.

[328] Chen, K.; Satlof, L.; *et al.* SAT-124 Optimization of Experimental Conditions for Mimicking Hypoxia in Cultured Breast Cancer Cells by Using Cobalt(II) Chloride (CoCl2). *J Endocr Soc* **2020**, *4*.

[329] Lunn, M.-L.; Mouritzen, P.; *et al.* MicroRNA Quantitation from a Single Cell by PCR Using SYBR® Green Detection and LNA-Based Primers. *Nat Methods* **2008**, *5* (2), 3.

[330] Ren, D.; Yang, Q.; *et al.* Oncogenic MiR-210-3p Promotes Prostate Cancer Cell EMT and Bone Metastasis via NF-KB Signaling Pathway. *Mol Cancer* **2017**, *16* (1), 1.

[331] Evangelista, A. F.; Oliveira, R. J.; *et al.* Integrated Analysis of MRNA and MiRNA Profiles Revealed the Role of MiR-193 and MiR-210 as Potential Regulatory Biomarkers in Different Molecular Subtypes of Breast Cancer. *BMC Cancer* **2021**, *21* (1), 1.

[332] Rothé, F.; Ignatiadis, M.; *et al.* Global MicroRNA Expression Profiling Identifies MiR-210 Associated with Tumor Proliferation, Invasion and Poor Clinical Outcome in Breast Cancer. *PLoS One* **2011**, *6* (6), 20980.

[333] Liu, W.; Gao, N. Clinical Significance of MiR-210 Expression in Breast Cancer Tissues and Its Influence on Malignant Be-Havior of Triple Negative Breast Cancer Cells. *Journal of International Oncology* **2018**, *12*, 525.

[334] Tang, T.; Yang, Z.; *et al.* Up-Regulation of MiR-210 Induced by a Hypoxic Microenvironment Promotes Breast Cancer Stem Cell Metastasis, Proliferation, and Self-Renewal by Targeting E-Cadherin. *The FASEB Journal* **2018**, *32* (12), 6965.

[335] Maxwell, P. H.; Wlesener, M. S.; *et al.* The Tumour Suppressor Protein VHL Targets Hypoxia-Inducible Factors for Oxygen-Dependent Proteolysis. *Nature* **1999**, *399* (6733), 271.

[336] Blancher, C.; Moore, J. W.; *et al.* Relationship of Hypoxia-Inducible Factor (HIF)-1 and HIF-2 Expression to Vascular Endothelial Growth Factor Induction and Hypoxia Survival in Human Breast Cancer Cell Lines. *Cancer Res* **2000**, *60*, 7106.

[337] Špaková, I.; Rabajdová, M.; *et al.* Effect of Hypoxia Factors Gene Silencing on ROS Production and Metabolic Status of A375 Malignant Melanoma Cells. *Scientific Reports 2021 11:1* **2021**, *11* (1), 1.

[338] Guo, K.; Searfoss, G.; *et al.* Hypoxia Induces the Expression of the Pro-Apoptotic Gene BNIP3. *Cell Death Differ* **2001**, *8* (4), 367.

[339] Sowter, H. M.; Ratcliffe, P. J.; *et al.* HIF-1-Dependent Regulation of Hypoxic Induction of the Cell Death Factors BNIP3 and NIX in Human Tumors 1. *Cancer Res* **2001**, *61*, 6669.

[340] Bellot, G.; Garcia-Medina, R.; *et al.* Hypoxia-Induced Autophagy Is Mediated through Hypoxia-Inducible Factor Induction of BNIP3 and BNIP3L via Their BH3 Domains. *Mol Cell Biol* **2009**, *29* (10), 2570.

[341] Koop, E. A.; van Laar, T.; *et al.* Expression of BNIP3 in Invasive Breast Cancer: Correlations with the Hypoxic Response and Clinicopathological Features. *BMC Cancer* **2009**, *9* (1), 1.

[342] Burton, T. R.; Eisenstat, D. D.; *et al.* BNIP3 (Bcl-2 19 KDa Interacting Protein) Acts as Transcriptional Repressor of Apoptosis-Inducing Factor Expression Preventing Cell Death in Human Malignant Gliomas. *The Journal of Neuroscience* **2009**, *29* (13), 4189.

[343] Bando, H.; Toi, M.; *et al.* Genes Commonly Upregulated by Hypoxia in Human Breast Cancer Cells MCF-7 and MDA-MB-231. *Biomedicine & Pharmacotherapy* **2003**, *57* (8), 333.

[344] Brown, J. M.; Wilson, W. R. Exploiting Tumour Hypoxia in Cancer Treatment. *Nature Reviews Cancer 2004 4:6* **2004**, *4* (6), 437.

[345] Muz, B.; Puente, P. de la; *et al.* The Role of Hypoxia in Cancer Progression, Angiogenesis, Metastasis, and Resistance to Therapy. *Hypoxia* **2015**, *3*, 83.

[346] Graham, K.; Unger, E. Overcoming Tumor Hypoxia as a Barrier to Radiotherapy, Chemotherapy and Immunotherapy in Cancer Treatment. *Int J Nanomedicine* **2018**, *13*, 6049.

[347] Jazbutyte, V.; Thum, T. MicroRNA-21: From Cancer to Cardiovascular Disease. *Curr Drug Targets* **2010**, *11* (8), 926.

[348] Dalvit, C. NMR Methods in Fragment Screening: Theory and a Comparison with Other Biophysical Techniques. *Drug Discov Today* **2009**, *14* (21–22), 1051.

[349] Buchholz, C. R.; Pomerantz, W. C. K. 19F NMR Viewed through Two Different Lenses: Ligand-Observed and Protein-Observed 19F NMR Applications for Fragment-Based Drug Discovery. *RSC Chem Biol* **2021**, *2* (5), 1312.

[350] Vulpetti, A.; Hommel, U.; *et al.* Design and NMR-Based Screening of LEF, a Library of Chemical Fragments with Different Local Environment of Fluorine. *J Am Chem Soc* **2009**, *131* (36), 12949.

[351] Dalvit, C.; Flocco, M.; *et al.* Fluorine-NMR Competition Binding Experiments for High-Throughput Screening of Large Compound Mixtures. *Comb Chem High Throughput Screen* **2002**, *5* (8), 605.